

~~SECRET/SPECIAL HANDLING~~

Document Control No 9400-68-717  
Copy 3 of \_\_\_\_\_

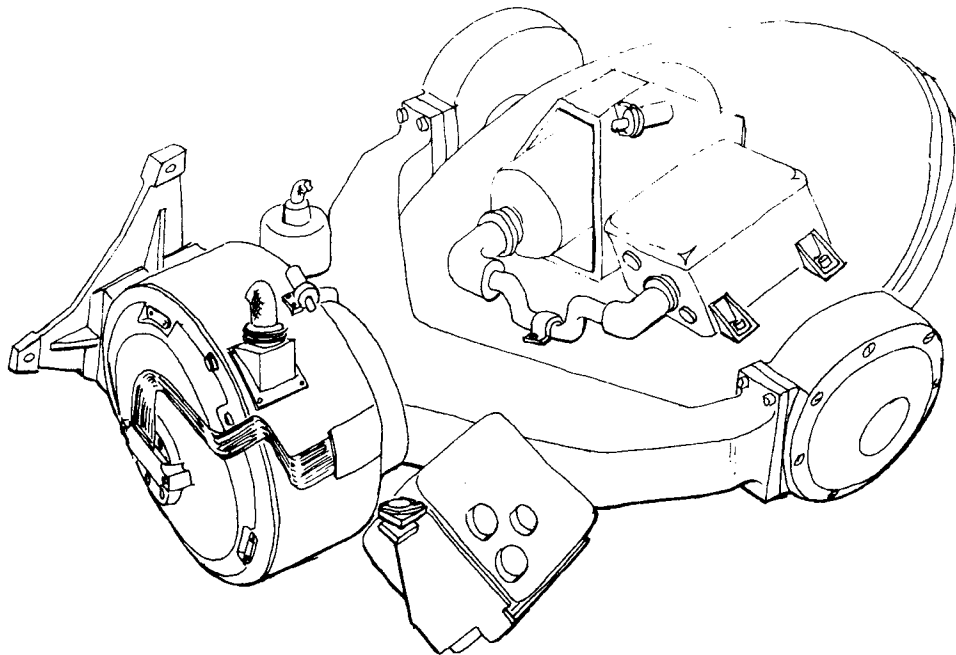
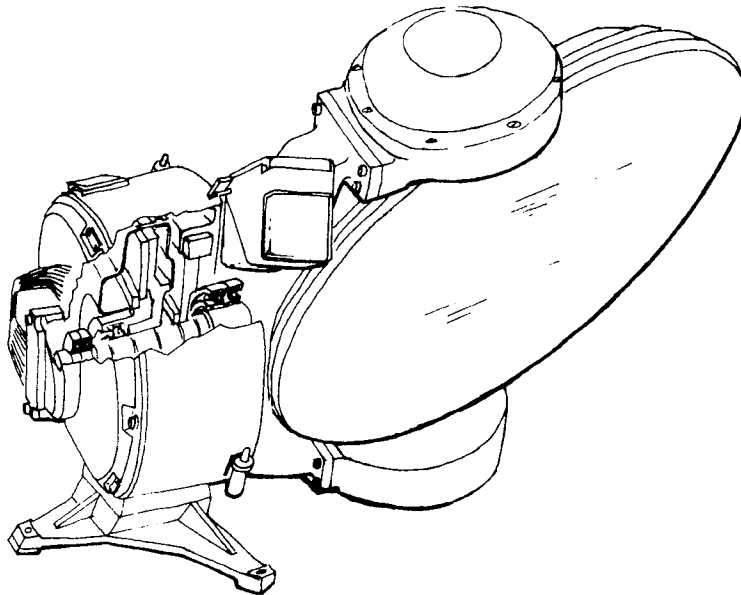
**PRELIMINARY DESIGN REVIEW REPORT**

**A/O SCANNER ASSEMBLY**

5 JULY 1968

~~SECRET/SPECIAL HANDLING~~

~~SECRET~~/SPECIAL HANDLING



Preliminary sketches of scanner assembly

~~SECRET~~/SPECIAL HANDLING

~~SECRET~~/SPECIAL HANDLING

## 1. INTRODUCTION

Itek Corporation has contracted, under the provisions of Contract No. 029 B 25000, to design, develop, test, qualify and delivery a complete Acquisition/Optics (A/O) Subsystem which will ultimately be utilized in a manned orbiting satellite. The mission objective, for which the Itek A/O is of paramount importance, is to provide constant surveillance of areas of military interest in denied territories. Although the general target areas are preselected and programmed under earth based computer control, the A/O Subsystem design must provide the capability for actual astronaut evaluation, discrimination and selection of prime targets among the multiple possibilities presented to him. Two such subsystems mounted on either side of the orbiting vehicle, i.e., a right hand and a left hand system, provide full field coverage.

The Itek A/O Subsystem is comprised of five major components located functionally as indicated schematically in Fig. 1-1. These major components are: (1) an internally mounted telescope, (2) a window in the vehicle wall, (3) a fixed fold mirror, (4) a scan mirror (both mirrors are mounted on the external vehicle wall), and (5) a protective shroud enclosing the external components during launch and passive portions of the mission.

During operation mode, with the shroud open, the scan mirror tracks and acquires targets on the ground under preprogrammed computer control. The optical image is reflected from the scan mirror to the fold mirror, through the window into the telescope where it is properly magnified and focussed as required to produce a clear sharp image for visual observation.

The design of each of these components is sophisticated and requires unique knowledge of optics and extensive experience in optical equipment design and fabrication. Among all of the A/O Subsystem designs, the design of the scan mirror is perhaps the most critical, since it forms an integral part of the complete servoloop; effecting control of the entire system.

Scanner performance, operation, and interface requirements are documented in specification EC-331B, AN's 1 through 9, and in Work Statement 331Q. The design of a scanner to meet these requirements has evolved through a number of configuration and tradeoff studies. It has become clear, as a result, that no reasonable design can meet the multiplicity of conflicting requirements without some relaxation of the governing specifications in key areas. The preliminary design of several alternate configurations has proceeded to the point where contractor definition and decision is required. Of the multiple preliminary designs evaluated, Itek has generated one which in our opinion, represents the optimum compromise possible.

In accordance with contractual requirements, Itek is prepared to submit its preliminary design. Also presented are alternative configurations studied and the specification tradeoffs required for contractor review. This report, which conforms to the requirements of Data Item MSM-S-137-2, is submitted in support of the formal Preliminary Design Review scheduled for 17 and 18 July 1968.

~~SECRET~~/SPECIAL HANDLING

~~SECRET~~/SPECIAL HANDLING

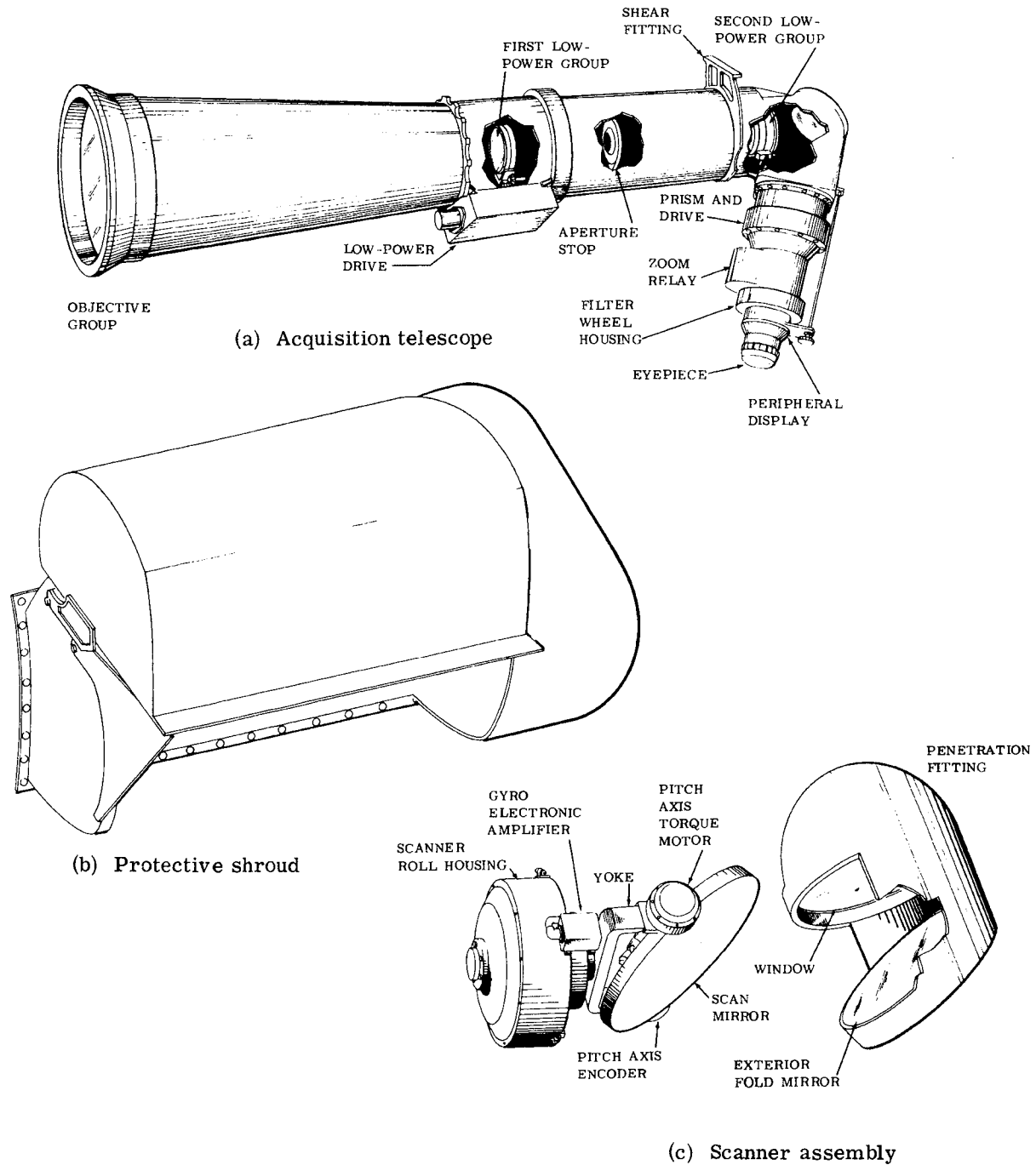


Fig. 1-1 — Present A.O. System

~~SECRET~~/SPECIAL HANDLING

~~SECRET~~/SPECIAL HANDLING

### 1.1 EVOLUTION OF THE DESIGN

The initial design approach subordinated weight, stiffness, inertia, and interference criteria to the specifications governing vignetting and obscuration since these parameters directly impacted system optical performance. A preliminary design evolved which satisfied all vignetting requirements except those associated with very high pitch angles. This design demonstrated satisfactory compliance with the weight, inertia, and stiffness requirements, although significant structural interferences did exist.

The significant characteristic of this scanner design (referred to hereafter as the "baseline" configuration) is its unbalanced roll axis (by approximately 40 inch-lbs). A balanced roll axis is possibly a more natural and desirable design. Many vignetting studies led to the conclusion however, that in the context of all the imposed restraints, a balanced roll-axis scanner design that met the requirements, particularly in the no-vignetting zone, could not be configured. The unbalanced design has no impact on the scanner's on-orbit operational capability, but it does assume significance in terms of ground testing in a 1-g environment. Other areas of the baseline configuration which required further design definition and resolution included alignment features, the use of pyrotechnic devices, bearing and cable noise characteristics, PSD allocation encoder performance, cable design maintainability, accessibility and fabrication/assembly techniques.

A review of the baseline configuration "in toto" led to the conclusion that although it offered the best promise for meeting a rigorous interpretation of specification EC331-B, it would fall short of fulfilling the overall needs for testing of the system. Itek thereupon directed its design efforts in two parallel directions: (1) to resolve deficiencies in the basic design, and (2) determine the areas in which specification tradeoffs could be made which would permit a design satisfying all requirements without a corresponding significant degradation of optical performance.

The first area resulted in the implementation of bearing, encoder, and cable test and development activities, evaluation of various mechanical design possibilities including the introduction of line-boring techniques, rearrangement of encoder and torques locations, introduction of cable runs, redesign of the mirror/bezel configuration, weight reduction techniques, finalizing launch lock, stow lock and energy absorber design concepts, material optimization, etc. The details and results of these efforts together with their implications with regard to specification changes and interface requirements are presented in appropriate sections throughout this report.

The second area resulted in the implementation of a complete series of vignetting and obscuration studies of various configurations, along with a parallel study effort to sufficiently assess the effects of vignetting and obscuration on ground resolved distance and image quality. As a result of these studies, and associated interference studies, Itek has selected one of these configurations as the best design compromise which will fulfill overall system needs. This preliminary design, hereinafter referred to as the "available" configuration is shown pictorially on the frontispiece.

The details of studies described above and their results are discussed in Section 3 of this report. A summary of these efforts along with a comparison of the "baseline" and "available" designs are presented in the following paragraphs.

~~SECRET~~/SPECIAL HANDLING

~~SECRET~~/SPECIAL HANDLING

## 1.2 TRADEOFF SUMMARY AND COMPARISONS

The ramifications of shifting design direction from the unbalanced, baseline design to the balanced, recommended design available are best illustrated by a summarized comparison of the two, and considerations of yet other alternatives. Many improvements have been incorporated into the scanner design over the past several months, and additional design detail completed. This is characterized by an overall reduction in scanner weight from 56.82 pounds to 52.32 pounds (exclusive of Contractor-furnished gyros, electronics and interconnecting cables).

The baseline configuration has a balanced pitch axis and an unbalanced (approximately 40 in.-lbs) roll axis. The pitch axis is located 0.9 inch above the roll axis which is coincident with the optical centerline. Numerous system trade studies conducted in recent months comparing the baseline configuration with various balanced configurations demonstrated the best compromise between minimizing structural interferences and vignetting was achieved by moving the roll axis up 0.45 inch and the pitch axis down 0.2 inch from their respective baseline locations. It is feasible that, using the results of the unbalanced design effort, an acceptable balanced design can be generated and would provide product improvement. Itek is prepared to proceed with this effort upon direction by the Customer. This design is hence defined as the available configuration.

It should be noted that all of the balanced configurations are characterized by a higher stiffness than the baseline configuration due to an inherently stiffer yoke (approximately 100 percent), reduced roll axis inertias by approximately 0.012 slug-ft<sup>2</sup>, and weigh approximately the same as the baseline design.

The baseline configuration meets the vignetting specification, whereas the available balanced configuration does not. The specification requires that no vignetting exist between +10 and +40 degrees in pitch, and ±35 degrees in roll. Vignetting of the balanced configuration is very small (approximately 1.1 percent maximum) for the nominal scanner mount location, but may increase to a few percent for scanner locations other than nominal (interface agreements on the tolerance for the scanner mount have not yet been reached). The resulting vignetting is not a serious factor, however, since it occurs only at extreme roll angles and the corresponding reduction in optical resolution is only a few hundreds of a foot. (See Section 3.3)

Detailed layouts of each configuration studied have been made to determine the extent and seriousness of any structural interference. Comparison of these layouts indicates the available configuration represents a significant improvement over the baseline configuration in that interference extends only through vehicle insulation and rib, and not into the vehicle wall as well.

A comparison of the salient features and characteristics of the various configurations studied is summarized in Table 1.2-1.

The best possible configuration in terms of interference is one where the pitch axis is moved down 0.9 inch relative to the baseline. The only interference is a slight penetration of the insulation of the vehicle by the encoder housing. The amount of vignetting of this configuration is excessive, however, being a maximum of 8.4 percent at +10-degree pitch, and -35-degree roll. The vignetting could be reduced significantly if the fixed fold mirror could be tilted approximately 1.0 to 1.5 degrees. Presently, specification EC-331B prohibits this but if the specification could be altered a detailed configuration layout study of this approach would be warranted.

A second approach to reducing interference with the vehicle involves reducing the gimbal travel at high positive pitch angles. Above 60 degrees in pitch, obscuration by the shroud very large. This combines with the deleterious effects of a long transmission distance through the atmosphere to seriously reduce ground resolution. A relaxation of maximum gimbal travel would thus improve the interference problem without sacrifice of significant optical capability.

~~SECRET~~/SPECIAL HANDLING

~~SECRET/SPECIAL HANDLING~~

Table 1.2-1 --Comparison of Configurations

Description	Vignetting					Interference or Clearance				Inertias	Stiffness	Weight	Configuration (approx.)	
	± 45° Roll		± 35° Roll		Vehicle	Ribs	Insulation	Shroud Shaft	Shroud Envelope					
	+70°p	+40°p	+10°p	0°p										+40°p
Unbalanced design P.A. up .900 (Baseline)	<.5	0	0	2.0	0	0	Interference	Clears	Clears	Clears	0.08 slug-ft <sup>2</sup> in pitch 0.02 slug-ft <sup>2</sup> minimum in roll	Greater than 150 cps Natural frequency	52.98 pounds	Layout No. 906037
Roll Axis up .900	3.7	3.7	7.6	8.3	3.8	4.3	Clears	Interference	Interference	Interference	Pitch axis = 0.08 slug-ft <sup>2</sup> (approximate) minimum for all balanced configurations	The yoke is approximately 100% stiffer for all balanced configurations. This increases the natural frequency by 5 to 10%	Approximately 52.3 pounds for all balanced configurations	Layout No. 906042 Gyro & elect. pkg on centerline of yoke
Roll Axis up .45 P.A. Down 0	2.3	2.5	2.1	8.5	<.5	<.5	Clears	Interference	Interference	Interference				Gyro .65" below roll axis elect. pkg & balance weight 4" below roll axis
Roll Axis up .45 P.A. Down .10	<.5	<.5	3.3	7.2	<.5	<.5	Clears	Interference	Clears	Clears				Layout No. 906040 Gyro .65" below roll axis elect. pkg 3" below roll axis
Roll Axis up .45 P.A. Down .30	<.5	<.5	8.5	8.5	<.5	2.9	Clears	Interference	Clears	Clears				Gyro .65" below roll axis elect. pkg 1" below roll axis
Roll Axis up .45 P.A. Down 20 (Recommended configuration)	<1.0	—	—	7.6	<.5	1.1	Clears	Interference	Clears	Clears				Layout No. 906045 Gyro .65" below roll axis elect. pkg 2" below roll axis
Roll Axis & pitch axis coincident with optical axis					0	8.4	Clears	Interference	Clears	Clears				Layout No. 906040 Gyro & elect. pkg on centerline of yoke

NOTE: P.A. = Pitch axis  
R.A. = Roll axis

+70°p = +70 degree pitch  
i.e., for +45-degree roll there are 4 pitch settings and for +35-degree roll there are 2 pitch settings  
<.5 etc. means less than

~~SECRET/SPECIAL HANDLING~~

~~SECRET~~/SPECIAL HANDLING

Potential interferences between the scanner and the protective shroud exist during the launch phase. The dynamic excursion of the scanner under launch loads has been determined, but since neither vehicle loads into the shroud nor hard mounting points have been established by the contractor, this has not been possible for the shroud. Until these factors are firmly defined, the required dynamic envelope cannot be established.

All interference and vignetting studies have been performed for the scanner in its nominal position. The tolerance on the mount position has yet to be defined by the contractor. Tolerances up to  $\pm 1/4$  inch have been mentioned as being necessary, but in view of the existing interference and vignetting problems, Itek considers this to be excessive and intolerable.

This summary is intended to emphasize the more critical tradeoff considerations. A full discussion of the studies performed and their implications is presented in Section 3.

~~SECRET~~/SPECIAL HANDLING

~~SECRET/SPECIAL HANDLING~~

### 1.3 STATUS OF THE DESIGN

At the present time, Itek has designed two complete preliminary scanner configurations, i.e., the unbalanced baseline and available balance, and has conducted sufficient design studies to implement variations of either of these without major impact of the program. The planned activity required to bring either of these designs through completion for Engineering Model hardware release is detailed in the Summary Network shown in Fig. 1.3-1.

It will be noted that effort should be expended in the area of the Itek available balance design during the intervening period between July 1st and the formal PDR presentation. This will serve to equalize the status of the two designs and will further provide additional pertinent information and data for that presentation.

Firm direction by the contractor is necessary at this stage of the design if the overall program schedule is not to be seriously impacted. Receipt of a configuration decision backed up by corresponding formal specification, changes to accommodate that decision by 1 August 1968 is considered critical. Important mechanical and electrical interface decisions and agreements must also be made by the dates specified on the summary network.

#### CRITICAL DESIGN AREAS

Certain areas of the scanner design have been critical in terms of achieving a satisfactory design from all view points. The status of these areas are as follows:

Unbalanced Roll Axis. Numerous balanced configurations are discussed in this report in terms of scanned system impact. A balanced roll axis is recommended.

Torque Ripple (PSD). Extensive effort has been devoted to bearing and cable tests over the past 6 months. A major portion of the bearing test work will be conducted by the contractor in order to benefit from its extensive past experience on problems of a similar nature. While Itek cannot yet conclusively demonstrate its ability to comply with the existing PSD specification, experimental results to date indicate that the probabilities of doing so are excellent.

Encoders. A redesign of the encoder electronics and an extensive test program over the past three months indicate that a satisfactory encoder velocity error is obtainable. The present specification EC-331B is grossly inadequate for either party and must be modified and better defined.

Torquers. A design study has been completed by Aeroflex on brushless torquers for both axes. Satisfactory torquers will be provided at less weight and power than previously anticipated.

Weight. The weight of the current scanner design is approximately 52.32 pounds and the trend is down but stabilizing. This weight is consistent with the total system weight budget of 166 pounds.

Inertias. Pitch axis inertia will be 0.08 slug-ft minimum for any configuration.

Roll axis inertia varies from  $>0.23$  slug-ft<sup>2</sup>, depending on mirror position and configuration (balanced or unbalanced). The minimum roll inertia is expected to drop further (0.17 to 0.175) as weight reductions are finalized.

To achieve the minimum specification value of 0.23 slug-ft<sup>2</sup>, weights will have to be added.

Stiffness. The present design will meet (or can be made to meet) the specified transmissibility. Since the overall transmissibility is greatly reduced by the soft vehicle mount, Itek feels the present transmissibility specification should be re-evaluated.

Transmissibility data with and without the vehicle ground spring is presented in this report.

~~SECRET/SPECIAL HANDLING~~

~~SECRET~~/SPECIAL HANDLING



Fig. 1.3-1— Program scanner network

~~SECRET~~/SPECIAL HANDLING

~~SECRET~~/SPECIAL HANDLING

Producibility. The scanner utilizes a large amount of beryllium in its construction. The design has been re-evaluated and many changes incorporated to improve ease of fabrication, assembly, and alignment. These are discussed in Section 4 of this report. The roll axis torquer and encoder positions have been reversed to improve encoder accessibility for maintenance.

It is planned to consult with Pittsfield Ordnance Department in relation to the production phase of the A/O effort.

Alignment. Both the pitch and roll axes will be line bored to eliminate critical alignment tolerances. An axial adjustment flexure has been incorporated in to the pitch axis. A third bearing has been added to the pitch axis assembly for mounting the encoder disc to eliminate disc deflection problems at launch.

Mirror/Bezel. A new bezel design has been incorporated to reduce mirror deformation under thermal loads and to reduce weight. A detailed mirror/potting/bezel analysis indicates a completely satisfactory design with passive thermal control is achievable.

In connection with any discussion about critical design areas, it is relevant to consider Itek's overall design approach to yield satisfactory, in-specification flight hardware. As a result of program funding restraints and resultant compression of schedules, Engineering Model hardware and a development test model will be fabricated to the Preliminary Design. In parallel with that activity, the design studies, analyses and development test effort required to further refine the design for flight hardware application and to resolve remaining questionable areas will be carried on at an intensive pace. This approach offers the requisite high degree of confidence that all program objectives, schedule and technical, can be met.

Compliance With Data Item MSM-S-137-2. Although this report does comply with the provisions of Data Item MSM-S-137-2, it does not necessarily follow that format. The following correlation index is provided to permit ready access to desired items of interest. An agenda for the scheduled PDR meeting is also included.

~~SECRET~~/SPECIAL HANDLING

~~SECRET~~/SPECIAL HANDLING

Table 1.3-1 — Response to MSM-S-137-2

DRL  
Item  
No.

Response

- 1 Item no. 1 is in essence the PDR report.
- 2 Item no. 2 is covered in Section 1.
- 3 Item no. 3 is covered in Section 3.2.
- 4 Item no. 4 is covered in each major section on each item of the scanner design
- 5 Item no. 5 is covered in Section 1. ~~and 2.~~
- 6 Section 2 comprises the response to Item no. 6.
- 7 This report ~~on~~ <sup>and</sup> appendixes cover the response to Item no. 7.
- 8 A plastic—metal model of the scanner is being fabricated.
- 9 Item no. 9 is fulfilled in Section 4.
- 10 Item no. 10 is covered in the network included in Section 1.
- 11 Item no. 11 is covered in Section 11.1.
- 12 In response to Item 12, the following schedule of long lead items is submitted:

Major long lead items previously released

1. SK-114148 18-bit optical shaft encoder
2. SK-114149 20-bit optical shaft encoder

The following units have been ordered:

Quantity	Description
1	Stainless steel experimental models
1	W/G in-house qualification model
3	Engineering models
12	Qualification, preproduction, and production models

Major long lead items not released

The following are the long lead items identified for the scanner procurement program

Item	Estimated time, weeks
Special bearings (pitch)	21
Special bearings (roll)	21
Torque motor (roll)	20
Torque motor (pitch)	17
Yoke (beryllium)	16
Bezel (beryllium)	14

~~SECRET~~/SPECIAL HANDLING

~~SECRET/SPECIAL HANDLING~~

Table 1.3-1 -- Response to MSM-S-137-2 (Cont.)

DRL Item No.	Response
13	Sections 10 and 6 provide data covering Item <del>12</del> <sup>13</sup> and an appropriate list will be available at PDR.
14	Item no. 14 is covered in the network in Section 1.
15 and 16	Items no. 15 and 16 are fulfilled by the accompanying documentation package and pertinent Appendixes to this report.
17	In response to Item no. 17, the recommended spares-support approach for the A/O Subsystem, including the scanner, was submitted as paragraph 5.11 of PDR Report (93W-67-296-6). Since no action has been taken by the contractor, no additional work has been done. Work Statement WS-331Q requires submittal of spares data per DRL Item MSM-L-104, which in turn calls out guidance meetings and further contract negotiations to determine the spares program. Upon direction from the contractor, Itek will reinstate work on the spares program. It is anticipated that this will take the form of an updated spares list.
18	An agenda is included in Section 1.

~~SECRET~~/SPECIAL HANDLING

AGENDA FOR SCANNER PDR - 17,18 JULY 1968

FIRST DAY

8:00 - 8:10	Welcome and General Introduction	T. G. Nelson
8:10 - 8:30	Technical Introduction and Summary	T. Vogt
8:30 - 8:50	Scanner Specifications and Status	R. Heath
8:50 - 9:10	Configuration Trade Studies - General	T. Vogt
9:10 -10:00	Balanced vs Unbalanced Design Studies	P. Clifford
10:00 -10:30	System Vignetting Studies	R. Carignan
10:30 -10:45	Vignetting Effects on Optical Performance	R. Heath
10:45 -11:00	<u>Coffee Break</u>	
11:00 -11:20	Mechanical Design Features	S. Staulo
11:20 -11:30	Overall Design Features	S. Staulo
11:30 -11:40	Mass Properties	A. Machera
11:40 -11:50	Optical Considerations	J. Zimmerman
11:50 -12:20	Mirror/Bezel Design	S. Kokkins
12:20-12:30	Alignment and Assembly Methods	S. Staulo
12:30 - 1:15	<u>Lunch</u>	
1:15 - 2:00	Encoder error and Encoder Design	D. Humez
2:00 - 2:30	Torque Levels and Torque Motors	R. Warren
2:30 - 2:45	<u>Coffee Break</u>	
2:45 - 3:00	Summary	T. Vogt
3:00 - 4:30	Questions and Answers	

~~SECRET~~/SPECIAL HANDLING

~~SECRET~~/SPECIAL HANDLING

SECOND DAY

8:00 - 8:20	PSD Definition	R. Warren
8:20 - 9:00	Bearings	D. Sokolow
9:00 - 9:30	Cable	R. Coates
9:30 - 10:00	PSD Allocation	D. Sokolow
10:00 - 10:15	<u>Coffee Break</u>	
10:15 - 11:00	Transmissibility and other Dynamic Considerations	F. Bovenzi
11:00 - 11:30	Thermal Considerations	J. Berenholz
11:30 - 12:00	Structural Considerations	R. Berks
12:00 - 12:45	<u>Lunch</u>	
12:45 - 1:15	Test Methods and Plans	R. Heath
1:15 - 1:45	Reliability and Maintainability	E. Powers
1:45 - 2:00	QA & QC	R. Capobianco
2:00 - 2:15	<u>Coffee Break</u>	
2:15 - 2:45	Technical Summation	T. Vogt
2:45 - 4:30	General Discussion	

} Move to  
1st day if  
possible

~~SECRET~~/SPECIAL HANDLING

~~SECRET/SPECIAL HANDLING~~

## 2. COMPARISON OF SPECIFICATIONS AND REQUIREMENTS TO PRELIMINARY DESIGN

This section demonstrates that design requirements are met by referencing the appropriate paragraphs contained in this report, and by summarizing, where necessary, data that appear in several different sections. The organization follows specification EC-331, and each discussion is preceded by the proper paragraph number from EC-331.

### 3.1.1.1.3 Scan Field

Gimbal coordinates for line-of-sight pointing within the required field limits differ from vehicle coordinates because of the 9° cant angle. A computer program written to calculate gimbal angles, field of view, and vignetting is presented in Section 3.2 and appropriate appendices, where it is demonstrated that the design meets all requirements for LOS pointing and field of view. A slight amount of vignetting (1.1%) is present inside +10°, +40° pitch and ±35° roll, and less than 60% vignetting obtains only out to +60° pitch. The effects of this vignetting are explained in Section 3.3.

### 3.1.1.1.4 Scanner Orientation

The orthogonality of the gimbal axes is easily established, as shown in Section 4.6. Alignment to the vehicle is a more difficult matter, involving both precision fabrication and careful alignment of the scanner pedestal to assure compliance with the requirements. The method of attachment and alignment to the vehicle is critical to the ability of the scanner to meet the requirements of this paragraph. Since recent information from the contractor has not yet been implemented, the final configuration for scanner alignment and adjustment has not been determined. The current design is described in Section 4.5.5 and shown in Drawing 906041.

### 3.1.1.1.5 Scanner Gimbal Acceleration

Section 6.3 discusses the selection of the proper motors. The requirements are more than easily satisfied, even with an unbalanced roll axis. The referenced discussions also explain how the current torque requirements can be lowered if a balanced system is chosen.

### 3.1.1.1.6 Scanner Gimbal Torques

The present requirement of no more than 2 in-oz of running friction torque for each gimbal is impossible to meet. Discussions with the Contractor have elicited a verbal agreement to 8 and 6 in-oz for roll and pitch respectively, as explained and elaborated in Section 5.4. The bearings, analyzed in Section 6.1, contribute 2 in-oz by themselves, leaving nothing for the cable friction. Ittek cannot at this time give positive assurance that the PSD specification

~~SECRET/SPECIAL HANDLING~~

~~SECRET/SPECIAL HANDLING~~

can be met, for the calculation process (explained in Section 5.3) is difficult and not entirely conclusive. Although preliminary calculations satisfy the requirements, the only way to measure accurately the PSD of a two-bearing shaft is experimentally.

3.1.1.1.7 Scanner Gimbal Inertia

The gimbal inertia requirements for the pitch and roll axes of no less than 0.08 and 0.23 slug-foot-squared respectively have not both been satisfied. The present design values are 0.08 and 0.19 slug-foot-squared respectively, and Section 4.7 explains the complete inertia problem in detail.

3.1.1.1.8 Scanner Structural Dynamics

The requirements on the structural dynamics are not satisfied by the present design model, for at one point the transmissibility curve goes above the profile in Figure 4 of EC-331. This is only a preliminary model, and data is available just from initial runs. The model does, however, include the interactions of the two axes and the effects of the mounting arrangement. Section 7 explains the details of the model and suggests methods to reduce the dynamic effects.

3.1.1.1.9 Scanner Gimbal Position Readout

Itek believes that the specified requirements, while simple enough to meet, are insufficient to assure adequate system performance. The requirements are satisfactory for random errors, but they neglect the more important systematic errors. Itek believes that a drastic revision of these specifications has become a matter of pressing concern, and Section 5.5.3 sets forth our views on the subject.

3.1.1.1.10 Gimbal Stops

The design requirements are satisfied without exception, as shown in Section 4.5.3.

3.1.1.1.26 Launch Locks

Launch locks with a remote redundant means of removal or deactivation are required for the scanner gimbals. Detailed design information is given in Section 4.5.1, where it is shown that all requirements are satisfied.

3.1.1.2.1 Alignment

The mirrors that are built onto the scanner gimbal housing to serve as alignment references assure compliance to the 0.25 arcminute maximum error in installation. No on-orbit alignment will be needed. Proper fabrication will allow the mirror surface to be parallel to the pitch axis within  $\pm 0.5$  arcminute.

3.1.1.2.5 Scanner Gimbal Drive

The requirements of the specification are fully satisfied by the inclusion of two independent stator windings in each torquer. Section 6.3 discusses the torque motors in detail.

~~SECRET/SPECIAL HANDLING~~

~~SECRET/SPECIAL HANDLING~~

#### 3.1.1.2.6 Scanner Gimbal Encoders

The requirements on the encoders can be met, three uncertainties notwithstanding. Section 6.4 presents a complete discussion of the design, and encoder specifications on Itek's subcontractor are given in SK114148 and SK114149.

The uncertainties are these. First, where is "the" zero reference position mentioned in EC-311? Second, which direction is defined as "clockwise"? Third, what accuracy is required on the auxiliary signals? These questions require answers, but it is certain that any reasonable response can be satisfied.

#### 3.1.1.2.7 Scanner Gimbal Mounted Gyro Assembly

Details of the location of the gimbal mounted gyro assemblies are in Sections 4.1.1 and 4.1.3, while the cable interconnection design is explained in Section 4.1.7.

#### 3.1.2.1 Reliability

The requirements in this section are met without exception. The whole of Section 11 is devoted to an analysis of reliability, where it is shown that the apportioned scanner reliability MTBF is 38,216 hours.

#### 3.1.2.2 Maintainability

The scanner assembly is designed for ease of maintenance and the recommended spares/support approach is defined in Table 1-2, DZTZ Item No. 17.

#### 3.1.2.3 Useful Life

The reliability estimate of Section 11 and the quality assurance provisions of Section 12 together satisfy the useful life provisions of the specification.

#### 3.1.2.4 Environmental

The scanner is designed to meet the environments of DR1100, Table III, as follows.

- a. Conditions during transportation and storage are controlled by the shipping containers.
- b. Thermal and atmospheric conditions during prelaunch, launch and ascent are controlled by the shroud and aerodynamics fairing, and on orbit by the shroud alone. Therefore the scanner is not designed to meet requirements relating to salt fog, sand and dust, rain, propellant compatibility, explosive atmosphere, and wind. As in Specification Item 1.3 of Table III, the scanner will be in class 100,000 atmosphere or better at all times.
- c. The scanner is being designed to withstand the specified dynamic environments detailed in Section 7.
- d. Thermal control of the gyro mounting surfaces is covered in Section 8.

#### 3.1.2.5 Transportability

These requirements can be fully satisfied, having been evaluated and approved by a potential container manufacturer, Container Research Incorporated. It should be noted that air transportation seems much more likely than railway shipment, in which case the shock requirements can be greatly relaxed. Proper packing for rail shipment is an expensive matter.

~~SECRET/SPECIAL HANDLING~~

~~SECRET~~/SPECIAL HANDLING

3.1.2.7 Safety

Section 11 summarizes the safety analysis, while Appendix II-A contains the complete safety report. All requirements are fulfilled.

3.2.2.3 Special Approval Components

The specifications for special approval components submitted on 4 April 1968 (reference 9400-68-566) are no longer valid. Revised specifications will soon be forthcoming.

3.3.1.1 Weight

The scanner weight allocation from the specified 166 pounds is 52.36 pounds. The current scanner weight estimate is presented in Section 4.7.

3.3.1.2 Power

The scanner power allocation from the specified 105 watts is 46.24 watts. The current scanner power estimate is presented in Sections 6.3 and 6.4.

3.3.1.4 Steady State Design Load Factors

That the proper load factors are used is demonstrated in the discussion in Section 7. The Design Loads of this paragraph were used unless load conditions derived from the dynamics environments specified in paragraph 3.1.2.4 were higher.

3.3.1.5 Wiring

Sections 4.1.7 and 6.2 present a complete discussion of wire and cabling design, with an explanation of why silicon rubber must be used rather than a fluorocarbon to insulate the flexible lead from the scanner to the mount.

3.3.3 Materials, Parts, and Processes

The discussions in the detailed design sections of this report reveal that these requirements can be satisfied.

3.3.4 Standard and Commercial Parts

All aspects of the scanner design are compatible with these requirements.

3.3.5 Moisture and Fungus Resistance

These requirements are met without exception. There are no materials in the scanner design that provide nutrients for fungus growth, according to MIL-STD-454, and all scanner surfaces resist detrimental moisture effects through use of the materials, coatings, and processes specified in MIL-S-5002.

3.3.6 Corrosion of Metal Parts

The design requirements of this paragraph are met by careful attention to selection of materials and finishes for all metal parts of the scanner. Major structural parts of the scanner are beryllium, while some small parts and fasteners are aluminum or corrosion-resistant steel.

~~SECRET~~/SPECIAL HANDLING

~~SECRET/SPECIAL HANDLING~~

### 3.3.7 Interchangeable and Replaceability

While the complete left and right hand scanners are not directly interchangeable due to their "mirror image" configurations, many individual parts are the same. For example, the encoders require only a simple change in electrical connections. Replacement of one scanner by another of the same handedness is highly dependent upon installation and alignment techniques that are yet to be determined.

### 3.3.8 Workmanship

All aspects of the scanner design load lend themselves to application of the required workmanship standards.

### 3.3.9 Electromagnetic Interference

The brushless D.C. torque motors are inherently insensitive to EMI. The radiated noise and the susceptibility to EMI of the encoder can be adequately controlled by conventional shielding techniques.

### 3.3.10 Identification and Marking

All aspects of the scanner design are compatible with these requirements.

### 3.3.11 Storage

All scanner materials, including mirror potting and lubricants will survive the required storage period.

### 3.3.12 Cleanliness

The scanner design is compatible with the assembly requirement of class 100 and the in-use requirement of class 100,000.

~~SECRET/SPECIAL HANDLING~~

~~SECRET~~/SPECIAL HANDLING

### 3. CONFIGURATION TRADE STUDIES

The baseline scanner configuration has a balanced pitch axis and an unbalanced roll axis. Neither axis is required to be balanced by the present specification, and, in fact, the roll axis cannot be balanced and meet other requirements (vignetting or space envelope).

Nevertheless, many advantages accrue if both axes can be balanced. For this reason, Itek has recently conducted extensive trade studies of various balanced configuration concepts. The results of these studies are presented in Section 3.1. In Section 3.2, vignetting studies over the full scanner field are presented for both optical vignetting and mechanical obscuration.

In Section 3.3, the effects of small vignetting on system resolution are discussed.

Based on the system trade studies that have been conducted, Itek recommended that the scanner design incorporate a balanced roll axis. The method of achieving this and the impact on scanner design, and required changes in the specification are presented below.

~~SECRET~~/SPECIAL HANDLING

## ~~SECRET/SPECIAL HANDLING~~

### 3.1 BALANCED VERSUS UNBALANCED ROLL AXIS CONSIDERATION

The previous scanner design had a balanced pitch axis and an unbalanced roll axis. It is desirable to balance both axes, but the specifications and envelope allocation made this unachievable.

The factors controlling the design of the gimbal assembly that are pertinent to balancing the scanner are as follows:

1. Balanced pitch axis. In order to test the scanner assembly on the ground, as an assembly, without counterweights, the pitch axis must be balanced. Fig. 3.1-1 shows the test orientation that would have to be used to compensate for the unbalanced roll axis. The roll axis unbalance would be taken out by maintaining the roll axis vertical, thus removing the need for the torquer to overcome the unbalanced moments.

#### Vignetting

The specification required 0 vignetting between line of sight (LOS) angles of +40 to +10 degrees in pitch and  $\pm 35$  degrees in roll. The pitch axis orientation and mirror size were formulated to meet this specification.

#### Interface

The maximum protrusion of the shroud shall not exceed 15.65 inches from the radiator surface of the module.

#### Orientation

1. 9-degree cant angle
2. The optical axis between the fixed fold and the scanner must be parallel to the vehicle axis.

With these requirements and specifications, the scanner was designed with a balanced pitch axis and an unbalanced roll axis.

During the past several months, it has been indicated the scanner assembly could not always be maintained in the vertical position and that use of counterweights on the roll axis would cause an increase in roll inertia that could not be compensated in the test results of the roll servo. As a result, a study was initiated to determine the consequences of going to a design having both axes balanced.

#### Balanced Scanner

Tradeoff studies or comparisons were made in four major areas in an attempt to obtain a balanced system. The four major areas were the following:

1. Vignetting
2. Gimbal—configuration
3. Shroud and vehicle interference
4. Weight and inertia changes.

A parallel effort was made on the investigation of the four controlling parameters. In an attempt to gain enough information to size the problem, many combinations of pitch and roll axis positions were studied.

~~SECRET/SPECIAL HANDLING~~

~~SECRET/SPECIAL HANDLING~~

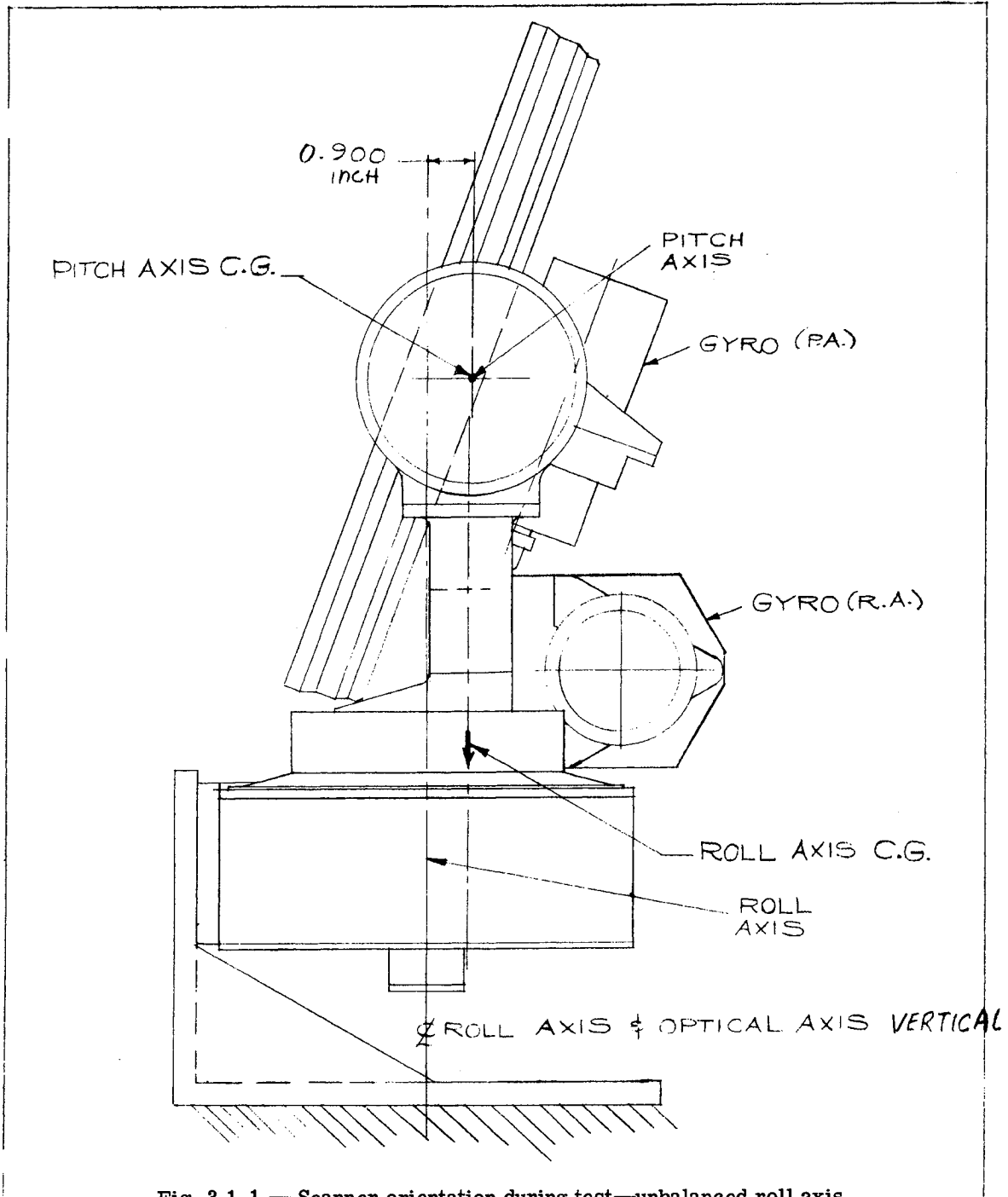


Fig. 3.1-1 — Scanner orientation during test—unbalanced roll axis

~~SECRET/SPECIAL HANDLING~~

~~SECRET/SPECIAL HANDLING~~

Vignetting Studies

A computer program was written to compute the vignetting for various locations of the mirror. The pitch and roll axis location was varied and runs made for various pitch and roll LOS angles. Table 3.1-1 shows the initial runs that were made. These data include only optical vignetting, not mechanical obstruction. Total optical vignetting and obstruction is considered in Section 3.2.

The baseline (unbalanced roll axis) design was used as a reference, where the roll axis and optical axis are coincident and the pitch axis is 0.9 inch above the optical axis (see Fig. 3.1-1).

The additional configurations that were considered are as follows:

1. Roll axis up 0.3 inch  
Pitch axis down 0.0 inch  
Pitch axis down 0.1 inch  
Pitch axis down 0.3 inch  
Pitch axis down 0.6 inch
2. Roll axis up 0.45 inch  
Pitch axis down 0.0 inch  
Pitch axis down 0.1 inch  
Pitch axis down 0.3 inch  
Pitch axis down 0.45 inch
3. Roll axis up 0.9 inch
4. Roll axis on optical axis  
Pitch axis down 0.3 inch  
Pitch axis down 0.6 inch  
Pitch axis down 0.9 inch

The runs point out that raising the roll axis increases the vignetting less than dropping the pitch axis. For example, with the roll axis raised 0.9 inch, pitched +10 degrees and rolled  $\pm 35$ , the vignetting is 2 to 4.8 percent, where dropping the pitch axis 0.9 inch with the same angular orientation has 7.0 to 8.4 percent vignetting. It also points out that a total combined displacement of the pitch and roll axis of up to 0.55 inch (i.e., roll axis up 0.45, pitch axis down 0.1 inch) can be achieved with only 2 percent vignetting and a displacement of 0.75 inch has roughly 3 percent vignetting in the +10 to +40 degree pitch range. With this knowledge and the results from the interference and configuration studies, more runs were made covering a larger range of pitch and roll angles. The results are shown in Table 3.1-2.

A rough comparison between +70 to +10 degrees pitch and  $\pm 45$  degrees roll is as follows:

Description	Vignetting (Max)	
	70°	10°
1. Unbalanced design (baseline)	<0.5	0
2. Roll axis up 0.9 inch	3.7	7.0
3. Roll axis up 0.45 inch Pitch axis down 0.0 inch	2.3	2.1
4. Roll axis up 0.45 inch Pitch axis down 0.1 inch	<0.5	7.2
5. Roll axis up 0.45 inch Pitch axis down 0.3 inch	<0.5	8.5

~~SECRET/SPECIAL HANDLING~~

~~SECRET/SPECIAL HANDLING~~

Table 3.1-1 — Vignetting Study for Various Pitch and Roll LOS Angles Initial Runs

Chart No.	Description	LOS Angles		Vignett.	Total	Vignett
		Pitch	Roll	Area	Area	Present %
1	Roll Axis up 0.9 inches	+10	+45	1.35	27.3	4.9
2	Roll Axis up 0.9 inches	+10	+35	.55	27.5	2.0
9	Roll Axis up 0.9 inches	+10	0	0.0	28.0	0.0
16	Roll Axis up 0.9 inches	+10	-35	1.3	27.4	4.8
17	Roll Axis up 0.9 inches	+10	-45	2.1	27.5	7.6
18	Roll Axis up 0.9 inches	+40	+45	1.48	23.8	.2
19	Roll Axis up 0.9 inches	+40	+35	1.28	23.4	.1
26	Roll Axis up 0.9 inches	+40	0	0.0	----	0.0
33	Roll Axis up 0.9 inches	+40	-35	0.9	23.6	3.8
34	Roll Axis up 0.9 inches	+40	-45	0.9	24.0	3.7
35	Pitch Axis down 0.3 in.	+10	+35	0.0	----	0.0
36	Pitch Axis down 0.3 in.	+10	0	0.0	----	0.0
37	Pitch Axis down 0.3 in.	+10	-35	1.4	27.4	.1
38	Pitch Axis down 0.3 in.	+40	+35	0.0	----	0.0
39	Pitch Axis down 0.3 in.	+40	+5	0.0	----	0.0
40	Pitch Axis down 0.3 in.	+40	-35	0.0	----	0.0
41	Pitch Axis down 0.6 in.	+10	+35	1.0	27.5	3.6
42	Pitch Axis down 0.6 in.	+10	+35	1.0	27.1	2.6
43	Pitch Axis down 0.6 in.	+10	-35	1.4	27.3	5.1
44	Pitch Axis down 0.6 in.	+40	+35	0.0	----	0.0
45	Pitch Axis down 0.6 in.	+40	0	0.0	----	0.0
46	Pitch Axis down 0.6 in.	+40	-35	0.0	----	0.0
47	Pitch Axis down 0.9 in.	+10	+35	2.0	27.6	7.2
48	Pitch Axis down 0.9 in.	+10	0	1.9	27.3	7.0
49	Pitch Axis down 0.9 in.	+10	-35	2.3	27.3	8.4
50	Pitch Axis down 0.9 in.	+40	+35	0.0	----	0.0
51	Pitch Axis down 0.9 in.	+40	0	0.0	----	0.0

Note: Total Mirror Area = 29.28" ( $\frac{1}{2}$ scale)  
Outer 0.1 inch of Mirror not used

~~SECRET/SPECIAL HANDLING~~

Table 3.1-1 -- (Cont.)

Chart No	Description	LOS Angles		Vignett Area	Total Area	Vignett Present %
		Pitch	Roll			
53	Roll Axis up 0.45, Pitch Axis down 0.0	+10	+35	---	---	<0.5
54	Roll Axis up 0.45, Pitch Axis down 0.0	+10	0	---	---	0.0
55	Roll Axis up 0.45, Pitch Axis down 0.0	+10	-35	---	---	<0.5
56	Roll Axis up 0.45, Pitch Axis down 0.0	+45	+35	---	---	<0.5
57	Roll Axis up 0.45, Pitch Axis down 0.0	+45	0	---	---	0.0
58	Roll Axis up 0.45, Pitch Axis down 0.0	+40	-35	---	---	<0.5
59	Roll Axis up 0.45, Pitch Axis down 0.1	+10	+35	0.5	27.3	1.8
60	Roll Axis up 0.45, Pitch Axis down 0.1	+10	0	---	---	0.0
61	Roll Axis up 0.45, Pitch Axis down 0.1	+10	-35	0.3	27.4	1.1
62	Roll Axis up 0.45, Pitch Axis down 0.1	+40	+35	---	---	<0.5
63	Roll Axis up 0.45, Pitch Axis down 0.1	+40	0	---	---	0.0
64	Roll Axis up 0.45, Pitch Axis down 0.1	+40	-35	---	---	<0.5
65	Roll Axis up 0.45, Pitch Axis down 0.3	+10	+35	0.4	27.5	1.5
66	Roll Axis up 0.45, Pitch Axis down 0.3	+10	0	---	---	<0.5
67	Roll Axis up 0.45, Pitch Axis down 0.3	+10	-35	0.8	27.5	2.9
68	Roll Axis up 0.45, Pitch Axis down 0.3	+40	+35	---	---	<0.5
69	Roll Axis up 0.45, Pitch Axis down 0.3	+40	0	---	---	0.0
70	Roll Axis up 0.45, Pitch Axis down 0.3	+40	-35	---	---	<0.5
71	Roll Axis up 0.45, Pitch Axis down 0.45	+10	+35	0.8	27.4	2.9
72	Roll Axis up 0.45, Pitch Axis down 0.45	+10	0	---	---	<1.0
73	Roll Axis up 0.45, Pitch Axis down 0.45	+10	-35	1.3		4.7
74	Roll Axis up 0.45, Pitch Axis down 0.45	+40	+35	---	---	0.0
75	Roll Axis up 0.45, Pitch Axis down 0.45	+40	0	---	---	0.0
76	Roll Axis up 0.45, Pitch Axis down 0.45	+40	-35	---	---	<0.5

Note:

Total Mirror Area = 29.28" ( $\frac{1}{2}$  Scale)  
Outer 0.1 inch of Mirror not used

~~SECRET/SPECIAL HANDLING~~

Table 3.1-1 — (Cont.)

Chart NO.	Description	LOS Angles		Vignett Area	Total Area	Vignett Present %
		Pitch	Roll			
77	Roll Axis up .03, Pitch Axis Down 0.0	+10	+35	---	---	0.1
78	Roll Axis up .03, Pitch Axis down 0.0	+10	0	---	---	0.0
79	Roll Axis up 0.3, Pitch Axis down 0.0	+10	-35	---	---	0.0
80	Roll Axis up 0.3, Pitch Axis down 0.0	+40	+35	---	---	0.0
81	Roll Axis up 0.3, Pitch Axis down 0.0	+40	0	---	---	0.0
82	Roll Axis up 0.3, Pitch Axis down 0.0	+40	-35	---	---	0.0
83	Roll Axis up 0.3, Pitch Axis down 0.1	+10	+35	---	---	0.5
84	Roll Axis up 0.3, Pitch Axis down 0.1	+10	0	---	---	0.0
85	Roll Axis up 0.3, Pitch Axis down 0.1	+10	-35	---	---	0.5
86	Roll Axis up 0.3, Pitch Axis down 0.1	+40	+35	---	---	0.5
87	Roll Axis up 0.3, Pitch Axis down 0.1	+40	0	---	---	0.0
88	Roll Axis up 0.3, Pitch Axis down 0.1	+40	-35	---	---	0.0
89	Roll Axis up 0.3, Pitch Axis down 0.3	+10	+35	---	---	1.0
90	Roll Axis up 0.3, Pitch Axis down 0.3	+10	0	---	---	1.0
91	Roll Axis up 0.3, Pitch Axis down 0.3	+10	-35	0.7	27.5	2.5
92	Roll Axis up 0.3, Pitch Axis down 0.3	+40	+35	---	---	0.0
93	Roll Axis up 0.3, Pitch Axis down 0.3	+40	0	---	---	0.0
94	Roll Axis up 0.3, Pitch Axis down 0.3	+40	-35	---	---	0.1
95	Roll Axis up 0.3, Pitch Axis down 0.6	+10	+35	1.2	27.4	4.4
96	Roll Axis up 0.3, Pitch Axis down 0.6	+10	0	0.7	27.1	2.6
97	Roll Axis up 0.3, Pitch Axis down 0.6	+10	-35	1.5	27.2	5.5
98	Roll Axis up 0.3, Pitch Axis down 0.6	+40	+35	---	---	0.0
99	Roll Axis up 0.3, Pitch Axis down 0.6	+40	0	---	---	0.0
100	Roll Axis up 0.3, Pitch Axis down 0.6	+40	-35	---	---	0.5

Note:

Total Mirror Area = 29.28" ( $\frac{1}{2}$  Scale)  
Outer 0.1 inch of Mirror not used

~~SECRET/SPECIAL HANDLING~~

~~SECRET/SPECIAL HANDLING~~

Table 3.1-2 — Vignetting Study Covering Larger Range of Roll Angles

Description	LOS Angles		%	Description	LOS Angles		%
	Pitch	Roll	Vig		Pitch	Roll	Vig.
Present	+70	+45	<0.5	Roll Axis up 0.9	+70	+45	2.8
Pitch Axis up 0.9	+70	0	<0.5	Roll Axis up 0.9	+70	0	2.8
Pitch Axis up 0.9	+70	-45	0.0	Roll Axis up 0.9	+70	-45	3.7
Pitch Axis up 0.9	+55	+45	0.0	Roll Axis up 0.9	+55	+45	4.9
Pitch Axis up 0.9	+55	0	<0.5	Roll Axis up 0.9	+55	0	3.2
Pitch Axis up 0.9	+55	-45	0.0	Roll Axis up 0.9	+55	-45	4.5
Pitch Axis up 0.9	+40	+45	0.0	Roll Axis up 0.9	+40	+45	0.2
Pitch Axis up 0.9	+40	+35	0.0	Roll Axis up 0.9	+40	+35	0.1
Pitch Axis up 0.9	+40	0	0.0	Roll Axis up 0.9	+40	0	0.0
Pitch Axis up 0.9	+40	-35	0.0	Roll Axis up 0.9	+40	-35	3.8
Pitch Axis up 0.9	+40	-45	0.0	Roll Axis up 0.9	+40	-45	3.7
Pitch Axis up 0.9	+10	+45	0.0	Roll Axis up 0.9	+10	+45	4.9
Pitch Axis up 0.9	+10	+35	0.0	Roll Axis up 0.9	+10	+35	2.0
Pitch Axis up 0.9	+10	0	0.0	Roll Axis up 0.9	+10	0	0.0
Pitch Axis up 0.9	+10	-35	0.0	Roll Axis up 0.9	+10	-35	4.8
Pitch Axis up 0.9	+10	-45	0.0	Roll Axis up 0.9	+10	-45	7.6
Pitch Axis up 0.9	0	+45	<0.5	Roll Axis up 0.9	0	+45	5.1
Pitch Axis up 0.9	0	0	1.7	Roll Axis up 0.9	0	0	5.1
Pitch Axis up 0.9	0	-45	2.0	Roll Axis up 0.9	0	-45	8.8
Pitch Axis up 0.9	-20	+45	14.5	Roll Axis up 0.9	-20	+45	25.3
Pitch Axis up 0.9	-20	0	18.8	Roll Axis up 0.9	-20	0	22.1
Pitch Axis up 0.9	-20	-45	13.7	Roll Axis up 0.9	-20	-45	16.8
Pitch Axis up 0.9	-40	+45	29.9	Roll Axis up 0.9	-40	+45	33.2
Pitch Axis up 0.9	-40	0	40.5	Roll Axis up 0.9	-40	0	42.2
Pitch Axis up 0.9	-40	-45	29.7	Roll Axis up 0.9	-40	-45	37.2

~~SECRET~~/SPECIAL HANDLING

Table 3.1-2 — (Cont.)

Description	LOS Angles		% Vig.
	Pitch	Roll	
Roll Axis up 0.45, Pitch Axis down 0.0	+70	+45	2.3
Roll Axis up 0.45, Pitch Axis down 0.0	+70	0	< 0.5
Roll Axis up 0.45, Pitch Axis down 0.0	+70	-45	< 0.1
Roll Axis up 0.45, Pitch Axis down 0.0	+55	+45	2.7
Roll Axis up 0.45, Pitch Axis down 0.0	+55	0	< 0.1
Roll Axis up 0.45, Pitch Axis down 0.0	+55	-45	< 0.1
Roll Axis up 0.45, Pitch Axis down 0.0	+40	+45	2.5
Roll Axis up 0.45, Pitch Axis down 0.0	+40	+35	< 0.5
Roll Axis up 0.45, Pitch Axis down 0.0	+40	0	0.0
Roll Axis up 0.45, Pitch Axis down 0.0	+40	-35	< 0.5
Roll Axis up 0.45, Pitch Axis down 0.0	+40	-45	< 0.1
Roll Axis up 0.45, Pitch Axis down 0.0	+10	+45	< 0.5
Roll Axis up 0.45, Pitch Axis down 0.0	+10	+35	< 0.5
Roll Axis up 0.45, Pitch Axis down 0.0	+10	0	0.0
Roll Axis up 0.45, Pitch Axis down 0.0	+10	-35	< 0.5
Roll Axis up 0.45, Pitch Axis down 0.0	+10	-45	2.1
Roll Axis up 0.45, Pitch Axis down 0.0	0	+45	8.5
Roll Axis up 0.45, Pitch Axis down 0.0	0	0	6.8
Roll Axis up 0.45, Pitch Axis down 0.0	0	-45	5.1
Roll Axis up 0.45, Pitch Axis down 0.0	-20	+45	22.2
Roll Axis up 0.45, Pitch Axis down 0.0	-20	0	24.3
Roll Axis up 0.45, Pitch Axis down 0.0	-20	-45	16.8
Roll Axis up 0.45, Pitch Axis down 0.0	-40	+45	35.4
Roll Axis up 0.45, Pitch Axis down 0.0	-40	0	42.4
Roll Axis up 0.45, Pitch Axis down 0.0	-40	-45	31.8

~~SECRET~~/SPECIAL HANDLING

~~SECRET~~/SPECIAL HANDLING

Table 3.1-2 — (Cont.)

Description	LOS Angles		% Vig.
	Pitch	Roll	
Roll Axis up 0.45, Pitch Axis down 0.1	+70	+45	< 0.5
Roll Axis up 0.45, Pitch Axis down 0.1	+70	0	0.0
Roll Axis up 0.45, Pitch Axis down 0.1	+70	-45	< 0.5
Roll Axis up 0.45, Pitch Axis down 0.1	+55	+45	< 0.5
Roll Axis up 0.45, Pitch Axis down 0.1	+55	0	0.0
Roll Axis up 0.45, Pitch Axis down 0.1	+55	-45	< 0.5
Roll Axis up 0.45, Pitch Axis down 0.1	+40	+45	< 0.5
Roll Axis up 0.45, Pitch Axis down 0.1	+40	+35	< 0.5
Roll Axis up 0.45, Pitch Axis down 0.1	+40	0	0
Roll Axis up 0.45, Pitch Axis down 0.1	+40	-35	< 0.5
Roll Axis up 0.45, Pitch Axis down 0.1	+40	-45	< 0.5
Roll Axis up 0.45, Pitch Axis down 0.1	+10	+45	< 0.5
Roll Axis up 0.45, Pitch Axis down 0.1	+10	+35	< 0.5
Roll Axis up 0.45, Pitch Axis down 0.1	+10	0	0
Roll Axis up 0.45, Pitch Axis down 0.1	+10	-35	< 0.5
Roll Axis up 0.45, Pitch Axis down 0.1	+10	-45	3.3
Roll Axis up 0.45, Pitch Axis down 0.1	0	+45	3.0
Roll Axis up 0.45, Pitch Axis down 0.1	0	0	2.4
Roll Axis up 0.45, Pitch Axis down 0.1	0	-45	7.2
Roll Axis up 0.45, Pitch Axis down 0.1	-20	+45	16.5
Roll Axis up 0.45, Pitch Axis down 0.1	-20	0	19.4
Roll Axis up 0.45, Pitch Axis down 0.1	-20	-45	19.6
Roll Axis up 0.45, Pitch Axis down 0.1	-40	+45	31.7
Roll Axis up 0.45, Pitch Axis down 0.1	-40	0	40.4
Roll Axis up 0.45, Pitch Axis down 0.1	-40	-45	31.9

~~SECRET~~/SPECIAL HANDLING

~~SECRET/SPECIAL HANDLING~~

Table 3.1-2 — (Cont.)

Description	LOS Angles		% Vig.
	Pitch	Roll	
Roll Axis up 0.45, Pitch Axis down 0.2	+70	+45	< 0.5
Roll Axis up 0.45, Pitch Axis down 0.2	+70	0	0.0
Roll Axis up 0.45, Pitch Axis down 0.2	+70	-45	< 0.1
Roll Axis up 0.45, Pitch Axis down 0.2	+55	+45	< 0.5
Roll Axis up 0.45, Pitch Axis down 0.2	+55	0	0.0
Roll Axis up 0.45, Pitch Axis down 0.2	+55	-45	< 0.5
Roll Axis up 0.45, Pitch Axis down 0.2	+40	+45	
Roll Axis up 0.45, Pitch Axis down 0.2	+40	+35	< 0.5
Roll Axis up 0.45, Pitch Axis down 0.2	+40	0	0.0
Roll Axis up 0.45, Pitch Axis down 0.2	+40	-35	< 0.5
Roll Axis up 0.45, Pitch Axis down 0.2	+40	-45	
Roll Axis up 0.45, Pitch Axis down 0.2	+10	+45	
Roll Axis up 0.45, Pitch Axis down 0.2	+10	+35	1.1
Roll Axis up 0.45, Pitch Axis down 0.2	+10	0	0.0
Roll Axis up 0.45, Pitch Axis down 0.2	+10	-35	0.4
Roll Axis up 0.45, Pitch Axis down 0.2	+10	-45	
Roll Axis up 0.45, Pitch Axis down 0.2	0	+45	5.5
Roll Axis up 0.45, Pitch Axis down 0.2	0	0	2.4
Roll Axis up 0.45, Pitch Axis down 0.2	0	-45	7.6
Roll Axis up 0.45, Pitch Axis down 0.2	-20	+45	14.3
Roll Axis up 0.45, Pitch Axis down 0.2	-20	0	21.0
Roll Axis up 0.45, Pitch Axis down 0.2	-20	-45	13.6
Roll Axis up 0.45, Pitch Axis down 0.2	-40	+45	41.5
Roll Axis up 0.45, Pitch Axis down 0.2	-40	0	42.3
Roll Axis up 0.45, Pitch Axis down 0.2	-40	-45	32.5

~~SECRET/SPECIAL HANDLING~~

~~SECRET~~/SPECIAL HANDLING

Table 3.1-2 — (Concl.)

Description	LOS Angles		% Vig.
	Pitch	Roll	
Roll Axis up 0.45, Pitch Axis down 0.3	+70	+45	0.0
Roll Axis up 0.45, Pitch Axis down 0.3	+70	0	0.0
Roll Axis up 0.45, Pitch Axis down 0.3	+70	-45	< 0.5
Roll Axis up 0.45, Pitch Axis down 0.3	+55	+45	< 0.5
Roll Axis up 0.45, Pitch Axis down 0.3	+55	0	0.0
Roll Axis up 0.45, Pitch Axis down 0.3	+55	-45	< 0.5
Roll Axis up 0.45, Pitch Axis down 0.3	+40	+45	< 0.5
Roll Axis up 0.45, Pitch Axis down 0.3	+40	+35	< 0.5
Roll Axis up 0.45, Pitch Axis down 0.3	+40	0	0.0
Roll Axis up 0.45, Pitch Axis down 0.3	+40	-35	< 0.5
Roll Axis up 0.45, Pitch Axis down 0.3	+40	-45	< 0.5
Roll Axis up 0.45, Pitch Axis down 0.3	+10	+45	3.6
Roll Axis up 0.45, Pitch Axis down 0.3	+10	+35	1.5
Roll Axis up 0.45, Pitch Axis down 0.3	+10	0	< 0.5
Roll Axis up 0.45, Pitch Axis down 0.3	+10	-35	2.9
Roll Axis up 0.45, Pitch Axis down 0.3	+10	-45	8.5
Roll Axis up 0.45, Pitch Axis down 0.3	0	+45	7.1
Roll Axis up 0.45, Pitch Axis down 0.3	0	0	5.1
Roll Axis up 0.45, Pitch Axis down 0.3	0	-45	8.5
Roll Axis up 0.45, Pitch Axis down 0.3	-20	+45	23.7
Roll Axis up 0.45, Pitch Axis down 0.3	-20	0	24.0
Roll Axis up 0.45, Pitch Axis down 0.3	-20	-45	21.6
Roll Axis up 0.45, Pitch Axis down 0.3	-40	+45	36.6
Roll Axis up 0.45, Pitch Axis down 0.3	-40	0	42.9
Roll Axis up 0.45, Pitch Axis down 0.3	-40	-45	32.5

~~SECRET/SPECIAL HANDLING~~

The vignetting results will be discussed further in conjunction with the interference and configuration studies.

Shroud and vehicle obscurations were also run; these are discussed in Section 3.2.

Configuration Studies

The orientation of the axis of rotation of the pitch axis with respect to the mirror, bezel, gyro, etc., has been kept the same for this study as that established by the initial design. Since the existing or unbalanced design has a balanced pitch axis, it was felt desirable to preserve the extensive study performed to establish the location of components on the pitch axis such that it would be balanced and meet the 0.08 slug-ft<sup>2</sup> inertia requirement.

Since the pitch axis is already balanced, the main objective of this study is to balance the roll axis. This can be done in two ways: (1) the pitch axis pivot can be brought closer to the roll axis, or (2) the roll gyro and electronic package can be lowered to the roll axis or placed below the roll axis, depending on the pitch axis locations.

In order to gain as much freedom of movement as possible for the gyro and electronic package, the yoke configuration was changed to make room to locate the two packages between the yoke and the roll housing (see Fig. 3.1-2). The yoke was swept forward as much as the mirror would allow.

The yoke section was increased, maintaining the equivalent strength and stiffness. This allowed space to move the electronics package and gyro perpendicular to the roll axis as required. The actual location will come out of the balance and interference analysis.

A first approximation for locating the gyro and electronic package was made by updating the mass property sheet, incorporating the yoke change and locating the CG for everything that rolls with the exception of the gyro, gyro mount, and electronic packages. If these three components are moved as one unit an approximate location for the CG of the three elements can be determined for each configuration.

The CG locations would be as follows:

1. Baseline design (pitch axis up 0.9 inch)
  - a. Gyro, mount, and electronic package 4.5 inches below the roll axis. This location would not be possible; the gyro and electronic package would interfere with the shroud when in the stowed position. Hence, a balanced roll axis for the baseline configuration is not feasible.
2. Roll axis up 0.9 inch
  - a. Gyro, mount, and electronic package would fall on the roll axis. This location would be possible in regards to gyro and electronic package position, but as will be shown later, the bezel cuts into the shroud shaft. The large diameter of the gyro would be contained within the yoke.
3. Roll axis up 0.45 inch (pitch axis down 0.1 inch)
  - a. Gyro, mount, and electronic package would fall 2.0 inches below the roll axis and the small portion of the gyro would be within the yoke area.

The gyro cannot move lower than 0.65 inch, in order to eliminate an interference with the shroud; therefore it will be maintained at 0.65 inch below the roll axis and the electronic package

~~SECRET/SPECIAL HANDLING~~

~~SECRET/SPECIAL HANDLING~~

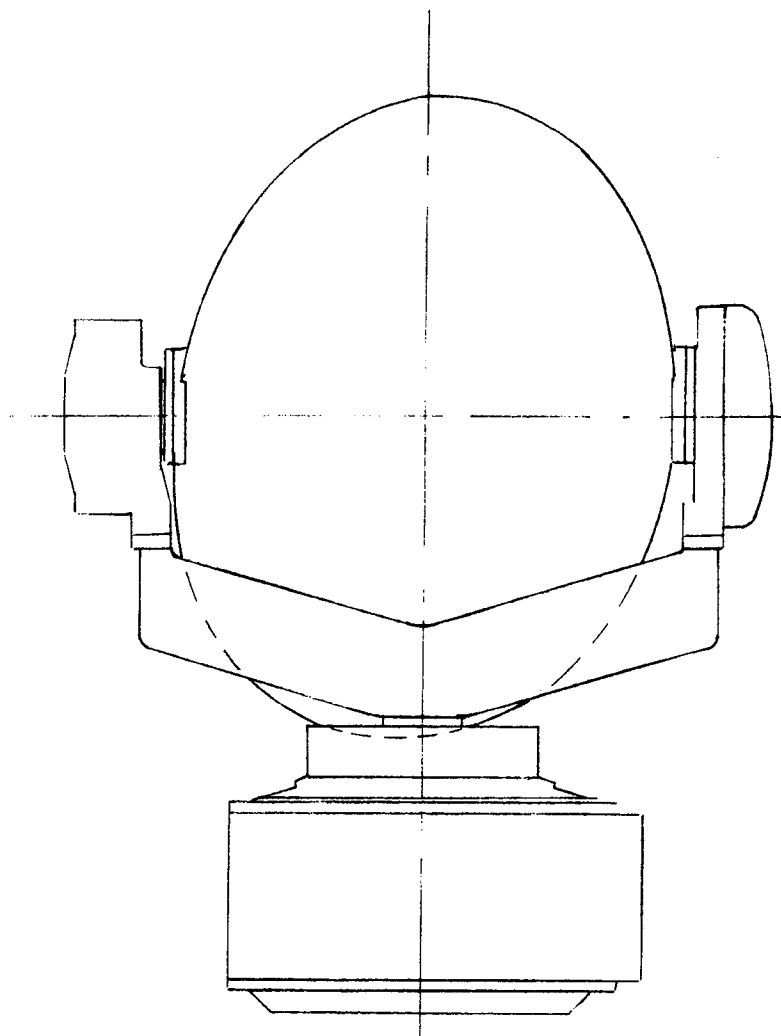


Fig. 3.1-2 — Yoke configuration, balanced roll axis

~~SECRET/SPECIAL HANDLING~~

~~SECRET~~/SPECIAL HANDLING

and a balance weight will be moved. This gives an approximate location for the electronic package of 3.0 inches below the roll axis. This location is acceptable from a clearance standpoint but the electronic package does hang quite a distance below the yoke. To remedy this the pitch axis was dropped another 0.1 inch.

4. Roll axis up 0.45 inch (pitch axis down 0.2 inch)(drawing no. 906031)
  - a. Gyro at 0.65 inch below roll axis.
  - b. Electronic package 2 inches below pitch axis and balance weight.

This is a possible location and brings the electronic package to within 2 inches of the roll axis.

These latter two combinations were layed out and are shown in drawing nos. 906041 and 906031.

Interference Studies

Most of the combinations that were checked for vignetting and balance were also checked graphically for interference with associated equipment. The results and appropriate drawings are listed below.

1. Baseline design (pitch axis up 0.9 inch) (drawing no. 906037) (see Fig. 3.1-3)
  - a. Bezel - interferes 0.12 inch with rib.
  - b. Encoder - interferes 0.18 inch with rib (separate trunnion); interferes 0.38 inch with insulation (combined trunnion).

NOTE

Specific engineering drawings are referenced herein.  
These drawings are included in an accompanying  
supplement package.

- c. Motor - clears shroud drive shaft 0.32 inch when rotating into the stowed position and 0.44 inch when in the stowed position (separate trunnion). Clears shaft 0.56 inch (combined trunnion).
2. Roll axis up 0.9 inch (drawing no. 906042) (see Fig. 3.1-4)
  - a. Bezel - clears vehicle, ribs, and insulation.
  - b. Encoder - interferes 0.16 inch with rib (separate trunnion).
  - c. Motor - interferes with shroud shaft 0.38 inch (separate trunnion) and 0.88 inch with door seal.
3. Roll axis up 0.45 inch (pitch axis down 0.2 inch) (drawing no. 906045) (see Fig. 3.1-5)
  - a. Bezel - interferes with insulation 0.18 inch.
  - b. Encoder - interferes with rib 0.12 inch (separate trunnion); interferes 0.38 inch with insulation (combined trunnion).
  - c. Motor - clear shroud shaft 0.12 inch (separate trunnion); clear shroud 0.32 inch (combined trunnion).

~~SECRET~~/SPECIAL HANDLING

~~SECRET/SPECIAL HANDLING~~

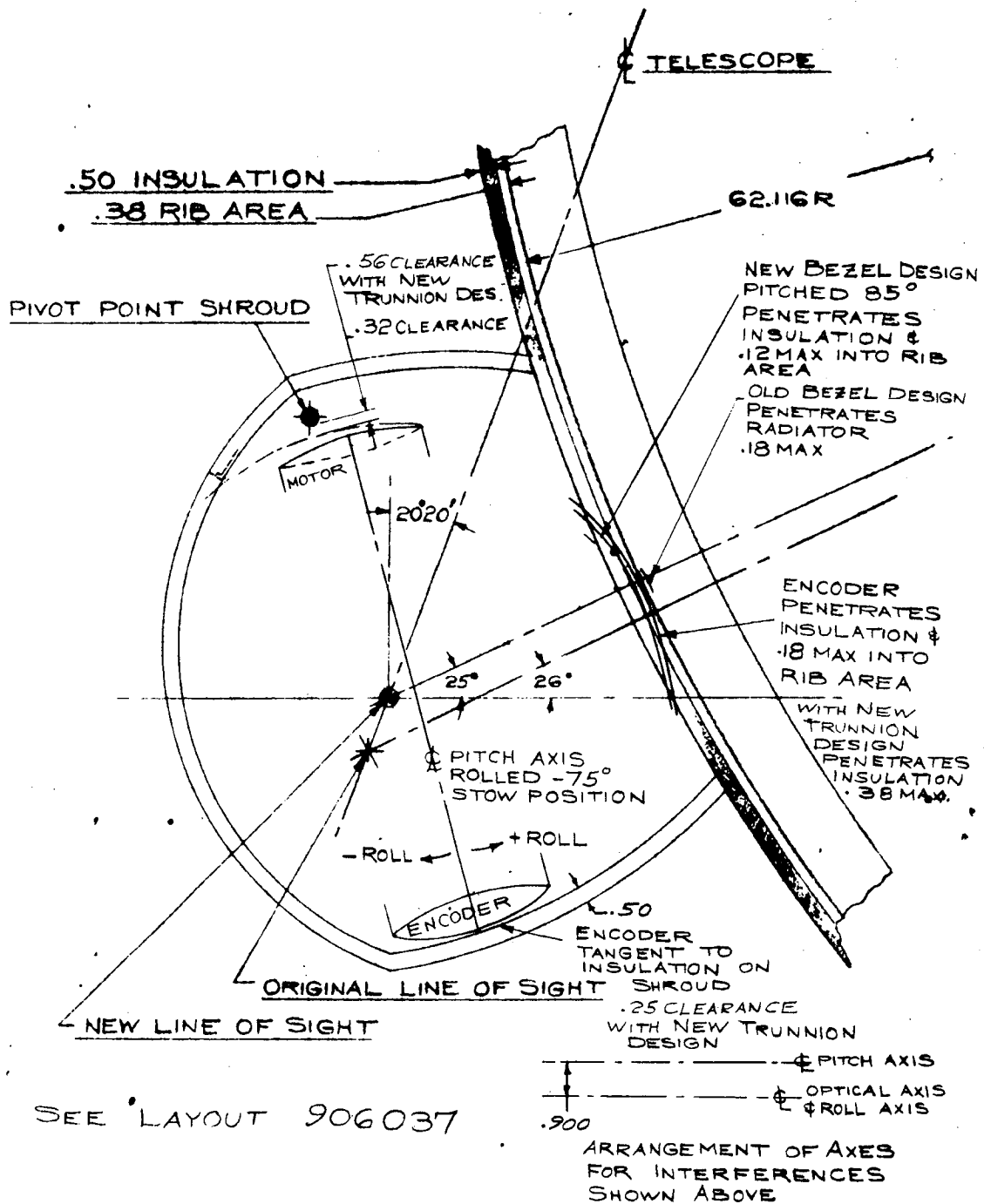


Fig. 3.1-3 — Initial design of arrangement for interference studies

~~SECRET/SPECIAL HANDLING~~

~~SECRET~~/SPECIAL HANDLING

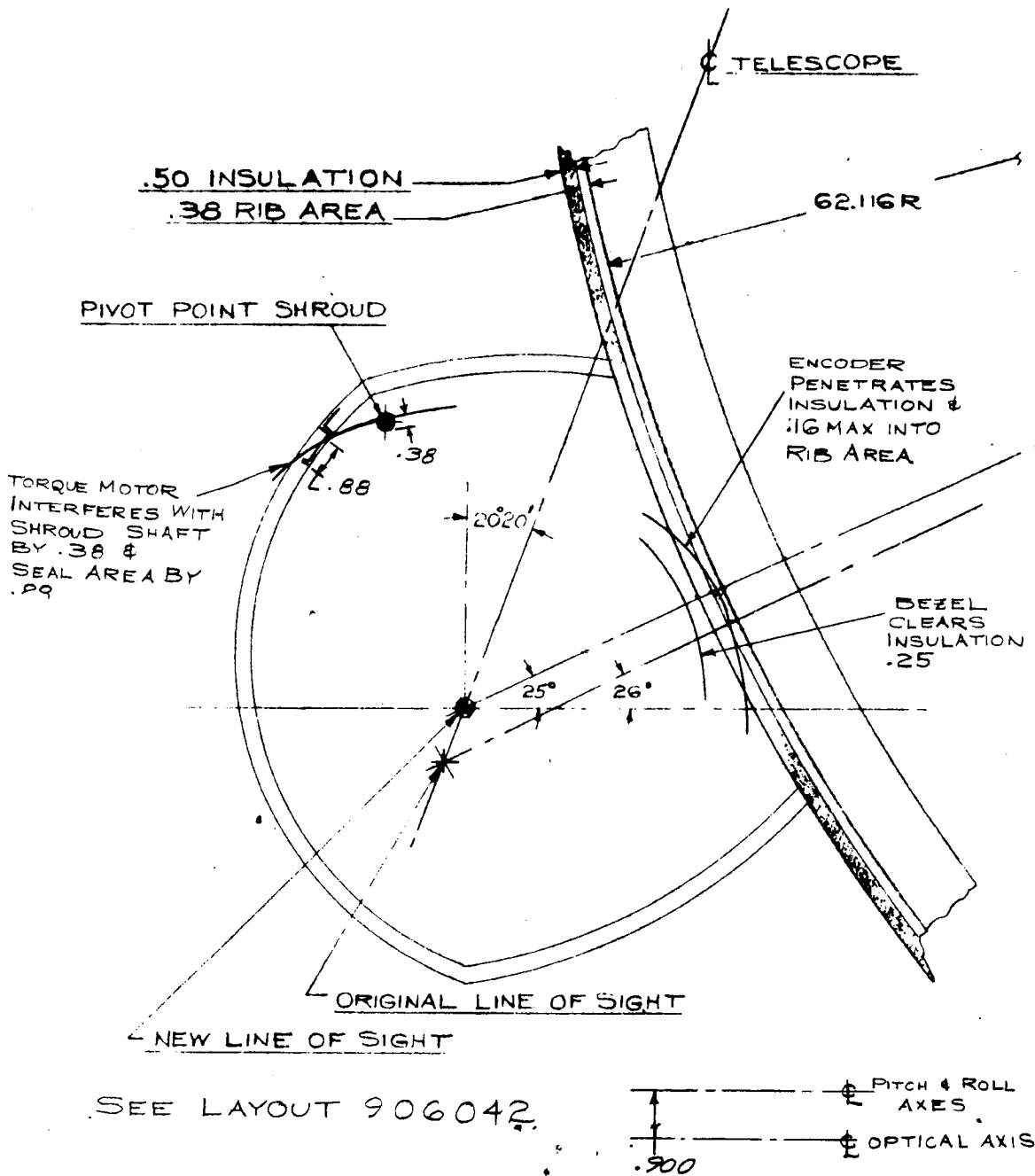


Fig. 3.1-4 — Arrangement for interference studies, roll axis up 0.9 inch

~~SECRET~~/SPECIAL HANDLING

~~SECRET/SPECIAL HANDLING~~

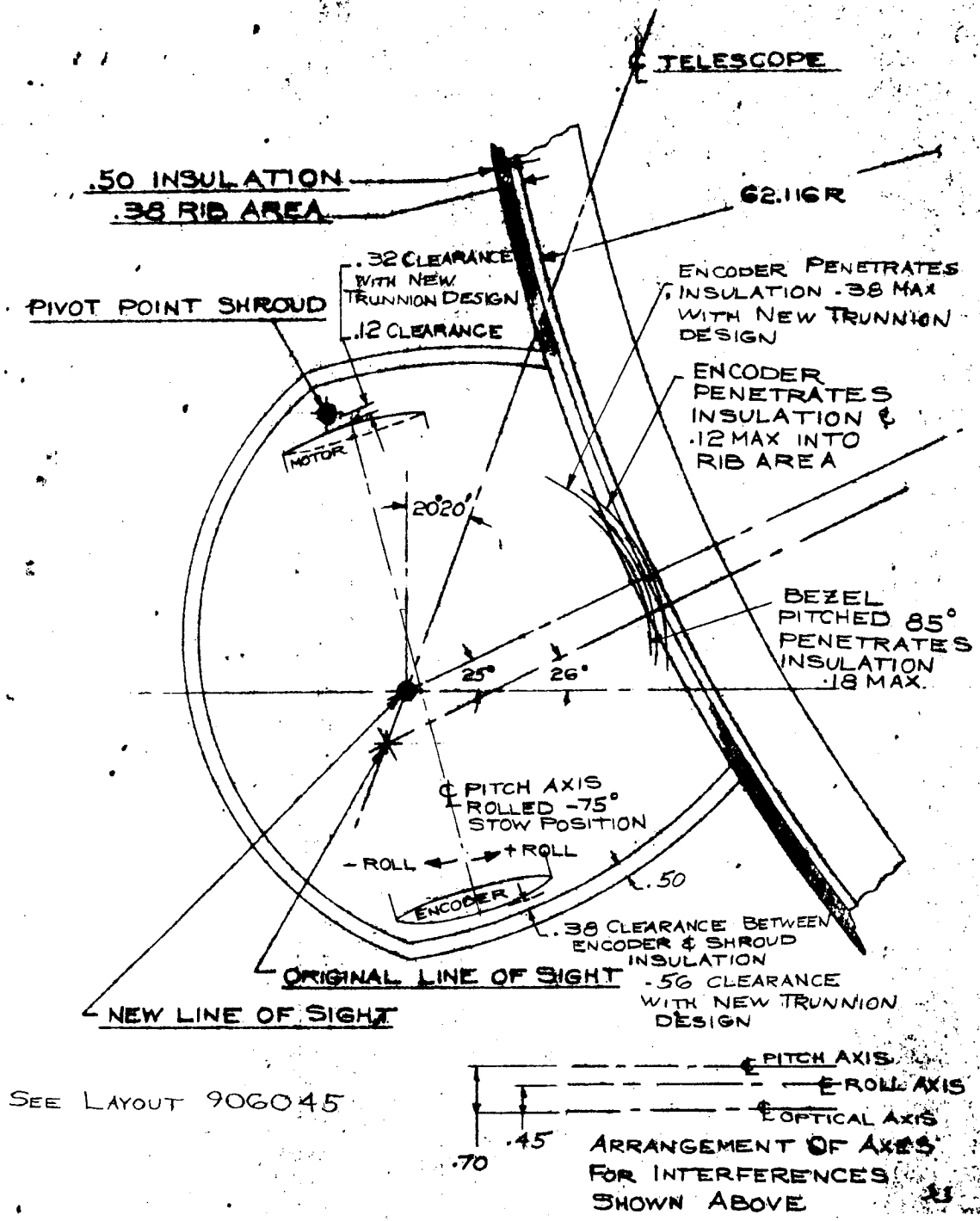


Fig. 3.1-5 — Arrangement for interference studies, roll axis up 0.45 inch—pitch axis down 0.2 inch

~~SECRET/SPECIAL HANDLING~~

~~SECRET~~/SPECIAL HANDLING

4. Pitch axis down 0.9 inch (drawing no. 906040) (see Fig. 3.1-6)
  - a. Bezel - clears everything.
  - b. Encoder - clears ribs, interferes with insulation 0.06 inch (combined trunnion).
  - c. Motor - clears shroud shaft by 0.75 inch (combined trunnion).
  - d. Encoder - in this on configuration the encoder is line to line with the insulation with the shroud when in the stowed position (0.25 inch clearance with combined trunnion).
5. Roll axis up 0.45 inch (pitch axis 0.1 inch) (drawing no. 906040) (see Fig. 3.1-7)
  - a. Bezel - interferes with insulation 0.28 inch.
  - b. Encoder - interferes with rib 0.16 inch (separate trunnion); interferes with insulation 0.41 inch (combined trunnion).
  - c. Motor - clears shroud shaft 0.12 inch (separate trunnion); clears shroud shaft 0.32 inch (combined trunnion).

Weight and Inertia Changes

The only structural change to the scanner for a balanced configuration involves the yoke. The new yoke weight is approximately the same as the old, hence the total weight of the scanner is not changed by this structural modification.

On making a closer check of the pitch axis balance and inertia, it was necessary to add 0.8 pound to achieve the required inertia of 0.08 slug-ft<sup>2</sup>. This is based on a pitch axis gyro and electronic package location as called out on drawing no. 906041. Future detailed analysis should reduce this amount of added weight. An interference check has shown that the pitch gyro can be moved approximately 0.94 inch forward on the scanner and the electronic package 1.18 inches. This will decrease the amount of additional weight required to meet the inertia specification but increase the weight needed to balance. Since the balance weight is proportional with the displacement of the gyro and electronic package, and the inertia varies with the square of the displacement, the additional weight should be less than 0.8 pound.

By incorporating the gyro mount into the yoke the equivalent weight of the gyro mount will be less since a joint will not have to be made between the bracket and the yoke. The yoke stiffness will also be increased.

The 1-pound weight that was carried for the gyro mount will be utilized on the electronic package side of the yoke to maintain roll balance.

The total roll inertia is still over 0.23 slug-ft<sup>2</sup> when the mirror is pitched to 80 degrees, and drops to approximately 0.19 slug-ft<sup>2</sup> when in a minimum pitch angle.

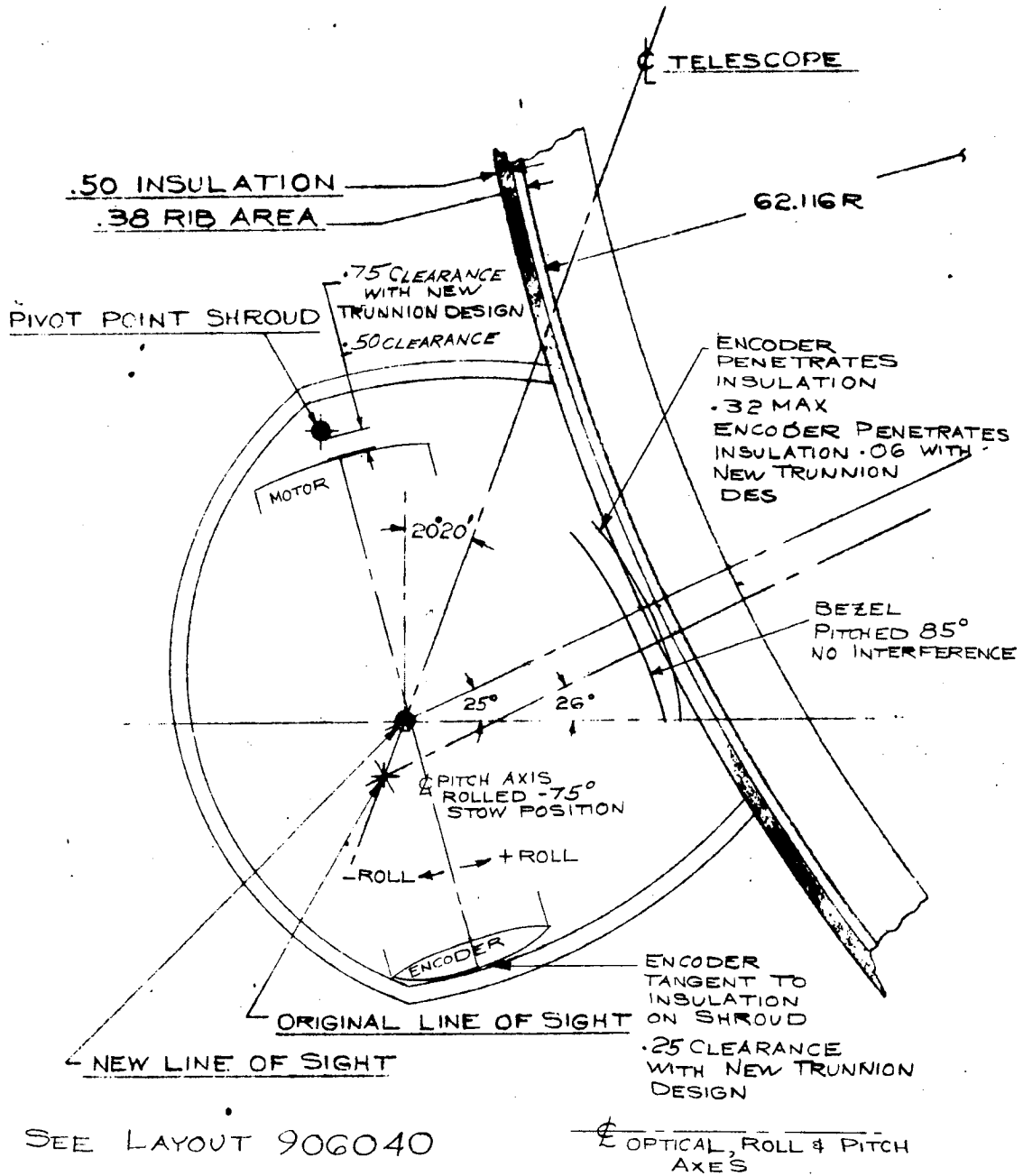
Summary

A comparison of various features such as interference, vignetting, and configuration, are shown in Table 3.1-3. For clarification, the advantages and disadvantages of each configuration are discussed below:

Configuration No. 1 (baseline)

Roll axis up 0.9 inch (see Fig. 3.1-4)

~~SECRET/SPECIAL HANDLING~~



ARRANGEMENT OF AXES  
FOR INTERFERENCES  
SHOWN ABOVE

Fig. 3.1-6 — Arrangement for interference studies, pitch axis down 0.9 inch

~~SECRET/SPECIAL HANDLING~~

~~SECRET~~/SPECIAL HANDLING

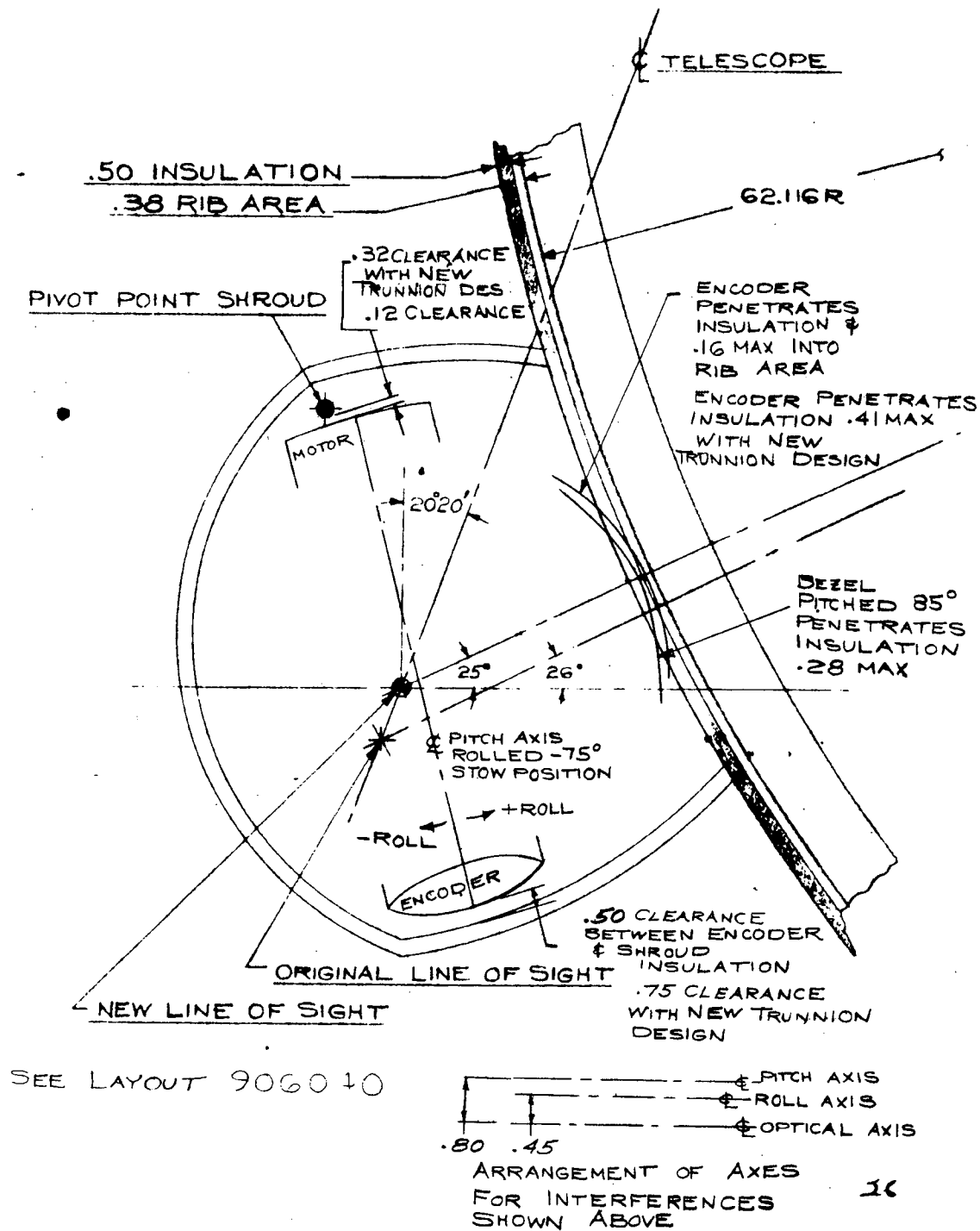


Fig. 3.1-7 — Arrangement for interference studies, roll axis up 0.45 inch—pitch axis down 0.1 inch

~~SECRET~~/SPECIAL HANDLING

~~SECRET/SPECIAL HANDLING~~

Table 3.1-3 — Comparison of Various Features and Interface Configurations

DESCRIPTION	VIGNETTING		INTERFERENCE OR CLEARANCE				SHROUD ENVELOPE	CONFIGURATION (APPROX)
	±45° ROLL 70P-140PH0P 0P	±35° ROLL 140PH0P 0P	VEHICLE	RIBS	INSULATION	SHROUD SHAFT		
UNBALANCED DESIGN PA. UP. 900 (Balance)	<.5	0	0	2.0	0	0	—	FIG. NO. 10 L/O NO. 906037
ROLL AXIS UP. 900	37	37	76	8.8	3.8	4.8	—	FIG. NO. 11 L/O NO. 906042 GYRO & ELECT PKG ON $\phi$ OF YOKE
ROLL AXIS UP. 45 PA. DOWN 0	23	2.5	2.1	8.5	<.5	<.5	—	GYRO .65" BELOW ROLL AXIS ELECT PKG & BALANCE WT .4" BELOW ROLL AXIS
ROLL AXIS UP. 45 PA. DOWN 10	<.5	<.5	3.3	7.2	<.5	<.5	—	FIG. NO. 14 L/O NO. 906040 GYRO .65" BELOW ROLL AXIS ELECT PKG 3" BELOW ROLL AXIS
ROLL AXIS UP. 45 PA. DOWN 30	<.5	<.5	8.5	8.5	<.5	2.9	—	GYRO .65" BELOW ROLL AXIS ELECT PKG 1" BELOW ROLL AXIS
ROLL AXIS UP. 45 PA. DOWN 20 (Balance)	<.10	—	—	7.6	<.5	1.1	—	FIG. NO. 12 L/O NO. 906045 GYRO .65" BELOW ROLL AXIS ELECT PKG 2" BELOW ROLL AXIS
ROLL AXIS & PITCH AXIS COINCIDENT WITH OPTICAL AXIS	—	—	—	—	—	—	0 8.4	FIG. NO. 13 L/O NO. 906040 GYRO & ELECT PKG ON $\phi$ OF YOKE

COMPARISON

~~SECRET/SPECIAL HANDLING~~

~~SECRET/SPECIAL HANDLING~~

- a. Advantages
  - Balanced roll axis
  - Bezel clears radiator, ribs, and insulation
- b. Disadvantages
  - Torque motor cuts through shroud drive shaft
  - Torque motor cuts through shroud door seal
  - Encoder interferes 0.16 inch into rib
  - Vehicle and shroud obscuration will increase
  - Vignetting is 4.8 percent in the +10 to +40 degree pitch,  $\pm 35$  degrees roll range.

Configuration No. 2

Roll axis up 0.45 inch, pitch axis down 0.1 inch (see Fig. 3.1-7)

- a. Advantages
  - Balanced roll axis
  - Motor clears shroud shaft 0.32 inch
  - Encoder clears bottom of shroud inner structure by 0.75 inch
  - Bezel clears ribs, but does penetrate the insulation by 0.28 inch
  - Encoder clears ribs but penetrates insulation 0.41 inch
  - Vignetting is less than 1 percent for pitch angles of +70 to +10 degrees with the exception of one 45-degree roll LOS (3.3 percent).
- b. Disadvantages
  - Location of gyro and electronic package is quite far below the roll axis.

Configuration No. 3

Roll axis up 0.45 inch, pitch axis down 0.3 inch

- a. Advantages
  - Balanced axis
  - Interference studies were not run on this configuration but the numbers would be close to that of Configuration No. 5 since there is only 0.1 inch difference in the location of the pitch axis.
  - Vignetting is less than 3 percent in the range of +70 to +10 degrees in pitch with a roll of  $\pm 35$  degrees. At 45-degree roll, it gets up to 8.5 percent at +10 pitch.
  - This is not as good as the no. 2 or no. 5 configuration but is better than no. 1.
- b. Disadvantages
  - The gyro location is such that the large portion of the gyro is within the yoke section; this cuts down the space between the gyro and roll housing and complicates the yoke design.

Configuration No. 4

Pitch axis down 0.9 inch (Fig. 3.1-6)

- a. Advantages
  - This configuration clears everything except for a slight penetration into the insulation of the vehicle. The encoder does come within 0.75 inch of the bottom of the shroud when in the stowed position, but it does clear.

~~SECRET/SPECIAL HANDLING~~

~~SECRET/SPECIAL HANDLING~~

b. Disadvantages

The vignetting is high. For example, at +10-degree pitch and -35-degree roll, the vignetting is 8.4 percent, about twice that of Configuration No. 1 where the roll axis is raised 0.9 inch.

NOTE

It should be noted that the vignetting can be reduced by tipping the fold mirror so that the optical bundle hits the scan mirror in the same place that it would have if the mirror had not been dropped. (See Fig. 3.1-8).

This configuration was submitted to the customer several months ago to remove the interference problem, and at that time we were told the impact to his software program would be quite severe. This configuration is probably overall the best, but would require a specification change to implement.

Configuration No. 5 (recommended)

Roll axis up 0.45, pitch axis down 0.2 inch (Fig. 3.1-5)

a. Advantages

Bezel clears radiator and ribs, but still penetrates the insulation 0.18 inch.

Encoder clears radiator, but penetrates the insulation and 0.12 inch maximum into the rib area.

Motor clears the shroud shaft by 0.32 inch.

Encoder clears the bottom of the shroud by 0.94 inch.

Vignetting is less than 1.1 percent from +70 to +10 degrees in pitch for roll angles of  $\pm 35$  degrees.

This configuration is a good package from a design point of view. The yoke design is more straightforward.

The last two advantages are the main reasons for selecting this configuration over the roll axis up 0.45 inch, pitch axis down 0.1 inch, or roll axis up 0.45 inch, pitch axis down 0.3 inch.

b. Disadvantages

No major ones

This configuration is the one that has been selected and is recommended as the best studied. It assumes that Configuration No. 4 is not in consideration because of the software problem.

~~SECRET/SPECIAL HANDLING~~

~~SECRET~~/SPECIAL HANDLING

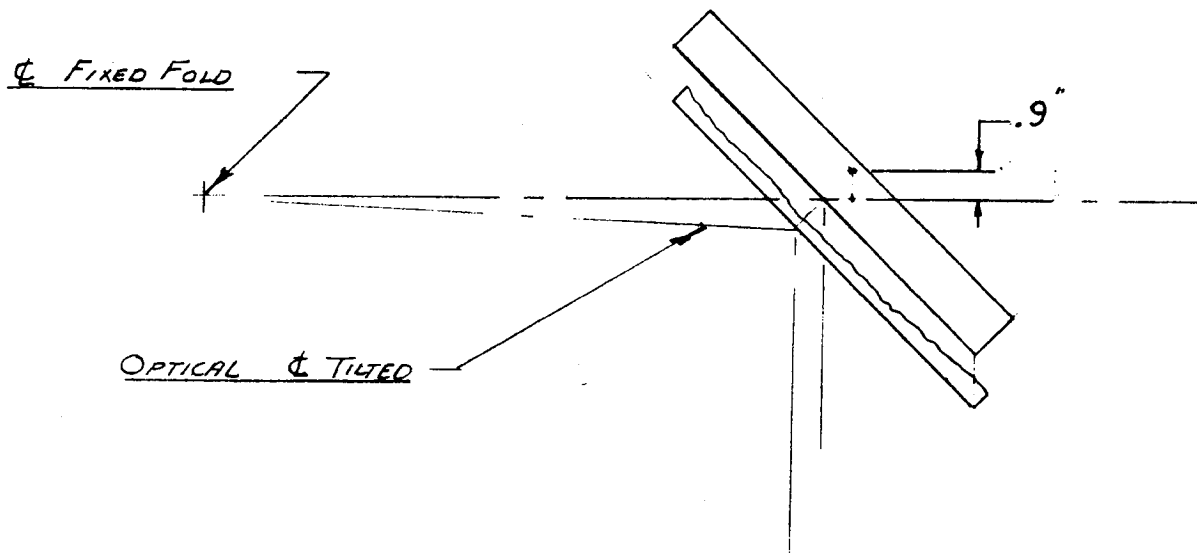


Fig. 3.1-8 — Solution for interference problem

~~SECRET~~/SPECIAL HANDLING

~~SECRET/SPECIAL HANDLING~~

## 3.2 SYSTEM VIGNETTING STUDIES

### 3.2.1 Vignetting/Obstruction Studies

Specification EC 331-B with appropriate AN changes states that no vignetting of the A/O bundle will occur in the LOS pitch range of +10 to +40 degrees within the LOS roll range -35 to +35 degrees. This specification further states that the maximum combined vignetting and obstruction of the A/O bundle will be limited to 60 percent at any operating LOS pitch/roll combination. This requirement has not been implemented in the present design based upon specific customer instruction not to do so. The total vignetting and obstruction effect has been determined, however, for the present design.

The geometry of the axes and mirror locations of the baseline configuration is shown in Fig. 3.2-1. This geometry satisfied all specified vignetting/obstruction criteria. As the merits of a configuration balanced about the roll axis became apparent, further axis geometries were studied.

To obtain a verification of graphical vignetting and obstruction studies as well as a flexible and efficient study method, a series of computer programs for the CDC 3300 computer were formulated. The use of these related programs permitted rapid evaluation of vignetting/obstruction performance for several trial system geometries.

Using vector matrix methods, the basic program projects an optical bundle having the proper (input) divergence from the telescope datum plane, reflects it onto the external fold mirror, and intersects it with the rotated/translated scan mirror surface for any combination of LOS and cant angles. The intersection of the bundle with the scan mirror surface, as viewed normal to the surface, is output as printed data and graphic data on a CALCOMP plotter. Two primary variations of this program were also developed. The first permitted generation of elongated plots for those LOS angles producing low angles of intersection between the A/O bundle and the scan reflecting surface, where maintaining a constant scale factor is expeditious in data reduction. The basic program and the first variation calculate "classical vignetting" defined as A/O bundle loss due to the finite size of the scan mirror in its gimballed position, and were used to evaluate "classical vignetting" for the roll balanced-versus-unbalanced study of Section 3.1.

The second variation, resulting in a major revision of the basic program, calculates the obstruction or "obscuration" of the bundle by external system components. A summary of the analytical basis for these computer programs appears as Appendix 3A.

For the obscuration study, three modes of operation of this latter variation were implemented:

1. The ability to intersect the optical bundle with any plane perpendicular to the X datum axis at any coordinate X
2. The ability to intersect the optical bundle with any plane perpendicular to the Z datum axis at any coordinate Z
3. The ability to analytically intersect the optical bundle with a plane perpendicular to the Z axis which is automatically calculated to be at the precise point in space of minimum vehicle/bundle clearance.

As an example of each option use, the first mode was used in determining possible obstruction of the optical bundle by the housing forward door frame and forward sunshield. The second mode was used in determining possible obstruction by the shroud outboard door edge, in the open position

~~SECRET/SPECIAL HANDLING~~

~~SECRET~~/SPECIAL HANDLING

(outboard roll angles). The third mode was used in determining possible obstruction by the vehicle (inboard roll angles). (Reference memo nos. 349-68-3048, 9400-68-652, 349-68-4207, and 349-67-121.) Geometrical axis configurations investigated are listed and discussed in Section 3.1 and are modifications of the axis geometry shown in Fig. 3.2-1.

Vignetting was calculated at specified points over the target range as indicated in Fig. 3.2-2. Obstruction was calculated over the target range as indicated in Figs. 3.2-3, 3.2-4, and 3.2-5.

3.2.2 Results of Vignetting/Obstruction Studies

"Classical vignetting" of the configurations studied was discussed previously in Section 3.1. Appendix 3B (Section 2) shows the "classical vignetting" study for the recommended balanced configuration of RAUP\* 0.45 and PADN† 0.2. The vignettted area is determined by overlaying the bundle plot on a transparency of the properly oriented mirror. The shaded area is vignettted. The nomenclature of the plot is as follows:

1. LOCY      Projection of the pitch axis on the mirror surface.  
              In the gimbal angle range of interest, + LOCY has + projection on Y axis.
2. LOCZ      A line normal to LOCY in the mirror plane and in a plane containing the  
              roll axis.  
              In the gimbal angle range of interest, + LOCZ has + projection on Z axis.
3. AAR      Gimbal roll angle.
4. AAP      Gimbal pitch angle.
5. AAC      Cant angle.
6. RLOS      LOS roll angle.
7. PLOS      LOS pitch angle.

Axis dimensions are in inches (1/2 scale). This series of plots are type no. 1 (see Fig. 3.2-2).

For values of LOS pitch 0 degrees, the elongated plot format variation (plot type 2) was incorporated, and the "classical vignetting" study is completed in Appendix 3B.

Obstruction studies were run for forward, inboard, and outboard LOS as indicated in Figs. 3.2-3, 3.2-4, and 3.2-5. Forward obstruction was determined by intersecting the optical bundle with a plane normal to the X axis located at X = -4.88 inches from the datum (program operation mode 1). This plane is located at the forward door frame of the shroud. Appendix 3C (part 1) shows the bundle intersection with this plane for the balanced configuration (RAUP 0.45 and PADN 0.2) forward obstruction study. Relative to the datum a one-half scale view of the shroud and sunshield was drawn and presented in Fig. 3.2-6. The sunshield, located at X = -6.21 inches, is projected into the plane at X = -4.88 inches for a LOS of 70, 55, and 40 degrees to reduce the number of computer runs required for the forward obstruction study. The determination of the obstruction for a given LOS is a simple three step operation as follows:

1. The axes INTZ and INTY intersect at the point where the central ray impinges upon the above established plane (XDA = -4.880) and are parallel to and in the same sense as the vehicle Y, Z axes.

---

\*Roll axis up 0.45 inch.

†Pitch axis down 0.2 inch.

~~SECRET/SPECIAL HANDLING~~

2. From the printed output the Y and Z coordinates of this impingement point are noted.
3. On the half scale drawing of the shroud (Fig. 3.2-6) place the intercept plot at the proper Y, Z coordinates and orientation. The obstruction can then be traced onto the plot and areas determined.

The outboard obstruction study, with the lower edge of the open door (point "A" on Fig. 3.2-6) is a similar operation as above but with a horizontal plane normal to the Z axis at ZDA = 14.50 (program operation mode 2). Similarly, this door edge is located and drawn relative to the impingement point of the central ray. This study is presented in part 2 of Appendix 3C.

The inboard obstruction study requires only the determination of areas since the program automatically determines the location of the horizontal plane (ZDA) and the line of vehicle obstruction (program operation mode 3). This study is presented in part 3 of Appendix 3C.

The obscuration program was also used during the evaluation of the various trial system geometries presented in Section 3.1. Obscuration percentages for the five other axis orientations are presented in Table 3.2-1. Classical vignetting is not included.

A study of Appendices 3B and 3C will reveal that for those cases showing significant obscuration, the classical vignetting is low (<2 percent). Actually, these two "bundle loss areas" can overlap and the bundle loss is less than the summation of the two percentages. Because little importance can be attached to such an error, a detailed investigation of vignetting/obstruction overlap was not performed. However, effort is continuing to determine if there are any LOS angle combination showing significant amount of such overlap.

### 3.2.3 Summary

In view of the above analyses no vignetting or obstruction, over the specified target area, occurs with the present unbalanced design. The maximum allowed vignetting requirement is violated. [LOS +70 degrees pitch exceeds this specification by 3.5 percent (roll -45 degrees) to 18.4 percent (roll 0 degrees).] In fact, all configurations studied violate this specification at LOS pitch angle -70 degrees.

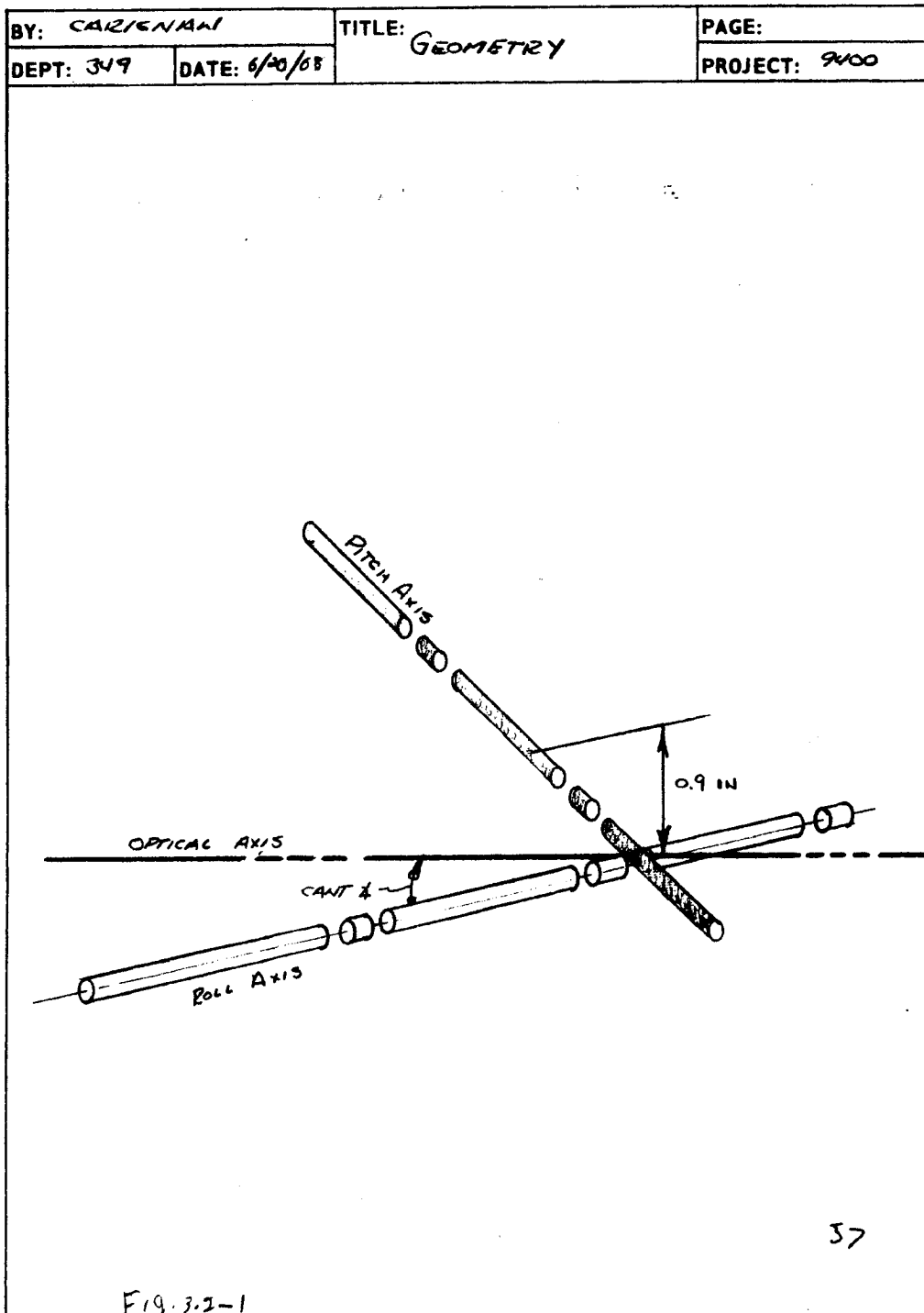
The question arises as to what LOS angles can the recommended balanced configuration attain and still satisfy the maximum vignetting specification as well as what percentage of vignetting occurs in the no vignetting target area (as a trade off for the balanced roll axis).

The recommended balanced configuration has the following vignetting/obstruction characteristics:

1. No obstruction over the LOS +40 degree pitch and roll LOS of  $\pm 35$  degrees.
2. A maximum of 1.1 percent "classical vignette" in the above LOS area occurring at LOS pitch +10 degrees LOS roll +35 degrees.
3. System vignette/obstruction exceeds 60 percent only with LOS pitch angle greater than 62 to 63 degrees, depending slightly on the LOS roll angle.

~~SECRET/SPECIAL HANDLING~~

~~SECRET/SPECIAL HANDLING~~



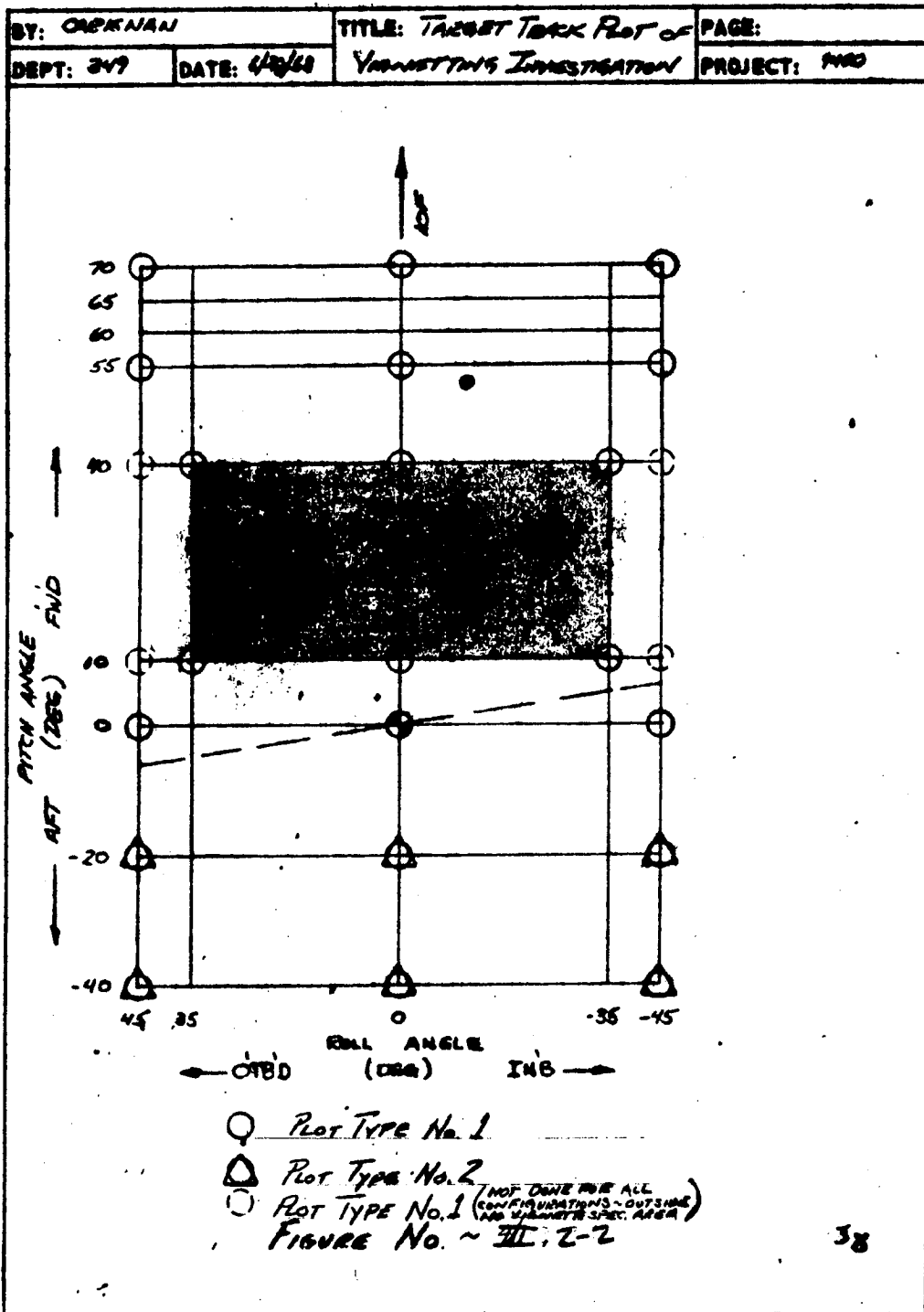
E 103 8/66 ENGINEERING ANALYSIS SHEET

Ittek

Fig. 3.2-1 -- Initial relationship between the optical axis, roll axis, and pitch axis

~~SECRET/SPECIAL HANDLING~~

~~SECRET/SPECIAL HANDLING~~

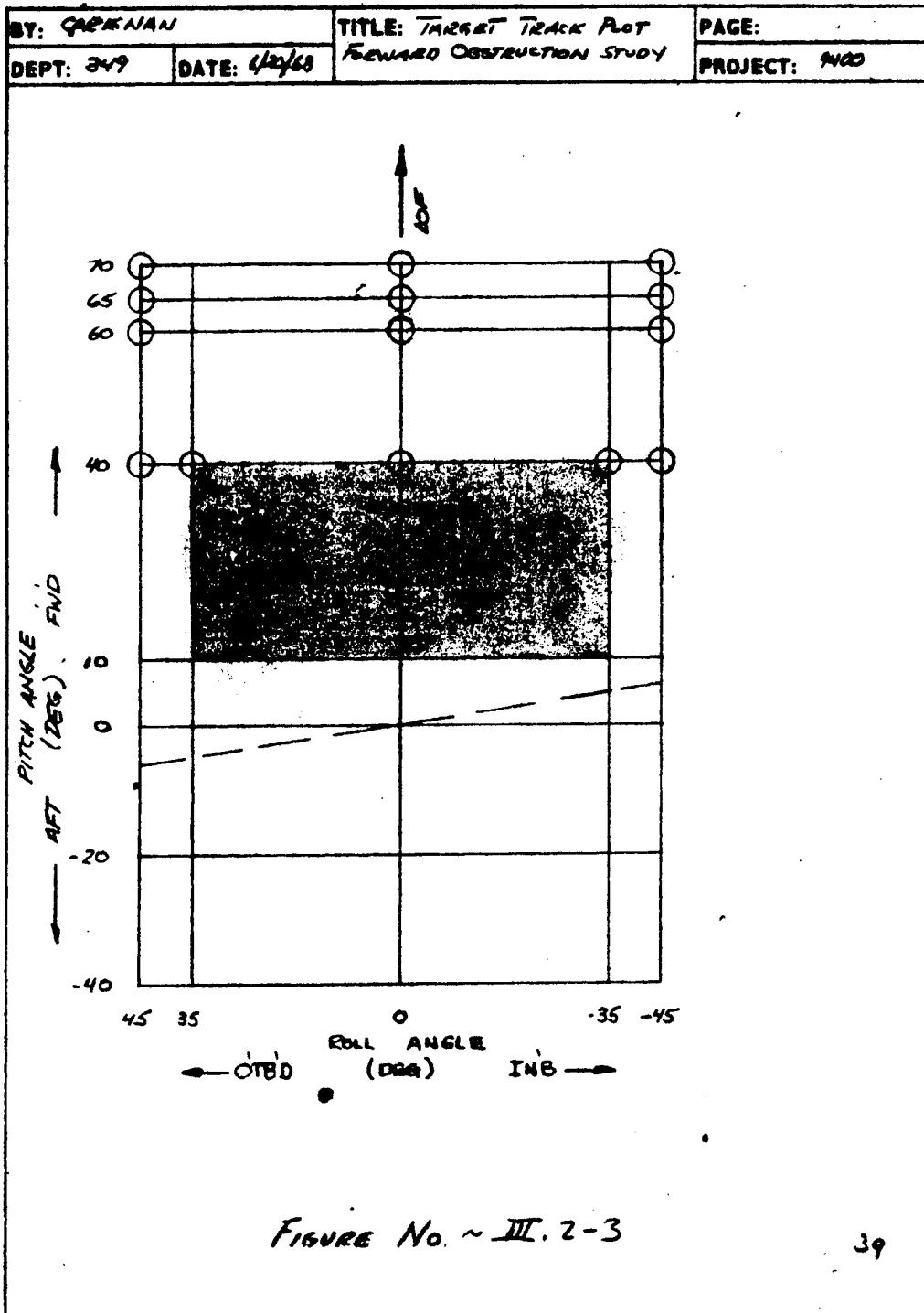


E 1038/66 ENGINEERING ANALYSIS SHEET  
Fig. 3.2-2 Target track plot of vignetting investigation

Fig. 3.2-2 — Target track plot of vignetting investigation

~~SECRET/SPECIAL HANDLING~~

~~SECRET/SPECIAL HANDLING~~



E 1038/66 ENGINEERING ANALYSIS SHEET 3.2-3 Target track plot, forward observation study

Fig. 3.2-3 — Target track plot, forward observation study

~~SECRET/SPECIAL HANDLING~~

~~SECRET/SPECIAL HANDLING~~

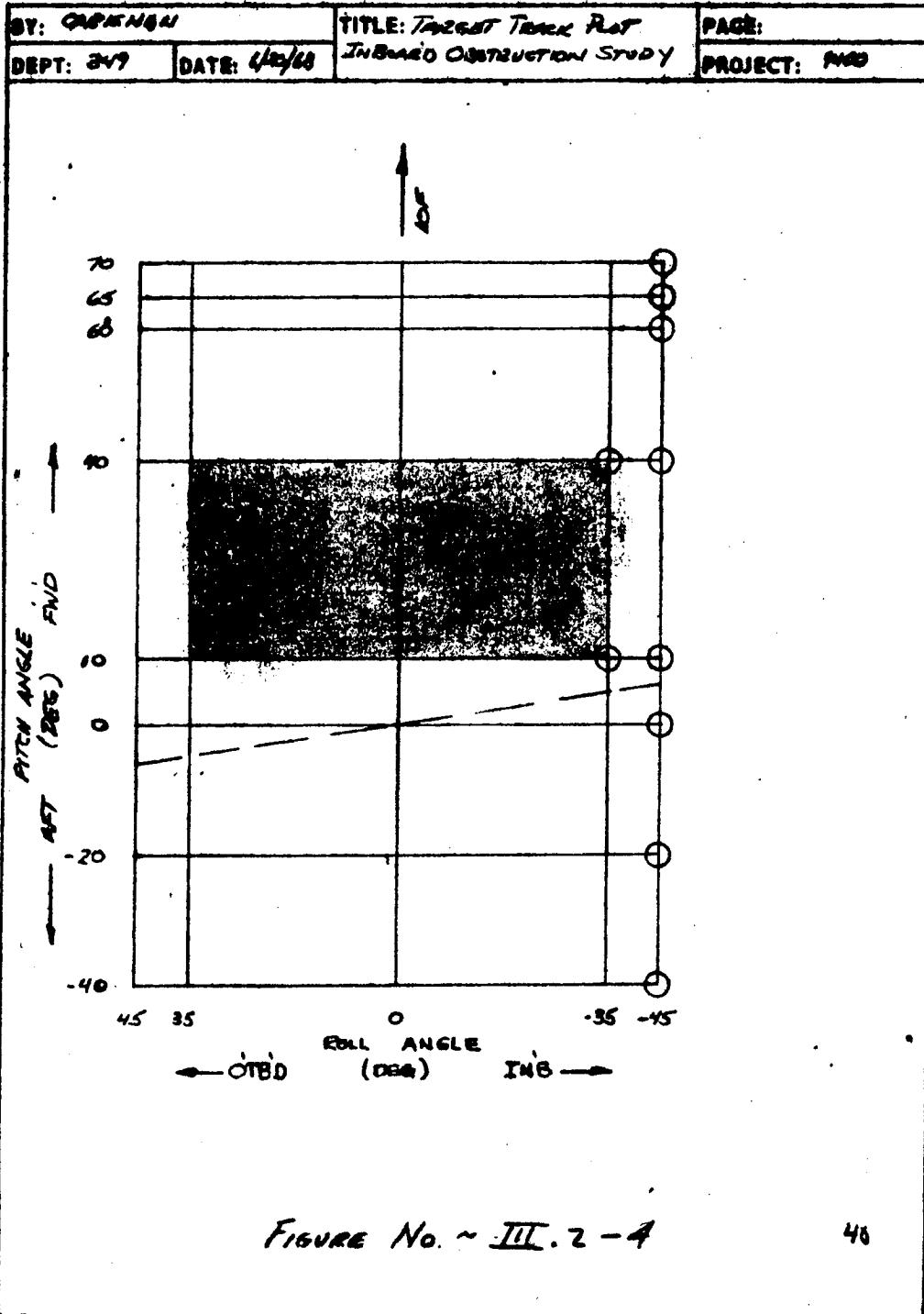


FIGURE No. ~ III.2-4

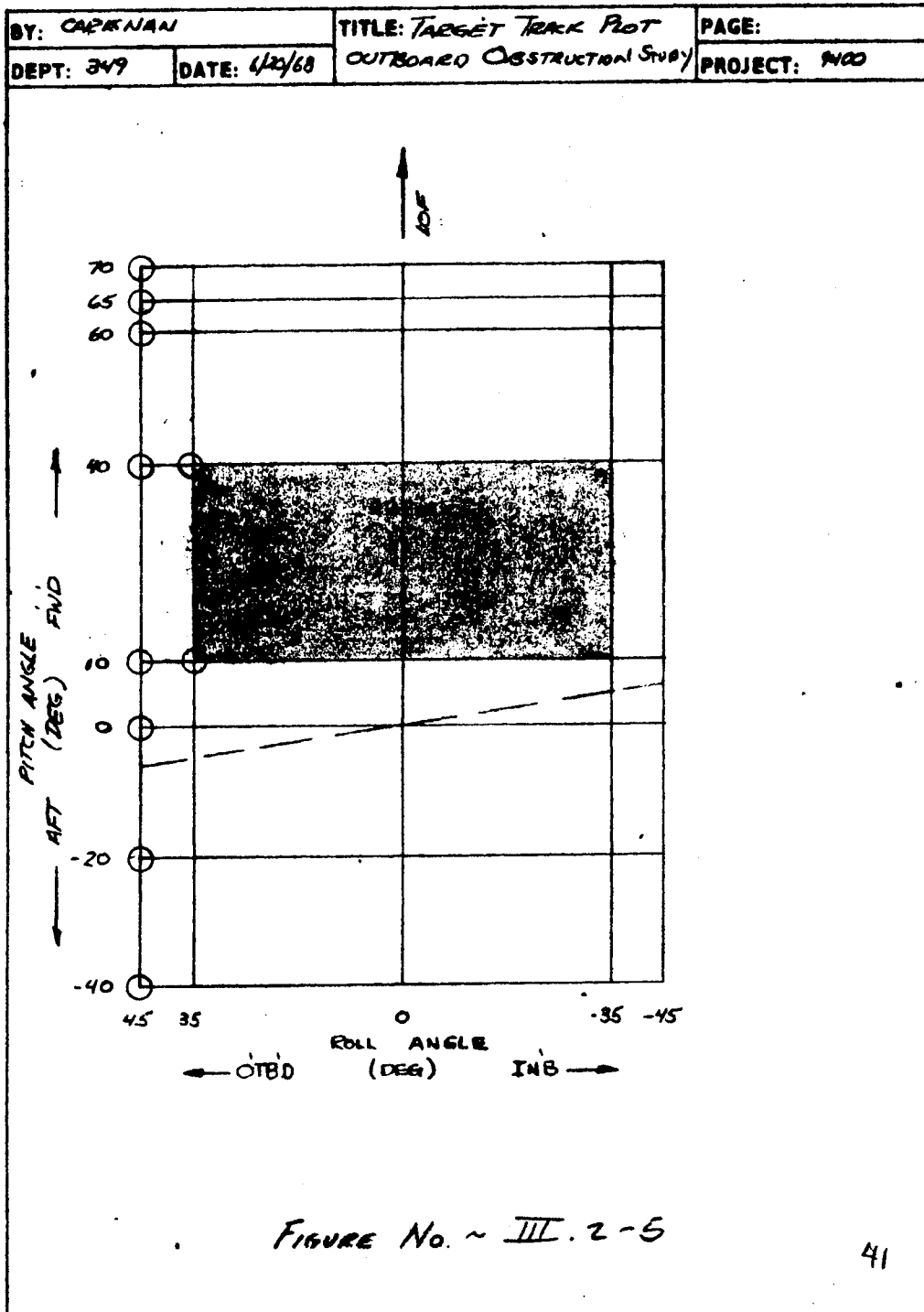
48

E 1038/66 ENGINEERING ANALYSIS SHEET  
Fig. 3.2-4 Target track plot; inboard obstruction study

Fig. 3.2-4 — Target track plot, inboard obstruction study

~~SECRET/SPECIAL HANDLING~~

~~SECRET/SPECIAL HANDLING~~



E 1038/66 ENGINEERING ANALYSIS SHEET

Fig 3.2-5 TARGET OBSTRUCTION PLOT, OUTBOARD OBSTRUCTION STUDY

Fig. 3.2-5 — Target obstruction plot, outboard obstruction study

~~SECRET/SPECIAL HANDLING~~  
3.2-8

~~SECRET~~/SPECIAL HANDLING

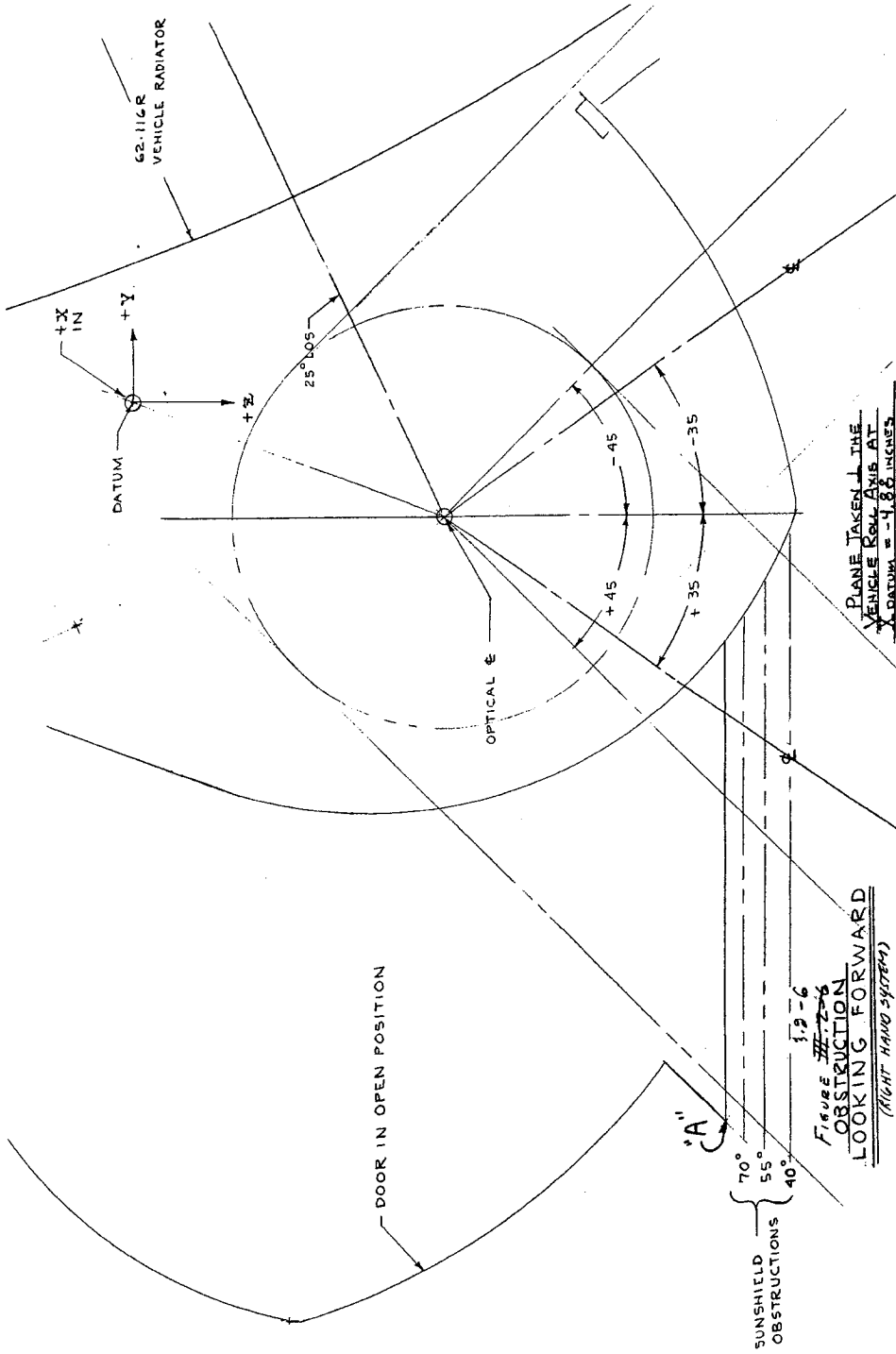


Fig. 3.2-6 — Obstruction looking forward

~~SECRET~~/SPECIAL HANDLING

3.2-9

~~SECRET~~/SPECIAL HANDLING

Table 3.2-1 — Obscuration Study

BY:		TITLE: 3, 2 - 1		PAGE:	
DEPT:	DATE:	TABLE III, 2 - T1		PROJECT:	
<u>Obscuration Study</u>					
CONFIGURATION	DITCH	LOS ANGLES ROLL	90 OBSCURATION	OBSCURATION FROM SHROUD FORWARD	
PRESENT	+70°	45 35 0 -35 -45	74.5 76.5 78.4 72.5 63.5		
RAUP0.9 PADN0.0	+40	ALL	0		
	+70	45	76.1		
		35	77.5		
		0	79.2		
		-35	72.4		
RAUP0.45 PADN0.0	+40	ALL	0		
	+70	45	75.7		
		35	77.2		
		0	78.7		
		-35	76.1		
RAUP0.45 PADN .1	+40	ALL	0		
	+70	45	76.4		
		35	77.4		
		0	78.5		
		-35	77.0		
RAUP0.45 PADN.3	+40	ALL	0		
	+70	45	76.9		
		35	76.8		
		0	79.2		
		-35	75.8		
		-45	64.2		
		+40	0		
ALL CONFIGURATIONS	+40	-45	} 15 TO 17	INBOARD	
	+10	-45		LOS	
	-40	-45			
SPEC REQUIREMENT	+40 ± 10	± 35	0	INBD & OTBD	

~~SECRET/SPECIAL HANDLING~~

### 3.3 VIGNETTING/OBSCURATION EFFECTS ON RESOLUTIONS

To understand the meaning of the vignetting and obscuration numbers given in the preceding section, it is necessary to express them in terms of their effect on ground resolved distance and then to weigh this against the perfect conditions.

#### 3.3.1 Theoretical Background

The loss of a portion of the optical bundle entering the telescope entrance pupil, either due to vignetting (running off a mirror) or obscuration (running into a surface), is equivalent to changing the size and shape of the aperture. This manifests itself in a change in the system modulation transfer function (MTF). The exact nature of this effect is complex and dependent upon the shape as well as the amount of aperture loss. For small amounts of peripheral beam loss, it is satisfactory to approximate the effect on MTF by assuming an area equivalent loss in circular aperture. Since vignetting and obscuration are expressed as

$$\text{Percent loss} = \frac{\text{area lost}}{\text{total area}} \times 100$$

and the area of a circle is proportional to the square of its diameter, then the equivalent new aperture diameter ( $r_2$ ) is:

$$r_2 = r_1 \sqrt{1 - \frac{\Delta A}{A}}$$

where  $r_1$  = actual system aperture  
 $\Delta A/A$  = fractional area loss

For a near diffraction limited system (the AO telescope qualifies) the MTF cut off spatial frequency is proportional to aperture diameter. Thus, the resolution is inversely proportional to aperture diameter and the following expression results.

$$\Delta \text{GRD} = 3.3 \left( \frac{1}{\sqrt{1 - \Delta A/A}} - 1 \right) \text{ feet}$$

This approximation is valid up to about 10 percent beam loss and is shown graphically in Fig. 3.3-1.

One more relationship is needed before looking at the predicted results. This is based on the simple fact that, for any system, as the range of the target increases the resolution achieved decreases proportionally. Slant range as a function of pitch ( $\phi_p$ ) and roll ( $\phi_r$ ) angles is given by

$$\text{SR} = h \sec \phi_r \sec \phi_p$$

Thus, the resolution loss relative to the nadir resolution is given by

$$\Delta \text{GRD} = 3.3 (\sec \phi_r \sec \phi_p - 1) \text{ feet}$$

~~SECRET/SPECIAL HANDLING~~

~~SECRET/SPECIAL HANDLING~~

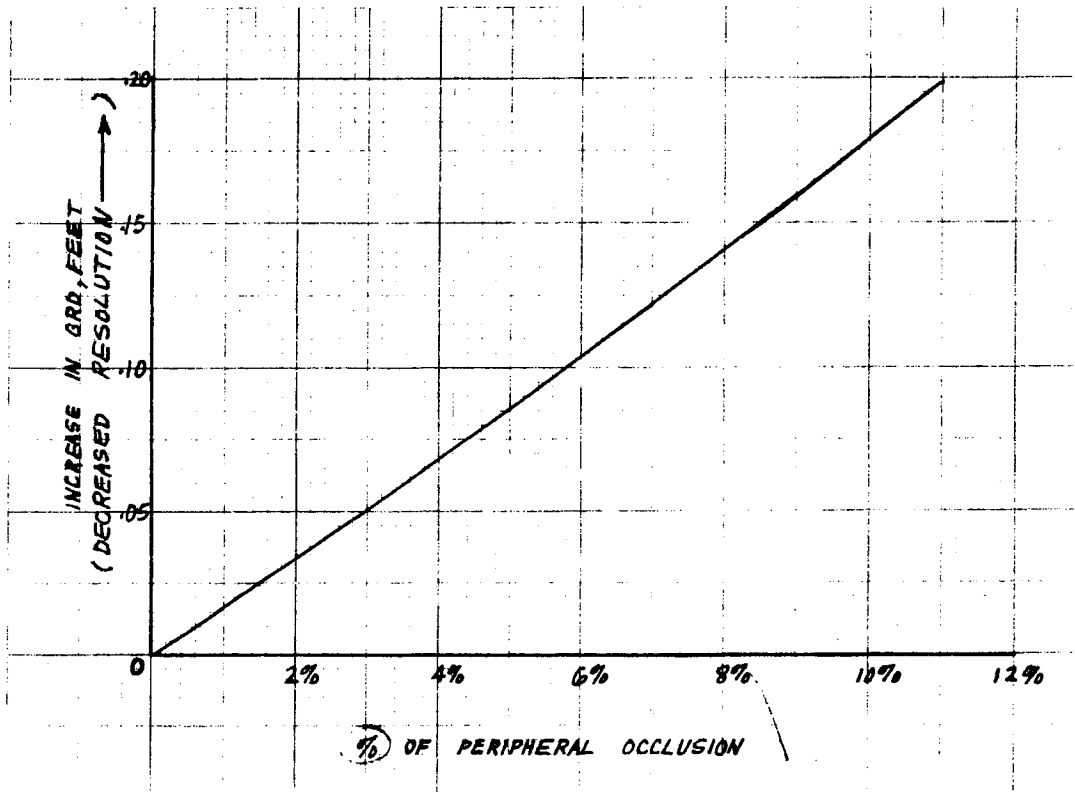


Fig. 3.3-1 — Resolution versus occlusion for a near diffraction limited system

~~SECRET/SPECIAL HANDLING~~

~~SECRET/SPECIAL HANDLING~~

### 3.3.2 Resolution Effects

First consider the performance at nadir and over the region of +10 to +40 degrees pitch and  $\pm 35$  degrees roll where no vignetting is specified. Fig. 3.3-2 shows the resolution loss for the vignetting predicted in Section 4, in parenthesis and for slant range increase.

It is evident from this figure that the effect of vignetting is essentially negligible with respect to the slant range effort. At the worst point (pitch +10 degrees, roll +35 degrees) the 1.1 percent vignetting results in a loss of resolution of only 0.02 foot. This is completely insignificant with respect to the information detection mission of the system. It is therefore recommended that the specification be modified to allow up to 2 percent vignetting over the currently specified angular region. This would effectively eliminate vignetting as a restraint on the balanced roll axis design.

Note that Fig. 3.3-2 also shows a degradation of resolution at nadir of 0.04 foot. Since nadir is outside the specified region of no vignetting this condition is within specification. In any event, such a small change in resolution will be undetectable in use.

Now consider the case of rather high obscurations at large positive pitch angles. Using the above at +60 degrees pitch, it can be seen that a resolution degradation factor of 2.00 to 2.45 will result due to slant range effects alone. This would be roughly equivalent to an aperture decrease of over 50-percent or an equivalent obscuration of over 75 percent. Thus, it can be seen that the obscuration values quoted in Section 4 result in a performance degradation roughly equivalent to that caused by slant range. It therefore seems reasonable to modify the vignetting specification to require no more than 60 percent out to 60 degrees pitch and to relax vignetting further forward.

~~SECRET/SPECIAL HANDLING~~

~~SECRET~~/SPECIAL HANDLING

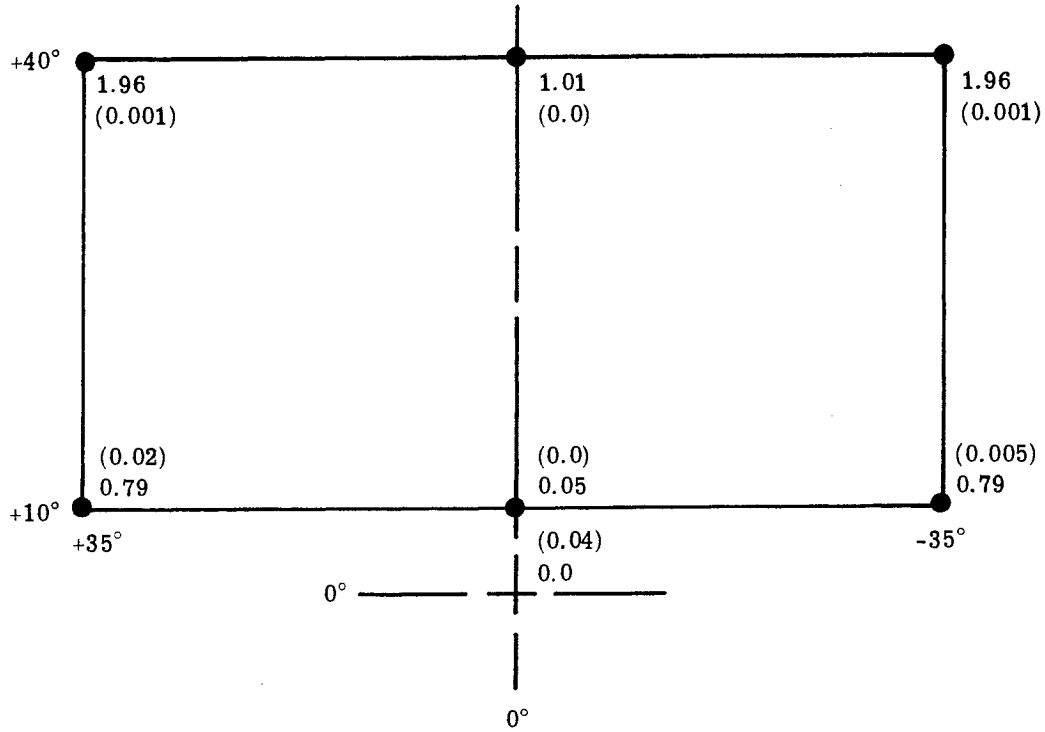


Fig. 3.3-2 — Resolution loss

~~SECRET~~/SPECIAL HANDLING

~~SECRET/SPECIAL HANDLING~~

#### 4. GENERAL CONFIGURATION BALANCED DESIGN

The overall arrangement of the recommended scanner design is shown in Fig. 4.1-1 (drawing no. 906041 Sheets 1 and 2 included in a separate package). The scanner is comprised of three major subassemblies, i.e., the pitch-axis, roll-axis, and pedestal, which are described in detail in the following subsections. The recommended design represents an optimum compromise based on a number of tradeoff studies performed to evaluate a variety of pertinent criteria. Its more salient features include both a balanced roll axis and a balanced pitch axis, as well as minimal optical vignetting.

The scanner is a two-axis roll and cross-roll gimbal system. At launch, the scanner is folded against the side of the vehicle in its stow position and the protective shroud is completely closed. The scanner is held secure in its stow position during launch and ascent by means of a locking device (protective launch locks) which pins the two axes to the fixed housing. Once on orbit, after the aerodynamic fairing has been ejected and the shroud door opened, the pyrotechnic launch locks are actuated to release the two axes. At appropriate times in orbit, upon computer command, the scanner is activated into its functional mode of operation, i.e., scanning preselected target areas on earth. The pitch and roll axes are driven by their respective torque motors at rates proportional to the command signal. Scanner acceleration and rate data is fed back into the control loop by means of the rate gyros in the primary mode, and the encoders in the secondary mode. Energy absorbers are provided at the limits of each axis of travel. At the end of the specified viewing period, the scanner is returned on command to its stow position and the protective shroud is then closed. The scanner is held in its stow position by means of small permanent magnets sized to resist any incident on-orbit loads. The scanner and shroud remain in the closed position until the next viewing period, at which time the cycle is repeated.

It is important that interlocks be provided to ensure proper operational sequencing of the shroud door and scanner, otherwise severe damage, with its subsequent loss of operational capability, could occur to either or both of the components, thus jeopardizing the mission.

With either the balanced or unbalanced roll axis scanner, there are areas of interference with adjacent vehicle elements. These interferences occur as a result of prescribed scanner pitch and roll angular excursions combined with the problem of trying to fit the required componentry into the allotted space without jeopardizing prime performance requirements. Areas of interference for the recommended balanced configuration are as follows:

1. Pitch axis encoder housing with vehicle insulation
2. Mirror bezel with vehicle insulation
3. Roll gyro with vehicle insulation.

Fig. 4.1-2 (drawing no. 906045) indicates the paths of these interferences. A drawing supplementing these data and showing patterns which will define total areas of insulation sweepout is in preparation. This drawing, Fig. 4.1-3 (SK-114519), shows the interference patterns for the unbalanced axis scanner configuration and will be similar to Fig. 4.1-2.

~~SECRET/SPECIAL HANDLING~~

~~SECRET~~/SPECIAL HANDLING

Fig. 4.1-1 is an engineering drawing (906041) which is included in an accompanying supplement package.

~~SECRET~~/SPECIAL HANDLING

~~SECRET~~/SPECIAL HANDLING

Fig. 4.1-2 is an engineering drawing (906045) which is included in an accompanying supplement package.

~~SECRET~~/SPECIAL HANDLING  
4.1-3

~~SECRET/SPECIAL HANDLING~~

Fig. 4.1-3 is an engineering drawing (SK114519) which is included in an accompanying supplement package.

~~SECRET/SPECIAL HANDLING~~

~~SECRET/SPECIAL HANDLING~~

In contrast to the unbalanced axis configuration scanner which showed interference with the actual vehicle structure, the present balanced configuration shows interference with insulation only. This amelioration of interference results from geometry changes inherent in the balanced configuration plus the foreshortening of the pitch axis trunnions resulting from a design change of the mirror bezel-trunnion structure.

Studies relating to the remedial action which can be taken to alleviate interference are in progress. For example, relocation of the roll gyro consistent with other constraints looks feasible; local chamfering of the mirror bezel may be feasible. A more obvious means of alleviating bezel interference would be to limit the pitch gimbal angle to an 80-degree maximum excursion rather than the present 85-degree limit. This would, of course, have to be reconciled with tolerable vignetting requirements. The encoder housing appears to be the least amenable to readjustment without major redesign of prime components such as the mirror. It appears that the most realistic course of action in this case is the local removal of insulation. The extent of insulation removal is presently being determined.

A full description of the mechanical design features and a complete discussion of the parameters influencing the scanner design follows.

~~SECRET/SPECIAL HANDLING~~

## ~~SECRET~~/SPECIAL HANDLING

### 4.1 ROLL AXIS SUBASSEMBLY

The major elements of the roll axis subassembly are the roll housing, roll shaft, roll axis bearings, roll axis torquer, roll axis encoder, yoke, roll gyro, roll gyro electronics, and cabling.

#### 4.1.1 Roll Housing

The roll housing is a two-piece assembly made up essentially of a cylindrical shell whose aft end is closed off by a piloted and keyed plate member. The plate serves not only as the aft bearing support but it incorporates a flexure providing for the axis adjustment required by thermal and assembly considerations. Both elements are precision machined from beryllium alloy stock. The two elements initially are individually premachined, then piloted, bolted, keyed by pinning, and line bored in order to optimize roll axis bearings alignment.

#### 4.1.2 Roll Axis Shaft

This is a beryllium alloy (XT-40) member mounted on the roll housing bearings. The roll shaft forward end terminates in an integral flanged adapter to which the yoke assembly is piloted and bolted. In addition to its primary function, the shaft serves as a cable raceway by means of an axial hole along its length.

#### 4.1.3 Roll Axis Support Bearings

These are preloaded DF pairs mounted against precision ground shoulders and retained by threaded members on the inner race and combination threaded and axially constrained pilots on the outer race. All bearing retainers incorporate labyrinth seals to prevent contamination while avoiding the frictional drag associated with conventional rubbing seals. The bearings are lubricated by stripped F-50 silicone oil with appropriate lubricant creep barriers applied to strategic areas of the bearing races. The fit-up problem of guaranteeing full inner race shaft contact and outer race housing contact or complete race conformity without distortion has been approached from several angles. One approach is match fitting, the other is potting. Other possibilities will be looked at and further tradeoffs will be made pending final decision. The recommended preliminary design will incorporate match-fitting techniques.

#### 4.1.4 Roll Axis Drive Motor

This motor is a dc brushless torquer whose rotor is keyed to the roll shaft. The torquer is positioned adjacent to the forward roll axis bearings in order to minimize shaft windup and to increase torsional stiffness.

#### 4.1.5 Roll Axis Encoder

This is a 20-bit optical type unit whose encoded glass disc is independently mounted on its own bearings. The mounting technique employed avoids the imposition of any significant loads which cause distortion sufficiently large to override the close gapping between the unit's glass disc and its detector array. The unit is of integral design providing a clean cut interface with the scanner roll housing and shaft. Interface is accomplished by accurate piloting of the encoder subassembly in the roll housing and through a zero backlash coupling to the roll axis shaft. Provision for the ready access requisite for zeroing the encoder with the roll axis neutral position is provided in the roll housing.

~~SECRET~~/SPECIAL HANDLING

~~SECRET/SPECIAL HANDLING~~

#### 4.1.6 Yoke

The yoke is a machined two-piece beryllium alloy structure consisting of a trussed channel section closed off by a cemented and bolted plate. The aft end of the yoke is piloted and bolted to the roll shaft while the front yoke arms are bolted and doweled to the pitch axis trunnion supports. Although these pitch axis trunnion supports subsequently become part of the pitch axis assembly, in the fabrication process they are previously bolted and doweled to the yoke, whereupon the assembly is line bored to optimize pitch axis bearings alignment. The yoke structure also carries the roll gyro in an integral bracket and the roll gyro electronic package mounted on suitable bracketry. Orientation of these elements normal to the roll axis adds flexibility in achieving the desired level of roll axis balance.

#### 4.1.7 Cabling

The cabling is configured about the limited angular rotation of both gimbals namely 60-degree pitch rotation and 140-degree roll rotation. The present roll axis cable design utilizes two paths for bringing wiring from the rotating elements to interface connectors on the fixed roll housing. The dual approach is desirable in that it permits segregation of the power lines from those carrying signals. Approximately 60 signal leads are brought out through a segmented raceway using a flat flexible cable in a "roll-along" configuration. The remainder (power) of the leads are brought out through a central axial hole in the roll shaft. Conventional planned effort in the cable development area is aimed towards arriving at a single path configuration, preferably through the axial hole in the shaft. This appears to offer the most potential for PSD and torque level control and reduction.

~~SECRET/SPECIAL HANDLING~~

~~SECRET/SPECIAL HANDLING~~

## 4.2 PEDESTAL DESIGN

### 4.2.1 Geometrical Considerations

In order to reconcile the geometric relationships of the A/O system to the vehicle axes and, hence, to the vehicle interface at which the scanner mounts, a detailed study of the resulting pedestal geometry has been accomplished. Essentially, the pedestal is the interface plate between the scanner assembly and the vehicle mounting surface and must geometrically match both surfaces while effectively transferring scanner loads into the vehicle structure.

A detailed report, "Investigation of Pedestal Geometry" is provided as an appendix.

### 4.2.2 Assembly and Adjustment Considerations

The pedestal design is dictated to a large extent by the degree of adjustment required, which is, in turn, dictated by the alignment concept of scanner to vehicle.

One concept, although crude, for instance, could be to assume no adjustments in the pedestal. The entire scanner assembly, including pedestal, is brought to the vehicle mounting pads and bolted in place. A certain amount of misalignment of components will result within the combined system tolerance limits. This, in turn, will result in a certain percentage of vignetting. If axes corrections can be made in the system software, and if vignetting is within tolerable limits, the pedestal can be of relatively simple design as shown in Fig. 4.2-1 (drawing no. 906050).

On the other hand, if, in the more likely case, the scanner is to be accurately mechanically aligned to the vehicle by the use of alignment mirrors, autocollimators, etc., then a means of adjustment of scanner position relative to fixed fold, telescope, and vehicle must be provided. To meet this requirement, a number of designs incorporating pedestal adjustability have been evolved. The most promising is shown on drawing no. 906050.

This design incorporates a spherical seat that carries a plate structure upon which the scanner roll housing is attached. The bottom support for the spherical seat is attached to the vehicle pads through the use of 5/16-inch-diameter body-bound bolts. To compensate for tolerance errors at this interface, a transfer plate for duplicating the bolt pattern spacing on both the vehicle pads and the mounting plate will be used. The top support, or scanner housing mounting surface, can be tipped or tilted; that is, adjusted in two planes by the three spherical-washer-seated adjustment screws. This arrangement would be for fine adjustment to be used subsequent to a gross correction using shims between the vehicle mounting pads and the spherical seat bottom plate. There will be a continuing effort to optimize the pedestal adjustability features, and this effort will have to be responsive to the evolution of final alignment concepts.

~~SECRET/SPECIAL HANDLING~~

~~SECRET~~/SPECIAL HANDLING

Fig. 4.2-1 is an engineering drawing (906050) which is included in an accompanying supplement package.

~~SECRET~~/SPECIAL HANDLING

~~SECRET/SPECIAL HANDLING~~

#### 4.3 PITCH AXIS ASSEMBLY

The major elements of the pitch axis subassembly are pitch housings (pitch axis trunnion supports), pitch trunnions, pitch axis bearings, pitch axis torquer, pitch axis encoder, scan mirror and bezel (Fig. 4.3-1, drawing no. 906001), pitch gyro, pitch gyro electronics package, and cabling.

##### 4.3.1 Pitch Axis Housings

The pitch axis housings or trunion supports are separate elements which are accurately pre-machined from beryllium alloy stock before being bolted and doweled to the yoke. They are then line bored in order to optimize pitch axis bearings alignment. Subsequent to doweling and line boring, they are removed from the yoke. One of these trunnion supports becomes the pitch torquer housing and the other becomes the pitch encoder housing. After assembly of torquer to the torquer housing and assembly of encoder to encoder housing, these subassemblies are then mounted via their respective bearings to the mirror bezel trunnions. This entire subassembly is then mounted and bolted to the yoke via the previously precision doweled pilots.

##### 4.3.2 Pitch Trunnions

The pitch trunnions or pitch shafting are an integral part of the scan mirror bezel structure. The entire structure is machined from a beryllium alloy block.

##### 4.3.3 Pitch Axis Support Bearings

The pitch axis support bearings are preloaded DF pairs mounted against precision ground shoulders and retained by threaded members on the inner race and combination threaded and axially constrained pilots on the outer race. Sealing, lubrication, lubricant creep barrier, and fit-up will generally follow the procedure and methods outlined for the roll axis bearings. The torquer housing incorporates a flexure providing for the axial adjustment required by thermal and assembly considerations.

##### 4.3.4 Pitch Axis Torquer

The pitch axis drive motor is also a dc brushless torquer similar to that used on the roll axis, whose rotor is keyed to the pitch shafting.

##### 4.3.5 Pitch Axis Encoder

The pitch axis encoder (Fig. 4.3-2, drawing no. 114148) is an 18-bit optical type unit whose encoded glass disc is independently mounted on its own bearings. The assembly and operational rationale for this encoder is identical with that of the roll axis encoder.

##### 4.3.6 Scan Mirror Bezel

The scan mirror bezel (Fig. 4.3-1) consists of a beryllium alloy structure which utilizes a "potted circumferential joint for holding the 1-inch-thick Cer-Vit mirror in its front face. The rear section of the bezel is closed off by a beryllium faced stainless steel honeycomb panel which is doweled and bolted through solid inserts to the bezel structure. The doweling is to facilitate removal and accurate replacement during the mirror plotting cycle. This panel, via appropriate inserts, mounts the pitch gyro holding bracket, pitch gyro, and the pitch gyro electronics package. The gyro bracket is again bolted and doweled to the panel inserts for accurate location and replacement.

~~SECRET/SPECIAL HANDLING~~

~~SECRET~~/SPECIAL HANDLING

Fig. 4.3-1 is an engineering drawing (906001) which is included in an accompanying supplement package.

~~SECRET~~/SPECIAL HANDLING

~~SECRET~~/SPECIAL HANDLING

Fig. 4.3-2 is an engineering drawing (114148) which is included in an accompanying supplement package.

~~SECRET~~/SPECIAL HANDLING

~~SECRET~~/SPECIAL HANDLING

#### 4.3.7 Cabling

The pitch axis cabling presently utilizes a slack loop design for bringing wiring from the rotating bezel structure to the yoke terminations. The cabling is then carried by means of the roll along cable and the axial roll shaft hole leads onto terminations on the roll housing. Possible areas of cabling improvement may involve passing wire bundles through axial holes in the pitch shafting, or through elongated slots in the side wall of the bezel. In this case, the concept would be similar to the axial shaft hole design in the roll axis in that the cable will be routed through a hole in the honeycomb structure.

~~SECRET~~/SPECIAL HANDLING

~~SECRET/SPECIAL HANDLING~~

4.4 MIRROR/BEZEL

4.4.1 Design and Sizing

The scan mirror design is given on Fig. 4.4-1 (Drawing no. SK 115279). The power and astigmatic variation in power given in note 4 are equivalent to:

$$\begin{array}{l} \text{Power} \\ \text{Astigmatic Variation} \end{array} \quad \begin{array}{l} \lambda/10 \\ \lambda/20 \end{array} \quad \lambda = 560 \text{ millimicrons}$$

These tolerances are based upon an astigmatic difference in focus of 1/4 dioptic at the eye, and are included in the static irregularity alleviation of the performance error budget.

The overall size of the mirror is based on having no vignetting for scan angles of +40 to +10 degrees in the high power mode for the baseline configuration. An empirical method was used to generate bundle/mirror intersections. This sizing was later confirmed by the analytical programs described in Section 3.

4.4.2 Fabrication Techniques and Problems

The scan mirror is to be fabricated by conventional optical grinding and polishing techniques, complicated only by the elliptical shape of the mirror. The approach presently contemplated is to grind and polish the mirror from a round blank, and then to cut and shape it to the required elliptical form. The mirror will be evaluated and recorrected in order to compensate for any surface irregularities caused by residual strain relief during the shaping process. A test mirror is being fabricated at the present to verify the process.

Two Cer-Vit mirrors have been fabricated using this technique. Number one was fabricated to the size and shape of the external fold mirror. However, the fabrication problems involved were identical to the problems involved in the scan mirror. This mirror was polished with a round shape with a resultant power of  $\lambda/6$  and astigmatism less  $\lambda/20$ . The mirror was edged to the size and shape of the fold mirror, during which the power increased to  $\lambda/3$  and the astigmatism to  $\lambda/4$ .

The other mirror was polished and gave  $\lambda/7$  power and less than  $\lambda/20$  astigmatism. This mirror was edged to the shape of the scan mirror with no detectable degradation. The refiguring now in process indicates that this mirror can successfully be figured to the required tolerance ( $\lambda/10$  power).

An alternate approach to fabrication consists of preshaping the mirror to the required form and blocking the blank using the removed edges as "make-up" pieced, so that the block has a circular shape. It is unlikely that this method will have to be employed.

4.4.3 Error Budget Allocation

On the performance error budget a total of 0.0075 rms was allowed for the thermal effects on the scan mirror. As shown in Section 3, the total center-to-edge deflection will be less than  $0.4 \times 10^{-6}$  inch. This corresponds to a peak wavefront error of about 0.05 wave, which is compatible with the budgeted error.

4.4.4 Primary Subsystem Functions

The primary subsystem functions are as follows:

~~SECRET/SPECIAL HANDLING~~

~~SECRET~~/SPECIAL HANDLING

Fig. 4.4-1 is an engineering drawing (SK115279) which is included in an accompanying supplement package.

~~SECRET~~/SPECIAL HANDLING  
4.4-2

---

~~SECRET/SPECIAL HANDLING~~

1. The mirror/bezel plotting subsystem must provide an optically flat reflecting surface under all mission observational conditions as described in Sections 3, 7, and 8.
2. Mounting must be provided for the pitch axis gyro and associated electronics unit.

4.4.5 Primary Design Considerations

The primary design considerations are as follows:

1. Nonoperational design criteria
  - a. Ensure no nonrecoverable deflections in any metallic structural components that would cause pitch gyro or pitch axis encoder misalignment with respect to the mirror surface.
  - b. Maintain noncritical stresses below the material yield point in all components due to 20 g equivalent static load in any direction (launch lock engaged).
  - c. Adequate rigidity in all planes must be provided in the bezel system to properly restrain the yoke assembly.
2. Operational design criteria have been described in Sections 3.2 and 4.4.

4.4.6 Description of the Determination of Basic Configuration

4.4.6.1 Mirror Potting Material and Nominal Potting Gap

The basic function of the potting material is to provide a circumferentially uniform mounting interface for the mirror which reduces the mechanical and thermal environmental effects on scan mirror wavefront distortions.

The required transmissibility, from Section 7, determines the potting shear spring constant per circumferential inch, expressed as  $G/t$ , where  $G$  equals the shear modulus (psi) and  $t$  equals the nominal potting gap. A value of  $G/t = 1200$  was considered adequate, according to Section 7. For small deflections, potting compounds that are suitable for optical shop potting techniques have values of  $G$  in the range of 100 to 250 psi. Thus, the gap range to satisfy  $G/t = 1200$  becomes 0.080 inch to 0.200 inch, depending on the potting material. The determination of the actual potting material and gap within this range, which varies with both axial and circumferential location, was performed on thermoelastic considerations (fully described later).

4.4.6.2 Ring Bezel

The ring bezel, machined from beryllium, was shaped considering thermoelasticity. The design goal was to shape the ring cross section in such a way as to cause the radial mirror load resultant due to nonsteady state thermal mismatch between the mirror potting and bezel components to pass through the neutral axis of the mirror. This was accomplished in two ways as follows:

1. The high in-plane stiffness of the bezel sandwich back was decoupled as much as possible from the bezel ring by the thin truncated cone transition section.

2. To counteract the remaining off-axis radial restraint due to the bezel back, the ring cross section was tailored so as to provide a radial load resultant at the mirror neutral axis under non-steady-state thermal conditions. In addition, to reduce local mirror edge-distortion effects due to the high Poisson's ratio ( $\alpha$ ) of the potting, the bezel-to-potting interface radius varies with axial location.

~~SECRET/SPECIAL HANDLING~~

## ~~SECRET/SPECIAL HANDLING~~

Beryllium material was chosen for the ring bezel and sandwich back face plates for the following reasons:

1. The coefficient of linear thermal expansion ( $\alpha$ ) of the potting ( $114 \times 10^{-6}$  in/in/ $^{\circ}$ F) and the  $\alpha$  of the bezel must be related by thermal-elastic considerations, since low radial loads at the mirror edge are desired under the entire temperature environment. The high  $\alpha$  of aluminum ( $13.3 \times 10^{-6}$  in/in/ $^{\circ}$ F) and magnesium alloys ( $14.5 \times 10^{-6}$ ) required a potting gap larger than the acceptable range indicated above, therefore, beryllium ( $\alpha = 6.4 \times 10^{-6}$ ) was chosen as a suitable light metal.

2. A beryllium bezel structure is thermo-elastically compatible with the scanner yoke assembly. Several titanium alloys having values of  $\alpha$  in the temperature range of interest of 4.9 to  $5.5 \times 10^{-6}$  in/in/ $^{\circ}$ F could otherwise satisfy (1) above.

3. With proper attention to the thermal design, it is conceivable that a bezel manufactured from a suitable titanium alloy could be made to satisfy (2) above. However, since the ring bezel is sized primarily from thermo-elastic considerations ( $\alpha$ ), the bezel weight for either beryllium or titanium would be approximately proportional to the material density,  $\rho$ . For titanium,  $\rho \approx 0.165$  lb/in<sup>3</sup> and for beryllium,  $\rho \approx 0.065$  lb/in<sup>3</sup>. While more ballast weight would be required for the beryllium bezel system to maintain the specified pitch axis rotational inertia, a given mass of material contributes to this pitch inertia (proportional to the distance from the mass to the pitch axis squared). Since the ballast weight location is at the extremity of the scan bezel, the overall pitching weight of the beryllium system will be lower than that of the titanium bezel system.

### 4.4.6.3 Bezel Back

A double-plate sandwich bezel back was chosen to provide a transversely rigid structure to support the pitch axis gyro and associated electronics under the high limit loads of Sections 7.9 and 7.10. In addition, the double plate configuration thermally decouples the mirror and the heat-producing gyro and electronics. The emissivities of the nonreflecting mirror face and the inner sandwich plate may then be varied to minimize the formation of axial mirror thermal gradients which result in wavefront spherical aberration ("edge sag").

Alternative bezel back configurations were also considered before choosing the sandwich (double plate) configuration. These alternatives were (1) single plate bezel back and (2) "strong-back" bezel back, consisting of a rigid member connecting the ring bezel trunnion points of sufficient width and rigidity for mounting the pitch axis gyro and associated electronics. This configuration therefore exposed a substantial part of the nonreflecting side of the scan mirror.

The temperature histories of the scan mirror/bezel system were determined for representative double-plate, single-plate and strongback configurations. The results of these analyses appear in Itek documents 9300-68-X292 (1-17-68) and 9400-68-X340 (4-5-68). The first assumed eight 25-minute active periods and eight inactive periods per operation. The second assumed ten 10-minute active operations and six inactive periods per operation.

The results of these analyses were then applied to the Itek transient thermal defocus program for preliminary determination of mirror bending ("sag") due to axial temperature gradients. The double-plate configuration provided the best compromise of gyro mount temperature range and edge sag and was therefore chosen for more refined development. The sandwich configuration is thermally very similar to the double-plate model since the sandwich core foil does not provide a significant heat transfer path from outer to inner plates.

The plate material chosen was 0.030 inch beryllium, for compatibility with the ring bezel.

~~SECRET/SPECIAL HANDLING~~

~~SECRET/SPECIAL HANDLING~~

The stainless steel vented core was chosen because its coefficient of linear thermal expansion ( $\alpha = 7 \times 10^6$  in/in/ $^{\circ}$ F) is similar to that of beryllium and is available in honeycomb core form. Attachment to the faceplates is with FM-1000 epoxy film, a standard sandwich bonding material.

#### 4.4.7 Design of Mirror/Bezel Potting System

After selection of the system component configurations, detail system design was initiated.

##### 4.4.7.1 Simplified Environmental Parameters for Operational Conditions

4.4.7.1.1 Mechanical. As described in Section 4.4.6, the scanner system transmissibility requirements determined the use of a potting  $G/t \approx 1200$ . This may be seen from Fig. 4.4-2, which shows the minimum permissible pitch frequency as a function of pitch shaft stiffness and potting  $G/t$  stiffness.

4.4.7.1.2 Thermal. The actual nonsteady state temperature distribution in the mirror/bezel system is extremely complex and, indeed, varies with design changes which affect component thermal masses ( $WC_p$ ), emissivities, conduction path lengths, etc. Therefore, for the initial design process, a thermal load consisting of a system uniform temperature change from 70 to 0 $^{\circ}$ F was chosen. The actual temperature distributions at selected times are then input to the final mirror/bezel potting system for checking purposes.

##### 4.4.7.2 Analytical Methods for Design Iteration

4.4.7.2.1 Construction of Representative Analytical Model. Ideally, the structural response of the mirror/bezel potting system would be evaluated for an elliptical model representing the actual system. This involves the development of the mathematical equivalent of an arbitrary three-dimensional elastic solid with complex internal boundaries separating areas of different material properties. To obtain the structural response of such a system to any but the most elementary loading conditions is generally conceded to be beyond the present state of the art. Itek's Advanced Technology Directorate is currently engaged in the development of a series of computer solution methods to this family of problems, incorporating the FRAN structural computer program as one stage in the process. However, even if this mathematical method were developed to a usable point, it has been estimated that, for a mirror/bezel potting model subdivided into enough discrete units to permit adequate accuracy, a single computer run would require two to three hours of IBM 360/65 processing time. Since the present study involved approximately 60 detail refined versions of the preliminary system configuration, the above approach was not considered practical.

The actual mathematical model used was axisymmetric. This technique was considered more than adequate for the following reasons:

1. The structure is reasonably similar to an axisymmetric structure, the ratio of major diameter to minor diameter being approximately 1.3.
2. Primary quantities to be controlled are the magnitude and location of the thermoelastic radial mirror loads as described in Section 4.4.6. These vary little with circumferential location and so an axisymmetric model of the minor diameter could be used for the system minor axis location, etc.
3. Bezel and potting temperatures are approximately axisymmetric. Only the mirror temperatures evidence nonaxisymmetric behavior. Since the thermoelastic interaction of the mirror/

~~SECRET/SPECIAL HANDLING~~

~~SECRET/SPECIAL HANDLING~~

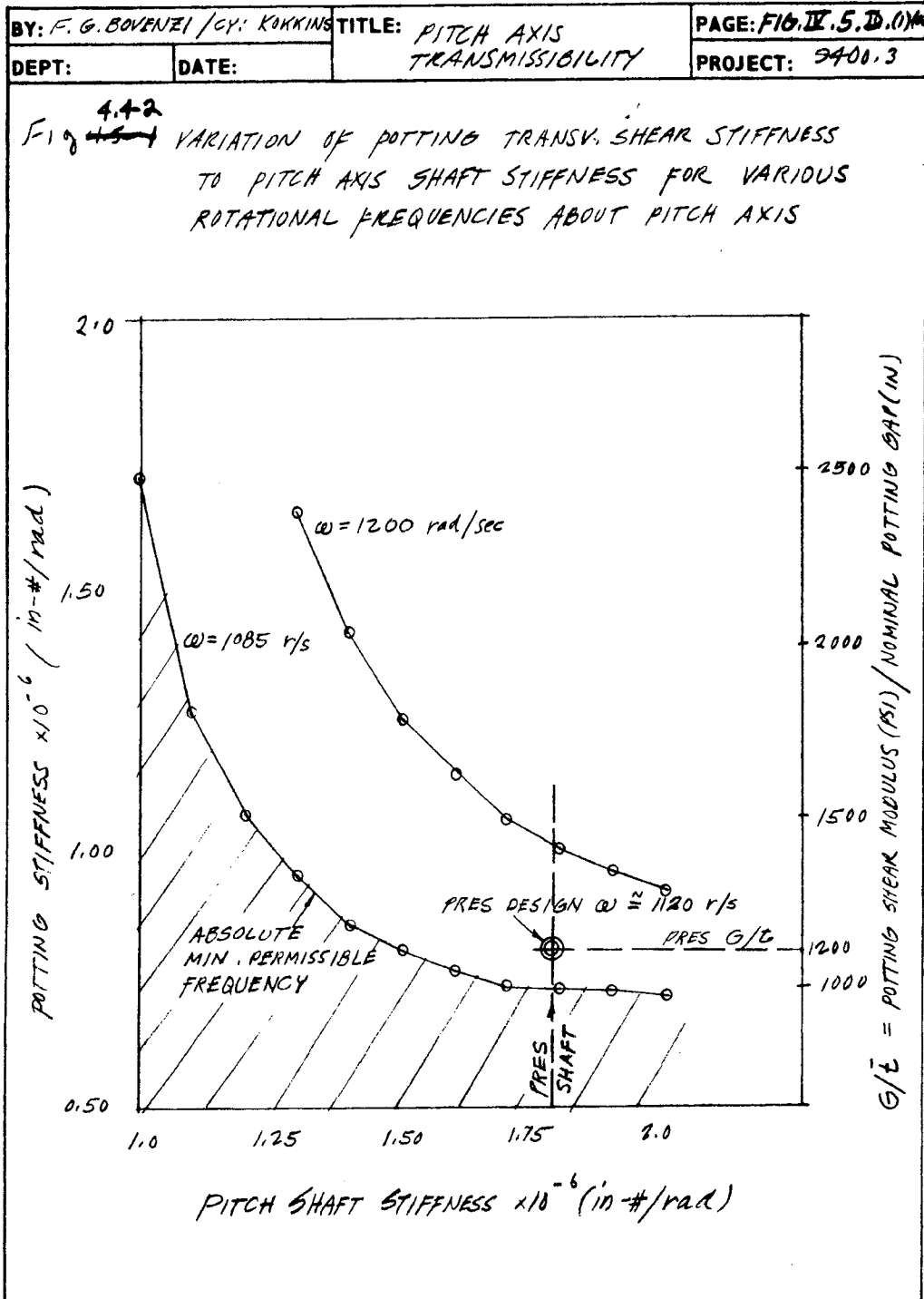


Fig. 4.4-2 — Variation of potting transverse shear stiffness to pitch axis shaft stiffness for various rotational frequencies about pitch axis

~~SECRET/SPECIAL HANDLING~~

~~SECRET/SPECIAL HANDLING~~

bezel plotting system is dependent mostly on the properties of the potting and bezel because of the extremely low  $\alpha$  ( $0.02 \times 10^{-6}$  in/in/ $^{\circ}$ F) of the Cer-Vit mirror material, the axisymmetric model was selected.

The solution to the thermoelastic response of a nonhomogeneous axisymmetric body has been performed by many writers and is mathematically equivalent to the solution of a two-dimensional general thermoelasticity problem.\* For example, the solution can be made of the partial differential equation series

$$\nabla^4 \Psi + \alpha E \nabla^2 T(r, z) = 0 \quad (1)$$

where  $\Psi$  is a stress function satisfying

$$\sigma_r = \frac{\partial}{\partial z} \left( \nu \nabla^2 \Psi - \frac{\partial^2 \Psi}{\partial r^2} \right)$$

$$\sigma_\theta = \frac{\partial}{\partial z} \left( \nu \nabla^2 \Psi - \frac{1}{r} \frac{\partial \Psi}{\partial r} \right)$$

$$\sigma_z = \frac{\partial}{\partial z} \left[ (2 - \nu) \nabla^2 \Psi - \frac{\partial^2 \Psi}{\partial z^2} \right]$$

$$\tau_{rz} = \frac{\partial}{\partial r} \left[ (1 - \nu) \nabla^2 \Psi - \frac{\partial^2 \Psi}{\partial z^2} \right]$$

and  $\nabla^2 =$  the Laplacian operator (axisymmetric)

$$\nabla^2 = \frac{\gamma^2}{\gamma r^2} + \frac{1}{r} \frac{\gamma}{\gamma r} + \frac{\gamma^2}{\gamma z^2}$$

and

$$\nabla^4 = \nabla^2(\nabla^2)$$

The generalized stress function satisfying Equation 4-1 will satisfy equilibrium and compatibility requirements.

The strain energy method is employed by the UCAL finite-element program used by Itek for the mirror/bezel potting thermoelastic analysis. A complete description of the UCAL program appears as Appendix 4A. Equations equivalent to 4-1 are solved by first generating certain integrals attaining their minimum values when the stress distribution in the body satisfies equilibrium conditions. These integrals are an expression of the potential strain energy produced in the body by the loadings. In the thermal loading situation, these loadings result from the enforcement of compatibility requirements on a set of finite elements whose initial shape is changed by temperature variations. The finite-element technique used in the UCAL program replaces the continuous structure by a system of axisymmetric ring elements interconnected at nodal points. Each finite

---

\* Gatewood, B. E., Thermal Stresses, McGraw-Hill, New York, 1957.

~~SECRET/SPECIAL HANDLING~~

element always has a uniform state of stress. Equilibrium equations, in terms of the unknown nodal point displacements, are generated at each nodal point. A matrix solution of this set of equations accomplishes the problem solution.

4.4.7.2.2 Development of UCAL Analytical Model. Since the UCAL program assumes a uniform state of stress to exist in each finite element, subdivision of the model must be "finer" in those areas where rapid stress variation is anticipated. This subdivision is diagrammed in Figs. 4.4-3 through 4.4-5. The indicated topology was retained for all detail refinements of the design; only node locations and material properties, when applicable, were varied to simulate the various trial model characteristics. Additional properties of the UCAL model follow:

1. Because of the structural peculiarities of the sandwich back honeycomb core material, a plate back of a fictitious material was analytically generated to simulate the sandwich back elastic behavior. The details of this process appear in Appendix 4B.
2. A single mirror radius for all analytical models was determined for development of the proper bezel and potting cross-sections. This mirror radius was set at approximately the geometric mean of the mirror major and minor radii

$$R = \sqrt{R_{\text{maj}}R_{\text{min}}} \cong \frac{(10.7)(14.2)}{2} \cong 6.2 \text{ inches}$$

Once the proper shapes were determined, the small variations in the potting gap required for the minor and major axis locations were established (i.e., the variation in potting gap as function of circumferential location).

4.4.7.2.3 Preliminary Establishment of Allowable Reflecting Surface Error Contribution. Only significant operational loads causing optical errors are thermal loads. The total allowable deviation from a flat plane surface was set to a preliminary value of  $\lambda/40 \cong 0.500 \times 10^{-16}$  inch, including worst-case error stackup. This includes nonsteady state thermal effects, but not manufacturing (figuring) errors. Several thermal error contributions must be considered. However, the relative magnitudes of these contributions could not be established without detailed structural analysis. Therefore, the thermoelastic errors were reduced through design to a feasible low value, whereupon the various error contributions were developed.

4.4.7.2.4 Preliminary Ring Bezel Cross Section Shape Determination. Based upon the initial sandwich bezel back configuration described in Appendix 4B, several series of trial ring bezels were constructed in an effort to have the effective radial mirror force resultant pass through the mirror neutral axis, as described in paragraph 4.4.6.2. At this point in the design, the required  $G/t$  shear transmissibility had not yet been established, and thermal elastic mismatch existed at the potting bezel interface. Sketches of these configurations appear as Appendix 4C. Although data obtained from these trial runs are not included in this report, they are in Itek Project 9400 files. Data reduction included reflecting surface transverse deflection, radial stress and deflection profile at potting-bezel interface, and linearized reflecting surface standard deviation. In these preliminary cases, the mirror surface transverse deflection proved to be extremely sensitive to potting gap and ring bezel cross-sectional details. This sensitivity was traced to the radial thermoelastic mismatch at the potting/bezel interface, aggravated by the high Poisson's ratio of the potting. It was therefore decided to determine the best potting gap shape before final selection of the ring bezel cross-section.

4.4.7.2.5 Potting Gap Investigation. Still using an axisymmetric model with geometric mean mirror radius, a mirror potting model with no bezel was subjected to the  $\Delta T = -70^\circ\text{F}$  simulated

~~SECRET/SPECIAL HANDLING~~

SECRET/SPECIAL HANDLING

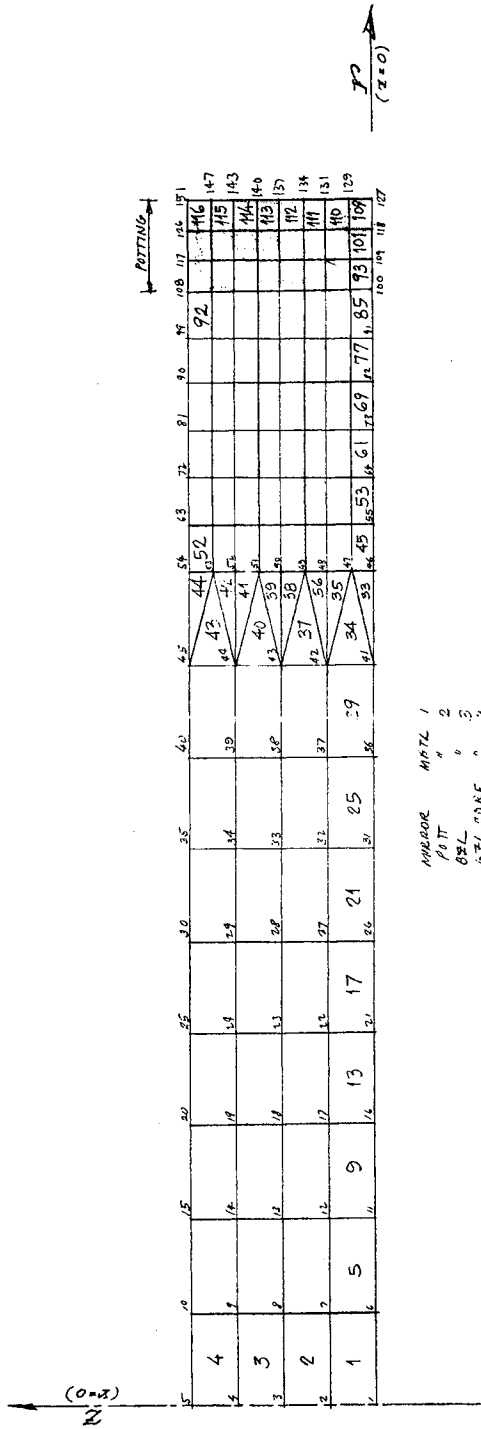


FIG. 4.4-3 — Revised master nodes and elements for FF&S mirrors (UCAL)

SECRET/SPECIAL HANDLING



~~SECRET/SPECIAL HANDLING~~

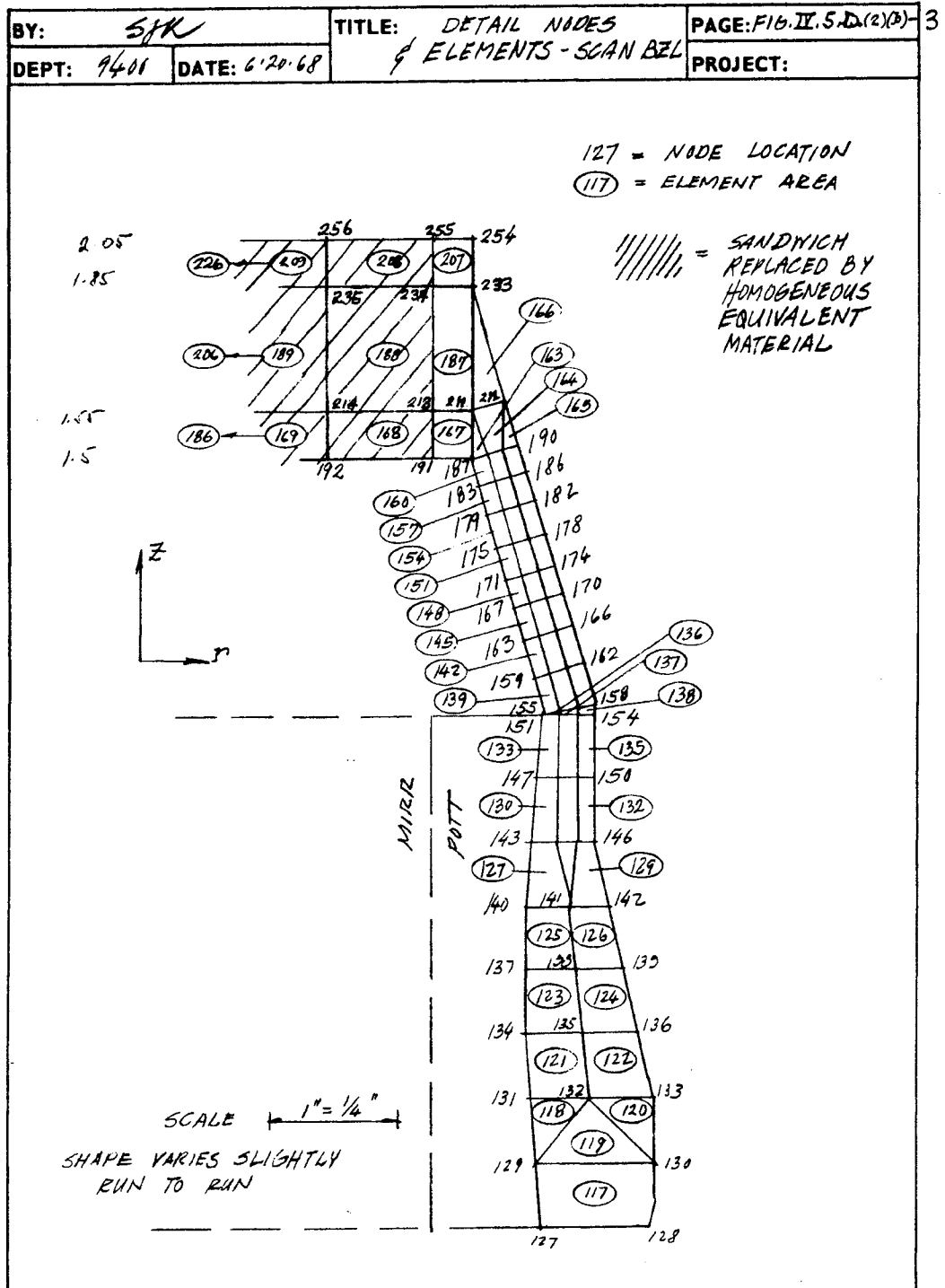


Fig. 4.4-5 — Detail nodes and elements—scan bezel

~~SECRET/SPECIAL HANDLING~~

~~SECRET/SPECIAL HANDLING~~

thermal load for a range of potting gaps. This UCAL model series appears in Fig. 4.4-6. After determination of the radial deflection profile at the potting outer radius for each gap, a comparison of these deflection profiles was made with the calculated radial displacement of the bezel along (to the same thermal load). This deflection is easily obtained as  $\delta_{BZL}^R = R_B \alpha_B \Delta T$ , where  $R_B$  = radius of bezel-potting interface. For present materials

$$\begin{aligned}\delta_{BZL}^R &= (6.2 \text{ in.})(6.4 \times 10^{-6} \text{ in./in./}^\circ\text{F})(-70^\circ\text{F}) \\ &= -2,780 \text{ min}\end{aligned}$$

Radial  $\delta_R$  profiles for potting-mirror model versus potting gap appear in Fig. 4.4-7. Comparison with  $\delta_{BZL}^R = -2,780 \text{ min}$  indicated that the nominal potting gap would fall in the range 0.120 to 0.125 inch. All further investigations with the full mirror-bezel-potting model varied the gap within this range.

4.4.7.2.6 Final Selection of Ring Bezel Potting Cross Section. After establishment of the proper potting gap range for the geometric mean radius model, further trials were made to:

1. "Home-in" to proper potting gap including axial variation to reduce the axial variations in potting strain evidenced in Fig. 4.4-7.
2. Finalize proper ring bezel cross-section shape.

These run series' culminated in the series 13.1 to 13.6 which bracketed trial model configurations yielding low values of surface out-of-plane deflection and surface linearized standard deviation. The latter is calculated internally for the reflecting surface by the UCAL program as modified by Itek.

The model configurations, 13.1 through 13.6, are shown in Fig. 4.4-8; of these, configurations 13.3 and 13.6 had the better potting/bezel interface shape, providing a reduction in the axial variation of radial potting strain. The variations of center-to-effective-edge deflection and linearized standard surface deviation with potting gap for the thermal load (70 to 0 $^\circ$ F) are shown in Fig. 4.4-9. Plots of the corresponding surface deflections from center to edge are shown in Fig. 4.4-10.

A final series of runs was made following the actual design of the sandwich back rim and surrounding area. This is the same configuration shown in Drawing no. 906001. Other minor changes included:

1. Mirror, from  $0.05 \times 10^{-6}$  to  $0.02 \text{ in./in./}^\circ\text{F}$ , reflecting Owens-Illinois Company certification of special Cer-Vit material.
2. Bezel truncated cone transition section reduced to 0.085 inch thickness from 0.100 inch. The configuration series', 15.1, 2, 3, 4, 6 are shown in Figs. 4.4-11 and 4.4-12. The linearized standard surface deviation and center-to-effective-edge deflection are shown in Fig. 4.4-13 as a function of g, and the actual surfacedeflections along a radius are shown in Fig. 4.4-13 as a function of g.

The actual nominal potting gap used was 0.123 inch for the 6.2-inch  $R_M$  model, and falls between cases 15.3 and 15.4. This surface deflection is also shown in Fig. 4.4-14.

A complete UCAL computer run for the 15.4 case is included in Appendix 4D.

4.4.7.2.7 Nonaxisymmetric Variation in Potting Gap. A preliminary estimate of the required circumferential variation in potting gap has been made to account for the different mirror/bezel radii at different circumferential locations. The same approach was used as that for the initial

~~SECRET/SPECIAL HANDLING~~

~~SECRET/SPECIAL HANDLING~~

potting gap sizing (paragraph 4.4.7.2.5). An axisymmetric mirror potting model series with an R mirror major radius of 7.1 inches was constructed with no bezel and with the same boundary conditions as Fig. 4.4-6. The radial outer potting displacements for a representative edge mode (average of 129 and 133) were evaluated as a function of potting gap. The gap giving a radial displacement was chosen. As may be seen from Fig. 4.4-15, the corresponding nominal gap at the major axis was set to 0.145 inch. Potting gap axial variation remains at  $\pm 0.015$  inch from this value, so Drawing no. 906001 shows the mirror-to-bezel gap of 0.130 inch at the closest point, for section M-M at the major axis. Note that other sections are aligned with radii.

A similar procedure was used to size the gap at the minor radius location.

#### 4.4.7.3 Surface Deflection Error Breakdown

A preliminary estimate of the relative error contributions of the several thermal effects has been made. It will be recalled that in 4.4.7.2.3, a total structural error of  $\lambda/40 \cong 0.500 \times 10^{-6}$  in.

1. Nominal center-to-effect edge thermal deflection error not including nonsteady-state effects is set at  $0.05 \times 10^{-6}$  inch from Fig. 4.4-14.

2. Center-to-edge spherical deflection due to axial thermal mirror gradients is calculated using the results of the Itek transient thermal defocus program. This error, calculated in Appendix 4E, is set at  $0.080 \times 10^{-6}$  inch.

3. Center-to-effective edge spherical deflection due to radial gradients (lensing) is also calculated in Appendix 4E. This error is set at  $0.035 \times 10^{-6}$  inch.

4. Center-to-effective edge deflection due to 10 percent variation in potting. This material property is the only one not established to 2 percent. This error may be estimated by relating it to the known effect of potting gap variation in Fig. 4.4-13.  $\Delta_{\text{gap}} = \nabla g^{\text{II}}$  (10 percent)  $\cong 0.012$  inch. This is valid because for a small range, radial strains shown in Fig. 4.4-15 go to zero for potting gap approaching zero. From Fig. 4.4-13,  $\nabla g = 0.012$  inch results in center-to-effective-edge deflection error  $0.220 \times 10^{-6}$  inch.

5. Center-to-effective-edge deflection due to 0.002 inch potting gap error. Again, from Fig. 4.4-13,  $\pm g = 0.002$  results in deflection error  $0.037 \times 10^{-6}$  inch. A preliminary summary of these errors yields

- a.  $0.050 \times 10^{-6}$
- b. 0.080
- c. 0.035
- d. 0.220
- e. 0.037

$$0.422 \times 10^{-6} \text{ inch} \cong 0.500 \times 10^{-6} \text{ inch}$$

#### 4.4.7.4 Conclusion

Refined thermal design is now in progress to evaluate more completely the scan mirror-bezel-potting system to revised nonsteady-state thermal loads. This is not expected to yield significantly greater values since:

1. Low temperature variations exist in the bezel due to the high coefficient of heat conductivity; the potting ring is very thin, ensuring that low effective temperature differences will exist between the potting and bezel. Their respective temperature values control the thermo-elastic interaction of the bezel and potting due to the extremely low mirror.

~~SECRET/SPECIAL HANDLING~~

~~SECRET/SPECIAL HANDLING~~

NODES AND ELEMENTS AS IN FIG. IV.5.d (2)(b)-1

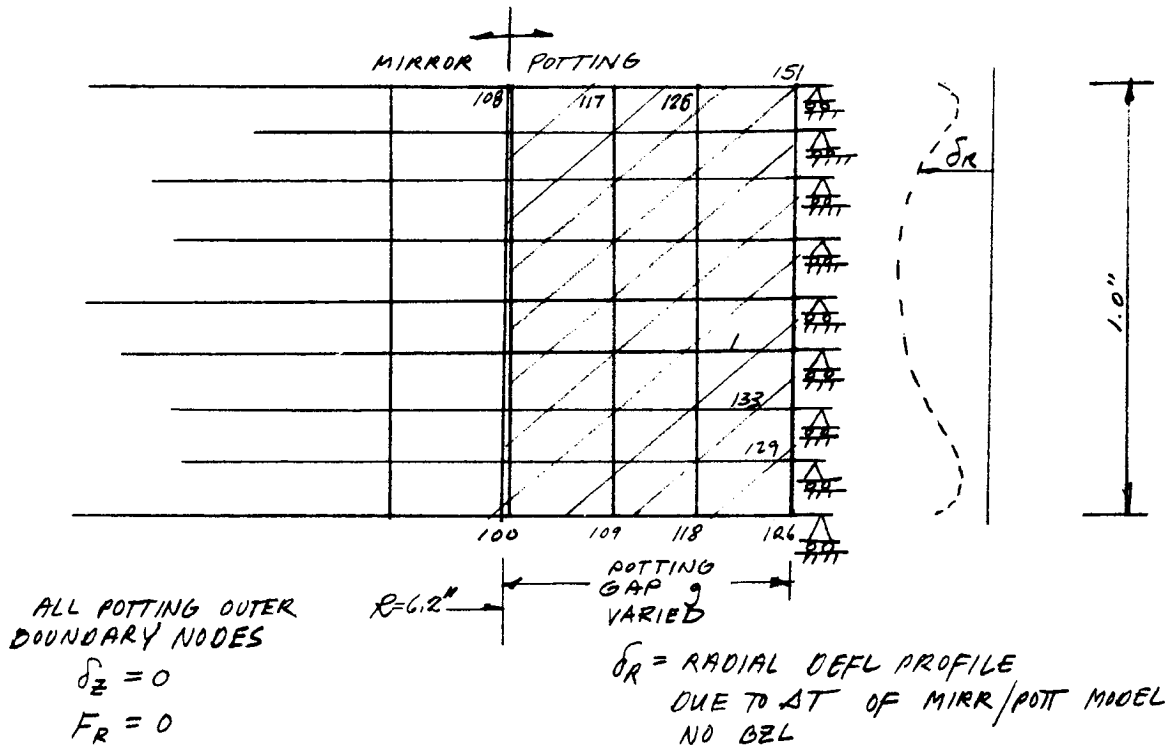


Fig. 4.4-6 — Mirror-potting model

~~SECRET/SPECIAL HANDLING~~

~~SECRET/SPECIAL HANDLING~~

K-E 10 X 10 TO THE 5/8 INCH 359-8DG  
KEUFFEL & ESSER CO. MADE IN U.S.A.  
12 X 12 TO THE INCH

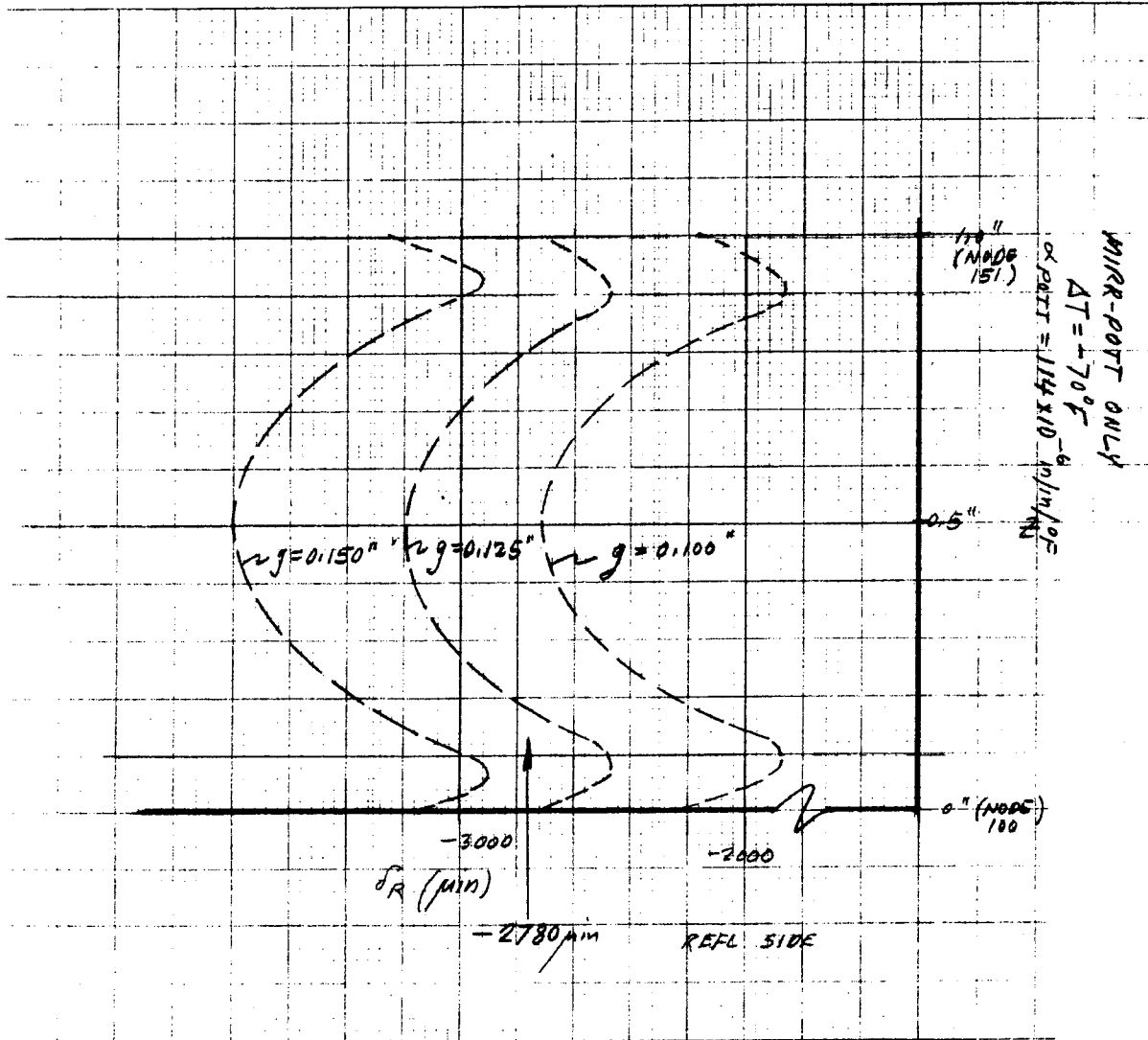


Fig. 4.4-7 — Radial  $\delta$ —outer potting nodes versus Z location

~~SECRET/SPECIAL HANDLING~~  
4.4-17

~~SECRET/SPECIAL HANDLING~~

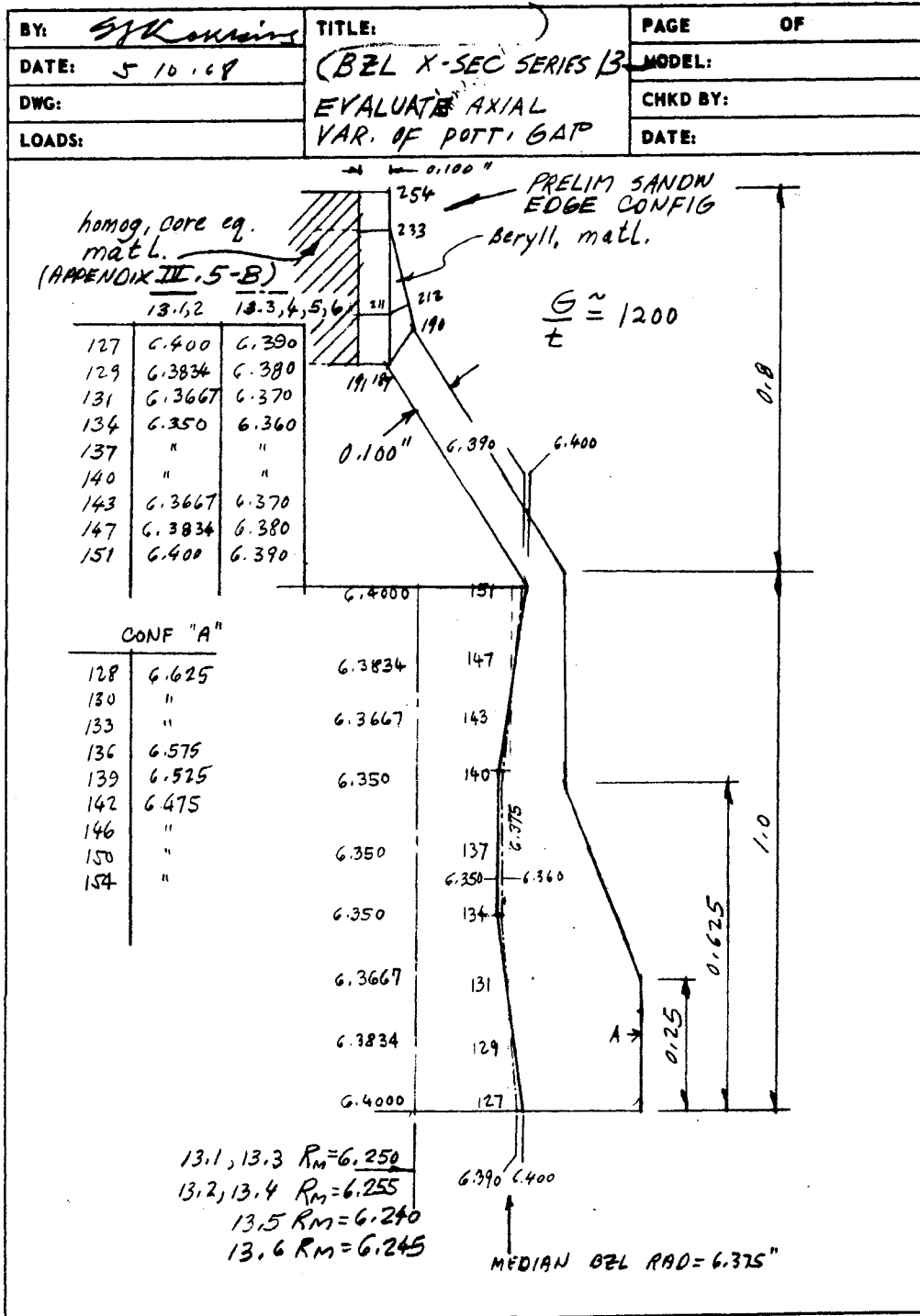


Fig. 4.4-8 — Bezel X-Section series 13—evaluation of axial variation of potting gap

SECRET/SPECIAL HANDLING

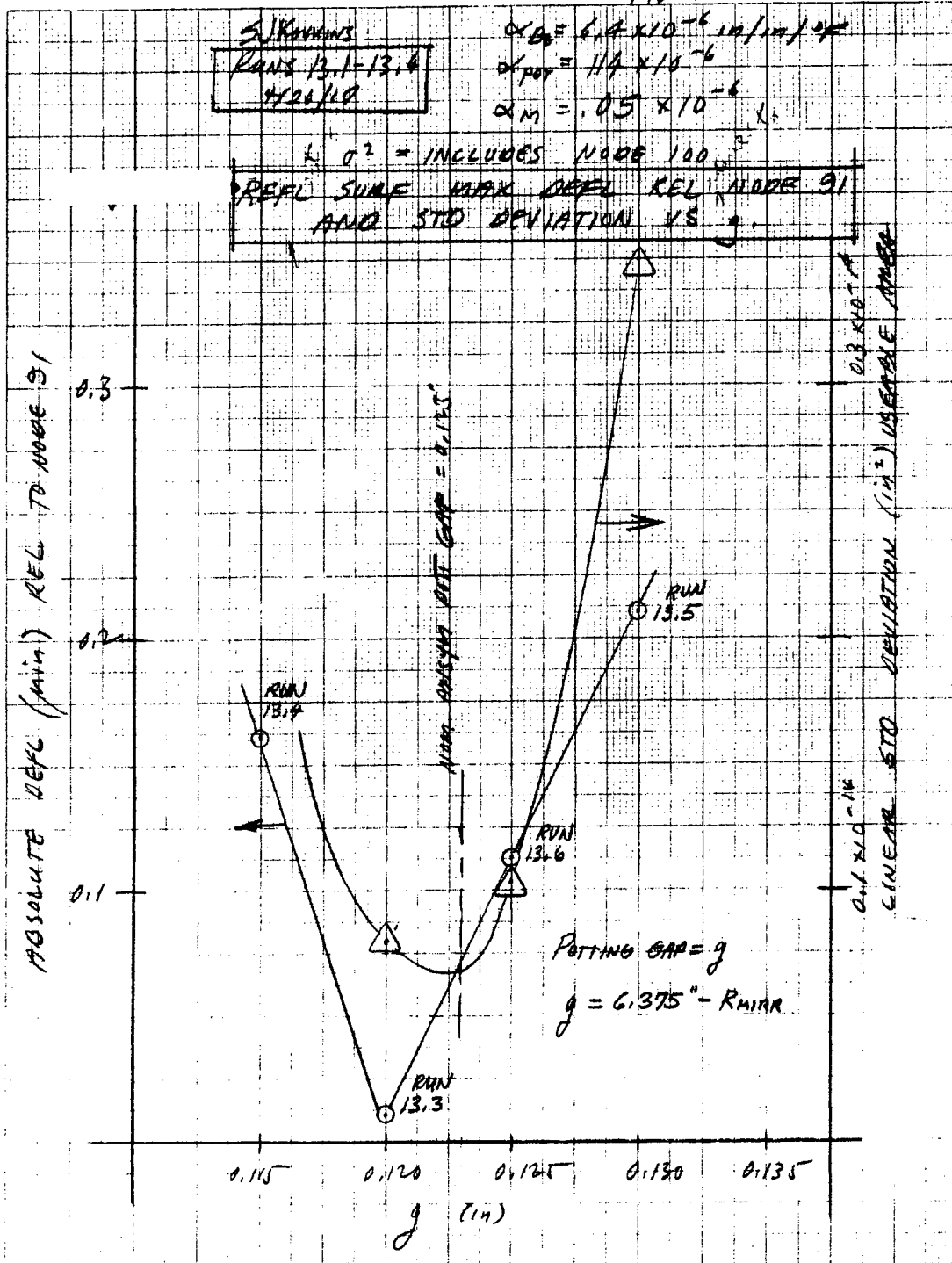
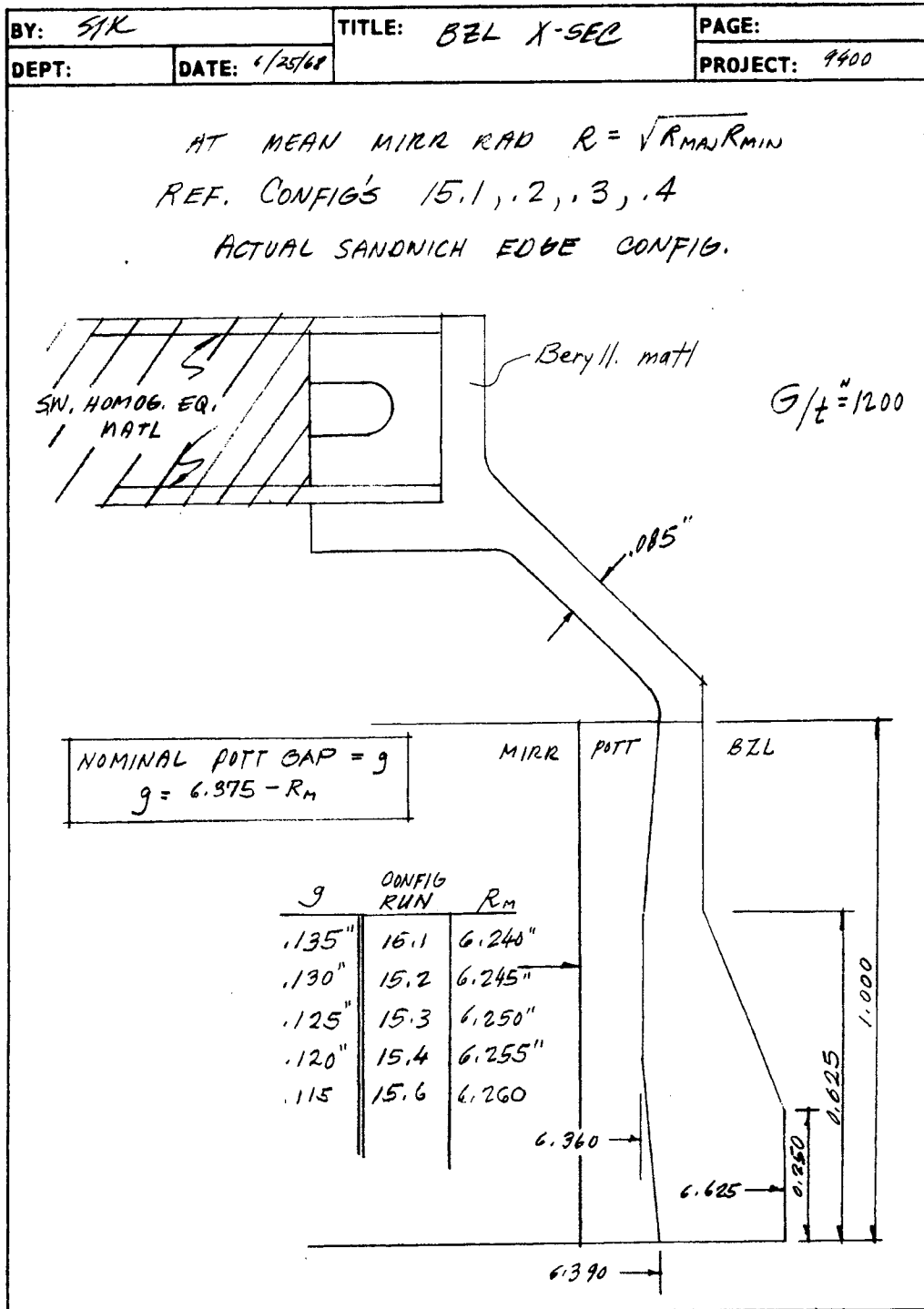


Fig. 4.4-9 — Reflecting surface maximum deflection relative to node 91 and standard deviation versus  $g$

SECRET/SPECIAL HANDLING



~~SECRET~~/SPECIAL HANDLING



Ittek

Fig. 4.4-11 — Actual sandwich edge configuration

~~SECRET~~/SPECIAL HANDLING

~~SECRET~~/SPECIAL HANDLING

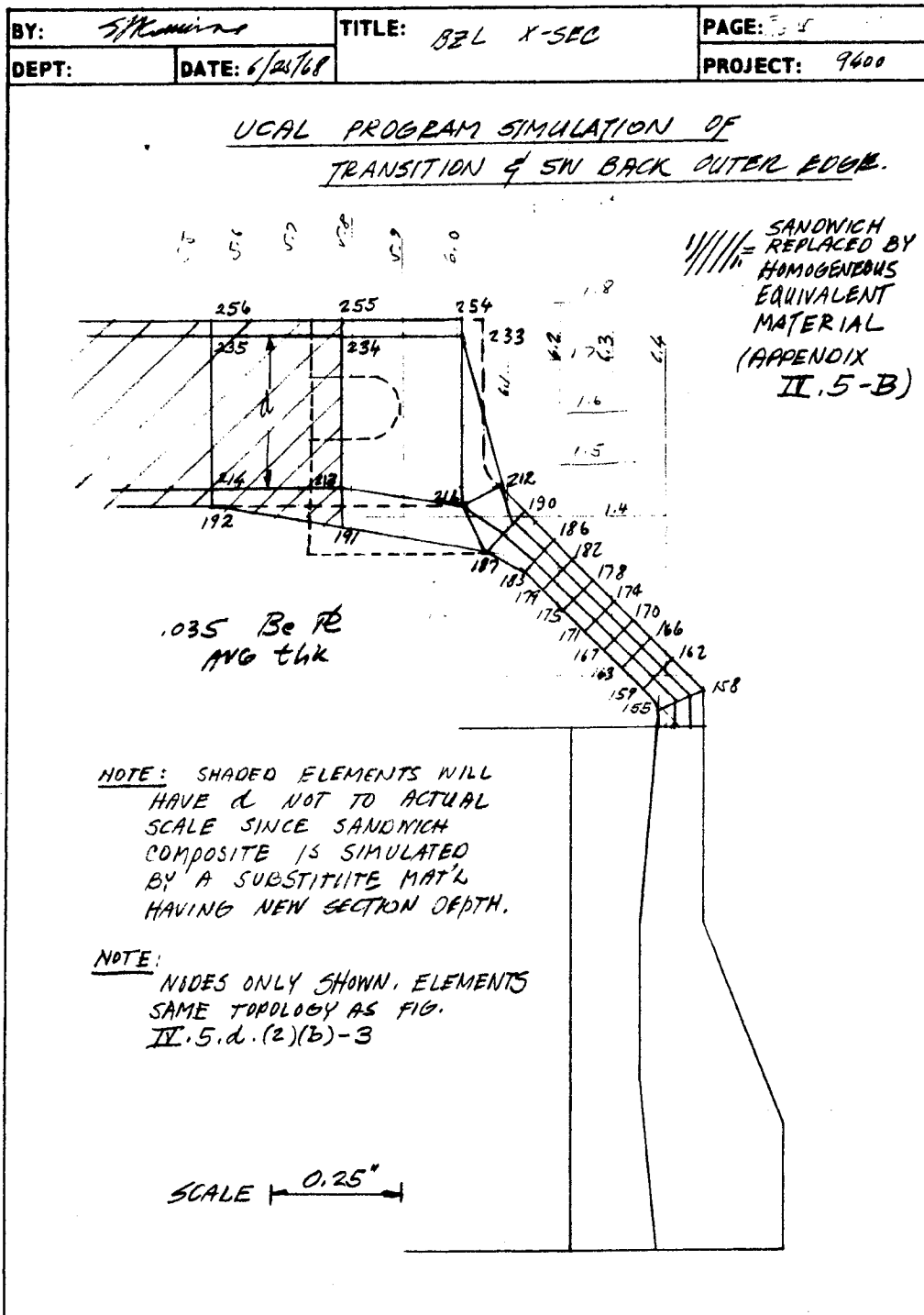


Fig. 4.4-12 — UCAL program simulation of transition and sandwich back outer edge

~~SECRET~~/SPECIAL HANDLING

~~SECRET/SPECIAL HANDLING~~

BY: <i>S. Rowlands</i>	TITLE:	PAGE:
DEPT:	DATE: <i>6/25/68</i>	PROJECT: <i>9400</i>

REVISED NODES FOR 906001 SCAN BZL IN  
TRANSITION & SW BACK OUTER EDGE REGIONS

<u>TRANSITION</u>		<u>r</u>	<u>z</u>	<u>r</u>	<u>z</u>
155	6.390	1.035	158	6.475	1.075
159	6.360	1.075	162	6.415	1.130
163	6.320	1.115	166	6.375	1.175
167	6.285	1.150	170	6.340	1.200
171	6.250	1.185	174	6.300	1.240
175	6.210	1.225	178	6.260	1.275
179	6.165	1.260	182	6.220	1.320
183	6.125	1.295	186	6.180	1.355
187	6.060	1.330	190	6.135	1.410

<u>BZL RIM</u>		<u>r</u>	<u>z</u>
191	5.780	1.380	
192	5.530	1.425	
211	6.085	1.460	
212	6.010	1.425	
213	5.980	1.460	
214	5.530	1.460	
233	6.010	1.745	
234	5.780	1.745	
235	5.530	(NOTE) p.3	
254	6.010	1.775	
255	5.780	1.775	
256	5.530	(NOTE) p.3	

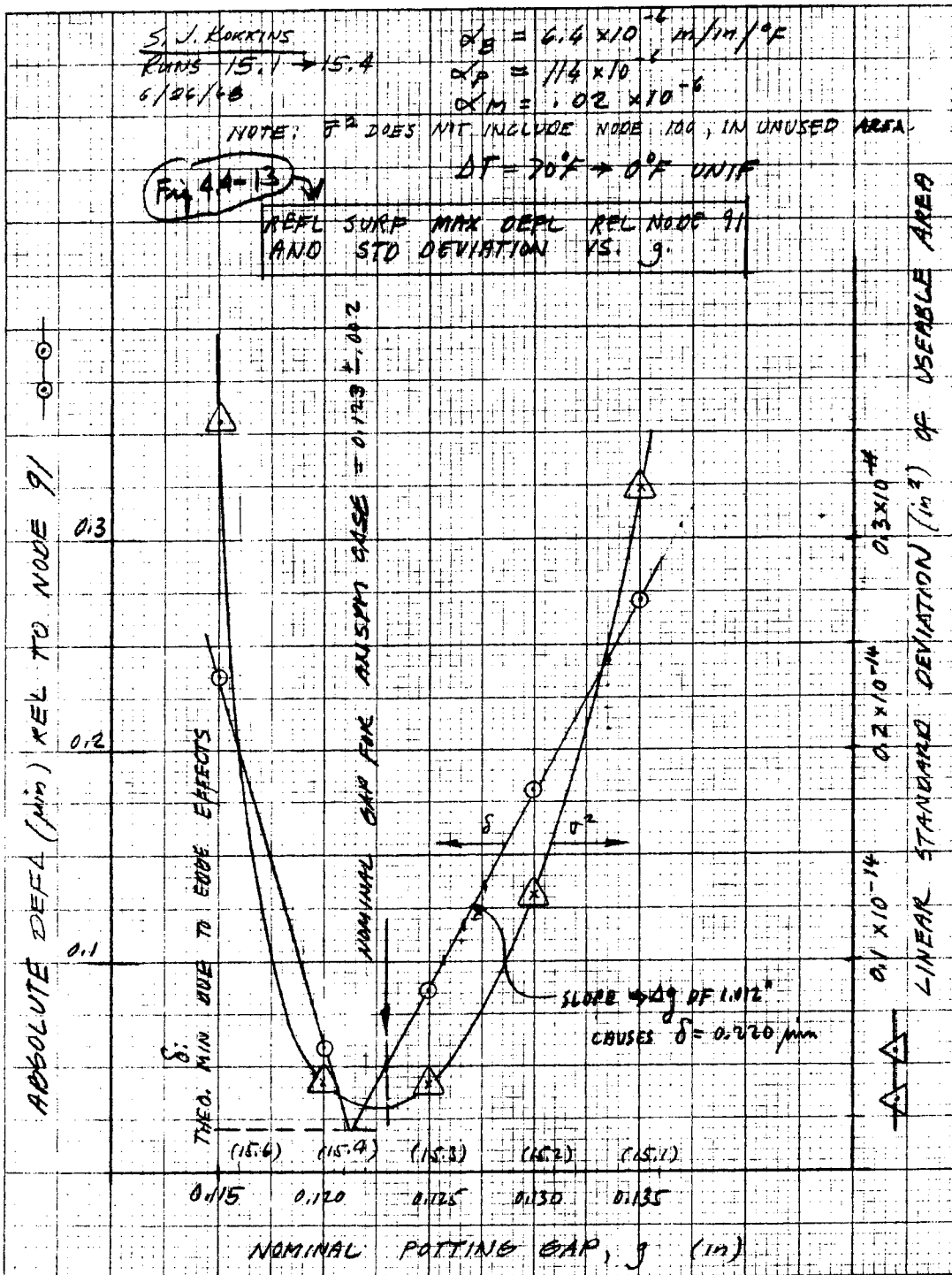
E 103 8/66 ENGINEERING ANALYSIS SHEET

Ittek

Fig. 4.4-12 — (Cont.)

~~SECRET/SPECIAL HANDLING~~

**SECRET/SPECIAL HANDLING**



M.S. 12 X 10 TO THE INCH 359-80G  
 REFERENCE: MIL-STD-883C, METHOD 2000

Fig. 4.4-13 — Reflecting surface maximum deflection relative to node 91 and standard deviation versus g

**SECRET/SPECIAL HANDLING**

~~SECRET/SPECIAL HANDLING~~

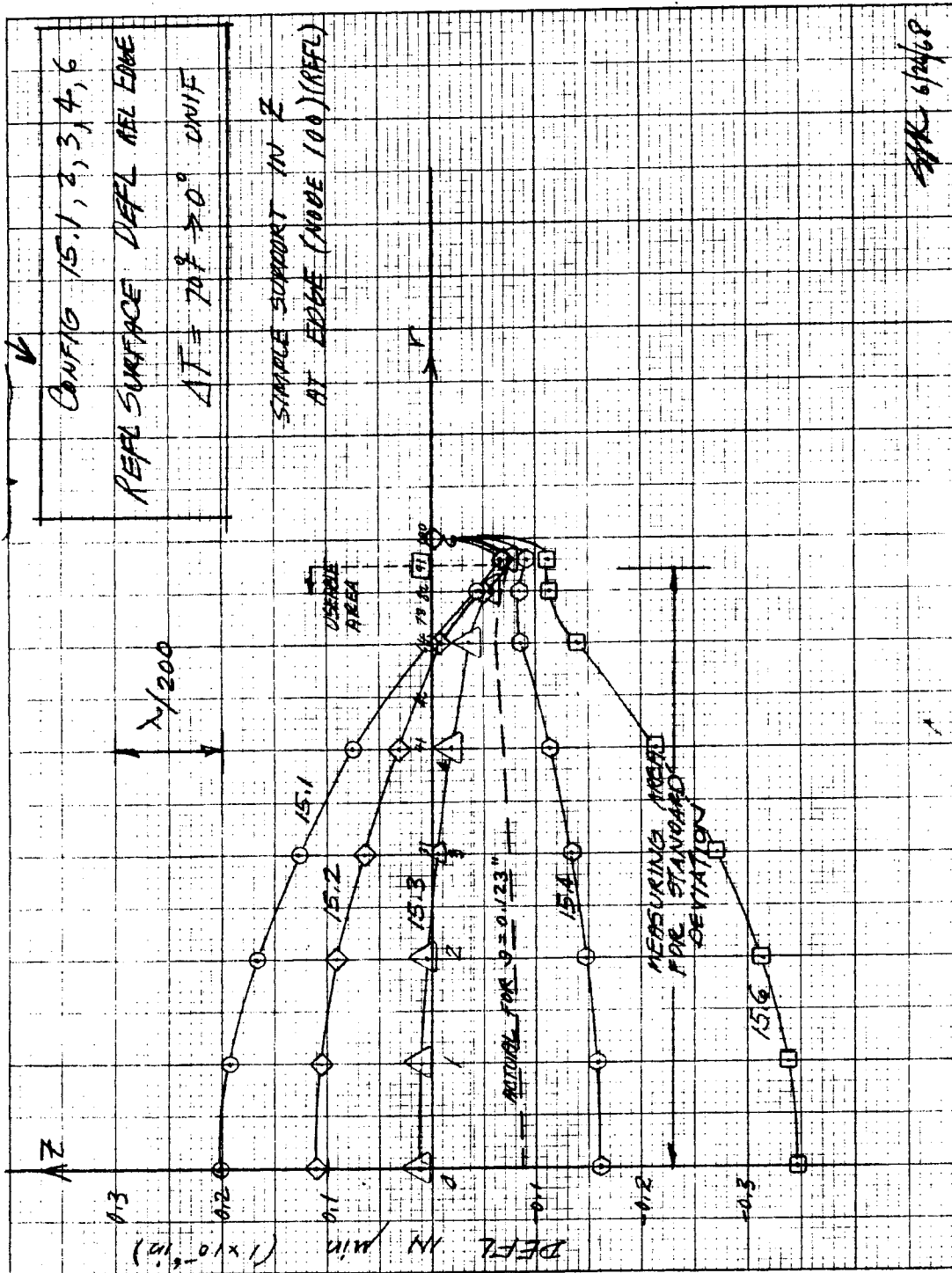


Fig. 4.4-14 — Configuration 15.1, 2, 3, 4, and 6—reflecting surface deflection relative to edge ( $\Delta T = 70^\circ F \rightarrow 0^\circ$  uniform)

~~SECRET/SPECIAL HANDLING~~

~~SECRET/SPECIAL HANDLING~~

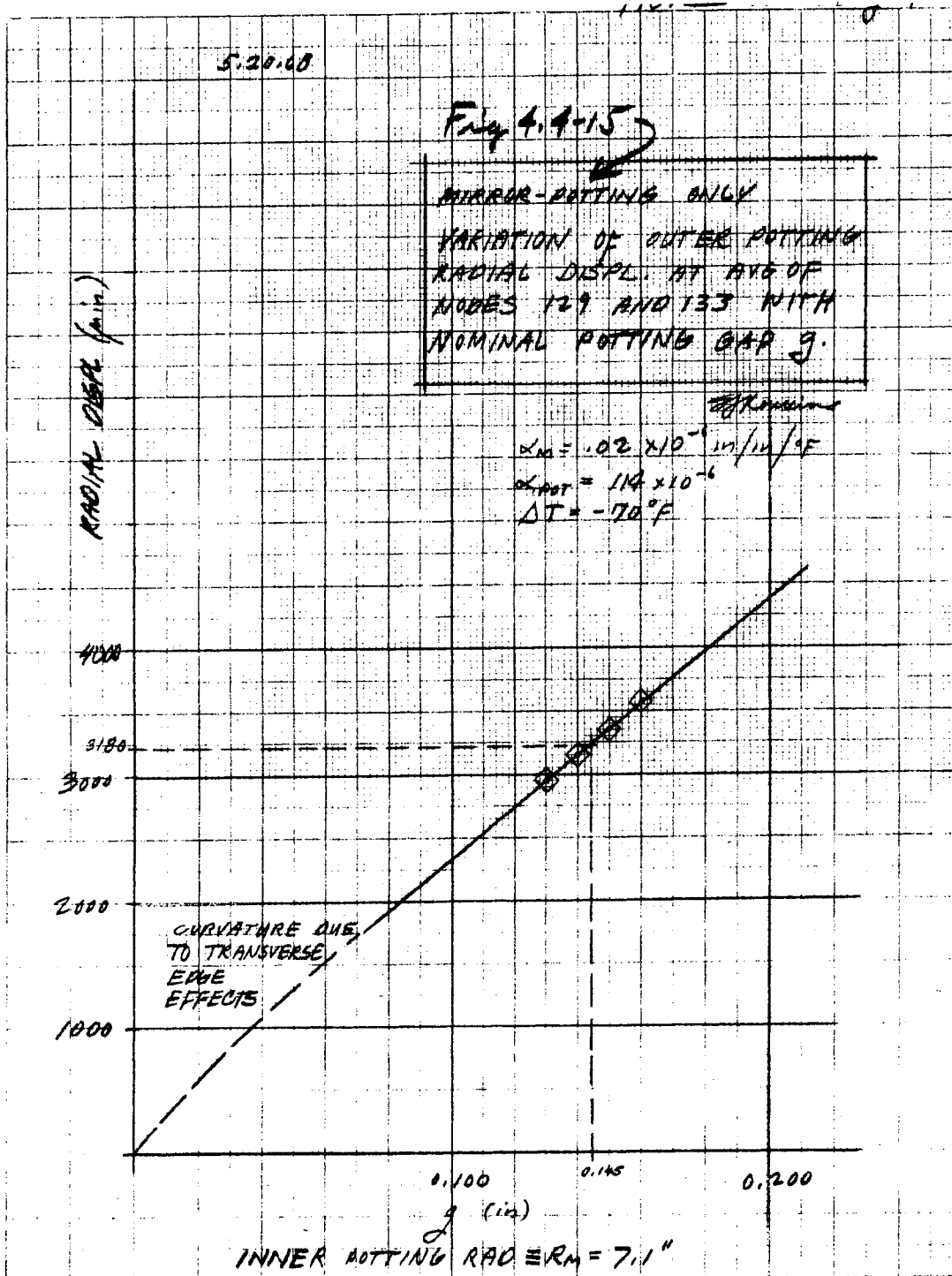


Fig. 4.4-15 — Mirror-potting only (variation of outer potting radial displacement at average of nodes 129 and 133 with nominal potting gap  $g$ )

~~SECRET/SPECIAL HANDLING~~

~~SECRET/SPECIAL HANDLING~~

2. Also, substantial axisymmetric and nonaxisymmetric temperature variations in the mirror may be tolerated as can be seen by the low values of terms (c) and (e) in paragraph 4.4.7.3. The exception is the larger effect of axial gradients; however, these values have been well established by analysis in Section 8.

4.4.7.5 Mechanical Loadings

As indicated in paragraph 4.4.4, significant mechanical loadings are applied only during non-operational periods. A conservative static equivalent load of 20g in any direction is substituted for all nonoperational equivalent loads.

Pertinent material allowables for HP-20 (Berylco) or S-200 (Brush) hot pressed beryllium are:

1. Precision elastic limit (PEL), defined as that stress where permanent set is  $= 1 \times 10^{-6}$  inch per inch, is approximately 2,500 psi.
2. Conventional yield stress ( $\gamma$ ) at 0.2 percent strain offset is approximately 42,000 psi.

The value of PEL is important when it is desired that initial alignment of the pitch gyro axis and encoder with the scan mirror surface be maintained after exposure to 20g equivalent static loads.

The bezel, bezel back and potting stress analyses are presented in Appendix 4F, along with pertinent material allowables for the other structural materials in the system.

In general, the thermo-elastic design produced a structural system conservatively rated at the present loads.

Minimum factors of safety appear below:

	Factor of Safety	Criteria
Ring bezel	10.4	Yield
Potting shear	50	Tensile allowable
Sandwich back		
Faceplate	1.68	PEL
Core	1.32	Shear allowable (1/2-inch diameter inserts)
Insert bonding	50	Shear allowable

## ~~SECRET/SPECIAL HANDLING~~

### 4.5 OVERALL FEATURES

#### 4.5.1 Launch Locks

Gimbal dynamic forces generated as a result of launch environments suggest the advisability of incorporating a gimbal launch lock device for the recommended scanner design. Because of indeterminate system stiffnesses, this appears advisable even though the scanner employs a balanced gimbal approach. Several locking schemes have been configured. Pyro actuation was selected over solenoid actuation from design considerations of weight, space, and ease of redundancy. An early configuration utilizing a pyro-actuated linkage for disengaging two pins, one from each gimbal, is shown on Fig. 4.5-1 (Drawing no. 906047A). The most current version utilizing a pyro-actuated compression spring driving a single pin for unlocking both gimbals is shown on Fig. 4.5-2 (drawing no. 906947). Several design iterations will be necessary to achieve the final geometry. In addition, further analytical and test efforts will continue for determining the feasibility of safe system functioning without the use of launch locks.

#### 4.5.2 Stow Locks

Conditions arising from on-orbit dynamics, when gimbal torquer power is removed, make it advisable to hold the scanner gimbals by some system of locks while in the stow position. This is to avoid inadvertent or uncontrolled gimbal slewing which might result in scanner or shroud door damage. Since the present scanner design is configured with a balanced gimbal system, the stow lock design presents less of a problem than the previous unbalanced baseline roll axis design approach. In either case, permanent magnet holding means are quite adequate. A small "Index 7" permanent magnet disc of approximately 0.75-inch diameter and 0.15 inch thick and capable of developing a pull of approximately 0.17 pound can represent a significant torque, when suitably positioned from the axis of rotation. The design can be gated about a torque limit from which the driving torque motor can easily free itself. The present design incorporates this permanent magnet stow lock arrangement on both pitch and roll axes, by having the magnetic material plungers of the respective kinetic energy absorbers make contact with the magnets when the pitch and roll gimbals are driven into their stow position. Size and location of present design stow locks are shown on Fig. 4.1-1. A series of tradeoffs will be made for further optimizing this approach.

#### 4.5.3 Energy Absorbers

Energy absorbing stops are provided at the extremes of roll and pitch gimbal travel. These energy absorbers are capable of coping with the total energy that the torquer can deliver in going from one extreme position to the other extreme position plus an overvoltage represented by the application of a constant 28 vdc to the motor terminals. Their energy absorbers being used are of the nonliquid type, utilizing selectively shaped damping materials. They are shown in their installed position on Fig. 4.1-1 and in detail on Figs. 4.5-3 through 4.5-6 (Drawing nos. 114582, 114583, 114579, and 114576).

#### 4.5.4 Alignment Mirrors

Two mirrors for facilitating scanner alignment to the vehicle have been shown (Drawing no. 906041). The mirror mounted on the 2-foot face of the roll housing will provide an orthogonality reference to the roll axis while the mirror mounted to the outboard side of the yoke structure will provide an orthogonality reference to the pitch axis. As presently configured, the mirrors are shown in individual holders before being attached to the structure. In order to facilitate achievement of the  $\pm 0.25$  arc-minute axes definition, the mirrors will be integrally mounted directly to pads machined adjacent and orthogonal to the respective axes bores.

~~SECRET/SPECIAL HANDLING~~

~~SECRET~~/SPECIAL HANDLING

Fig. 4.5-1 is an engineering drawing (906047) which is included in an accompanying supplement package.

~~SECRET~~/SPECIAL HANDLING  
4.5-2

~~SECRET~~/SPECIAL HANDLING

Fig. 4.5-2 is an engineering drawing (906947) which is included in an accompanying supplement package.

~~SECRET~~/SPECIAL HANDLING  
4.5-3

~~SECRET~~/SPECIAL HANDLING

Fig. 4.5-3 is an engineering drawing (114582) which is included in an accompanying supplement package.

~~SECRET~~/SPECIAL HANDLING

~~SECRET/SPECIAL HANDLING~~

Fig. 4.5-4 is an engineering drawing (114583) which is included in an accompanying supplement package.

~~SECRET/SPECIAL HANDLING~~

~~SECRET~~/SPECIAL HANDLING

Fig. 4.5-5 is an engineering drawing (114579) which is included in an accompanying supplement package.

~~SECRET~~/SPECIAL HANDLING  
4.5-6

---

~~SECRET~~/SPECIAL HANDLING

Fig. 4.5-6 is an engineering drawing (114576) which is included in an accompanying supplement package.

~~SECRET~~/SPECIAL HANDLING  
4.5-7

~~SECRET~~/SPECIAL HANDLING

#### 4.6 ALIGNMENT AND ASSEMBLY METHODS SUMMARY

Specification requirement for orthogonality between pitch and roll axes of the scanner assembly is  $\pm 0.5$  arc-minutes. On the basis of preliminary tolerancing studies, it has been concluded that this tolerance is readily achievable with current state-of-the-art fabrication techniques as regards the maintenance of positional tolerances, which in turn make up the error input to scanner axes orthogonality. This being the case, a built-in adjustment to achieve axes orthogonality is not deemed necessary. The above applies also to the specification requirement for holding the tracking mirror reflecting surface parallel to the pitch axis within  $\pm 0.5$  arc-minutes.

An additional specification requirement is that the scanner incorporate means for defining the scanner axes within  $\pm 0.25$  arc-minutes in order to permit optical alignment to the vehicle. This has been provided for in the current design, as described above, by two accurately mounted mirrors. One mirror is mounted on the aft portion of the roll housing and will be orthogonal to the roll axis bores and, hence, the roll axis within the specified limit. The other is mounted on the outboard portion of the yoke structure and will be orthogonal to the pitch axis bores and hence the pitch axis to within a specified limit. It is additionally planned to make these mirrors optically accessible with shroud door open for possible post alignment checks of the scanner without the necessity for complete shroud removal. Modifications or improvements to this proposed alignment mirror arrangement will be made as the Customer alignment plan and techniques approach finalization.

~~SECRET~~/SPECIAL HANDLING

~~SECRET/SPECIAL HANDLING~~

#### 4.7 SCANNER MASS PROPERTIES

The scanner weights and mass properties shown on Tables 4.7-1 through 4.7-6 reflect information pertaining to varying the balanced scanner configurations.

Table 4.7-1 represents weight and mass properties data for that portion of the scanner assembly which pitches, that is, rotates about the  $y_0 - y_0$  axis. Tables and Figs. 4.7-1 and 4.7-2 show the reference axes definition and relationship. It should be noted that a weight of 1.8 pounds is required to balance this portion about the pitching centerline. Also an additional pound of trim weights is required in order to meet the specification defining a minimum mass moment of inertia of 0.08 slug-ft<sup>2</sup> for this axis. This area of weight and component redistribution for optimizing the weight, balance, and inertia consistent with system clearances, will be given continuing attention as the current scanner design assumes its final configuration.

Tables 4.7-2 and 4.7-3 represent weight and mass properties data for that portion of the scanner assembly which rolls, that is, rotates about the  $x_0 - x_0$  axis. The data presented on Tables 4.7-1 and 4.7-2 is obtained when the pitching portion of the scanner is pitched at the lowest angle demanded by the LOS operating range, namely a gimbal angle of 22° 15'.

Table 4.7-2 presents data for the condition when balance in the roll plane was achieved by reducing the displacement between pitch and roll axes from 0.9 in to 0.35 inch. Additionally, the roll gyro and roll gyro electronics package and a 1-pound balance weight were also redistributed. Table 4.7-3 or Case II, which is our present configuration scanner, presents data for the condition where balance in the roll plane was achieved by reducing the displacement between pitch and roll axes from 0.90 into 0.25 inch. Here also there was a redistribution of the roll gyro and roll gyro electronics package and a one pound balance weight.

It should again be noted that the roll axis mass moment of inertia is a function of the pitch gimbal angle. Lowering the pitch gimbal angle obviously lowers the value computed for roll inertia. The data presented herein represents the worst case condition, that is the condition of

~~SECRET/SPECIAL HANDLING~~

~~SECRET/SPECIAL HANDLING~~

least inertia where the pitch gimbal is positioned at the low extreme of  $22^{\circ} 15'$ . It should also be noted that in attempting to realize a minimum weight scanner design within specified geometry and clearance conditions, the minimum inertia value called out in the specification becomes difficult to achieve. Presently the roll axis inertia is  $0.188 \text{ slug-ft}^2$ , versus the specification requirement of  $0.23 \text{ slug-ft}^2$ . This will obviously be an area for continued investigation and study in order to strive for specification compliance. Tables 4.7-4 and 4.7-5 represent the scanner weight summaries for the configuration defined in Tables 4.7-1, 4.7-2, and 4.7-3. It should also be noted that these weight summaries include a 10.16 pound weight for the pitch and roll gyro and pitch and roll gyro electronics, so that total scanner weight within our control would be 62.48 less 10.16 or 52.32 pounds.

Table 4.7-6 presents mass properties summaries of the various scanner concepts studied. Condition 1 data presents the unbalanced, baseline configuration with the tracking mirror at a 20 degree gimbal angle. It is important to note that 2 pounds of trim weight attached to the outer ends of the mirror were used in order to meet the specified minimum pitch inertia ( $I_{Ox} = 0.081 \text{ slug-ft}^2$ ). It should also be noted that the specified minimum inertia of  $0.23 \text{ slug-ft}^2$  was not met in the roll plane ( $I_{Oy} = 0.21 \text{ slug-ft}^2$ ).

Conditions 2 and 3 of Table 4.7-6 summarize the two balanced concepts previously mentioned. It was necessary in both conditions to add 1.8 pounds of weight to the bezel in order to obtain balance about the pitch plane. It was also necessary to add four 1/4-pound trim weights in order to obtain the required minimum pitch inertia ( $I_{Ox} = 0.0812 \text{ slug-ft}^2$ ). Because of clearance problems it was necessary to add these weights to the back of the bezel and not at the outer extremities of the mirror as was the case in condition 1. The minimum roll inertia of  $0.23 \text{ slug-ft}^2$  again was not met (condition 2,  $I_{Ox}$  being equal to  $0.191 \text{ slug-ft}^2$  and condition 3,  $I_{Ox}$  being equal to  $0.188 \text{ slug-ft}^2$ ). It was necessary to add 1 pound of weight at the yoke in order to obtain balance.

Conditions 4 and 5 were derived from conditions 2 and 3 by the use of the mass moment of inertia transfer formula ( $I = WD^2 + I_O$ ). The distances (d) used being the difference between the balanced and unbalanced axis (condition 4 being  $0.90 \text{ inch} - 0.55 \text{ inch} = 0.35 \text{ inch}$  and conditions 5 being  $0.90 \text{ inch} - 0.65 \text{ inch} = 0.25 \text{ inch}$ ). In each of these two conditions the 1 pound of weight used for balance can be removed resulting in a lighter scanner assembly weight. It should also be noted that there is no appreciable change in the roll mass moments of inertia between the balanced and unbalanced gimbals of conditions 2 through 5 of Table 4.7-6.

~~SECRET/SPECIAL HANDLING~~

~~SECRET/SPECIAL HANDLING~~

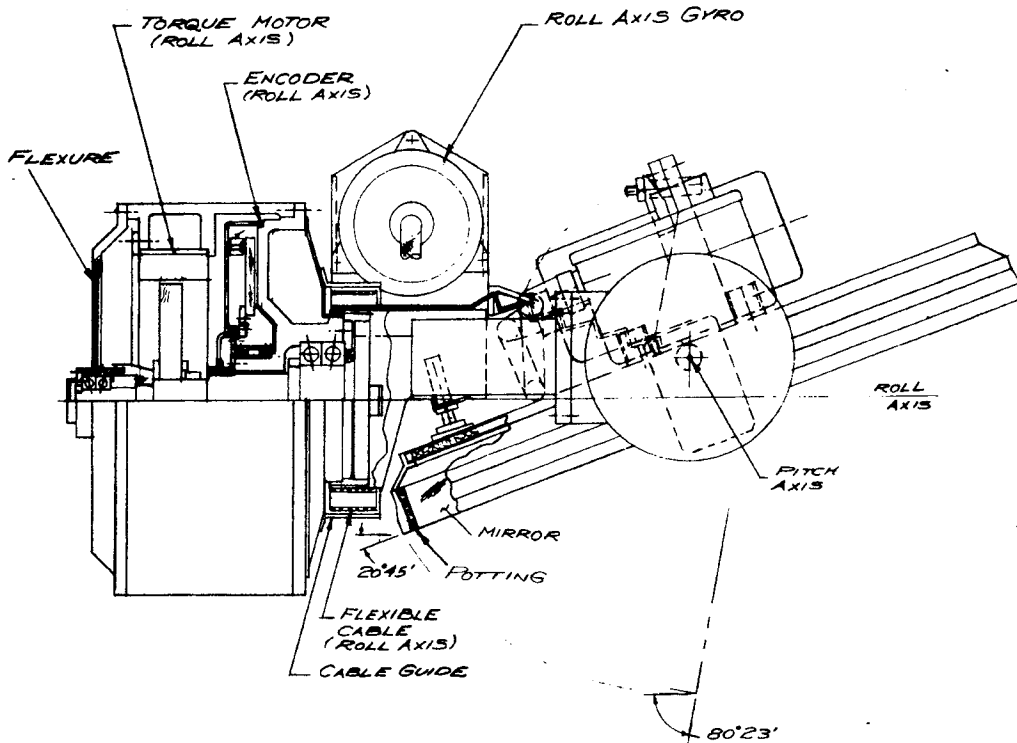


Fig. 4.7-1 — Scanner side view (for a reference only)

~~SECRET/SPECIAL HANDLING~~

~~SECRET/SPECIAL HANDLING~~

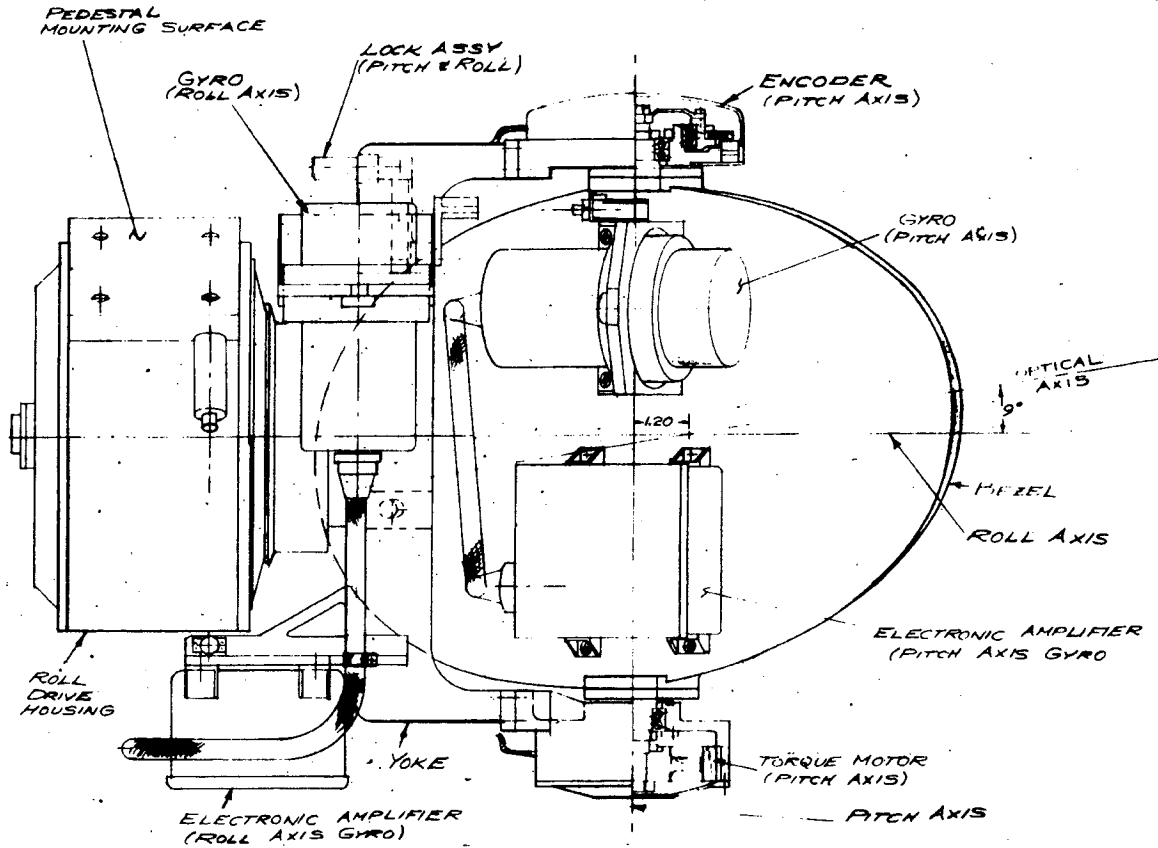


Fig. 4.7-2 — Scanner plan view (for reference only)

~~SECRET/SPECIAL HANDLING~~

~~SECRET~~/SPECIAL HANDLING

Table 4.7-1 — Pitch Axis Assembly—Rotating Items

ENGINEER *A. M. ...*  
DATE *6-15-68*

IT&T CORPORATION  
LEXINGTON 73, MASSACHUSETTS

Itak

PITCH ASSEMBLY - 22° 15'

PAGE

SECT.	COLUMN	CONDITION														MODEL
		1	2	3	4	5	6	7	8	9	10	11	12	13	14	
	DESCRIPTION	W	X	Y	Z	WX	WY	WZ	WX <sup>2</sup>	WY <sup>2</sup>	WZ <sup>2</sup>	WXZ	Δ I <sub>xx</sub>	Δ I <sub>yy</sub>	Δ I <sub>zz</sub>	
	<i>Pitch Axis Assembly - Rotating Items - Pitch Angle = 22° 15'</i>															
	MIRROR	11.4	4.57	10.00	7.47	50.91	111.40	83.21	232.62	111.40	621.59		103.50	143.50	204.25	
	GRATING	.85	4.57	10.00	7.47	3.88	8.50	6.35	17.73	85.00	47.43		9.63	4.69	31.23	
	GRATE - PITCH STOP	.03	4.81	10.00	7.47	1.11	3.0	0.22	0.67	3.00	1.64		0.00	0.00	0.00	
	BEAR - MOTOR END	1.65	4.81	10.00	7.47	7.94	16.50	13.12	38.19	145.00	104.30		24.97	29.31	48.72	
	SHAFT - MOTOR END	.14	5.00	3.50	8.35	0.80	5.6	1.34	4.00	1.96	11.19		0.11	0.15	0.11	
	LOCK NUT - B&G	.02				0.55	.34	0.22	0.75	1.03	7.69		0.02	0.04	0.02	
	LOCK NUT - B&G	.02				0.10	.03	0.17	0.50	0.06	1.42		0.01	0.02	0.01	
	BEARINGS - MOTOR END	.05				0.25	.07	0.22	1.25	0.10	3.51		0.06	0.14	0.06	
	BEARINGS - MOTOR END	.31				1.70	1.07	2.84	8.50	4.02	23.71		0.33	0.46	0.33	
	EXTER - TORQUE MOTOR	.15				0.65	0.13	1.07	3.25	34.88	9.70		0.20	0.10	0.10	
	SHAFT - EXCODER	.13				0.65	0.31	1.07	3.25	37.44	9.70		0.11	0.21	0.11	
	DISK EXCODER	.25				1.25	0.28	2.09	6.25	73.10	17.45		0.00	0.00	0.00	
	MOUNT - EXCODER DISK	.03				0.15	.51	0.35	0.75	8.77	2.04		0.06	0.14	0.06	
	BEARINGS - EXCODER END	.30				1.50	5.34	3.51	7.50	95.14	20.94		3.14	5.72	5.03	
	GYRO	2.65	3.85	12.75	10.20	8.84	15.96	22.55	37.92	123.73	23.91		4.03	5.41	4.51	
	ELECTRONIC PKG	.37	8.18	10.50	9.34	3.89	3.41	2.63	12.73	40.77	3.60		1.52	0.03	1.52	
	INTERCONNECTING CABLE	1.80	3.81	12.75	10.20	3.51	12.75	10.55	12.32	162.56	113.42		3.57	2.02	2.61	
	MOUNT - GYRO	.50	1.00	10.00	10.00	0.50	0.50	0.50	0.50	180.00	74.68					
	WEIGHT - MAIN ASSE (2.88 x 3)	.50	1.00	10.00	10.00	0.50	0.50	0.50	0.50	50.00	54.74					
	WEIGHT - MAIN ASSE (1.88 x 3)	.50	1.00	10.00	10.00	0.50	0.50	0.50	0.50	50.00	54.74					
	WEIGHT - MAIN ASSE (1.88 x 3)	.50	1.00	10.00	10.00	0.50	0.50	0.50	0.50	50.00	54.74					
	SUMMARY - Σ	24.91				125.74	249.62	206.05	756.04	2665.66	1795.20		154.00	182.51	304.87	

**SUMMARY**

WEIGHT 249.1 lb.

$I_{xx}$  154.00

$I_{yy}$  182.51

$I_{zz}$  304.87

$I_{xy}$  154.00

$I_{yz}$  182.51

$I_{zx}$  304.87

SLUG FT<sup>2</sup>

$I_{xx}$  372.32

$I_{yy}$  372.32

$I_{zz}$  372.32

$I_{xy}$  372.32

$I_{yz}$  372.32

$I_{zx}$  372.32

~~SECRET~~/SPECIAL HANDLING

SECRET/SPECIAL HANDLING

Table 4.7-2 -- Roll Axis Assembly -- Rotating Items

Ittek  
ITTEK CORPORATION  
LEXINGTON 73, MASSACHUSETTS  
ENGINEER: \_\_\_\_\_ PAGE: \_\_\_\_\_  
DATE: \_\_\_\_\_

CASE I  
PITN AXIS ASSEMBLY  
PITN AXIS ASSEMBLY  
MICROSE ASSEMBLY @ 22.15"

SECT.	DESCRIPTION	CONDITION														MODEL
		1	2	3	4	5	6	7	8	9	10	11	12	13	14	
		W	X	Y	Z	WX	WY	WZ	WXZ	WYZ	WZ <sup>2</sup>	WXZ	Δ I <sub>xx</sub>	Δ I <sub>yy</sub>	Δ I <sub>zz</sub>	
	ROLL AXIS ASSEMBLY - ROTATING ITEMS															
	MICROSE ASSEMBLY @ 22.15"															
	SUMMARY - PITN ASSEMBLY	24.31	5078	1002	8.35	125.75	239.60	208.00	634.77	2,520.91	1794.80	374.38	374.67	590.33		
	Yoke	2.12	11.11	10.98	8.99	23.55	22.32	18.00	31.65	232.87	152.82	10.71	2.89	46.85		
	DRIVE SHAFT - PITN AXIS FLY FLYWHEEL	1.83	5.72	3.00	8.35	10.97	5.97	15.28	57.87	74.47	127.57	3.77	4.63	9.77		
	ENCODER ASSEMBLY - PITN AXIS	3.73	5.98	16.97	16.97	19.71	94.72	28.71	81.68	735.44	189.63	7.44	12.62	7.99		
	LAUNCH LOCK - PITN AXIS	50	12.00	16.40	4.54	6.25	5.00	2.32	78.13	50.00	10.74	.83	.21	6.3		
	SMART - BALL AXIS	94	14.36	8.00	13.50	9.40	9.40	7.52	193.87	94.00	60.16	.95	4.15	4.15		
	BEARINGS, SHA - BALL AXIS	1.10	10.28	8.00	14.61	11.00	8.80	193.87	170.73	110.00	70.40	.68	.36	.36		
	BEARINGS, RET - BALL AXIS	1.52	10.12	8.00	14.61	9.42	5.20	4.46	170.73	52.00	33.28	.20	.13	.13		
	ENCODER ASSEMBLY WITH MOUNT - BALL AXIS	1.44	15.10	8.00	14.61	14.40	14.40	28.12	373.94	164.00	104.94	18.71	2.55	2.55		
	FLUTE - TORQUE ARM - BALL AXIS	2.50	16.02	10.00	8.00	17.55	25.00	20.00	870.53	2520.00	1680.00	12.33	6.39	6.39		
	SHAFT ASSEMBLY - TOP	.12	8.70	11.00	10.33	1.07	1.32	1.24	9.57	14.52	12.87	.18	.18	.18		
	SHOCK ASSEMBLY - BOTTOM	.08	10.81	9.00	7.85	1.90	1.08	0.95	14.92	8.00	7.85	.18	.18	.18		
	RETURNER, RES - FWD	.13	15.78	10.00	8.00	1.70	0.80	0.64	15.13	8.00	8.32	.05	.03	.03		
	RETURNER, ENCODER DISK	.06	12.20	10.00	8.00	1.03	1.30	1.04	32.37	8.00	8.32	.08	.07	.07		
	RETURNER, ENC - RET	.03	10.91	10.00	8.00	1.03	.60	0.48	17.75	6.00	3.84	.07	.02	.02		
	MISC.	.34	13.91	24.00	8.00	4.73	.30	0.24	10.20	3.00	1.72	.03	.01	.01		
	GYRO - BALL AXIS	2.65	10.61	14.90	7.35	39.47	19.48	19.48	357.34	588.33	193.03	1.05	1.96	1.26		
	ELECTRONIC RES - BALL GYRO	2.06	13.91	4.91	5.14	28.65	9.08	10.63	328.82	440.06	54.85	5.42	2.77	5.72		
	BACKLASH WEIGHT	1.00	13.91	4.71	5.14	13.91	4.77	5.14	193.47	33.75	34.63	---	---	---		
	SUMMARY - Σ	49.37	367.23	493.68	362.51	3853.17	493.30	362.51	3853.17	493.30	2732.62	472.17	423.30	674.78		

**SUMMARY**

WEIGHT 465.37 lb.

X 14.000

Y 7.970

Z 2.970

I<sub>xx</sub> 694.17 IN IN<sup>2</sup>/409

I<sub>yy</sub> 632.03 IN IN<sup>2</sup>/409

I<sub>zz</sub> 1222.27 IN IN<sup>2</sup>/409

E 0.197 DEG

Σ (6<sup>2</sup> + 1) = 8.657

Σ (6<sup>2</sup> + 1) = 19.000

Σ (7<sup>2</sup> + 1) = 7.170

Σ (ROLL MOMENT OF INERTIA) (IN IN<sup>2</sup>)

Σ (PITCH MOMENT OF INERTIA) (IN IN<sup>2</sup>)

Σ (YAW MOMENT OF INERTIA) (IN IN<sup>2</sup>)

Σ (PRODUCT OF INERTIA) (IN IN<sup>2</sup>)

Σ (INCLINATION OF THE PRINCIPAL AXES)

Σ (PITCH MOMENT OF INERTIA) (IN IN<sup>2</sup>)

Σ (YAW MOMENT OF INERTIA) (IN IN<sup>2</sup>)

Σ (PRODUCT OF INERTIA) (IN IN<sup>2</sup>)

Σ (INCLINATION OF THE PRINCIPAL AXES)

Σ (PITCH MOMENT OF INERTIA) (IN IN<sup>2</sup>)

Σ (YAW MOMENT OF INERTIA) (IN IN<sup>2</sup>)

Σ (PRODUCT OF INERTIA) (IN IN<sup>2</sup>)

Σ (INCLINATION OF THE PRINCIPAL AXES)

SECRET/SPECIAL HANDLING

~~SECRET/SPECIAL HANDLING~~

Table 4.7-3 — Roll Axis Assembly—Rotating Items

ITK CORPORATION  
LEXINGTON 73, MASSACHUSETTS

Case II  
Roll Axis Assembly  
MILCOE ASSEMBLY G. 22.0.55

DATE: 1/15/63  
ENGINEER: G. H. G.

SECT.	COLUMN	CONDITION													
		1	2	3	4	5	6	7	8	9	10	11	12	13	14
	DESCRIPTION	W	X	Y	Z	WX	WY	WZ	WXZ	WY <sup>2</sup>	WZ <sup>2</sup>	WXZ	Δ I <sub>yo</sub>	Δ I <sub>zo</sub>	Δ I <sub>xy</sub>
	SUMMARY - PITCH ASSEMBLY	24.91	5.04	10.25	12.57	249.60	205.57	639.79		2500.97	1695.94		376.39	77.17	5.33
	Yoke	2.12	11.11	10.18	8.19	23.35	22.22	18.00	261.64	232.97	152.82		40.71	2.29	0.95
	DRIVE AX. PITCH AX. FLY BUSH	1.83	5.72	3.00	8.35	10.47	5.71	15.28	57.97	16.77	127.57		3.47	4.63	3.97
	ENCODER ASSEMBLY - PITCH AX. EN. BUSH	2.72	5.48	14.41	8.35	14.97	44.72	22.71	87.68	735.14	159.43		7.44	22.62	7.44
	SLIPRING GEAR - PITCH ASSEMBLY	.50	12.50	10.00	4.00	6.25	5.00	2.32	78.03	529.00	10.76		.83	.21	.63
	SLIPRING - BALL AXES	.94	14.36	8.00	13.50	9.16	7.52	123.84		94.00	60.76		.95	4.15	4.15
	BEARING, END - BALL AXES	1.10	13.18	8.00	14.61	11.00	8.80	123.14		110.00	70.40		.69	.36	.36
	BEARING, END - BALL AXES	.82	18.12	8.00	9.42	5.30	4.16	123.73		52.00	33.30		.20	.71	.71
	ENCODER GEAR - BALL AXES	1.14	15.70	8.00	24.72	14.70	13.72	373.47		257.00	144.16		15.71	9.55	9.55
	ENCODER GEAR - BALL AXES	2.50	14.84	10.00	9.00	41.55	25.00	28.00	679.56	250.00	160.00		12.33	6.37	6.37
	SLIPRING ASSEMBLY - PITCH	.12	8.50	10.00	10.33	1.07	1.32	1.54	9.57	14.52	12.97		.17	.78	.07
	SLIPRING ASSEMBLY - BOTTOM	.08	13.75	10.00	8.00	1.10	1.08	.95	14.02	9.72	7.55		.18	.03	.03
	RETURNER ASSEMBLY - PITCH	.13	15.78	10.00	8.00	1.10	1.04	1.57	15.13	8.00	5.72		.05	.03	.03
	RETURNER ASSEMBLY - PITCH	.06	17.20	10.00	8.00	1.03	1.30	1.04	32.37	13.20	5.32		.05	.03	.03
	MISC.	.03	18.44	10.00	8.00	0.55	.30	2.77	10.20	3.00	1.74		.03	.01	.01
	GYRO - BALL AXES	2.65	11.61	14.00	7.35	30.77	39.49	19.48	357.24	515.33	123.15		10.05	1.94	1.94
	GEOSTATIONARY - BALL AXES	2.06	13.31	14.00	6.00	28.15	9.06	12.57	388.52	37.64	76.13		57.92	2.37	5.32
	GEOSTATIONARY - BALL AXES	1.00	13.31	14.00	5.88	13.31	4.77	5.88	193.47	22.44	54.22		3.94	5.74	4.62
	SUMMARY - Σ	45.37			369.23	493.65	362.65	3853.47		4493.30	2920.70		472.17	92.10	679.73

Σ (5) + (1) = 6.1547  
 Σ (6) + (1) = 7.1593  
 Σ (7) + (1) = 7.1593

ROLL MOMENT OF INERTIA (lb IN<sup>2</sup>)  
 I<sub>yo</sub> = 472.17 + 2920.70 + 42.32 = 495.37 (6.07 x 7.99)<sup>2</sup>  
 I<sub>zo</sub> = 92.10 + 2920.70 + 42.32 = 495.37 (6.07 x 7.99)<sup>2</sup>  
 I<sub>xy</sub> = 679.73

(INCLINATION OF THE PRINCIPAL AXES)  
 E = 8 TAN<sup>-1</sup> (I<sub>xy</sub> / (I<sub>yo</sub> - I<sub>zo</sub>))  
 E = 8 TAN<sup>-1</sup> (679.73 / (495.37 - 92.10))

(VAN MOMENT OF INERTIA) (lb IN<sup>4</sup>)  
 I<sub>yo</sub> = 362.65 + 3853.47 + 2920.70 = 7537.82 (8.15 x 9.0)<sup>2</sup>  
 I<sub>zo</sub> = 362.65 + 3853.47 + 2920.70 = 7537.82 (8.15 x 9.0)<sup>2</sup>  
 I<sub>xy</sub> = 3853.47

~~SECRET/SPECIAL HANDLING~~

~~SECRET~~ SPECIAL HANDLING

Table 4.7-4 -- Scanner and Pedestal Assembly

SECT.	COLUMN	CONDITION														MODEL
		1	2	3	4	5	6	7	8	9	10	11	12	13	14	
	DESCRIPTION	W	X	Y	Z	WX	WY	WZ	WX <sup>2</sup>	WY <sup>2</sup>	WZ <sup>2</sup>	WXZ	Δ I <sub>xx</sub>	Δ I <sub>yy</sub>	Δ I <sub>zz</sub>	
	SCANNER & PEDESTAL ASSY															
	SUMMARY - Roll Axis Assembly	461.37	81.84	10.00	7110	3619.13	453.62	262.61	3853.17	4913.30	2222.62		884.67	1294.03	1872.71	
	Housing - Pedestal	3.37	16.13	10.00	8.13	38.55	23.90	11.43	621.82	232.00	157.77		49.83	38.42	39.22	
	Camera - Axis Assembly - Horn - Horn	0.81	18.80	10.00	18.13	15.23	8.10	6.57	338.29	171.00	53.54		8.88	4.34	4.25	
	BASE - Pedestal	1.81	15.74	15.74	10.81	28.85	28.85	19.57	459.57	459.57	21.57		38.68	14.57	14.57	
	EVAPORATOR - Roll - TROUBLE	4.36	14.20	10.00	8.00	61.81	93.60	34.88	879.15	436.00	279.04		58.87	20.57	20.57	
	STATOR - Roll - TROUBLE	3.50	16.43	10.00	8.00	58.17	35.00	26.00	716.79	350.00	224.00		45.88	23.69	23.69	
	SHOCK ABSORBER - Roll - OK	0.12	13.81	12.19	12.05	1.66	1.96	1.93	22.89	12.83	19.51		0.18	0.18	0.18	
	SHOCK ABSORBER - Roll - OK	0.12	13.81	12.19	12.05	1.66	1.96	1.93	22.89	12.83	19.51		0.18	0.18	0.18	
	Camera - Axis Assembly - Horn - Horn	0.50	13.75	10.00	3.09	4.88	5.50	1.55	94.53	60.50	4.77		0.21	0.63	0.83	
	HARNESSES - Connectors	3.50	17.50	10.00	9.35	50.75	35.00	34.13	735.88	350.00	332.72		44.04	44.04	87.50	
	SUMMARY - Σ	62.98				633.57	616.62	508.57	7943.31	6944.62	4216.99		1100.42	1433.34	2064.22	

ENGINEER: A. J. ...  
DATE: 6-19-68

PITCH ANGLE = 22° 15'  
PITCH AXIS AT 8.35" (distance 2.10")

WEIGHT DISTRIBUTION AND MOMENT OF INERTIA

ITEM CORPORATION  
LEXINGTON 73, MASSACHUSETTS

Σ (G) + (I) = 16.14  
Σ (G) + (I) = 16.17  
Σ (I) = 6.14

ROLL MOMENT OF INERTIA (lb in<sup>2</sup>)  
Σ WX<sup>2</sup> + Σ WY<sup>2</sup> + Σ WZ<sup>2</sup> + Σ W(X<sup>2</sup> + Y<sup>2</sup>)  
= 4216.99

PITCH MOMENT OF INERTIA (lb in<sup>2</sup>)  
Σ WXZ + Σ WYZ + Σ WYZ + Σ W(X<sup>2</sup> + Y<sup>2</sup>)  
= 4216.99

(INCLINATION OF THE PRINCIPAL AXES)  
K TAN<sup>-1</sup> (Σ WYZ / (Σ WXZ - W(X<sup>2</sup> + Y<sup>2</sup>)))  
= 10.17°

(YAW MOMENT OF INERTIA) (lb in<sup>2</sup>)  
Σ WY<sup>2</sup> + Σ WZ<sup>2</sup> + Σ W(X<sup>2</sup> + Y<sup>2</sup>)  
= 1100.42

(PRODUCT OF INERTIA) (lb in<sup>2</sup>)  
Σ WXY + Σ WYZ + Σ WZX  
= 1433.34

WEIGHT SUMMARY

W = 62.98 lbs  
Y = 10.17 lbs  
Z = 8.10 lbs

SLUG FT<sup>2</sup>  
W = 30.34  
Y = 5.034  
Z = 4.020

DEC.

SECRET/SPECIAL HANDLING

4.7-11

~~SECRET~~/SPECIAL HANDLING

Table 4.7-5 — Scanner and Pedestal Assembly

SECT.	COLUMN	CONDITION														MODEL
		1	2	3	4	5	6	7	8	9	10	11	12	13	14	
	DESCRIPTION	W	X	Y	Z	WX	WY	WZ	WX <sup>2</sup>	WY <sup>2</sup>	WZ <sup>2</sup>	WXZ	Δ I <sub>xx</sub>	Δ I <sub>yy</sub>	Δ I <sub>zz</sub>	
	<b>SCANNER &amp; PEDESTAL ASSEMBLY</b>															
	SUMMARY - Roll Axis Assembly	45.37	8.59	10.00	7.93	368.93	463.68	362.15	3253.71	4923.30	2720.70		470.57	236.53	144.77	
	HOUSING - PEDESTAL	2.39	14.13	10.00	8.13	38.55	23.70	14.43	624.82	237.00	157.77		49.83	25.92	37.92	
	COVERS - 441 & 400 - GREENWALD	0.81	14.10	10.00	8.13	15.23	8.10	4.57	216.27	81.00	53.57		8.48	4.37	4.37	
	BASE - PEDESTAL	1.81	15.94	10.00	10.81	28.95	28.55	19.57	959.87	257.83	211.51		28.48	14.57	14.57	
	ENCODER - ENG - END PLATE	4.34	14.10	10.00	8.10	61.97	43.60	34.88	174.15	436.00	274.04		38.37	20.57	20.57	
	STATOR, SERVO - TORQUE	3.50	14.10	10.00	8.10	58.19	35.00	28.00	164.21	350.00	224.00		45.88	23.60	23.60	
	SHOCK ASSEMBLY BALL - BASE	0.16	13.81	14.10	12.15	1.66	1.46	1.53	33.31	19.83	19.31		0.18	0.08	0.08	
	SHOCK ASSEMBLY BALL - OUTER	0.16	13.81	14.10	12.15	1.66	1.46	1.53	33.31	19.83	19.31		0.18	0.08	0.08	
	LAUNCHER - BALL - BASE	0.50	13.81	14.10	12.15	6.81	6.50	7.55	140.50	40.50	47.77		0.51	0.23	0.23	
	HARNESSES & CABLES	3.50	14.00	10.00	9.95	59.75	35.00	34.13	735.88	357.00	332.72		44.04	24.57	24.50	
	<b>SUMMARY - Z</b>	63.48				633.51	656.02	508.71	7942.37	6946.00	4205.07		1026.32	1408.24	211.00	

ITK CORPORATION  
LEWINGTON 73, MASSACHUSETTS

PITCH ANGLE = 22° 15'  
CASE II PITCH AXIS = 8.25" (DIMENSIONAL)

FOR CASE 16  
SIGNED BY  
DATE 4-17-62

ENGINEER R. ROACH  
DATE 4-17-62



**SUMMARY**  
WEIGHT = 62.02 lb.  
I<sub>xx</sub> = 7942.37  
I<sub>yy</sub> = 1408.24  
I<sub>zz</sub> = 211.00

(YAW MOMENT OF INERTIA) (lb IN<sup>2</sup>)  
I<sub>xx</sub> = Σ(WY<sup>2</sup> + ZW<sup>2</sup>) + Σ(I<sub>xx</sub>)<sub>0</sub> - W(R<sub>z</sub> + R<sub>y</sub>)<sup>2</sup>  
I<sub>yy</sub> = Σ(WX<sup>2</sup> + ZW<sup>2</sup>) + Σ(I<sub>yy</sub>)<sub>0</sub> - W(R<sub>x</sub> + R<sub>z</sub>)<sup>2</sup>  
I<sub>zz</sub> = Σ(WX<sup>2</sup> + WY<sup>2</sup>) + Σ(I<sub>zz</sub>)<sub>0</sub> - W(R<sub>x</sub> + R<sub>y</sub>)<sup>2</sup>

(ROLL MOMENT OF INERTIA) (lb IN<sup>2</sup>)  
I<sub>xx</sub> = Σ(WY<sup>2</sup> + ZW<sup>2</sup>) + Σ(I<sub>xx</sub>)<sub>0</sub> - W(R<sub>z</sub> + R<sub>y</sub>)<sup>2</sup>  
I<sub>yy</sub> = Σ(WX<sup>2</sup> + ZW<sup>2</sup>) + Σ(I<sub>yy</sub>)<sub>0</sub> - W(R<sub>x</sub> + R<sub>z</sub>)<sup>2</sup>  
I<sub>zz</sub> = Σ(WX<sup>2</sup> + WY<sup>2</sup>) + Σ(I<sub>zz</sub>)<sub>0</sub> - W(R<sub>x</sub> + R<sub>y</sub>)<sup>2</sup>

(PITCH MOMENT OF INERTIA) (lb IN<sup>2</sup>)  
I<sub>xx</sub> = Σ(WY<sup>2</sup> + ZW<sup>2</sup>) + Σ(I<sub>xx</sub>)<sub>0</sub> - W(R<sub>z</sub> + R<sub>y</sub>)<sup>2</sup>  
I<sub>yy</sub> = Σ(WX<sup>2</sup> + ZW<sup>2</sup>) + Σ(I<sub>yy</sub>)<sub>0</sub> - W(R<sub>x</sub> + R<sub>z</sub>)<sup>2</sup>  
I<sub>zz</sub> = Σ(WX<sup>2</sup> + WY<sup>2</sup>) + Σ(I<sub>zz</sub>)<sub>0</sub> - W(R<sub>x</sub> + R<sub>y</sub>)<sup>2</sup>

(INCLINATION OF THE PRINCIPAL AXES)  
E = 1/2 TAN<sup>-1</sup> (I<sub>yy</sub> - I<sub>xx</sub>) / I<sub>xy</sub>

(ROLL ANGLE) (DEG)  
E = 1/2 TAN<sup>-1</sup> (I<sub>yy</sub> - I<sub>xx</sub>) / I<sub>xy</sub>

(PITCH ANGLE) (DEG)  
E = 1/2 TAN<sup>-1</sup> (I<sub>zz</sub> - I<sub>xx</sub>) / I<sub>xy</sub>

~~SECRET~~/SPECIAL HANDLING

SECRET/SPECIAL HANDLING

Table 4.7-6 — Mass Properties Summary

COND	CONCEPT	PITCH PORTION				ROLL PORTION				TOTAL SCANNER ASSEMBLY					
		INERTIA ~ SCUG-FT <sup>2</sup>		INERTIA ~ SCUG-FT <sup>2</sup>		INERTIA ~ SCUG-FT <sup>2</sup>		INERTIA ~ SCUG-FT <sup>2</sup>		WTL COS	WTL COS	I <sub>Y0</sub>	I <sub>Z0</sub>	I <sub>Y0</sub>	I <sub>Z0</sub>
		I <sub>X0</sub>	I <sub>Y0</sub>												
1	UNBALANCED CONFIGURATION 20° GIMBAL ANGLE	26.13	0.081	—	—	47.23	0.210	—	—	—	—	—	—	—	
2	BALANCED CONFIGURATION ~ 0.35 IN DISPLACEMENT BETWEEN PITCH AND ROLL AXIS	24.91	0.0812	0.0801	0.1273	45.37	0.191	0.279	0.1407	62.48	0.349	0.1654	0.870	0.870	
3	BALANCED CONFIGURATION ~ 0.25 IN DISPLACEMENT BETWEEN PITCH AND ROLL AXIS	24.91	0.0812	0.0801	0.1273	45.37	0.188	0.276	0.1407	62.48	0.343	0.1649	0.870	0.870	
4	UNBALANCED CONFIGURATION ~ 0.35 IN DISPLACEMENT BETWEEN PITCH AND ROLL AXIS	24.91	0.0812	0.0801	0.1273	44.37	0.192	0.281	0.1407	61.48	—	—	—	—	
5	UNBALANCED CONFIGURATION ~ 0.25 IN DISPLACEMENT BETWEEN PITCH AND ROLL AXIS	24.91	0.0811	0.0801	0.1273	44.37	0.188	0.277	0.1407	61.48	—	—	—	—	

\* NOTE - DATA DERIVED FOR A GIMBAL ANGLE OF 22.15°

\*\* NOTE - 1/16 COS MUST BE SUBTRACTED FOR PITCH AND ROLL GYRO FOR PITCH AND ROLL GYRO ELECTRONICS

SECRET/SPECIAL HANDLING

~~SECRET/SPECIAL HANDLING~~

## 5. SCANNER EFFECTS ON SERVOLOOP

### 5.1 INTRODUCTION

The scanner represents a critical element in a complex closed loop servo. Scanner requirements influencing overall loop performance include torque variation from both bearing and cables, frictional torque levels, scanner transmissibility, encoder velocity error, and torquer characteristics.

A great deal of effort has been spent since last PDR in generating experimental and analytical data to support the design effort in the above areas. The results of these studies indicate the need to revise the existing specification, and discussions with the contractor have been held accordingly.

A preliminary allocation of PSD for each axis has been made based on experimental data tempered with engineering judgment. Both cables and bearings and their degrading environments have been considered. Based on recent decisions, further experimental and analytical studies of the bearings used in this scanner design will be performed by the contractor under direction of the subcontractor. These results, together with experimental cable work being performed at Itek, will form the basis for any future revision to the PSD allocation.

~~SECRET/SPECIAL HANDLING~~

~~SECRET/SPECIAL HANDLING~~

## 5.2 PSD DEFINITION

### 5.2.1 Physical Interpretation

The Power Spectral Density (PSD) of a stochastic (i.e., random) process describes the general frequency composition of the process in terms of the density of power with respect to angular frequency. It is important to note that it is the area under the PSD curve and not the ordinate value that represents power. Since this is the case, the amount of power in any frequency band can be found by calculating the area under the PSD curve over that band. Furthermore, the power at any specific frequency is zero. As a consequence of this last fact, the PSD of a periodic function must show an infinite power density at a frequency equal to one over the period. Clearly then, if information as to actual magnitude is sought, PSD is applicable to functions that are purely random (i.e., contain no periodic components).

### 5.2.2 Mathematical Definition

The Power Spectral Density of a random process is defined as the Fourier transform of the statistical autocorrelation function. If the process in question is ergodic in autocorrelation and stationary in the wide sense then the time autocorrelation is equal to the statistical autocorrelation with probability one. Therefore, under these assumptions, the PSD can be expressed as in Equation (5.2.1):

$$S(\omega) = \int_{-\infty}^{\infty} R(t) E^{-j\omega t} dt = 2 \int_0^{\infty} R(t) \cos \omega t dt \quad (5.2.1)$$

where  $S(\omega)$  = power density at  $\omega$

$R(t)$  = time autocorrelation at time shift interval  $t$

The last equality is true since  $R(t)$  is an even function.

#### NOTE

This is a mathematical definition of PSD in a frequency space containing both positive and negative frequencies.

The one-sided spectrum having physical significance is defined as:

$$S_1(\omega) = 4 \int_0^{\infty} R(t) \cos \omega t dt, \omega \geq 0 \quad (5.2.2)$$

### PSD Computation Data Reduction Capability

Itek, at present, has two computer routines for the computation of PSD. The primary routine called Autocor computes the PSD of a data sample either bearing data or cable data by autocorrelation followed by cosine transformation. In effect, Autocor is the digital computer solution of Equation (5.2.1) above. The backup routine, called FRAP, which is used as a check of the Autocor results, is an in-house generated program which computes PSD by first computing the Fourier transform of the data and then squaring the transform and normalizing by  $T$ , the length of the data

~~SECRET/SPECIAL HANDLING~~

~~SECRET~~/SPECIAL HANDLING

sample. In effect, FRAP is the digital computer solution of Equation (5.2.3) below, which is an alternative mathematical statement of PSD.

$$S(\omega) = \lim_{T \rightarrow \infty} \frac{1}{T} |X(\omega)|^2 \quad (5.2.3)$$

where  $X(\omega)$  = the Fourier transform of  $X(t)$

Solution Philosophy—Autocor

The Autocor program computes digitally the PSD of a random process utilizing the basic definition that PSD equals the Fourier transform of the time autocorrelation. The time autocorrelation is defined as:

$$R(\tau) = \lim_{T \rightarrow \infty} \frac{1}{T} \int_{-\infty}^{\infty} X(t) X(t-\tau) dt \quad (5.2.4)$$

Since a time autocorrelation of infinite extent is not realizable from a finite data sample, it is necessary to alter the basic definition to account for correlations outside the time interval of the data sample. That is the autocorrelation is estimated by the formula Equation (5.2.5):

$$R(\tau) = \frac{1}{N-\tau} \sum_{i=0}^{N-\tau} X_i \cdot X_{i+\tau} \quad (5.2.5)$$

where  $N$  = number of data points

$\tau$  = lag number = 0,  $\Delta t$ ,  $2\Delta t$ , . . .  $m\Delta t$

$\Delta t$  = lag interval = number of points/sampling rate

$M+1$  = max number of lags

$X_i$  =  $i$ th member of the data record after the mean value has been removed

Having started the analysis with  $N$  equally spaced data points, we now have computed  $M+1$  equally spaced estimates of the autocorrelation. The next step is to compute a discrete finite cosine transform of the autocorrelation according to Equation (5.2.6):

$$V(f) = \Delta t \left[ R(0) + 2 \sum_{i=1}^{m-1} R(i) \cos \frac{if\pi}{m} + R(m) \cos \pi f \right] \quad (5.2.6)$$

where  $V(f)$  = raw spectral estimate

$f$  = 0,  $\Delta f$ ,  $2\Delta f$ , . . .  $m\Delta f$

$\Delta f$  =  $1/2 m\Delta t$

We now have arrived at  $M+1$  "raw" estimates of the PSD. The estimates are raw in the sense that they are arrived at by a finite transform of a truncated autocorrelation without any thought as

~~SECRET/SPECIAL HANDLING~~

to the effect of such truncation. It has been shown\* that an easy way to view this truncation is to consider the autocorrelation to have been multiplied by an even function of time which possesses the following properties:

$$\begin{aligned}D(0) &= 1 \\D(t) &= D(-t) \\D(t) &= 0 \quad t > m\Delta t, \text{ the max lag used}\end{aligned}$$

That is, our estimate of the autocorrelation is the result of a multiplication in time by a shaped window. Since multiplication in time corresponds to a convolution in frequency and if  $Q(f)$  is the Fourier transform of  $D(t)$  then the resultant PSD can be seen as Equation (5.2.7):

$$S(f) = Q(f) \otimes V(f) \quad (5.2.7)$$

where  $\otimes$  implies convolution

A convenient and often used even function is the hamming window. When our raw estimate of the PSD is convolved with the hamming window, the result is  $M+1$  smoothed estimates of PSD.

$$S(f) = 0.54 \quad V(f) + 0.23 \quad V(F-\Delta f) + V(f+\Delta f) \quad (5.2.8)$$

#### NOTE

The PSD so computed is one half of a two-sided spectrum, if PSD is to be referred to a one-sided spectrum, then we get:

$$S_1(f) = 2 S(f)$$

#### Computer Program—Autocor

Autocor is a computer program that determines the two-sided PSD of a sampled time function. It is available on disc at the Itek Scientific Computation Center. The data to be analyzed is presented as a series of ordinate values for equal increments of the abscissa. The program will handle up to 5,000 data points. The PSD estimate is presented both as a printed tabulation and a plot on log-log format. The plot routine includes the drawing of the PSD specification line on the plot.

A simplified Autocor flow chart is shown in Fig. 5.2-1. The card deck set up for Autocor consists of two sets of decks. The starter deck consists of the necessary control cards to open the file on disc. The starter deck is followed by one or more job decks containing the following cards:

1. Plot Label Card which allows the user the opportunity to print comments on the plot (e.g., Test Variables).

---

\*Blackman, R. B., and Tukey, J. W., The Measurement of Power Spectra, Dover Publications Inc., New York, 1958, p. 12.

~~SECRET/SPECIAL HANDLING~~

~~SECRET~~/SPECIAL HANDLING

2. Program Alteration Card which allows the user to alter certain constants within the program (e.g., Scale Factor conversion from volts to foot-pounds).
3. Data Deck which contains the data to be analyzed. The data deck may contain any number of points, but as previously mentioned, the program will only process the first 5,000 points.
4. End Card which simply specifies the end of a Job Deck.

As indicated in the program flow chart (Fig. 5.2-1), after the data is read in and stored, the ordinate value is scaled according to Equation (5.2.9):

$$X_i \text{ (ft-lbs)} = X_i \text{ (mv)} \cdot K \left( \frac{\text{oz-in.}}{\text{mv}} \right) \times \frac{1}{192} \left( \frac{\text{ft-lbs}}{\text{oz-in.}} \right) \quad (5.2.9)$$

The mean of the data is then computed and removed. Following removal of the mean value, the correlation is computed. For good stability of the estimate,  $m+1$  is set equal to one tenth the number of data points. The raw estimates,  $V(f)$  are the computed for  $\Delta f = 1/2m\Delta t$  where  $\Delta t$  represents the time between adjacent data points. The maximum frequency estimated corresponds to the Nyquist frequency  $1/2\Delta t$ .

The raw estimates are then smoothed by hamming and the resulting PSD estimate is stored and the program is initiated again for the next data sample. When the last data sample has been processed, the PSD for each data sample is outputted onto the line printer and the X-Y plotter.

Solution Philosophy—FRAP

The FRAP program computes digitally the PSD of a random process utilizing the alternative definition of PSD given in Equation (5.2.3). The Fourier transform in that equation involves an infinite length of record. Since our data samples are necessarily of finite length, a modification of that equation is necessary. After modification, the estimate of PSD satisfies the expression:

$$S(\omega) = \frac{1}{T} |X_T(\omega)|^2 \quad (5.2.10)$$

$$\text{where } X_T(\omega) = \int_{-T/2}^{T/2} X(t) E^{-j\omega t} dt$$

Simpson's rule integration is used to evaluate the transform of Equation (5.2.10). It is known that the estimator given by Equation (5.2.10) is not as "good" in a statistical sense as the estimator in Autocor, nevertheless, the results of the two programs correlate rather well (see Figs. 5.2-2 and 5.2-3) in this present application. It must again be noted that the PSD given by Equation (5.2.10) is a two-sided PSD. The physical one-sided spectrum is again given by:

$$S_1(\omega) = 2 S(\omega) = \frac{2}{T} |X_T(\omega)|^2$$

Computer Program—FRAP

FRAP, a general Fourier Analysis Program, developed at Itek to solve optical problems, can be used to compute PSD. The FRAP Program is available on disc at the Itek Scientific Computation Center. The program in its present form will handle up to 3,000 data points.

~~SECRET~~/SPECIAL HANDLING

~~SECRET/SPECIAL HANDLING~~

The computer outputs both the computed PSD and the PSD specification onto an X-Y plotter as a log-log plot of PSD versus frequency.

A simplified FRAP flow chart is shown in Fig. 5.2-4. After the data is read into the computer, the mean value of the data is removed. The data is then transformed into frequency. The FRAP program computes  $N/2$  discrete values of the Fourier Transform at frequency increments of  $1/T$ , up to a maximum frequency of  $N/2T$  which as in Autocor is the Nyquist frequency. ( $N$  equals the total number of data points and  $T$  equals the length in time of the data sample.) The transformed data has units of millivolt/hertz (mv/hz). In order that the PSD resulting from the square of the transform divided by  $T$  is in units of PSD (ft-lb)<sup>2</sup>/rad/sec, it is necessary to multiply the transformed data by appropriate conversion factors. The scaling operation Equation (5.2.11), also includes division by the square root of  $T$  which is equivalent to the required division of the squared transform by  $T$ .

$$F_i \frac{\text{ft-lbs}}{(\text{rad/sec})^{1/2}} = F_i (\text{mv/hz}) \times K \frac{\text{ft-lbs}}{\text{mv}} \times \frac{1}{2\pi} \frac{\text{hz}}{\text{rad/sec}} \times \frac{1}{T^{1/2}} (\text{sec}^{-1/2}) \quad (5.2.11)$$

After this scaling operation, the transformed data is squared and the resulting PSD is plotted on the X-Y plotter.

The FRAP program is also used in another area of data reduction. The harmonic analysis of encoder error is performed by FRAP. The raw data from the encoder is presented as 1024 ordinate values proportional to the cumulative bit width errors of 1024 adjacent bits of the encoder where cumulative bit width error is defined in Equation (5.2.12).

$$\text{Cumulative bit width error at the } n^{\text{th}} \text{ bit} = nW - \sum_{i=1}^n w_i \quad (5.2.12)$$

where  $W$  = bit width for a perfect encoder  
 $w$  = actual width of the  $i^{\text{th}}$  bit

A simplified flow chart for FRAP harmonic analysis is shown in Fig. 5.2-5. After the data is read in, it is transformed into frequency. Since the values of a Fourier transform at equal increment of a fundamental frequency are equal to the amplitudes of the harmonics in a Fourier series, the data resulting from the transform of the input represents the amplitudes of the Fourier series of the input data. The Fourier transform is evaluated at  $N/2$  equal increments of  $1/1024$  cycles per bit. These amplitudes are multiplied by a scale factor so that they are in units of arc seconds. The computer then outputs the data on the X-Y plotter as a plot of amplitude in seconds versus frequency in cycles per bit. This plot is used to determine the RSS (root-sum-squared) error of the encoder (see Section 5.5).

Plans are under way to include determining RSS values weighted by the specified filter and also to slide the frequency scale under the curve so as to find the maximum RSS value for the range of possible encoder fundamental frequencies.

#### Cable and Bearing Data Reduction to PSD

The raw data from the cable and bearing test fixtures is in the form of an analog voltage  $V = f(t)$ . This voltage is in each case proportional to torque. The analog voltage is first filtered

~~SECRET/SPECIAL HANDLING~~

~~SECRET~~/SPECIAL HANDLING

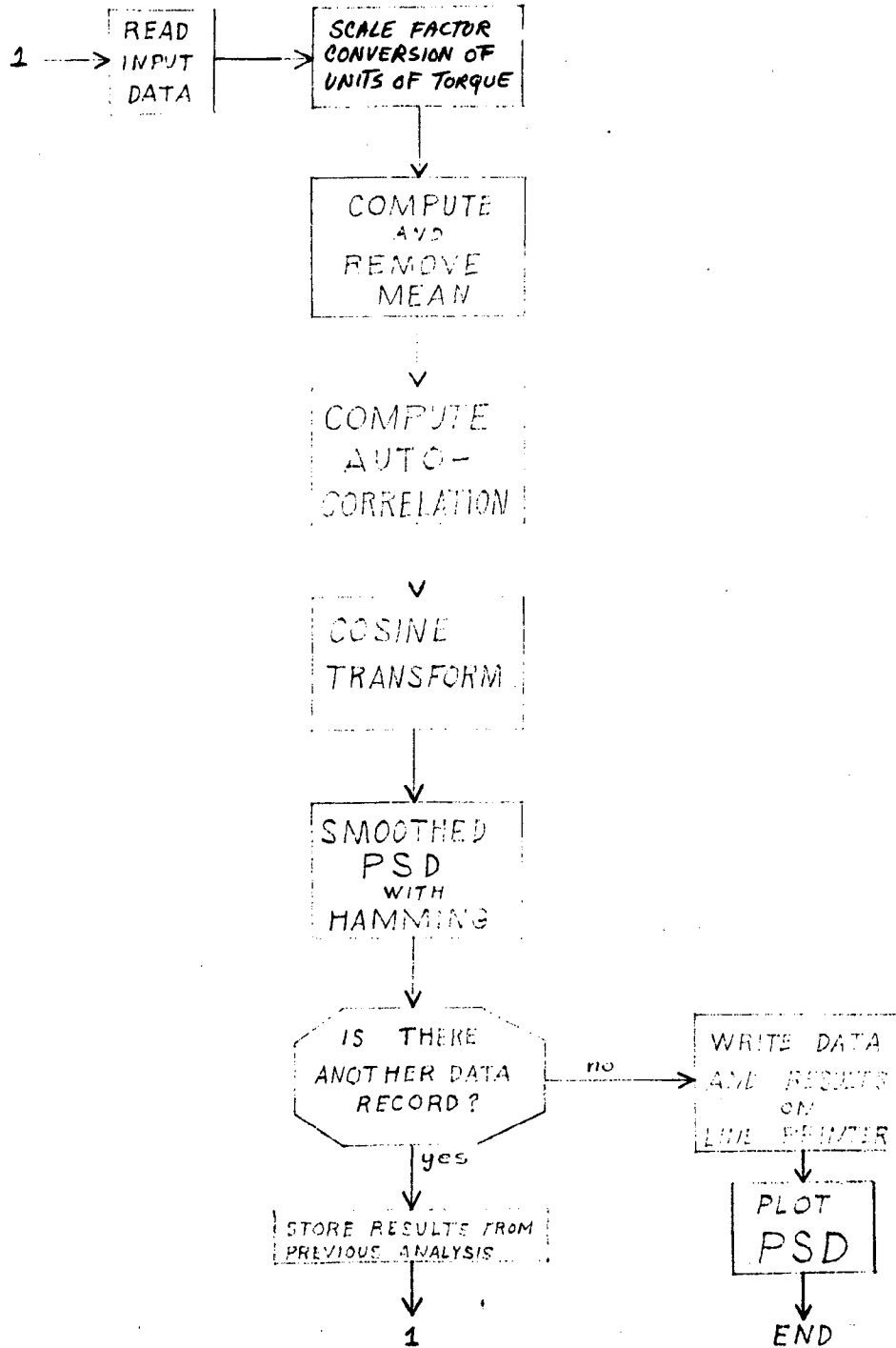


Fig. 5.2-1 — Autocor flow chart

~~SECRET~~/SPECIAL HANDLING

~~SECRET/SPECIAL HANDLING~~

PSD BY AUTOCOR  
2MM9104 BEARING WITH F50 OIL  
1.70/S CCW, 7-12LB PRELOAD 1  
R. J. JONES 5-26-68

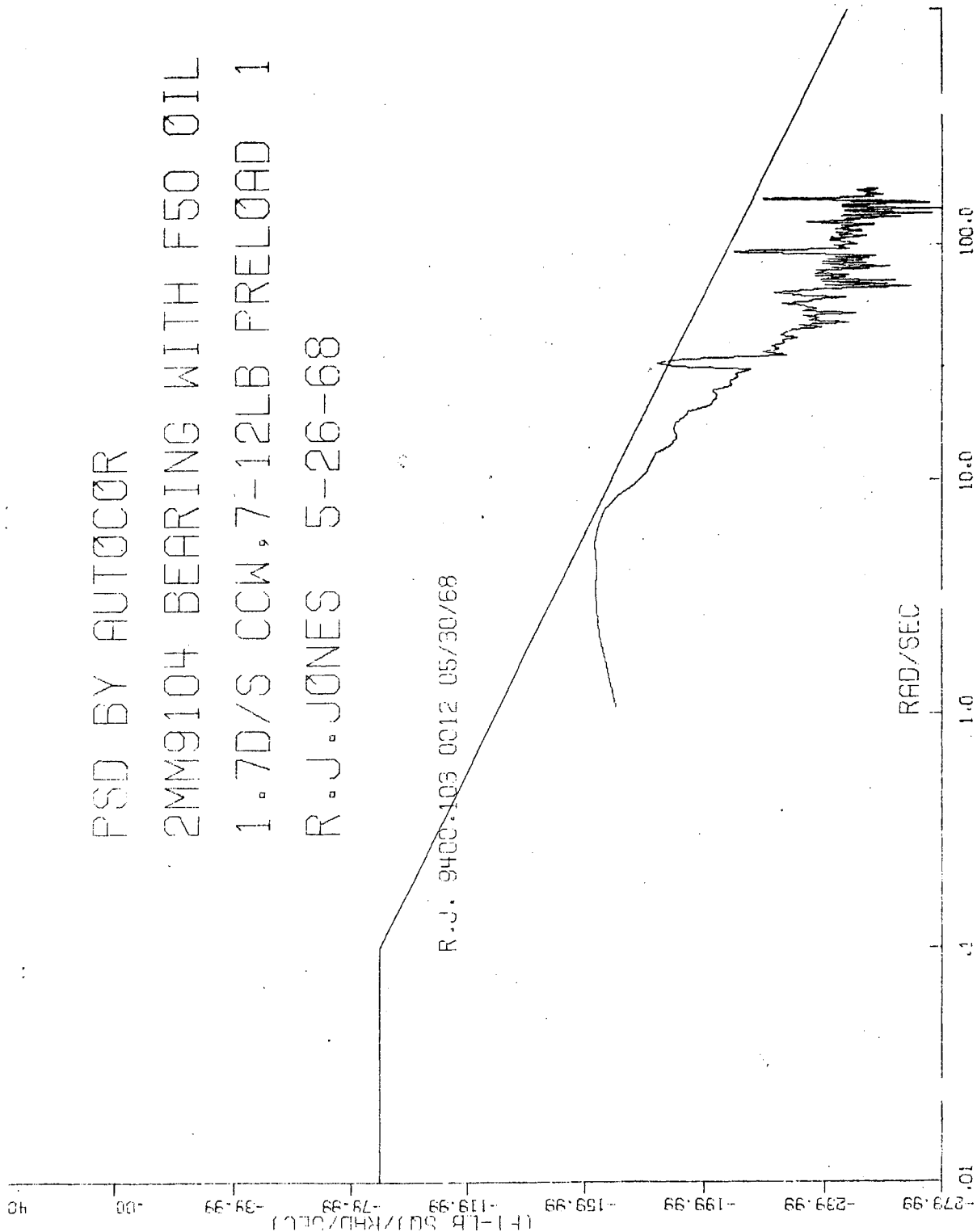


Fig. 5.2-2 — PSD by Autocor program

~~SECRET/SPECIAL HANDLING~~

~~SECRET~~/SPECIAL HANDLING

1.7 DEG/SEC CCW RUN 1  
2MM 9104 WITH F50 OIL AND 7-12 LB PRELOAD  
R.J. JONES 5-19-68

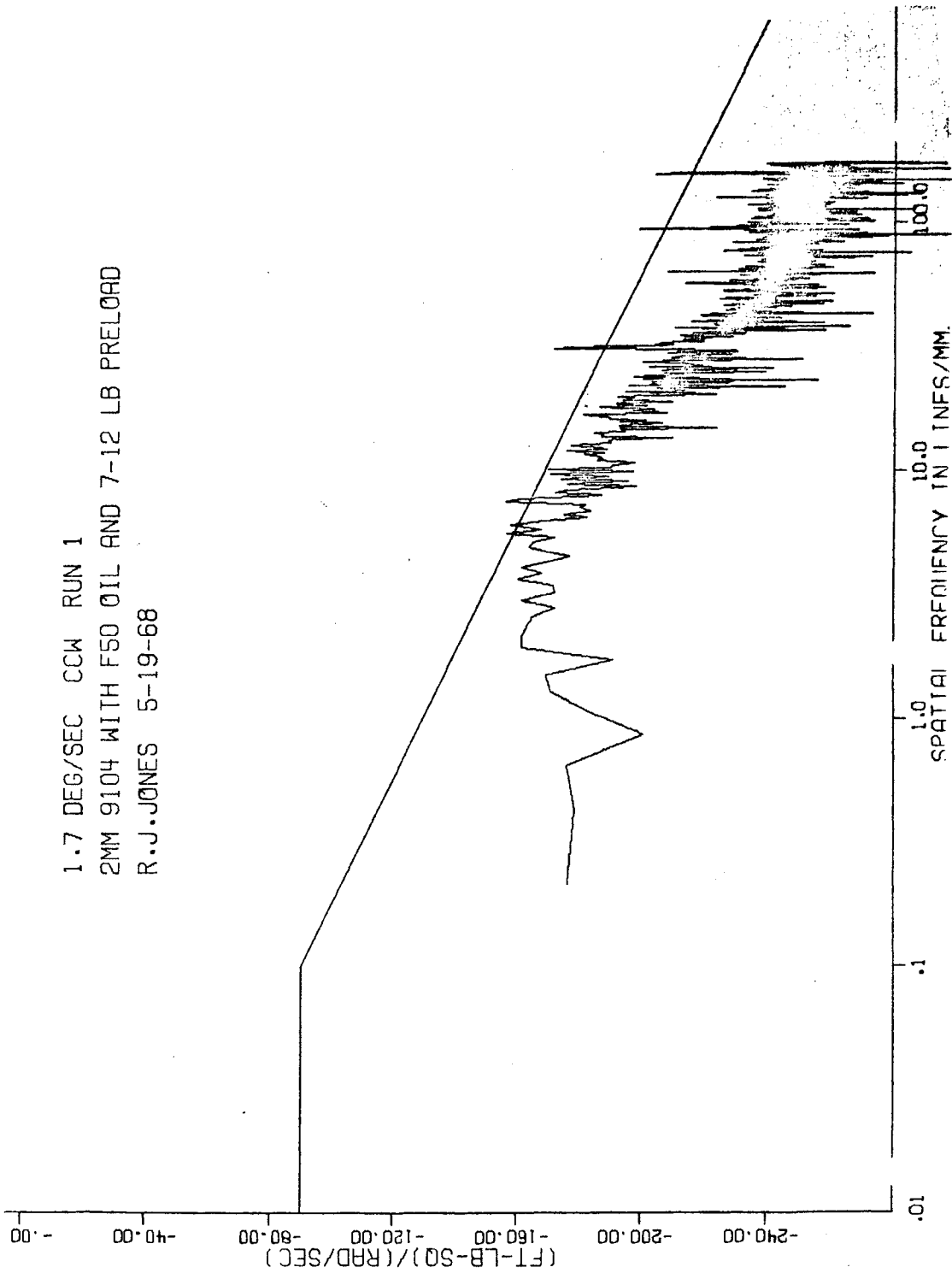


Fig. 5.2-3 — PSD by FRAP program

~~SECRET~~/SPECIAL HANDLING

~~SECRET~~/SPECIAL HANDLING

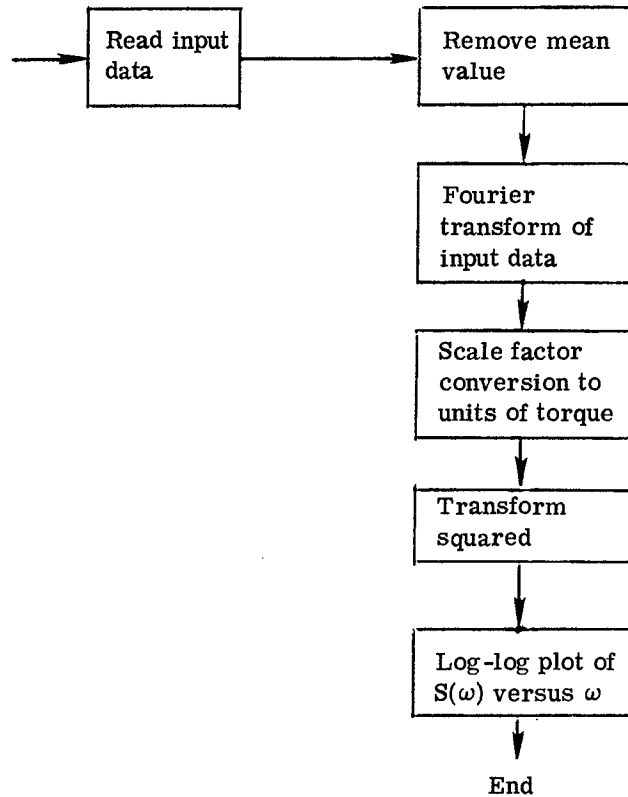


Fig. 5.2-4 — FRAP PSD flow chart

~~SECRET~~/SPECIAL HANDLING

~~SECRET~~/SPECIAL HANDLING

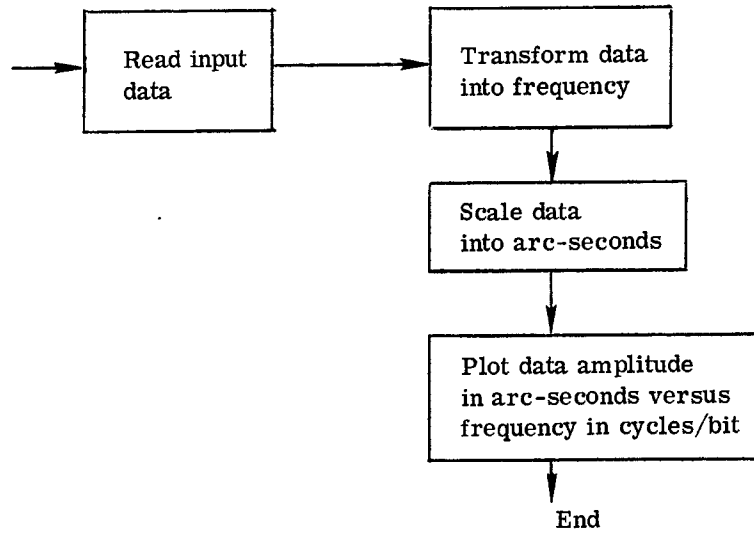


Fig. 5.2-5 — FRAP harmonic analysis flow chart

~~SECRET~~/SPECIAL HANDLING

~~SECRET~~/SPECIAL HANDLING

to avoid aliasing in the resulting PSD estimate and then applied to the input of an A-D converter and digitized. The data is then sampled and punched onto paper tape. The paper tape is seven level tape which uses two lines (14 characters) to store one sample value. One character is used for parity, one for sign, two to indicate the beginning of a word and the remaining 10 are used to record the number in octal. Therefore, the tape can record a maximum octal number of 1777. The paper tape is read by a console tape reader into a CDC 924 computer. A short routine in Mint, the language designed for use with the CDC 924, calls for the computer to read a predetermined number of points from the tape, to compute the mean value and then to output that mean value and the data points on the line printer, and to punch the data onto cards on the on-line card punch (see Fig. 5.2-6).

This data deck along with the appropriate control deck (FRAP or Autocor) is then read into the CDC 3300 computer. The data is processed according to the particular program used and upon termination of the program, the computer outputs PSD as a log-log plot on the X-Y plotter (see Fig. 5.2-7).

#### Accuracy of Computed PSD

An analysis of the errors in PSD computation for any random process is not possible. However, if the process is assumed to be Gaussian then approximate expressions of errors can be found. It can be shown that under this Gaussian assumption, the 90 percent range of an individual estimate in db can be found by

$$(90 \text{ percent range in db}) = 2 \left( \frac{200}{T \cdot \frac{1}{m\Delta t} - 5/6} \right)^{1/2}$$

For the Autocor program,

$$T = 30, \quad M = 160, \quad \Delta t = 1/55$$

So that the 90 percent range in db is 9.5 db.

#### 5.2.3 PSD Interpretation

As mentioned previously, the PSD specification is drawn on the plots of computed PSD. Since the PSD specification as presented to Itek corresponds to a physically realizable one-sided spectrum, and since the computed spectrum is a two-sided spectrum, it is necessary to modify one or the other such that a graphical comparison is possible. We have lowered the PSD specification line as given to us by 6 db so that it corresponds to a two-sided spectrum (see Fig. 5.2-8).

The PSD specification gives the maximum allowable PSD per axis. The combined PSD of three bearings on each axis plus cable must not exceed the specification. Our effort to date has been to determine the PSD of each contributor acting independently. This effort has enabled us to investigate the operation of our test fixtures and to determine the PSD levels involved. This effort has also given us a convenient starting point from which we can go to the more difficult problem of determining just how the PSD of the contributing components will add. It is known that if the torque due to one contributor adds linearly to the torque due to the other, then the resultant PSD will be the sum of the individual spectra and the cross spectrum. In equation form,

~~SECRET~~/SPECIAL HANDLING

~~SECRET~~/SPECIAL HANDLING

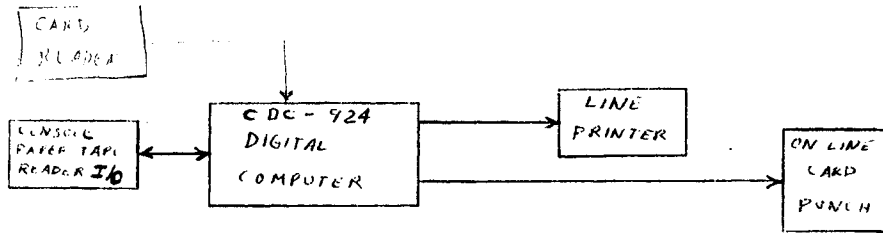


Fig. 5.2-6 — Data conversion from paper tape to cards

~~SECRET~~/SPECIAL HANDLING

~~SECRET/SPECIAL HANDLING~~

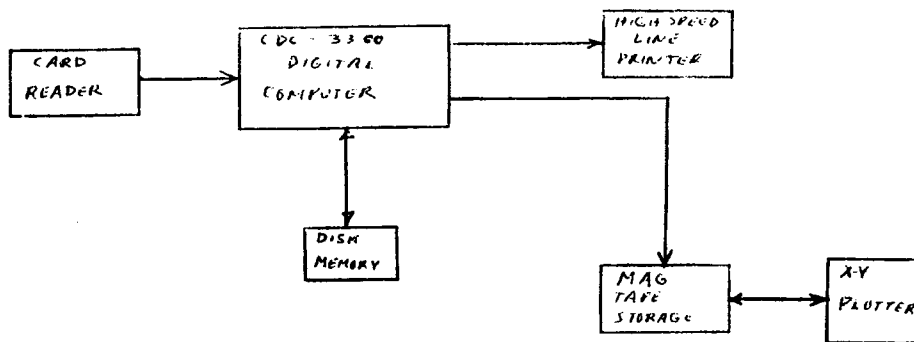


Fig. 5.2-7 — PSD computation system block diagram

~~SECRET/SPECIAL HANDLING~~

~~SECRET~~/SPECIAL HANDLING

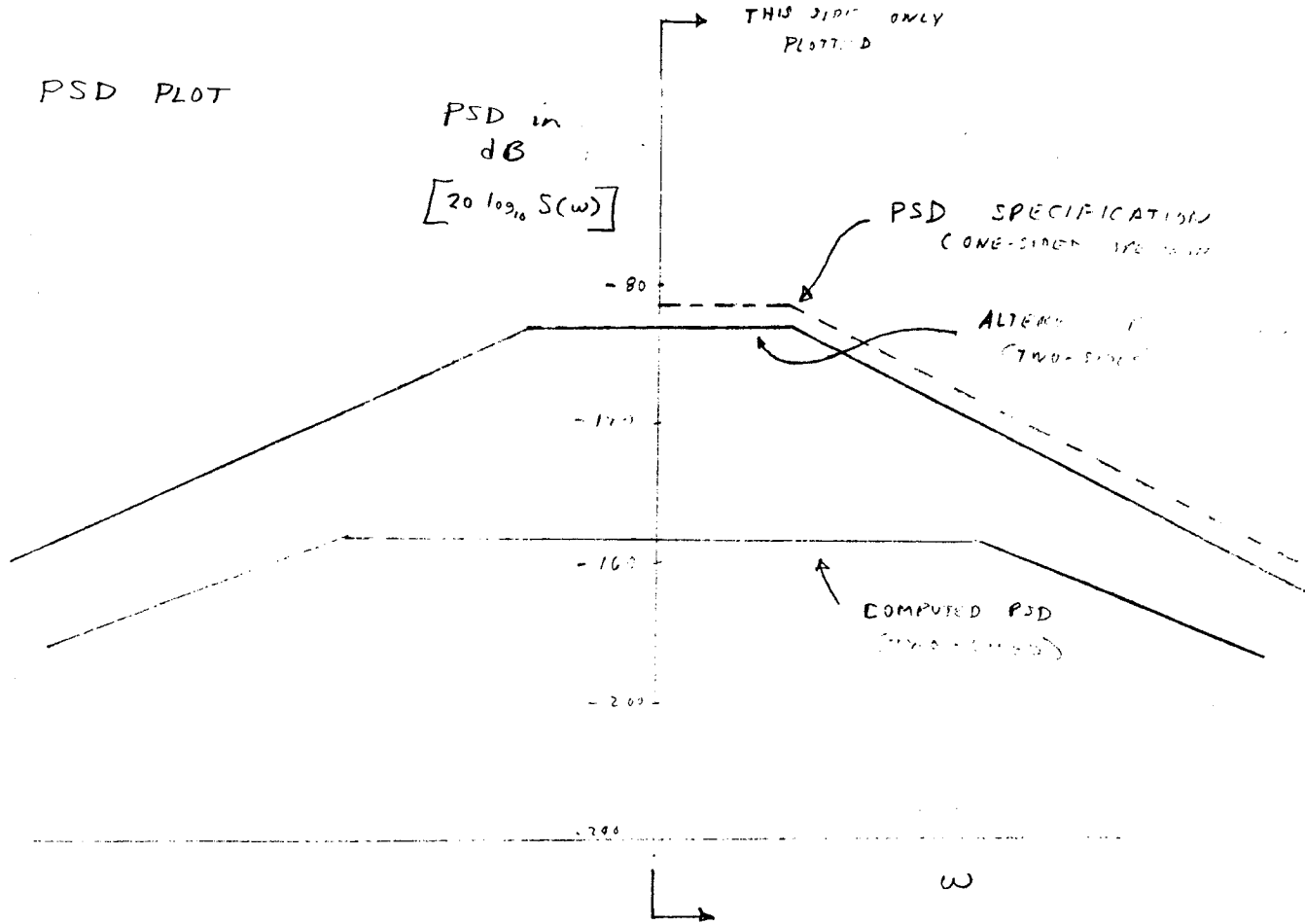


Fig. 5.2-8 — PSD plot

~~SECRET~~/SPECIAL HANDLING

~~SECRET/SPECIAL HANDLING~~

if  $X(t)$  and  $Y(t)$  are two stationary processes then if:

$$Z(t) = X(t) + Y(t)$$

(5.2.13)

$$S_Z(\omega) = S_X(\omega) + S_Y(\omega) + 2 \operatorname{Re} [S_{XY}(\omega)]$$

provided of course the cross correlations are stationary. We feel, however, that the PSD of the combined contributors cannot be found by this method since it is not known if the torque due to the individual contributors will add linearly. Therefore, it is our determination that to accurately compute total PSD, the torque of the contributing components acting together must be measured experimentally. This experimental effort is in progress.

~~SECRET/SPECIAL HANDLING~~

~~SECRET/SPECIAL HANDLING~~

### 5.3 PSD ALLOCATION

The present scanner gimbal torque specification (Paragraph 3.1.1.1.6) states that the power spectral density of random torque variation about the mean value of running friction shall be completely enclosed by the given PSD curve.

In order that individual contributors to the PSD such as bearings and cables might be tested, the total scanner specification must be divided up and allotted to the individual contributors. The first question that must be answered in order to make an allocation is how does the PSD add. It is known that if the torque due to one contributor adds linearly to the torque due to another, the resultant PSD will be the sum of the individual spectra plus a cross-spectra. In equation form, if  $X(t)$  and  $Y(t)$  are two stationary processes and if

$$Z(t) = X(t) + Y(t)$$

then

$$S_Z(\omega) = S_X(\omega) + S_Y(\omega) + 2 \operatorname{Re} [S_{XY}(\omega)] \quad \text{where } S(\omega) = \text{PSD}$$

provided of course, the cross correlations of  $X(t)$  and  $Y(t)$  are stationary. The interpretation of this expression says that if  $X(t) = Y(t)$  then the cross correlation is the same as the autocorrelation and the PSD curve for  $X(t) + Y(t)$  will be 12 db above the PSD curve for  $X(t)$ . However, the probability of the cross correlation equaling the autocorrelation is very small. If the cross correlation is zero the PSD of  $X(t)$  and  $Y(t)$  would be directly additive and if the PSD's were equal the resultant PSD would be higher by 6 db than either individual PSD. From these assumptions it appears that PSD's would add so as to increase PSD somewhere between 6 and 12 db for two PSD's. In order that a reasonable PSD allocation can be made, it will be assumed that the PSD's of the contributors will add as twice the algebraic sum. The factor of two is an allowance for the presence of cross spectra. It is felt that a PSD allocation based on such an assumption is quite conservative.

#### 5.3.1 Cable PSD Contributors

Fig. 5.3-1 shows the PSD allocation for the cables on the roll axis. This allocation consists of 2 cables summed together, twist and roll along, and a factor for variation due to temperature. The allocations shown are design goals that have not yet been met. Figs. 6.2-21 and 6.2-23 show the PSD we are currently measuring for these cable configurations.

Fig. 5.3-2 shows the PSD allocation for the cable on the pitch axis. This allocation covers one cable and a factor for variation due to temperature. No test has been conducted on the pitch twist cable to date, and thus no data is available. It is felt that designing cables to meet the roll axis specification will allow us to meet the pitch axis requirement due to the smaller wire bundle.

#### 5.3.2 Bearing Contribution to PSD

The total contributors to PSD on each axis are the cables and bearings. The cable allocation in our preliminary PSD allocation is discussed in Section 5.3-1.

The bearings employed on the roll axis are one pair 2 mm 9108 main load carrying bearings, one pair 2 mm 9105 aft bearings on the roll shaft, and one pair SBB 29-36 for the encoder mount. We have measured typical torque ripple characteristics of these bearings, and have formulated a

~~SECRET/SPECIAL HANDLING~~

~~SECRET/SPECIAL HANDLING~~

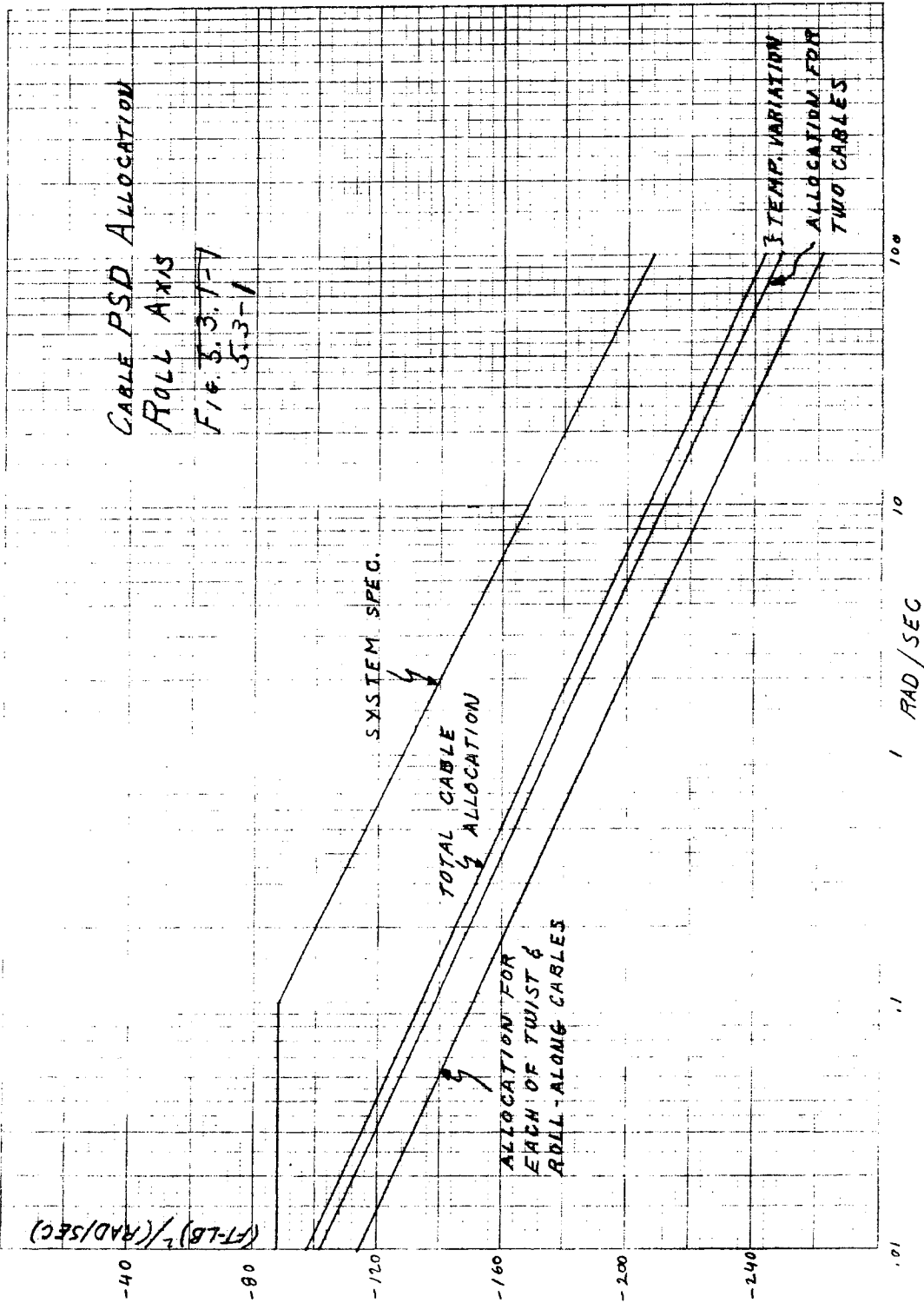


Fig. 5.3-1 — Cable PSD allocation, roll axis

~~SECRET/SPECIAL HANDLING~~

~~SECRET/SPECIAL HANDLING~~

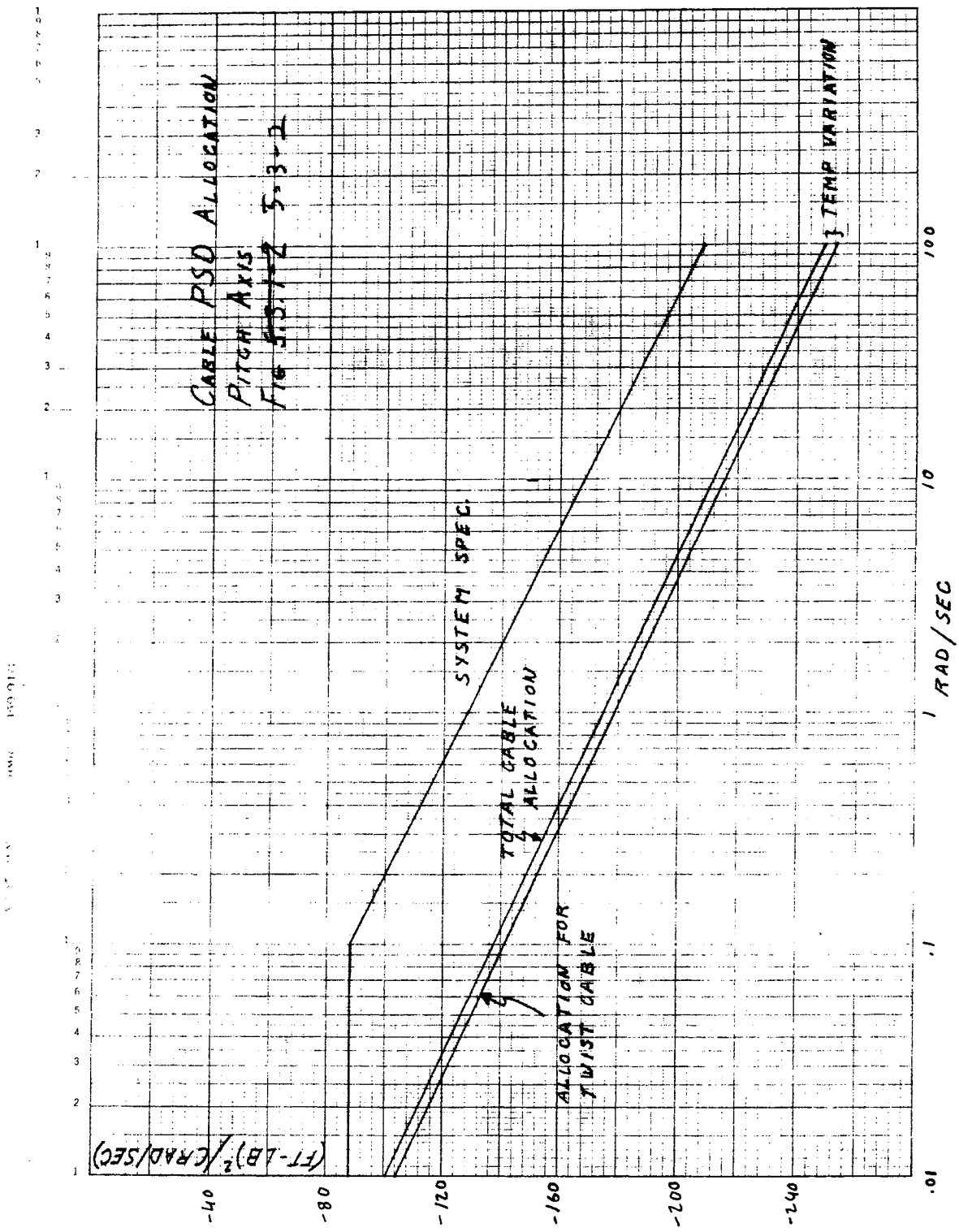


Fig. 5.3-2 — Cable PSD allocation, pitch axis

~~SECRET/SPECIAL HANDLING~~

~~SECRET/SPECIAL HANDLING~~

preliminary PSD budget on that basis. The total contributors to PSD that we have considered in this allocation are:

1. Measured data of individual bearings of catalog quality
2. Torque ripple improvement of improved bearings for flight hardware
3. Thermal degradation effects based on analysis
4. Misalignment effects based on analysis
5. Degradation of bearings mounted in scanner
6. Brinelling of bearings during launch environment.

Roll Axis Allocation

Figs. 5.3-3 and 5.3-4 show the measured PSD of a pair of 2 mm 9108 ABEC-7 bearings of 20 pounds preload. Data have been obtained with both the factory lube and after cleaning and re-lubricating with F-50 oil. The data is taken at 0.1 degree/second, a mean speed for the roll axis. No significant change is expected in PSD at other speeds, and our allocation covers the full speed range of the roll axis (0.05 to 0.15 deg/sec). Fig. 5.3-5 is a synthesized plot of the measured data.

The specification for engineering model bearings requires significant improvements in raceway topography. Additionally, the bearings will be assembled and operated under class 100 clean room conditions. Finally, we will control preload very carefully, and intend to reduce preload from 20 pounds to approximately 15 pounds on the 9108 bearings if our dynamic analysis substantiates this possibility. Although it is difficult to quantitatively assess the impact of these improvements over existing data, we conservatively estimate this improvement to be 12 db and perform our allocation accordingly.

Figs. 5.3-6 through 5.3-11 show measured data for a 2 mm 9104 bearing and a SBB 29-36 bearing. We have recently substituted a 2 mm 9105 bearing in our design instead of the 9104, but the preloads are identical and no substantial difference in performance between a 9104 and 9105 are expected. Both the 9105 and 29-36 bearings are expected to yield the same 12 db improvement for engineering model bearings as the 9108. Fig. 5.3-12 presents the individual bearing allocation for engineering model hardware.

Temperature changes in the bearings influence PSD by changing ball loading. Ball loading (and hence PSD) increases when the inner race is warmer than the outer race, and decreases for the reverse situation. In terms of torque allocation, we are thus concerned only when the inner race is warmer. Figs. 8.4-12, -13, -14 in Section 8 show predicted bearing temperatures. The inner race is typically the hotter. For 9108 bearing, the temperature difference is a maximum of about 6 degrees. For the 9105, it is about 7.5 °F maximum, and for the 29-36 it is about 4 °F maximum. In each case, this represents approximately a factor of 2 increase in bearing preload equivalent, as seen in Section 6. Isothermal temperature changes (soak temperatures vs. assembly temperature) also increase ball loading. With a scanner assembly temperature of 35 °F, the maximum isothermal difference is about 13 °F. From Section 6, it is seen that the ball load increase is approximately 20 to 25 percent for both the 9105 and 9108 bearing, and approximately 50 percent for the 29-36. The worst case thermal ball loading for each of the three bearings is thus approximately:

2 mm 9108	20 pounds initial preload increases to 48 pounds
2 mm 9105	10 pounds initial preload increases to 24 pounds
SBB 29-36	10 pounds initial preload increases to 30 pounds

~~SECRET/SPECIAL HANDLING~~

~~SECRET/SPECIAL HANDLING~~

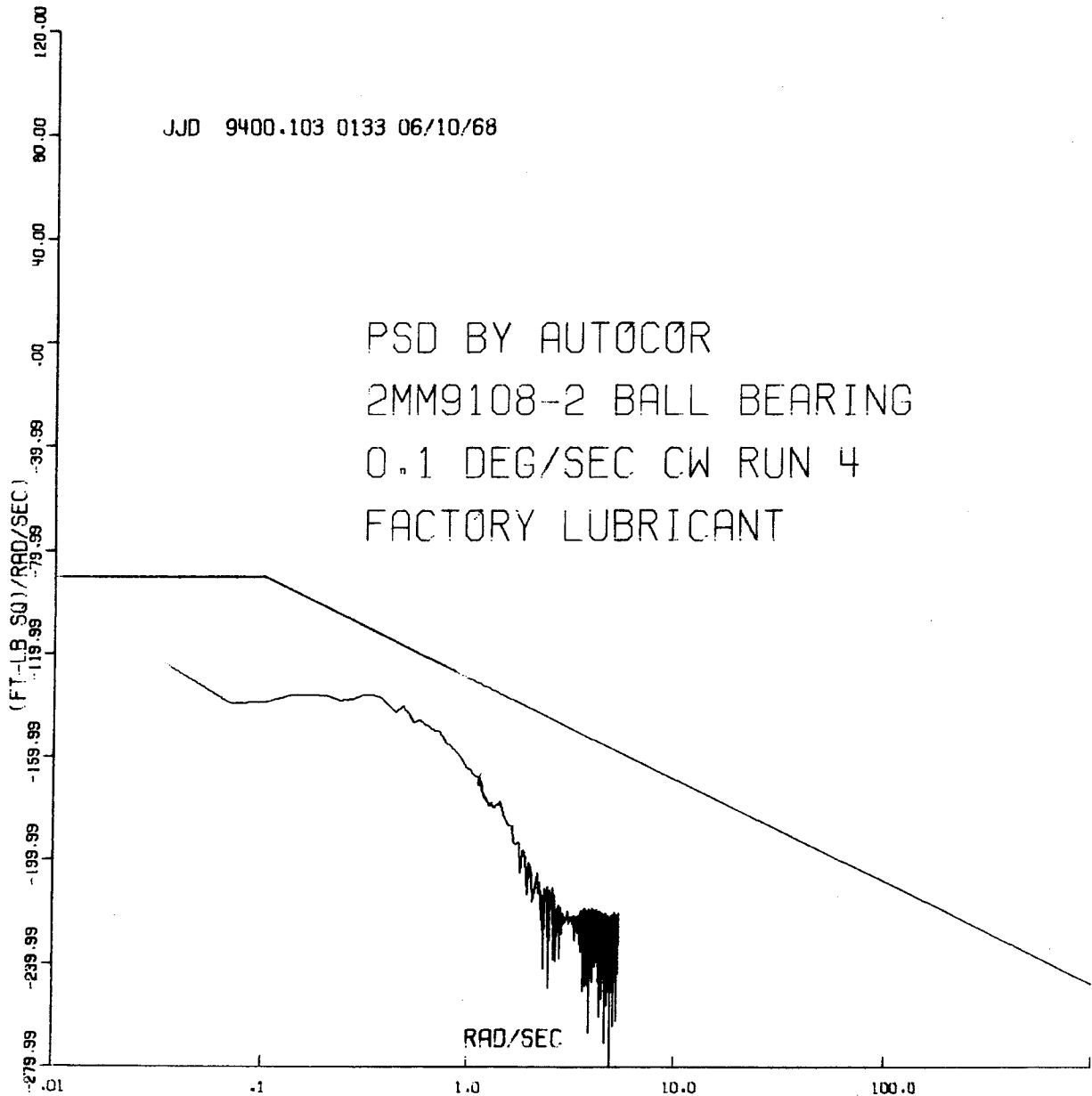


Fig. 5.3-3 — PSD by Autocor, run no. 4

~~SECRET/SPECIAL HANDLING~~

~~SECRET/SPECIAL HANDLING~~

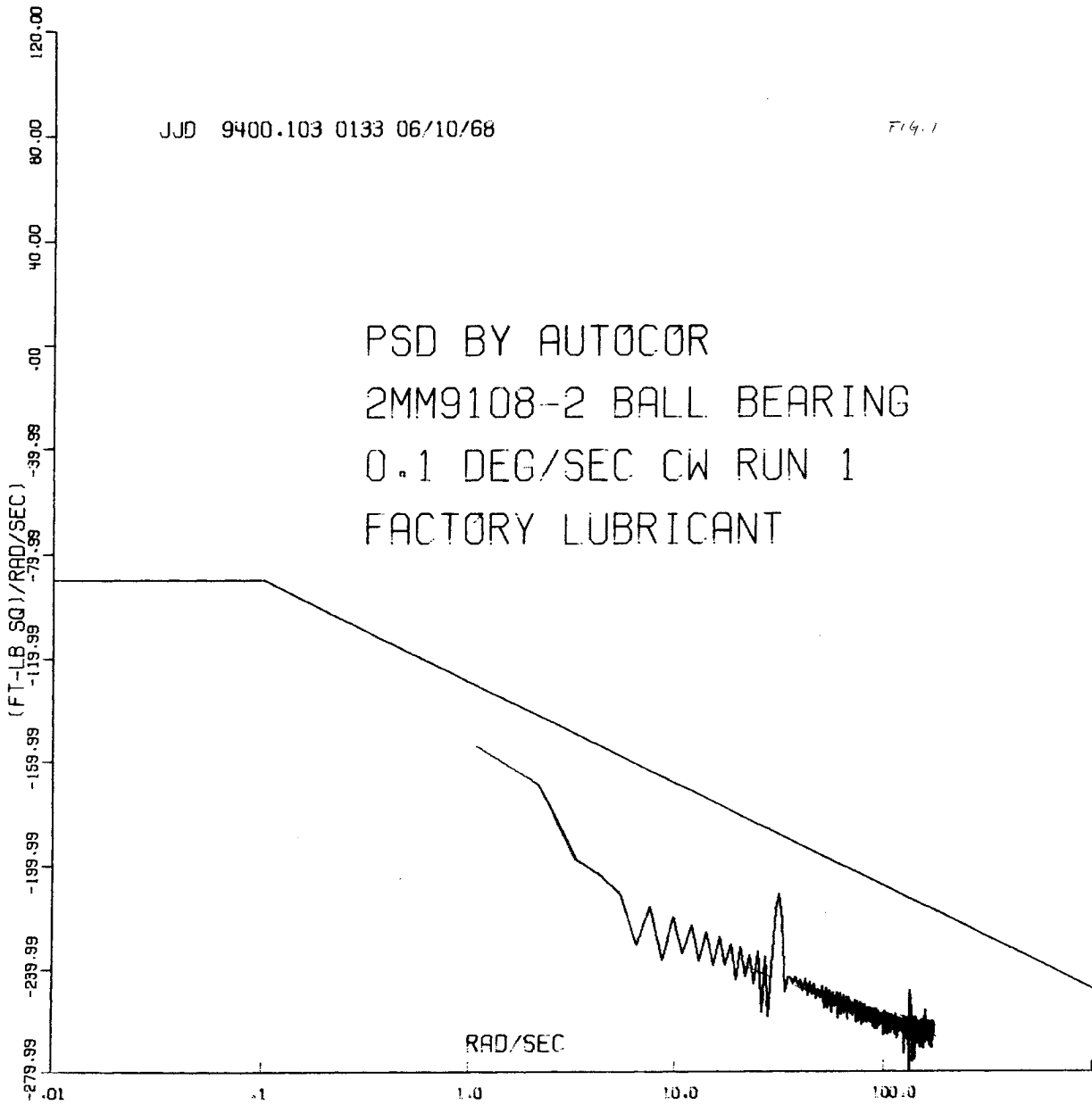


Fig. 5.3-4 — PSD by Autocor, run no. 1

~~SECRET/SPECIAL HANDLING~~

~~SECRET/SPECIAL HANDLING~~

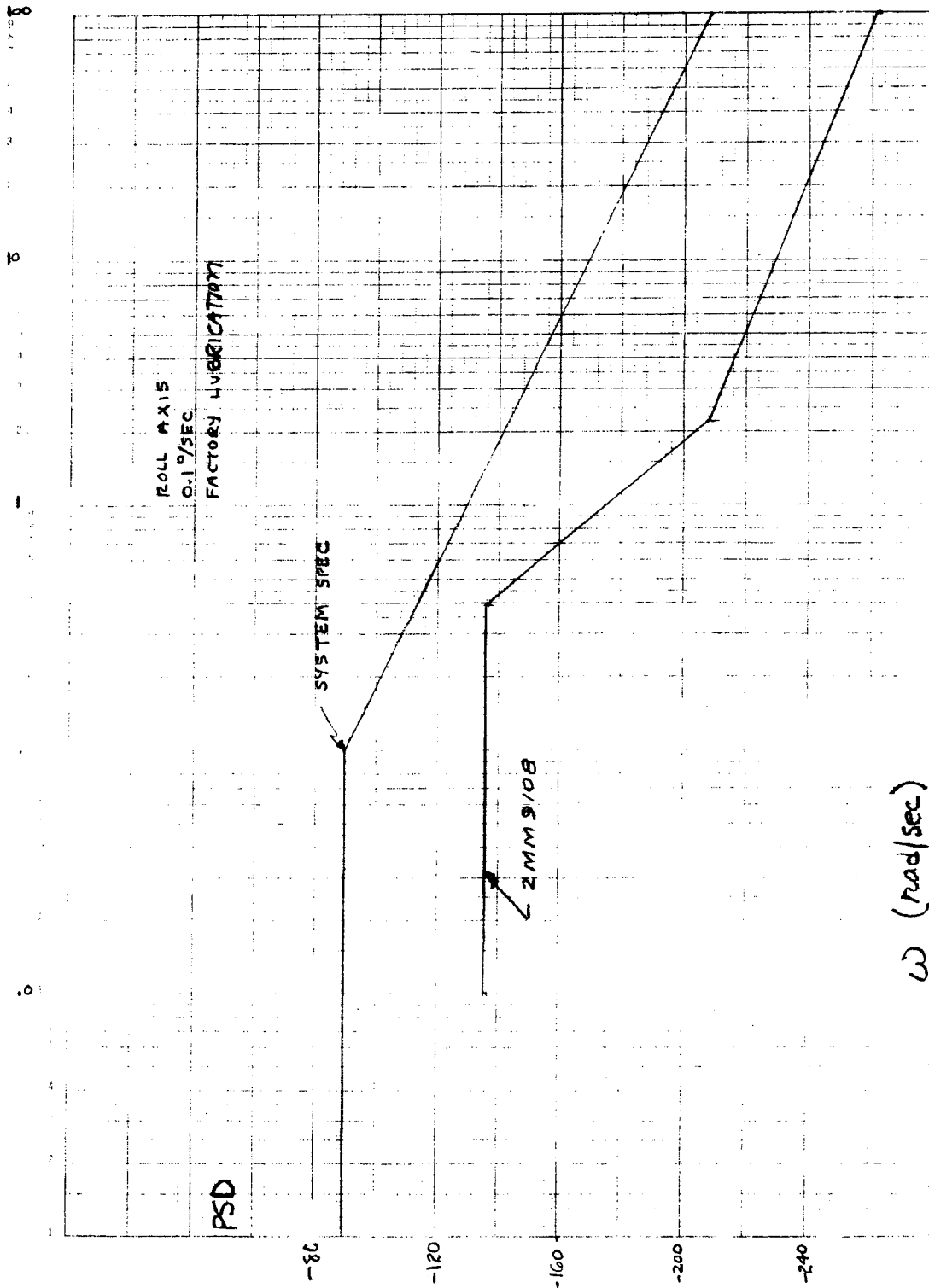


Fig. 5.3-5 — Synthesized PSD plot of 9108 bearing

~~SECRET/SPECIAL HANDLING~~  
5.3-7

~~SECRET/SPECIAL HANDLING~~

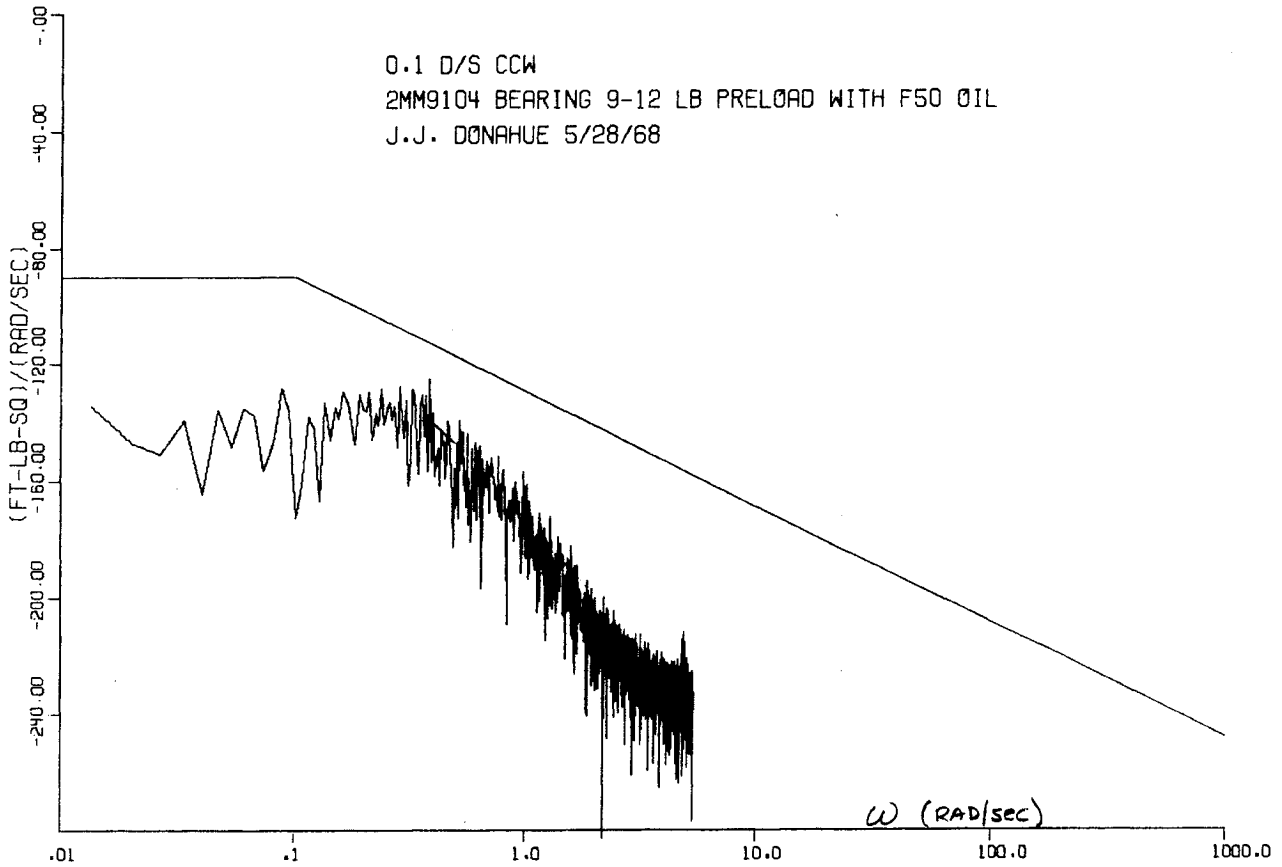


Fig. 5.3-6 — Data for 2mm 9104 bearing, 9- to 12-pound preload

~~SECRET/SPECIAL HANDLING~~

~~SECRET/SPECIAL HANDLING~~

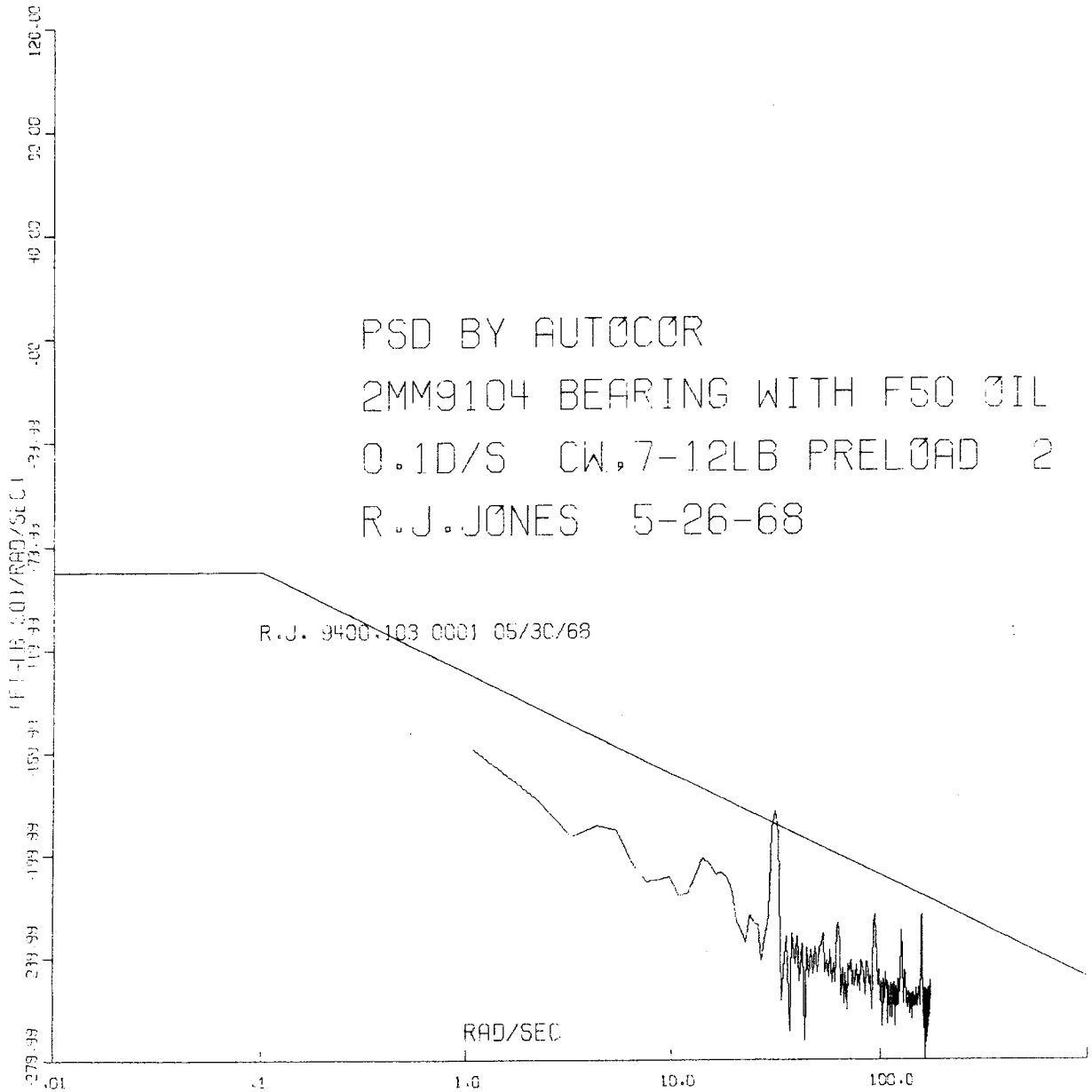


Fig. 5.3-7 — Data for 2mm 9104 bearing, 7- to 12-pound preload

~~SECRET/SPECIAL HANDLING~~

~~SECRET/SPECIAL HANDLING~~

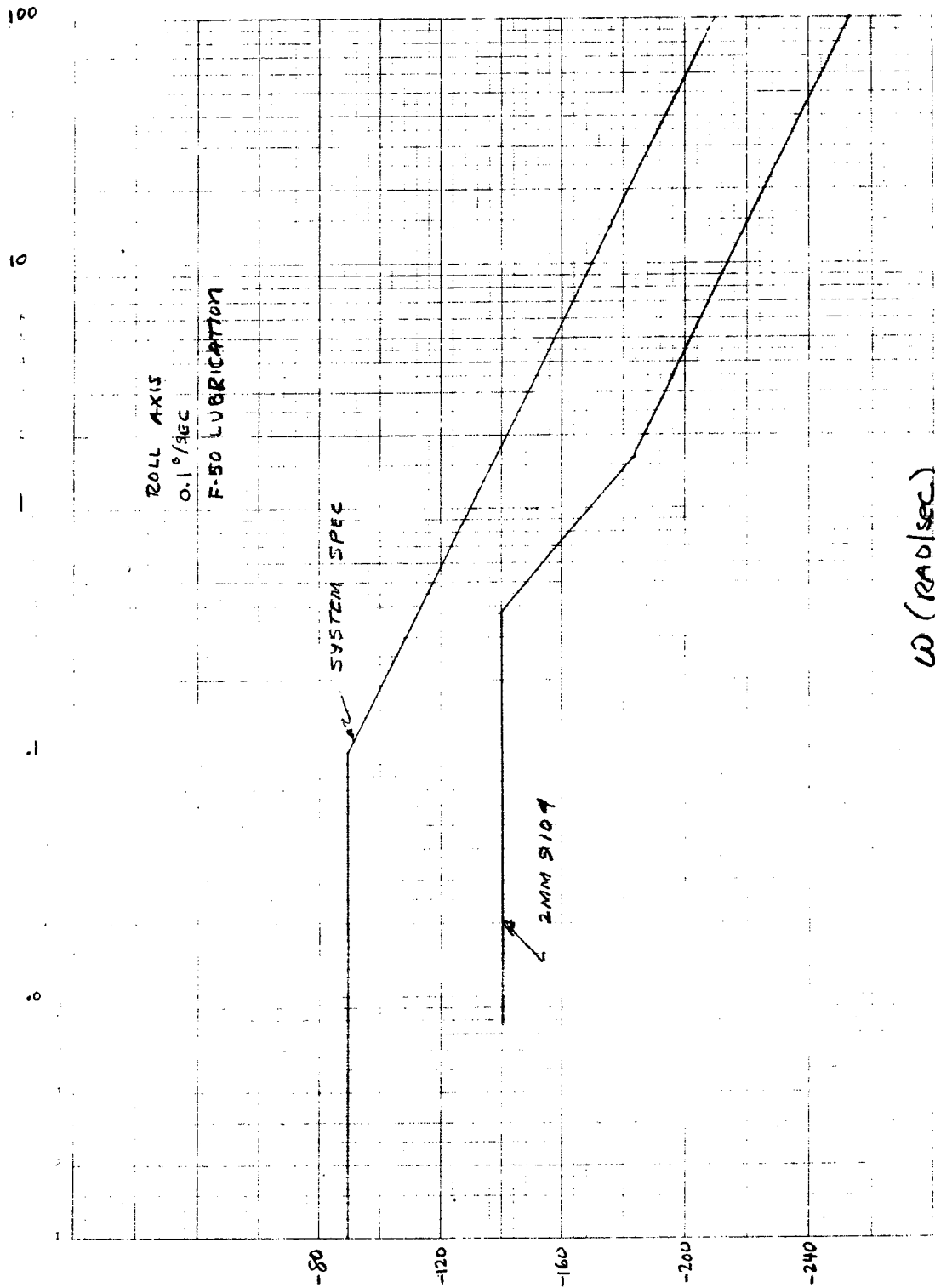


Fig. 5.3-8 — Synthesized PSD plot of 9104 bearing

~~SECRET/SPECIAL HANDLING~~

~~SECRET/SPECIAL HANDLING~~

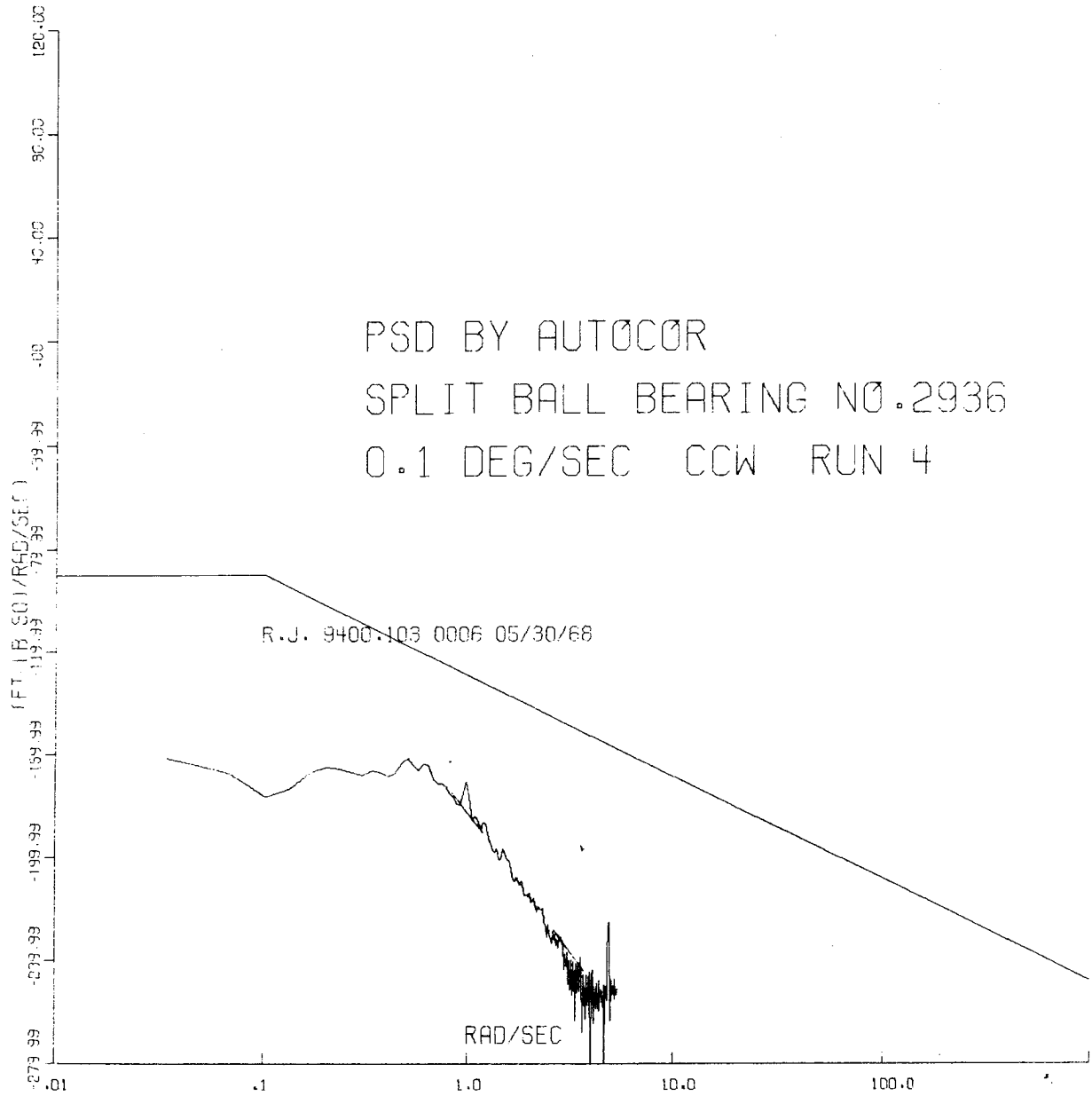


Fig. 5.3-9 — Data for 9236 bearing, run no. 4

~~SECRET/SPECIAL HANDLING~~

~~SECRET/SPECIAL HANDLING~~

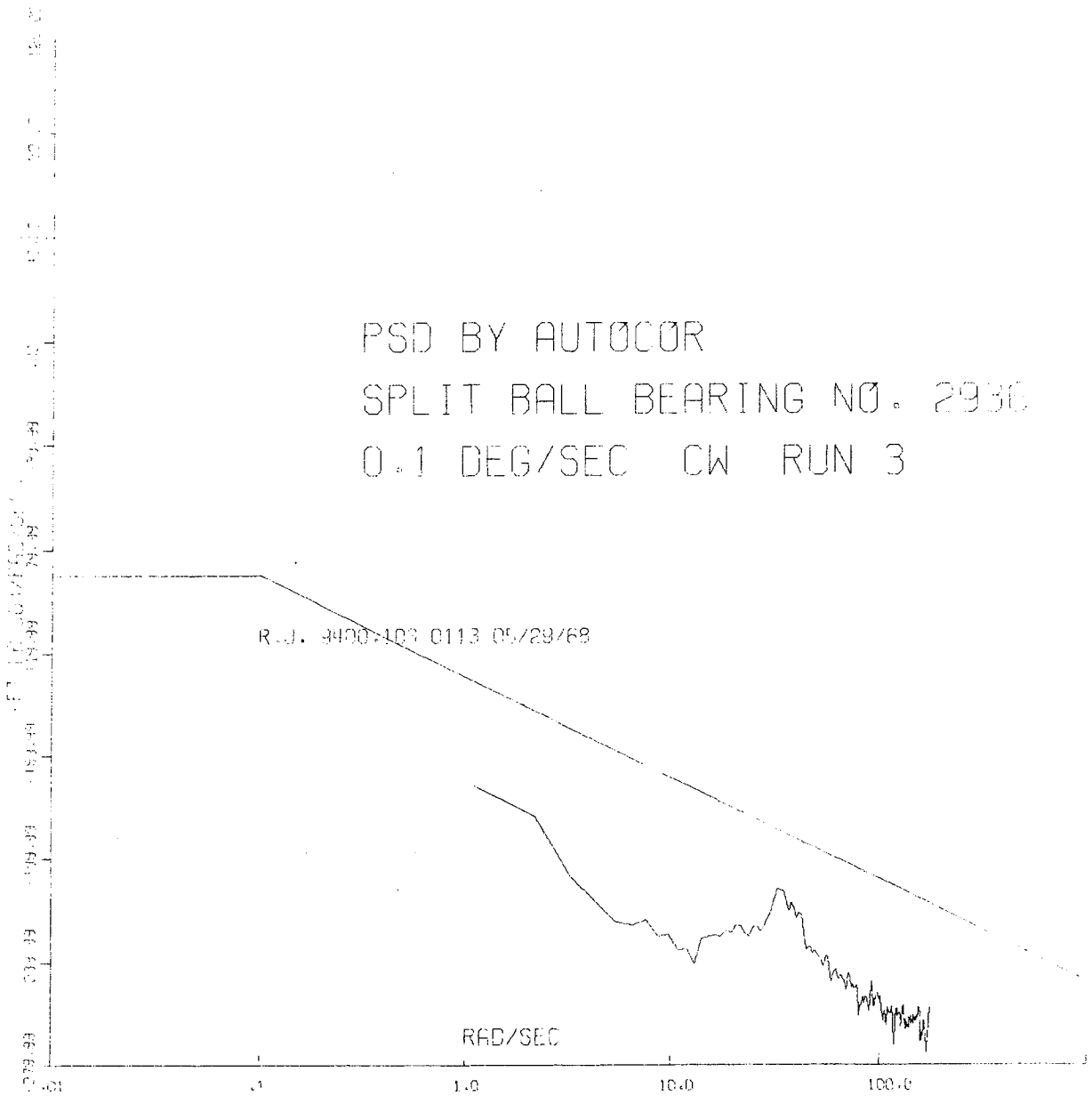


Fig. 5.3-10 — Data for 9236 bearing, run no. 3

~~SECRET/SPECIAL HANDLING~~

~~SECRET/SPECIAL HANDLING~~

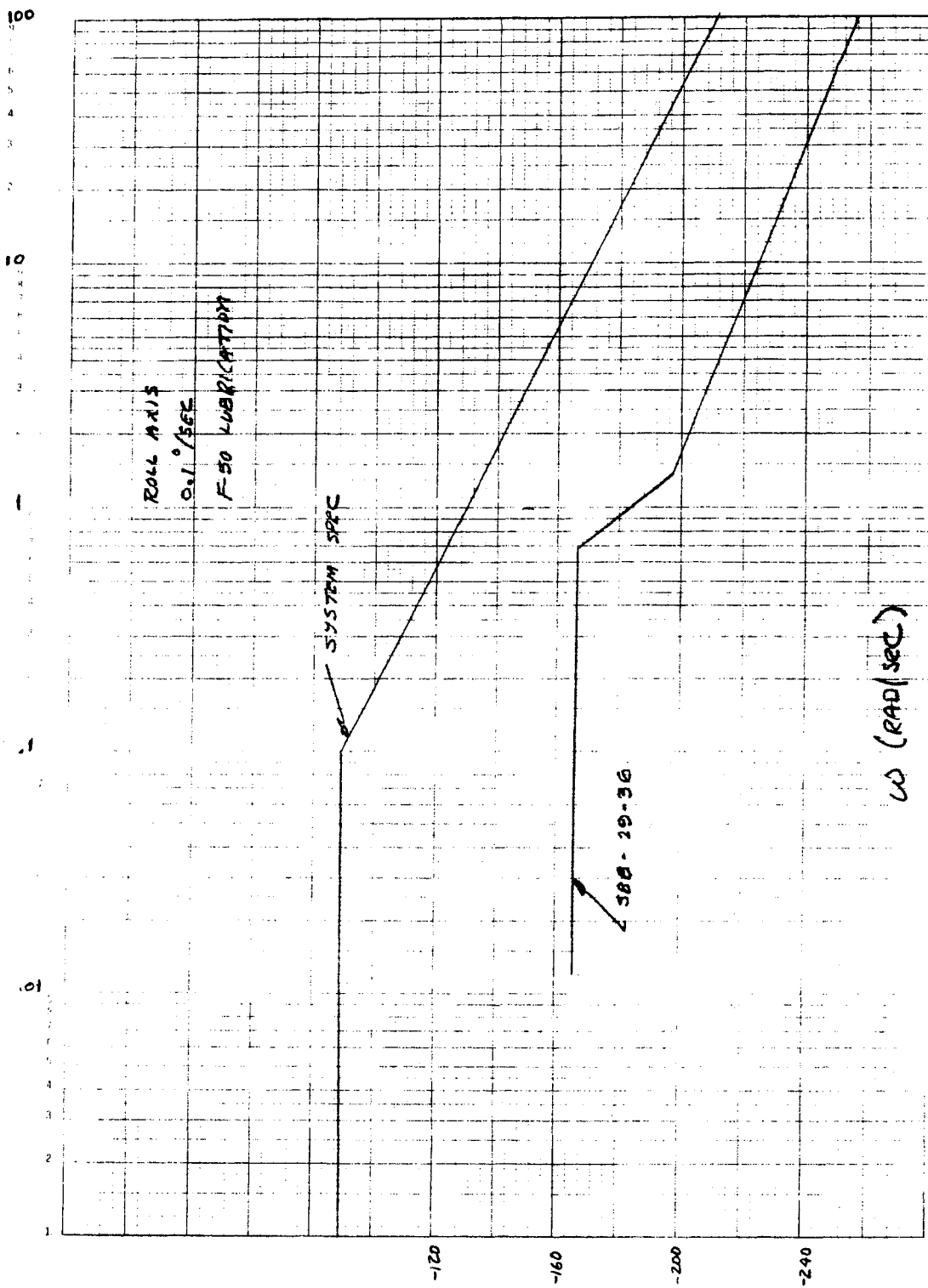


Fig. 5.3-11 — Synthesized PSD plot of 29-36 bearing

~~SECRET/SPECIAL HANDLING~~

~~SECRET~~/SPECIAL HANDLING

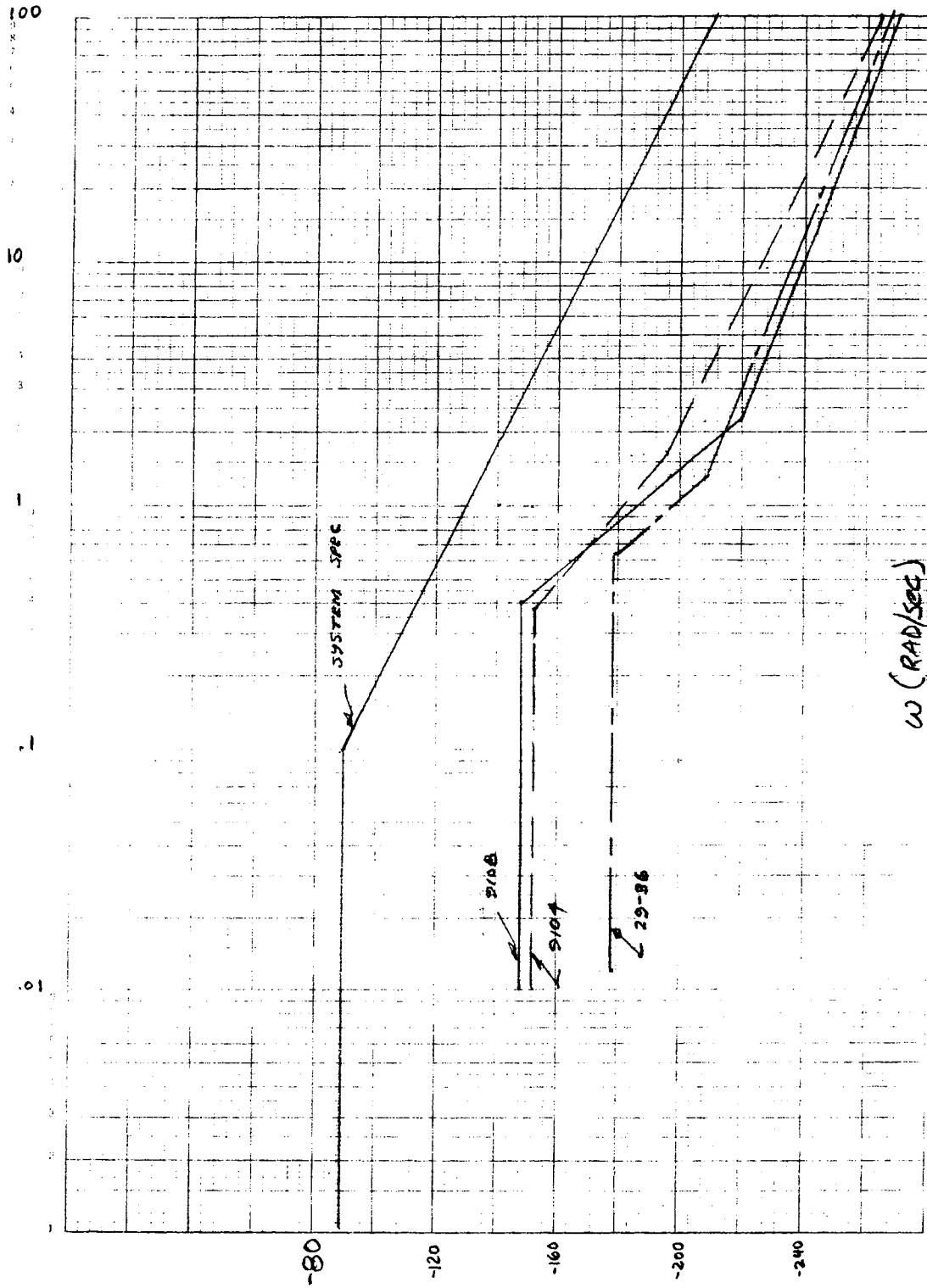


Fig. 5.3-12 — Engineering model bearing allocation

~~SECRET~~/SPECIAL HANDLING

~~SECRET/SPECIAL HANDLING~~

We do not have experimental data relating ball loading to PSD, but we know that running torque increases as the 4/3 power of ball load. It is reasonable to assume the same relationship for PSD. Hence:

$$\left(\frac{48}{20}\right)_{9108}^{4/3} = 3.22 \quad \text{or 10.1 db increase for thermal effects}$$

$$\left(\frac{24}{10}\right)_{9105}^{4/3} = 3.22 \quad \text{or 10.1 db increase for thermal effects}$$

$$\left(\frac{30}{10}\right)_{29-36}^{4/3} = 4.34 \quad \text{or 12.7 db increase for thermal effects}$$

Bearing cocking influences PSD in a similar manner to thermal effects, i.e., by changing ball load. In Section 6 of this report, ball load data vs. cocking angle are presented which show misalignments of 60 arc-seconds or more do not cause ball unloading in any of the load carrying bearings. Tests conducted by our contractor indicate only a slight increase of ball load and PSD in the absence of ball unloading. In our allocation, we allow a conservative 25 percent increase in PSD (2 db) for each of the two load carrying bearings on the roll axis. We intend to experimentally verify this allocation in the immediate future.

The degradation effects on bearings when installed in the scanner are difficult to assess quantitatively. It depends on the care and technique utilized in the installation. Based on discussions with our contractor, and based on his experience, we feel an allowance of 10 db per bearing pair is a conservative allowance for this decrease in performance.

The bearings in the scanner have been sized based on expected shock and vibration loads which will not cause detectable brinelling marks and therefore not increase PSD. The bearing loads and sizing analysis are presented in Section 6 of this report. Briefly they show all bearings will see maximum loads significantly less than 30 percent of their rated values. Tests conducted by the contractor show no detectable brinell marks or PSD increase from these light loads, on larger bearings, and we will make no allowance for degradation from this source. We intend to perform brinelling tests in the immediate future to verify this assumption.

Fig. 5.3-13 is a summary allocation of the bearing PSD for the roll axis. It includes the EM bearing allocation (Fig. 5.3-12), the degrading effects of the thermal environment, 2 db degradation for misalignment, and 10 db degradation for each bearing due to installation. Also plotted is the cable allocation of the roll axis from Section 5.3-1, and the sum of all contributors to total PSD on the roll axis.

Pitch Axis Allocation

The bearings used on the pitch axis are all thin section types. The load carrying bearing pairs are a SBB 14-21 on the encoder end, a SBB 21-28 on the torquer end, and a SBB 29-36 for the encoder mount.

We have obtained data on an ABEC-7 29-36 bearing at 1.7 deg/sec rotation speed (again, a nominal speed), but no data on the other two. We assume the other two bearings will each contribute

~~SECRET/SPECIAL HANDLING~~

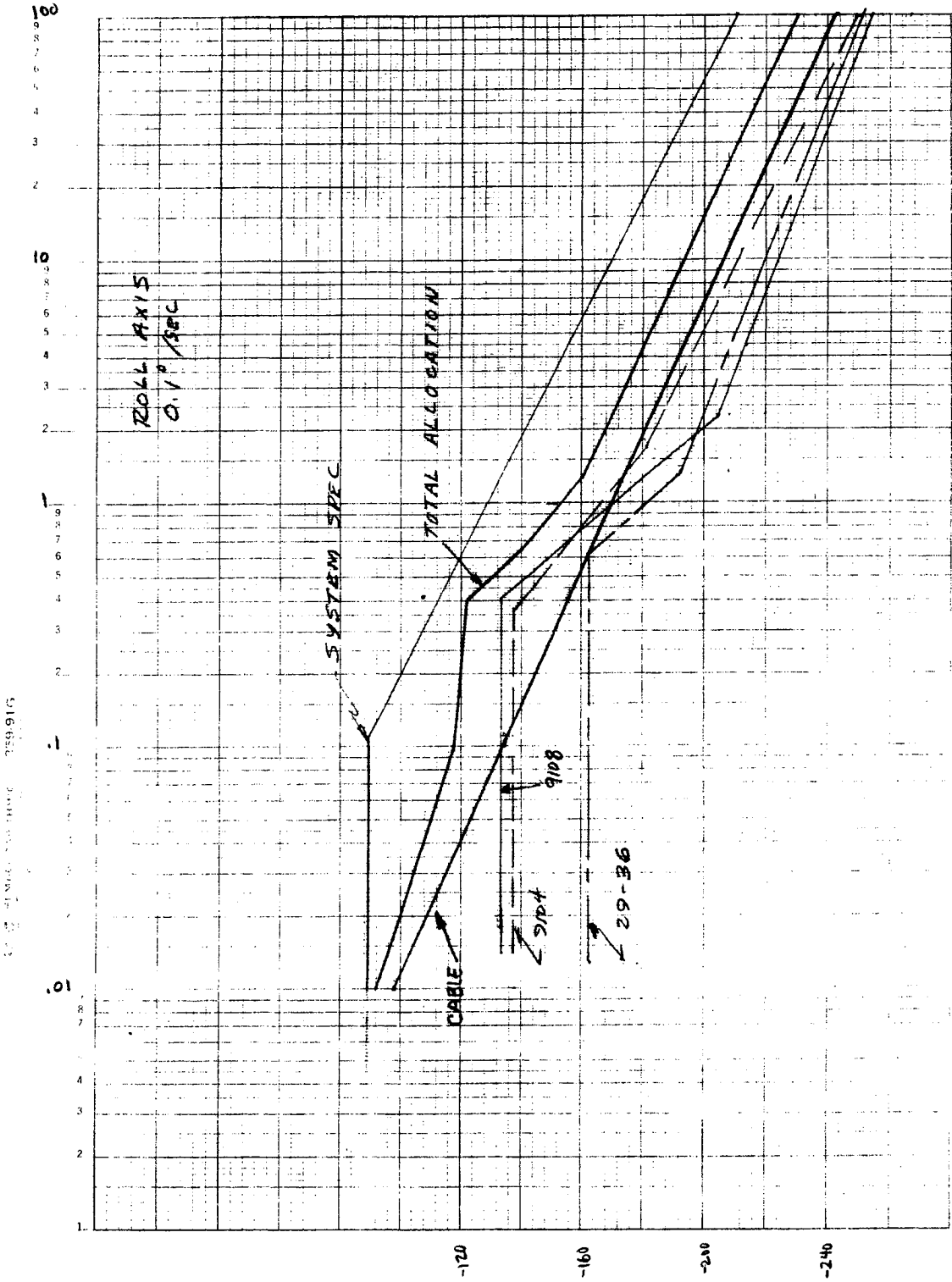


Fig. 5.3-13 — Summary allocation of bearing PSD for roll allocation

~~SECRET/SPECIAL HANDLING~~

~~SECRET/SPECIAL HANDLING~~

an identical PSD as the 29-36. This is felt to be a worst case assumption, since the preloads are identical, and the bearings are smaller. Fig. 5.3-14 shows the measured PSD of the 29-36 bearing, and Fig. 5.3-15 is the synthesized plot.

For the same reasons as discussed for the roll axis bearings, we have allocated a 12 db improvement in pitch axis bearings procured for the engineering model. The PSD specification for each of the three bearings is shown in Fig. 5.3-16.

Thermal effects on the bearings can be determined by reference to Figs. 8.4-10 and 8.4-11 of Section 8 and the ball load vs. temperature plots shown in Section 6. The inner race of the SBB 21-28 is a maximum of 7°F hotter than the outer race, and the maximum departure in operating temperature from assembly temperature is also 7°F. The former effect increases preload to 24 pounds and the latter produces a further increase of 20 percent to nearly 30 pounds. The resulting increase in PSD is 12.7 db.

The maximum gradient in either the SBB 14-21 or SBB 29-36 bearing is about 2°F. In the worst case they get 13°F hotter than the assembly temperature. This latter effect produces an increase in preload to 11 pounds and 14 pounds, respectively. The gradient effect increases these to approximately 13 pounds and 22 pounds respectively. The PSD is thus degraded by 3 db for the 14-21 bearing pair, and 9 db for the 29-36 bearing pair.

In a manner similar to that described for the roll axis, we have allocated 2 db, 10 db, and zero db for bearing degradation due to cocking, assembly, and brinelling, respectively.

Fig. 5.3-17 summarizes the pitch axis allocation. It includes all effects and magnitudes described above, and includes the cable allocation from Section 5.3-1.

~~SECRET/SPECIAL HANDLING~~

~~SECRET/SPECIAL HANDLING~~

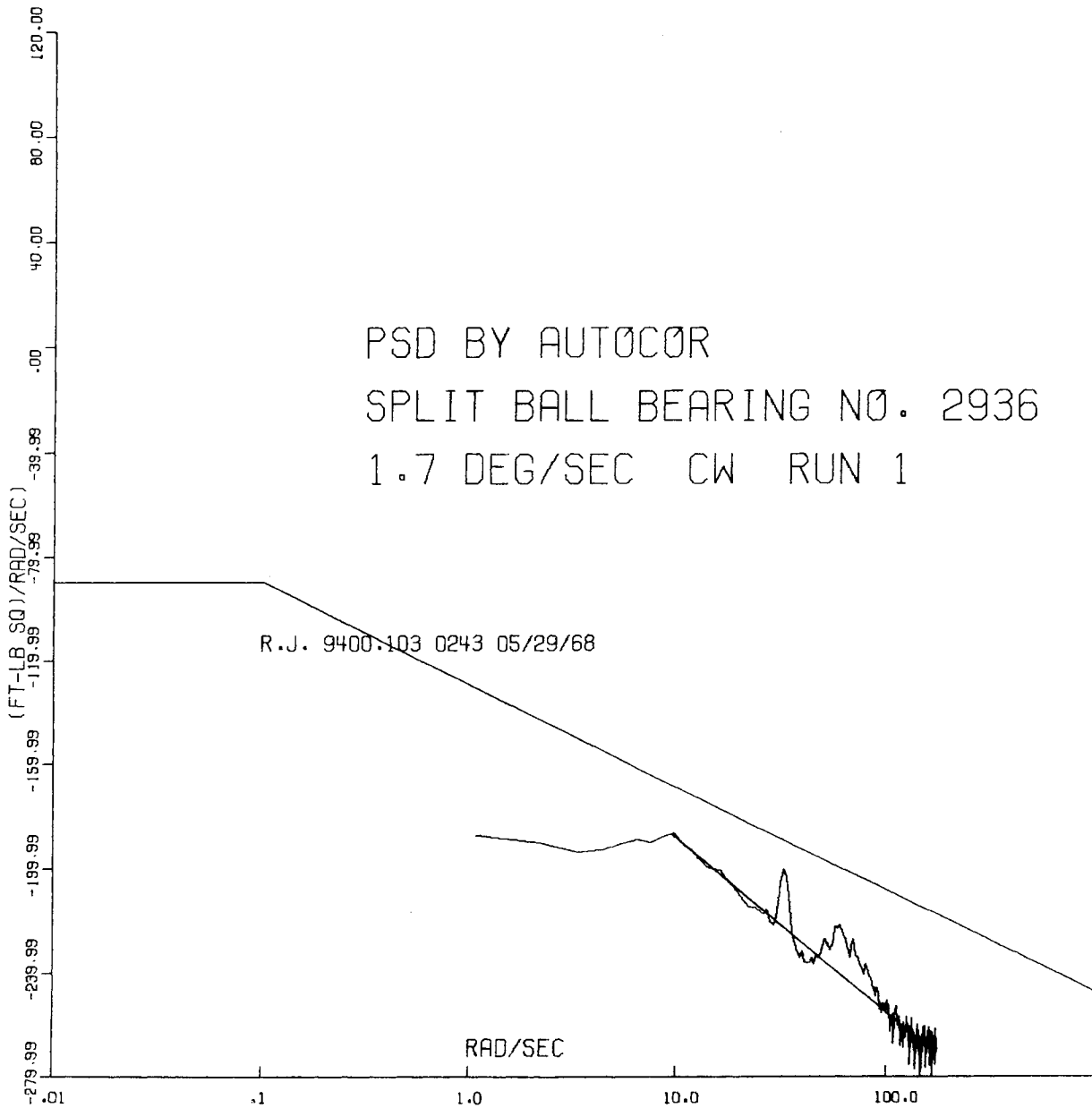


Fig. 5.3-14 — Measured PSD of 29-36 bearings

~~SECRET/SPECIAL HANDLING~~



~~SECRET/SPECIAL HANDLING~~

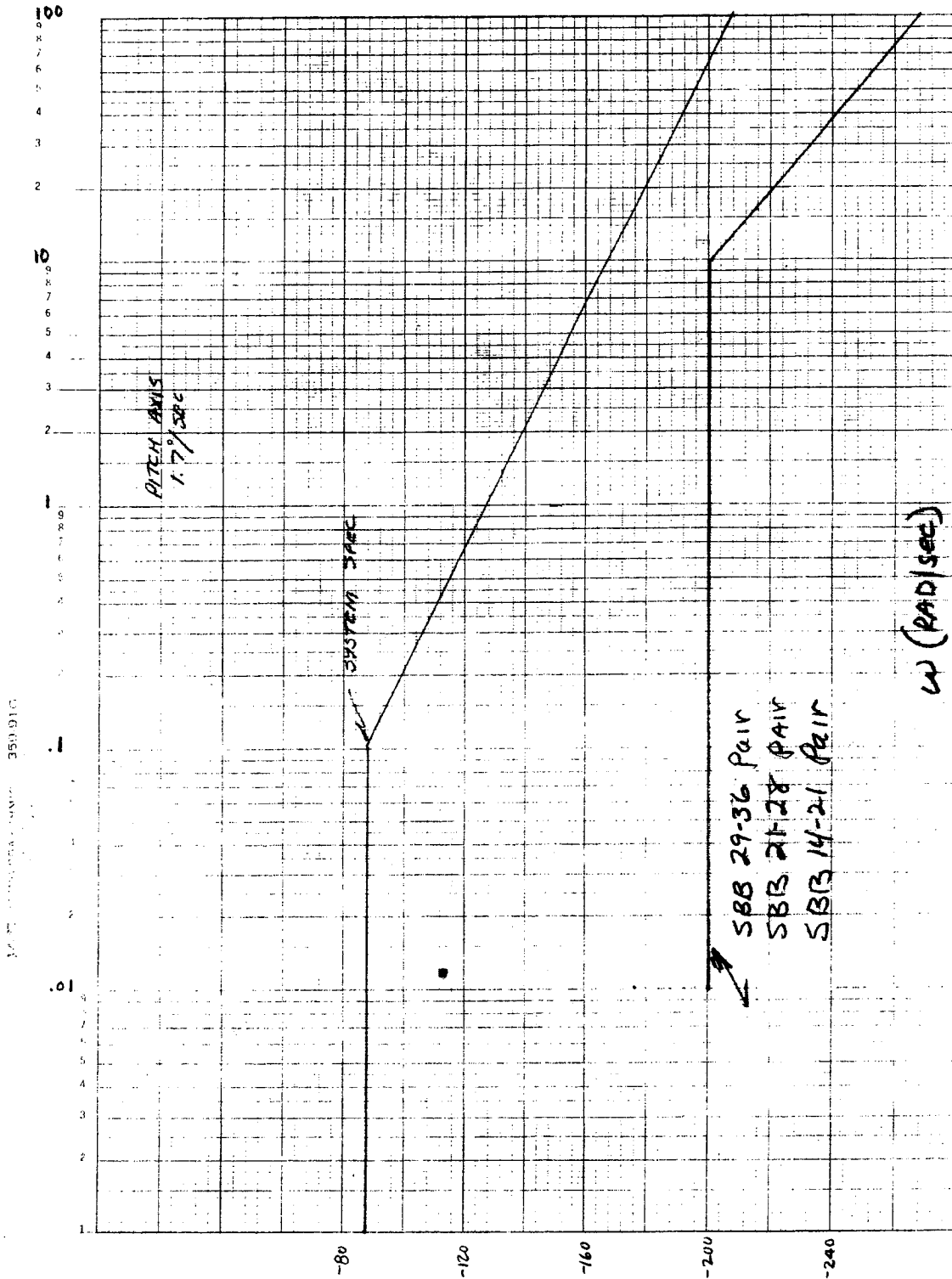


Fig. 5.3-16 — PSD specification for three bearings

~~SECRET/SPECIAL HANDLING~~

~~SECRET~~/SPECIAL HANDLING

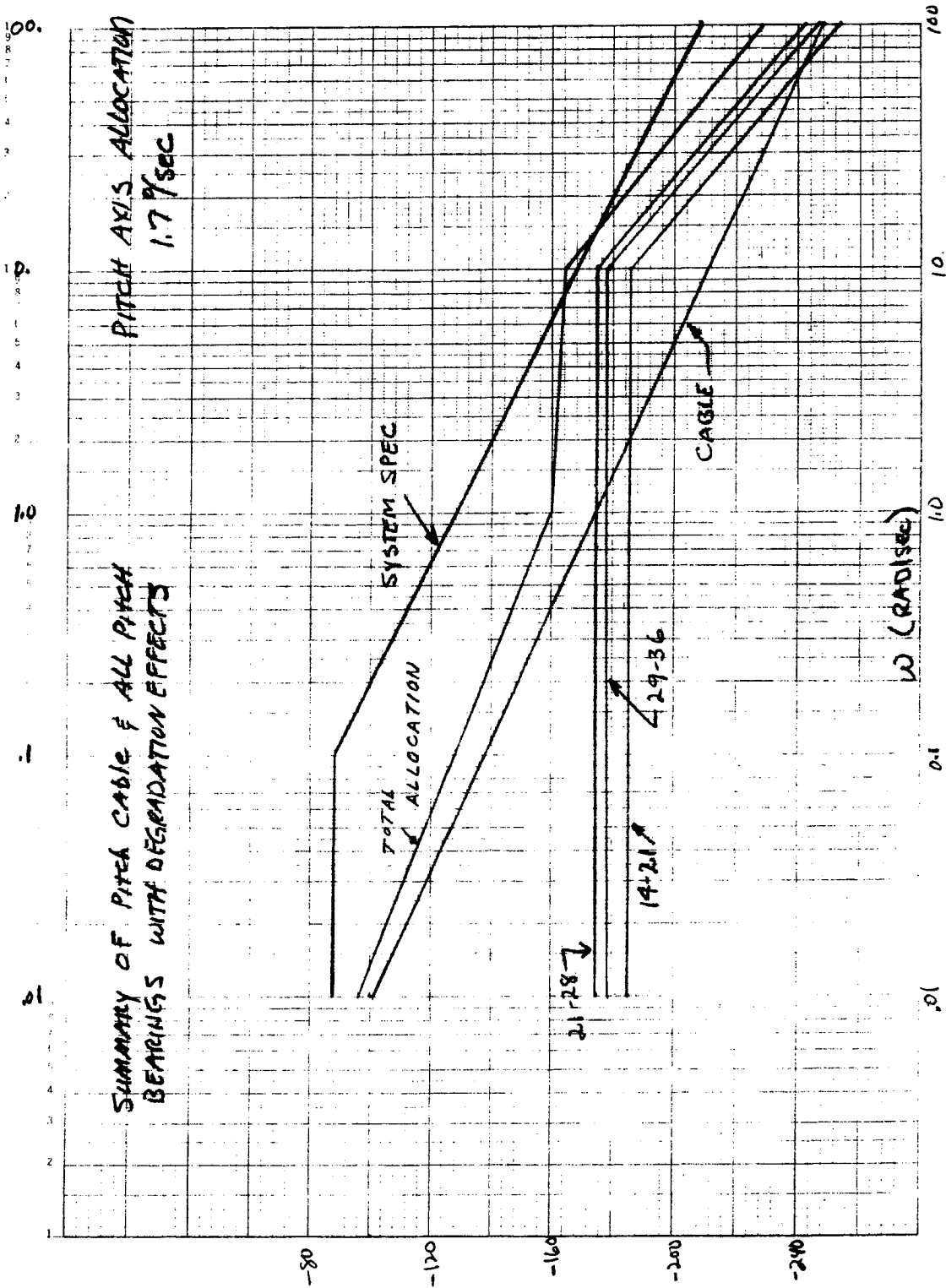


Fig. 5.3-17 — Summary of pitch cable and all pitch bearings with degradation effects

~~SECRET~~/SPECIAL HANDLING

~~SECRET/SPECIAL HANDLING~~

#### 5.4 TORQUE LEVELS

The present specification requires that the mean value of running friction torque for either gimbal axis shall be no greater than 2 oz-in. and that starting friction torque shall be no greater than 1.5 times the mean value of running friction torque for each gimbal.

The contractor has been notified that the running torque levels of 2 oz-in. are not realizable. The bearing state of the art and our present gimbal design indicates that bearing friction of the roll axis will be in excess of 2 oz-in. This is the total torque allotment for the roll axis but we must also have an allotment for the cable torques. Preliminary cable tests have indicated that the mean running torque contributed by the cable will be at least 4 oz-in. for the roll axis. For the cross roll gimbal the bearings will contribute 1.5 oz-in. and the cable at least 2.5 oz-in.

The running friction problem has been discussed at Contractor—Itek interface meetings. It has been mutually agreed that a specification change was in order. It was agreed that the specification for running friction torques should include a 2 oz-in. contingency for each gimbal axis and read as follows:

The mean value of running friction torque for the roll gimbal shall be no greater than 8 oz-in. The mean value of running friction torque for the cross roll gimbal shall be no greater than 6 oz-in. The mean value of running friction torque is defined as the sum of running frictional torques measured at equally spaced intervals over the total gimbal range divided by the number of measured values. Starting friction torque shall be no greater than 1.5 times the mean value of running friction torque.

~~SECRET/SPECIAL HANDLING~~

~~SECRET~~/SPECIAL HANDLING

## 5.5 ENCODER ERROR ANALYSIS

### 5.5.1 Experimental

#### 5.5.1.1 Static Bit Length Measurement

A brief investigation was conducted to determine the error inherent in the Wayne-George master dividing engine used to generate encoding discs. Autocollimator measurements were made of bit error over a 96 point run of successive bits. Error curves were analyzed and the frequency spectra plotted. Further test of this type did not appear likely to be profitable because of two difficulties. The 2-sigma error of the autocollimator is 0.1 arc-second, which is also the operator's limit of ability to read, and the capture angle, i.e., the angle over which readings can be made without moving the instrument is only a few minutes of arc. Accuracy of such measurements is probably further degraded by operator fatigue and temperature effects both of which are aggravated by the length of time (many hours) required to take the data. Such investigations were therefore abandoned in favor of a dynamic test facility and technique which, besides the conceptual advantages of testing in the same mode, i.e., velocity, as the intended end use, also promised to provide as least as great accuracy and at enormously higher rates of data acquisition.

#### 5.5.1.2 Dynamic Bit Length Measurement

A Wayne-George  $2^{18}$  bit absolute position encoder, Type BD-18CP-80 was purchased from a customer who had bought it as backup in November 1965 and had not needed it. Although techniques of fabrication and design of encoders have advanced since 1965, it was felt that this encoder would be useful in establishing testing techniques and that some extrapolation to expected present generation performance could be made.

The encoder was mounted on an air-bearing table of approximately 2 slug-ft<sup>2</sup> inertia. Table drive was provided by a brushless ac torquer in a servoloop phase locked to the  $2^{15}$  bit (outermost optical) track. Time constant of the loop was of the order of 0.2 second. The lowest angular wheel velocity at which stable operation (without hunting) could be achieved was 25 hz, corresponding to approximately 0.5 degree per second and 20 hz at the frequency of the least significant ( $2^{18}$ ) bit track. Some smoothing of possible variation in the outermost optical track frequency was inevitable. Variations in disturbing torques due to encoder bearings, variations in air pressure, vibration, etc., placed a limit on allowable length of servo time constant. At bandwidths less than 2 to 5 hz the system would lose phase lock. Even though variation in outer track line spacing of more than a few lines span were smoothed, the effect of such variations was not lost, as will be discussed in the analytical section below. Ideally, of course, the table should be driven at absolutely uniform angular velocity. However, such uniformity implies much higher inertia and/or a perfect tachometer to which the nearest approximation available was the encoder itself. As a consequence the actual table angular velocity was constrained to follow the line frequency of the outer optical track averaged over approximately four cycles (8 bits of the  $2^{15}$  bit track).

The output of the LSD ( $2^{18}$ ) was processed and/or recorded in a number of ways. See Fig. 5.5-1.

##### 5.5.1.2.1 Discriminator and Wave Analyzer Tests

LSD output was processed by a General Radio type 1142-A frequency meter whose output was analyzed by a General Radio Model 1900 Wave Analyzer equipped with a General Radio Model 1521-B Graphic Level Recorder. The frequency meter accepts the input signal, limits, amplifies,

~~SECRET~~/SPECIAL HANDLING

~~SECRET/SPECIAL HANDLING~~

Dynamic Bit Length Measurement  
and  
Error Frequency Analysis

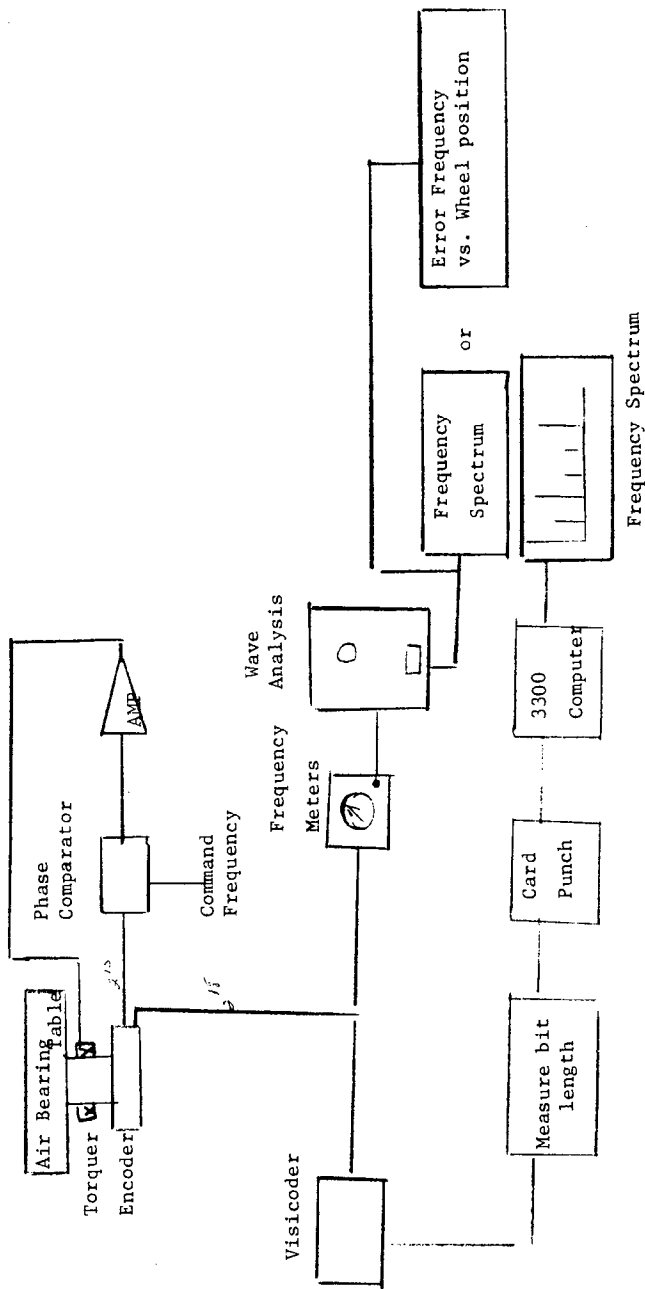


Fig. 5.5-1 — Dynamic bit measurement and error frequency analysis

~~SECRET/SPECIAL HANDLING~~

~~SECRET~~/SPECIAL HANDLING

squares and differentiates it. The resulting pulses are used to trigger a monostable multivibrator of carefully controlled amplitude and duration. The output signal then consists of pulses of uniform charge per pulse, whose repetition rate is equal to the input frequency, and whose average value is proportional to the input frequency. Such a signal may be analyzed for its various frequency components by such an instrument as the General Radio Wave Analyzer. This instrument operates on the heterodyne principle. The incoming signal is mixed with the output of a calibrated tuneable local oscillator to produce a 100 Khz intermediate frequency. The I. F. amplifier section contains a crystal filter of bandwidths variable from 3 to 50 hz. The 100 Khz output signal is then a measure of the energy contained within the indicated bandwidth centered at the indicated frequency. The instrument is calibrated in rms volts of input signal at the frequency of interest. An output signal is available and may be recorded by the Graphic Level Recorder either as a function of time or by means of a chain drive unit coupling the chart drive to the local oscillator frequency knob shaft, as a function of frequency. Both types of recording were made.

#### 5.5.1.2.2 Visicorder Recording

The LSD output was recorded directly on paper by means of Honeywell Visicorder. Maximum recording chart speed is 80 inches per second. At the minimum achievable wheel velocity, the frequency of the LSD was 400 bits per second. To facilitate measurement of bit length (0.2 inch per bit) the square output signal was processed by an integrator and the integrator output recorded simultaneously with the LSD signal. The triangular wave form resulting from integration was adjusted to give lines about 2 inches long. Lengths of these lines were then measured with a scale and the bit lengths recorded and punched into cards for computer analysis. It is estimated that total bit length processing and reading errors were between 0.01 and 0.02 corresponding to 0.05 to 0.1 arc-second, an accuracy comparable to that of autocollimator measurements.

Data as described above was taken and analyses made of the performance of the encoder equipped with three different electronic multipliers; the original equipment multiplier, a new multiplier fabricated by Wayne-George and employing integrated circuits in both logic and amplifier section, and an experimental multiplier designed and fabricated by Itek project personnel. The experimental multiplier was designed, built and tested for the purpose of gaining further insight into the various sources of error in the multiplier and the effects of design parameter variation thereon. Measurements by oscilloscope and by interval times were made of individual bit length and of squaring amplifier symmetry. Analysis of the performance of this experimental multiplier has suggested that further experimental and analytical work can result in still further improvement and that higher precision of components and care in adjustment than has been characteristic of multipliers in the past may be required in order to keep pace with advance in the encoder disc art.

#### 5.5.1.2.3 Sine and Cosine Signal Analysis

Observations of the sine and cosine signals both individually and as lissajous figure were made and these observations suggested a wave analysis. Although the lissajous figure was clearly distorted (somewhat square) the sine and cosine waves proved to contain surprisingly little distortion. Second harmonic was down 40 decibels and the third harmonic was down 20 decibels. Higher harmonics were down 60 decibels or more. In principle it is possible to adjust the sampling resistors in the multiplier so that the effects of this wave shape distortion are nullified. In practice this does not appear necessary. First, because the effect, already small, promises to be even smaller in present day and future encoders, and second, because other effects such as departure

~~SECRET~~/SPECIAL HANDLING

~~SECRET/SPECIAL HANDLING~~

of the sine versus cosine from 90 degrees, differences in amplitude between sine and cosine signals, and tolerance due to aging and/or temperature effects appear to be considerably larger.

Phase angle between the sine and cosine waves varied as a function of wheel position over a range of approximately plus and minus 6 degrees. Amplitude difference varied over a range of approximately plus and minus 5 percent. It is estimated that present generation encoders have approximately half these errors with further improvement expected in the encoders to be supplied under this contract.

#### 5.5.1.3 Projected Experimental Procedures

Two further improvements in data acquisition are planned with a view to reducing the time required and increasing the accuracy. Bit length will be measured in real time and recorded as a binary word. An intermediate solution will be the recording of these words (6 bit) on a six channel visicorder and transcribing the words on to computer cards. Equipment to perform these functions has been completed but not yet used. It will be checked out with the 18-bit encoder on hand. It is hoped that within the next two months a present generation 20-bit encoder will be available from Wayne-George for test. A similar system but recording directly on computer compatible tape is being designed. Such a system will make practical the evaluation of the encoder over its entire angular range. In addition, such a system will facilitate evaluation of multipliers driven from pure sine wave sources and of simulated multiplier performance needed to establish design parameter variation error budgets. (See analytical section.)

The air bearing table used for testing to date is available only at limited times since it is engaged on another project and, in addition, far from optimum design for encoder testing. We plan to acquire either by purchase or in-house design and fabrication a table of much higher inertia, greater torquer capacity and higher axis stiffness than those of the table presently being used. For example commercial tables are available of 40 slug ft<sup>2</sup> inertia, 7.5 foot-pounds torquer and 200 pounds/second stiffness. This table is guaranteed to less than 1 arc-second axis wobble. Such a table could not only serve as an ideal testing table, but could also be the principle component in a new generation disc-generating engine.

#### 5.5.2 Analytical

Since the number of lines per unit length that could be printed and resolved is limited by the resolution of the photographic process used and/or the wavelength of light, high angular resolution can be obtained either by increasing the diameter of the disc or by some form of electrical subdivision of the signals derived from the outermost track. Two basically different methods of performing this electrical subdivision are in common use. Both methods use as basic inputs signals from two photoelectric read stations spaced  $(n + 1/4)$  lines apart, i.e. some convenient number of lines plus 90 spatial degrees of the outermost track spatial frequency.

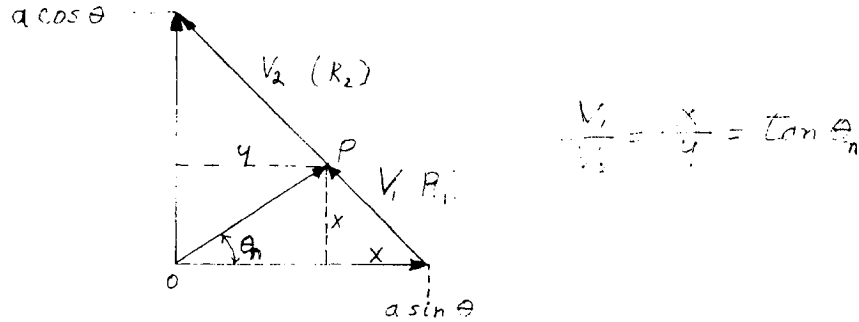
##### 5.5.2.1 Phase Shift Multiplier

In the system typified by Wayne-George multipliers the read stations consist of a lamp energized by direct current and a silicon photo detector. Outputs from these two detectors vary sinusoidally (since the system is diffraction limited to the extent that practically all of the higher harmonics of the triangular wave form are removed by what amounts to a spatial low pass filter) and, by virtue of their spacing, bear the relationship to each other of sine to cosine. From these two basic signals a number of phase shifted waves are derived by electrically adding or subtracting a suitable fraction of one signal from the other. For example, if a wave at 45 degrees is

~~SECRET/SPECIAL HANDLING~~

~~SECRET~~/SPECIAL HANDLING

desired the sine and cosine signals are simply added or subtracted to give new sine waves leading and lagging respectively. In general, if one wishes a sine wave shifted by  $\theta_n$  degrees, samples of the sine and cosine signals of ratio  $\tan \theta_n$  may be added or subtracted to produce such a signal. This is apparent from the following vector diagram:



Vector to point P is the desired wave and can be conveniently obtained as the voltage between the common ground of the two generators and the junction of two resistors  $R_1/R_2 = \tan \theta$  whose other ends are connected to the outputs of the two generators. The various phase shifted signals so obtained are zero detected by squaring amplifiers and the higher bit track synthesized from the shifted squared signals by appropriate logic.

Errors in the finest track may be due to the sine and cosine signals not being pure sinusoids or exactly 90 spatial degrees apart or exactly the same magnitude or by errors in the  $R_1/R_2$  ratios or by errors in zero detection, i.e., asymmetry in the squaring amplifiers or by combinations of these sources. Note that the sine waves and the finer bits are spatially determined. As a result the rate of data acquisition in bits of information per unit time is directly proportional to angular velocity.

#### 5.5.2.2 Modulation Multiplier

The other method, typified by Baldwin, also starts with sine and cosine read stations but uses pulsed light sources pulsed in time quadrature. If the lights are pulsed such that their outputs contain fundamental components at a  $\omega t$  and a  $\cos \omega t$ , two photocell signals result, i.e., a  $\sin \omega t$  and  $\cos \omega t$ . If these two signals are added electrically, a signal  $\sin(\omega t + \theta)$  results. This signal at the same frequency ( $\omega t$ ) as the pulse source is zero detected and its phase difference,  $\theta$ , from the pulse source counted by a clock derived from the same master clock which provides the light pulsing voltage. If, for example a counting frequency equal to 32 times the pulse rate is used the 360 electrical degrees of  $\sin(\omega t + \theta)$  from  $\theta = 0$  to  $\theta = 2\pi$  corresponding to a full cycle of the finest optical track can be divided into 32 parts to give a LSD  $1/32$  of the optical track. Like the phase shift multiplier such a multiplier is subject to errors due to sine and cosine amplitude and phase errors. Error in the zero detecting amplifier produce merely a fixed phase error which is of no consequence in an incremental recorder, whereas the errors introduced by the many zero detectors (one per bit) required in the phase shift multiplier generate subharmonic error frequencies. Because the system depends on pulse phase relationship care must be taken to assure

~~SECRET~~/SPECIAL HANDLING

~~SECRET/SPECIAL HANDLING~~

preservation or at least rapid reacquisition of proper phasing in the presence of noise pulse interference. In this type of multiplier there is no counterpart of the error introduced by errors in the sampling resistors in the phase shift multiplier. However, this is only a minor advantage since these resistors need not be individually accurate or stable as long as their ratio is, a situation comparatively easier to achieve.

Perhaps the most significant difference, especially for encoders operated over a wide range of speeds is that data acquisition rate in the modulation multiplier is limited by the pulse rate. In effect the system is interrogated at the pulse rate and can therefore not supply information as to LSD changes that occur between pulses. At a rate of 50 degrees per second and a  $2^{20}$  LSD, bits are changing at about a 200,000 bits per second rate, an inconveniently high rate for a pulsed light source. Although Gallium Arsenide diodes operated in the laser mode are capable of such rates, power requirements are high and life expectancy low.

### 5.5.2.3 Comparison of Sine-Cosine Errors in Wayne-George and Baldwin Multipliers

#### 5.5.2.3.1 Baldwin Multiplier

As we have seen, the Baldwin multiplier takes advantage of the trigonometric identity  $\sin \omega t \cos \theta + \cos \omega t \sin \theta = \sin (\omega t + \theta)$ . If amplitude and phase errors exist, the expression has the form  $a \sin \omega t \cos (\theta + \phi) + b \cos \omega t \sin \theta = f(t, \theta)$ . The function  $f(t, \theta)$  may be found as follows:

$$f(t, \theta) = \left[ \sin \omega t + \frac{b \sin \theta}{a \cos (\theta + \phi)} \cos \omega t \right] a \cos (\theta + \phi)$$

let

$$\frac{b \sin \theta}{a \cos (\theta + \phi)} = \tan \psi = \frac{\sin \psi}{\cos \psi}$$

then

$$\begin{aligned} f(t, \theta) &= \left( \sin \omega t + \frac{\sin \psi}{\cos \psi} \cos \omega t \right) a \cos (\theta + \phi) \\ &= \left( \sin \omega t \cos \psi + \cos \omega t \sin \psi \right) \frac{a \cos (\theta + \phi)}{\cos \psi} \\ &= \sin (\omega t + \psi) \frac{a \cos (\theta + \phi)}{\cos \psi} \end{aligned}$$

but since  $\cos \psi$  may be written as

$$\begin{aligned} &\frac{a \cos (\theta + \phi)}{\sqrt{a^2 \cos^2 (\theta + \phi) + b^2 \sin^2 \theta}} \\ f(t, \theta) &= \sqrt{a^2 \cos^2 (\theta + \phi) + b^2 \sin^2 \theta} \sin \left[ \omega t + \tan^{-1} \frac{b \sin \theta}{a \cos (\theta + \phi)} \right] \end{aligned}$$

~~SECRET/SPECIAL HANDLING~~

~~SECRET/SPECIAL HANDLING~~

The term under the square root is the amplitude which in the ideal case is constant but now varies with  $\theta$ . Since amplitude information is discarded in the squaring (zero detection amplifier) this variation is of no consequence. The angle  $\tan^{-1} [b \sin \theta / a \cos (\theta + \phi)]$  which ideally should be simply,  $\theta$  is in error by the quantity  $\theta - \tan^{-1} [b \sin \theta / a \cos (\theta + \phi)]$ . The author has not so far been able to reduce this quantity to an intuitively manageable form, but computer plots for various values of  $a$ ,  $b$ , and  $\phi$  disclose that it varies sinusoidally at twice the frequency of  $\theta$ , i.e., the error appears to have the form  $= K \sin (2\theta + a)$  and for small errors in  $a/b \neq 1$  has a peak-to-peak amplitude of  $\phi$ .

#### 5.5.2.3.2 Wayne-George Encoder

Similarly the simple tangent relationship which is appropriate in the ideal case for the Wayne-George encoder must be modified as follows. If a nominal value of  $\theta_n$  is chosen and the ratio of resistors set at  $\tan \theta_n$ , the actual angle of the resulting wave will be a value  $\theta$  such that  $a \cos (\theta + \phi) \tan \theta_n = b \sin \theta$ . Solving this expression for  $\theta$  yields  $\theta = \tan^{-1} (a \tan \theta_n \cos \phi / b + a \tan \theta_n \sin \phi)$  and the error is  $\theta_n - \theta$ . Again this form, although easily computed, is not intuitively very instructive. If however the original expression is rewritten as

$$\theta_n = \tan^{-1} \left[ \frac{b \sin \theta}{a \cos (\theta + \phi)} \right]$$

and the error

$$\theta - \theta_n = \theta - \tan^{-1} \left[ \frac{b \sin \theta}{a \cos (\theta + \phi)} \right]$$

the form is seen to be identical to that of the Baldwin encoder error except that the quantity  $\theta$  is a dependant variable and must be calculated from an explicit expression in  $\theta_n$  and  $\phi$ . The magnitude and frequencies are identical in the two cases and the actual error curves differ only by a small constant angle. (Note: at an earlier discussion of this point a curve was shown which purported to show approximately a factor of two difference in the two methods. This difference proved to be due to a computation error).

#### 5.5.2.4 Error Spectrum of Wayne-George Encoder

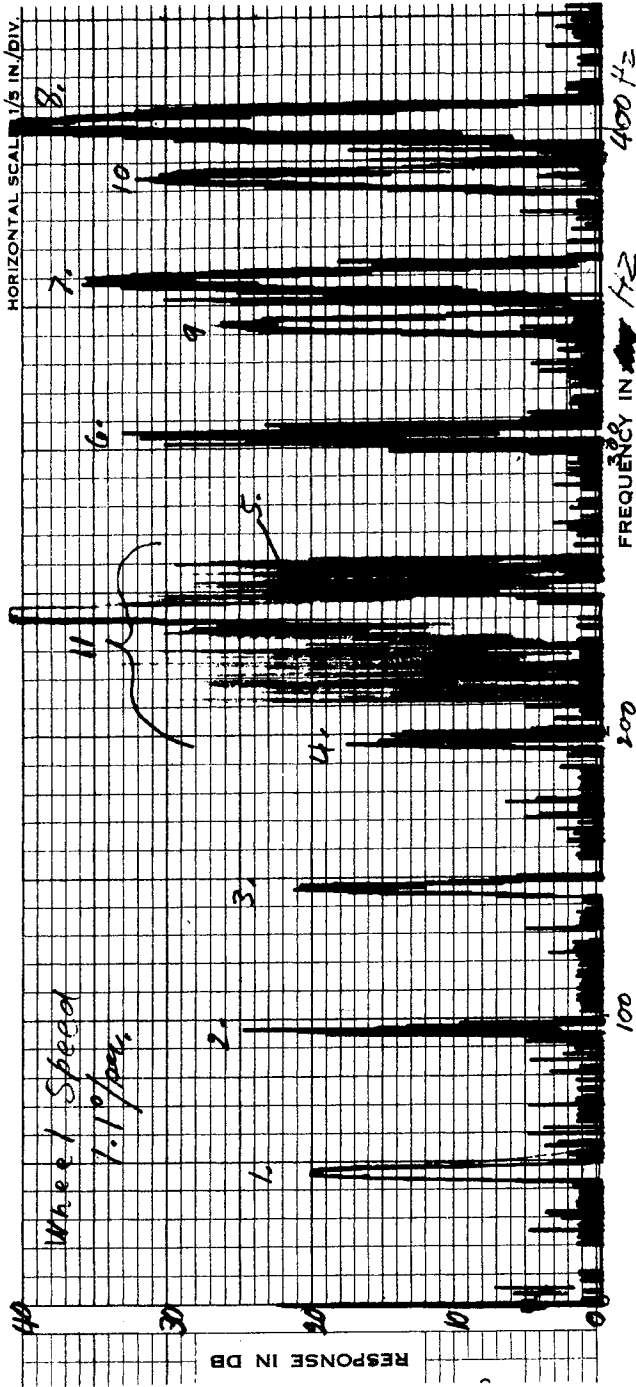
Analysis of data obtained by the discriminator and wave analyzer (5.5.1.2.1) disclosed essentially a line spectrum (see Fig. 5.5-2) i.e., the encoder output signal contained a series of discrete frequencies consisting of the frequency of the outermost optical track and all its multiples. Those signals were 20 to 40 decibels above the random components and were clearly going to be the principle source of error torques in any servoloop using such an encoder as the rate feedback device. Subsequent computer analysis of bit-length data obtained from visicorder traces (5.5.1.2.2) has repeatedly confirmed the line nature of the noise spectrum.

##### 5.5.2.4.1 Multiplier Errors

One of these error frequencies, namely that at twice the optical track frequency, can be accounted for, as was shown above, assuming a perfect multiplier but errors in phase and or magnitude in the sine and cosine signals. The other frequencies, however, must be ascribed to errors in the multiplier itself, e.g., sampling ratio or detecting errors. Consider a hypothetical (but possible) case of a multiplier which divides the optical track spacing into 16 parts, i.e., a times 16 multiplier, with errors in ratios and zero crossing such that 15 of the 16 bits are all

~~SECRET/SPECIAL HANDLING~~

~~SECRET/SPECIAL HANDLING~~



Wave Analysis Trace

- Peak nos. 1 - 8 - 30 db = 3 V R M S
- Peak nos. 9 - 10 - 30 db = 10 V R M S
- Peak no. 11 - 30 db = 0.1 V R M S
- Peak no. 9 is same frequency as no. 7 ) frequency recalibration
- Peak no. 10 is same frequency as no. 8 )
- Peak no. 1 is 2<sup>1.5</sup> fit frequency
- Peak no. 8 is 2<sup>1.8</sup> fit frequency

Fig. 5.5-2 — Wave trace analysis

~~SECRET/SPECIAL HANDLING~~

~~SECRET/SPECIAL HANDLING~~

the same lengths but a little too short and the 16th bit a little too long. The error curve of such a multiplier would show a single pulse of angular duration 1/16 of the optical cycle and repeated once per cycle. The spectrum of a repetitive short pulse is given by:

$$y = Ak + \frac{2A}{\pi} \left( \sin k\pi \cos x + \frac{1}{2} \sin 2k\pi \cos 2x \right. \\ \left. + \frac{1}{3} \sin 3k\pi \cos 3x + \dots + \frac{1}{n} \sin nk\pi \cos nx \right)$$

where  $y$  = the complex signal amplitude

$2\pi k$  = the width of the pulse (i.e.,  $k$  = the fraction of a cycle occupied by the pulse)

$A$  = the pulse amplitude

For an  $2^{18}$  bit encoder and the situation described above, an error of 1 percent of the optical cycle in one of the 16 bits would yield errors at the optical frequency of 0.033 arc-seconds rms at the second harmonic of 0.032, at the third of 0.030 etc. Of course the typical multiplier will not in general present such a simple picture. Bit lengths will vary due to combinations of the various sources of error. All sources of error, however, result in error components at the same frequencies but at various phases and amplitudes. It was reasoned that with a given set of ratio and zero crossing errors it should be possible by adjusting the relative amplitudes and zero crossings of the sine and cosine signals, to minimize a given error frequency at the expense of increasing others. This was verified experimentally as inspection of Figs. 5.5-3 and 5.5-4 shows. Figs. 5.5-5 and 5.5-6 show the improvement obtained with electronics characterized by smaller ratio and zero detection errors. Still further improvement is anticipated particularly in accuracy of zero detection.

#### 5.5.2.4.2 Disc Errors

Fig. 5.5-7 shows a recording of the frequency, viz, twice that of the outermost optical track which, as discussed above, would be present even with a perfect multiplier if phase and/or amplitude errors were present in the sine and cosine signals. In this case, the multiplier is not perfect and there is a component at this frequency due to this imperfection. Variations in the signal, however, must be due to changes in the sine-cosine errors as a function of wheel position. It is noteworthy that both the error signals themselves and the variations in them as a function of wheel position are by no means random. The magnitude of this error signal is clearly periodic at the frequencies of the various more significant digit tracks. Particularly obvious are the periods of the  $2^4$ ,  $2^5$ ,  $2^6$ ,  $2^7$ , and  $2^8$  tracks. Periods longer than that of the  $2^4$  track can be detected by close inspection. In addition to the binary tracks there appears to be a 60-degree period presumably due to the use of a six sided optical polygon at some point in the history of the disc generation procedure.

This periodicity occurs because of the conventional method of generating a binary disc, namely by successive division. Errors in division at the more significant digit tracks when subdivided are propagated out to the less significant digit tracks.

Periodicity of order higher than  $2^8$  bits per revolution do not appear to be significant. Presumably this comes about from the Wayne-George method of disc fabrication which is to step and repeat a wedge of 64 lines (128 bits)  $2^8$  times around the disc. The 64 line wedge appears to be virtually free of cyclic errors.

~~SECRET/SPECIAL HANDLING~~

~~SECRET/SPECIAL HANDLING~~

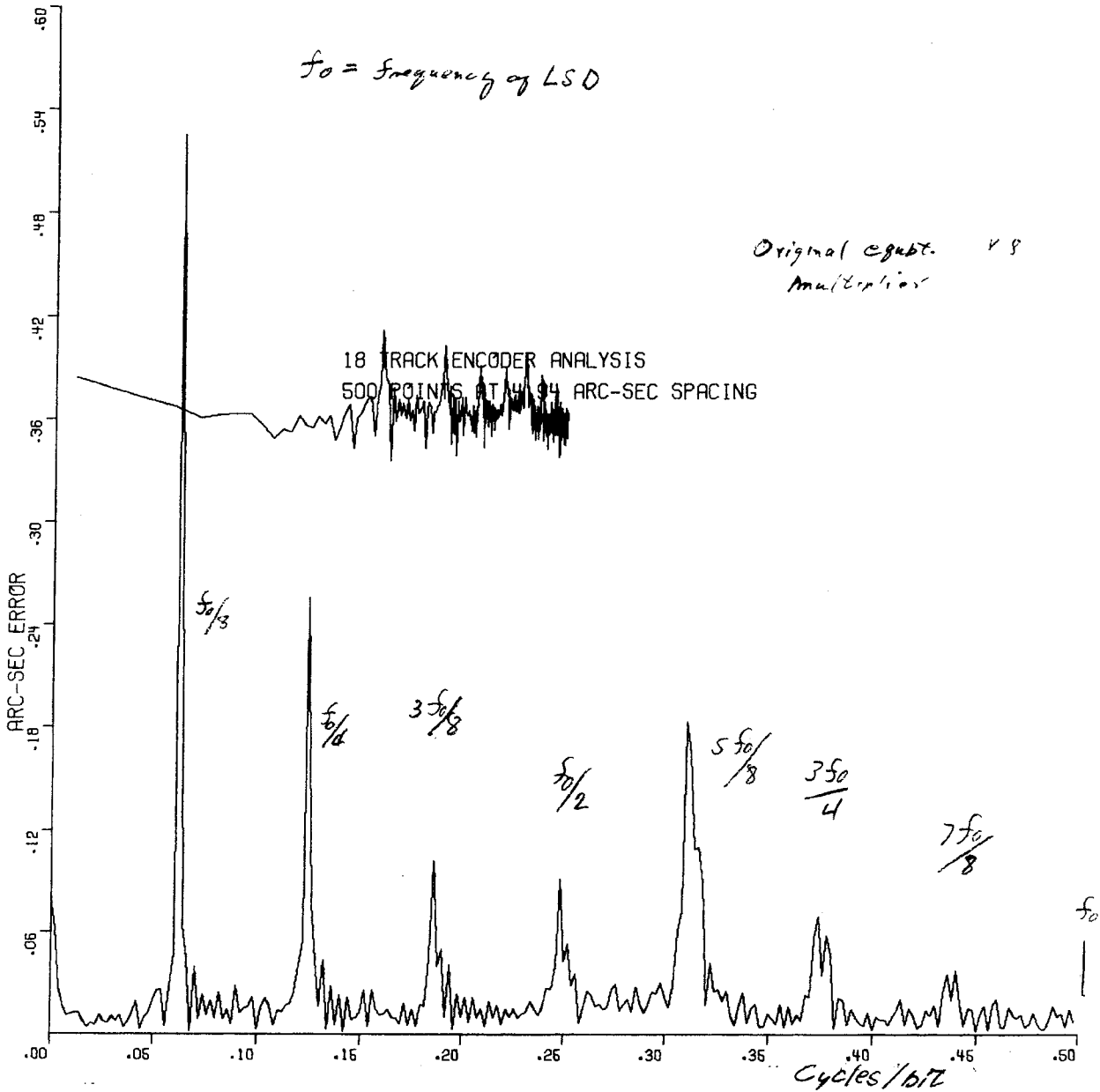


Fig. 5.5-3 — 18-track encoder analysis

~~SECRET/SPECIAL HANDLING~~

~~SECRET/SPECIAL HANDLING~~

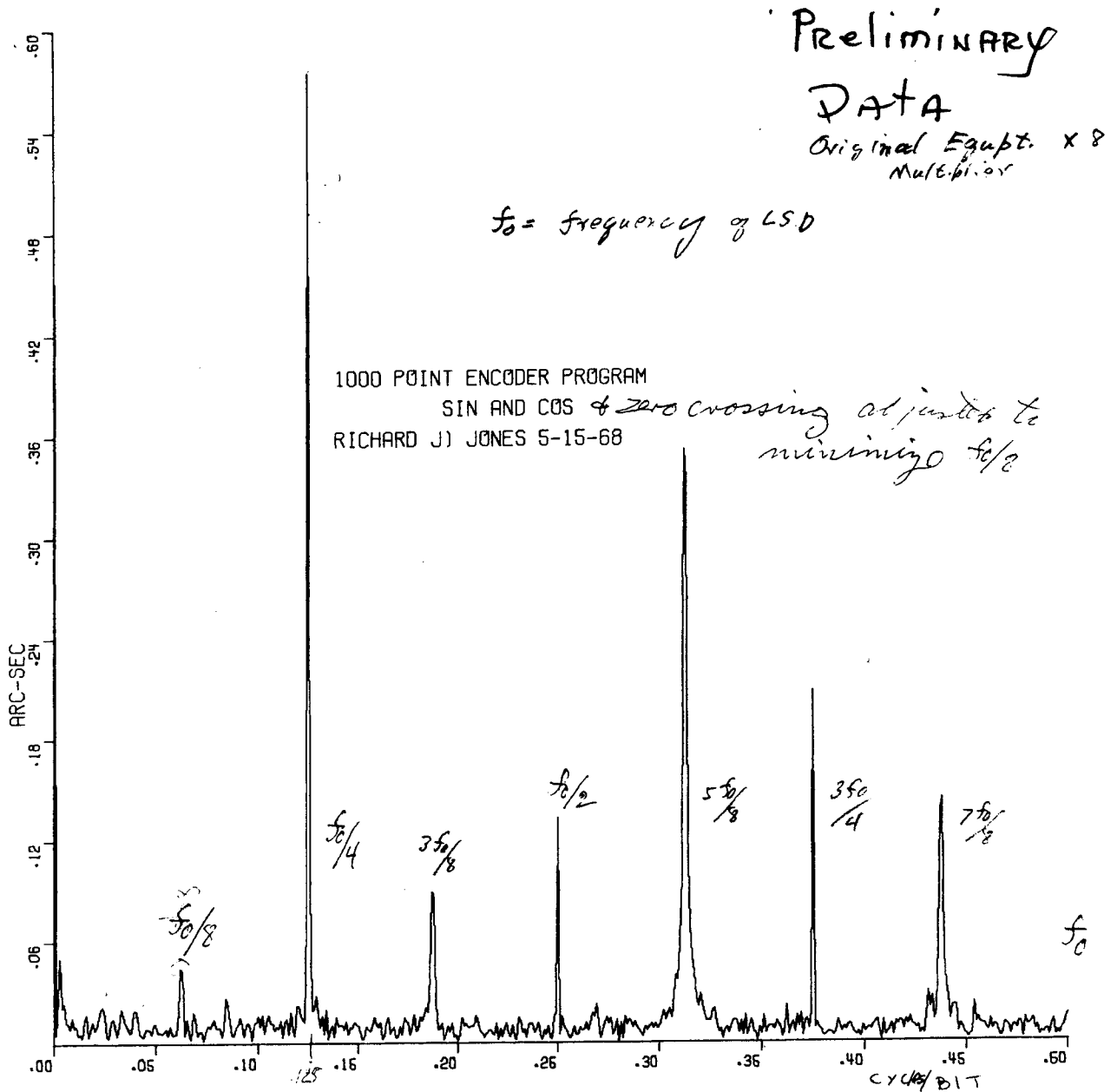


Fig. 5.5-4 — 1,000-point encoder program

~~SECRET/SPECIAL HANDLING~~

~~SECRET/SPECIAL HANDLING~~

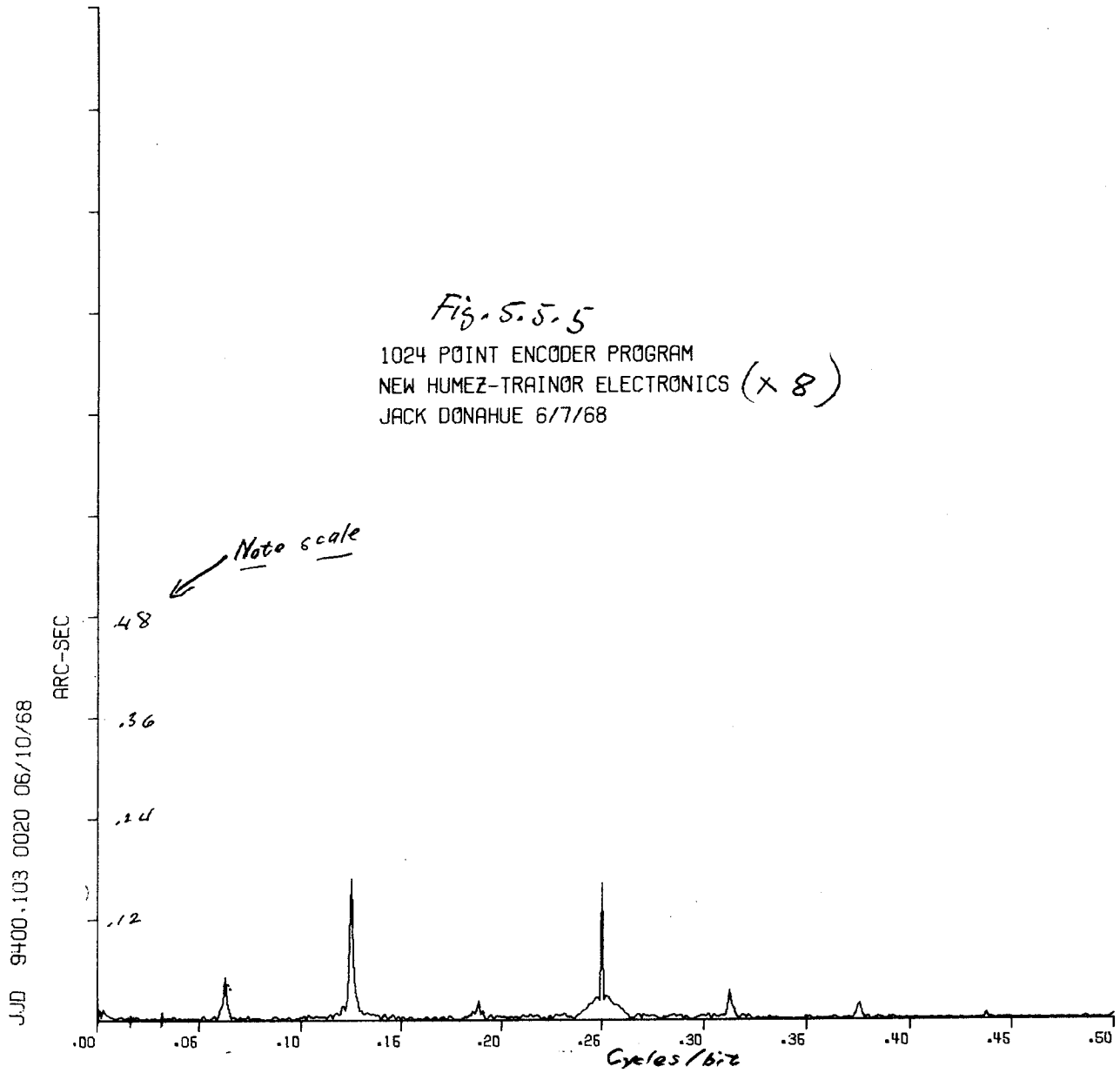
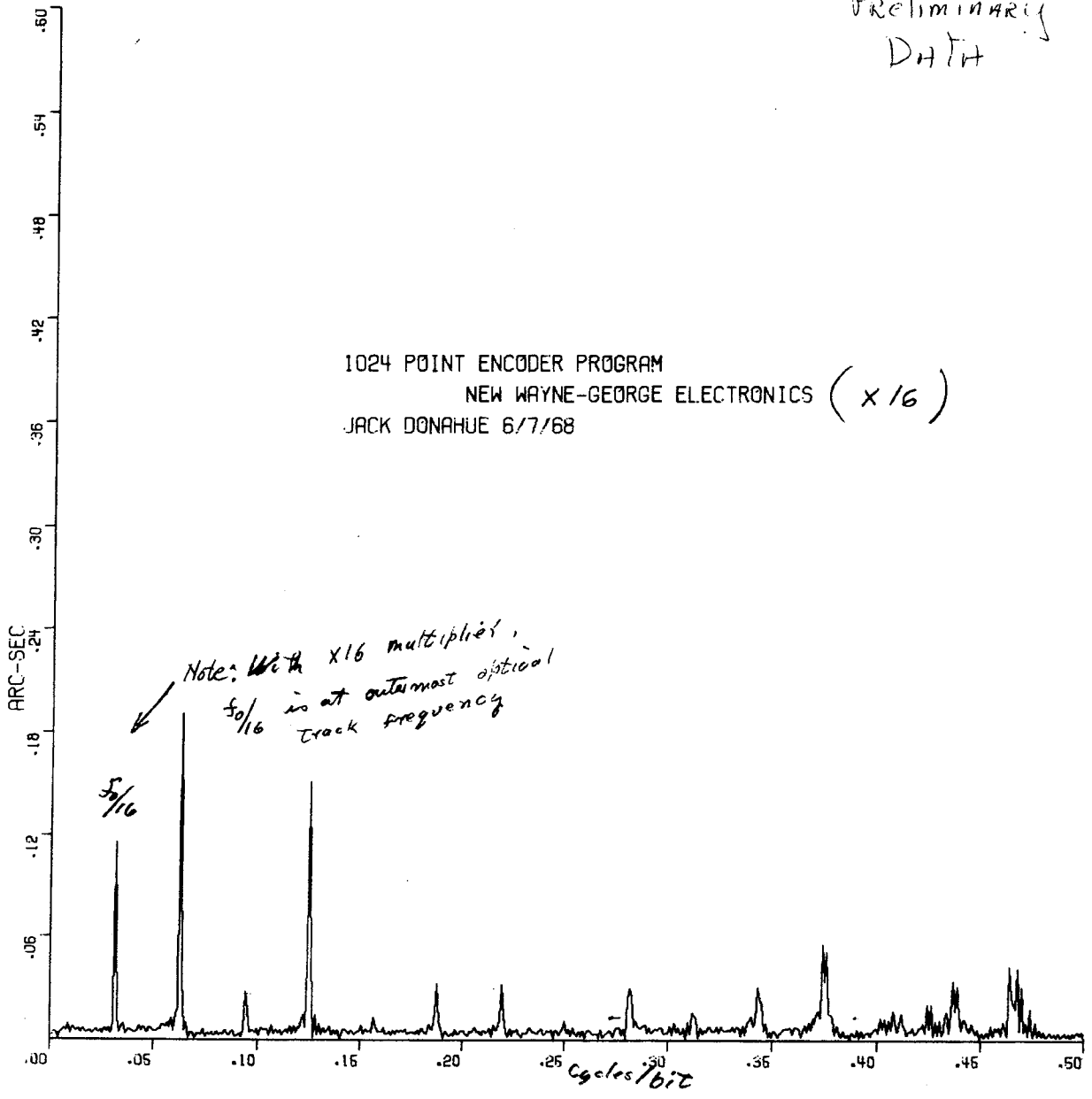


Fig. 5.5-5 — 1,024-point encoder program (x 8)

~~SECRET/SPECIAL HANDLING~~

~~SECRET/SPECIAL HANDLING~~

Preliminary  
DATA

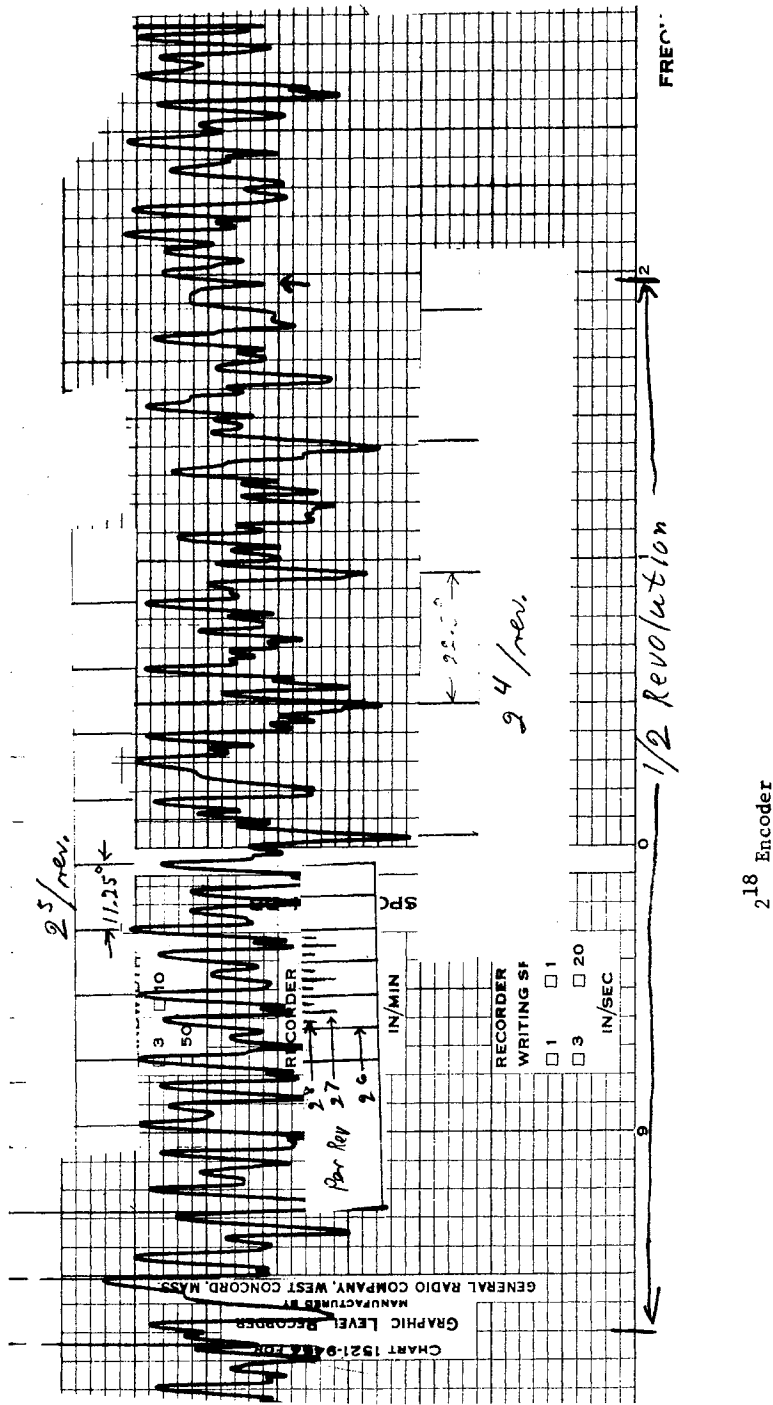


1024 POINT ENCODER PROGRAM  
NEW WAYNE-GEORGE ELECTRONICS (X16)  
JACK DONAHUE 6/7/68

Fig. 5.5-6 — 1,024-point encoder program (x16)

~~SECRET/SPECIAL HANDLING~~

~~SECRET/SPECIAL HANDLING~~



Error Frequency Vs. Wheel Position  $f =$  twice that of outermost Optical Track

Fig. 5.5-7 — Error frequency versus wheel position

~~SECRET/SPECIAL HANDLING~~

~~SECRET/SPECIAL HANDLING~~

Improvements in master discs have been made since this disc was fabricated and it is anticipated that disc imperfections will be a factor of four or more smaller than those observed.

It was mentioned in the experimental section that error information at frequencies lower than the bandwidth of the servoloop would not be lost. It will now be seen that because of the finite separation of the sine and cosine read stations, any optical spatial frequency variation will be disclosed by the resulting phase error as a change in the appropriate error frequency amplitude.

#### 5.5.2.5 Projected Analytical Procedures

In addition to continuation of computer analysis of bit length data, a program will be developed to simulate performance of an encoder with predetermined sine-cosine and multiplier errors in order to establish design parameter tolerance budgets. Such a program will assist the encoder designer to achieve optimum performance at minimum cost and will serve to predict performance as a function of component aging and/or unfavorable environments notably temperature variation.

#### 5.5.3 Encoder Specification

It is abundantly demonstrated that the error spectrum of the encoder tested is essentially a line spectrum and that the amplitudes of these lines vary periodically. Document EC 331 paragraph 3.1.1.1.9 subparagraph b specified that the random components of the error spectrum be expressed as a power spectral density plot and that a certain envelope not be exceeded. Interpreted literally, this specification could easily be met by present day encoders in which random errors are typically very small but in which disasterously large periodic errors could exist.

A solution to this difficulty has been suggested by the customer's engineering personnel and consists of specifying that the noise spectrum be attenuated by a filter which reflects the sensitivity of the servo system to error torques and a limit placed upon the root sum square of the error components so attenuated.

It is strongly urged that the specification be revised as suggested above to take properly into account the line nature of the error spectrum.

EC 331 paragraph 3.1.1.1.9 also specifies that the error spectrum requirements must be met not only at scanning rates, at which the smoothest performance possible is essential but also at slewing rates at which maintaining the same stringent requirements is not needed and may be unrealizable because of large angle errors which, though within the mean error limit, generate periodic errors in excess of those characteristic of the small angles over which tracking is required.

A number of minor specification points need to be resolved and, it is hoped, will be completed in the immediate future. The points mentioned above, however, are of major conceptual importance and urgently require action.

~~SECRET/SPECIAL HANDLING~~

~~SECRET~~/SPECIAL HANDLING

## 6. MAJOR COMPONENT SELECTION AND DESIGN

### 6.1 BEARINGS

#### 6.1.1 Summary of Bearing Problem

The requirement for total torque variation is defined in Fig. 3 of Specification EC-331B. This figure, in effect, shows an envelope of allowable torque ripple with frequency of occurrence in radians per second for each axis. The envelope or curve is to be applied to the total torque ripple of all disturbances on each axis, bearings and cable. Physically then, bearings are required that rotate smoothly enough so that the mirror does not jitter significantly when it rotates about either the roll or pitch axis. Since tracking of the scanner is controlled by a closed loop, the servo will be able to filter out much of the jitter, particularly that which is very low frequency. Similarly, high frequency ripple disturbances will not be present at the mirror surface as jitter because of the inertia involved. For this reason, low torque ripple requirements only apply between certain frequencies and as reflected in Fig. 3 of Specification EC-331B these lie 0.01 to 100 radians per second. Below and above these frequencies, ripple is of less interest.

The ripple is, of course, a torque disturbance or change of magnitude; but for the purposes of the Contractor's error budget, the specification was written as PSD (power spectral density), or the actual frequency density of power in the ripple. The total power in the ripple is the integral of the power spectrum over the frequencies involved or the area under the curve of Fig. 3 of the specification. This is mathematically equivalent to the rms value of bearing torque ripple. More detailed discussion of PSD is included in Section 5.2 of this report.

The specification curve, Fig. 3 mentioned before, is the total allowable PSD for each scanner axis. This total PSD must be allocated to the various contributors on each axis, namely, the three pairs of bearings, and the cabling. The PSD allocation is detailed in Section 5.3 of this report.

In addition to the PSD requirements, there is a maximum allowable running torque of 2 inches on each axis, which must also be allocated between each pair of bearings and the cables. This allocation is detailed in Section 5.4.

The scope of the bearing problem includes maintaining PSD performance after initial assembly within the specification, under operating environmental conditions. Factors for PSD degradation due to environmental conditions have been reflected into the PSD budget.

#### 6.1.2 Desired Bearing Characteristics

The bearings must be capable of supporting the loads imposed on them during storage, handling, and launch and still meet PSD, torque and operational specifications. These include not only rotational freedom but adequate positional control of the rotating components after being subjected to the above conditions. The geometry and materials of the bearings must be compatible with size and weight limitations and environmental conditions.

~~SECRET~~/SPECIAL HANDLING

~~SECRET~~/SPECIAL HANDLING

Many parameters must be considered to meet all the requirements, among them are axial and radial stiffnesses, type and size of bearing, class or precision, preload, contact angle, mounting arrangement, ball separator type and material, lubricant and retention method, raceway topography, curvature relationships or conformity of balls to raceways, dirt exclusion devices, brinelling effects during launch condition, and provision for thermal changes. All these factors have a direct relation to PSD and torque values. Many of these factors can be examined very minutely, such as raceway topography. This is probably one of the most important factors influencing torque ripple. The raceway finish, direction of grain, smoothness, waviness, and lobing all go to make up this one factor of topography essential to low PSD attainment.

Lobing is a periodic out of roundness of the raceway occurring at a number of points around the circumference. It is typical in a quality bearing. The machines used to grind raceways, although precision-made for the tool industry, have chatter, instabilities, non-rigidities, etc. which cause lobing. Special machines can be built to eliminate such lobing, but the resulting disturbances are felt to be of a low frequency and not serious. Fafnir Bearing Co. has indicated that in a bearing the size of 2MM9108, 16 point and other lobing may occur. Sixteen point lobing is referred to the lowest frequency and its peak to trough amplitude is expected to be 20 micro-inches or so in a 9108 or 9105 size. Out of roundness is in reality a form of low number of point lobing, and Fafnir indicates that a 200 microinch amplitude for 2 or 3 point out of roundness is state of the art for this bearing size. This information has been roughly corroborated by information from the Contractor.

Waviness consists of peaks and valleys, spaced at a distance sufficient so to promote torque ripple of possible disturbing frequencies. The critical distance is dependent on the number of balls, their contact area with the raceway, and more particularly, the dimension of the minor axis of the contact ellipse. Waviness and lobing both show up on a talyround trace that can be supplied with each bearing.

During ball rolling in the raceways, the ball and race are in intimate contact, with the ball rolling as an ellipse. The size of the elliptical foot-print (related to ball size, raceway conformity, and load) and its orientation (related to contact angle) will determine ball skidding or slip, all related to PSD. Ball separator or retainer, its coefficient of friction, oil absorption quality, geometric design and dimensional control may all influence torque disturbances.

Some of the desirable characteristics unfortunately do not go hand in hand with other. For example, stiffness which is required to fulfill important dynamic and structural considerations, increases ball loading on the raceways, with a resultant increase in torque and PSD. This required a compromise or tradeoff to keep the preload light yet meet dynamic requirements. Also, during thermal excursion, it is important that the bearing pair not be unloaded from its initial preload, or positional control is lost—some ball loading is required at the expense of PSD.

Dirt is a direct contribution to low torque ripple, and conversely, cleanliness is the essence of smooth bearing performance. Other factors affecting PSD include ball load and rotational speed. Mounting misalignments, cocking of the bearings and the previously mentioned isothermal or adiabatic temperature changes may increase ball loads and PSD. Some test data show that PSD increases with rotational speed.

Section 6.1.8 presents a preliminary specification for the procurement of Engineering model bearings which describe in detail how parameters affecting PSD and torque performance will be controlled.

~~SECRET~~/SPECIAL HANDLING

~~SECRET~~/SPECIAL HANDLING

### 6.1.3 Bearing Sizing and Preload Requirements

During operation, the only loads imposed on the bearings are those caused by built-in preloads, cocking and misalignment, and/or the torque motor side loads (on the order of ounces) due to stator and rotor eccentricities. The bearings must nevertheless be sized to ensure that the raceway topography is not changed or damaged by shock and random vibration loads encountered during launch.

The bearing loads anticipated during launch were determined from a dynamic excitation that includes shock, random vibration, and steady state accelerations, but which excludes acoustic noise. Earlier bearing compliances were calculated for a 10 pound preload. The aft bearing on the roll axis was assumed to have no thrust carrying capability. The loads have been recalculated in an updated, more detailed dynamic analysis recently. The new loads are far lighter than the originals.

Although the bearings will be statically loaded during launch, selection as to size and load cannot be based directly on bearing manufacturers' static load ratings (capacity). A derating to approximately 30 of the rated static capacity is necessary to avoid micro-brinelling of the raceway. The catalog ratings allow a brinell mark of 0.0001 times the ball diameter, to which the AFBMA has agreed. For smooth running, slow speed bearings, this criteria cannot be used, since even disturbances this small would result in an increase of PSD. Extensive literature investigation has revealed that a derating to 30 is recommended for smooth performance as a practical value although theoretically only 3 should be used. The Contractor has performed tests in which stress levels equivalent to 30 of rating have been induced on his bearings. These tests have indicated no signs of brinelling. Plans are underway to repeat this type of test for the bearing in the scanner. Although theory predicts micro-brinell marks at exceedingly small loads, Contractor tests with single balls on flat plates have failed to produce such measureable marks.

Since the Contractor bearing selections are derived from the wealth of test data and results, theoretical predictions, and literature surveys, none of which we have the time or funding to duplicate, and since the information was transmitted to us to take advantage therefrom, plan to apply the information to this bearing program and then verify the results by our own testing. Itek plans to verify its bearing selection criteria with data generated by the Contractor as a result of his extensive bearing development program. To assure full continuity to the overall system, the Contractor will also perform bearing tests for Itek as required. The final selection of scanner bearings is shown in Table 6.1-1, Scanner Bearing Summary. The static load ratings, actual dynamic loads and percentages of static loads used on the bearings are shown on Table 6.1-2 for original loads and Table 6.1-3 for latest loads.

Note that the thrust loading on the pitch axis torquer end changed because of a design change. All capacities and loads are per bearing, not per bearing pair. In the case of radial loads it is assumed that both members of the pair share the load equally; in the case of a thrust load, one member takes all the load.

Table 6.1-3 shows that in most cases far less than 30 percent of the bearing capacity is used and this is because in these cases, the bearings were sized according to the necessary shaft sizes. The shafts must be minimum sizes for structural, dynamic and transmissibility reasons, and if the bearing with the required bore appears to be oversized relative to its percent load it is because of shaft stiffness requirements. Thus the final selection of the bearings were arrived at as shown in Table 6.1-1.

In all cases the bearings are sufficiently stiff to satisfy dynamic requirements of the bearing itself, hence light preloads on all bearings were adequate without unloading during expected

~~SECRET~~/SPECIAL HANDLING

~~SECRET/SPECIAL HANDLING~~

Table 6.1-1 — Scanner Bearing Summary

	ROLL AXIS FORWARD	ROLL AXIS REAR	ROLL AXIS ENCODER	PITCH AXIS ENCODER END	PITCH AXIS, TORQUER END	PITCH AXIS
Bearing Manufacturer Type Number	FAFNIR 2MM 9108WO CR FS-130	FAFNIR 2MM9105WO- CR FS-130	SBB CO. 3TA0 29-36	SBB CO. 3TA0 14-21	SBB CO. 3TA0 21-28	SBB CO. 3TA020-36
Race & Ball Material	CEVM 440C	CEVM 440C	CEVM 440C DB, used with 1/2 lg. spacer	CEVM 440C	CEVM 440C	CEVM440C
Type of Mount	DF	DF	DF	DF	DF	DB
Preload	20 lbs.	10 lbs.	10 lbs.	10 lbs.	10 lbs.	10 lbs.
Retainer	One piece paper base Phenolic	One piece paper base Phenolic	Toroids	Toroids	Toroids	Toroids
Lubrication	G.E. F-50 Versilube Stripped					
Inside Diameter	1.5748	.9843	1.8125	.8750	1.3125	1.8125
Outside Diameter	2.6772	1.8504	2.2500	1.3125	1.7500	2.2500
Outside Race Diameter	2.4385	1.6674	2.147	1.218	1.656	2.147
Inside Race Diameter	1.8135	1.1674	1.897	.968	1.406	1.897
Pitch Diameter	2.1260	1.4174	2.031	1.093	1.531	2.031
Ball Quantity	16	13	38	20	28	38
Ball Diameter	.3125	.250	.125	.125	.125	.125
Contact Angle	15°	15°	15°	15°	15°	15°
Conformity Inner Race $r_1/d$	.52	.52	.525	.525	.525	.524
Conformity Outer Race $r_o/d$	.52	.52	.525	.525	.525	.525
Axial Dimension Between Balls of Bearings	.591	.472	.500	.250	.250	.290
Stiffness of Pair - Axial (lbs./in.)	$2.58 \times 10^5$	TBD	$2.55 \times 10^5$	$1.77 \times 10^5$	$2.14 \times 10^5$	$2.4 \times 10^5$
Stiffness of Pair - Radial (lbs./in.)	$1.50 \times 10^6$	TBD	$1.48 \times 10^6$	$.954 \times 10^6$	$1.20 \times 10^6$	$1.48 \times 10^6$
Stiffness of Pair Rotational (in.lbs/rad) Resistance to Overturning Moment						
Static Radial Capacity ( $C_o$ ) per Single Bearing	2680 lbs.	1396 lbs.	1000 lbs.	488 lbs.	716 lbs.	1000 lbs.
Static Thrust Capacity ( $T_o$ ) per Single Bearing	2870 lbs.	1492 lbs.	1850 lbs.	980 lbs.	1360 lbs.	1850 lbs.
ABEC # Designation	ABEC-9	ABEC-9	ABEC-7T	ABEC-7T	ABEC-7T	ABEC-7T
Race Finish	✓	✓	✓	✓	✓	✓
Ball Grade	5	5	5	5	5	5

~~SECRET~~/SPECIAL HANDLING

Table 6.1-2 — Bearing Loads, Original

ITEM	DESCRIPTION	ROLL AXIS FORWARD FAPNIR 2MM 9108 CR FS-130	ROLL AXIS REAR FAPNIR 2MM 9105 WC-CR FS-110	PITCH AXIS ENCODER SND SBB CO. 3740 14-21	PITCH AXIS TORQUE AND SBB CO. 3740 21-28
1	STATIC RADIAL LOAD CAPACITY PER SINGLE BEARING (LBS)	LBS. 2680	LBS 1396	LBS. 488	LBS. 716
2	STATIC THRUST CAPACITY PER SINGLE BEARING	2870	1510	980	1360
* 3	RADIAL LOADS DUE TO DYNAMIC ENVIRONMENT	650	425	125	125
* 4	THRUST LOADS DUE TO DYNAMIC ENVIRONMENT	900	0	225	250
5	RADIAL LOADING % OF STATIC CATALOG CAPACITY	$\frac{650}{2680} = 24\%$	$\frac{425}{1396} = 30\%$	$\frac{125}{488} = 26\%$	$\frac{125}{716} = 18\%$
6	THRUST LOADING % OF STATIC CATALOG CAPACITY	$\frac{900}{2870} = 31\%$	$\frac{0}{1492} = 0\%$	$\frac{225}{980} = 23\%$	$\frac{250}{1360} = 18.5\%$

\* ITEM 3 & 4 THESE LOADS WERE PRELIMINARY  
REF. 142170 349-67-418 : AUG 1967

~~SECRET~~/SPECIAL HANDLING

Table 6.1-3 — Bearing Loads, Latest

ITEM	DESCRIPTION	ROLL AXIS	ROLL AXIS	PITCH AXIS	PITCH AXIS
		FORWARD FAENIR DINA DINA WD DR. FC. 14	REAR FAENIR DINA DINA W	EMGOLA E 140 SFB 00 P. 140 14 0	TOR. 140 140 SER. 00 P. 140 14 0
1	RADIAL LOADS DUE TO DYNAMIC ENVIRONMENT	562.5 POUNDS	356.5 POUNDS	103.5 POUNDS	103.5 POUNDS
2	THRUSTS LOADS DUE TO DYNAMIC ENVIRONMENT	408.7 POUNDS	0	250. POUNDS	0
3	RADIAL LOADING % OF STATIC CATALOG CAPACITY	$\frac{562.5}{2680} = 21\%$	$\frac{356.5}{1396} = 26\%$	$\frac{103.5}{488} = 21\%$	$\frac{103.5}{716} = 15\%$
4	THRUST LOADING % OF STATIC CATALOG CAPACITY	$\frac{408.7}{2930} = 14\%$	$\frac{0}{1492} = 0\%$	$\frac{250}{950} = 26\%$	$\frac{0}{1360} = 0\%$

~~SECRET~~/SPECIAL HANDLING

temperature excursions. It may be that further work will also show that we can go to somewhat lighter preloads in the final selection of bearings but there is some degree of uncertainty in the pre-load deflection curves at very light preloads.

6.1.4 Bearing Analysis

Thermal, environmental, alignment, and other parameters will affect bearing performance in the assembled AO scanner. Bearing stiffnesses (compliances) and therefore scanner structural dynamic characteristics will vary with temperature excursions. Similarly, bearing ball loads will change due to thermal effects and cocking or misalignment problems, and with a change in ball loading will inevitably come a change in torque, torque ripple, and PSD.

Analytical tools are available for calculating these effects. They are elucidated in "Analysis of Stresses and Deflections," by A. B. Jones "Rolling Bearing Analysis," by T. Harris, and other works. Computer programs have been written which make the equations in these works tenable in terms of engineering usefulness. Accordingly, the consulting engineering firm of Jones and Harris of Newington, Connecticut was engaged to analytically explore these environmental effects in our scanner bearings. They are the authors of many books on rolling element bearings and have also written computer programs which they used in our analyses.

Fig. 6.1-1 through 6.1-12 following, show the results of their computations. All results are for the preloaded bearing pairs elucidated in Table 6-1-1. Some of the parameters of Fig. 6.1-12 make a big difference in a bearing performance, and therefore great care should be taken in trying to extrapolate these results to bearings that do not have the exact properties of those of Fig. 6-12. For example, contact angles other than 15 degrees give the bearings widely different radial and axial stiffnesses than those shown in Fig. 6.1-1 and 6.1-2 and change the thermal and cocking effects too. Furthermore, ball bearings being what they are, many of the effects calculated are non-linear, so extrapolation of, for example, the thermal results to bearings of the same geometry but different preloads is not permitted. Extrapolation of any data from a 9104 bearing to, for example, a 9105 is risky too. In the event of any bearing changes from what is shown in Fig. 6.1-12, it would be a simple matter to have Jones rerun the program for the new data.

The first effect explored was the change in axial and radial stiffness with preload. The results are shown in Fig. 6.1-1 and 6.1-2. The stiffnesses shown for the 2MM9108 at 20 pounds preload and all the other bearings at 10 pounds preload are the ones used in the dynamic analysis of the scanner. These stiffnesses are the reciprocal of the compliances normally used in bearing work. The compliances of our bearings will not correlate with the manufacturer's catalog compliances for the same size bearings because the contact angles are different.

As the scanner undergoes temperature excursions to different temperatures from those at which it was assembled, bearing characteristics will change. If it gets colder, the beryllium housing will tend to shrink the outer race more than the race would shrink by itself because of beryllium's higher coefficient of expansion. The beryllium shaft will shrink away from the inner race and thus have no effect. This extra outer race compression will have a net effect of "squashing" the balls, increasing effective preload. In case of heating, extra expansion of the inner race due to expansion of the beryllium shaft (while the housing expands away from the outer race) will have a similar net effect of ball "squash" and increased preload. These isothermal (i.e., bearing inner race, outer race, and housing are all at the same temperature, but it is a different temperature than the one at which the scanner was assembled) effects are plotted in Fig. 6.1-3. The isothermal temperature change is the change from assembly to flight. These curves are for our bearings starting at our preloads. If we desired to know the preload change

~~SECRET~~/SPECIAL HANDLING

~~SECRET~~/SPECIAL HANDLING

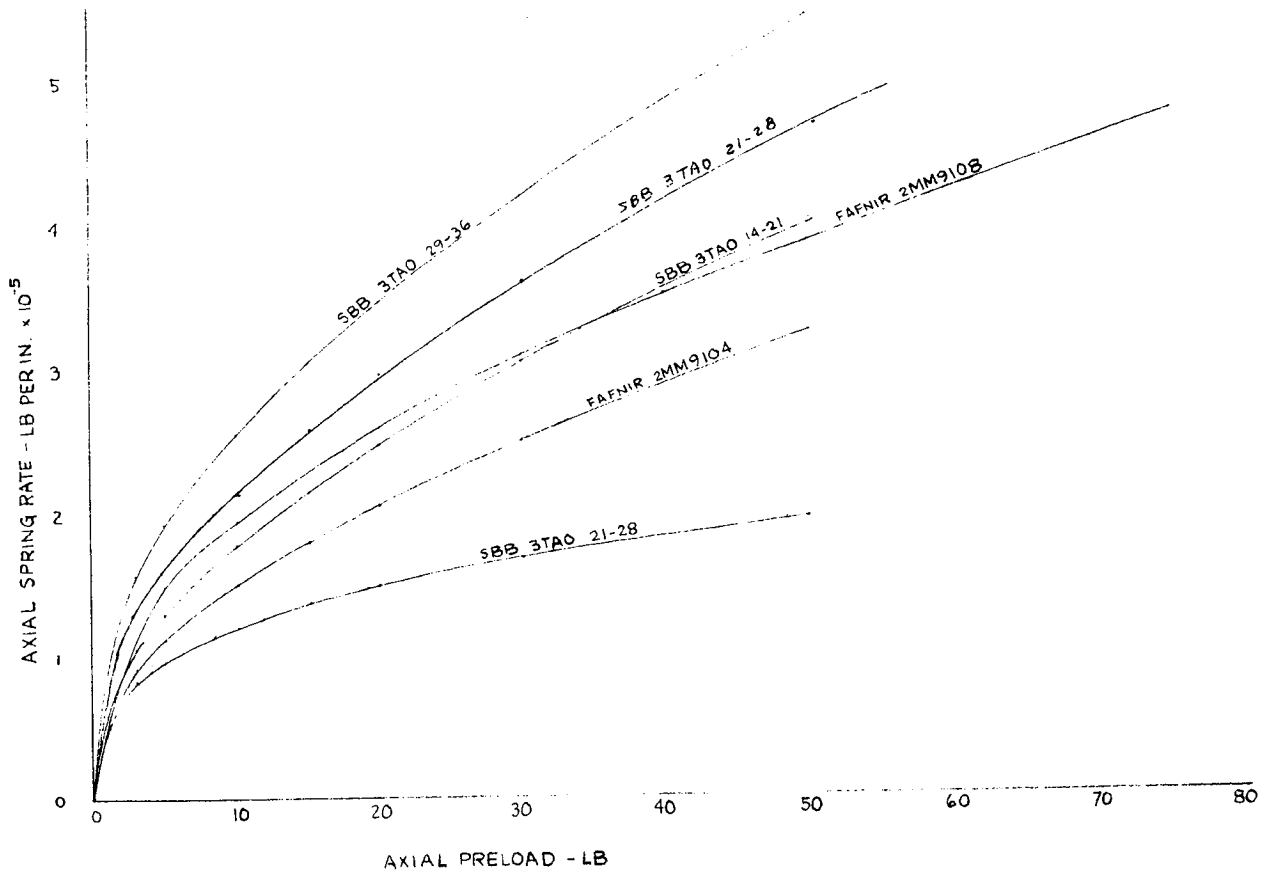


Fig. 6.1-1 — Axial spring rate versus preload

~~SECRET~~/SPECIAL HANDLING

~~SECRET~~/SPECIAL HANDLING

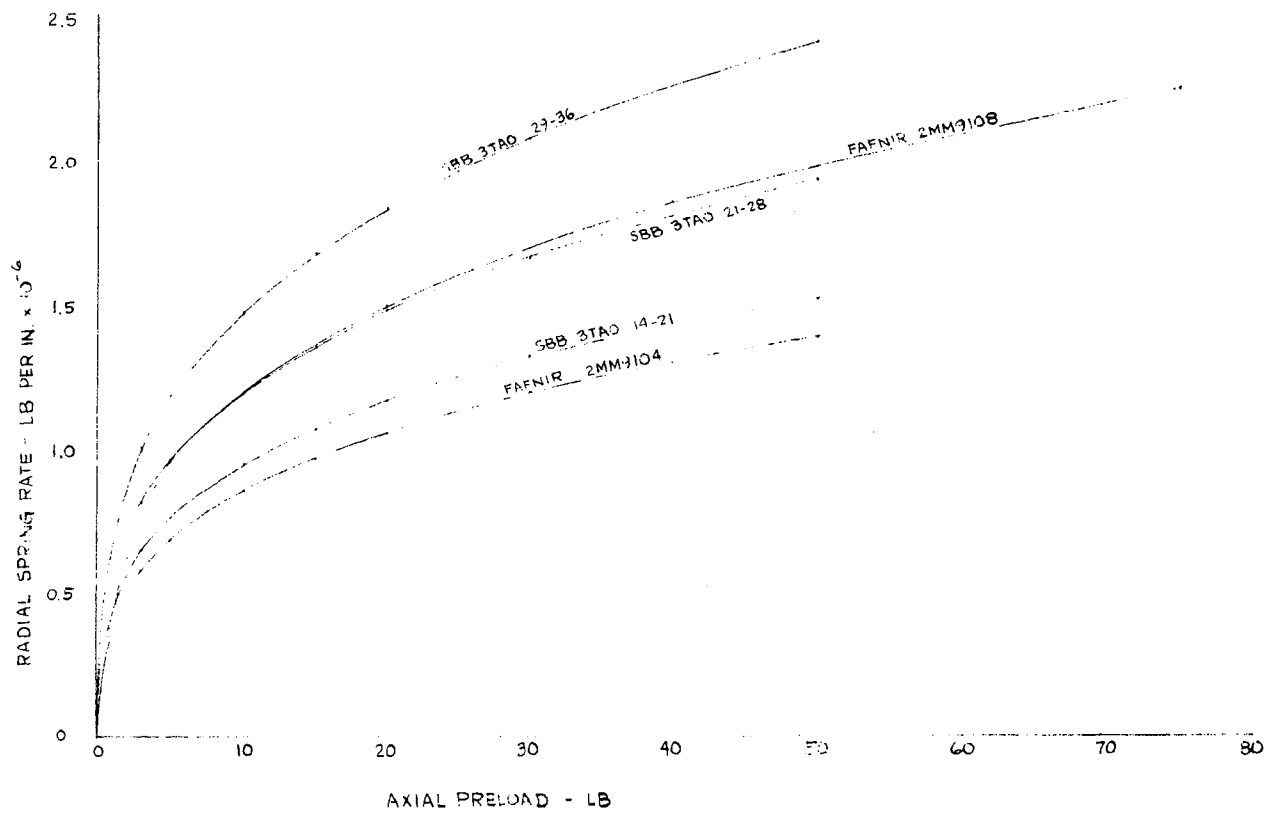


Fig. 6.1-2 — Radial spring rate versus preload

~~SECRET~~/SPECIAL HANDLING  
6.1-9



~~SECRET/SPECIAL HANDLING~~

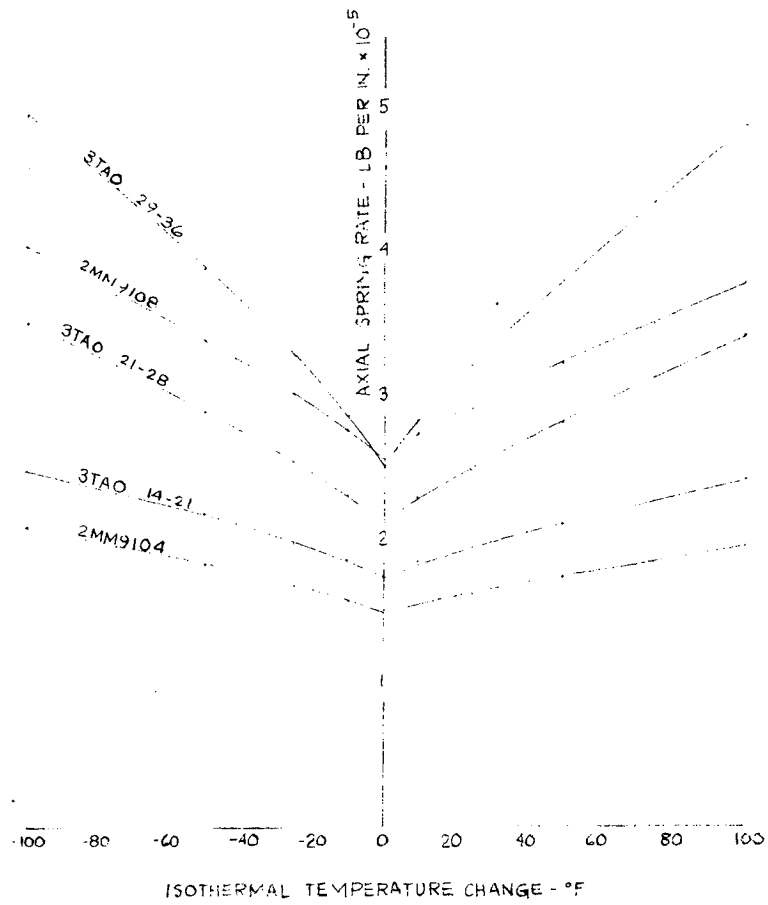


Fig. 6.1-4 — Axial spring rate versus isothermal temperature change

~~SECRET/SPECIAL HANDLING~~

~~SECRET/SPECIAL HANDLING~~

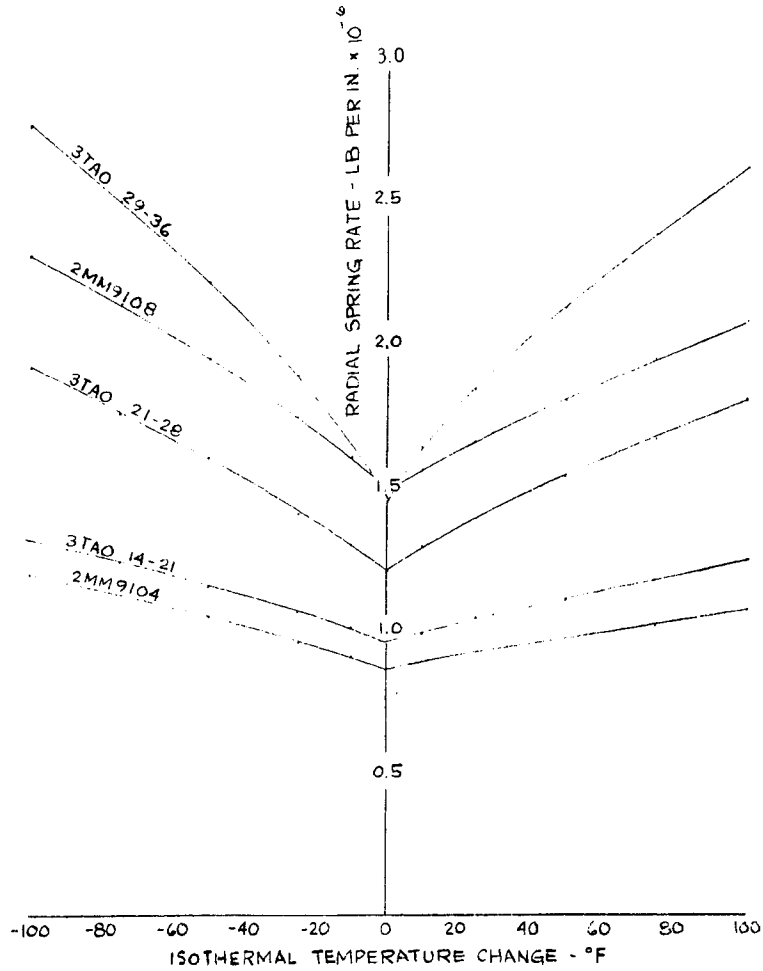


Fig. 6.1.5 — Radial spring rate versus isothermal temperature change

~~SECRET/SPECIAL HANDLING~~

~~SECRET~~/SPECIAL HANDLING

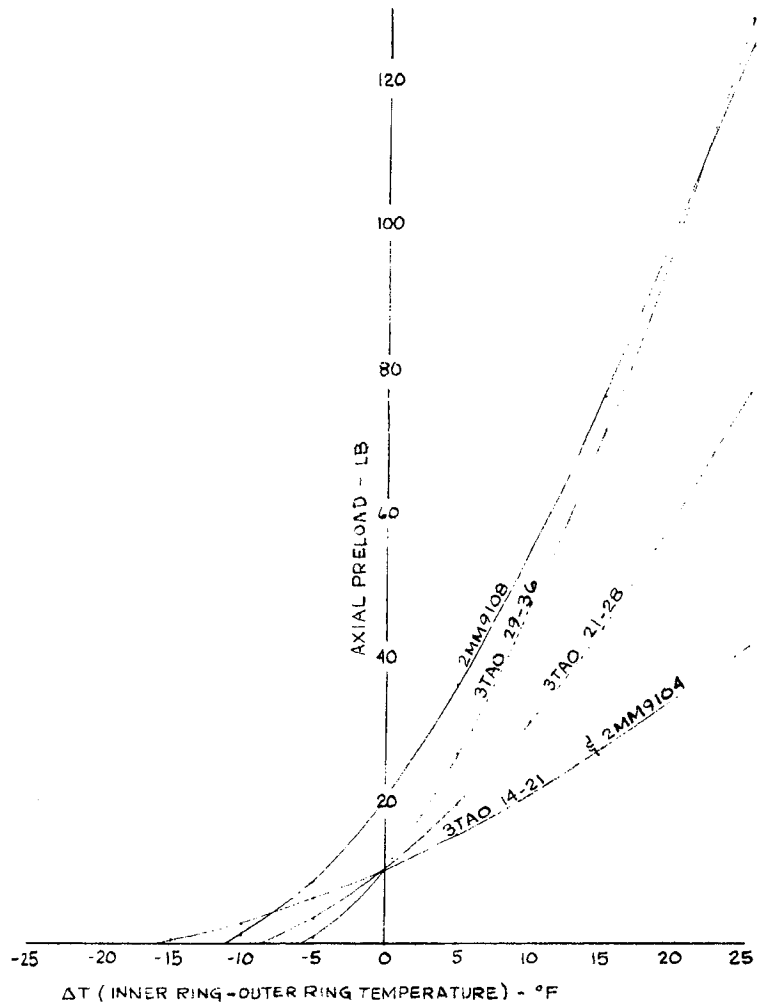


Fig. 6.1-6 — Axial preload versus temperature differential

~~SECRET~~/SPECIAL HANDLING

~~SECRET/SPECIAL HANDLING~~

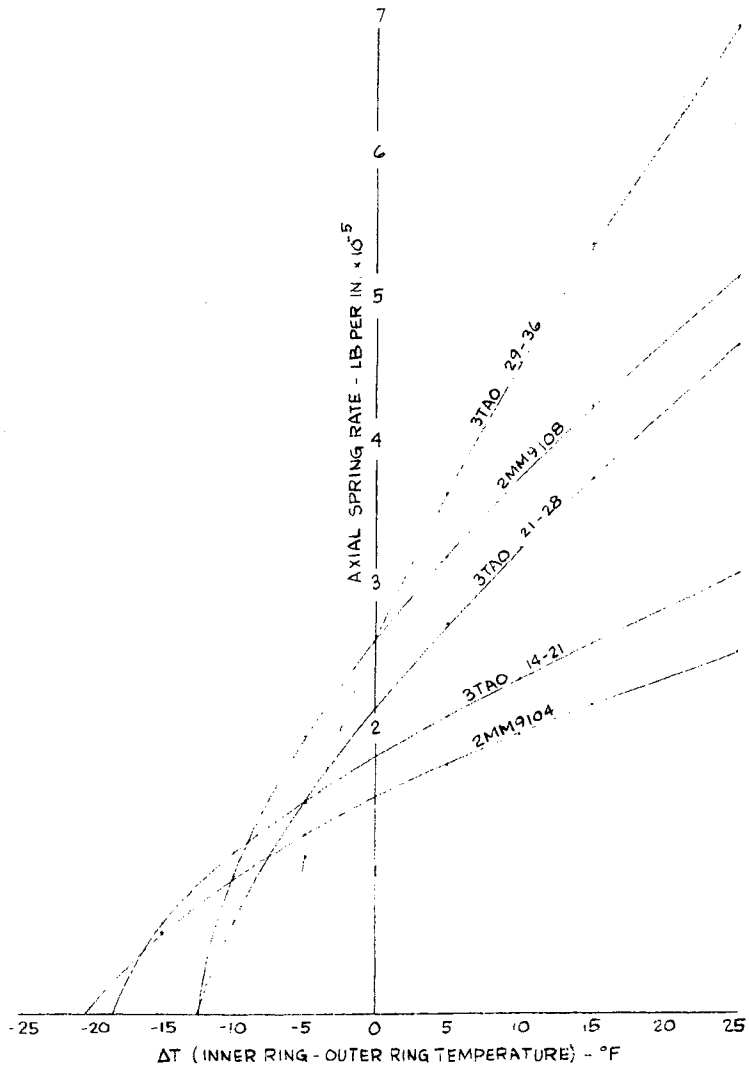


Fig. 6.1-7 — Axial spring rate versus temperature differential

~~SECRET/SPECIAL HANDLING~~

~~SECRET~~/SPECIAL HANDLING

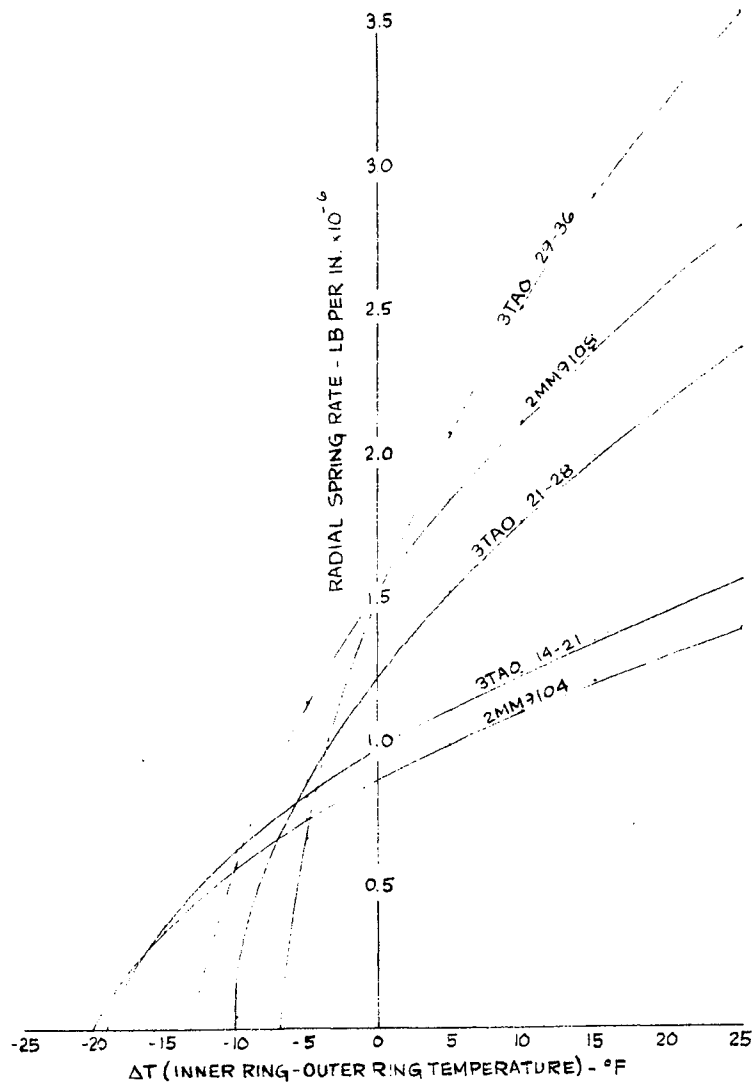


Fig. 6.1-8 — Radial spring rate versus temperature differential

~~SECRET~~/SPECIAL HANDLING

~~SECRET/SPECIAL HANDLING~~

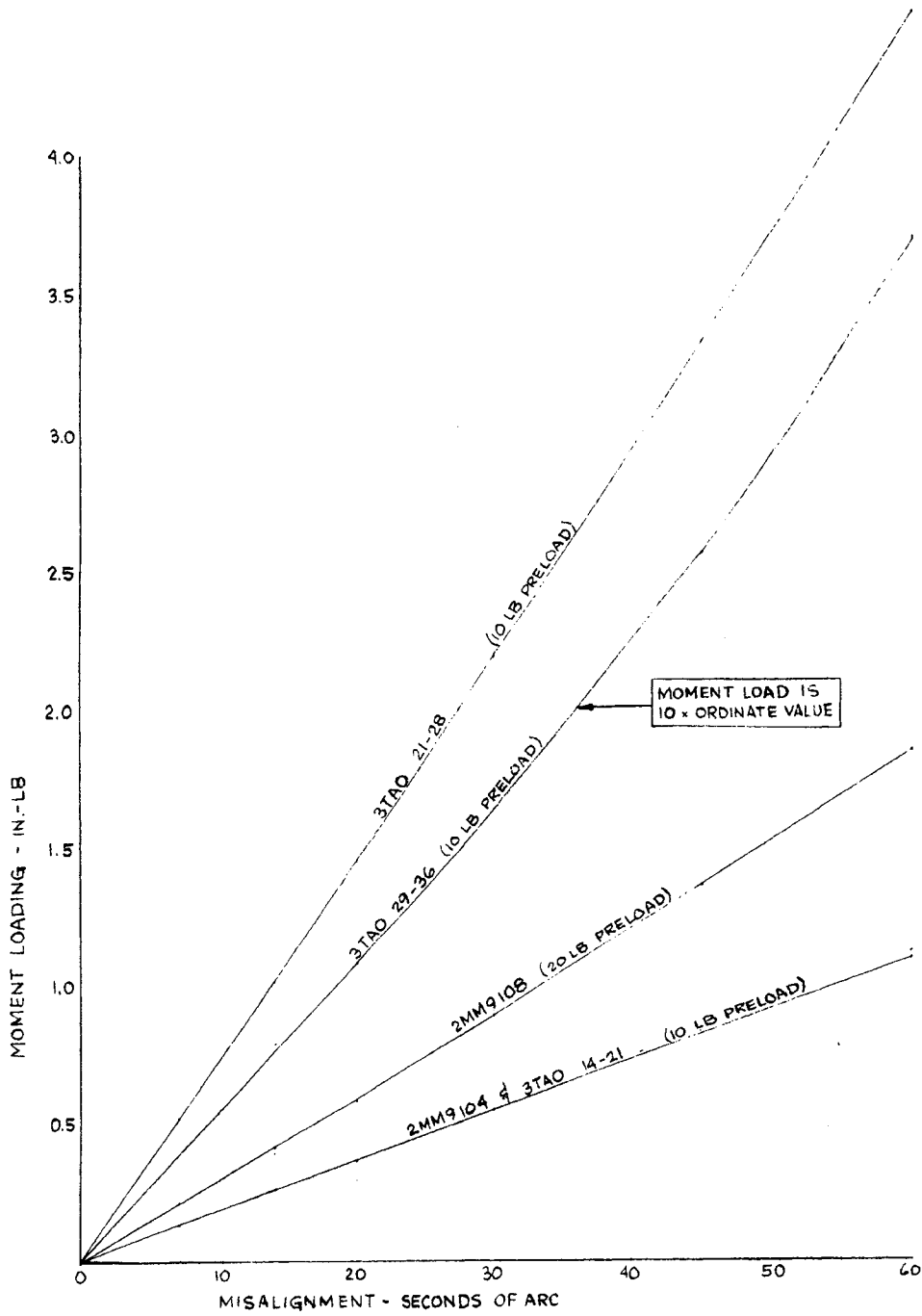


Fig. 6.1-9 — Moment loading versus misalignment

~~SECRET/SPECIAL HANDLING~~

~~SECRET~~/SPECIAL HANDLING

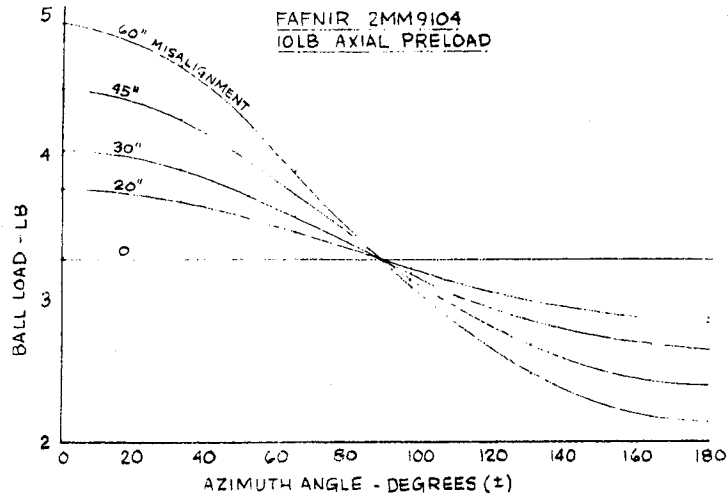
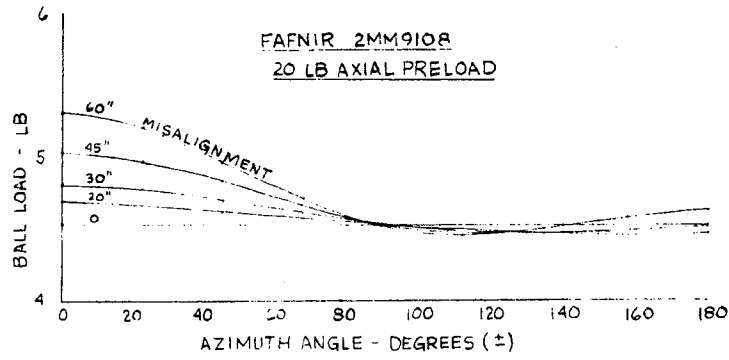


Fig. 6.1-10 — Ball load versus azimuth angle and misalignment

~~SECRET~~/SPECIAL HANDLING

~~SECRET~~/SPECIAL HANDLING

SBB 3TA0 29-36  
10 LB AXIAL PRELOAD

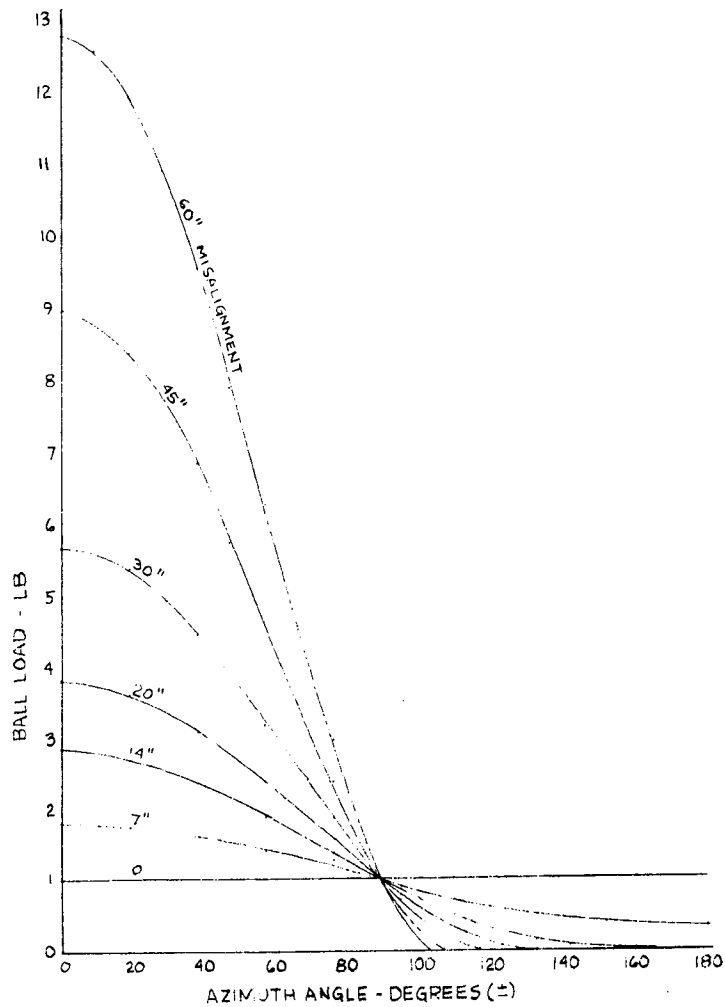


Fig. 6.1-11 — Ball load versus azimuth angle and misalignment

~~SECRET~~/SPECIAL HANDLING

~~SECRET~~/SPECIAL HANDLING

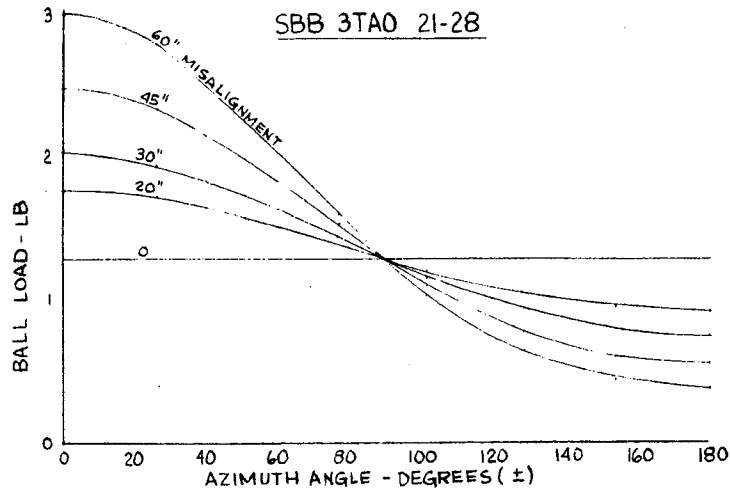
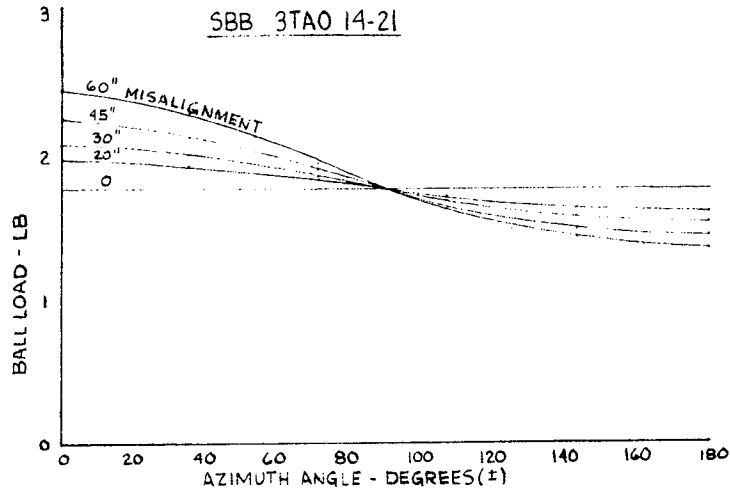


Fig. 6.1-12 — Ball load versus azimuth angle and misalignment (10-pound axial preload)

~~SECRET~~/SPECIAL HANDLING

~~SECRET~~/SPECIAL HANDLING

for a bearing starting at a different preload, we could not use these curves because the effect is non-linear. Similarly, ball squash or preload tightening due to cooling is dependent on the geometry of the housing (a massive housing will shrink the outer race more than a thin weak ring type housing) and these curves were calculated using the approximate scanner geometry shown in 9400-68-DR-231, drawing no. 129841, A. M. O'Lari 29 April 68. Any appreciable changes in the outer diameters of the bearing housings would change this data. Of course material changes, such as going to a steel shaft, would also change it.

Fig. 6.1-4 is a combination of Fig. 6.1-1 and 6.1-3 showing axial stiffness and how it changes with isothermal temperature excursions. Fig. 6.1-5 shows the same data for radial stiffnesses.

A temperature differential from inner race to outer race will cause changes in the preload and stiffnesses. In case of inner race being cooler than outer race, the ball bearing annular space will get bigger, relaxing the preload and making the bearing less stiff. If the inner race is warmer than the outer, ball squash similar to the isothermal excursion effect will take place. Preload is plotted versus raceway temperature difference in Fig. 6.1-6. Negative differences indicate inner races cooler than outer and note that for a big enough negative difference, the preload inevitably drops to zero. For positive differences the preload rises quite sharply in some cases, with serious implications for PSD. Again, extrapolation of this data to bearings starting at other preloads is not permitted due to non-linearity. Also, this data is for an average of outer race and inner race temperatures is always 70 °F) and, strictly speaking, should not be applied to other ambients. However, the error will probably be small and, in the interest of not getting drowned in data, we did not do computations for other ambients.

Fig. 6.1-7 is a combination of Figs. 6.1-1 and 6.1-2 showing axial stiffness versus raceway temperature differential. Fig. 6.1-8 is the same for radial stiffness.

Figs. 6.1-9 through 6.1-12 deal with cocking or mis-alignment. Raceway cocking is the angle between the outer raceway face and the inner raceway face. Either the housing clamps the outer raceway rigidly and the shaft cocks the inner raceway, or visa versa. It is assumed that the bearing pair is subjected to a pure cocking or moment loading, there is no concurrent radial or axial load and no shift of the bearing pair center. It should be pointed out that this is not a real-life situation; if a bearing is cocked, radial loads will arise due to a consequent moment resistance and the interactions with other bearings in the structure. However, these loads will be small and their inclusion would tie our results even more tightly to the present scanner geometry than they are now, so consequently, to avoid the uncontrollable proliferation and multiplication of data we have investigated only the pure cocking case.

Fig. 6.1-9 shows the moment loading versus cocking angles up to 60 seconds of arc. The slope of these curves is the "overturning moment stiffness". The resistances to overturning moment are very low in all cases except the 29-36 bearing because of the DF mounts. The 29-36 has a DB mount. This means that our bearings are relatively insensitive to cocking. Once again, these results apply only to bearings of the sizes, contact angles, and preloads of Table 6.1-1.

Figs. 6.1-10 through 6.1-12 show the actual ball loads in a cocked bearing versus an azimuth angle. It is assumed that the ball at the top, or 0 degree azimuth angle, sees the most increase in load due to cocking and the one at the bottom or 180 degrees sees the greatest decreased in load, or the most tendency to unload completely. The ball at 90 degrees theoretically sees no change in load due to cocking. A family of curves was drawn for each bearing pair, corresponding to cocking angles up to 60 arc-seconds. Note that in no case in our load carrying DF mounted bearings does a ball unload, even for 60 seconds of cocking. These results confirm the calculations

~~SECRET~~/SPECIAL HANDLING

~~SECRET/SPECIAL HANDLING~~

reported by R. Rosenthal in memo no. 349-67-774 "Response to PDR Action Items no. 21 and 37" 29 December 1967 in which he stated that our bearings are far less sensitive to cocking than the Customer's and that we could stand 1.3 arc-minutes of cocking for the same performance degradation that would result from customer's bearing cocking of 20 arc-seconds. Note, however, that the encoder bearings are very sensitive due to their geometry and DB mount and that a ball unloads even for about 14 seconds of arc cocking. This bearing, however, is not mounted on the main shaft, carries no significant load, and is not subject to any forces liable to cause cocking.

Now that we have related ball load to cocking, we must relate it to PSD. We know that running torque goes roughly with the 4/3 power of ball load, hence we can get a handle on it by integrating the contributions for each ball, knowing the number of balls. However, more grossly, the Customer's tests have shown little increase in PSD until a ball is on the verge of unloading. If this is so, we can permit misalignments up to 1 minute of arc or more in our scanner assembly with practically no change of PSD. No cocking tests have been done so far to support our contention, but this is planned in the immediate future.

Dynamic analyses of our scanner show no transmissibility problems if the bearing stiffnesses vary only by the amounts shown here for normal thermal excursions and raceway temperature differentials. Increasing preloads with thermal effects increase stiffness, hence transmissibility.

Jones and Harris have informed us that they will be happy to do further analytical work for us along these lines. In case of parameter or bearing changes, we should re-calculate the data instead of attempting to extrapolate.

Memorandum no. 349-68-996, Bearing Data includes preliminary thermal calculations using bearings very close to those in the present design, and is included in the Appendix 6-A for reference. These are essentially hand calculations that the firm of Jones and Harris has incorporated into their computerized program. Also some calculations of the ball area contact in the raceways leading up to temperature gradient across the races are included in Table 6.1-4 and the present information of temperature gradient across the races is in Table 6.1-5. An earlier analysis using a somewhat now obsolete model gave a good approximation of the pitch axis bearing temperature. It was determined that the outer race would be 6 °F higher than the inner race and that the bearings would range in temperature from 0 to 70 °F. For optimum performance we are considering assembling the scanner at a midtemperature of 35 degrees approximately.

Finally, some bearing cocking analysis were performed prior to the Jones-Harris report and is presented in the appendix for information purposes. These earlier hand analysis was supported by later sophisticated programs and points out the relative insensitivity to cocking of the DF bearings to up to 60 seconds of arc.

#### 6.1.5 Brinelling Test

In order to assess the actual effect of launch loads on the bearing raceways, a development brinelling test will be undertaken. This will consist of a simulated pitch axis assembly mounted in bearings of the type and size used in the engineering model. A special exchange fixture will accept the assembly for mounting to a shake table, where shock and vibration conditions on both radial and axial direction similar to launch will be experienced.

An initial torque and PSD test will establish a base line before the vibration test, and then another PSD test will be made after vibration. If there is any change, then most likely it is due to brinelling since the bearings, mounting and preload were undisturbed in their fixture.

~~SECRET/SPECIAL HANDLING~~

~~SECRET~~/SPECIAL HANDLING

Table 6.1-4 — Ball Contact Areas for Scanner Bearings

BY:		TITLE:		PAGE:			
DEPT: 9-349		DATE: 3/10/68		PROJECT: 9400			
		Ball dia. .375	Ball dia. .125	Ball dia. .250	Ball dia. .125	Ball dia. .125	
			<u>ROLL AXIS</u>		<u>PITCH AXIS</u>		
		Inboard	Encoder	Outboard	Forever	Encoder	
BALL TO I N E R R A C E	ONE CON- TACT  EL- LIPSE  Area (in. <sup>2</sup> )  TOTAL AREA (in. <sup>2</sup> ) 16 Balls	Semi- Major Axis (in.)  Semi- Minor Axis (in.)  (in. <sup>2</sup> )  16 Balls	.0138  .0015  .0000672  .00108	.01341  .000452  .0000048  .000185	.0114  .00105  .0000447  .000492	.00050  .000853  .0000174  .000400	.00683  .000883  .0000190  .000379 20 Balls
BALL TO O U T E R R A C E	ONE CON- TACT  EL- LIPSE  Area (in. <sup>2</sup> )  TOTAL AREA (in. <sup>2</sup> ) 16 Balls	Semi- Major Axis (in.)  Semi- Minor Axis (in.)  (in. <sup>2</sup> )  16 Balls	.0135  .00179  .0000761  .00122	.00340  .000485  .0000052  .000197	.01119  .00134  .0000343  .000195	.00644  .000934  .0000189  .000435	.00675  .000987  .0000209  .000419 20 Balls

Inboard Bearing Closings to Yoke

~~SECRET/SPECIAL HANDLING~~

Table 3.1-5 — Bearing Thermal Gradients

Bearing Set	Gradient Across the races Of the Bearing
Pitch Motor	7.3
Pitch Encoder	2
Inboard	6.3
Roll Encoder	3.8
Outboard	7.4

NOTE: Outer race becomes hotter when door opens

~~SECRET/SPECIAL HANDLING~~

~~SECRET/SPECIAL HANDLING~~

If there is no appreciable change in PSD then it indicates that brinell indentations no deeper than the rms surface finish were imprinted into the raceway.

The contractor has run similar bearing brinelling tests on his own Drive A bearings and has found that if the 30 percent derating criterion previously mentioned is used in sizing a bearing, then PSD will not be affected by the vibration test. It is not expected that our brinelling tests will differ.

Fixtures for conducting these tests were designed and will be transmitted to the contractor for adaption or incorporation into his brinelling test fixtures since it appears likely that he will be performing the tests for us.

6.1.6 Bearing PSD and Torque Level Test Program

The measurement of torque ripple for preloaded bearings pairs in itself is not new. The testings of bearings for running torque variation under load is a standard test for many different applications, but the digesting of this torque ripple data into a power spectral density (PSD) plot versus frequency was a completely new concept and requirement at Itek. This PSD requirement made it necessary for us to devise a method of testing which would yield meaningful data in a short time period. Since we did not have a facility for testing bearings in our own house, we conducted a search in the area for a vendor with the necessary facility.

This facility consisted of a class 100 clean room and a low speed dynamometer for the bearing tests. The Nortronics Division of the Northrop Corporation of 100 Morse Street, Norwood, Massachusetts, was chosen to do our bearing testing.

The low speed dynamometer consisted of a motor to turn the outer race of the bearing and a force transducer located at the end of an arm from the inner race to readout torque. Fig. 6.1-13 is a sketch of the setup with the important components noted.

The force transducer is a cantilevered beam with a strain gage bridge located on the beam to yield a signal proportional and linear to the force applied to the beams.

The driving force applied to the calibrated strain gage beam is that caused by friction between the bearing's inner and outer races. It is noted that the torque coupling between the bearing inner race and the beam is through the inertia of the outer race. This inertia and the beam stiffness constitute a resonant mechanical circuit whose response will control the instruments ability to respond to torque variations. Since our prime requirement is to obtain PSD from torque friction variation data, evaluation of this response is of great importance. The differential equation of motion is of the type:

$$T = J \frac{d^2\theta}{dt^2} + \frac{Rd\theta}{dt} + K\theta$$

where T = applied torque, ft-lbs

J = bearing outer race inertia, slug-ft<sup>2</sup>

R = damping, ft-lbs/rad/sec

K = beam stiffness, ft-lb/radian

Assuming the damping to be small, the resonant frequency is shown to be:

$$f(r) = (1/2\pi) \sqrt{K/J}$$

~~SECRET/SPECIAL HANDLING~~

~~SECRET/SPECIAL HANDLING~~

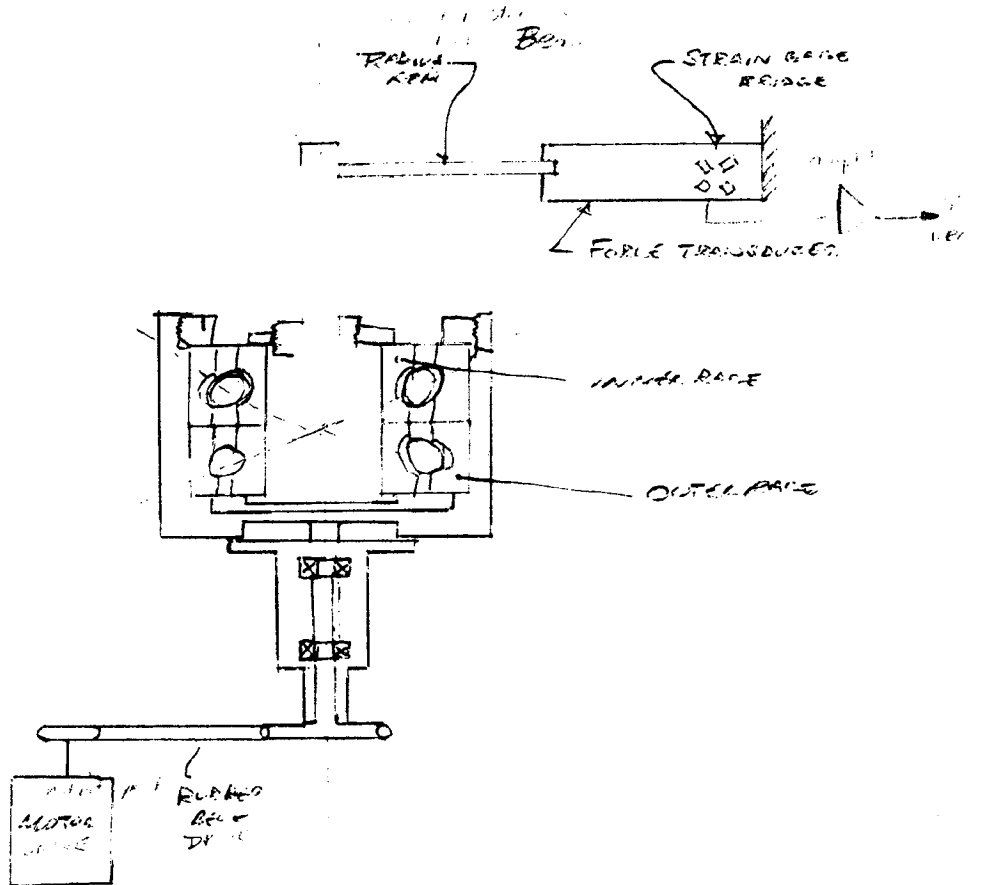


Fig. 6.1-13 — Low speed dynamometer with bearing test fixture

~~SECRET/SPECIAL HANDLING~~

~~SECRET~~/SPECIAL HANDLING

It may be shown (See Appendix 6-A-4) that the torque constant K is equal to:

$$K = \frac{3 EI r^2}{L^3}$$

where E = Youngs modulus of beam material

I =  $bh^3/12$ , beam moment of inertia (b = thickness, h = height)

r = outer radius of bearing

L = strain gauge length

The rectangular steel strain gauge beam is 0.01-inch thick and is 0.5 inches high. Using this data:

$$K = 32 \text{ in.-ob/radian} = 2.68 \text{ ft-lbs/radian}$$

The Fafnir 2MM 9106 bearing as a typical size has a catalog weight of 0.26 pound and an outer radius of 1.083 inches. For inertia calculations, we shall estimate 50 percent of the weight to be concentrated in the outer race at a 1-inch radius. The computed inertia is  $2.83 \times 10^{-5}$  slug-ft<sup>2</sup>.

Accordingly,

$$f(r) = (1/2\pi) \frac{2.68}{2.83} 10^5 = 49 \text{ cps}$$

All of the damping is felt to be due to the cantilevered strain gauge beam, since the friction in the bearing is the driving force, and is not stabilizing as in more classically oriented situations. Assuming small damping (0.05 or critical), inspection of universal transmissibility curves shows reasonable behavior ( $T \leq 1.5$ ) up to about half of resonance. Since our PSD limit is 16 cps (100 radians second) and the raw data was heavily filtered, the setup was considered acceptable.

The output of the strain gage bridge is then amplified and fed into an fm audio tape recorder. The tape recorder is then played back into a digitizer and a paper tape is made to be used as the input for the punch cards that are used for the program which enables us to get from the bearing torque test to the PSD specification. The test and calibration procedure will now be described in more detail.

#### Calibration of Strain Sensor

1. Linearity. The Nortronics Company shall provide a calibration curve for the strain measuring apparatus indicating in.-oz of torque as a function of actuation of the system by stimuli of known magnitudes. This calibration curve shall cover the range from zero to 5 in.-oz in steps of 0.1 in.-oz.

2. Sensitivity. The output signal as delivered to the magnetic tape recorder from the strain gage measuring instrumentation in response to a 1 in.-oz torque level shall have a signal-to-noise ratio in excess of 60 db.

3. Drive System Noise. The output from a rate gyro shall be made available during all tests which accurately depicts the effect of variations in the velocity of the drive system.

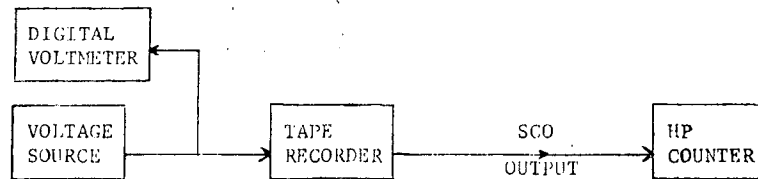
~~SECRET~~/SPECIAL HANDLING

## ~~SECRET~~/SPECIAL HANDLING

4. Absolute Accuracy and Stability. The absolute accuracy of the amplitude of the resulting measurements shall be 1 percent as referenced to the calibration curve mentioned above.

### Calibration of the Magnetic Tape Recorder

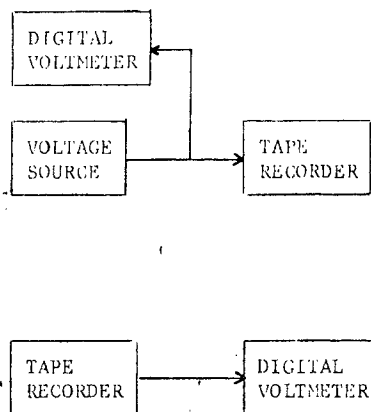
1. Compatibility. In order that the magnetic tapes of our bearing data may be compatible with standard IRIG ground station equipment, the following procedure is required.



Using the above described test equipment, accurate dc voltages shall be fed into the tape recorder and the resulting output of the SCO monitored. With zero volts in, and SCO upper frequency shall be adjusted to correspond with its appropriate IRIG designation and this value shall be recorded.

Then by varying the voltage source input, a calibration shall be made in 0.1 volt steps of the frequency deviation of the SCO. This procedure shall apply to each channel used for data.

2. Accuracy and Linearity



~~SECRET~~/SPECIAL HANDLING

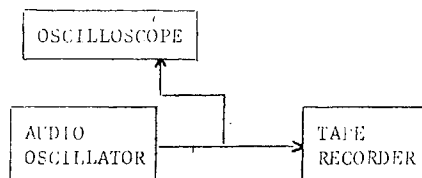
Using a stable voltage source and a digital voltmeter as depicted in the above sketch, a record shall be made of the voltage source output as it is varied from zero to 10 volts in steps of 0.1 volts at a rate of one step every 10 seconds. The resulting data shall be played back into the digital voltmeter and the results used to determine the linearity and dc accuracy of the recording process. They shall be less than one percent of full scale and one percent respectively. This information shall form a part of the log on any subsequent tests to be performed with the instrument.

3. Sensitivity



Using a stable fixed voltage source such as a battery as an input to the tape recorder, a 30-minute record shall be made. This tape shall be appropriately processed and analyzed as would actual data. The resulting power spectral density shall be at least 20 db below the specification limits for bearings throughout the frequency range of interest.

4. Frequency Response

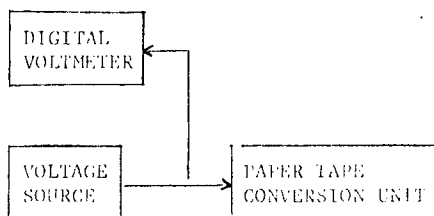


## ~~SECRET~~/SPECIAL HANDLING

Using an audio oscillator and an oscilloscope to monitor its amplitude, a record shall be made as the audio oscillator frequency is varied from zero to 100 hertz in 5-hertz steps, at a rate of one step every 15 seconds. The peak-to-peak amplitude of the oscillator shall be maintained at 5 volts throughout this period.

When the tape record is played back to an oscilloscope, the amplitude shall not deviate more than 1/2 db.

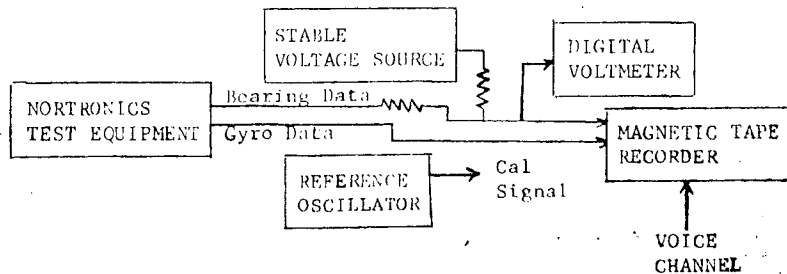
### Paper Tape Conversion Unit



1. Accuracy. Using a stable voltage source and a digital voltmeter, a voltage from 0 to 1 volt in steps of 0.05 volts shall be applied to the paper tape conversion unit at a rate of one step every 10 seconds. The resulting paper tape record shall reproduce the input voltage within the quantization constraints of the output.

2. Noise. With an output derived from a stable source such as a battery applied to the input of the paper tape unit at a level of about 1/2 volt, a paper tape record shall be generated at a sample rate of 55 samples/second for a 2-minute period. Examination of this record shall disclose no change in the output greater than 1 part in  $2^9$  in any 55 sample sequence, nor any change greater than 1 part in  $2^{10}$  for any 10 sample sequence.

### Test Procedure



~~SECRET~~/SPECIAL HANDLING

## ~~SECRET~~/SPECIAL HANDLING

The bearing data and the output from a stable dc voltage source shall be applied to one channel of the magnetic tape recorder through a summing junction as depicted in the above sketch. A digital voltmeter shall be used to measure the rms value of the summed signal, and the voltage from the dc source shall be set so that this value is zero volts. Thus the value of the dc source voltage can be used as a measure of the dc component of the friction.

In addition, the dc source provides dc suppression so that the gain of the tape recorder can be increased for optimum ac signal-to-noise ratio. The specific steps in the data taping process are:

1. Measure approximate amplitude for the ac components of the bearing and gyro data and set the amplitude into the tape recorder accordingly.
2. Using the reference oscillator at a frequency of 10 hertz and a peak-to-peak amplitude suitable for the ranges as measured in step 1, apply it to the bearing and gyro channels for a 15-second recording period to provide an amplitude calibration reference.
3. Connect the equipment as in the above sketch and adjust the dc voltage source for dc suppression.
4. Record the value of the digital voltmeter for purposes of dc friction computation, and record data for 30 minutes.
5. The voice channel shall be used to provide appropriate data concerning the particular test in progress.

### Improved Instrumentation

An improved, low noise data acquisition scheme was designed and fabricated as depicted in Fig. 6.1-14, 6.1-15 and 6.1-16. A strain gauge bridge is stimulated by a 1 khz signal. Unbalance of the bridge causes a difference signal to be amplified and applied to the detector and filter stage. The active filter rejects noise outside of the range of interest. The subsequent band-pass filter limits the data acquisition to the frequency range of interest.

The work done at Nortronics was covered by a work statement similar to the one attached to the appendix of this report. The work statement covered the testing for all of the bearings tested for torque ripple.

### Early Data

Much early data was obtained from the Nortronics tests, some not very meaningful, since we were on the learning curve of the problem, but two graphs are shown as representatives of the type of effort. Fig. 6.1-17 shows a plot of PSD versus  $\omega$  with respect to the allowable total PSD on each axis. This served to establish early torque values and to get the feel of PSD and the testing techniques.

The second graph (Fig. 6.1-18) shows a change in speed which generally shows an increase in PSD, something which later proved to be correct by the contractor testing. It also shows some similarity between CCW rotation and CW rotation, although not following the signature exactly. The contractors complete testing does show exact signature duplication in either direction, so again the indications of our early graph were correct.

Other data was obtained using a FRAP program; however, this is not considered as accurate as our later Autocor program and therefore is not discussed herein.

~~SECRET~~/SPECIAL HANDLING

## ~~SECRET~~/SPECIAL HANDLING

The next six figures are representative of that produced by the Autocor program. The Autocor program uses the classic definition that PSD is equal to the cosine transform of the autocorrelation function operated on by an appropriate weighting function, this

$$\text{PSD} = H \otimes \int_{-T}^{+T} R(t) e^{j\omega t}$$

where  $H^*$  = operation by the weighting function  
 $R(t)$  = autocorrelation of  $f(t)$

Fig. 6.1-19 shows graphs of our 29-36 bearing. Some of the repetitive runs do not show the same curve, this is thought to be due to different azimuth orientation of the bearing races under test. Data handling limitations prevented obtaining data below 1.0 radians per second on these graphs.

It should be noted that the peak that is observed around 40 radians per second on some graphs, is electrical noise in the instrumentation and is not bearing noise. This anomaly was subsequently eliminated.

### 6.1.7 Summary and Conclusions

The material presented herein indicates the care and detail which prevailed in the setting up and the testing of ball bearings for torque ripple and presented as a plot of power spectral density (see Fig. 6.1-20). The bearing test was set up to determine if the size bearings called out for the scanner design would or could meet the customer's PSD Specification.

The bearings which were procured for the test program were standard off-the-shelf ABEC 7 and ABEC 9 class bearings which are of lesser quality than would be specified for the actual hardware. The lead time of 20 weeks prevented us from procuring the actual precision bearings. The bearings used for the test are not necessarily of the best race-way finish or race-way geometry (probably two of the most important factors influencing PSD). Further, the cleanliness, contact angle material, preload, and lubricant were different. The results of the test indicates that bearings can be made and when properly installed will meet the existing specification.

The procurement of super-precision ball bearings which have the required lubrication and cleanliness precaution, with special emphasis placed on raceway geometry and raceway finish points to a bearing which will be lower in PSD than the bearings we have been testing. The super-precision bearings will be the ultimate in bearing procurement and will definitely be state-of-the-art hardware. Any improvement in any of the critical areas such as raceway finish and geometry will be an advancement in bearing technology.

The bearings manufactured by different vendors will also present differences in PSD, as each vendor has his own proprietary methods of fabricating bearings. However, we have not tested bearings from many vendors since time did not permit.

### Bearing Lubrication and Potting

Lubricant. The selection of lubricant has been based mainly on a literature search and recommendations from the contractor based on his own investigations and testing. The final selection has been to use the recommended stripped F-50 Versilube oil as this has been tested

~~SECRET~~/SPECIAL HANDLING

~~SECRET~~/SPECIAL HANDLING

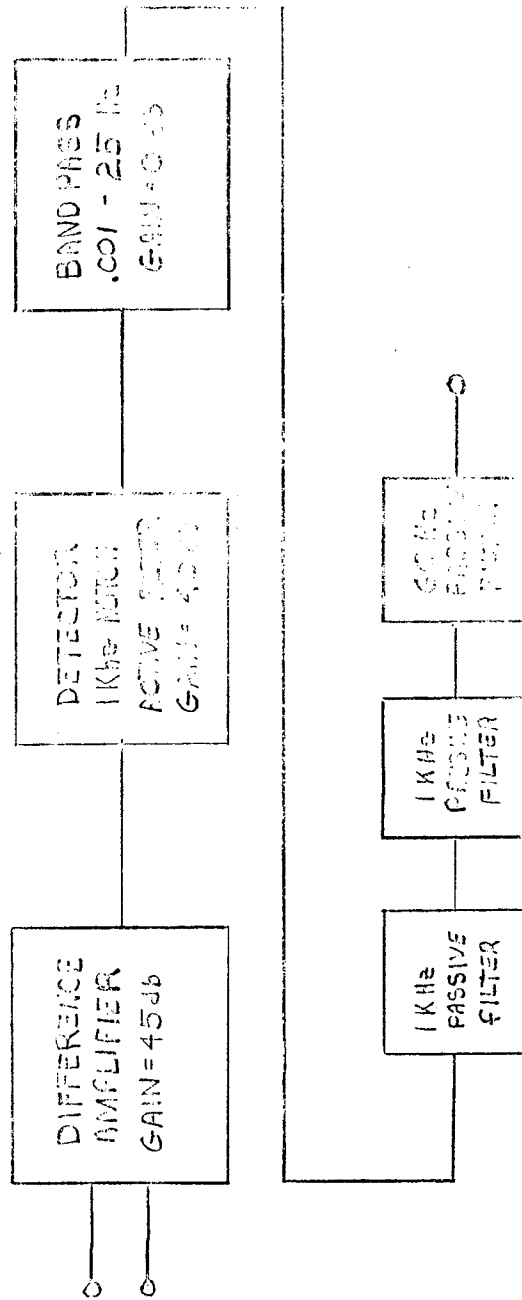


Fig. 6.1-14 -- Strain gauge amplifier block diagram

~~SECRET~~/SPECIAL HANDLING

~~SECRET~~/SPECIAL HANDLING

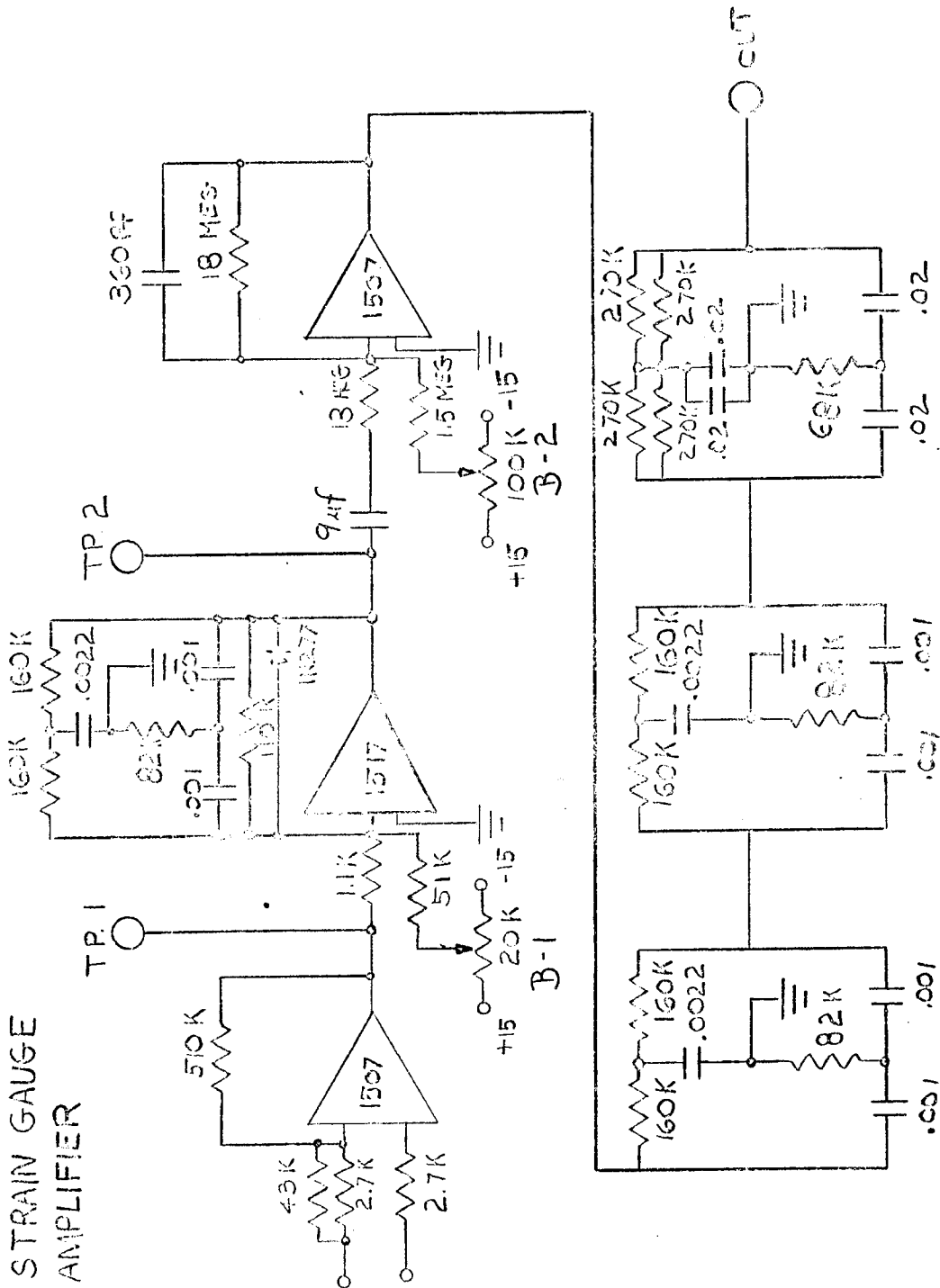


Fig. 6.1-15 — Strain gauge amplifier

~~SECRET~~/SPECIAL HANDLING

~~SECRET/SPECIAL HANDLING~~

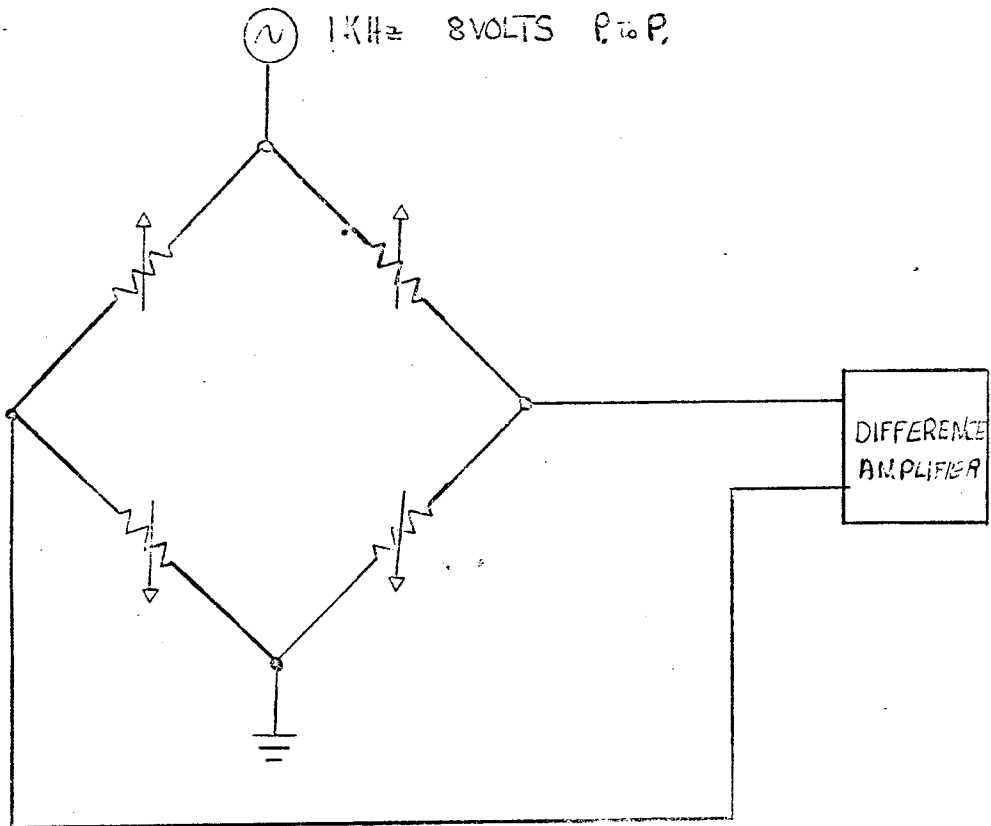


Fig. 6.1-16 — Strain gauge bridge

~~SECRET/SPECIAL HANDLING~~

~~SECRET/SPECIAL HANDLING~~

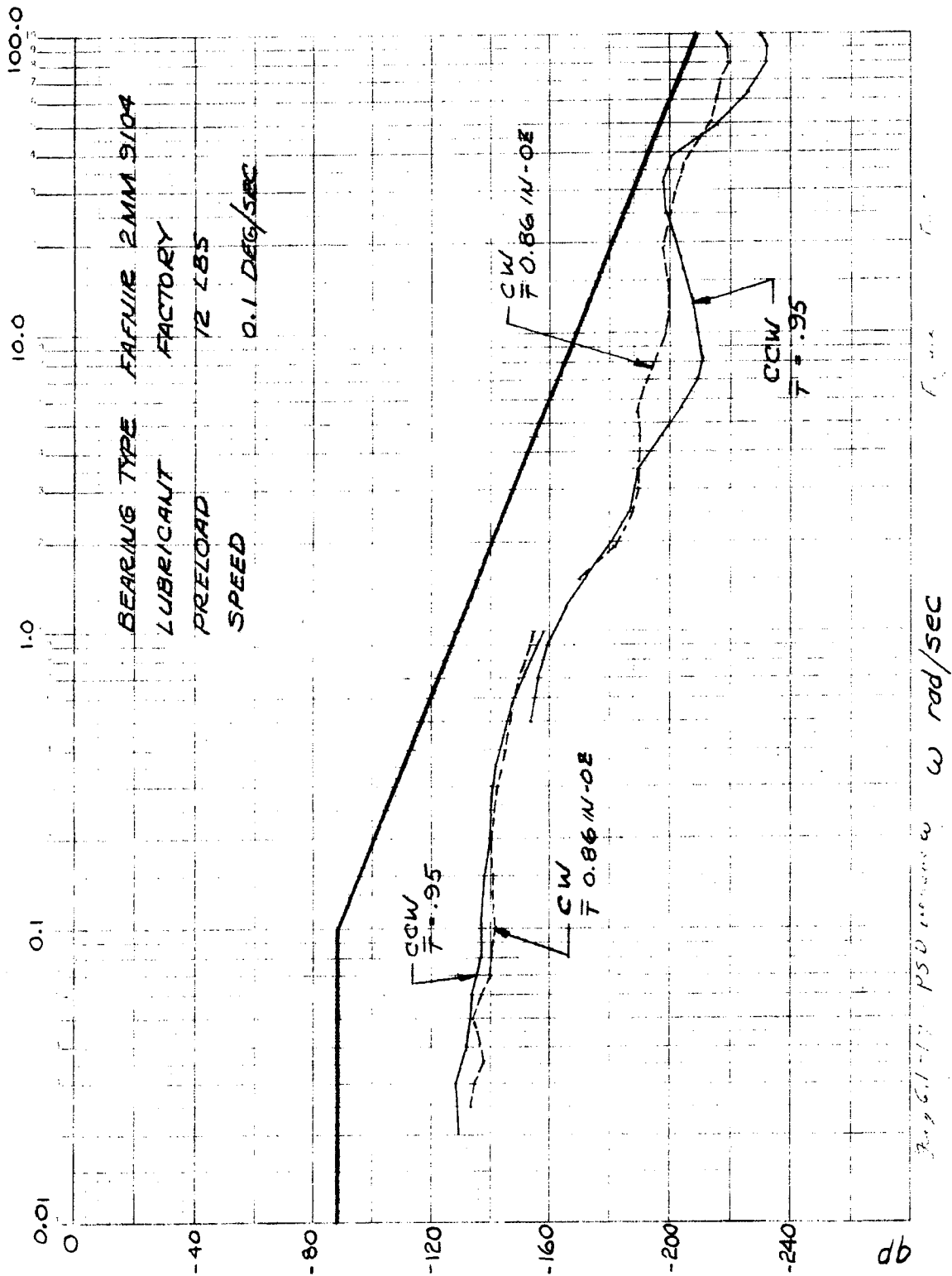


Fig. 6.1-17 -- PSD versus  $\omega$

~~SECRET/SPECIAL HANDLING~~



~~SECRET/SPECIAL HANDLING~~

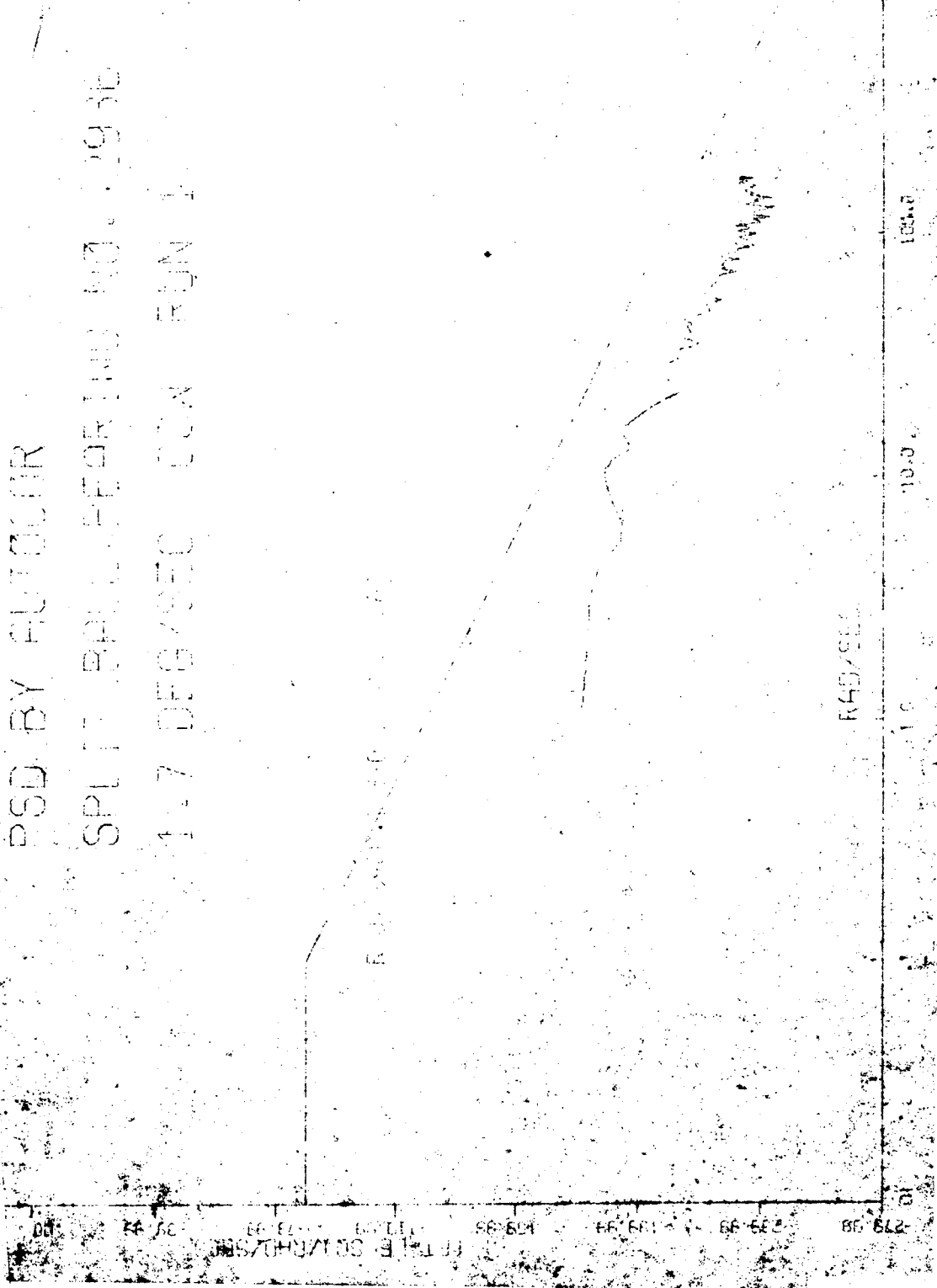


Fig. 6.1-19 -- Power spectral density plot of torque ripple for ball bearing 2936

~~SECRET/SPECIAL HANDLING~~

~~SECRET~~/SPECIAL HANDLING

Fig. 6.1-19 — (Cont.)

~~SECRET~~/SPECIAL HANDLING

~~SECRET/SPECIAL HANDLING~~

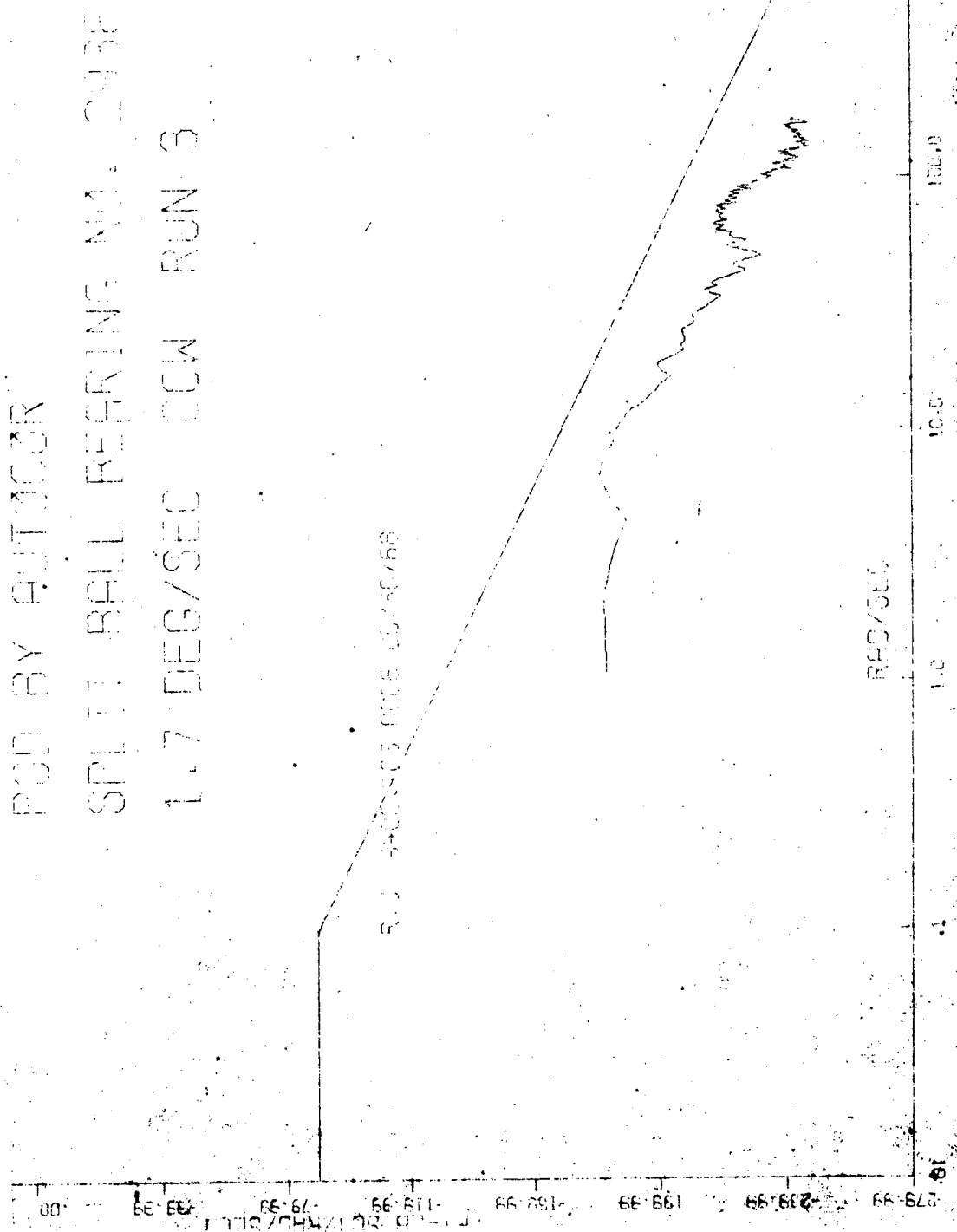


Fig. 6.1-19 — (Cont.)

~~SECRET/SPECIAL HANDLING~~

~~SECRET/SPECIAL HANDLING~~

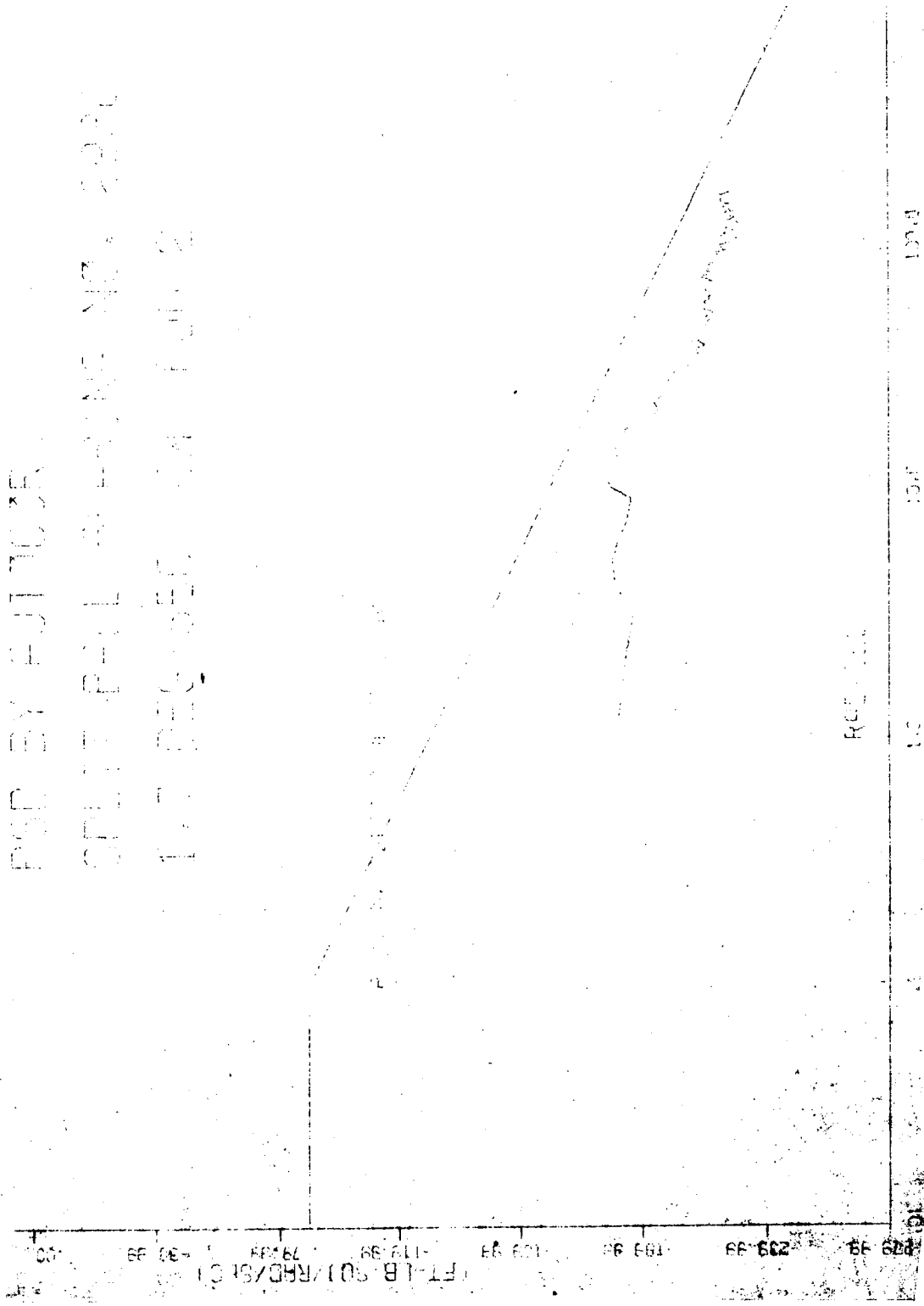


FOO BY HHT 1000  
SWI IT BALL RECOVERY 1000 1000  
1000 RELEASED ON 10/10/68

Fig. 6.1-19 — (Cont.)

~~SECRET/SPECIAL HANDLING~~

~~SECRET/SPECIAL HANDLING~~



100  
 110  
 120  
 130  
 140  
 150  
 160  
 170  
 180  
 190  
 200

Fig. 6.1-19 — (Cont.)

FOL

~~SECRET/SPECIAL HANDLING~~

~~SECRET/SPECIAL HANDLING~~

Fig. 6.1-19 — (Concl.)

~~SECRET/SPECIAL HANDLING~~

~~SECRET~~/SPECIAL HANDLING

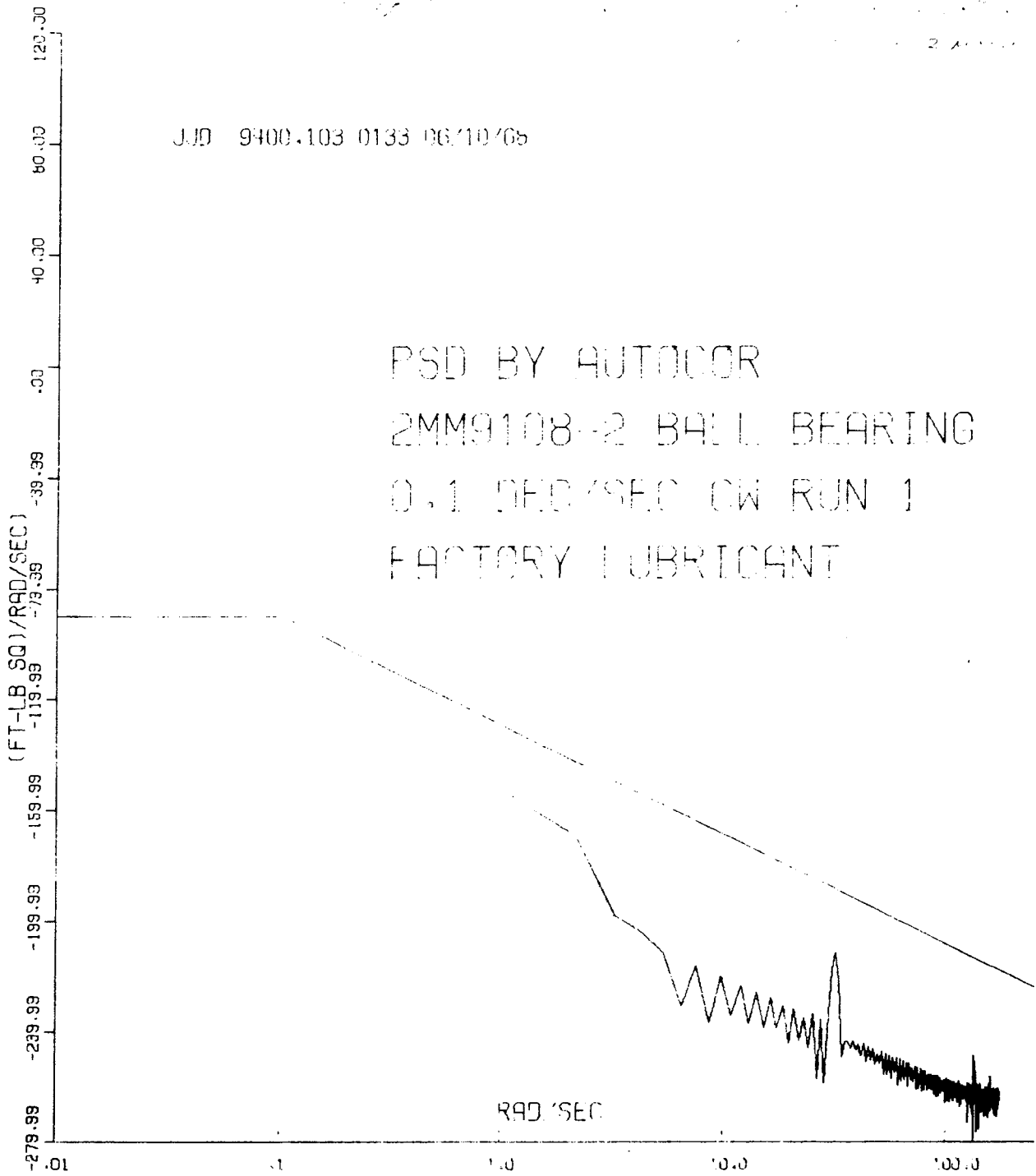


Fig. 6.1-20 — Power spectral density plot of torque ripple for ball bearing 2MM9188-2

~~SECRET~~/SPECIAL HANDLING

~~SECRET~~/SPECIAL HANDLING

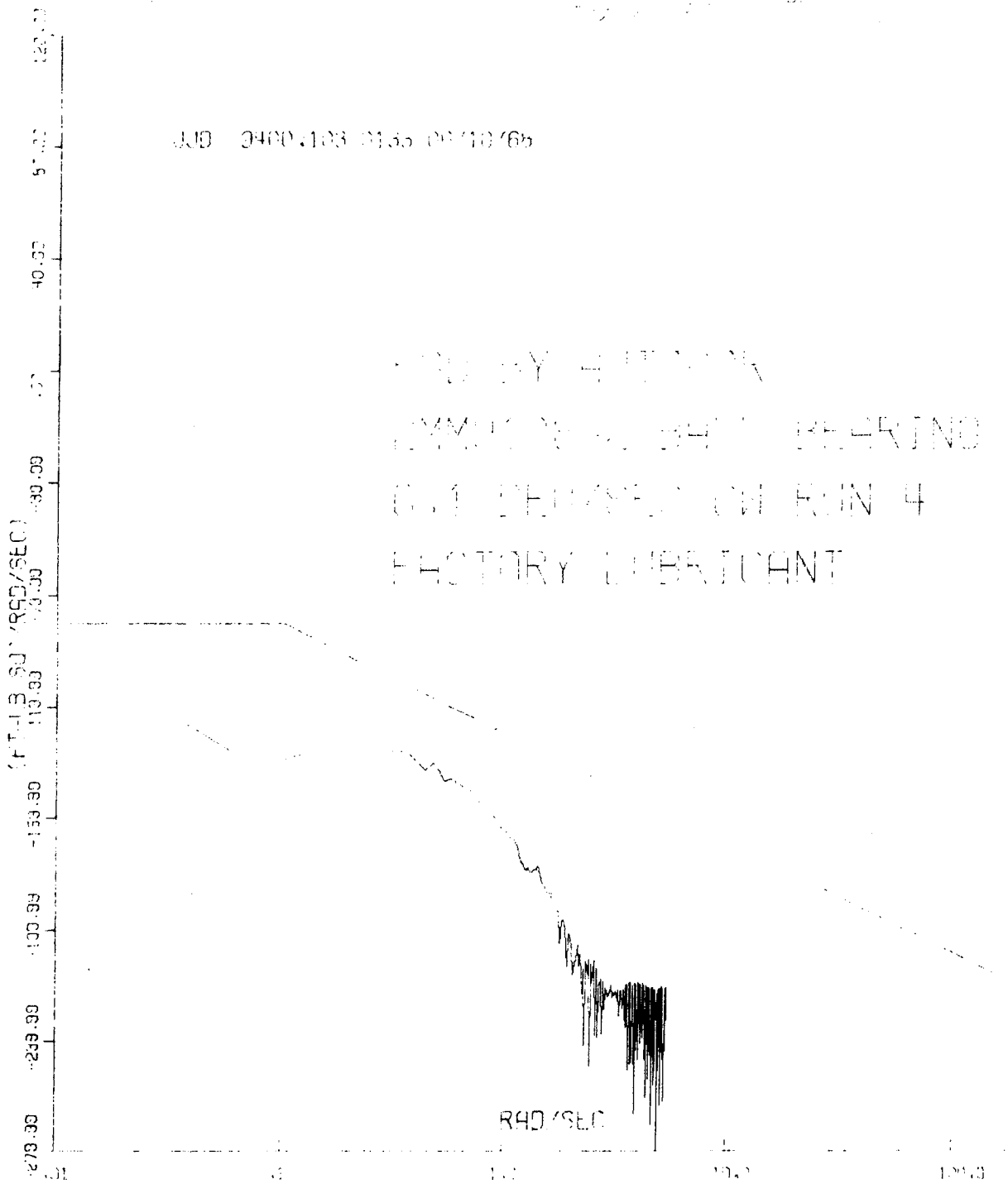


Fig. 6.1-20 — (Cont.)

~~SECRET~~/SPECIAL HANDLING





~~SECRET/SPECIAL HANDLING~~

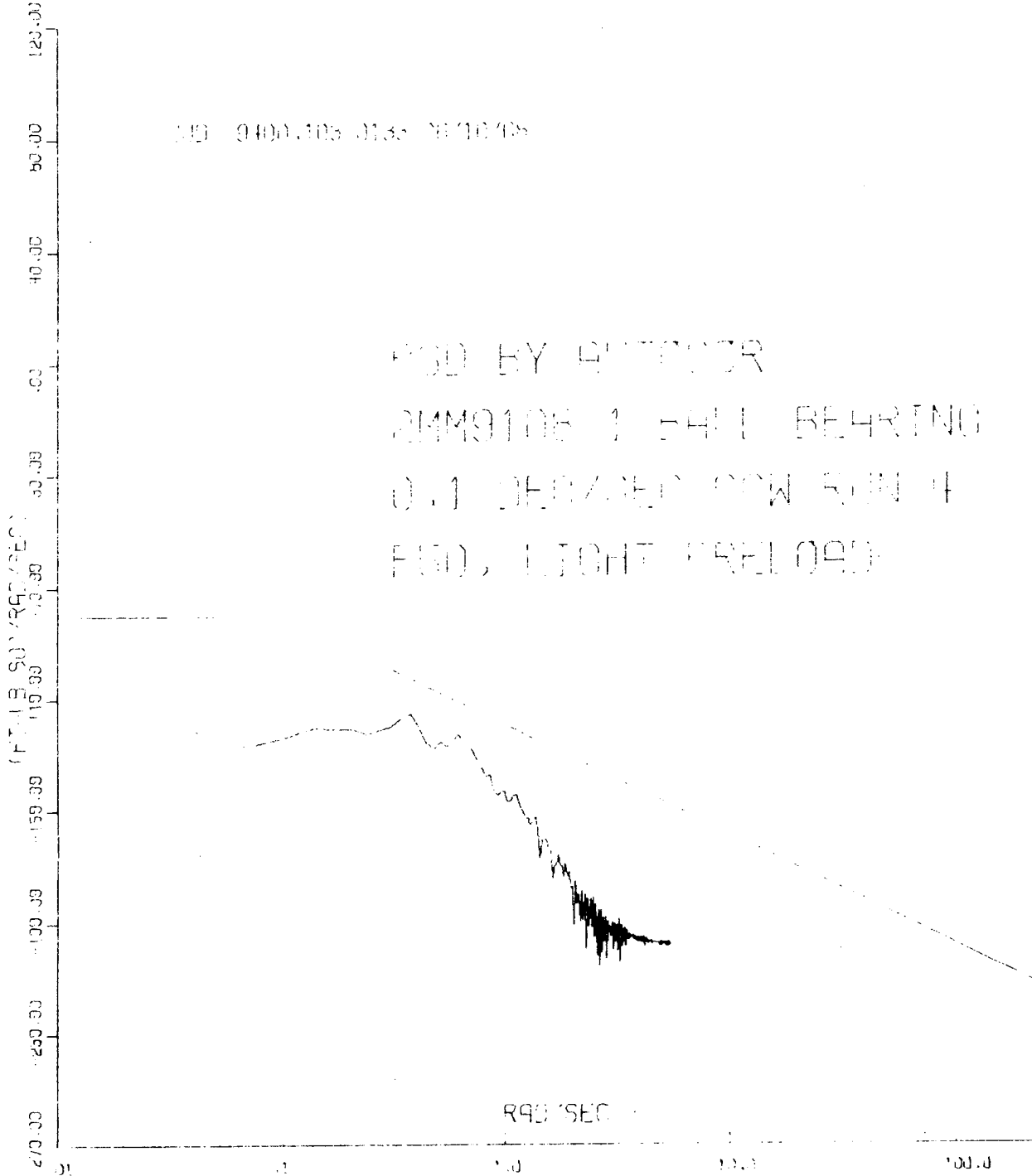


Fig. 6.1-20 — (Cont.)

~~SECRET/SPECIAL HANDLING~~

~~SECRET~~/SPECIAL HANDLING

Fig. 6.1-20 F5

JJD 9400.103 0133 06/10/68

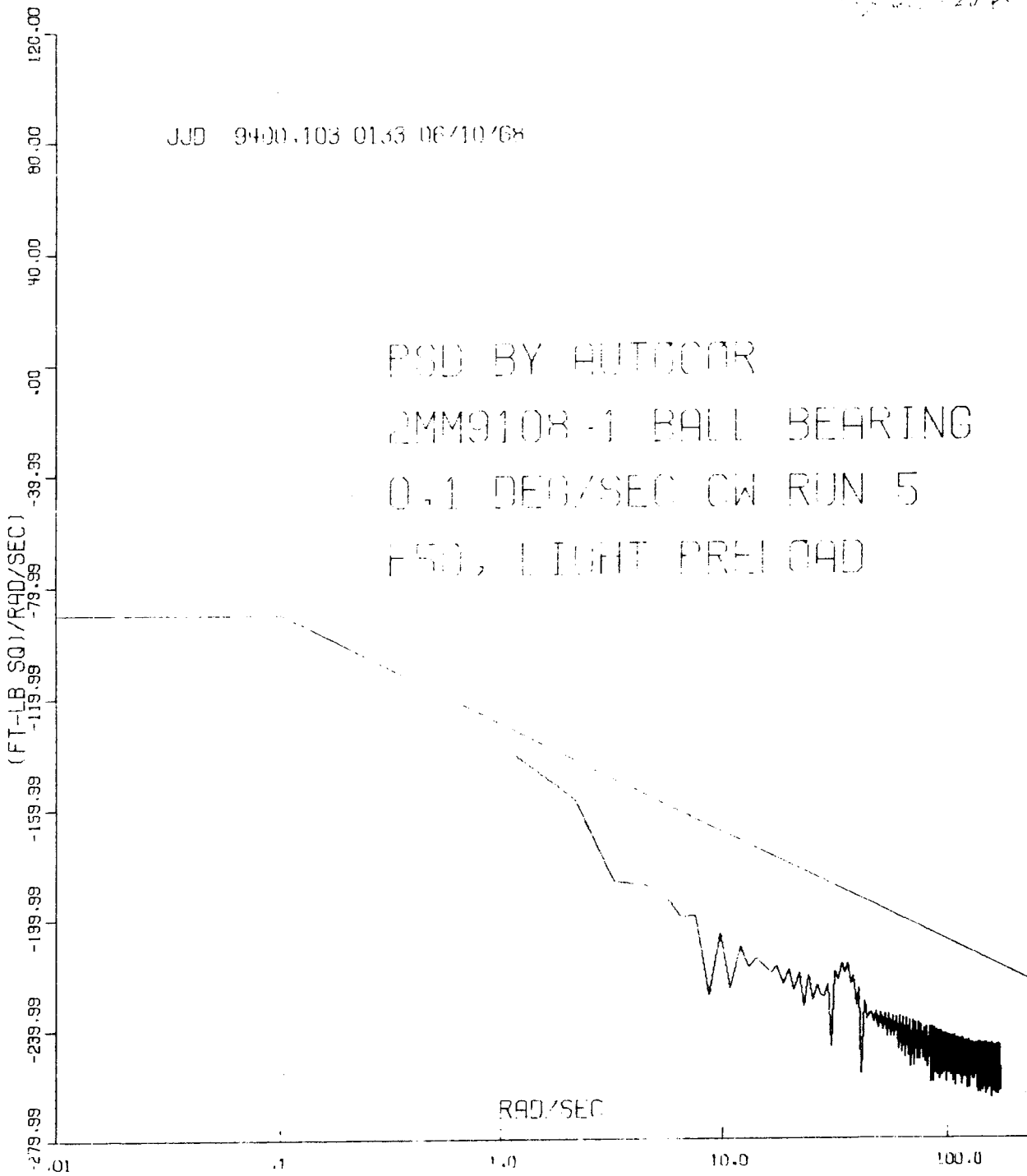


Fig. 6.1-20 — (Concl.)

~~SECRET~~/SPECIAL HANDLING

~~SECRET/SPECIAL HANDLING~~

to yield the lowest PSD values over a solid film lubricant  $AS_1$  and  $M_0S_2$ ; results have proved consistently reliable. The bearing manufacturers contacted are themselves in agreement with the selection based on our requirement and environmental conditions.

During our early test program, many candidate lubricants were to be investigated and tested, from Apiezon oils to Silver-coated balls, and from fused tungsten disulfide on raceways to fine particles of  $M_0S_2$  impregnated in TFE. However, this program was abruptly curtailed during a funding constraint; contractor tests showed rather conclusively that F-50 was the best lubricant.

Creep Problem. There exists the problem of keeping the lubricant inside the bearing at all times in order for it to be effective. F-50 oil creeps or flows very readily and will spread out of the bearing unless contained by a rubbing seal, which is impossible, or other device such as an anticreep barrier which will not allow the oil to wet it. FX-706A by 3M Company and W. F. Nye Company, New Bedford, Massachusetts, in conjunction with the U. S. Navy, had been studying the phenomenon of a fluid of higher surface energy not creeping or wetting a surface of lower surface energy. Published information from the Navy indicates that the FX-706A barrier film can be used satisfactorily up to 350°F, and information from W. F. Nye Company indicates that 2 to 5 years shelf life does not adversely affect the film. The application of the film to the faces of the bearings will be done by the contractor for us with the procurement of the bearing as presently planned.

Potting Material Selection. The retention of the outer races in their housings, and the retention of the shaft within the inner races of the bearings without introducing additional ball loading during or after assembly and without any clearances after installation, has been a problem which has not been solved to date. We have not made any decision to pot, although the contractor has recommended a potting material Stycast no. by Emerson Cumings, Canton, Massachusetts, if this is our direction.

#### Bearing Specifications for Engineering Model

Presented herein, is a preliminary bearing specification prepared for the procurement of bearings for the A/O subsystem engineering model. It is the culmination of our test program and of many consultations with the Fafnir Bearing Company and the Split Ball Bearing Division of Miniature Precision Bearings, Incorporated, as well as much literature digestion and contractors information and suggestions.

The specification details the geometry, material, precision, lubricant, lubricant quantity, cleanliness, barrier film, raceway topograph and other parameters requiring close control to achieve our overall specification.

It is expected that this specification will be interfaced with the contractor for modification regarding the barrier film application and recleaning cycle thought to be necessary based on prior receipt of many bearings.

After the bearings are received from the vendor, they will be disassembled by the contractor, recleaned, reassembled, lubricated and barrier-filmed. Running tests will then be conducted to determine their meeting the specified PSD requirements. Selection of pairs of bearings will probably be made for appropriate models.

#### Activity Preceding Flight Hardware Bearing Specification

Recently the contractor has suggested carrying on the bearing development testing program including the writing of the specification and recommendations for the selection of the bearings.

~~SECRET/SPECIAL HANDLING~~

~~SECRET~~/SPECIAL HANDLING

This will include methods of measuring and applying preloads, recommendations of potting, continued necessary performance analysis and verification tests, brinelling, thermal and cocking tests, etc. All in which he can apply his already established facilities and capability from his own drive A bearing test program. A working arrangement and bearing program with this type of liaison or interface is being arranged at this writing. There are many areas of investigation that could be made to improve bearing performance, but the present bearing specification as written 3-A.2 of the appendix should allow performance to Fig. 3 of EC-331B. To improve the performance by searching investigations in race topography, significant configuration mounting and bearing changes is not within the scope of the present specified requirements and is not our intention.

~~SECRET~~/SPECIAL HANDLING

~~SECRET~~/SPECIAL HANDLING

## 6.2 CABLING

In the scanner design we are faced with the problem of transmitting electrical signals and power to the gimbals. This problem is made unique in the manner that it is defined in the specification, that is 2-in. oz average running torque per axis for all contributors and a curve defining the PSD per axis for all contributors.

At the present time, the electrical interface, 1F332, requires passing of: 12 twisted pairs, 2 twisted triples, 6 shield twisted pairs and 14 single conductors across the roll axis, and 3 twisted pairs, 2 twisted shield pairs, and 7 single conductors across the pitch axis. The resistance of most of the wires have been defined but the remaining ones and any requirement for spares and were to terminate the spares are effecting the final scanner cable design.

There seem to be only two practical means of transmitting wires to the gimbals. The first is by means of slipring. There would be some problems to using a slipring such as: high PSD caused by the brushes rubbing on the rings; the electrical noise induced in the signal leads; the possible failure to meet the EMI spec; the size required to carry the number of circuits and current in them would require a larger shaft. An advantage to using sliprings is that there is record of success of passing wires across a rotary joint. Because of this we have obtained a slipring from the Electro-Tec Corporation of Blacksburg, Virginia. The slipring contains 32 circuits and is constructed with materials suitable for our application. We will test this slipring for PSD as well as running torque.

The other means of transmitting power is through appropriate bending of wires. Three methods of bending wires have been considered.

First, form the wires into flat flexible cables and then form the cable into a spiral similar to a clock spring. One end being anchored to the gimbal and the other to the stationary member. Calculations were made to optimize the length of the cable and the number of turns needed for flexing. For identification this configuration is called the spiral and Fig. 6.2-1 shows it on the roll axis.

Second, using flat flexible cable, as in the first method, form it into a "U" shape. By anchoring one end to the gimbal and the other end to the stationary member the cable rolls as the gimbal moves thus this configuration was termed "roll-along." Fig. 6.2-2 shows such a configuration on the roll axis.

Third, using flat flexible cables or individual wire and passing them down the center of the shaft that supports the gimbal. By anchoring one end to the gimbal and the other end to the stationary member as the gimbal rotates the wires will twist in the shaft. Fig. 6.2-3 shows such a configuration on the roll axis.

Flexing wires to transmit power over a limited rotation joint is not a new concept, but measuring the torque required to bend them and the torque variations that occur as they move apparently is. It has been determined that wire and or cable manufacturerers are completely unfamiliar with such a requirement. It has also been determined that the torque required to flex the wires can be approximated by calculations, but torque variations (PSD) must be determined empirically. Because of this a test fixture was constructed to test the three configurations.

Fig. 6.2-4 shows a photograph of the test fixture designed to simulate the roll axis. The fixture was driven by a position servo using a brushless torque motor with a potentiometer as the feedback device. (See Fig. 6.2-5 for the schematic.) To obtain a voltage directly related to torque a resistance was placed in series with the motor. Since torque is directly proportional

~~SECRET~~/SPECIAL HANDLING

~~SECRET/SPECIAL HANDLING~~

to motor current, the voltage impressed across the resistor gave the motor torque when multiplied by a constant. This arrangement enabled measurement of PSD and torque due to cables.

Fig. 6.2-6 shows the method used to calibrate the sensitivity of the torque motor. A torque watch was used to determine the no load torque of the fixture. Several readings were taken to obtain an average. A known weight was attached to the motor shaft with a string and the motor driven to just hold the weight, while the voltage across the series resistor was recorded. This was repeated with the string wound in the opposite direction and the motor rotation reversed.

To prevent aliasing problems in the digitized data an active filter was installed across the output of the series resistor. This is a 2-pole filter with a break frequency of either 1 rad/sec or 100 rad/sec, depending on the type of data to be recorded. The gain of the filter was set at one. The output of the filter is recorded on a Brush recorder and or sampled by an analog to digital conversion when PSD measurements are to be made. The digitizer (A to D converter) will accept analog signals with a range of -1 volt to +1 volt. The series resistor is chosen such that the output voltage will not saturate the digitizer. The value is determined with a bridge and the proper scale factor (oz-in./volt) calculated and recorded.

#### 6.2.1 Early Testing

Figs. 6.2-7, and 6.2-8 show the baseline data that was recorded on the fixture alone (no cables). Fig. 6.2-7 is the fixture PSD. As can be seen the fixture alone is too high and exceeds the specification curve for all contributors (bearings and cables). Recognizing the fact that the fixture PSD was high we attempted to gain an insight into the nature of PSD due to cables by testing representative wire bundles.

The spiral configuration was tested using cable samples obtained from Sanders Associates. The cables were flexible printed wiring using 2-oz copper for conductors and 3-mil thick kapton insulation. The cables were only 1/2-inch wide rather than 1 1/4 inches intended and contained copper equivalent to 4 number 26 AWG conductors. Fig. 6.2-9 shows the running torque required to rotate through 120 degrees of travel for the cable only, the fixture torque has been subtracted. Fig. 6.2-10 shows the PSD of the cable and the test fixture.

The roll-along configuration was tested using cables purchased from Sanders Associates. The cables were flexible printed wiring using 2-oz copper, 1-mil thick kapton insulation, containing copper equivalent to 9 number 26 AWG conductors. Fig. 6.2-11 shows the running torque required to rotate through 120 degrees of travel for the cable only. Fig. 6.2-12 shows the PSD of the cable and the test fixture.

The twist configuration was tested using samples obtained from Cicoil Corp. The cables were highly stranded round conductors imbedded in strips of silicone rubber, each strip containing 10 number 28 AWG conductors. Fig. 6.2-13 shows the running torque of the cables only, the fixture running torque has been subtracted. Fig. 6.2-14 shows the PSD of the cables and the test fixture. It should be pointed out that the twist cable was not contained by a shaft during this test.

Although the PSD of this test fixture was too high, valuable data were obtained. From the data it can be seen that PSD due to cables add little to the test fixture PSD and in fact the twist configuration seemed to reduce it at the lower frequencies. We were able to determine the relative PSD levels of the different cable configurations and thus determine the best configuration. Relative running torque of the different configurations was also obtained. The torque gradient

~~SECRET/SPECIAL HANDLING~~

~~SECRET~~/SPECIAL HANDLING

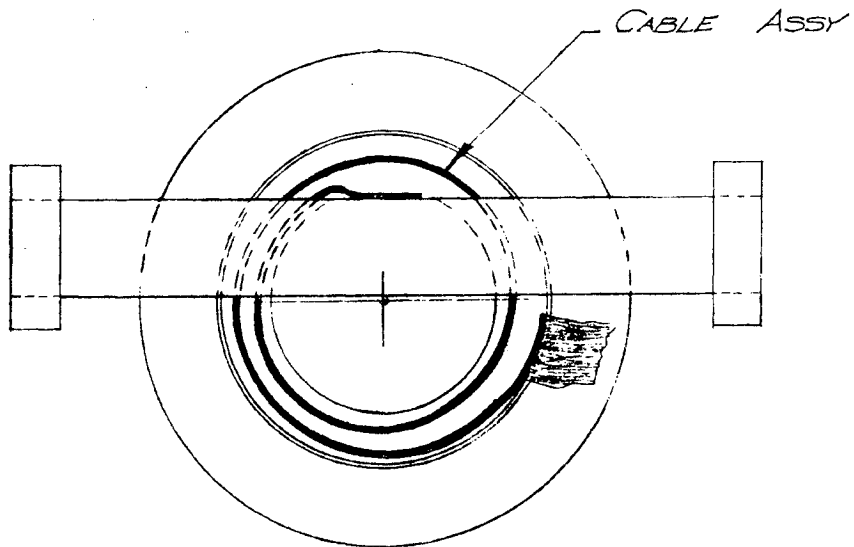


Fig. 6.2-1 — Spiral configuration, flexible cable assembly (roll axis)

~~SECRET~~/SPECIAL HANDLING

~~SECRET~~/SPECIAL HANDLING

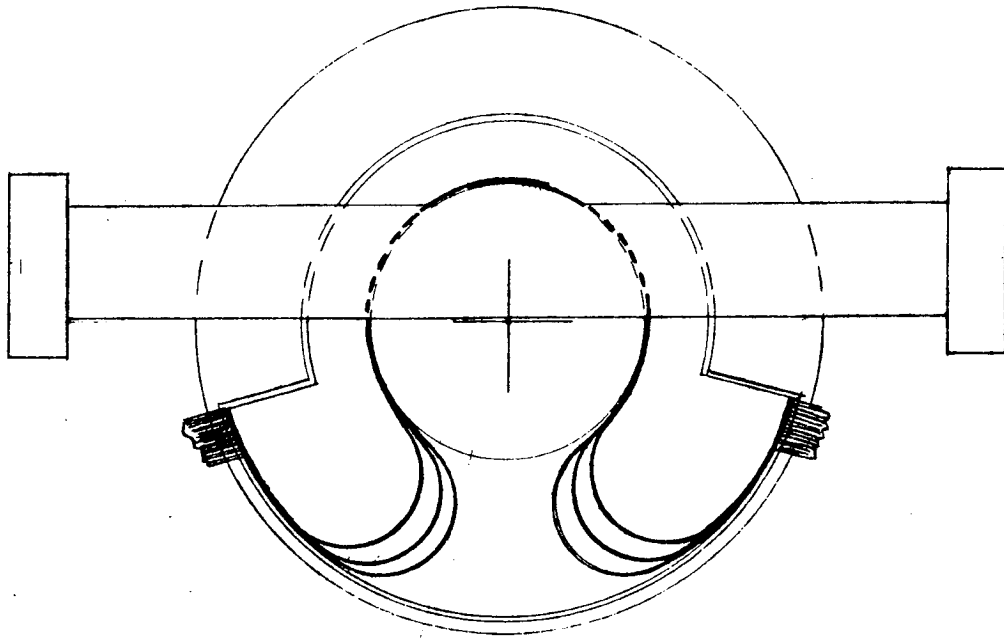


Fig. 6.2-2 — Roll-along configuration cable assembly (roll axis)

~~SECRET~~/SPECIAL HANDLING

~~SECRET/SPECIAL HANDLING~~

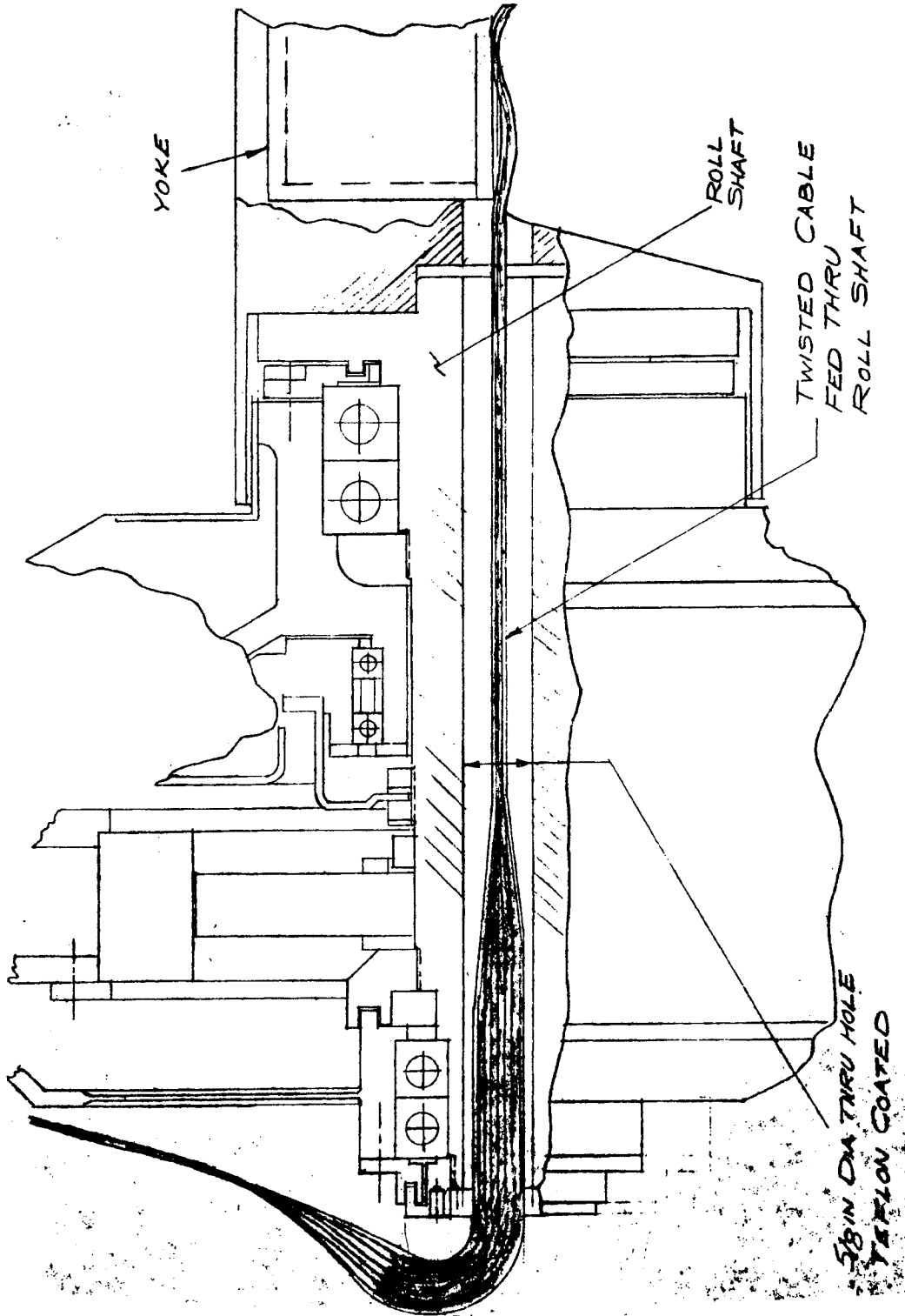


Fig. 6.2-3 — Twist configuration cable assembly (roll axis)

~~SECRET/SPECIAL HANDLING~~

~~SECRET~~/SPECIAL HANDLING

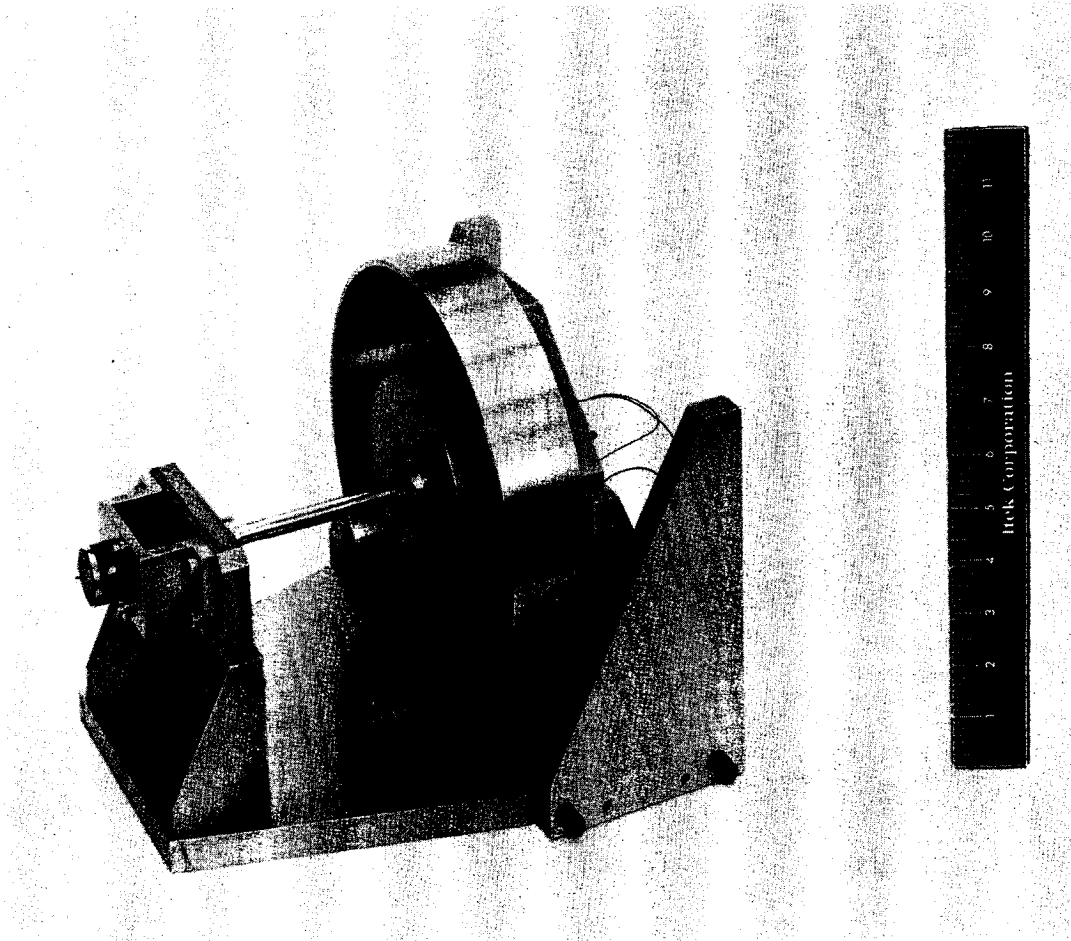


Fig. 6.2-4 — Cable test fixture photograph

~~SECRET~~/SPECIAL HANDLING

~~SECRET~~/SPECIAL HANDLING

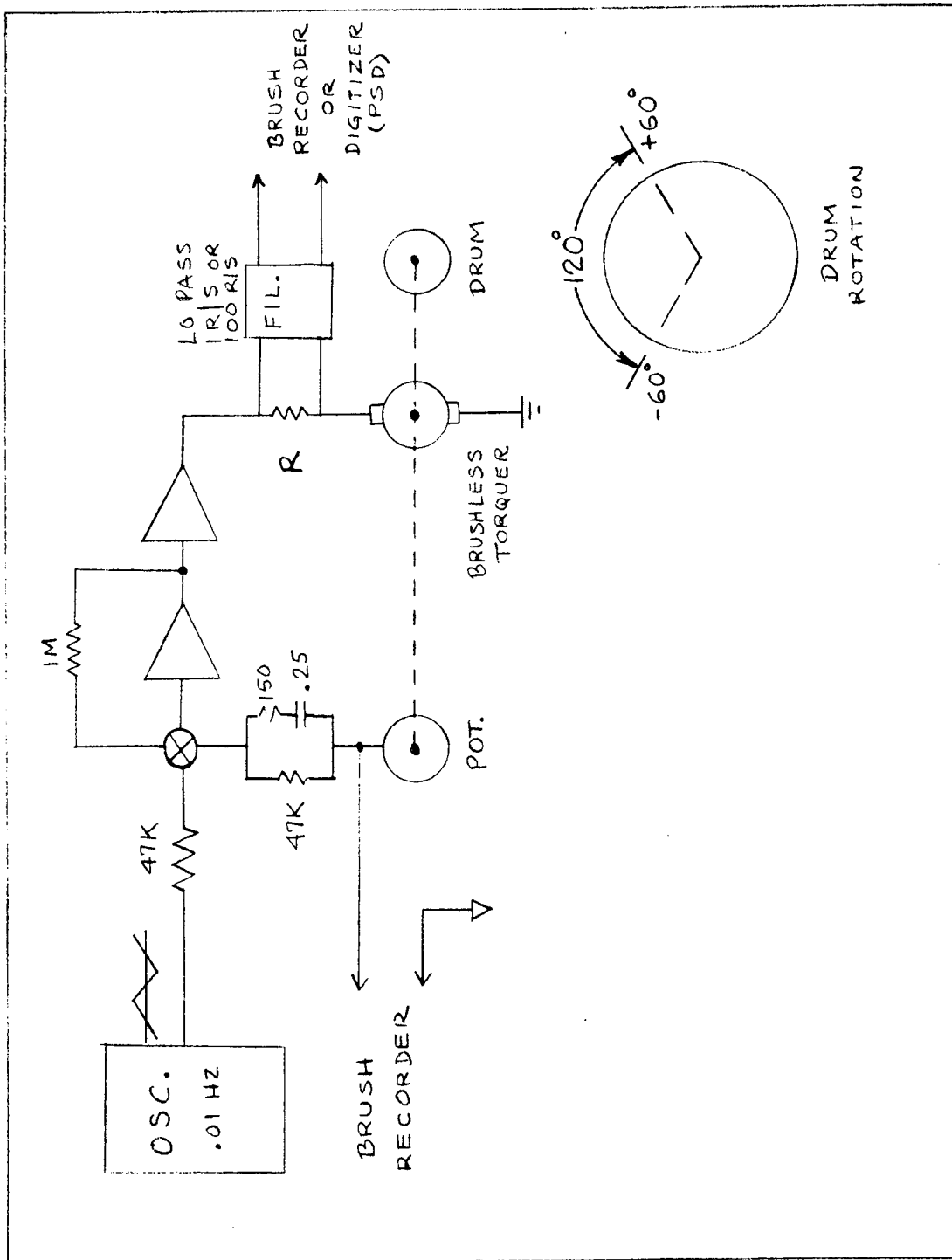


Fig. 6.2-5 — Cable test fixture schematic

~~SECRET~~/SPECIAL HANDLING

~~SECRET/SPECIAL HANDLING~~

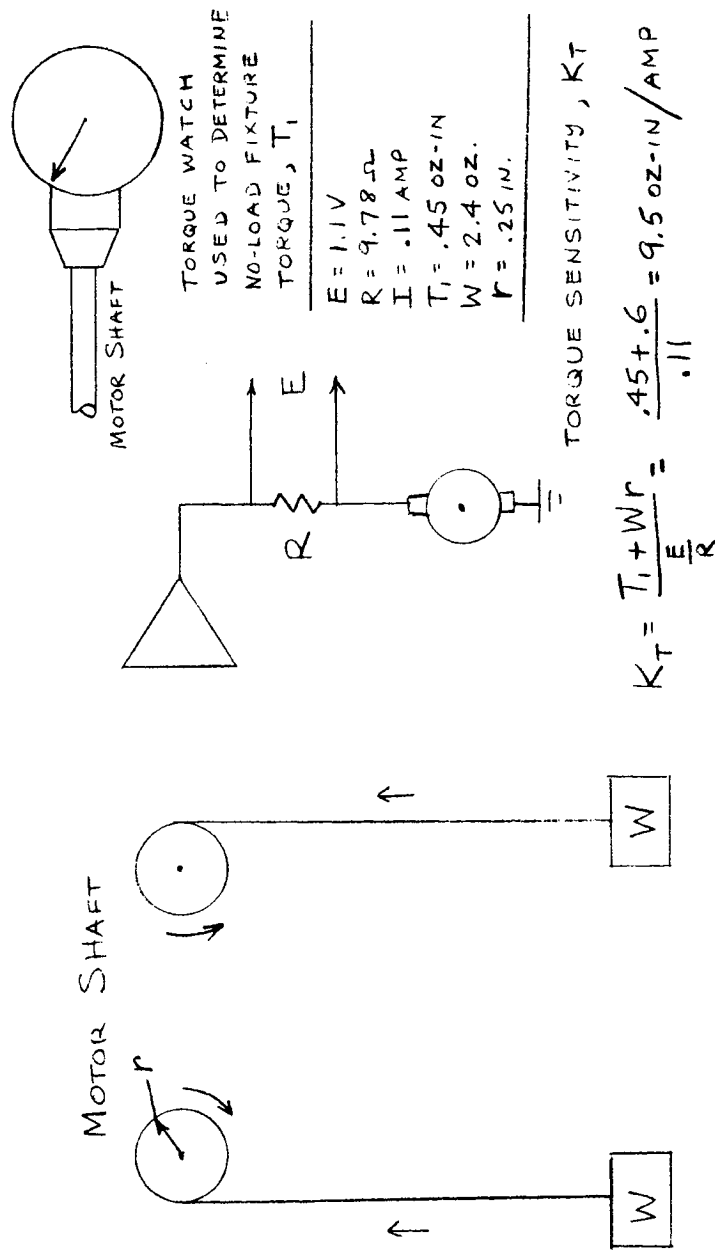


Fig. 6.2-6 — Torque sensing calibration

~~SECRET/SPECIAL HANDLING~~

~~SECRET/SPECIAL HANDLING~~

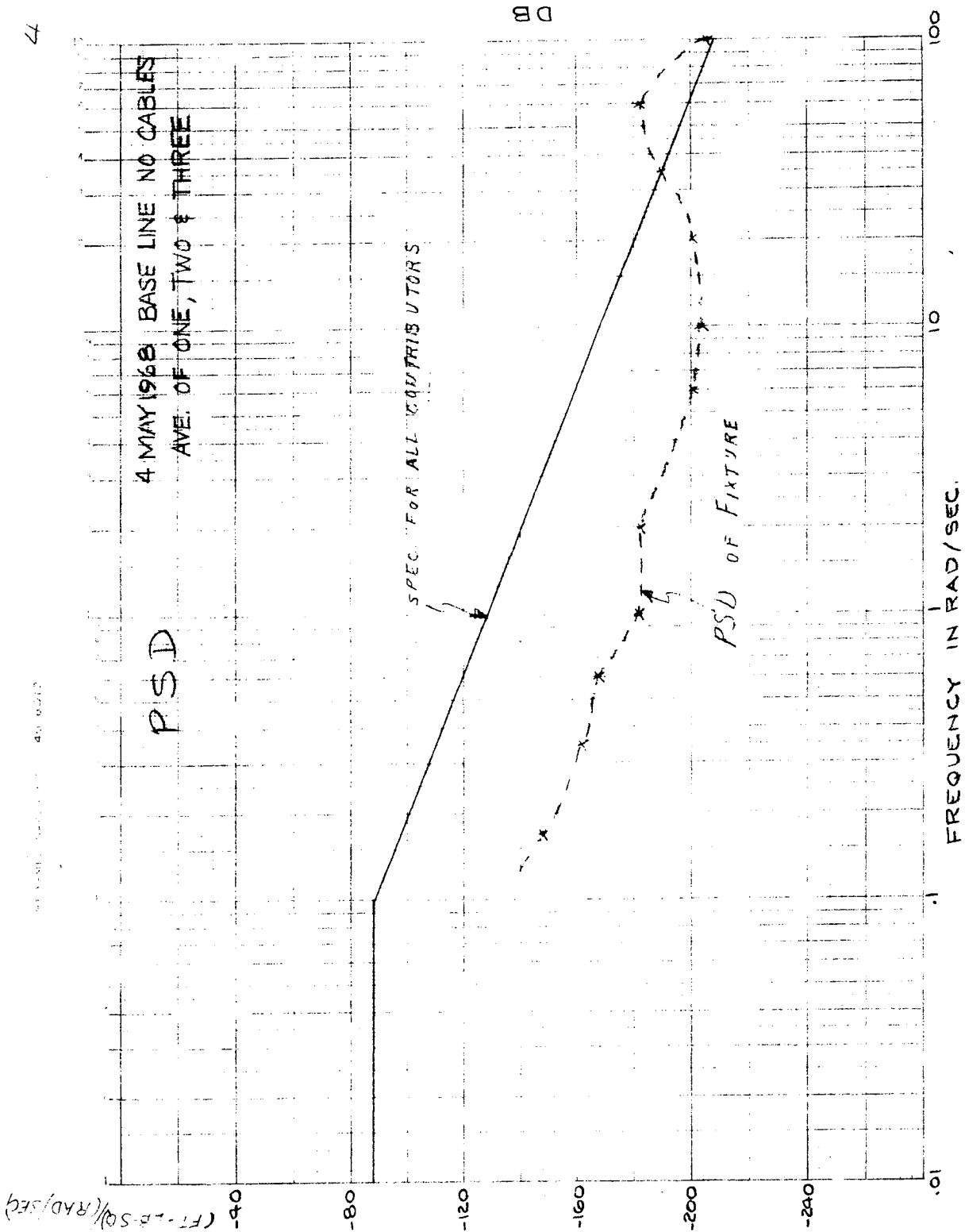


Fig. 6.2-7 — Baseline data for test fixture alone (PSD)

~~SECRET/SPECIAL HANDLING~~

~~SECRET~~/SPECIAL HANDLING

TEST FIXTURE

AVERAGE RUNNING TORQUE

0.25 oz.-IN.

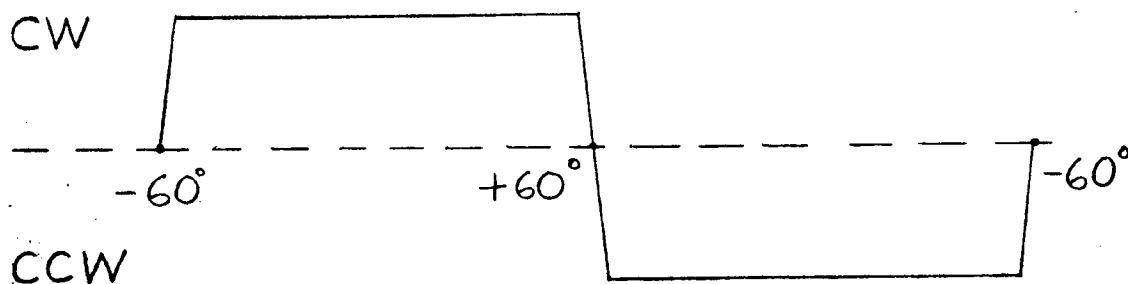


Fig. 6.2-8 — Average running torque for test fixture alone

~~SECRET~~/SPECIAL HANDLING

~~SECRET~~/SPECIAL HANDLING

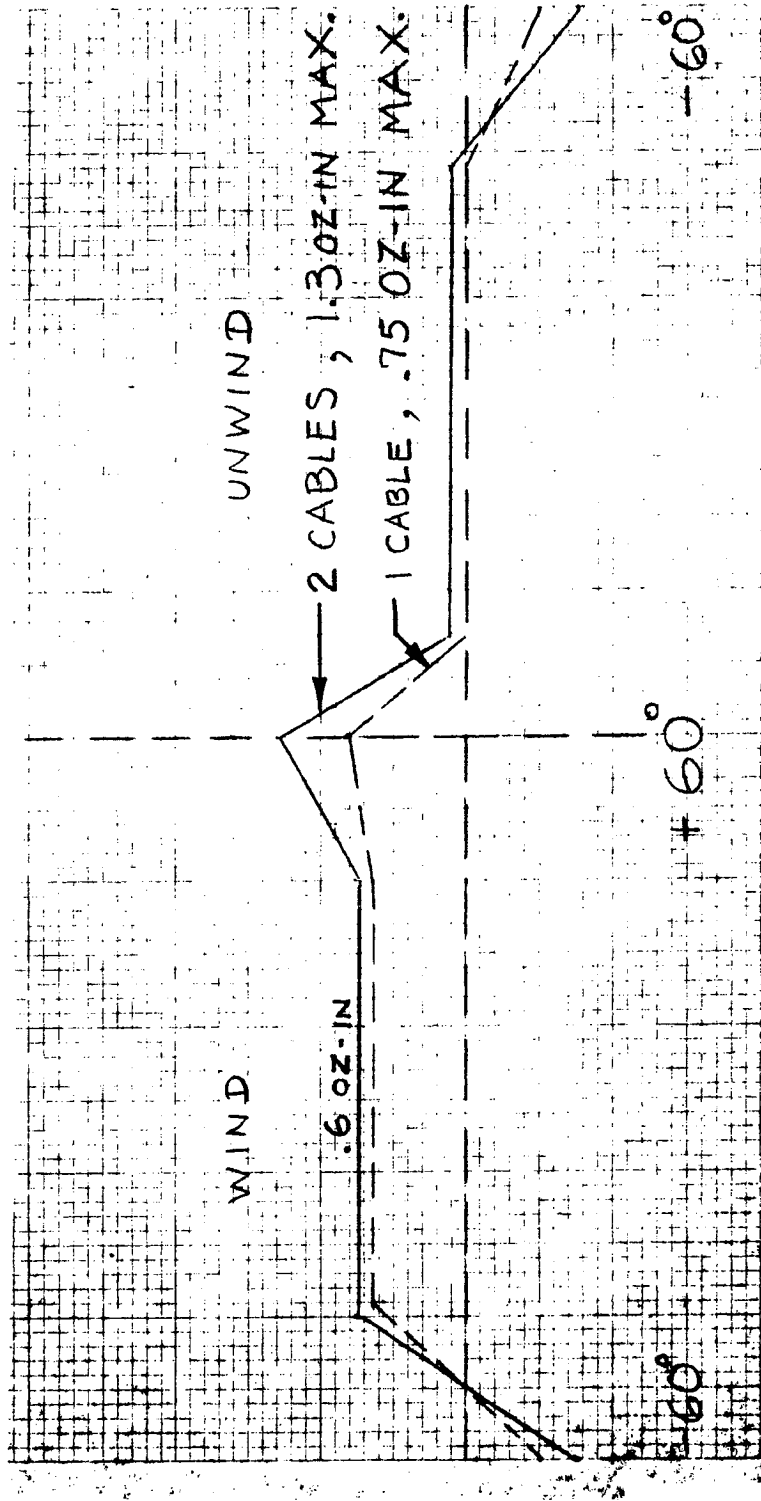


Fig. 6.2-9 — Running torque required to rotate through 120 degrees, for cable only (spiral configuration)

~~SECRET~~/SPECIAL HANDLING

~~SECRET/SPECIAL HANDLING~~

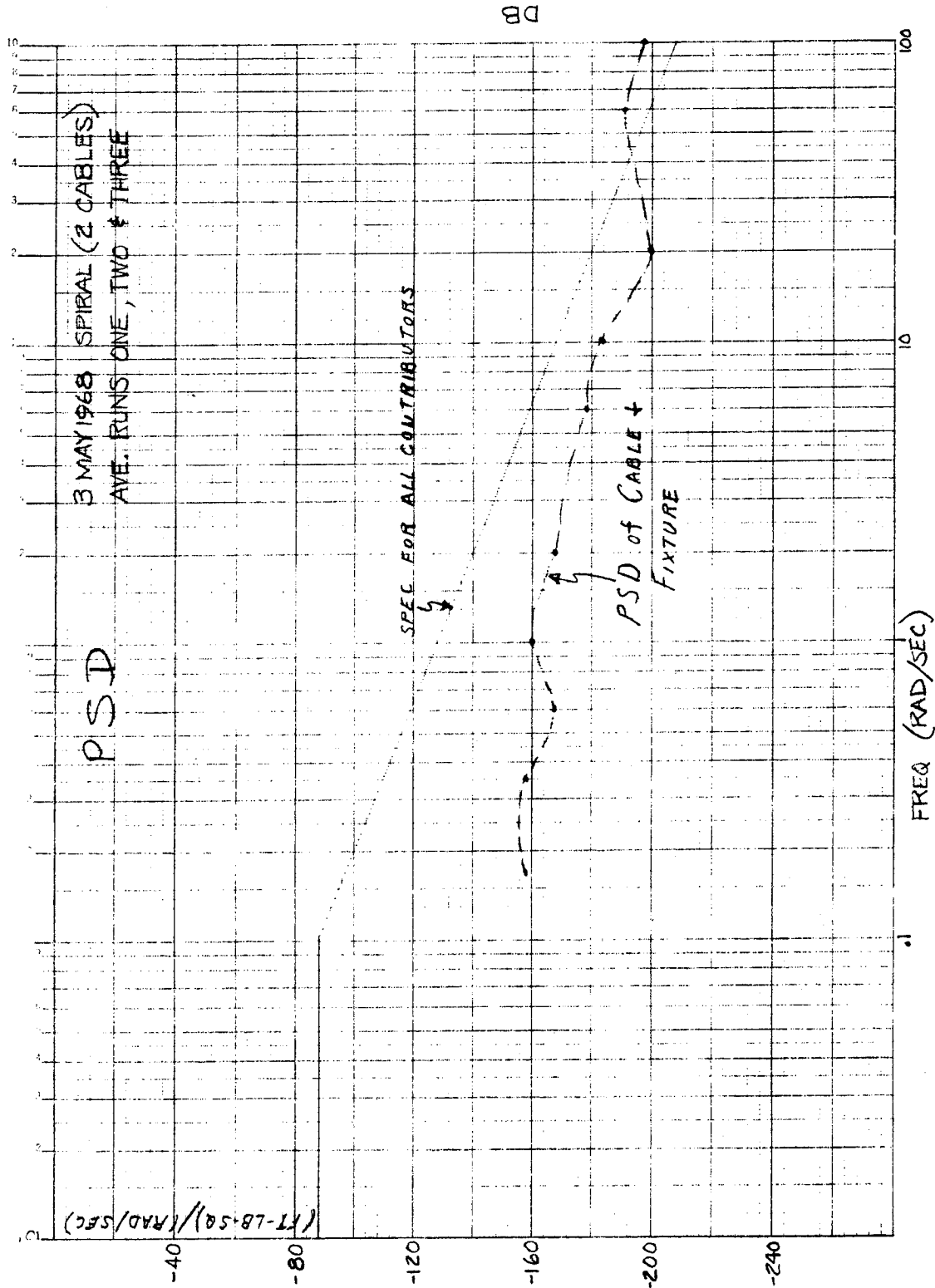


Fig. 6.2-10 — Cable and test fixture PSD, spiral configuration

~~SECRET/SPECIAL HANDLING~~

~~SECRET/SPECIAL HANDLING~~

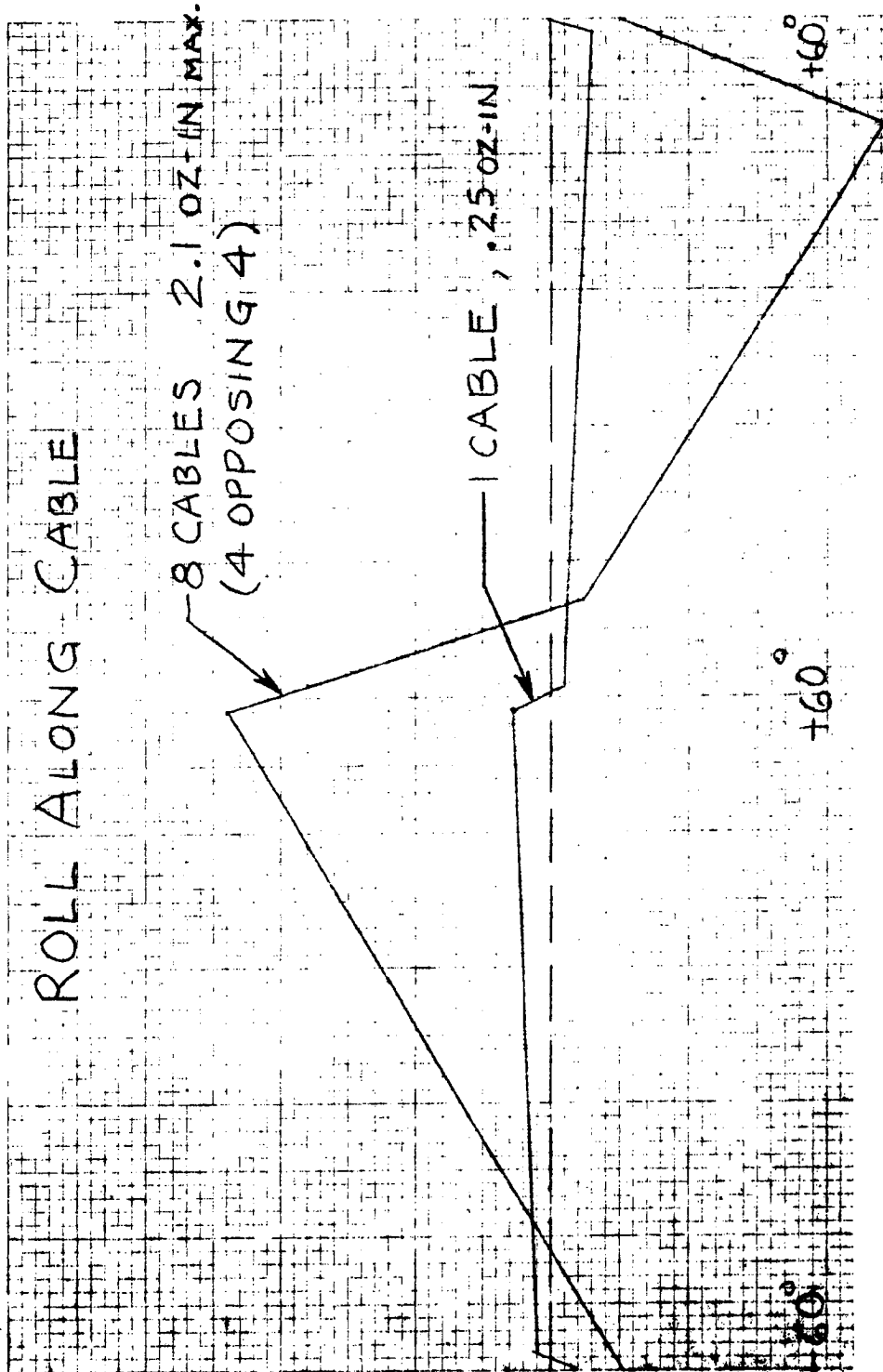


Fig. 6.2-11 — Running torque required to rotate through 120 degrees  
(roll-along configuration)

~~SECRET/SPECIAL HANDLING~~

~~SECRET/SPECIAL HANDLING~~

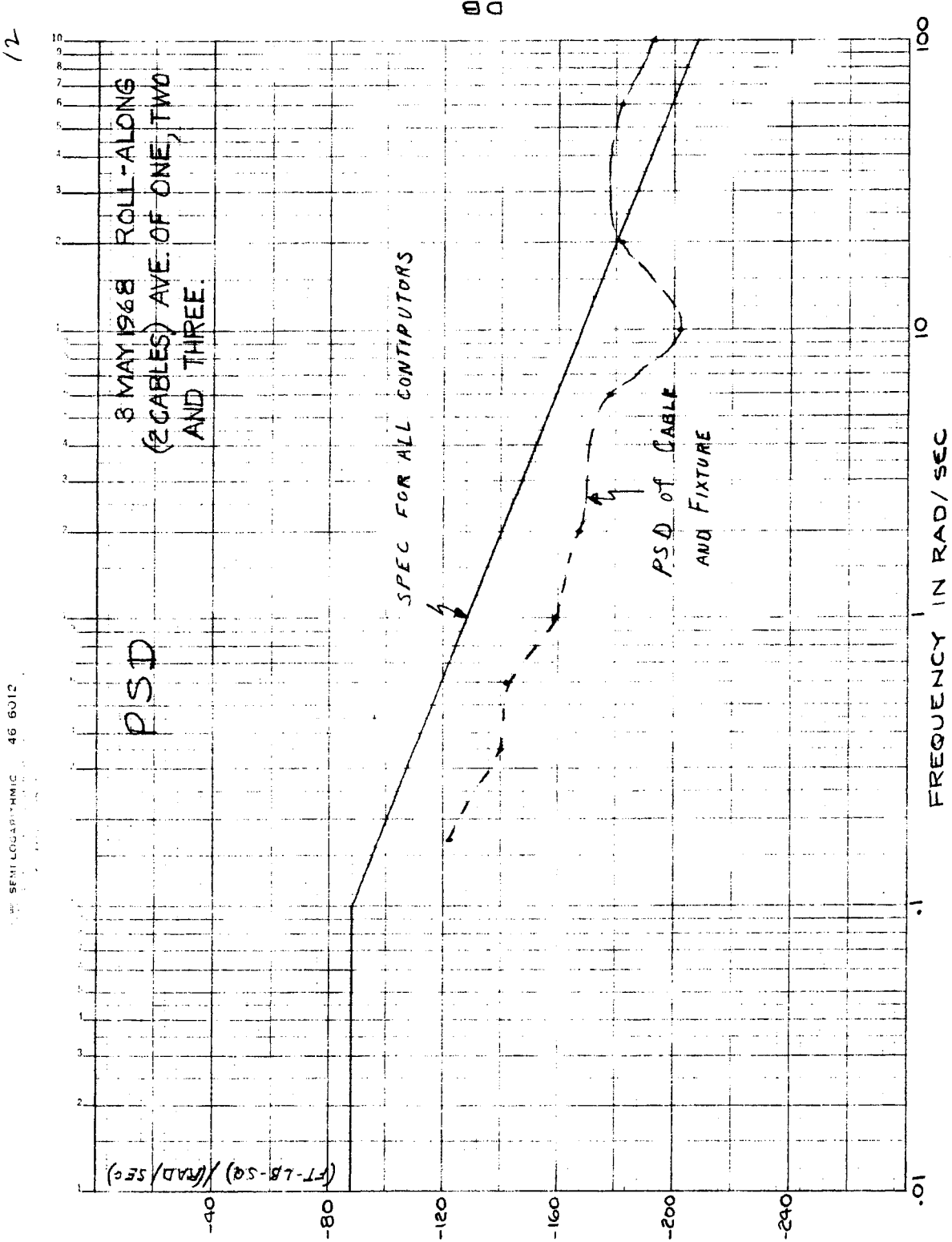


Fig. 6.2-12 — Cable and test fixture PSD, roll-along configuration

~~SECRET/SPECIAL HANDLING~~

~~SECRET~~/SPECIAL HANDLING

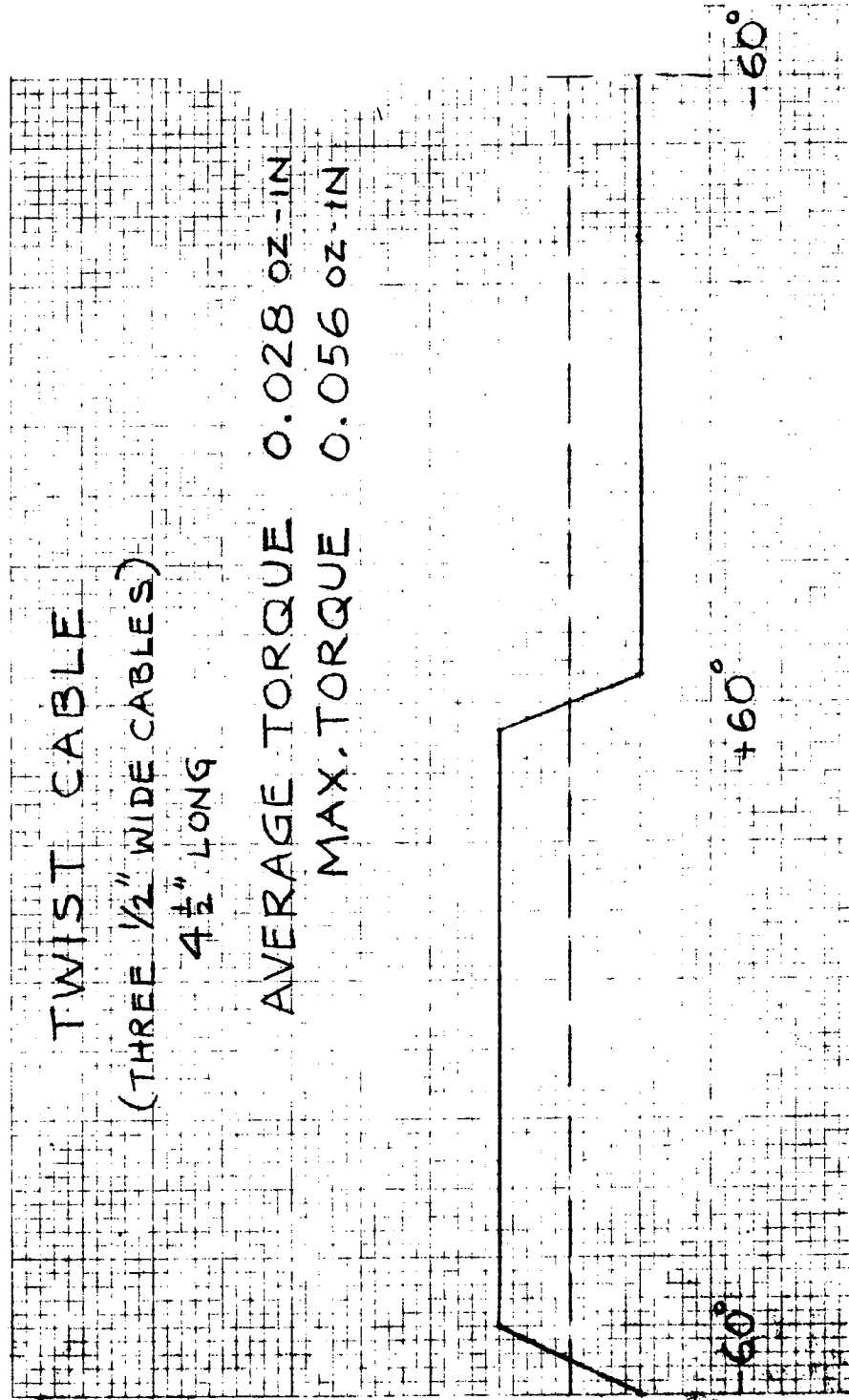


Fig. 6.2-13 — Running torque for cables only, twist configuration

~~SECRET~~/SPECIAL HANDLING

~~SECRET/SPECIAL HANDLING~~

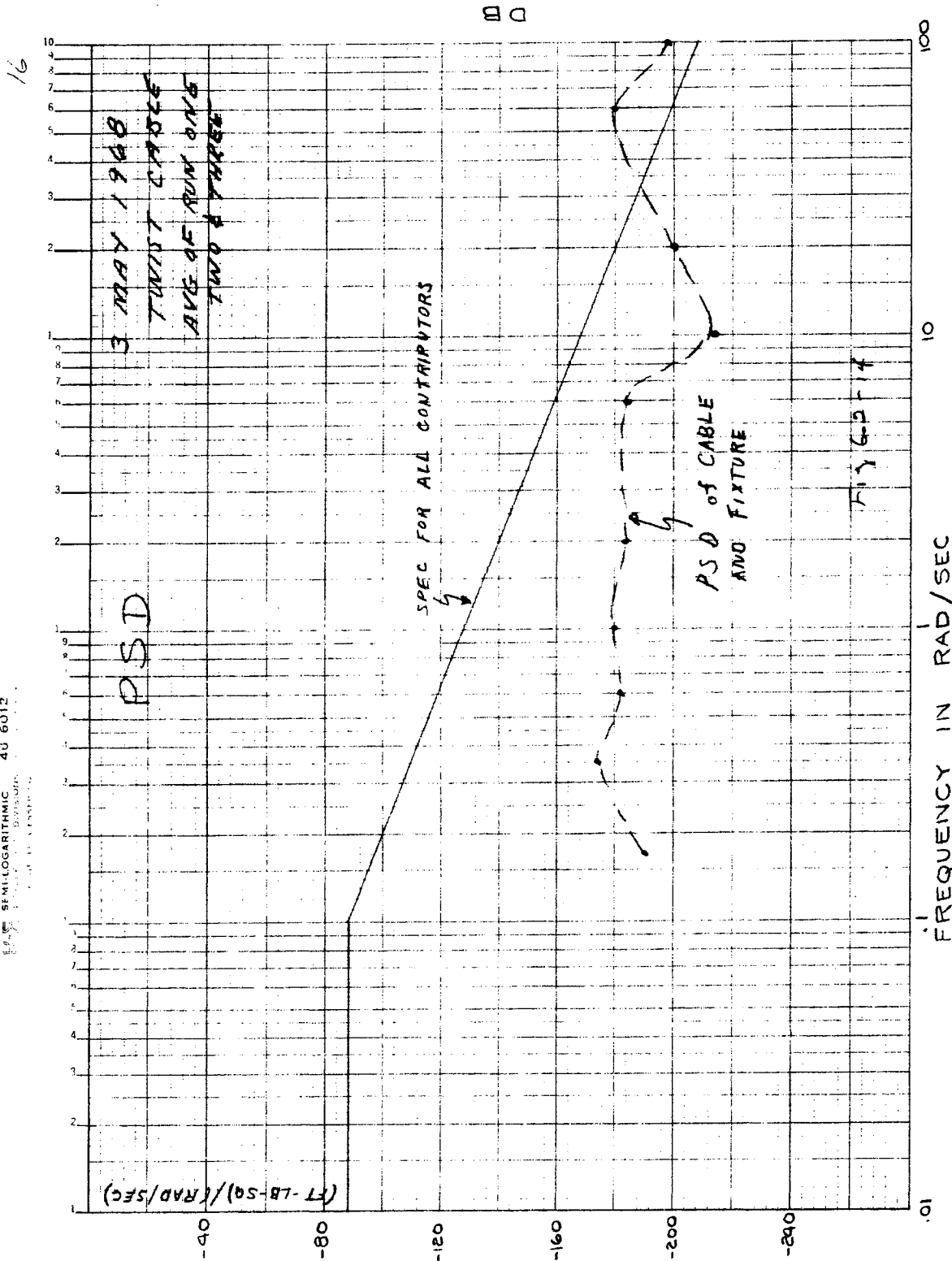


Fig. 6.2-14 — Cable and test fixture PSD, twist configuration

~~SECRET/SPECIAL HANDLING~~

~~SECRET~~/SPECIAL HANDLING

recorded in the spiral configuration was anticipated due to the spring-like configuration. The torque gradient recorded in the roll-along configuration was not anticipated. It is believed that this torque gradient is due to the cable taking a set in one position and acting as a spring when moved from that position. It has been demonstrated by testing that this set, or memory, is a function of the insulating material. While no torque gradient was observed in the twist cable it is probably due to the very low running torque, as anticipated.

The test results indicate the best cable configuration, from a PSD and torque consideration is the twist configuration, that is, to have all the wires pass through the shaft. At this time there are some unknown variables that may not allow such a cable configuration. The electrical interface is not complete, and thus the size of the total wire bundle is undefined. The amount of clearance needed between the wire bundle and shaft wall needed for minimum PSD and torque is still unknown. What effects the proximity between power and signal leads, which would result from all the wires in one bundle, may have on EMI are unknown.

With the above consideration in mind, a preliminary cable design has been made that is a combination of a twist and roll-along configurations for the roll axis and a twist configuration for the pitch axis. (Fig. 6.2-15, Itek drawing 906009) shows this design. A connector, RTK00-18-85S will be mounted on the stationary part of the roll housing. This connector will be used to connect or disconnect all power and signal leads to the scanner: a separate connector will supply the gyros. The roll torque motor and encoder leads will run directly to the connector as self leads. The power leads for: two gyros, pitch and roll, and the pitch torque motor and encoder will pass through the shaft to a terminal board mounted on the bottom of the roll axis yoke. Fig. 6.2-16 (Itek drawing 906010) shows a layout of the stationary bushing that will retain the twist cable to the roll housing. The twist cable contains 2 trippletwisted wires of 28 AWG, 6 twisted pairs of 22 AWG and 2 twisted pairs of 24 AWG wire. The wires in the twist cable will be individual, twisted as specified, and constructed of thin-wall teflon insulation with the conductor made of many strands. The signal leads will be formed into a roll-along cable as shown in Fig. 6.2-17 (Itek drawing 906008). This cable will be formed into a roll along as shown in Fig. 6.2-15 and terminated on the top of the roll axis shaft at a terminal board. The roll along cable will be of a highly specialized construction as follows: twisted pairs will be thin wall teflon with high stranding. Twisted shield pairs will be the same as above with a braided shield. Individual conductors will be uninsulated with high stranding. The cable is then encased in a silicon rubber insulation. Cables of this construction have been ordered from Cicoil Corporation. The wires from the pitch axis torque motor and encoder will run along the roll axis yoke and terminate at the appropriate terminal boards. The leads from the pitch axis gyro will be formed into a loop, as shown in Fig. 6.2-15, and held in a manner, not yet determined, so they will twist as they cross the pitch axis to the roll yoke. They will then follow the roll yoke, top and bottom, to the appropriate terminal board.

This cable design was selected to allow for the maximum freedom for future growth or change. It can be seen that the use of connectors has been held to a minimum in order to save weight and space. On engineering models it may be desirable to replace the terminal strips with Amp taper pin blocks or some other type of quick-disconnect terminals.

#### 6.2.2 Current Test Effort

As mentioned previously, the PSD previously, the PSD of the first fixture was too high. Fig. 6.2-18 shows a photograph of our new test fixture. To eliminate as much friction as possible, the ball bearings supporting the simulated roll shaft were replced with air bearings. The potentiometer was replaced with a brush less tachometer. In this design the shaft completely floating

~~SECRET~~/SPECIAL HANDLING

~~SECRET~~/SPECIAL HANDLING

and is only restrained by the magnetic field of the motor and tach plus the unbalance of the shaft. Included in the design of this fixture was a provision for simulating different size holes in the shaft.

Fig. 6.2-19 shows the baseline PSD of the new fixture. This baseline was taken with no filter in the output and as was mentioned previously an aliasing problem can be seen, the spike at 31.4 rad/sec. It seems from this plot of PSD.

The roll-along cable shown in Fig. 6.2-17 has been tested. The running torque is shown in Fig. 6.2-20 and a plot of the PSD is shown in Fig. 6.2-21. The apparent upward break in the PSD plot is a function of the autocor program used to reduce the data and not a function of the cable and test fixture PSD.

A twist cable consisting of 6 number 22 AWG twisted pairs, 2 number 24 AWG twisted pairs and 2 number 28 AWG twisted triples has been tested using a shaft with a 7/16 dia hole. The running torque is shown in Fig. 6.2-22 and the PSD plot is shown in Fig. 6.2-23. The wire used for the twist cable was PVC wire per MIL-W-16878 type B. It is recognized that PVC wire is more flexible than the proposed teflon wire but it is hoped that the increased stranding and thin insulation will more than compensate for the stiffer teflon. At the present time, the purchasing department is conducting a search to determine how many wire manufacturers will make the desired wire.

At this time, the control system used to drive the new test fixture is being optimized and calibrated.

When this is completed, a series of test will be conducted to optimize the cable design, such as: minimum shaft size versus cable size, coatings on the inside of the shaft to reduce PSD, and different insulation material to reduce torque and PSD.

Because the cables now being planned for use in the scanner will not conform to the wire recommended in the approved parts list a qualification program must be conducted. The qualification program will include the following test.

1. Life cycling: Representative cables will be cycles a minimum of 100,000 cycles. The resistance will be monitored during the life test to determine if and when a failure takes place.
2. Environmental: Representative cables will be subjected to program levels of vibration, temperature and vacuum to determine the effects, if any, on the cables.

NOTE: The three figures listed below are engineering drawings and are included in a supplement accompanying this report.

Fig. 6.2-15 — Cable design showing combination of 2-twist and roll-along configuration for roll axis, and 2-twist configuration for pitch axis (Dwg. no. 906009)

Fig. 6.2-16 — Stationary bushing to retain twist cable to roll housing (Dwg. no. 906010)

Fig. 6.2-17 — Roll-along cable (Dwg. no. 906008)

~~SECRET~~/SPECIAL HANDLING

~~SECRET~~/SPECIAL HANDLING

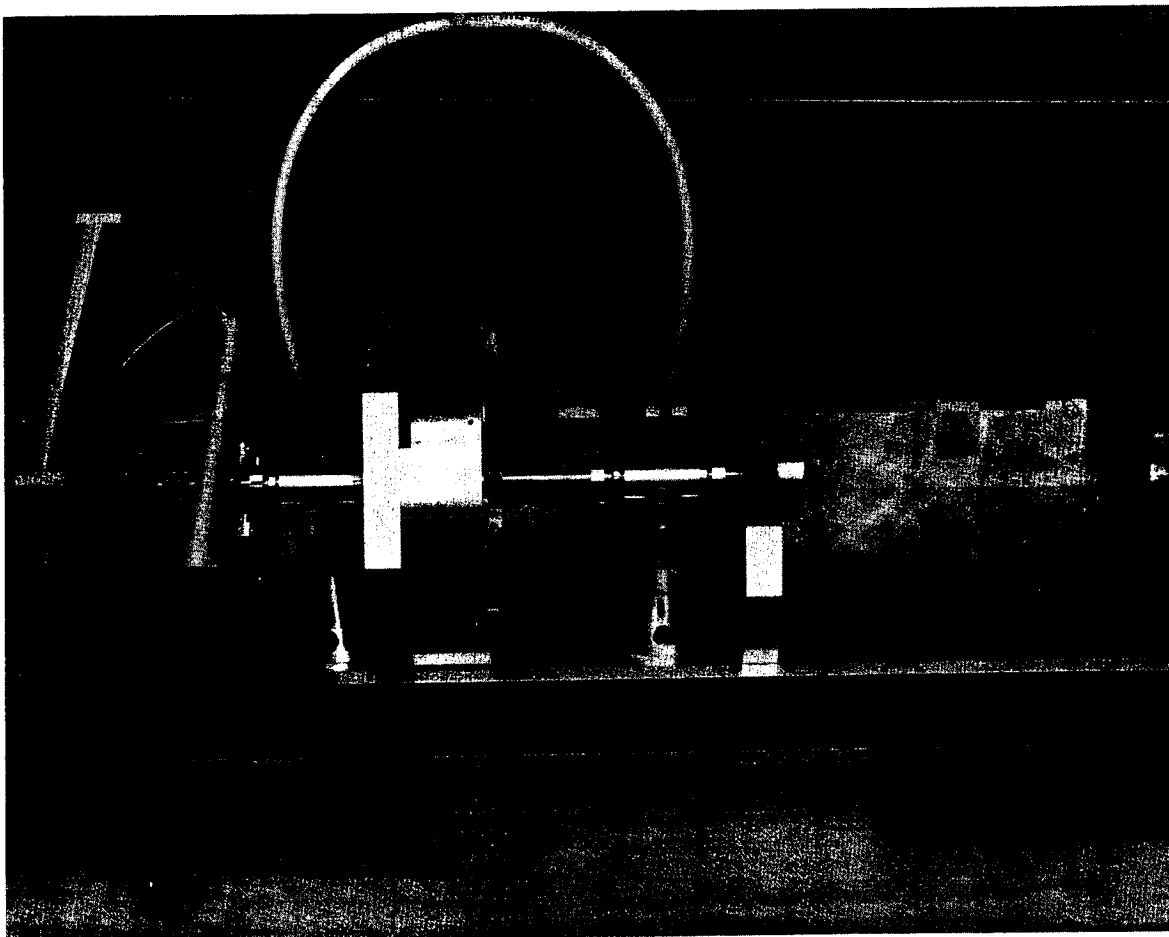


Fig. 6.2-18 — Photograph of new test fixture, roll-along cable

~~SECRET~~/SPECIAL HANDLING

~~SECRET/SPECIAL HANDLING~~

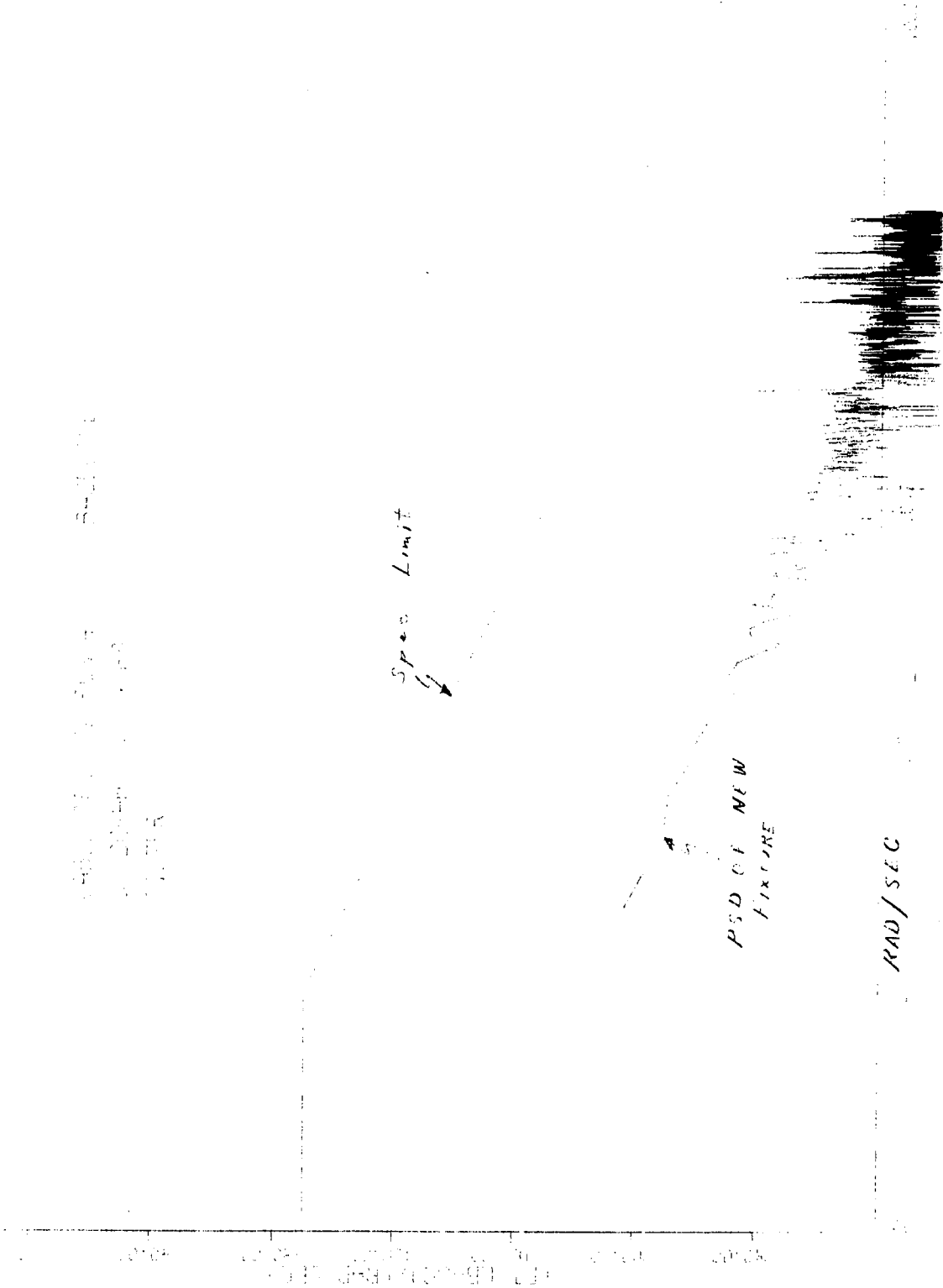


Fig. 6.2-19 -- Baseline PSD of new fixture, roll-along cable

~~SECRET/SPECIAL HANDLING~~

~~SECRET/SPECIAL HANDLING~~

RENE D ETZBEN CO.

RENE D ETZBEN CO.

ROLL ALONG CABLE

USINS

Itek PART 906008

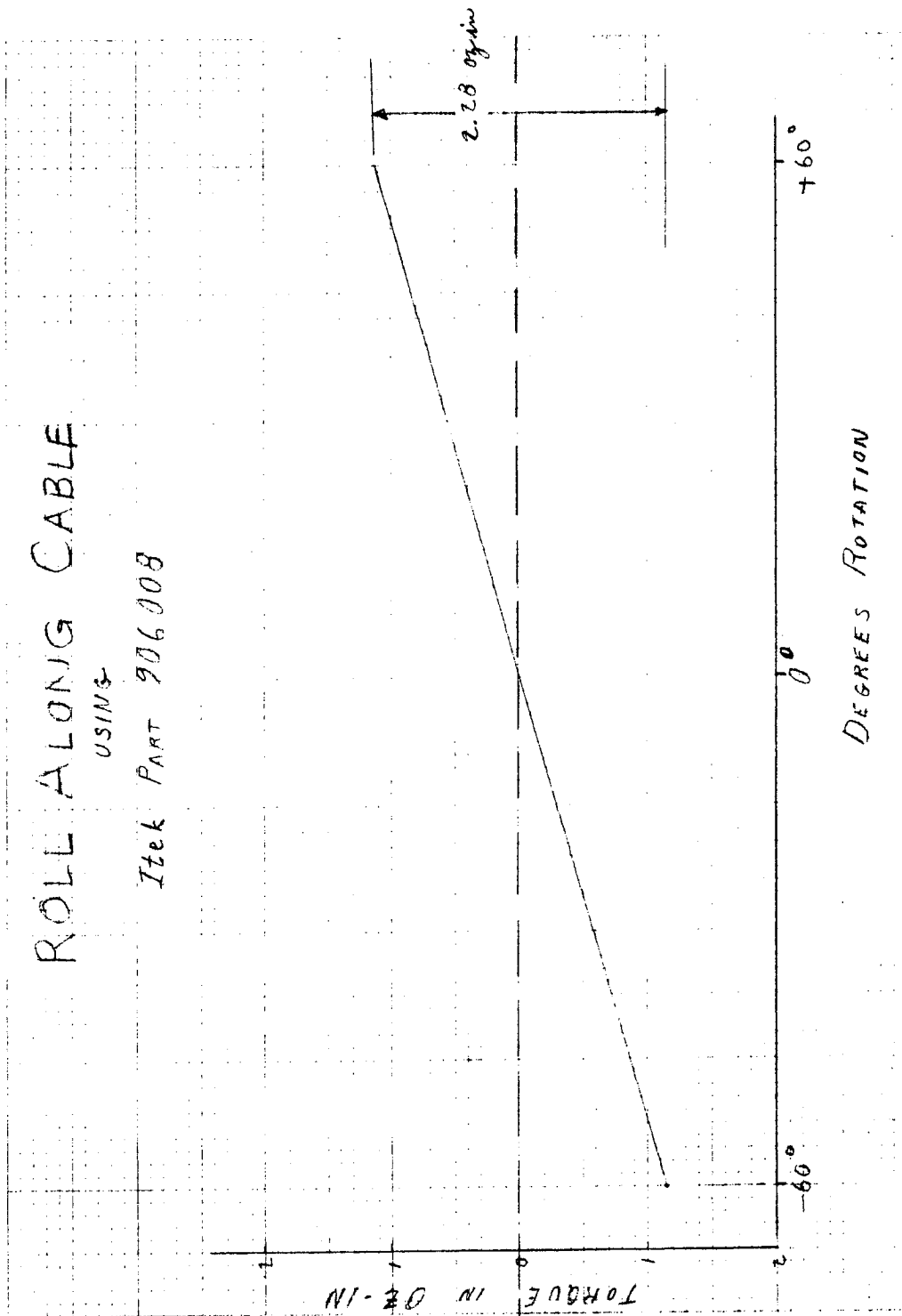


Fig. 6.2-20 — New fixture running torque, roll-along cable

~~SECRET/SPECIAL HANDLING~~

~~SECRET~~/SPECIAL HANDLING

PSD BY AUTOCOR  
CABLE TEST W02  
ROLL ALONG, SPEED=1.5 D/S

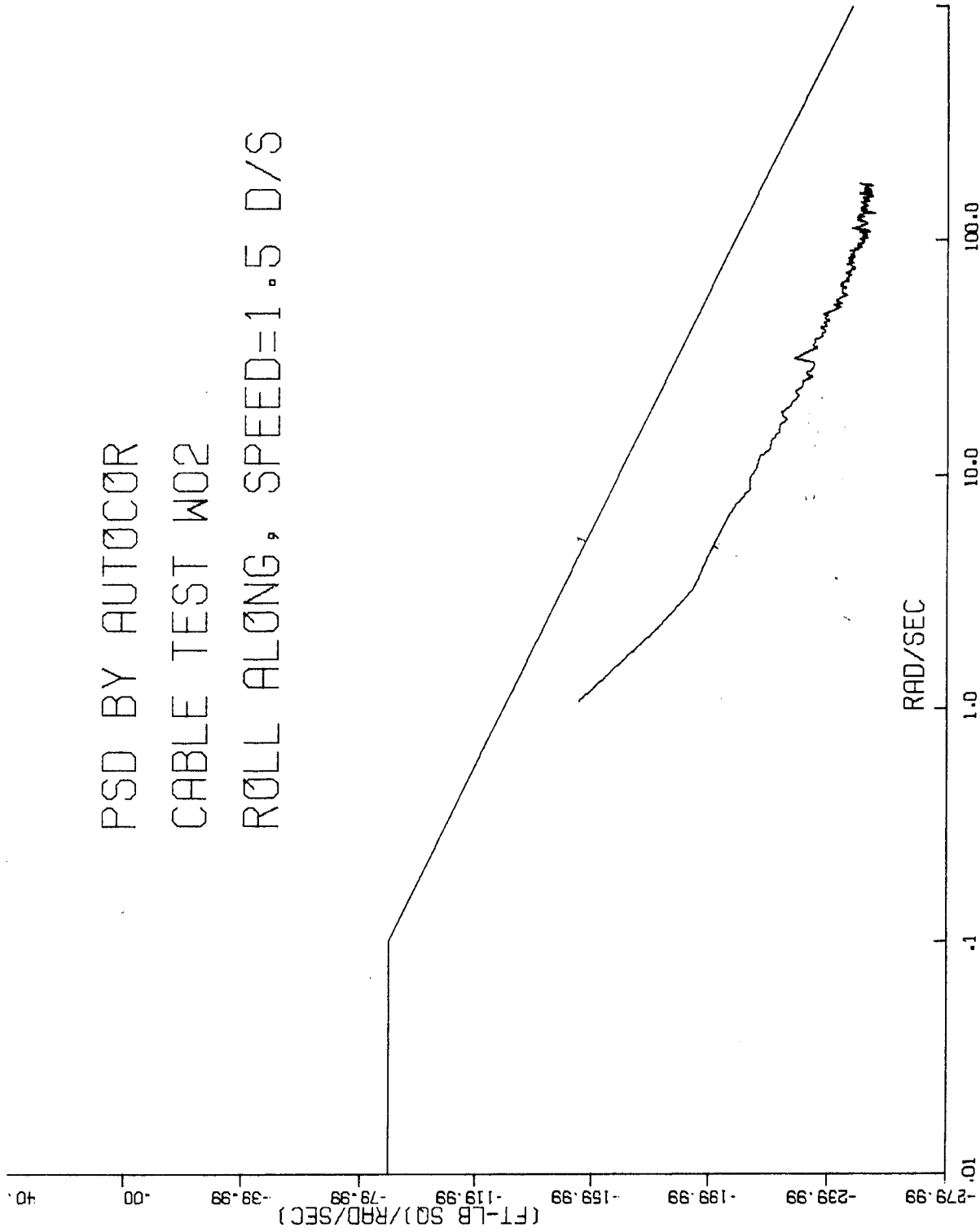


Fig. 6.2-21 — Plot of baseline PSD of new fixture, roll-along cable

~~SECRET~~/SPECIAL HANDLING

~~SECRET/SPECIAL HANDLING~~

NO. 20017-2 DIETZEN SPARK PAPER  
EURENE DIETZEN CO  
MAY 1954

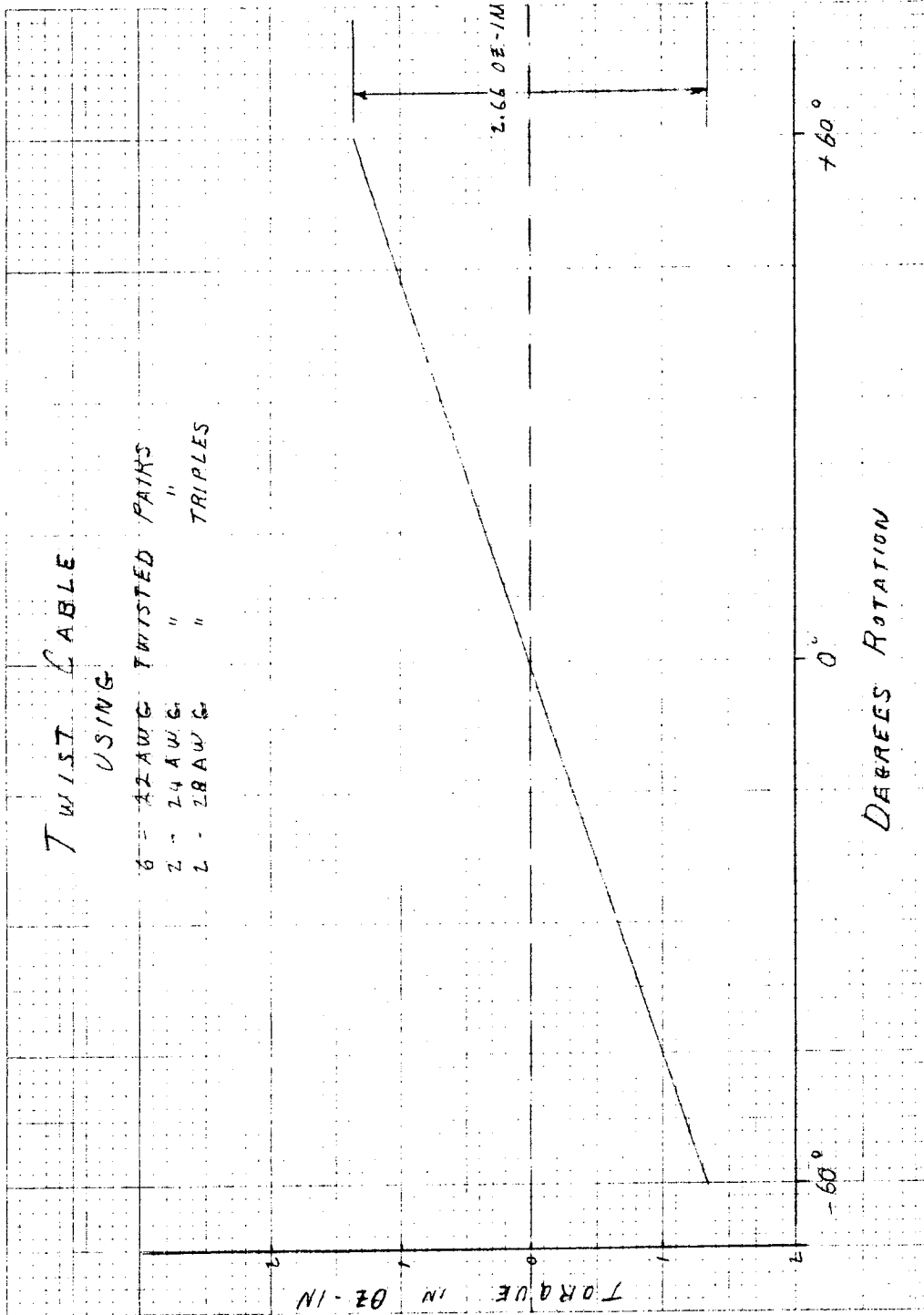


Fig. 6.2-22 — Running torque, twist cable

~~SECRET/SPECIAL HANDLING~~

~~SECRET/SPECIAL HANDLING~~

PSD BY AUTOCOR  
CABLE TEST W07  
TWIST CABLE  
MIN SPEED VARIATIO

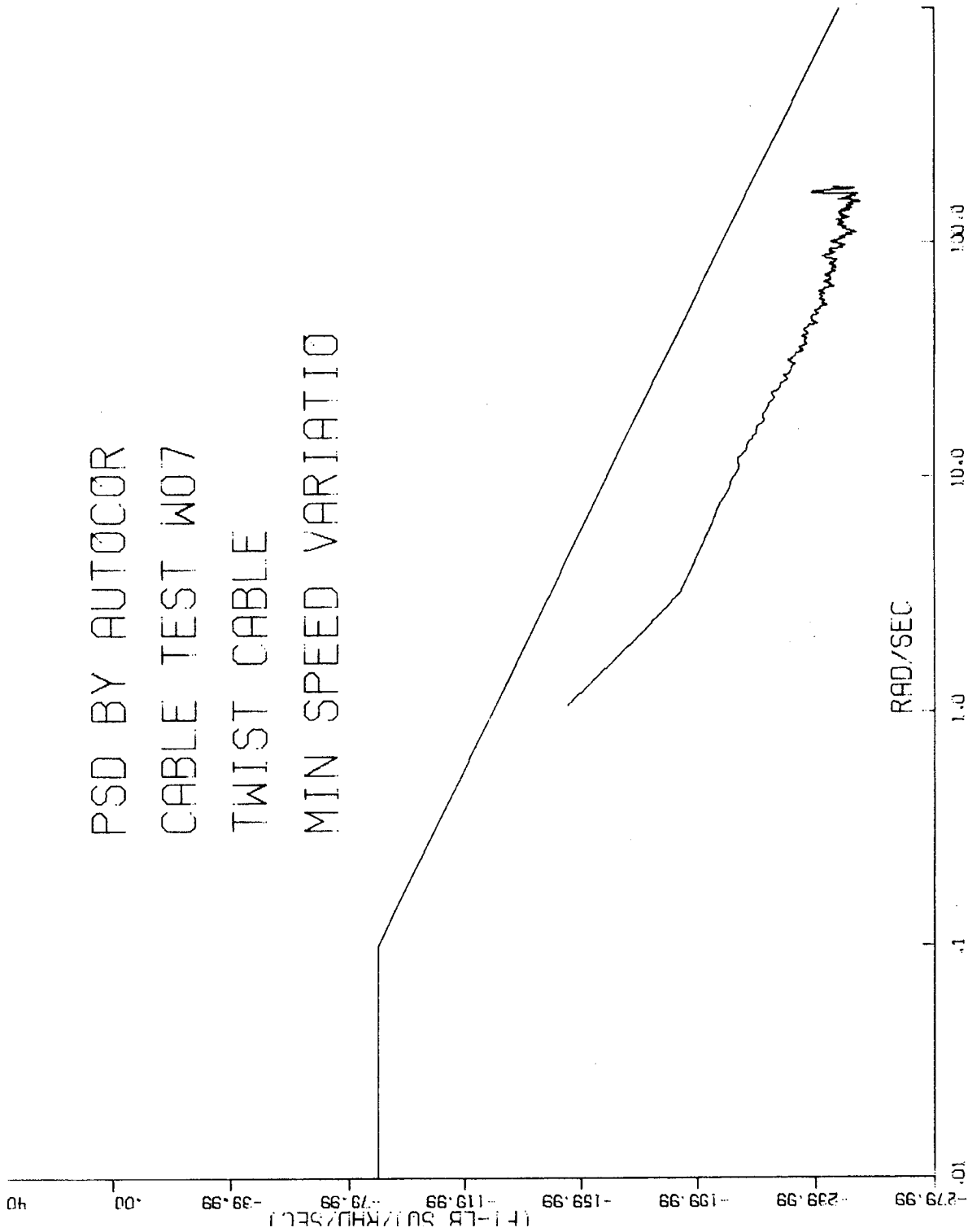


Fig. 6.2-23 — PSD plot, twist cable

~~SECRET/SPECIAL HANDLING~~

~~SECRET~~/SPECIAL HANDLING

### 6.3 TORQUE MOTORS

Specification EC-331-B, Paragraph 3.1.1.2.5 specifies that the gimbal torquers shall consist of one or two brushless noncommutated motors. If one torquer is used, two independent stator windings shall be provided for each gimbal, each of which shall be capable of driving its associated gimbal at one-half the specified acceleration in the event of failure in the other winding.

The requirements which dictate the minimum torque capability of the torquers are twofold. The roll gimbal is specified to accelerate over a range of  $\pm 40$  degrees at an acceleration of 2 radian/sec<sup>2</sup> with a simultaneous cross roll acceleration of 1 radian/second<sup>2</sup> within the scan field, or  $\pm 27.5$  degrees pitch angle. The second requirement dictating minimum torque is that of running torque. It is assumed that the present specification will be changed to 8 oz-in. in roll and 6 oz-in. in pitch.

The inertias are specified (Para. 3.1.1.1.7) to be no less than 0.23 slug-ft<sup>2</sup> for roll and 0.08 slug-ft<sup>2</sup> for cross roll. Considering the existing balanced roll and pitch axis scanner, the minimum torques which will meet the above requirements are:

$$\begin{aligned} T_{(\text{roll})} &= I_{(\text{roll})} (\text{roll}) + \text{Friction} \\ &= 0.23 \text{ slug-ft}^2 \times 192 \frac{\text{oz-in.}}{\text{ft-lb}} \times 2 \text{ rad/sec}^2 + 8 \text{ oz-in.} \end{aligned}$$

(Note: 0.23 slug-ft<sup>2</sup> is maximum roll inertia of present design. Roll inertia varies with pitch angle.)

$$= 96.32 \text{ oz-in.}$$

$$\begin{aligned} T_{(\text{pitch})} &= I_{(\text{pitch})} d_{(\text{pitch})} + \text{Friction} \\ &= 0.08 \text{ slug-ft}^2 \times 192 \frac{\text{oz-in.}}{\text{ft-lb}} \times 1 \text{ rad/sec}^2 + 6 \text{ oz-in.} \\ &= 22.36 \text{ oz-in.} \end{aligned}$$

Existing sizing calculations were based on an unbalanced roll axis, and cross product inertia terms were included in these calculations. The unbalanced roll configuration caused the stow requirements at 75 degrees to be an overriding factor in the roll torquer requirements. These requirements dictated that the roll torquer should have a maximum capability of 155 oz-in. and have a flat sensitivity curve out to  $\pm 40$  degrees so as to provide the required torque to overcome the stow magnet force at 75 degrees torquer angle.

The pitch axis calculations were also based on cross products of inertia due to unbalance of the roll axis. Again, stow requirements indicated that 38 oz-in. maximum torque would be required so as to give the necessary 27 oz-in. torque to overcome the stow magnet at 29.5 degrees.

The above requirements were submitted to Aeroflex Laboratories for an optimization study to determine a maximum weight and minimum power configuration. The gimbal torquer motor design study was preceded by several meetings with Aeroflex such that goals were set up in the form of the following work statement.

~~SECRET~~/SPECIAL HANDLING

~~SECRET~~/SPECIAL HANDLING

## STATEMENT OF WORK

### Gimbal Torque Motor Design Study

#### 1.0 INTRODUCTION

This document establishes the design services that the Aeroflex Laboratory, Inc. (Aeroflex) is to provide for Itek Corporation, Project 9400 (Itek).

#### 2.0 APPLICABLE DOCUMENTS

Itek Drawing SK114315, General Requirements for Brushless DC Torque Motor.

#### 3.0 REQUIREMENTS

##### 3.1 General Requirements

The tasks to be covered by this statement of work represent the first phase of what is envisioned as a multi step procurement to confirm design parameters, perform detail designs, qualification test, and deliver production quantities of brushless DC torque motors. The motors are to be used in a program where maximum torque in terms of minimum weight and power consumption must be achieved. To this end, premium materials shall be used to the fullest extent practical. The present study has as its primary goal that of confirming that motors with size and weight parameters as defined in paragraphs 3.1 and 3.2 are within the state of the motor art. As such, the environmental requirements of referenced drawing SK114315 apply to the extent that they will influence detailed design of the production phase motors.

##### 3.2 Pitch Motor

The pitch motor shall meet the following requirements:

- A) The developed torque at "O" angle shall be at least 38 in-oz.
- B) The developed torque at angles  $\pm 29.50$  degrees from "O" degrees shall be at least 0.75 that of maximum.
- C) The weight shall not exceed 2.0 lbs. Pancake mounting shall be used. Maximum diameter shall not exceed 5.25" and maximum thickness shall not exceed 0.935". The rotor bore shall be 0.525" with provisions for a machined slot to engage a shaft pin.
- D) Power consumption at 38 oz-in shall not exceed 6.0 watts; the duty cycle is 2 sec. on, 10 sec. off. The motor will eventually be wound for 16 to 17 volts; the design study shall make available the nearest available voltage rating and expected back voltage coefficient.

~~SECRET~~/SPECIAL HANDLING

~~SECRET/SPECIAL HANDLING~~

### 3.3 Roll Motor

The roll motor shall meet the following requirements:

- A) The developed torque at "O" angle shall be at least 155 oz-in.
- B) The developed torque at angles  $\pm 62.3$  degrees from zero degrees shall be at least 0.80 of maximum. The developed torque at angles  $\pm 75$  degrees from "O" shall be at least 50 oz-in.
- C) The weight shall not exceed 4.3 lbs. Pancake mounting shall be used. Maximum diameter shall not exceed 8.187", thickness shall not exceed 1.375 inches. The rotor bore shall be 1.28" diameter with provision for a machined slot to engage a shaft pin.
- D) Power consumption at 155 oz-in shall not exceed 30 watts; the duty cycle is 2 sec. on, 10 sec. off. The motor will eventually be wound for 16 to 17 volts; the design study shall make available the nearest available voltage rating and expected back voltage coefficient.
- E) Power and/or weight savings associated with reducing the rotor bore to 1.00 inches shall be investigated. The results of this investigation shall be made available at the interim design review, at which time Itek shall give direction as to which approach will be pursued.

## 4.0 PRESENTATION OF RESULTS

### 4.1 Interim Design Review

The first task to be accomplished is to ascertain that the Itek requested design parameters are within the state of the art. The optional 1" rotor bore of item 3.3-E shall also be investigated. Approximately 14 days after receipt of order, Itek and Aeroflex shall hold a design review meeting at a site mutually acceptable to both parties. Aeroflex shall present Itek with its preliminary results; engineering sketch level data will be adequate. This data shall also contain information as to what changes in direction or parameters would help optimize the designs for the intended application. Itek will accept this information and will give Aeroflex direction as to what alternatives should be chosen. This direction will be given within 7 days.

### 4.2 Final Report

Aeroflex shall present Itek with a final report within 21 days after receipt of Itek's technical direction. The report shall contain enough data to enable Itek to specify the parameters that can be expected on production motors manufactured from detailed design. It is required that the data be of sufficient detail and accuracy to permit parallel design of all hardware that interfaces with the motors, e.g., shaft size, housing, rotor bore, voltage, power, weight, etc. It is planned that the data in the final report will be used to prepare detailed purchase specifications, from which the design phase will be conducted.

~~SECRET/SPECIAL HANDLING~~

~~SECRET~~/SPECIAL HANDLING

The results of the Aeroflex study are presented here for completeness and to indicate that these two motors constitute the present torque motor designed. A torque versus angle for each motor is presented in Fig. 6.3-1.

In view of the balanced scanner, it is obvious that the design is conservative. It appears reasonable to proceed with the present design for engineering model hardware. There are considerations that must be investigated before a final sizing can be made. Since the motors are conservatively sized, the mounting dimensions will remain fixed and Aeroflex can perform a final trimming by changing the taper profile of the rotor magnets. The magnet is a very dense material and shaping of the rotor can be a very effective technique for final trimming to the desired torque rating and to minimize weight.

One of the considerations that effects motor sizing when considering a balanced roll axis is that weight in the pitch motor will affect the roll balance and roll inertia. Investigations will have to be made with these considerations in mind and the approach of minimum weight may not be the determining consideration. Added weight in the motor could be advantageous from an inertia and balance standpoint and in turn would give added torque capability. These studies will be accomplished, and along with information from engineering model tests, a final torque requirement will be determined and submitted to Aeroflex for final trimming of the rotor.

Another consideration for the roll torquer is associated with the size of the shaft through the torquer. Since it is planned to route cables through this shaft, an investigation must be accomplished on how much bigger this hole through the armature can be made and still maintain the required torque for the balanced gimbal configuration. This hole size will have to now be traded off with cable PSD improvement torque requirements, stiffness, and weight-power requirements. However, none of the above investigations will affect mounting dimensions of the torquer.

~~SECRET~~/SPECIAL HANDLING

~~SECRET/SPECIAL HANDLING~~

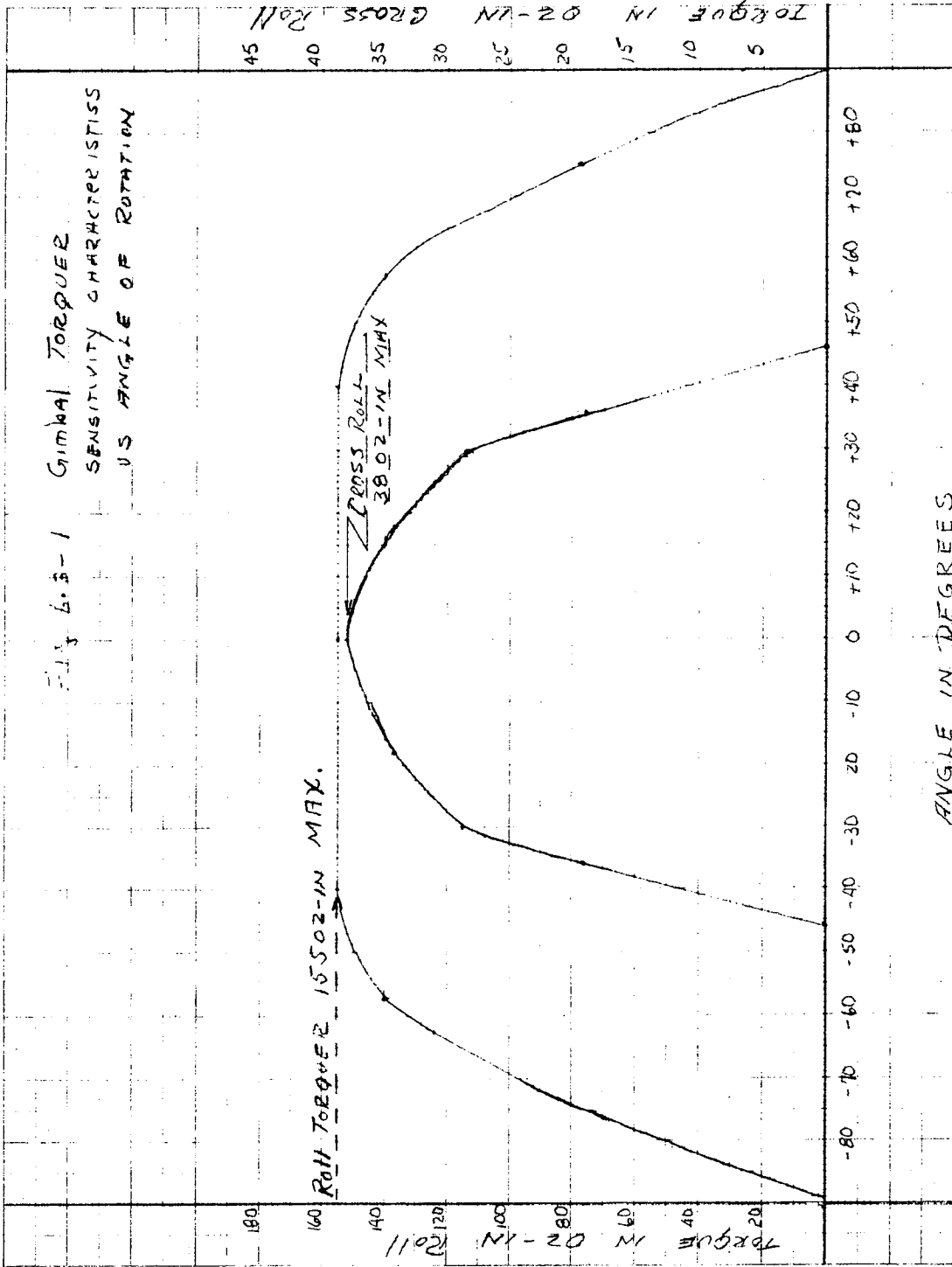


Fig. 6.3-1 — Gimbal torque sensitivity characteristics versus angle of rotation

~~SECRET/SPECIAL HANDLING~~

~~SECRET/SPECIAL HANDLING~~

#### 6.4 PITCH AND ROLL ENCODERS

Preliminary investigation of the availability of incremental encoders suggested that only optical encoders with some form of electronic division of the finest optical interval would be capable of the accuracy and resolution required. Of the many manufacturers of optical encoders, Wayne George and Baldwin appeared to be the leaders. Since there appeared to be no clear total superiority of one basic approach to the electronic digit multiplying problem over the other (see Section 5.5.2.3) and since both companies have demonstrated capability in precision fabricating, Wayne George was selected as the supplier for the obvious advantages of working with a member of the same corporation. It was further realized that the known fact that Wayne George is a member of the same corporation places severe limitations on the freedom of communication with a competitive supplier.

##### 6.4.1 Encoder as Velocity Sensor

Digital shaft encoders have been mainly used to indicate shaft angular position, and design and fabrication techniques have been directed at minimizing error in the total indicated angle measured from zero. Errors in least significant bit length are made as small as possible but with no concern for whether such errors are random or periodic.

Because of the special properties of a rate controlled servo loop, an encoder used as the rate feed back element must possess special properties not required in a position encoder. In any physically rate controlled system there exists a range of frequencies over which the system is most sensitive to disturbing torques. Therefore, for the same total energy in an error signal, loop performance will be better if the energy is more or less randomly distributed in frequency than if it is concentrated in the sensitive range.

Since errors in a digital shaft encoder tend to be periodic at frequencies related by powers of 2, special attention must be given to reducing those components which may occur in the most sensitive region, (approximately 37 radians per second in the anticipated servo system).

Section 5.5 discusses encoder errors and the methods of evaluating and reducing them. Best estimates of achievable performance appears to be 0.05 to 0.1 root-sum-squared-arc-seconds for the error in 1024 consecutive least significant bits suitably attenuated with the appropriate filter and for appropriate scanning velocities. Absolute position error at any velocity in the scanning or slewing range and any operating range of angle can be less than 3 arc-seconds, peak. Design goals are for the best performance possible and there appears to be reason to hope that the above figures may be surpassed.

##### 6.4.2 Design Criteria

Computer studies simulating performance of the encoder electronics over an operating temperature range of -20 to +55 °C will be conducted to ensure optimum design including temperature compensation, if required.

Mechanical and electrical design are directed to an MTBF of at least 47,000 hours. Highest possible use will be made of integrated microcircuits in order to achieve the highest reliability as well as savings in space and weight. All electronic components will be of the highest reliability achievable and will be carefully inspected, using x-ray inspection where applicable, prior to assembly.

~~SECRET/SPECIAL HANDLING~~

~~SECRET/SPECIAL HANDLING~~

Optical and electronic channels will be redundant and means for switch-over to standby channel will be provided by a switch-over of external power leads. Test points will be provided to indicate when a failure has occurred so that switch-over may be initiated.

6.4.3 Fabrication and Test

Precautions to avoid contamination of bearings or optics will include performing all sensitive assembly or test procedures in a class 100 (or equal) clean room.

One unit will be tested in accordance with applicable sections of Mil-Std 810 and Mil-Std 826 to assure qualification of the design. Any design changes indicated by the results of such testing will require requalification of the modified design.

Workmanship and assembly procedures will equal or surpass military practice for aerospace equipment in accordance with Itek Workmanship Standards QAWS -50.

~~SECRET/SPECIAL HANDLING~~

~~SECRET/SPECIAL HANDLING~~

## 7. DYNAMIC SPECIFICATIONS AND CRITERA

### 7.1 INTRODUCTION

The significant dynamic excitations which the scanner must survive are:

1. Acoustic loads during lift off and at maximum  $\alpha$  g
2. Random vibration loads derived from the acoustic loads and transmitted to frame/mounted components
3. Shock loads developed from vehicle staging and other pyrotechnic devices.

The effects of each of these excitations are considered separately. Throughout all these load periods the scanner is not operating; it is in the stow position and has the launch locks engaged to preclude roll or pitching motions.

#### Acoustic Loading

The direct effects of acoustic loading on the scanner will be very small. The scanner is protected from the direct effects of the fluctuating air pressure by the aerodynamic shroud and also by the shroud of the A/O system. The attenuation effects of these two paralld walls is expected to be significant.

Acoustic loadings are known to have their greatest effect on panel type structures, having a large surface area-to-weight ratio. Assemblies such as the scanner are virtually unaffected by acoustic environments. This fact and the already reduced levels to which the scanner will be exposed have discouraged the expenditure of analytical time in this direction.

The indirect effects of acoustic loading have been carefully examined. The energy accepted by resonating panels in an acoustic environment is transmitted through the frames to units like the scanner as random vibration. The analytical evaluation of that environment should more than account for the direct effects of acoustic excitation.

#### Random Vibration

An input PSD for random vibration is given in Fig. 10 of DR1100B, which is to be applied at the base of all components weighing less than 50 pounds. The scanner weighs slightly over 50 pounds and thereby qualifies as a heavy component in paragraph 4.4.3.5.3. This paragraph states, "For test specimens weighing 50 pounds or more, vibration test levels shall be determined by an analysis based on the acoustic curves of Fig. 14." This paragraph deals specially with random test input levels and although a similar statement does not exist anywhere in the specification for the input excitation for an analysis, a consistant approach must be maintained. It was therefore decided that random vibration inputs to the scanner would be reduced from the specification levels of Fig. 10 to account for the high weight of the unit.

~~SECRET/SPECIAL HANDLING~~

## ~~SECRET/SPECIAL HANDLING~~

The acoustic curve of Fig. 14 applies to internal components and therefore should not apply to the scanner. Further, the conversion of acoustic to random levels is an arbitrary procedure and is highly dependent upon the geometry of the parent structure. These considerations coupled with the fact that the scanner is only slightly overweight made it undesirable to attempt a recalculation of random levels from the acoustic specification.

An alternate approach was taken, based upon the reasons behind the special treatment of overweight components. The factor requiring the reduced levels is that there is not enough energy available in the acoustic excitation to excite large articles to the levels indicated by the random spectrum. For components of less than 50 pounds, sufficient energy is available; therefore, the random levels as given were scaled downward by the ratio of

$$\left( \frac{50}{\text{scanner weight}} \right)^2$$

and a new lower random PSD was developed for the input (see Fig. 7.1-1).

### Shock Loads

The shock excitation input to the scanner was taken from Figs. 13a and 13b of DR1100B. The middle curve of Fig. 13a was used. It was extended down from 100 to 0 cps in a straight line at the customer's direction. The levels given by this curve were then lowered according to Fig. 13b and the final curve for shock input to the scanner base was developed (see Fig. 7.1-2). This excitation was applied to each of the three scanner axes, one at a time, through the attach point.

### Structural Dynamics

The performance/design and qualification requirements state that the scanner assembly, scanner assembly mount, gyro assembly mount and mount location shall be such that the frequency response of each axis of the gyro output signal to motor excitation, normalized to the response at 1 radian per second and compensated for the motor electrical time constants and the gyro transfer function shall have no amplitude excursions above the profile of Fig. 7.1-3. The curve is a unitized response envelope in terms of  $g(x)$  versus  $\omega$  in which  $g(x)$  is  $20 \log_{10} |X|$  and  $\omega$  is excitation frequency given in radians/second. The value  $|X|$  must be further clarified as:

$$|X| = \frac{\dot{\theta}}{V_m} = \frac{\tau_e s + 1}{\left( \frac{\dot{\theta}}{V_m} \right) \omega = 1}$$

in which

$$\frac{\dot{\theta}}{V_m} = \frac{\text{gimbal rate (rad/sec)}}{\text{motor voltage}}$$

and  $\tau_e$  = the motor electrical time constant

In order to apply this curve directly to the scanner structural response, it is proper and desirable to treat the ordinates as structural gains or transmissibilities. In that regard the axis  $g(x)$  will become  $x_0/x_i$  in which  $x_0$  is the displacement at the gimbal point of interest and  $x_i$  is the displacement at the torquer. The abscissa will remain as frequency.

~~SECRET/SPECIAL HANDLING~~

~~SECRET~~/SPECIAL HANDLING

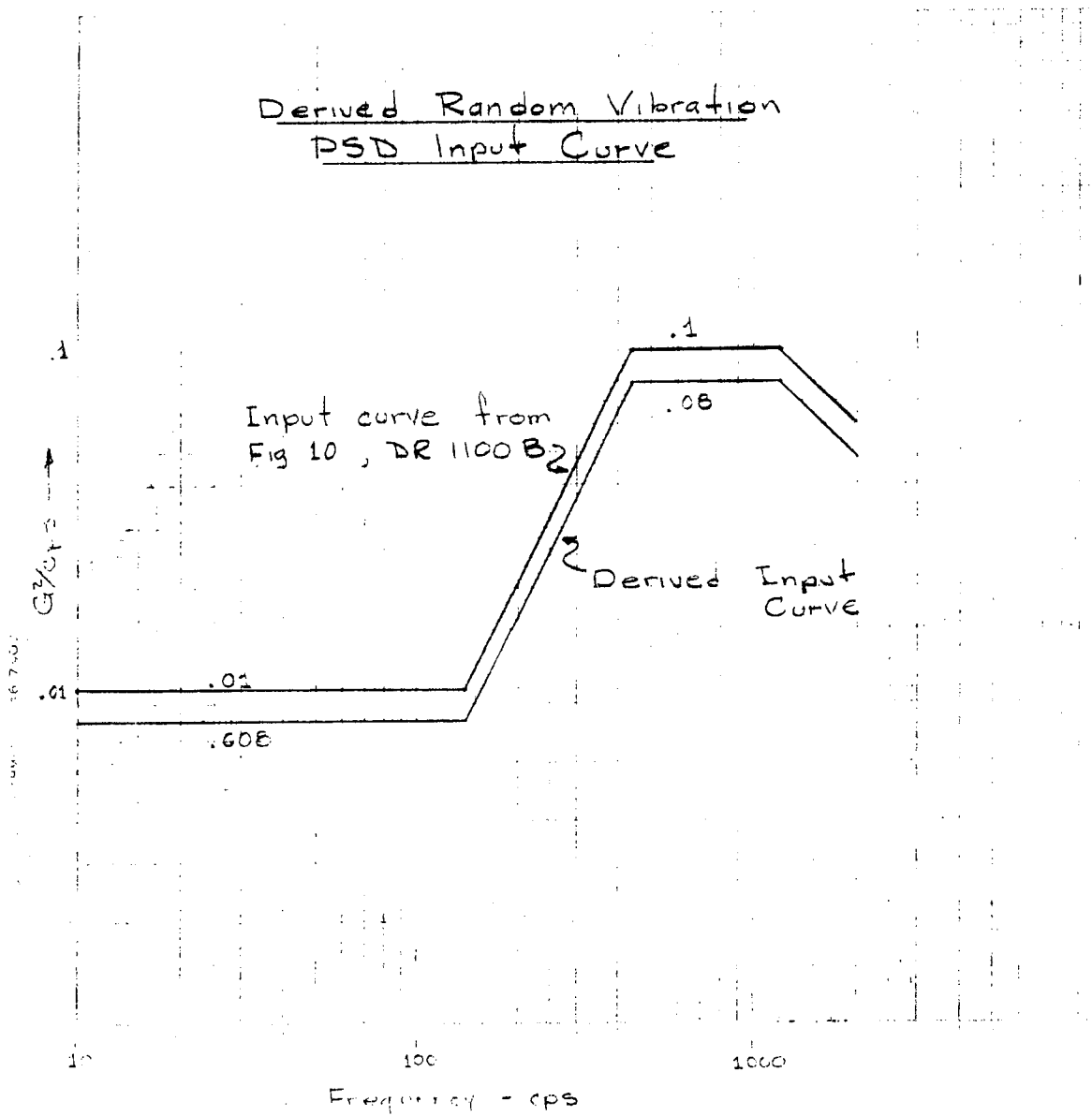


Fig. 7.1-1 — Derived random vibration PSD input curve

~~SECRET~~/SPECIAL HANDLING

~~SECRET/SPECIAL HANDLING~~

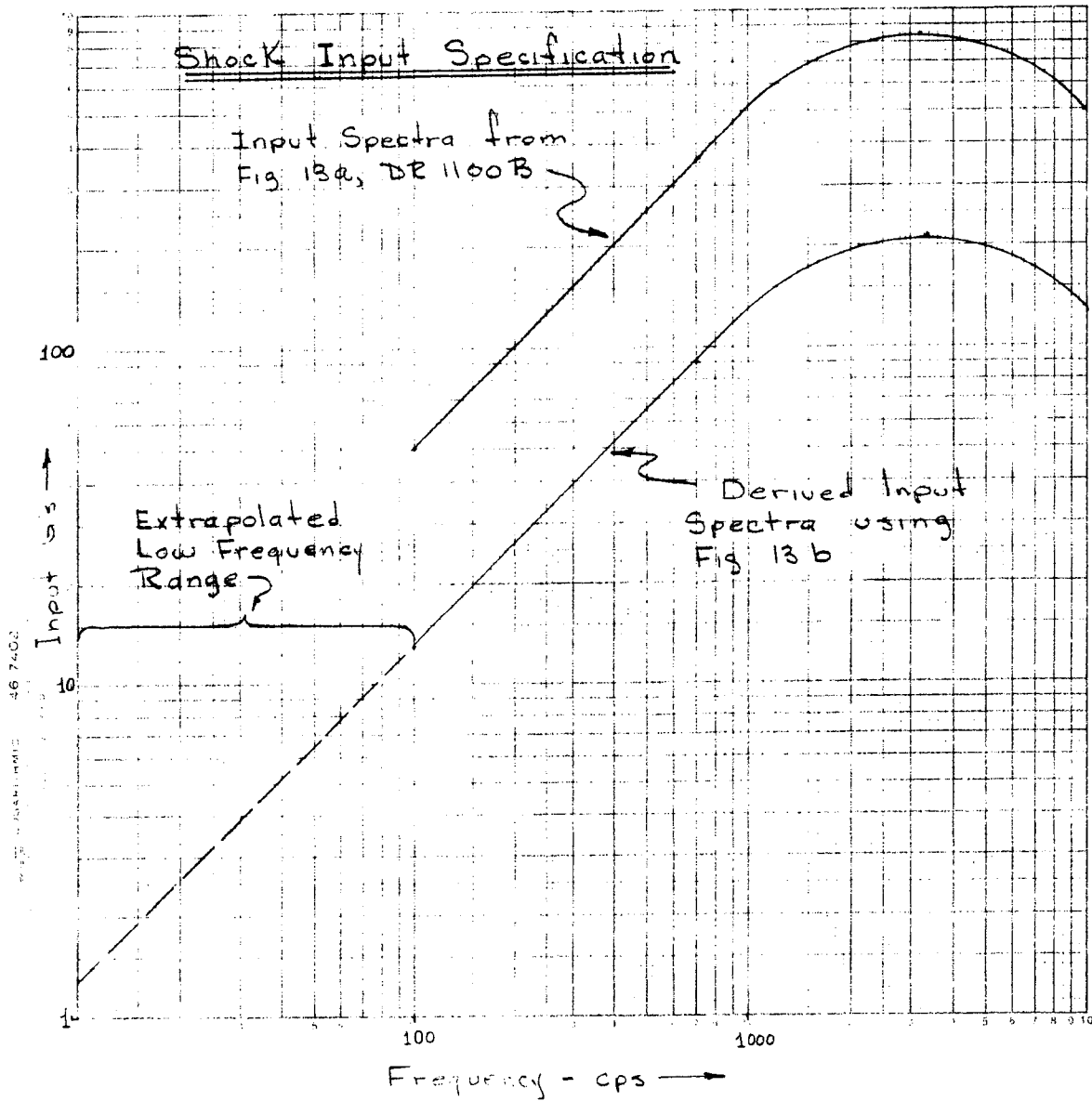
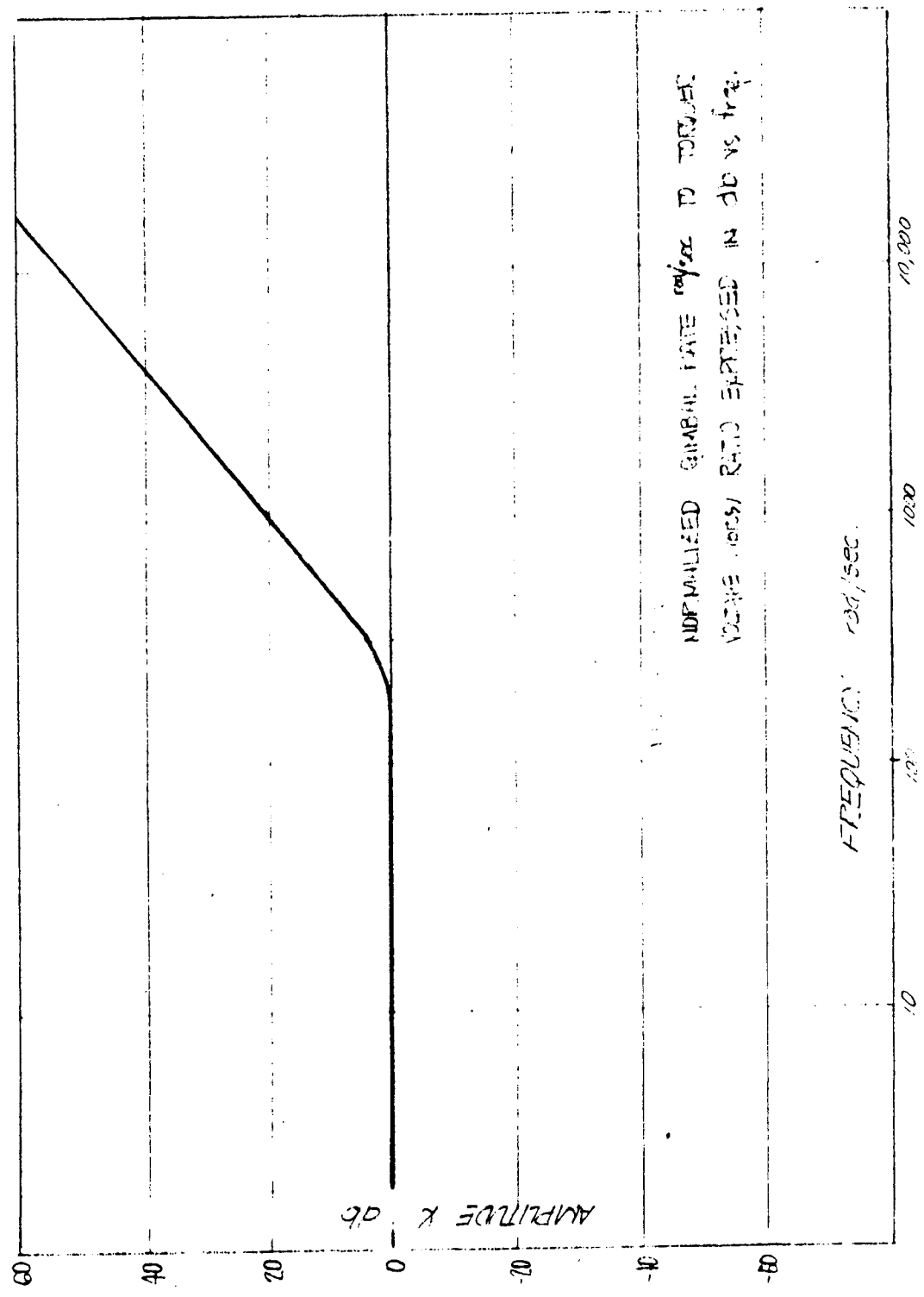


Fig. 7.1-2 — Shock input specification

~~SECRET/SPECIAL HANDLING~~

~~SECRET/SPECIAL HANDLING~~



NORMALIZED GIMBAL RATE  $\frac{\text{volts}}{\text{rad/sec}}$  TO TORQUER  
VOLUME LOSS/ RATIO EXPRESSED IN db vs freq.

Fig. 7.1-3 — Normalized gimbal rate rad/sec to torquer voltage (volts) ratio expressed in db versus frequency

~~SECRET/SPECIAL HANDLING~~

~~SECRET~~/SPECIAL HANDLING

## 7.2 SCANNER DYNAMIC ANALYSIS PLAN

The analytical effort, directed toward meeting environmental requirements and establishing stiffness and frequency needs proceeded according to the plan of Fig. 7.2-1.

Initial analysis to determine major load paths and to evaluate the relative importance of the various masses and structural elements was conducted on a large system. It consisted of sixteen masspoints with six dynamic coordinates at each point for a total of ninety-six differential expressions which represented the scanner's dynamic behavior. The system's lowest six natural frequencies and associated mode shapes were determined by a digital routine that utilizes the Mykelstal-Probability approach.<sup>1</sup> These results were used as a guide to construct simple working models representing the structure in a single direction with orthogonal coupling omitted. That is, each model was planar with no provisions for out-of-plane contributions. In the direction radial to the vehicle, a model consisting of twelve node points connected by massless springs was utilized. In the other directions, two degree systems were employed. The working models along with the necessary property calculations are shown in the "Dynamics Appendix".

The analytical effort was divided into two major categories:

1. Design Loads and Deflection Determination
2. Structural Dynamics Characteristics.

The first is the system's response to the flight environments: acoustic excitation and random vibration during launch and ascent, pyrotechnic shocks due to staging and spent structure shedding, and steady launch accelerations. The second is the system's response to harmonic excitation at the torquers.

The two categories each required a unique model because the scanner attitude during launch is different from those associated with operational modes. In addition, the scanner is mechanically locked during launch while it is unlocked, but controlled, during use. These factors influence the mass and stiffness representation to an extent which precludes utilization of a universal model.

The loads model consisted of eleven masses with 30 translational coordinates and 10 rotational coordinates. Detailed discussion of the ensuing operations is presented in Section 7.3.

The structural dynamics analysis was directed toward determining system transmissibilities. Two uncoupled models were used to conduct optimization studies pointed toward developing the most agreeable set of transmissibility properties. Following this, a larger model, which incorporated the effects of stiffness and mass coupling was generated. This model also included damping values that were influenced by the potting damping development tests. Results from this model and the loads models were then channeled to the design to end the dynamic analytical efforts prior to Preliminary Design.

~~SECRET~~/SPECIAL HANDLING

~~SECRET/SPECIAL HANDLING~~

FIGURE 2. Scanner Analysis Plan

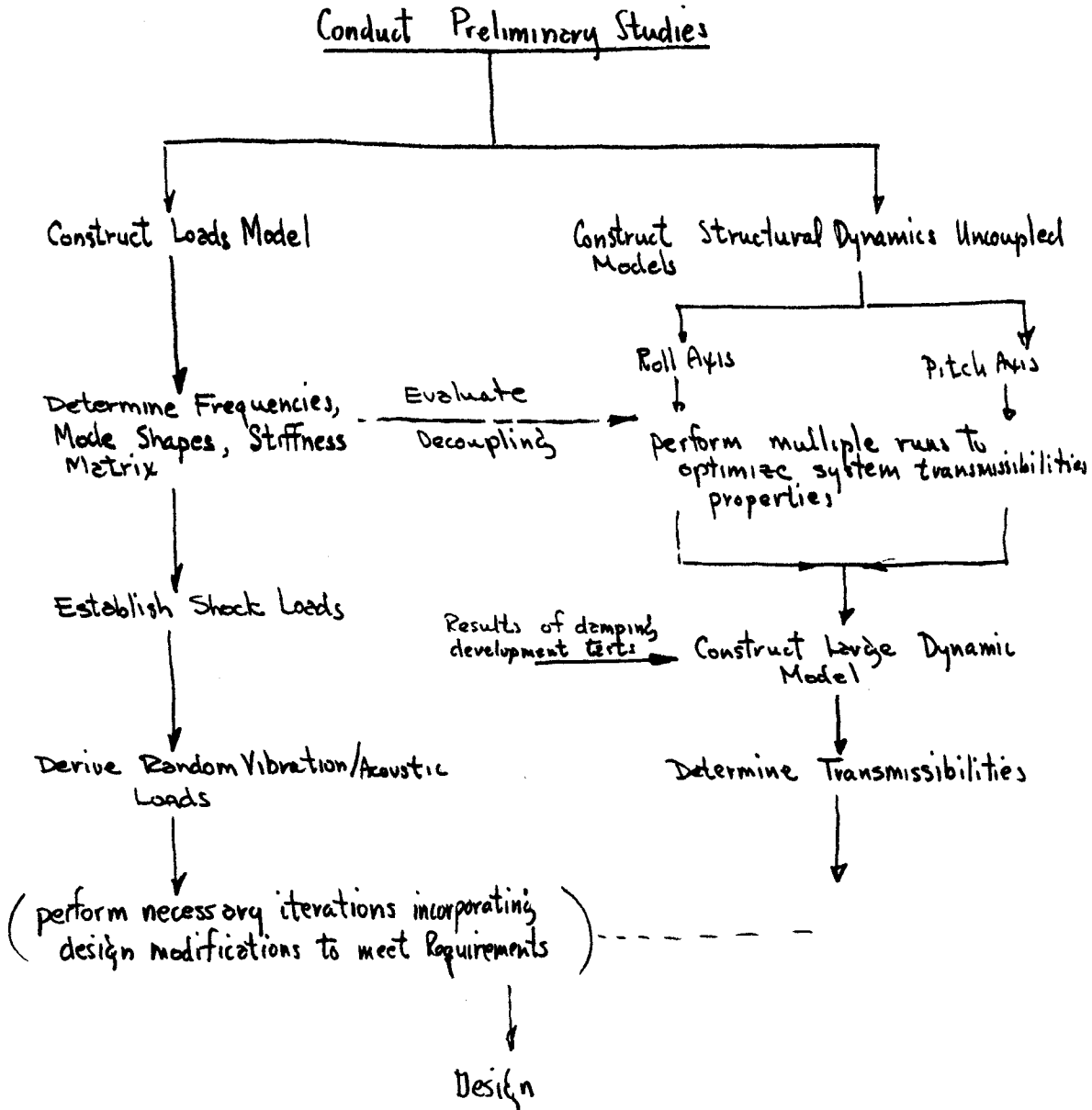


Fig. 7.2-1 — Scanner analysis plan

~~SECRET/SPECIAL HANDLING~~  
7.2-2

~~SECRET/SPECIAL HANDLING~~

### 7.3 DYNAMIC LOADS AND DISPLACEMENTS

#### 7.3.1 Scanner Frequencies and Modes

The scanner frequency and model characteristics were developed for the 11 mass, 40 degree of freedom system modeled as in Fig. 7.3-1. The model was first run on a general structures program to determine a flexibility matrix. To insure maximum accuracy, 21 joints and 25 bars were used in the model (See Fig. 7.3-2). After this large flexibility matrix was developed, it was reduced to the 40 coordinates required for the dynamic problem, then inverted to form the necessary stiffness matrix.

The first fifteen natural frequencies of the system are:

1	11 cps
2	16
3	22
4	40
5	45
6	68
7	90
8	105
9	108
10	120
11	121
12	124
13	125
14	134
15	145

The first 5 modes are sketched in Fig. 7.3-3. These are rigid body type rotation modes principally attributable to the cantilevered geometry acting on the ground springs. Some of these rotational motions are combined with either translational motions along the roll axis or some small twisting of the yoke.

The cantilevered geometry of the scanner combined with the relatively soft ground springs forces the installation to resonate at low frequencies and will therefore be an extremely important factor in minimizing random vibration and shock response loads.

#### 7.3.2 Random Excitation Analysis

The model used to describe the scanner for the random vibration analysis is shown in Fig. 7.3-4. The size of the model was dictated by the limitations of the computer program on which it was to be run and also by the reliability of structural information at the time. That is, some of the larger, more important members were not completely designed which required assumptions to be made; this meant that some of the finer aspects of the model, attributable to less important structural elements, could not be considered.

##### 7.3.2.1 Development of Stiffness Matrix

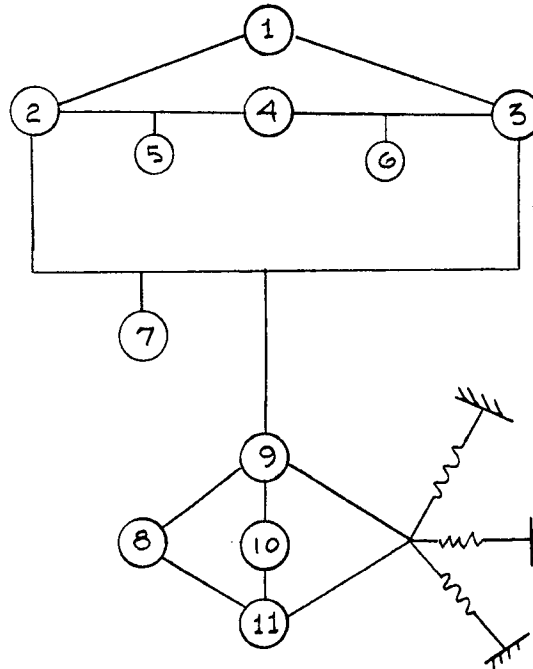
The steps taken in the development of the stiffness matrix were:

- (a) A flexibility matrix was developed for the model shown in Fig. 7.3-2.

~~SECRET/SPECIAL HANDLING~~

~~SECRET/SPECIAL HANDLING~~

Dynamic Model - Scanner Frequencies  
& Modes - 40 d.o.f.



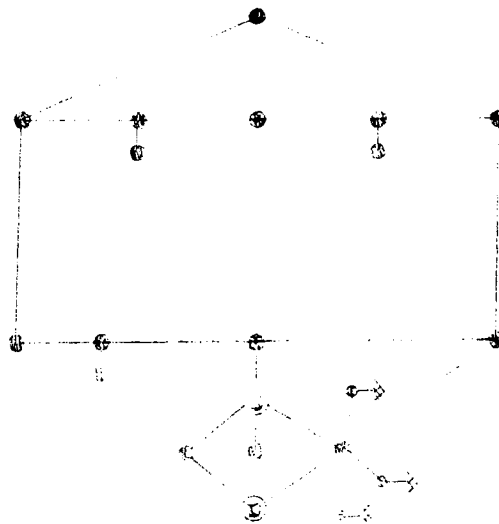
- |            |                      |                 |
|------------|----------------------|-----------------|
| 1. Mirror  | 5. Pitch Electronics | 9. Fwd. Bearing |
| 2. Torquer | 6. Pitch Gyro        | 10. Torquer     |
| 3. Encoder | 7. Roll Gyro         | 11. AH. Bearing |
| 4. Bezel   | 8. Roll Electronics  |                 |

Fig. 7.3-1 — Dynamic model—scanner frequencies and modes—40 d.o.f.

~~SECRET/SPECIAL HANDLING~~

~~SECRET~~/SPECIAL HANDLING

Structural Model for Scanner  
Dynamic Flexibility Matrix



See Fig. 7.3-1 for  
identification of  
major mass points.

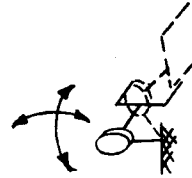
Fig. 7.3-2 — Structural model for scanner dynamic flexibility matrix

~~SECRET~~/SPECIAL HANDLING

~~SECRET~~/SPECIAL HANDLING



1<sup>st</sup> Mode - 11 cps  
Cantilevered twisting



4<sup>th</sup> Mode - 40 cps  
Cantilever bending  
in two directions



2<sup>nd</sup> Mode - 16 cps  
Cantilevered bending



5<sup>th</sup> Mode - 45 cps  
Rotation +  
Translation

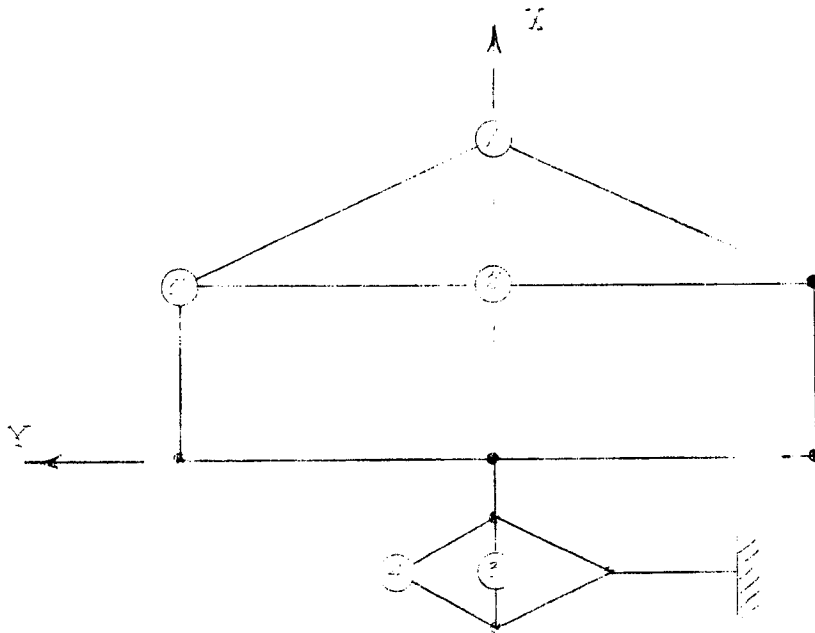


3<sup>rd</sup> Mode - 22 cps.  
Cantilever bending  
+ Translation

Note: These first 5  
modes depend almost  
entirely on ground  
springs.

Fig. 7.3-3 — Scanner modes 1-5

~~SECRET/SPECIAL HANDLING~~



1. Motor

4. Yoke Eccentric

2. Spring - pin  
assembly

5. Yoke Axis  
assembly

3. Blade - of  
Scanner

Fig. 7.3-4 — Scanner—random vibration model

~~SECRET/SPECIAL HANDLING~~

~~SECRET~~/SPECIAL HANDLING

- (b) An  $18 \times 18$  flexibility matrix was assembled by hand from the elements of the larger matrix of step #1
- (c) This  $18 \times 18$  matrix was inverted to form the stiffness matrix for the problem. The basic model for the stiffness matrix was the same model used as a basis for the stiffness matrix for the mode and frequency calculations.

#### 7.3.2.2 Development of Damping Matrix

A full damping matrix of individually calculated damping terms was used. The individual terms were developed with consideration to both spring rate and mass associated with the concerned damper. The method used is shown in Fig. 7.4-5. A damping constant of 5 percent was assumed for the potting spring and 2 percent for structural springs.

#### 7.3.2.3 Calculation of Random Response

The response was calculated using the AVCO 1536 random response program. A description of the operations of this program is given in the appendix. The specified random PSD was input to the base. Three separate sets of response were calculated, one for each direction of base excitation.

The set of response levels giving the highest loads are presented in Table 7.3-1.

A typical response PSD as drawn by the computer is shown in Fig. 7.3-5. The input PSD has been superimposed over the output to show the relative importance of the individual modes.

#### 7.3.2.4 Discussion of Random Response Results

The output PSD in Fig. 7.3-5 shows the major contribution of the 400 cps mode. The effect of this mode was determined by calculating its contribution and subtracting it from the total response at each coordinate. By this procedure the following contributions to each load were calculated (see Table 7.3-2).

The source of the 400 cps mode was investigated by solving the frequencies and modes of this small system on the AVCO 1384 program. It was determined that mass 4 was dominating this mode and was responsible for its presence. Subsequent removal of mass 4 from the model completely eliminated the mode.

It should be noted that mass 4 has been relocated in the design since this calculation was made. It has been relocated in a relatively neutral position on the yoke. The effect should be to lower the calculated loads by the percentages indicated.

#### 7.3.3 Shock Excitation

The model used to investigate the scanner's shock response characteristics is the same that is used to determine natural frequencies and modes. The stiffness matrix was also the same.

The reduced shock spectra of Fig. 7.1-2 was input at the base along each of the three scanner axes, one at a time. Three sets of responses were calculated.

The program output consisted of inertial loads, accelerations, displacements, and bar forces for each member for each of the 40 modes. The method of combining the individual modal contributions is left to the user.

~~SECRET~~/SPECIAL HANDLING

~~SECRET/SPECIAL HANDLING~~

Table 7.3-1 — Set of Response Levels Giving the Highest Load

	DIRECTION	RESPONSE LEVEL G's
MIRROR	X	7.0
MASS 1	Y	11.3
	Z	3.8
BERE L	X	6.1
MASS 2	Y	11.1
	Z	3.8
HOUSING (MASS 3)	X	12.7
	Y	5.5
	Z	4.5

Table 7.3-2 — Contributions to Each Load

	DIRECTION	% OF TOTAL RESPONSE IN 400 cps MODE
MIRROR (1)	X	1
	Y	12
	Z	1
BERE L (2)	X	7
	Y	14
	Z	1
HOUSING (3)	X	72
	Y	1
	Z	1

~~SECRET~~/SPECIAL HANDLING

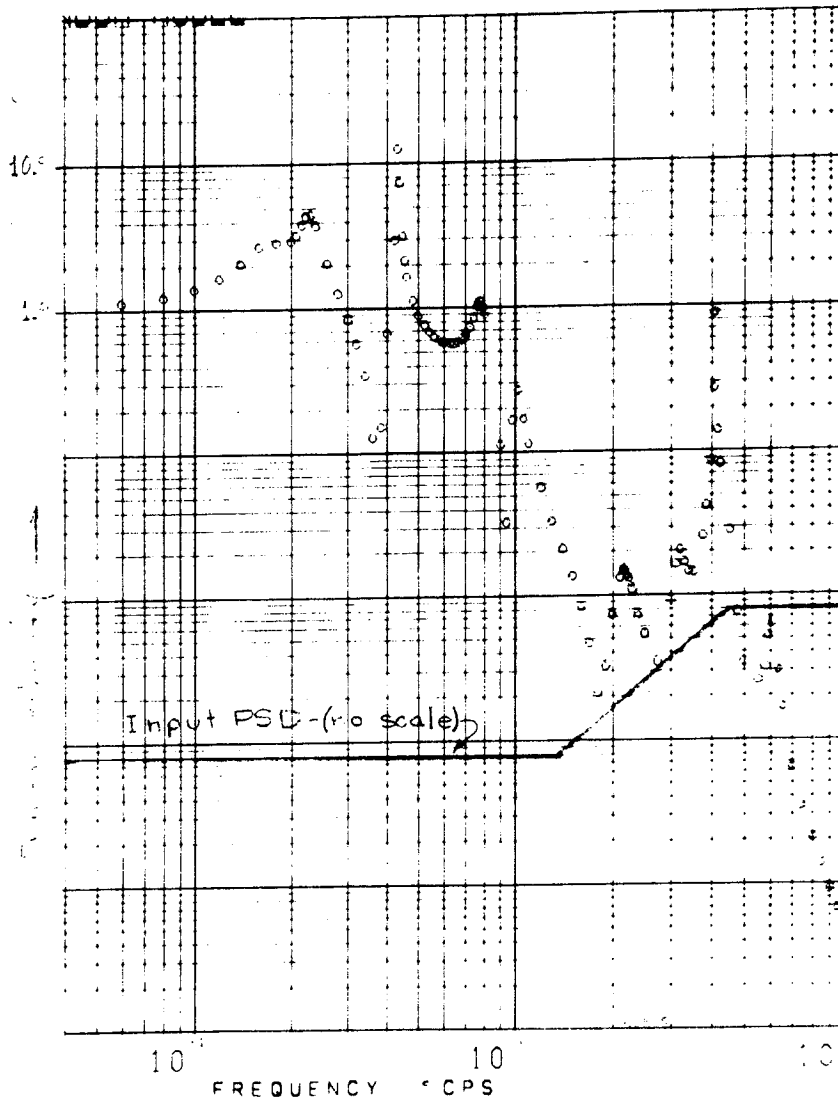


Fig. 7.3-5 — Typical coordinate transmissibility random model

~~SECRET~~/SPECIAL HANDLING

~~SECRET~~/SPECIAL HANDLING

The results showed that the response loads were clearly a result of the first seven or fewer modes. (Typically the eighth mode contribution was less than 1 percent of the total.) The frequencies involved are 90 cps and below.

The method used to combine contributions of individual loads was

$$F_{\text{Total}} = F_{\text{Max}} + \sum_{n=1} F_n^2 \text{ }^{1/2}$$

The loads calculated in this analysis were much lower than those developed during the random excitation response periods. For purposes of comparison, the highest mirror response loads are compared in Table 7.3-3.

The mirror is by far the largest single mass of the scanner. Its cantilevered position makes it the most important single mass of the unit.

#### 7.3.4 Effects of Balancing Roll Axis On Shock and Random Vibration Response Levels

Balancing the roll axis has its greatest effect upon rotation of the roll axis. During all periods of shock and random loadings, roll shaft rotation is restrained by the launch lock and therefore can have no effect on the frequency or mode characteristics of the unit. The numbers discussed thus far will not be significantly affected by the balancing process itself. The attendant changes in stiffness and coordinates of the masses will have some effect on the flexible modes of the structure. The changes have not been evaluated yet, but we do know that the lowest, most important response modes tend to be rigid in nature, and the flexible modes are secondary in importance.

We may expect the change to a balanced configuration to bring about some small load increases; no significant differences are expected.

#### 7.3.5 Effect of Changing Ground Springs on Shock and Vibration Response

The first few modes are by far the most important in determining shock and vibration loads. The input excitation levels (See Figs. 7.1-1 and 7.1-2) at these frequencies determine the level of the response loads. It is important therefore, that the scanner's first few frequencies lie in a low power region of the input spectrum if we are to minimize the response levels.

As described previously, the lowest modes of the scanner are a rigid body type of rotation about the support point; that is, the unit is acting as a single mass system responding only to the ground springs.

If random vibration inputs continue to be the source of maximum loads, it is important that the lower frequencies stay on the flat part of the input spectrum; i.e., below 140 cps. If we assume that the first seven modes account for most of the load, as was the case in shock response, we determine that the highest significant mode is presently about 90 cps. A frequency shift from 90 to 140 cps requires a change in ground springs of

$$\frac{140^2}{90}$$

or  $2.4 \times$  the present values. If ground spring values change more than this amount, loads will increase at an intolerable rate.

~~SECRET~~/SPECIAL HANDLING

~~SECRET~~/SPECIAL HANDLING

The shock input spectra does not have a flat response in the low frequency range. Shock loads will begin to increase immediately if ground springs are stiffened. The slope of the input spectra shows a doubling of level for each doubling of frequency or for each quadrupling of spring values. Since the shock loads are only 1/2 the random vibration loads, it would take a spring change of about 4X present value to equal random levels. This great a spring change would be intolerable from the viewpoint of random response.

It appears then, that response of the scanner will be relatively unaffected by reasonable changes in the ground springs; however, major changes (over  $2.4 \times$  present values) will be intolerable.

Table 7.3-3 — Comparison of Highest Mirror Response Loads

Mirror Response Levels - G's

	Shock Excitation	Random Excitation
x	6.4	7.0
y	2.4	11.25
z	2.1	3.75
Total Response (Vector Sum)	7.15G	13.77G

~~SECRET~~/SPECIAL HANDLING

~~SECRET/SPECIAL HANDLING~~

#### 7.4 TRANSMISSIBILITY REQUIREMENTS

During operation of the scanner, positional adjustments are made to limit, within acceptable tolerances, the variations of the scanner's pointing angle at any time. The effect of these adjustments is a motion approximating a decaying sinusoid in that it oscillates about a desired angle with decreasing amplitudes. The decay envelope of that response is shaped by the structural and electrical characteristics of all the contributing components of the servo control system.

Any practical, linear structure when mechanically excited, will respond in a manner unique to the structures' physical properties and nature of excitation. In a structural system evaluation, this response has traditionally been determined for a steady harmonic force or motion excitation and is expressed as the ratio of response amplitude to excitation amplitude. The variation of this ratio with excitation frequency is termed the transfer function or generalized frequency response.

The scanner is an elliptical mirror mounted in an orthogonal gimbal system which allows rotation about the orthogonal axes. Two torque motors provide the drive of the scanner; one about the pitch axis and the other about the roll axis. Frequency response. Frequency response curves have been developed for both the pitch and roll assemblies and are compared to Figure 1.

##### Analytical Approach

Analysis directed toward developing pitch/roll axes assemblies, involved the following steps:

1. Construct a representative dynamic model
2. Mathematically describe the system's motions
3. Calculate transmissibility as a function of frequency for each pertinent mass point.

Each of these steps will be discussed in detail.

##### Dynamic Models

The construction of the dynamic models was carried out at four levels resulting in the necessary mathematical tools that are called Models I through VI. Models I and VI are large models which entail the most structural detail while the other models served in investigating effects of specific areas. Table 7.4-1 is a table of these models. Model VI, the large coupled model, is discussed in detail in its own section, however some comments about its status and applicability will be made at this time. The model is the result of recent efforts and is yet in the preliminary operational phases. It represents the unbalanced scanner design with a modification (i.e., it has the torquer positioned closer to the roll axis forward bearing as in the balanced design).

Some preliminary data, which can be used as guiding information, has been generated in the initial runs. Fig. 7.2-21, 7.4-22, and 7.4-23\* are preliminary plots derived from this data. They show the presence of a resonance at 105 hz (660 radians/second) and another at about 180 hz (1130 radians/second). The second resonances are the uncoupled frequencies of the respective axes. The first is suspected to be the scanner rotating on its pedestal. In view of the fact that present data is insufficient to validate or invalidate this premise, further effort is being expended in this area.

The level of the first peak (13 db in pitch and 11 db in roll) falls under the curve. All the data to date indicate that this point is fairly insensitive to damping values assumed, and therefore

\* Reference only, figures presented further on in this Section.

~~SECRET/SPECIAL HANDLING~~

~~SECRET~~/SPECIAL HANDLING

Table 7.4-1 — Transmissibility models

<u>TRANSMISSIBILITY MODELS</u>	
Model No.	Remarks
I	Large model to determine load path and critical mass locations
II	Uncoupled pitch axis assembly - 7 mass locations
III	Working pitch axis model - 3 mass locations
IV	Uncoupled roll axis assembly - 6 mass locations
V	Working roll axis model - 3 mass locations
VI	Large coupled model to determine effects of coupling and bearing stiffnesses

~~SECRET~~/SPECIAL HANDLING

~~SECRET/SPECIAL HANDLING~~

will not violate the curve for reasonable estimates of system damping. The low level of this peak indicates that its degree of coupling to the input torques is small and does not pose a foreseeable problem.

The second peak falls outside of the envelope by approximately 8 db. Fig. 7.4-1 is a plot of  $\delta$  (percent of critical damping) and T (transmissibility expressed in decibels) for a single degree to freedom model responding at resonance. Indicated on the curve is the allowable T at 1,000 radians/second and also at 1,180 radians/second. The third line is the present value for T. Using a single degree of freedom analogy, our system has a  $\rho = 0.012$  and requires  $\rho = 0.030$ . These values of  $\rho$  are not to be interpreted as the values of  $\rho$  used in the analysis but rather a quality factor by which to judge amounts of relative damping. Applying this quality factor indicates that the necessary damping at this frequency is approximately 2.5 times that present.

A point to note is that the envelope curve shown in Fig. 7.4-21, 7.4-22, and 7.4-23 is that shown in the unmodified specification. Other sections of the report show the curve with a knee at 1,000 radians/second as discussed at the October PDR. That curve has never been officially transmitted and therefore will not be used.

Model I — The scanner was idealized as a system of lumped masses, including the major mass locations, connected by massless springs accounting for critical load path stiffnesses. This model was programmed for dynamic calculations which predicted system frequencies and associated mode shapes. The results indicated that the degree of stiffness coupling between the pitch axis assembly and the scanner proper was small. That is, any rotational motions about the pitch axis would not greatly effect yoke and pedestal movements. Based on this uncoupling, smaller systems consisting of several masses were constructed. Those models were more adaptable to multiple calculations necessary to parameter studies.

Model II — The pitch axis assembly was treated as a seven mass system driven at the torquer with a sinusoidal motion of varying frequency. Fig. 7.4-2 shows the model configuration with the major responding masses and the following dynamic degrees of freedom:

$\theta_1$  = Rotation of the bezel about the pitch axis at the electronic package foundation

$\theta_2$  = Rotation at the center of gravity of the electronic package about an axis parallel to the pitch axis

$\theta_3$  = Rotation about the pitch axis, of the center portion of the bezel at the potting interface

$\theta_4$  = Rotation of the mirror about the pitch axis

$\theta_5$  = Rotation of the bezel about the pitch axis at the gyro foundation

$\theta_6$  = Rotation at the center of gravity of the pitch axis gyro about an axis parallel to the pitch axis

$\theta_7$  = Rotation of the encoder internals about the pitch axis

The springs used in the model are comprised of the following structural elements:

$k_1$  = Torsional spring representing a serial addition of the torquer shafting, the shaft coupling, and the torque end of the bezel

$k_2$  = Torsional spring representing the bezel between points 1 and 3

$k_3$  = Torsional spring representing electronic package mount and bezel pan

~~SECRET/SPECIAL HANDLING~~

~~SECRET/SPECIAL HANDLING~~

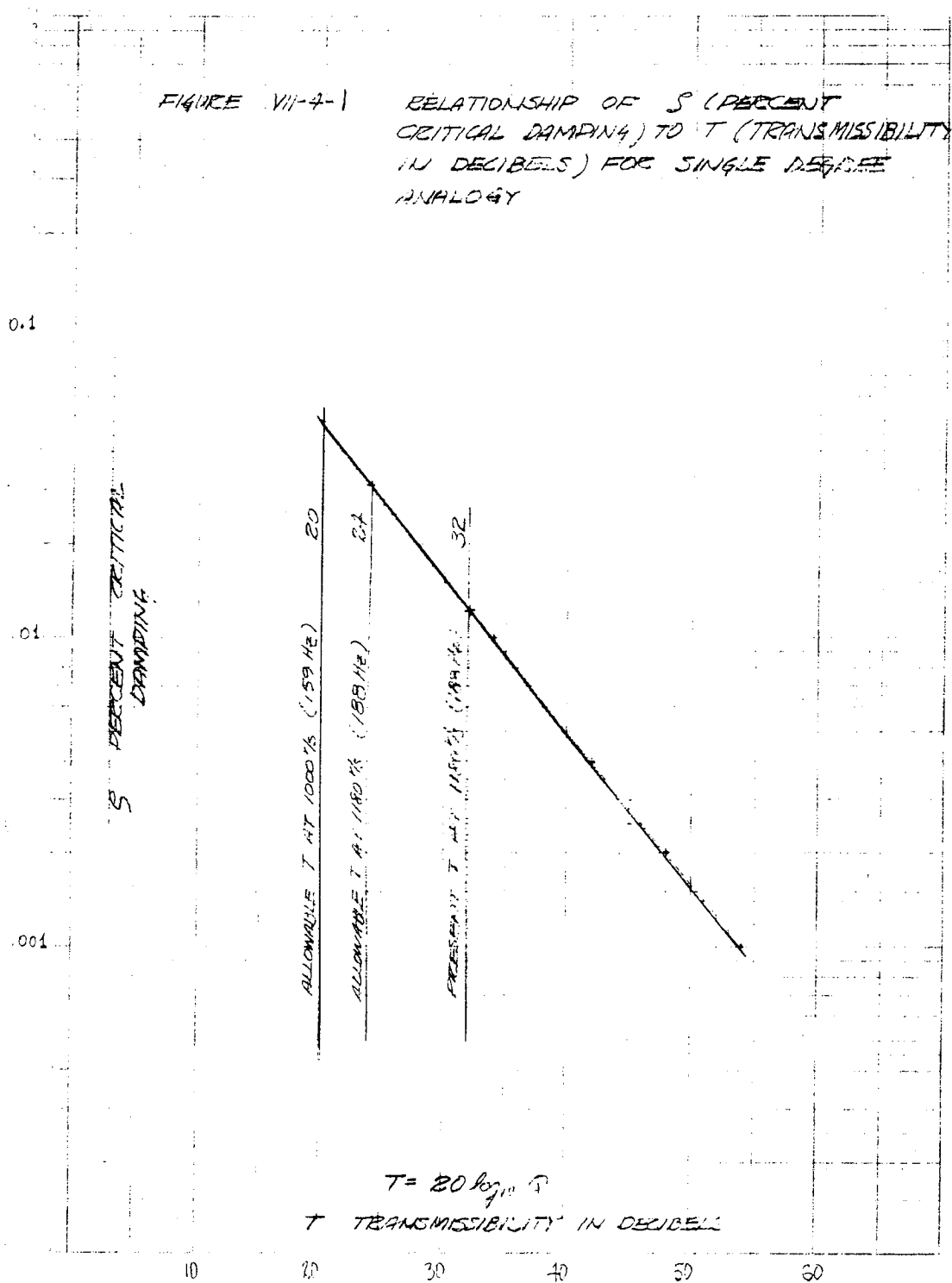


Fig. 7.4-1 — Relationship of  $\delta$  (percent critical damping) to T (transmissibility in decibels) for single degree analogy

~~SECRET/SPECIAL HANDLING~~

~~SECRET/SPECIAL HANDLING~~

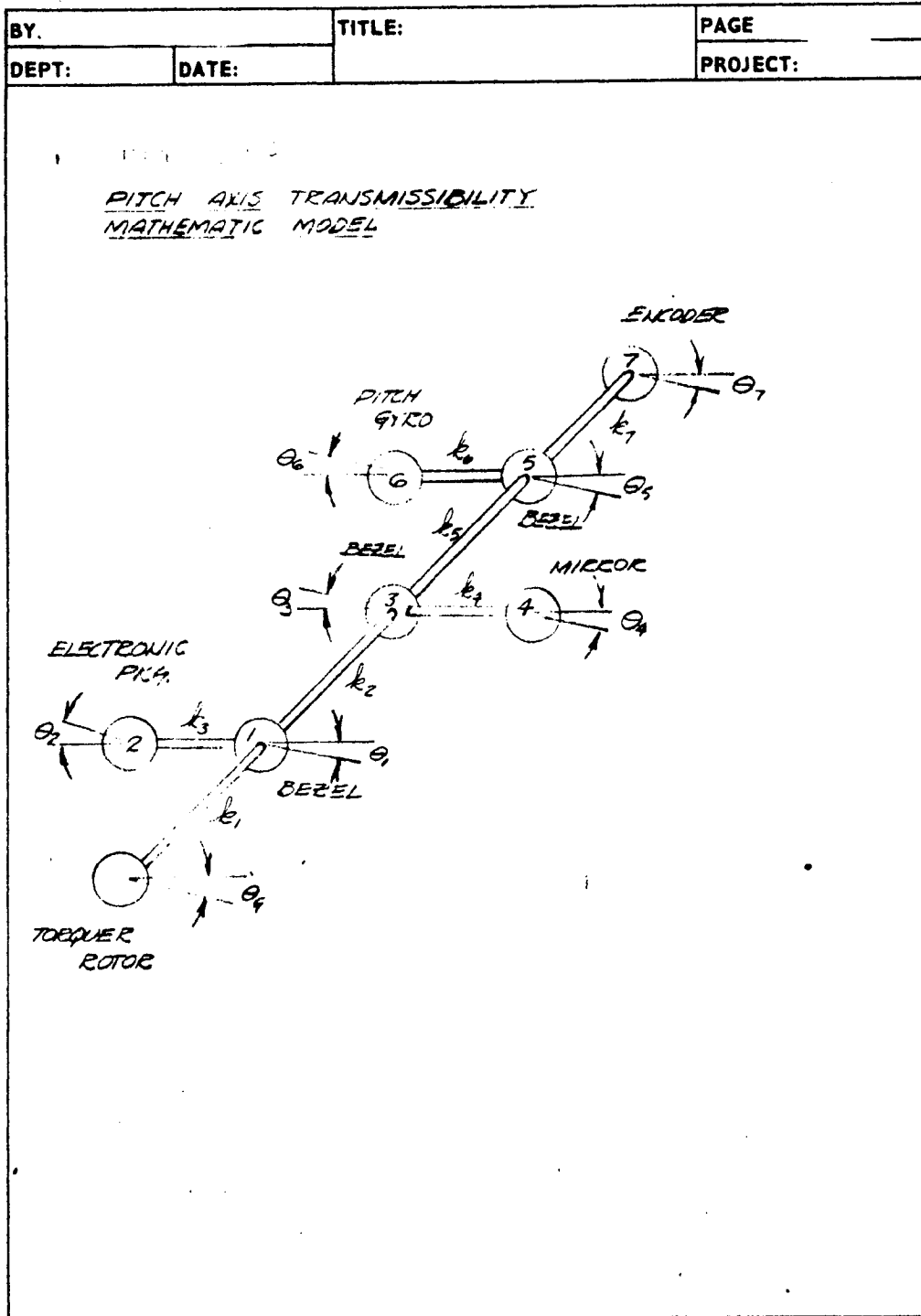


Fig. 7.4-2 — Pitch axis transmissibility mathematic model

~~SECRET/SPECIAL HANDLING~~

~~SECRET~~/SPECIAL HANDLING

$k_4$  = Torsional spring representing the potting

$k_5$  = Torsional spring representing the bezel between points 3 and 5

$k_6$  = Torsional spring representing pitch gyro package mount and bezel pan

$k_7$  = Torsional spring representing encoder end of bezel and encoder shafting

Analysis of this model resulted in system transmissibilities that exceeded the envelope of Fig. 7.4-3. It also indicated which springs and masses were responsible for the specification violation and which springs and masses had little effect on the transmissibility. Calculations given in the dynamic appendix indicated that two mechanisms were instrumented in fixing the system's fundamental frequency. These were:

1. The entire pitch axis assembly "winding up" on the torquer shafting stud, and
2. The mirror pitching in its bezel at the potting interface.

These two mechanisms appeared to completely dominate the lower mode responses and were used as the basis of constructing Model III.

Model III — A workable equivalent system was generated consisting of two masses and two springs which was used in a parametric study directed toward determining the optimum stiffness values allowing specification compliance. The elements of the model are the following components:

$k_1$  = Torsional spring representing the torque shafting stud and the torquer end of the bezel

$I_1$  = The entire pitch axis inertia shown in Model II excluding the mirror

$k_2$  = Torsional spring representing the potting

$I_2$  = Mirror inertia

Models II and III were uncoupled pitch analogs and were primarily used as expedient tools in guiding the design. It will be instructive to discuss these models and their response before continuing to the remaining models.

#### Equations of Motion

The equations of motion developed for the system are described in the following form:

$$[M] \{\ddot{x}\} + [C] \{\dot{x}\} + [k] \{x\} = [A] \{X_G\}$$

where  $[M]$  = the inertia matrix

$[C]$  = the viscous damping matrix

$[k]$  = the stiffness matrix

$\{x\}$  = the displacement vector

$[A]$  = the ground coefficient matrix

$\{X_G\}$  = the input motion vector

The mass and stiffness matrices were determined by routine procedures and are presented in the appendix. The damping matrix was constructed to reflect the energy dissipation properties of the potting material, the structural members and the friction losses inherent to the movable components, i.e., the bearings, the encoders, and the cabling.

Allowable friction losses Fig. 7.4-3 are given in terms of torque PSD which is a plot of  $(\text{ft-lb})^2$  per radian per second versus frequency. This may be thought of as the frequency

~~SECRET~~/SPECIAL HANDLING

~~SECRET/SPECIAL HANDLING~~

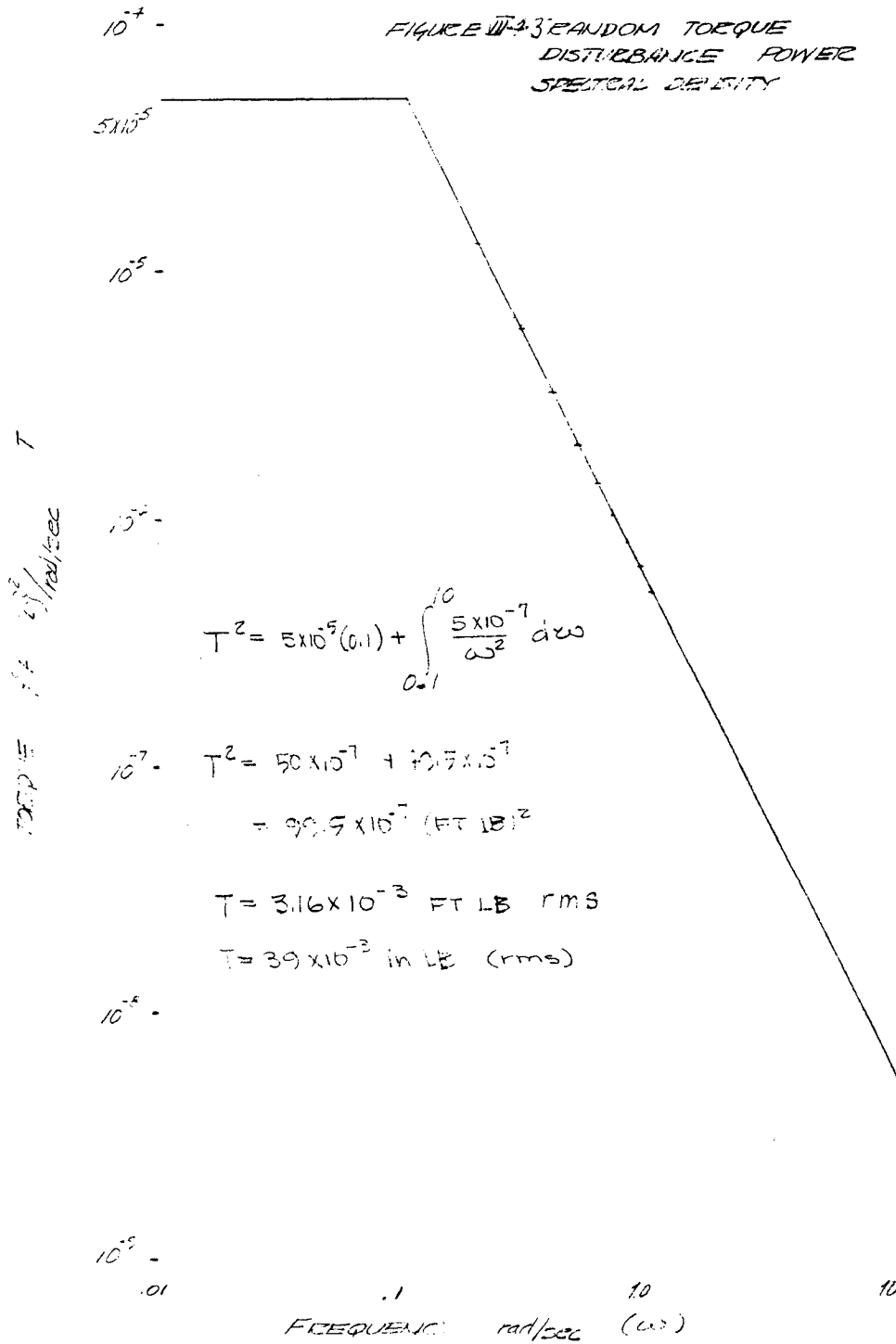


Fig. 7.4-3 — Random torque disturbance power spectral density

~~SECRET/SPECIAL HANDLING~~

~~SECRET~~/SPECIAL HANDLING

content of the frictional torque variations caused by the movable elements. The square root of the area under the curve is the overall rms torque level of these variations. This level is related to the operation speed of roll and pitch and may be equated to an equivalent viscous damping factor by the expression:

$$T = c\omega$$

where T = overall rms torque variation

$\omega$  = operational speed

c = damping factor

Probably the most important damping contributor is the potting material which is used to affix the mirror in its bezel. Assumed friction values directly effect the magnification of response. Preliminary values of damping were based on previous experience in similar applications. This experience also indicated that maximum Q was dependent on the potting's stiffness, the volume of material, the configuration, the level of excitation and properties unique to a particular design. To this end, a potting damping test was conducted to provide evaluation of the analytical assumption.

The specimen built for the damping study consisted of a 1 inch circular glass mirror blank, 12 inches in diameter. The mirror was potted into a heavy aluminum plate which attached directly to the shaker head. The central surface for the aluminum bezel was machined and finished to provide a good bonding surface. The mirror was potted with RTV-30 at a 0.2 inch gap exercising similar preparation and care that will be used on the prototype. After the prescribed 48 hour cure, the gap was X-rayed to ascertain the absence of voids and inclusions. The mirror was then cured for an additional 48 hours to finish its 96 hour cure period.

The test specimen was bolted to the shaker head and fitted with seven accelerometers as shown in Fig. 7.4-4. The steps in the procedure are as follows:

- a. A frequency sweep was performed to locate the system's natural frequency.
- b. A sinusoidal wave was input at this frequency and both inputs and output levels were recorded.
- c. The sinusoidal input was terminated abruptly and the decay of the output amplitude was recorded on a visicorder.
- d. Steps b and c were repeated for different levels of input.
- e. Steps a thru d were repeated for the other axis by bolting the specimen to a slip table, rotating the shaker and exciting the assembly in a horizontal direction.
- f. Steps b and c were repeated with output being read optically. Pieces of emery cloth were affixed to the accelerometers. The excursions of a particular, marked grit particle on the cloth were then measured with use of a calibrated microscope. The microscope and operator were situated on the same seismic block that supported the shaker.

The results of the tests are given below in terms of gain for out-of-plane and in-plane excitation:

~~SECRET~~/SPECIAL HANDLING

~~SECRET~~/SPECIAL HANDLING

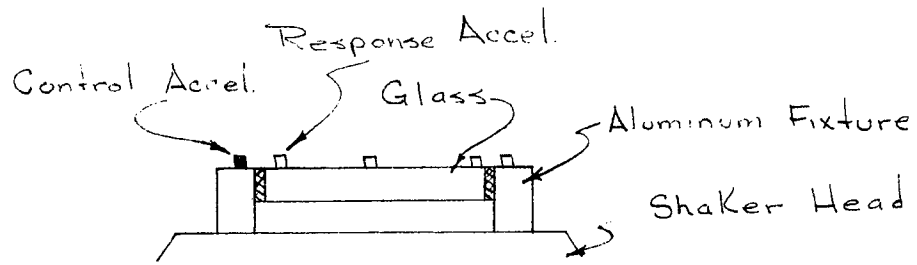
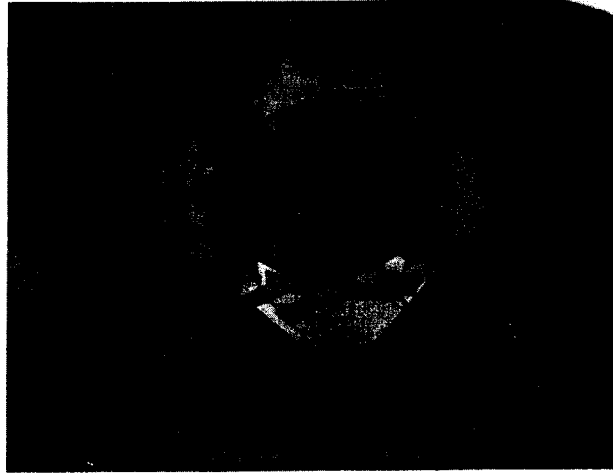


Fig. 7.4-4 — Damping test setup

~~SECRET~~/SPECIAL HANDLING

~~SECRET~~/SPECIAL HANDLING

Out of Plane Testing

	Range of Gain (Q)
Decay test	32-55
Resonance dwell	47-60
Optical reading	47-54

The optical readings are by far the most reliable and produce readings within the range of the other two methods; therefore a gain (Q) of approximately 50 or a damping constant of 1 percent of critical is correct for this axis.

In Plane Testing

	Range of Gain (Q)
Decay test	11-18

The in plane tests show approximately 2.8 percent to 4.7 percent of critical damping. The fact that exact figures for gain could not be established in this phase of the developmental tests is discouraging in a general sense; however, it does not negate the results. Approximate figures were established and were useful in validating the analytical assumptions. From this phase of the development damping test these conclusions are drawn with confidence:

1. The damping values of the potting material are dependent upon the direction of the major straining mechanism.
2. A damping value of 3 percent of critical is conservative for the slip axis direction.
3. A damping valve of 1 percent of critical is conservative for the direction of the normal axis.

The amount of damping in a silicone is dependent upon the volume of strained material, the magnitude of the strain, and the ratio of constrained surfaces to free surfaces in each responding mechanism. The latter explains why the out-of-plane case (case 2) exhibits less damping than the in-plane case (case 1). For, in case 2, both top and bottom surfaces are in the direction of strain and are unrestrained, while in case 2, those surfaces are orthogonal to the major strain direction. In the case of the mirror in the scanner, responding modes utilize a greater volume of potting than case 1 and have less free edges in direction strain than either case. For this reason 3 percent of critical damping was incorporated into the studies.

The third source of damping was due to material hysteresis. Normally bolted and bonded sections have high values of equivalent viscous damping, however, in this application conservative values have been selected. The hysteresis damping has taken as 0.5 percent of critical for all the structural members including the yoke. This assumption is particularly conservative in the yoke area for it neglects the damping contributions from the bonding material, eccobond 45, used to hold down the yoke top plate.

~~SECRET/SPECIAL HANDLING~~

Two mathematical approaches were considered to include the effects of damping, a model technique and an equivalent parallel dashpot technique. In both cases 0.5 percent damping was used.

The model technique uses a diagonal matrix of model damping coefficients derived from the normal modes and frequencies. A corresponding physical damping matrix operation:

$$[C] = [\phi^{-1}]^t [\bar{c}] [\phi^{-1}]$$

where  $[C]$  = the physical damping matrix

$[\phi]$  = the vibration mode shape matrix

$[\bar{c}]$  = the diagonal matrix of model damping coefficients

The stiffness coefficient analogy (4) assures that the system contained a viscous damper in parallel with each physical spring in the system as shown in Fig. 7.4-5.

The damper ( $C_{ij}$ ) was related to the spring constant ( $k_{ij}$ ) in the following manner:

$$C_{ij} = 2 \frac{c}{c_r} \sqrt{k_{ij} \frac{M_i M_j}{M_i + M_j}}$$

In the above,  $c/c_r$  is the ratio of the actual damping to the critical value of damping.

In general the  $[C]$  matrix obtained through the model technique is a full matrix indicating coupling between all degrees of freedom, while the equivalent system has damping valves that correspond only to stiffness terms. Model II was run as a test case with both sets of damping. The potting in the system was assumed to have similar properties to the structural elements. That is, all the members were considered to have 0.5 percent of critical. Figs. 7.4-6 and 7.4-7 shows the response in terms of transmissibility at the electronic package for a ground input. They show that the modal model has a  $Q$  of 35 while the Equivalent model has a  $Q$  of 75. The results of this isolated case indicate that the equivalent system has approximately half the damping than the model. Based on this, it is concluded that the use of an equivalent analogue is conservative.

#### Discussion of Results of Models II and III

Fig. 7.4-8 is the transmissibility plot of the mirror relative to the torquer as calculated for Model II. Superposed is the required scanner frequency response envelope. It is evident that the envelope is exceeded at 75 cps, the system's fundamental frequency. The mode associated with this frequency displays the entire pitch axis assembly torsionally winding up at the pitch torquer shaft (spring  $k_1$  in Figure 2). The frequency at which the second peak occurs is dominated by the mirror responding on the potting spring. This peak is significantly lower than the first because of the superior energy dissipating characteristics of the potting. The higher frequencies are beyond the range of interest and have little effect on the system structural response. This is seen from the sharp drop-off after the second peak.

Fig. 7.4-9 shows the response of the mirror (circles) and the pitch axis gyro (diamonds). This plot and the phase angle information shown in Fig. 7.4-10 indicates that the mirror and gyro, in general, move together up to 300 cps with the exception of the gyro having an antiresonance at 130 cps (the fixed base frequency of the mirror/potting). Motions at frequencies beyond 300 cps are not significant as they do not approach the specification levels.

~~SECRET/SPECIAL HANDLING~~

~~SECRET~~/SPECIAL HANDLING



Fig. 7.4-5 — Model used to derive damping matrix elements

~~SECRET~~/SPECIAL HANDLING

~~SECRET/SPECIAL HANDLING~~

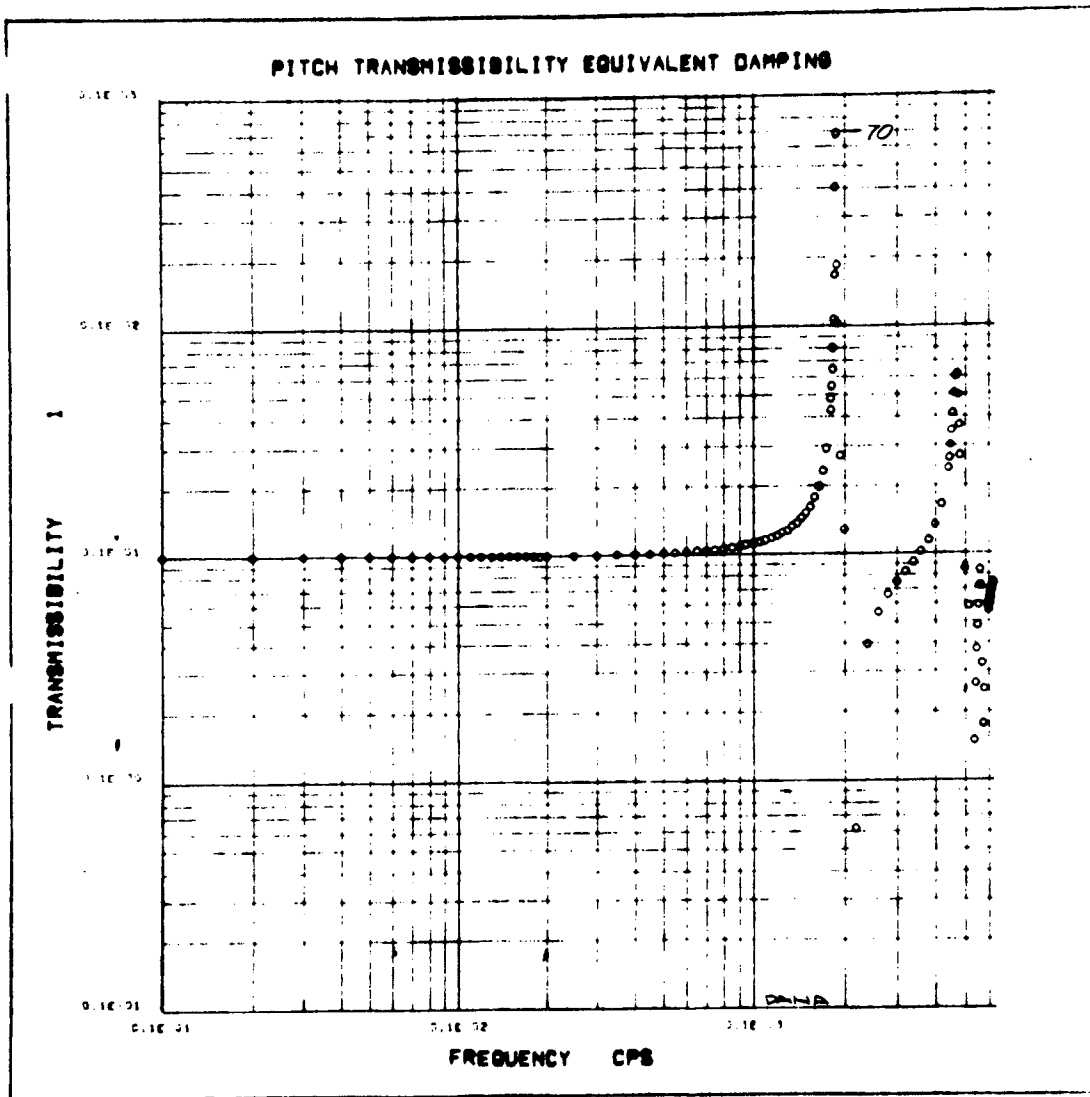


Fig. 7.4-6 — Test case—pitch axis encoder equivalent damping .005 c/cc

~~SECRET/SPECIAL HANDLING~~

~~SECRET/SPECIAL HANDLING~~

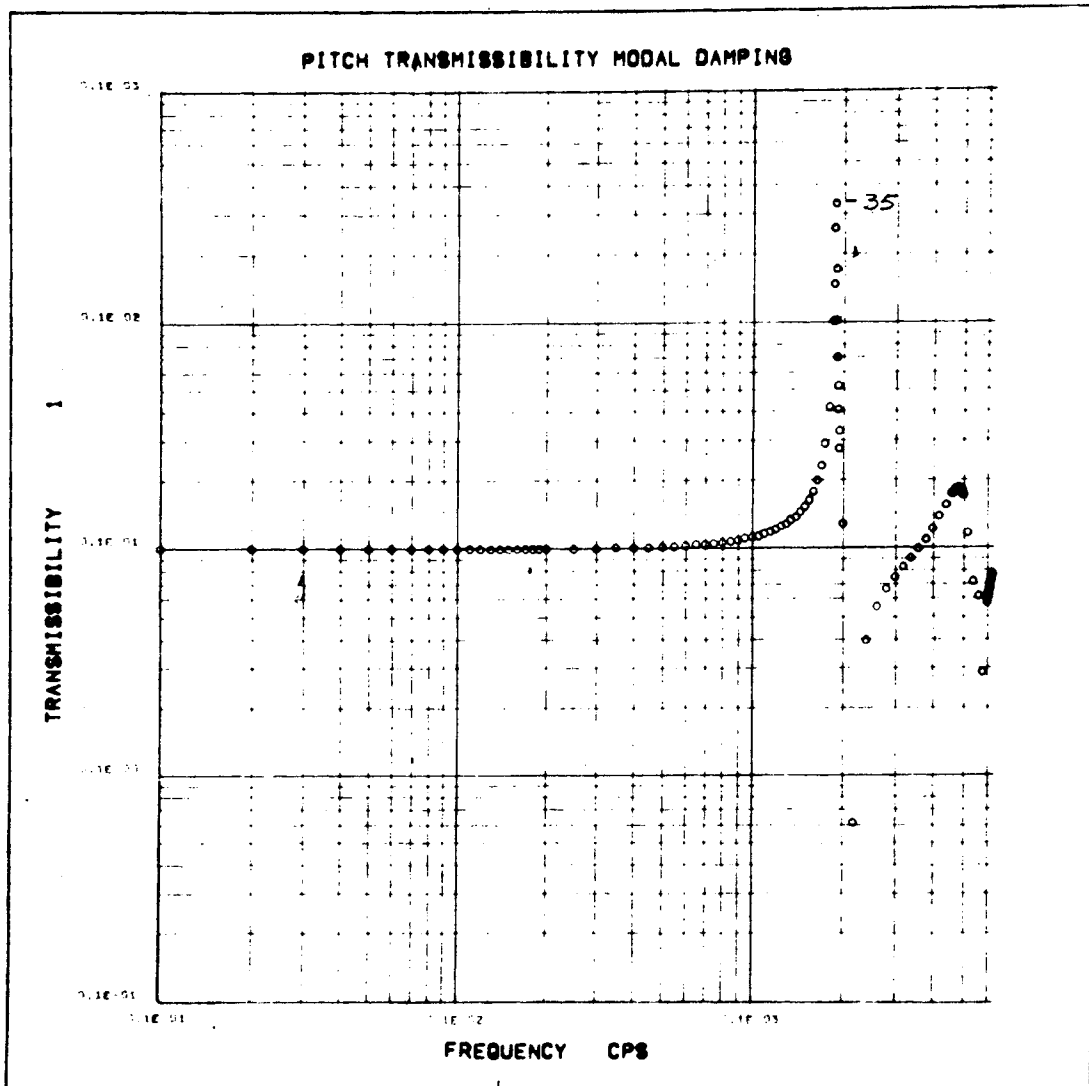


Fig. 7.4-7 — Test case—pitch axis encoder modal damping .009 c/cc

~~SECRET/SPECIAL HANDLING~~

~~SECRET~~/SPECIAL HANDLING

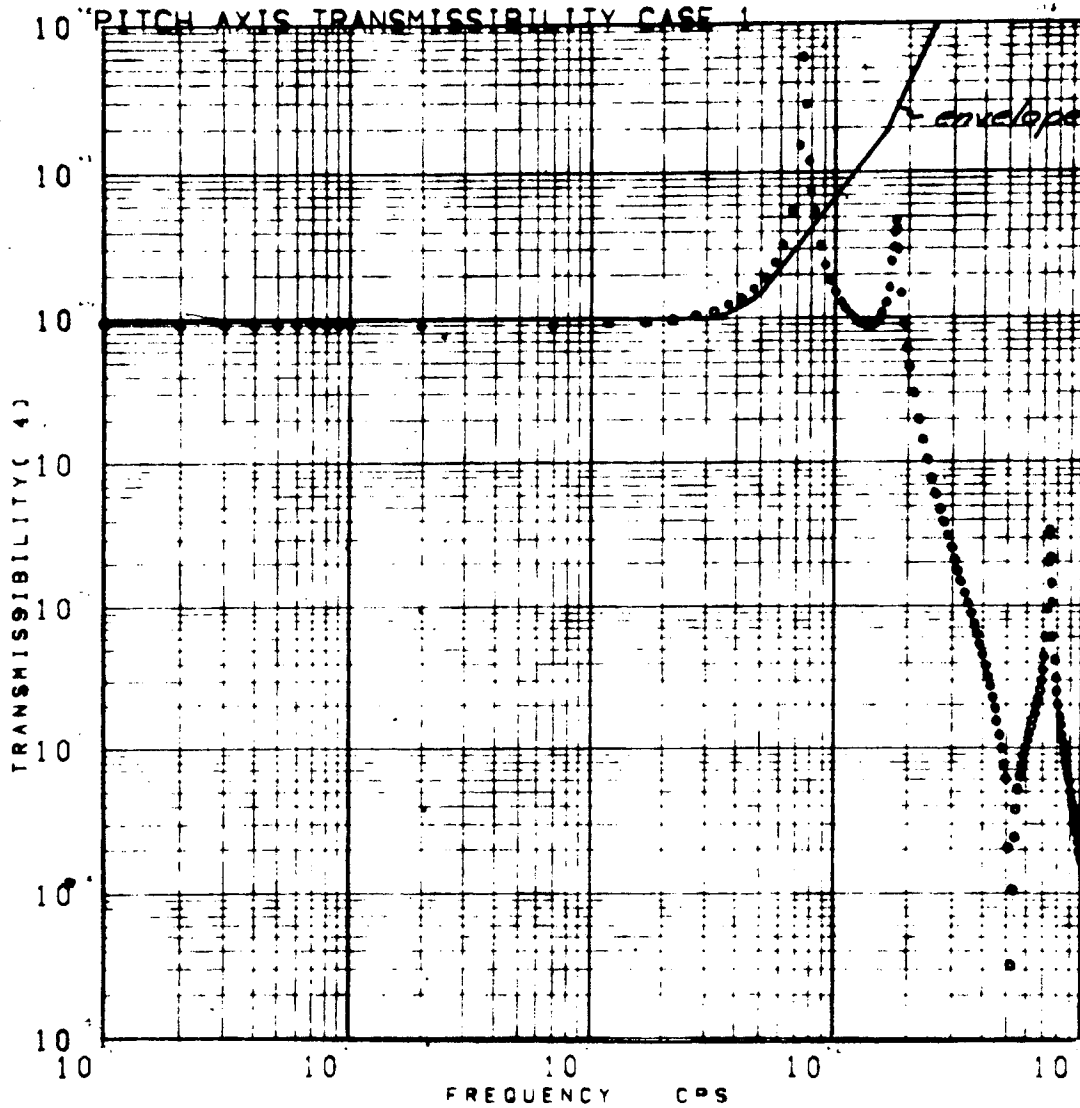


Fig. 7.4-8 — Transmissibility of mirror relative to torquer rotor

~~SECRET~~/SPECIAL HANDLING

~~SECRET~~/SPECIAL HANDLING

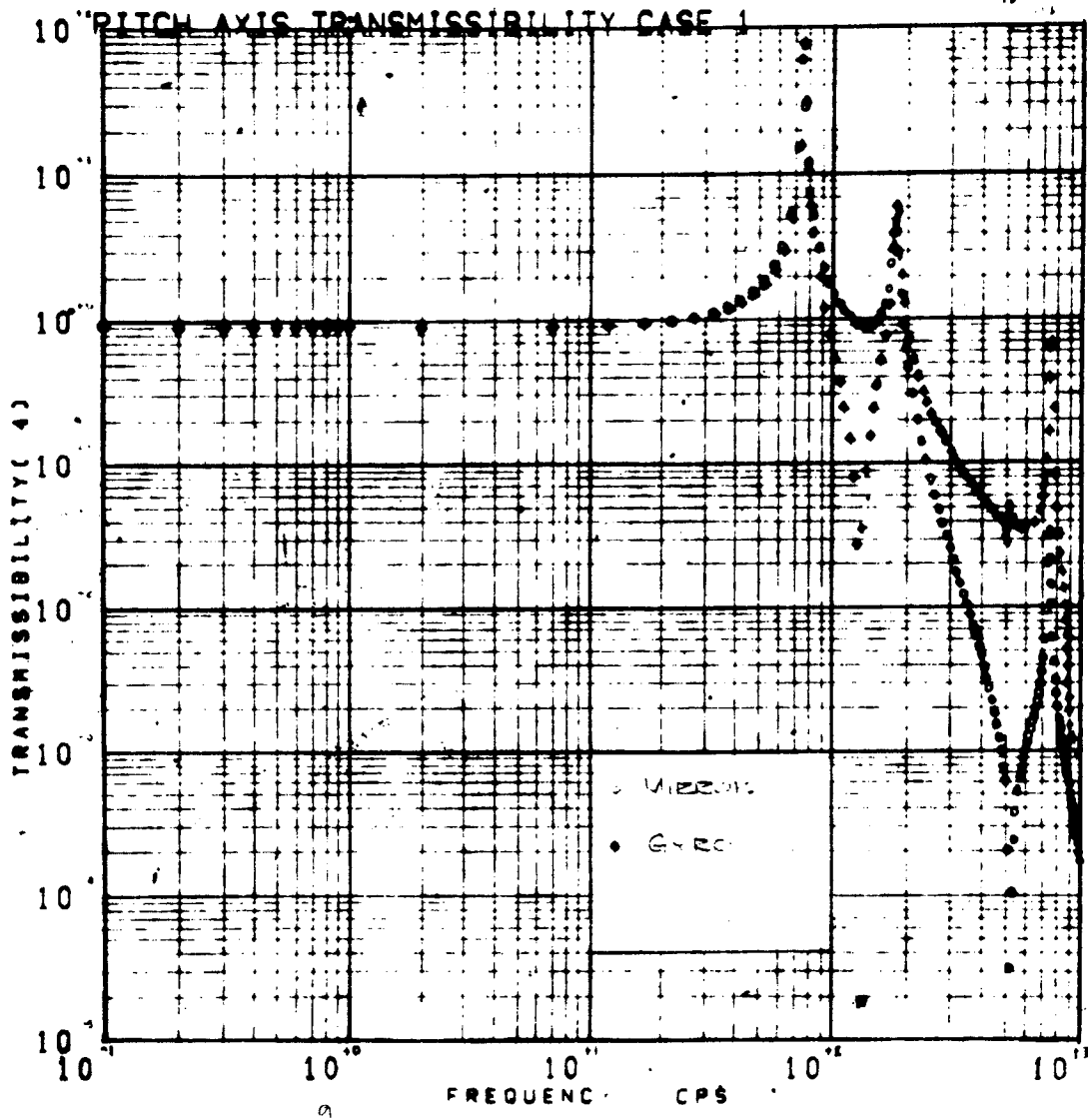


Fig. 7.4-9 — Transmissibilities of mirror and pitch axis gyro

~~SECRET~~/SPECIAL HANDLING

~~SECRET/SPECIAL HANDLING~~

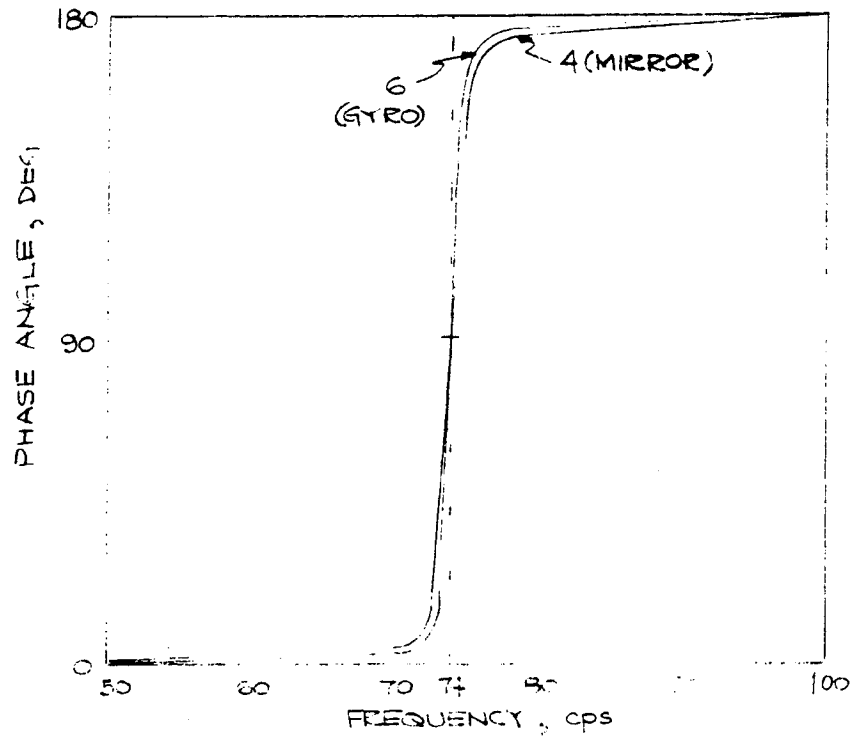


Fig. 7.4-10 — Phase angle plot of mirror (point 4) and gyro (point 6)

~~SECRET/SPECIAL HANDLING~~

~~SECRET~~/SPECIAL HANDLING

Although the requirements specifically call out the motion of the gyro alone, it is recognized that the relative movements of the gyro and mirror are of importance. The gyro's function is to monitor the mirror's movements by sensing the motion of its own foundation. An undesirable situation would be to have both gyro and mirror independently fall under the transmissibility envelope but have their respective peaks and notches line up so unfavorably as to result in a relative motion that would exceed the envelope. The notch corresponds to an amplification factor of 30 which when applied to the design system does not exceed the required envelope.

Based on the two mode dominance and the magnitude of the relative responses of gyro and mirror. Model III was constructed and utilized in a parametric study directed toward establishing optimum stiffness requirements of both pitch torquer shafting and potting. This study showed the required fundamental frequency could not be achieved by holding either value at the levels of Model II. It also showed the sensitivity approximately the same for each spring. This dictated treating the values simultaneously to obtain optimum properties.

Fig. 7.4-11 is a plot of the derived transmissibility for the two mass systems. The peak was taken at the system's fundamental frequency with its amplitude derived from a weighted damping consistent with Model II. Based on single degree of freedom considerations, Fig. 7.4-8 indicates the shafting resonance has an amplification of 60 while the mirror has an amplification of 5. The response of Model III indicates that the mirror/potting resonance had greater influence on the fundamental frequency that it did in Model II. This means that the first peak will have an amplification factor significantly lower than 60. Taking this into account an amplification factor of 30 was used.

The lowest acceptable frequency with this amplification was 1,085 radians/second. Fig. 7.4-12 is a plot of the relationship between the pertinent stiffnesses for the lowest acceptable fundamental frequency. Also shown is a curve for 1,200 radians/second. In addition to stiffness, the potting parameter  $G/t$  (shear modulus of rigidity divided by thickness) is indicated as the ordinate. The 1,200 radians/second curve indicates the magnitude of necessary stiffness increases to raise the system frequency approximately 100 radians/second. The potting values must be increased by approximately a factor of two. This large increase is physically unattainable with this design.

The design modifications engendered by use of Model III were then incorporated into Model II and rerun. Fig. 7.4-13 shows that the envelope is satisfied.

#### Model IV

A mathematical analog representing the uncoupled roll axis assembly was developed to describe the uncoupled roll response.

Fig. 7.4-14 shows the idealized roll model of the scanner, the mass points chosen represent the major mass contributions to the roll axis inertia. Structural elements included, reflect the critical load path stiffnesses. The following dynamic motions were included in the model:

- $O_1$  = rotation of the scan mirror in its bezel about the roll axis
- $Z_2$  = linear motion of the pitch axis torquer and torquer trunnion assembly
- $Z_3$  = linear motion of the pitch axis encoder and encoder trunnion assembly
- $\theta_4$  = rotation of the bezel about the roll axis
- $\theta_5$  = rotation of the roll axis gyro about an axis parallel to the roll axis
- $\theta_6$  = rotation of the roll axis shaft, yoke and electronic package about the roll axis

~~SECRET/SPECIAL HANDLING~~

The springs used in the model are comprised of the following structural elements:

$k_{12}$  = flexural spring representing a serial addition of one half of the potting, the torquer bezel plate, and the pitch axis torquer shafting

$k_{13}$  = flexural spring representing a serial addition of one half of the potting, the encoder bezel plate, and the pitch axis encoder shafting

$k_{24}$ ,  $k_{34}$  = flexural springs representing the bezel

$k_{25}$ ,  $k_{35}$  = flexural springs representing the yoke

$k_{56}$  = torsional spring representing the roll axis shafting.

Fig. 7.4-15 is a plot of the motion transmissibility of the roll axis gyro. Superposed on the plot is the required frequency response envelope. Note that this envelope has the knee at 300 radians/second. The curve shows an amplification factor of 25 at 175 cps. This maximum point lies approximately 3 db below the envelope. The analysis dictated the roll axis component stiffness requirements necessary to meet the specification.

The roll axis model neglected the effects of bearing stiffnesses. Preliminary information indicated that the compliance of the bearings had little effect on the transmissibility. Recently acquired information relating bearing preload to isothermal changes as well as a temperature differential was incorporated into the analysis. The ultimate results of thermal effects are felt in the system's overall stiffness and encumbant transmissibility. A variation of the roll axis bearing stiffness will not effect the transmissibility greatly. However, if the pitch bearing's stiffness drops significantly it will adversely effect the roll axis transmissibility. An exploratory study was conducted to determine the effects of isothermal heating on the roll axis transmissibility. This is best accomplished with a small model (Model V) which consisted of three inertias coupled with two springs as the elements of the model are the following components:

$I_1$  = the roll axis torquer rotor and a portion of the shaft

$k_1$  = a serial addition of the pitch axis shafting, the pitch axis bearings, the yoke, and the roll axis shafting

$I_2$  = the inertia of the yoke, a portion of the shaft, the roll gyro and electronic package assemblies, and the pitch axis trunnion mounts

$k_2$  = rotational spring representing the potting

$I_3$  = mirror inertia about the roll axis

Fig. 7.4-16 shows this pitch axis bearings torsional spring rate versus an isothermal temperature change. The curves indicate that the system's stiffness increase with both negative and positive temperatures differentials. This can do nothing but increase the system's frequency. An interesting calculation was done at this point: the bearing stiffness was treated as infinitely stiff. The resulting frequency was less than 1 percent higher than the  $0^0$  isothermal case.

Further studies were conducted with this model to determine the effects of a reduction in preload. This reduction can arise by faulty assembly, a temperature gradient across the bearings or other deleterious events. Fig. 7.4-17 shows the variation of the system's frequency with radial preload. The curve shows the region (hatched line) boundary at which the frequency response curve is exceeded. This boundary is based on an amplification factor of 25. This has no built-in conservatism and may be considered as an absolute lower bound.

~~SECRET/SPECIAL HANDLING~~

SCANNER PITCH TRANSMISSIBILITY  
(2 MASS SYSTEM)

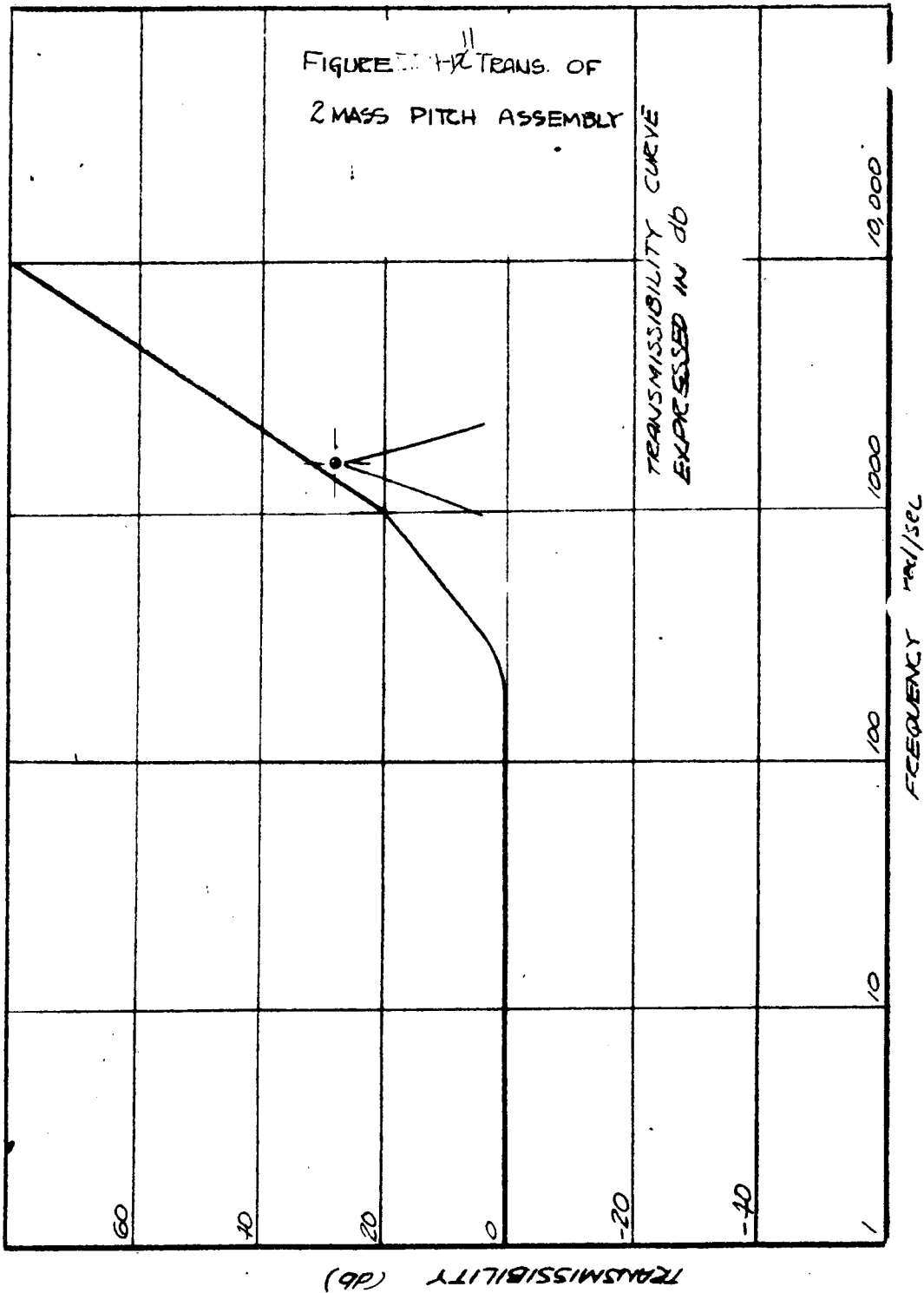
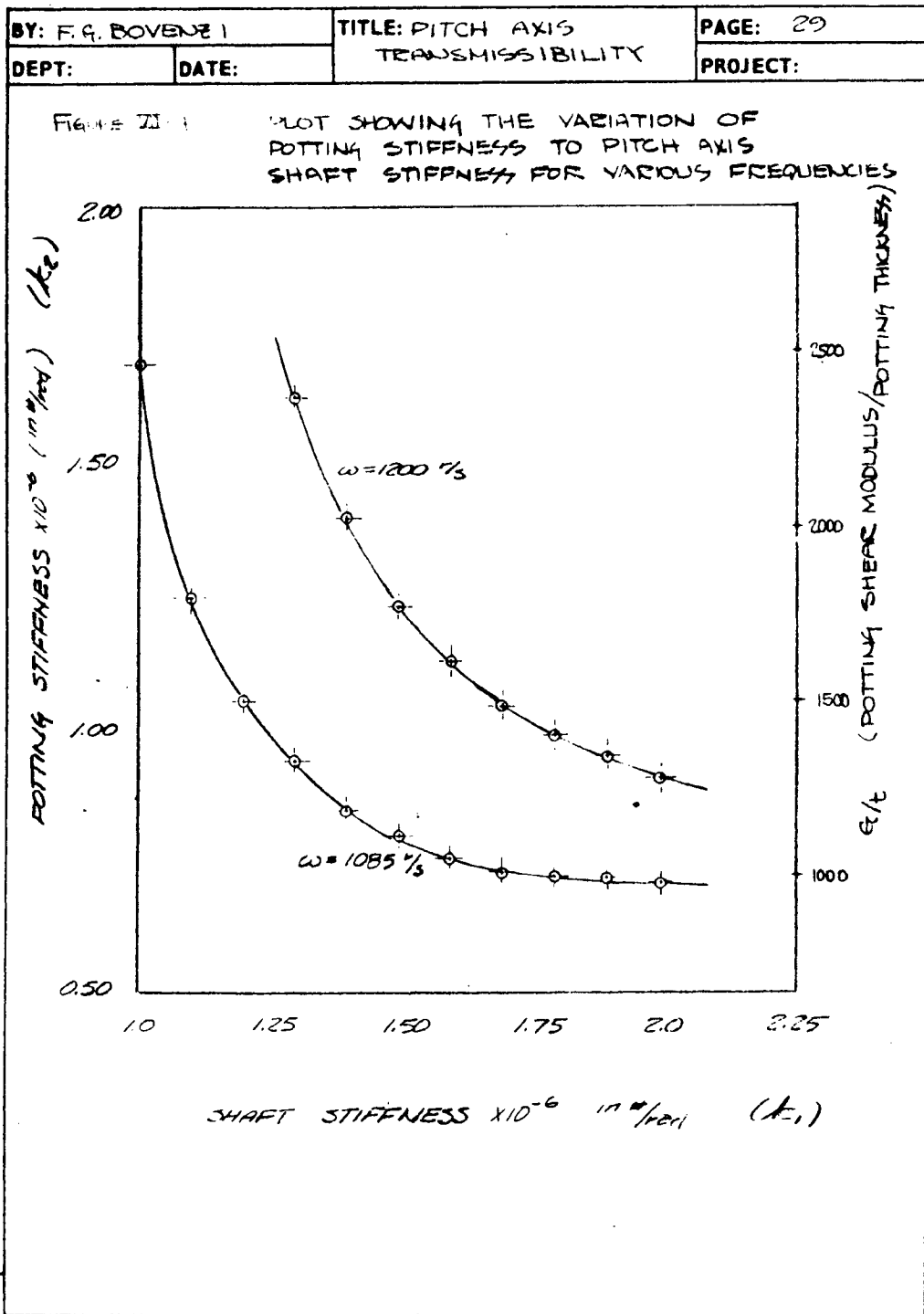


Fig. 7.4-11 -- Transmissibility of 2 mass pitch assembly

~~SECRET/SPECIAL HANDLING~~

~~SECRET/SPECIAL HANDLING~~



E 103 B 66 ENGINEERING ANALYSIS SHEET

ltek

Fig. 7.4-12 — Plot showing the variation of potting stiffness to pitch axis shaft stiffness for various frequencies

~~SECRET/SPECIAL HANDLING~~

~~SECRET/SPECIAL HANDLING~~

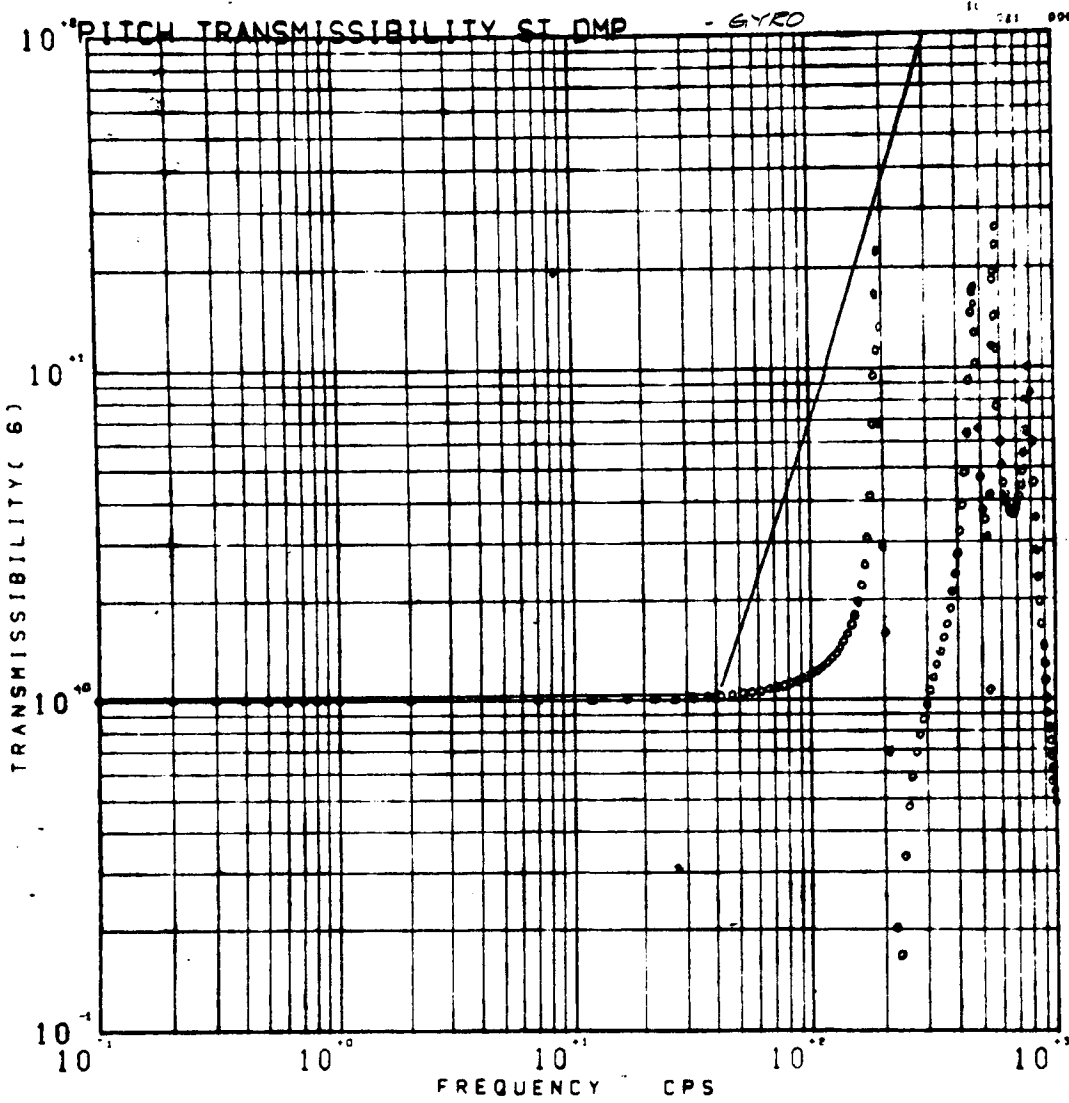
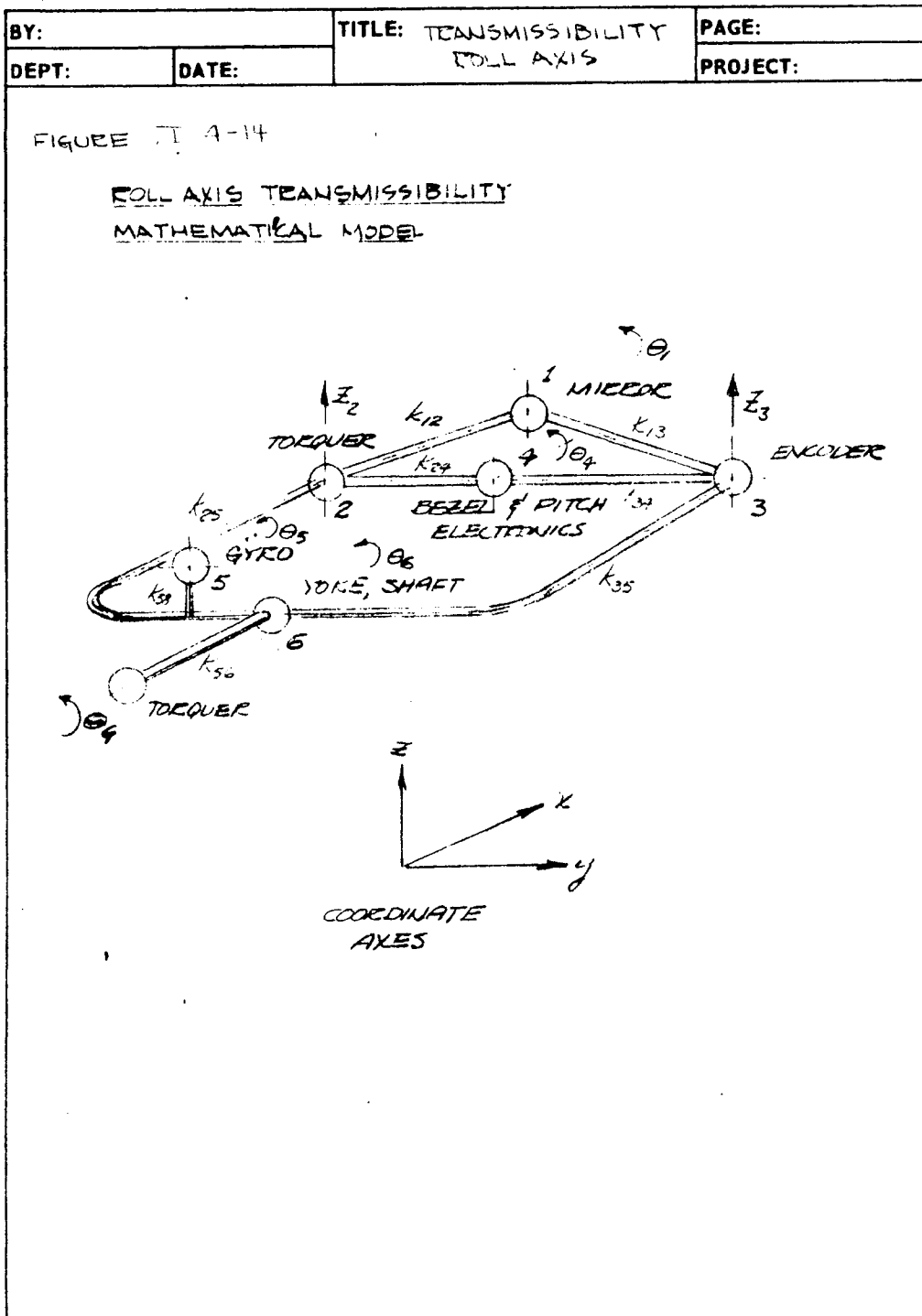


Fig. 7.4-13 — Pitch gyro—Model II

~~SECRET/SPECIAL HANDLING~~

~~SECRET/SPECIAL HANDLING~~



E 103 8/66 ENGINEERING ANALYSIS SHEET

liek

Fig. 7.4-14 — Roll axis transmissibility mathematical model

~~SECRET/SPECIAL HANDLING~~

~~SECRET/SPECIAL HANDLING~~

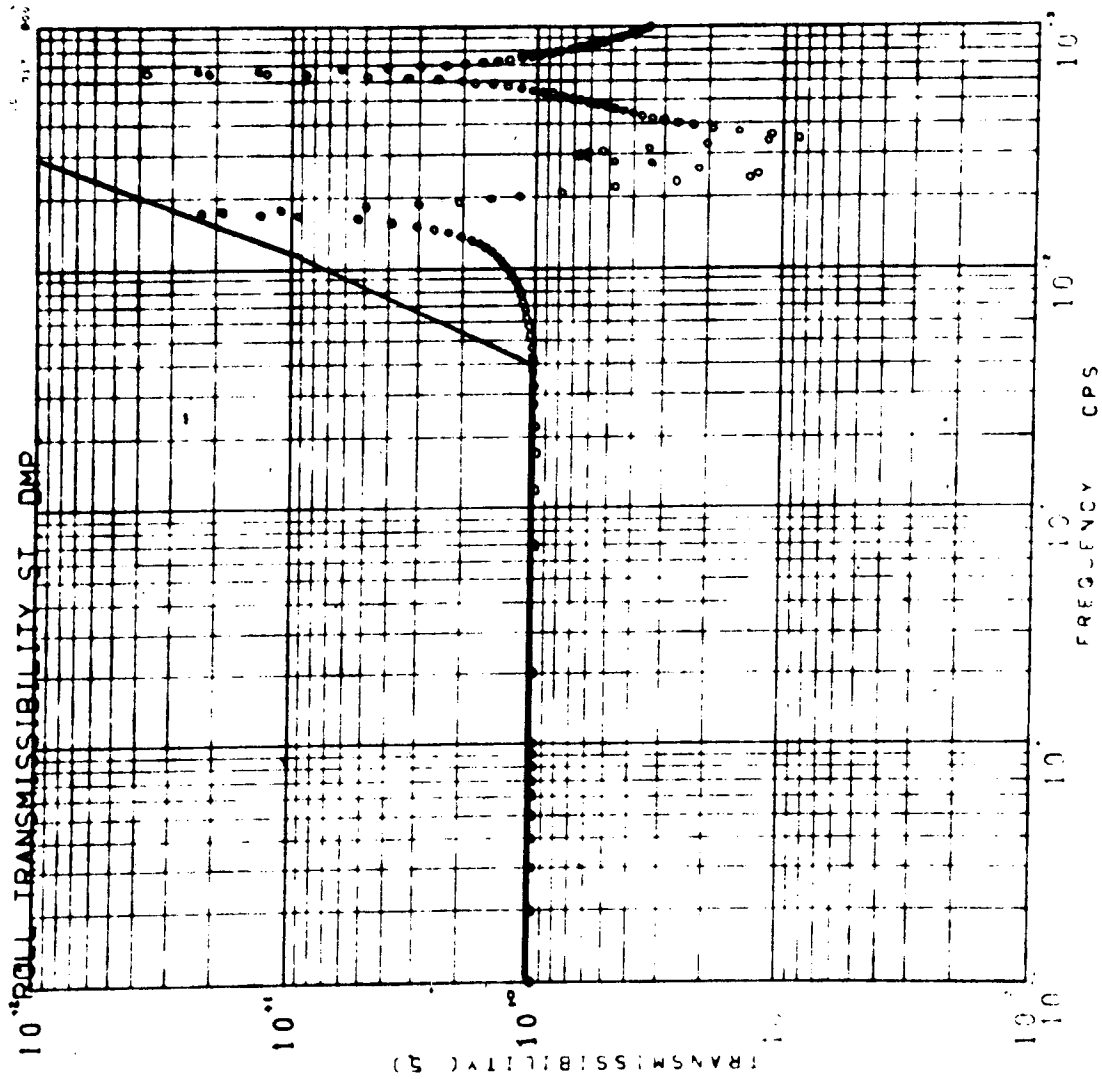
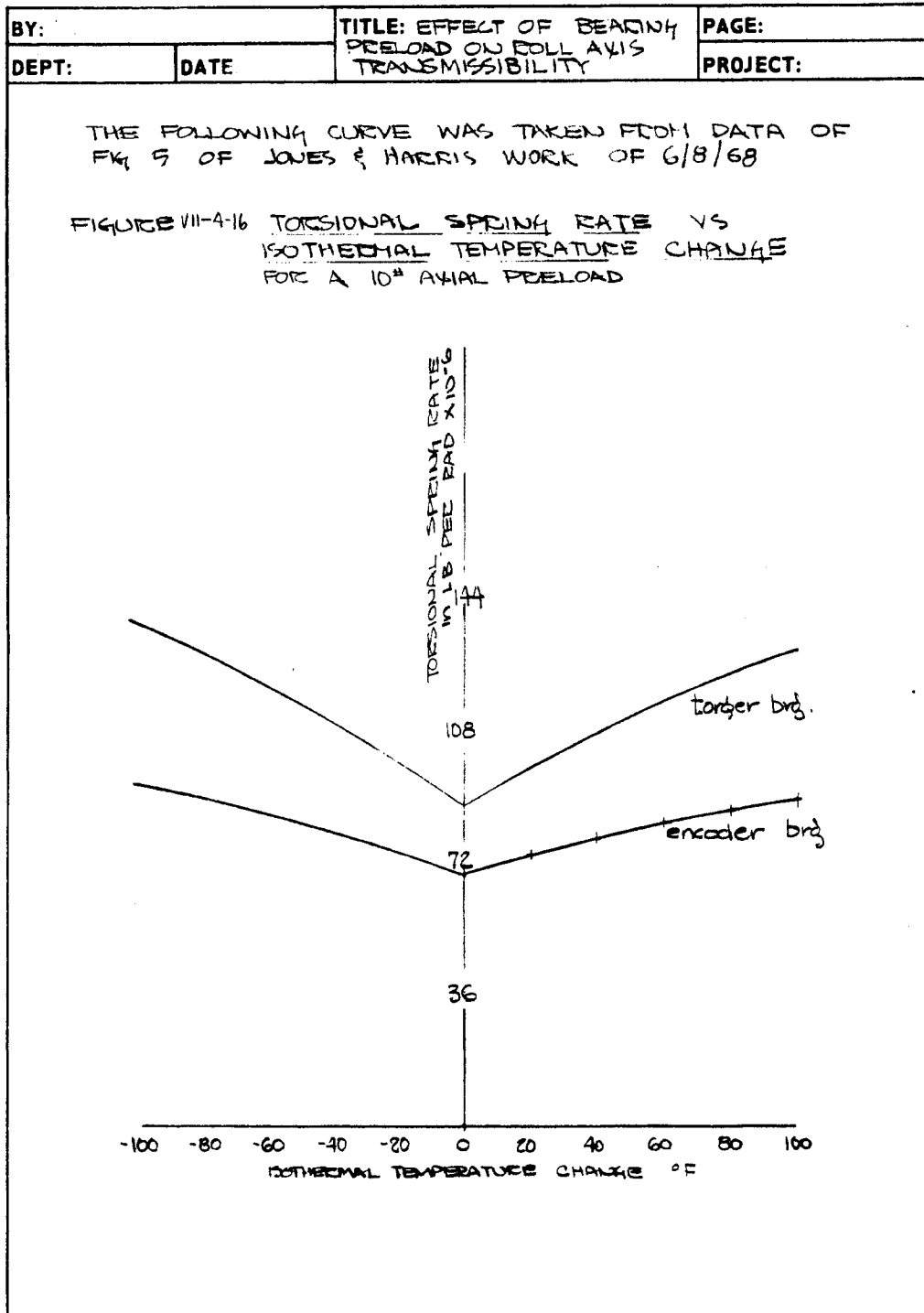


Fig. 7.4-15 — Transmissibility plot roll axis gyro

~~SECRET/SPECIAL HANDLING~~

~~SECRET/SPECIAL HANDLING~~



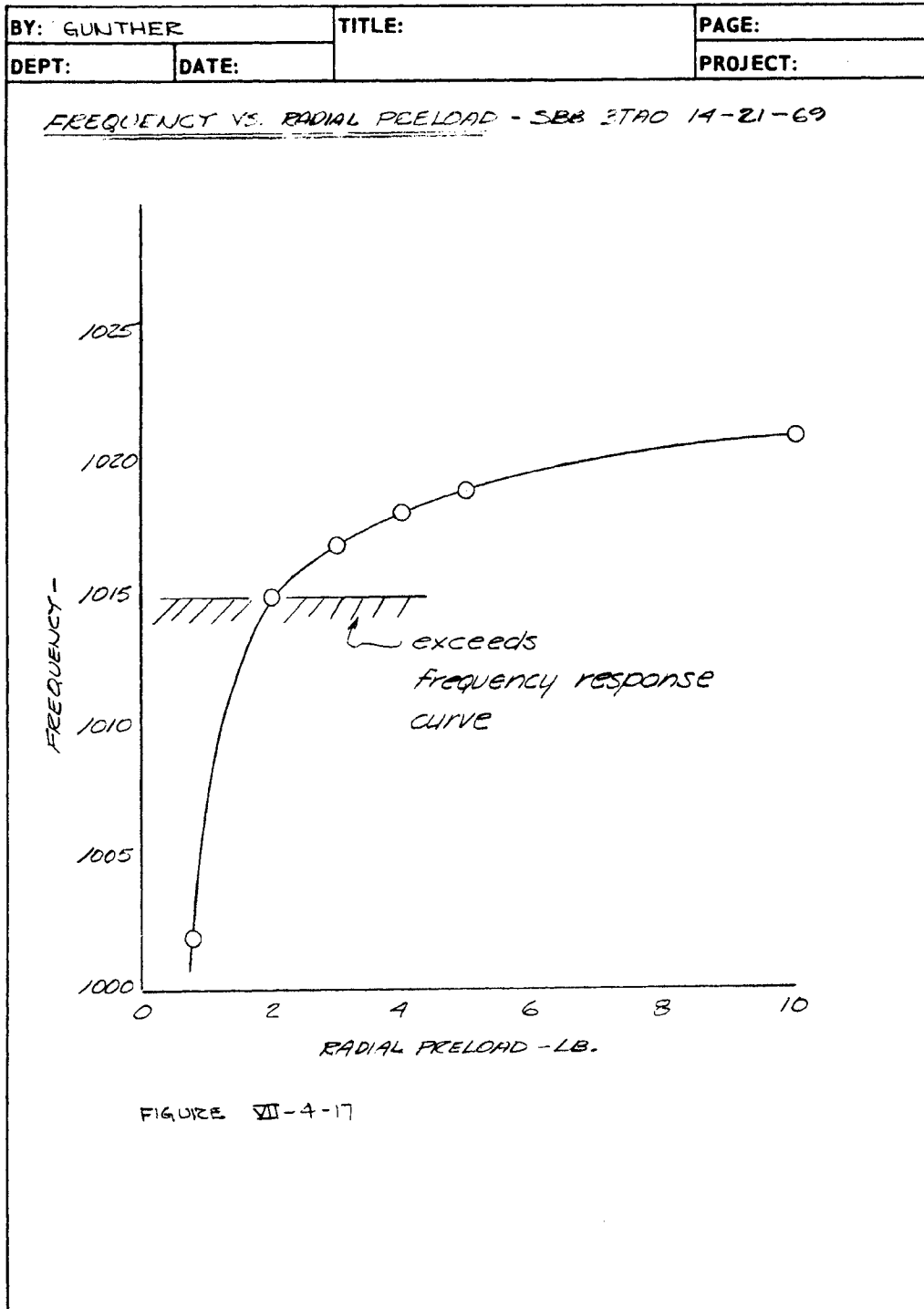
E 103 8/66 ENGINEERING ANALYSIS SHEET



Fig. 7.4-16 — Torsional spring rate versus isothermal temperature change for a 10-pound axial preload

~~SECRET/SPECIAL HANDLING~~

~~SECRET/SPECIAL HANDLING~~



E 103 8 66 ENGINEERING ANALYSIS SHEET



Fig. 7.4-17 — Frequency versus radial preload—SBB 3TAO 14-21-69

~~SECRET/SPECIAL HANDLING~~  
7.4-26

~~SECRET/SPECIAL HANDLING~~

The results of analysis performed on Models I through V were implemented into the design as stiffness requirements at the component assembly level, e.g., the pitch axis electronic package mount including the bezel pan must be a system in excess of 300 cps. It is instructive to review the tacit assumptions that these requirements were based on:

1. The pitch axis assembly and the roll axis assembly were uncoupled in a dynamic sense which includes both stiffness and mass coupling.
2. The full complement of bearing compliance, with design preloads, had little effect and was therefore excluded.
3. The cross products of inertia terms had little effect. This is, in a sense, an elaboration of 1.

To incorporate the effects, in terms of stiffness requirements of the above considerations, into the design, Model VI was constructed. In addition, the effects of the shell flexibility were to be incorporated. Although the specification deals only with the scanner proper, it is of great interest, to evaluate the relative importance of the shell's flexibility to the overall system's fundamental frequency.

#### Model VI Coupled Model

For this dynamic analysis study, the scanner was idealized as a lumped parameter system. The structure was treated as a series of discrete masses interconnected by elements having stiffness and damping characteristics which are expressed as matrix coefficients in the system's motion relationships. Since the evaluation of these coefficient matrices was a prerequisite to determining the system response, the following discusses the procedure used in that evaluation.

Prior to obtaining the various structural parameters, a geometrical orientation of the scanner was established. As shown in Fig. 7.4-18, the scanner was positioned with respect to a reference coordinate system designed as XYZ.

As inspection of the component mass data (Tables 7.4-2 thru 4) along with the structural geometry, established points where the largest mass concentrations occur. As a result, mass points as shown in Fig. 7.4-18 were selected and designated as JAA through JAN. Coordinates of these points were chosen where possible to coincide with the intersection of structural axes. Table 7.4-5 gives these coordinates in terms of the reference axes.

In addition to determining mass point concentrations, mode points were established at locations where three or more stiffness elements intersected. These node points were designated as JB—and the respective coordinates are given in Table 7.4-6.

#### Mass Properties

Once the geometrical locations of the various mass concentrations were established, the component parts to be acting at these points were selected and the mass acting at each point was numerically evaluated.

Each mass point was assumed to have six degrees of freedom, i.e., three translations and three rotations. Consequently, in addition to evaluating the mass, inertia quantities about the reference axes had to be determined.

The various scanner components assumed to act at each mass point are indicated in Tables 7.4-2 thru 4. In addition, these tables list the component weights and inertias used to evaluate the mass point properties.

~~SECRET/SPECIAL HANDLING~~



~~SECRET/SPECIAL HANDLING~~

Table 7.4-2 — Scanner — Component

BY: <i>W. D. J. [unclear]</i>		TITLE: <i>SCANNER</i>		PAGE:							
DEPT:		DATE:		PROJECT: <i>9400</i>							
PART	DESCRIPTION (COMPONENTS)	COORDINATE		WEIGHT		MOMENT OF INERTIA		PRODUCT OF INERTIA			
		X	Y	Z	W	I <sub>XX</sub>	I <sub>YY</sub>	I <sub>ZZ</sub>	I <sub>XY</sub>	I <sub>YZ</sub>	I <sub>XZ</sub>
		IN	IN	IN	LB	IN <sup>2</sup> -LB	IN <sup>2</sup> -LB	IN <sup>2</sup> -LB	IN <sup>3</sup> -LB	IN <sup>3</sup> -LB	IN <sup>3</sup> -LB
<i>1AA</i>	<i>MIRROR 1/2 REMAIN</i>	<i>0.21</i>	<i>0.00</i>	<i>0.73</i>	<i>11.12</i>	<i>223.19</i>	<i>143.35</i>	<i>89.53</i>	<i>1.67</i>	<i>51.51</i>	<i>-9.28</i>
		<i>0.21</i>	<i>0.00</i>	<i>0.73</i>	<i>11.00</i>	<i>222.20</i>	<i>82.22</i>	<i>141.76</i>	<i>0.0</i>	<i>0.0</i>	<i>0.0</i>
		<i>0.21</i>	<i>0.00</i>	<i>0.73</i>	<i>0.12</i>	<i>4.94</i>	<i>1.87</i>	<i>3.09</i>	<i>0.0</i>	<i>0.0</i>	<i>0.0</i>
<i>1AB</i>	<i>BEZEL (1/6) SHAFTING ENCODER Disc ENCODER Mount CLAMP RINGS BEARINGS</i>	<i>1.20</i>	<i>-6.55</i>	<i>0.90</i>	<i>1.07</i>	<i>40.82</i>	<i>10.32</i>	<i>31.61</i>	<i>0.10</i>	<i>-11.61</i>	<i>-0.58</i>
		<i>1.20</i>	<i>0.00</i>	<i>0.90</i>	<i>0.58</i>	<i>15.51</i>	<i>9.65</i>	<i>6.30</i>	<i>0.10</i>	<i>-11.61</i>	<i>-0.58</i>
		<i>1.20</i>	<i>-6.38</i>	<i>0.90</i>	<i>0.13</i>	<i>0.10</i>	<i>0.15</i>	<i>0.10</i>	<i>0.0</i>	<i>0.0</i>	<i>0.0</i>
		<i>1.20</i>	<i>-6.97</i>	<i>0.90</i>	<i>0.14</i>	<i>0.20</i>	<i>0.40</i>	<i>0.20</i>	<i>0.0</i>	<i>0.0</i>	<i>0.0</i>
		<i>1.20</i>	<i>-7.10</i>	<i>0.90</i>	<i>0.10</i>	<i>0.04</i>	<i>0.08</i>	<i>0.04</i>	<i>0.0</i>	<i>0.0</i>	<i>0.0</i>
		<i>1.20</i>	<i>-7.12</i>	<i>0.90</i>	<i>0.04</i>	<i>0.0</i>	<i>0.0</i>	<i>0.0</i>	<i>0.0</i>	<i>0.0</i>	<i>0.0</i>
		<i>1.20</i>	<i>-6.62</i>	<i>0.90</i>	<i>0.08</i>	<i>0.02</i>	<i>0.04</i>	<i>0.02</i>	<i>0.0</i>	<i>0.0</i>	<i>0.0</i>
<i>1AC</i>	<i>BEZEL (1/6) SHAFTING LOCK NUT, BRG LOCK NUT, MOTOR BEARINGS ROTOR</i>	<i>1.20</i>	<i>6.55</i>	<i>0.90</i>	<i>2.05</i>	<i>42.22</i>	<i>10.48</i>	<i>33.04</i>	<i>0.10</i>	<i>-11.61</i>	<i>-0.58</i>
		<i>1.20</i>	<i>0.0</i>	<i>0.90</i>	<i>0.58</i>	<i>15.51</i>	<i>9.65</i>	<i>6.30</i>	<i>0.10</i>	<i>-11.61</i>	<i>-0.58</i>
		<i>1.20</i>	<i>6.50</i>	<i>0.90</i>	<i>0.16</i>	<i>0.11</i>	<i>0.15</i>	<i>0.11</i>	<i>0.0</i>	<i>0.0</i>	<i>0.0</i>
		<i>1.20</i>	<i>6.94</i>	<i>0.90</i>	<i>0.11</i>	<i>0.02</i>	<i>0.04</i>	<i>0.02</i>	<i>0.0</i>	<i>0.0</i>	<i>0.0</i>
		<i>1.20</i>	<i>8.31</i>	<i>0.90</i>	<i>0.02</i>	<i>0.02</i>	<i>0.04</i>	<i>0.02</i>	<i>0.0</i>	<i>0.0</i>	<i>0.0</i>
		<i>1.20</i>	<i>6.56</i>	<i>0.90</i>	<i>0.34</i>	<i>0.06</i>	<i>0.14</i>	<i>0.06</i>	<i>0.0</i>	<i>0.0</i>	<i>0.0</i>
		<i>1.20</i>	<i>7.75</i>	<i>0.90</i>	<i>0.84</i>	<i>0.33</i>	<i>0.46</i>	<i>0.33</i>	<i>0.0</i>	<i>0.0</i>	<i>0.0</i>
<i>1AD</i>	<i>BEZEL (2/3) TRIM WEIGHT</i>	<i>1.20</i>	<i>0.00</i>	<i>0.90</i>	<i>3.82</i>	<i>64.04</i>	<i>132.75</i>	<i>121.33</i>	<i>0.39</i>	<i>-6.43</i>	<i>-2.33</i>
		<i>1.20</i>	<i>0</i>	<i>0.90</i>	<i>2.32</i>	<i>62.02</i>	<i>38.61</i>	<i>25.21</i>	<i>0.39</i>	<i>-6.43</i>	<i>-2.33</i>
		<i>1.20</i>	<i>0</i>	<i>-7.00</i>	<i>1.50</i>	<i>2.02</i>	<i>0.52</i>	<i>2.50</i>	<i>0.0</i>	<i>0.0</i>	<i>0.0</i>

~~SECRET/SPECIAL HANDLING~~

~~SECRET/SPECIAL HANDLING~~

Table 7.4-2 — Scanner — Component (Cont.)

BY: D. DUGAN		TITLE: SCANNER		PAGE:								
DEPT:		DATE:		PROJECT: 9400								
POINT	DESCRIPTION (Component)	COORDINATE			WEIGHT W	MOMENT OF INERTIA			PRODUCT OF INERTIA			
		X	Y	Z		I <sub>xx</sub>	I <sub>yy</sub>	I <sub>zz</sub>	I <sub>xy</sub>	I <sub>yz</sub>	I <sub>xz</sub>	
		IN	IN	IN	LB	IN <sup>2</sup> LB	IN <sup>2</sup> LB	IN <sup>2</sup> LB	IN <sup>2</sup> LB	IN <sup>2</sup> LB	IN <sup>2</sup> LB	IN <sup>2</sup> LB
3AE	GYRO MOUNT CABLE (V2)	3.32	-2.75	3.00	3.51	12.47	11.72	6.21	-0.01	-0.29	-1.07	0.0
		3.32	-2.75	3.00	2.65	5.42	5.42	2.77	0.0	0.0	0.0	0.0
		2.83	-2.75	3.19	0.57	1.62	1.35	2.53	0.0	0.0	0.0	0.0
		8.26	-1.63	-2.00	0.19	0.46	0.01	0.46	0.0	0.0	0.0	0.0
3AF	ELECTRONIC PWA CABLE (V2)	3.32	2.25	2.50	2.25	9.40	9.26	4.92	-0.08	-0.16	1.37	0.0
		3.20	2.25	2.50	2.06	4.62	5.41	3.94	0.0	0.0	0.0	0.0
		3.26	0.63	-2.00	0.19	0.46	0.01	0.46	0.0	0.0	0.0	0.0
3AG	YOKE (V2) LAMPEN LOCK ENCLOSURE ASSEMBLY SHROUS	1.20	-6.44	0.90	4.70	85.89	78.88	132.98	19.14	-13.09	-5.24	0.0
		5.79	0.0	0.88	1.14	12.74	2.85	12.80	0.0	0.0	0.0	0.0
		8.70	-3.00	-2.81	0.50	0.83	0.21	0.03	0.0	0.0	0.0	0.0
		1.68	-6.44	0.90	2.94	8.04	13.64	8.04	0.0	0.0	0.0	0.0
		5.10	-1.00	2.88	0.12	0.18	0.18	0.04	0.0	0.0	0.0	0.0
3AH	YOKE (V2) DRIVE ASSEMBLY SHROUS	1.20	7.80	0.90	4.24	93.50	89.69	123.09	-46.56	-0.38	0.50	0.0
		5.79	0.0	0.88	1.14	12.74	2.85	12.80	0.0	0.0	0.0	0.0
		1.92	7.80	0.90	2.98	5.65	7.94	5.65	0.0	0.0	0.0	0.0
		7.01	1.00	0.50	0.12	0.18	0.18	0.04	0.0	0.0	0.0	0.0
3AI	GYRO MOUNT	7.81	-2.56	4.06	3.32	6.78	5.31	7.04	0.0	0.0	0.0	0.0
		7.81	-2.56	4.06	2.65	5.42	2.77	5.42	0.0	0.0	0.0	0.0
		7.81	-2.56	3.69	0.67	1.35	2.53	1.02	0.0	0.0	0.0	0.0

~~SECRET/SPECIAL HANDLING~~

~~SECRET/SPECIAL HANDLING~~

Table 7.4-3 — Scanner — Component Data-3

BY: D. DUQUETTE		TITLE: SCANNER		PAGE:										
DEPT:		DATE:		PROJECT: 9400										
Point	Description (Components)	Coordinates			Weights			Moments of Inertia			Product of Inertia			
		X	Y	Z	W	I <sub>xx</sub>	I <sub>yy</sub>	I <sub>zz</sub>	I <sub>xy</sub>	I <sub>yz</sub>	I <sub>xz</sub>	I <sub>xy</sub>	I <sub>yz</sub>	I <sub>xz</sub>
		IN	IN	IN	LB	IN <sup>2</sup> -LB	IN <sup>2</sup> -LB	IN <sup>2</sup> -LB	IN <sup>2</sup> -LB	IN <sup>2</sup> -LB	IN <sup>2</sup> -LB	IN <sup>2</sup> -LB	IN <sup>2</sup> -LB	IN <sup>2</sup> -LB
3A)	Electronic Pkg.	10.11	7.31	0.05	2.58	4.99	7.37	5.88	0.0	0.0	0.0	0.0	0.0	0.0
3AK		12.82	0.00	0.00	7.03	32.59	43.65	43.65	0.0	0.0	0.0	0.0	0.0	0.0
	SMARTING	10.56	0.0	0.0	0.94	0.45	4.15	4.15	0.0	0.0	0.0	0.0	0.0	0.0
	BEARING - FWD.	9.78			1.10	0.68	0.36	0.36						
	BEARING - AFT	14.32			0.52	0.20	0.13	0.13						
	ENCLOSURE DISC	11.30			1.64	18.71	9.55	9.55						
	RETOR	12.82			2.50	12.33	6.39	6.39						
	RETAINER - FWD. BOW	9.95			0.08	0.05	0.03	0.03						
	RETAINER - DISC	11.88			0.13	0.08	0.04	0.04						
	RETAINER - MOTOR	13.80			0.07	0.04	0.02	0.02						
	RETAINER - AFT BOW	14.64			0.05	0.05	0.01	0.01						
3AL		10.20	0.00	0.00	8.95	123.18	100.36	100.36	0.23	0.0	0.0	0.0	0.0	0.0
	Pico-Housing (1/2)	12.33	0.0	0.13	1.35	26.09	15.41	15.41	0.0	0.0	0.0	0.0	0.0	0.0
	ENCLOSURE	10.40	0.0	0.0	4.36	38.27	20.59	20.59						
	SHIELD - RAIN BOW	10.01	-2.19	4.75	0.12	0.18	0.04	0.18						
	SHIELD - RAIN OUT	10.01	2.81	-4.09	0.12	0.18	0.18	0.04						
	LAUNCH LOUL	9.95	-1.00	-4.91	0.50	0.21	0.63	0.83						
	HARDNESS (1/2)	10.70	0.0	1.75	2.50	31.46	31.46	62.90	0.0	0.0	0.0	0.0	0.0	0.0
3AM		7.80	0.00	0.00	7.35	111.11	105.70	129.26	0.0	0.0	0.0	0.0	0.0	0.0
	Pico-Housing (1/2)	14.32	0	0.13	1.35	26.09	15.41	15.41	0.0	0.0	0.0	0.0	0.0	0.0
	SHIELD - RAIN	12.82	0	0	3.50	45.88	23.00	23.00	0.0	0.0	0.0	0.0	0.0	0.0
	HARDNESS (1/2)	10.70	0	1.75	2.50	31.46	31.46	62.90	0.0	0.0	0.0	0.0	0.0	0.0

~~SECRET/SPECIAL HANDLING~~

~~SECRET/SPECIAL HANDLING~~

Table 7.4-4 — Scanner — Component Data-4

BY: D. [Signature]		TITLE: SCANNER		PAGE:	
DEPT:		DATE:		PROJECT: 9400	

Point	Description	COORDINATE			Weight	Moment of Inertia			Product of Inertia		
		X	Y	Z		I <sub>xx</sub>	I <sub>yy</sub>	I <sub>zz</sub>	I <sub>xy</sub>	I <sub>yz</sub>	I <sub>xz</sub>
	(Components)	IN	IN	IN	W	I <sub>xx</sub>	I <sub>yy</sub>	I <sub>zz</sub>	I <sub>xy</sub>	I <sub>yz</sub>	I <sub>xz</sub>
					LB	IN <sup>2</sup> -LB					
SAN		11.97	-5.91	2.53	1.81	14.85	25.87	17.21	-1.79	-0.86	-5.39
	PERCENT BASE	* 12.14	-5.94	2.51	1.81	26.68	14.57	14.57	0.0	0.0	0.0

\* INERTIA VALUES ABOUT LOCAL PRINCIPAL AXES; ALL OTHER INERTIA VALUES REFERRED TO GLOBAL XYZ AXES.

Component Mass Properties — REF. F. GAULIN



~~SECRET/SPECIAL HANDLING~~

~~SECRET/SPECIAL HANDLING~~

Table 7.4-5 — Scanner—mass point coordinates and properties

TABLE 7.4-5

SCANNER— MASS POINT COORDINATES  
AND PROPERTIES

BY: DOUGLETTE		TITLE: SCANNER		PAGE:						
DEPT:		DATE: 5-4		PROJECT: 9400						
		5-9-80								
MASS POINT	COORDINATES			WEIGHT LBS	MASS MOMENTS OF INERTIA LB-IN <sup>2</sup>			MASS PRODUCTS OF INERTIA LB-IN <sup>2</sup>		
	X IN.	Y IN.	Z IN.		I <sub>XX</sub>	I <sub>YY</sub>	I <sub>ZZ</sub>	I <sub>XY</sub>	I <sub>XZ</sub>	I <sub>YZ</sub>
JAA	0.21	0.00	0.73	11.12	223.19	146.92	89.62	0.66	51.52	-9.81
JAB	1.20	-6.55	0.90	1.07	40.82	10.32	31.61	0.10	-1.62	-0.58
JAC	1.20	6.55	0.90	2.05	42.22	10.48	32.01	0.10	-1.62	-0.58
JAD	1.20	0.00	0.90	3.82	64.04	132.75	121.33	0.39	-6.43	-2.33
JAE	3.32	-2.75	3.00	3.51	12.47	11.72	6.21	-0.01	70.29	-1.07
JAF	3.32	2.25	2.50	2.25	9.59	9.26	5.12	-0.02	70.18	1.39
JAG	1.20	-6.44	0.90	4.70	85.89	78.88	132.98	49.14	-13.09	-5.24
JAH	1.20	7.80	0.90	4.24	93.50	39.69	123.09	-45.56	70.38	0.50
JAI	7.81	-2.56	4.00	3.32	6.78	5.31	7.04	0.0	0.0	0.0
JAJ	10.11	7.31	0.05	2.98	4.99	7.37	5.88	0.0	0.0	0.0
JAK	12.82	0.00	0.00	7.03	52.59	43.65	43.65	0.0	0.0	0.0
JAL	10.20	0.00	0.00	8.95	123.18	100.36	108.23	0.23	3.16	2.50
JAM	13.80	0.00	0.00	7.35	111.11	98.24	129.26	0.0	-13.47	0.0
JAN	11.97	-5.91	2.83	1.81	14.28	25.87	17.21	-1.79	-0.86	-5.39

~~SECRET/SPECIAL HANDLING~~

~~SECRET~~/SPECIAL HANDLING

Table 7.4-6 — Scanner node coordinates

BY: D. DUQUETTE		TITLE: SCANNER		PAGE:																																																															
DEPT:	DATE: 5-9			PROJECT: 9400																																																															
<table border="1" style="margin: auto; border-collapse: collapse;"> <thead> <tr> <th rowspan="3">Node Point</th> <th colspan="3">COORDINATES</th> </tr> <tr> <th>X</th> <th>Y</th> <th>Z</th> </tr> <tr> <th>IN</th> <th>IN</th> <th>IN</th> </tr> </thead> <tbody> <tr><td> </td><td> </td><td> </td><td> </td></tr> <tr><td>JBF</td><td>1.20</td><td>-2.75</td><td>0.90</td></tr> <tr><td>JBF</td><td>1.20</td><td>2.25</td><td>0.90</td></tr> <tr><td>JBG</td><td>6.75</td><td>-6.44</td><td>0.90</td></tr> <tr><td>JBH</td><td>6.75</td><td>6.44</td><td>0.90</td></tr> <tr><td>JBI</td><td>6.75</td><td>-2.86</td><td>0.90</td></tr> <tr><td>JBS</td><td>6.75</td><td>5.00</td><td>0.90</td></tr> <tr><td>JBL</td><td>9.48</td><td>0.0</td><td>0.0</td></tr> <tr><td>JBM</td><td>14.48</td><td>0.0</td><td>0.0</td></tr> <tr><td>JBR</td><td>9.72</td><td>-4.17</td><td>7.21</td></tr> <tr><td>JBS</td><td>9.72</td><td>-8.23</td><td>-1.27</td></tr> <tr><td>JBT</td><td>16.18</td><td>-5.37</td><td>2.57</td></tr> <tr><td>JBZ</td><td>6.75</td><td>0.0</td><td>0.90</td></tr> </tbody> </table>						Node Point	COORDINATES			X	Y	Z	IN	IN	IN					JBF	1.20	-2.75	0.90	JBF	1.20	2.25	0.90	JBG	6.75	-6.44	0.90	JBH	6.75	6.44	0.90	JBI	6.75	-2.86	0.90	JBS	6.75	5.00	0.90	JBL	9.48	0.0	0.0	JBM	14.48	0.0	0.0	JBR	9.72	-4.17	7.21	JBS	9.72	-8.23	-1.27	JBT	16.18	-5.37	2.57	JBZ	6.75	0.0	0.90
Node Point	COORDINATES																																																																		
	X	Y	Z																																																																
	IN	IN	IN																																																																
JBF	1.20	-2.75	0.90																																																																
JBF	1.20	2.25	0.90																																																																
JBG	6.75	-6.44	0.90																																																																
JBH	6.75	6.44	0.90																																																																
JBI	6.75	-2.86	0.90																																																																
JBS	6.75	5.00	0.90																																																																
JBL	9.48	0.0	0.0																																																																
JBM	14.48	0.0	0.0																																																																
JBR	9.72	-4.17	7.21																																																																
JBS	9.72	-8.23	-1.27																																																																
JBT	16.18	-5.37	2.57																																																																
JBZ	6.75	0.0	0.90																																																																

~~SECRET/SPECIAL HANDLING~~

Essentially, the mass and inertia acting at each point were obtained by summing the effects of the individual components. For translational degrees of freedom, the component weights were summed directly. However, for rotational degrees of freedom the component inertias were individually evaluated about the mass point and then summed. Thus, the inertia transfer was performed as follows:

$$[I'_n] = [I_n] + [d_n][m_n][d_n]$$

$$[I_n] = \begin{bmatrix} I_{xx}^c & -I_{xy}^c & -I_{xz}^c \\ -I_{yx}^c & I_{yy}^c & -I_{yz}^c \\ I_{zx}^c & -I_{zx}^c & I_{zz}^c \end{bmatrix}$$

= mass moments and mass products about component c.g.

$$[d_n] = \begin{bmatrix} 0 & z & -y \\ -z & 0 & x \\ y & -x & 0 \end{bmatrix}$$

= distances along x, y, z, from mass point to component c.g.

$$[m_n] = \begin{bmatrix} m & 0 & 0 \\ 0 & m & 0 \\ 0 & 0 & m \end{bmatrix}$$

= mass of component

$$[\tilde{d}_n] = \text{Transpose of } [d_n]$$

$$[I'_n] = \begin{bmatrix} I'_{xx} & -I'_{xy} & -I'_{xz} \\ -I'_{yx} & I'_{yy} & -I'_{yz} \\ -I'_{zx} & -I'_{zy} & I'_{zz} \end{bmatrix}$$

= mass moments and mass products about mass point coordinates

The net inertia at each masspoint was then obtained by summing the component inertias.

$$[I'] = \Sigma [I_n]$$

In some instances, it was advantageous to evaluate inertias about the principal axes (u, v, w) and then transform these values to the (x, y, z) reference system. Mass points treated in this fashion are denoted by an asterisk (\*) in Tables 7.4-2 thru 4.

This rotational transformation of inertias was evaluated by

$$[I'] = [j][I][j]$$

where

$$[j] = \begin{bmatrix} \cos_{ux} & \cos_{vx} & \cos_{wx} \\ \cos_{uy} & \cos_{vy} & \cos_{wy} \\ \cos_{uz} & \cos_{vz} & \cos_{wz} \end{bmatrix}$$

~~SECRET/SPECIAL HANDLING~~

~~SECRET~~/SPECIAL HANDLING

= direction cosine matrix of axes u, v, w with respect x, y, z

$$[I] = \begin{bmatrix} I_{uu} & -I_{uv} & -I_{uw} \\ -I_{vu} & I_{vv} & -I_{vw} \\ -I_{wu} & -I_{wv} & I_{ww} \end{bmatrix}$$

= Inertias with respect to u, v, w axes

$\tilde{[j]}$  = Transpose of  $[j]$

$[I']$  = Intertias with respect to x, y, z axes

Detail calculations for the mass point quantities are presented in Appendix 7.4-3 and summarized in Table 7.4-5. These values were forwarded to the customer to be used in their integrated analysis. These data represent mass properties associated with a dynamic model having fourteen mass points each with six degrees of freedom, or a total of eighty-four degrees of freedom.

In order to remain within matrix limitations of the 1,536 transmissibility program (Reference Appendix 7.4-1), it was necessary for Itek to reduce the total number of degrees of freedom. To accomplish this, the mass property quantities as shown in Table 7.4-5 were redistributed such that only degrees of freedom as shown in Fig. 7.4-19 would result. Fig. 7.4-19 indicates by arrows the order of steps taken by which the eighty-four degrees of freedom mass quantities were transferred to yield an equivalent thirty-nine degree of freedom system. Fig. 7.4-20 schematically shows the mass points applicable to the thirty-nine degree of freedom system. Table 7.4-7 summarizes the mass properties while the detail calculation are given in Appendix II.

#### Stiffness Properties

In order to obtain the stiffness coefficient matrix (K), elements between mass points and nodes were idealized into equivalent beam-type members. Structural characteristics of the members were individually evaluated, and then the stiffness matrix was formulated using the computer program as described in Appendix I.

The data necessary for evaluating the stiffness matrix consisted of member coordinates, direction cosines, and section properties. These data were used to form, for each structural element, stiffness matrices (6 × 6) which represented a three-dimensional stiffness between each set of mass/node points.

The coordinates (initial and final) for each structural element are given in Tables 7.4-8 and 9, along with the mass points and nodes between which they exist. In addition, a set of direction cosines associated with each element is necessary for proper orientation of the element with respect to the x, y, z reference axes.

The various types of deformations that each structural element may be subjected are considered in the formulation of the element stiffness matrix. These consist of effects due to axial, flexural, torsional, and shear deflections. Section property data for each element consists of; area, area moment/inertia about two mutually perpendicular axes, shear deformation constants, and equivalent structural polar moment of inertia. These section properties are obtained by calculation given in Appendix II and summarized in Tables 7.4-8 and 9.

Utilizing the computer program for matrix techniques as applied to structural analysis, each element stiffness matrix was evaluated and an eighty-four element square array was formulated to represent the scanner stiffness coefficient matrix (K).

~~SECRET/SPECIAL HANDLING~~

BY: <u>D. DUQUETTE</u>	TITLE:	PAGE:
DEPT:	DATE: <u>6/18</u>	PROJECT: <u>9400</u>

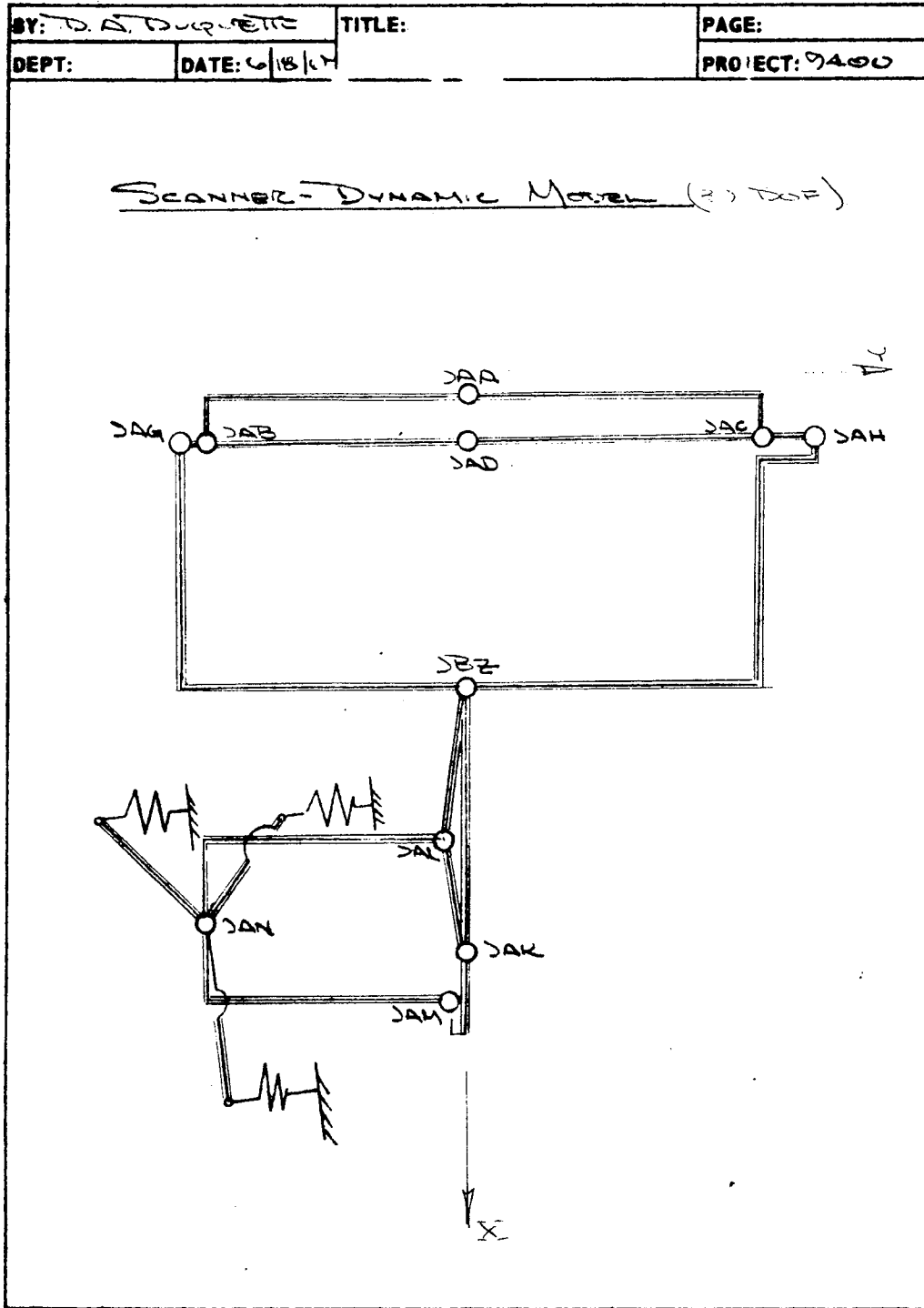
SYNTHESIS OF MASS PROPERTIES  
- 16 -

	$\Delta_x$	$\Delta_y$	$\Delta_z$	$\Theta_x$	$\Theta_y$	$\Theta_z$	STEP
JATB	0	0	0				3
JAA	0	0	0	0	0	0	1
JAG	0	0					2
JAC	0	0	0				5
JAD	0	0	0	0	0	0	6
JAH	0	0					4
JBE	0	0	0	0	0	0	8
JAK				0			7
JAL	0	0					9
JAM	0	0					10
JAN	0	0	0	0	0	0	11

○ 29 DEGREES OF FREEDOM  
→ INDICATES MASS/INERTIA TRANSFER

Fig. 7.4-19 — Synthesis of mass properties to 39 d.o.f.

~~SECRET/SPECIAL HANDLING~~



E 103 B 66 ENGINEERING ANALYSIS SHEET



Fig. 7.4-20 — Scanner—dynamic model (39 d.o.f.)

~~SECRET/SPECIAL HANDLING~~  
7.4-38

~~SECRET/SPECIAL HANDLING~~

Table 7.4-7 — Mass properties

BY: D.A. DURJETTE		TITLE: SCANNOR		PAGE:								
DEPT:		DATE: 6/18		PROJECT: 9400								
<u>Mass Properties</u>												
Mass Point	COORDINATES			Mass			MASS MOMENTS OF INERTIA			MASS PRODUCTS OF INERTIA		
	X	Y	Z	W <sub>x</sub>	W <sub>y</sub>	W <sub>z</sub>	I <sub>xx</sub>	I <sub>yy</sub>	I <sub>zz</sub>	I <sub>xy</sub>	I <sub>xz</sub>	I <sub>yz</sub>
	IN	IN	IN	LB	LB	LB	LB- <sup>2</sup>	LB- <sup>2</sup>	LB- <sup>2</sup>	LB- <sup>2</sup>	LB- <sup>2</sup>	LB- <sup>2</sup>
3AA	0.21	0.00	0.73	11.12	11.12	11.12	223.19	143.35	89.53	1.57	51.51	-9.26
3AB	1.20	-6.55	0.90	1.07	1.07	4.63	—	—	—	—	—	—
3AC	1.20	6.55	0.90	2.05	2.05	5.15	—	10.40	—	—	—	—
3AD	1.20	0.00	0.90	9.58	9.58	9.58	373.46	262.08	—	1.54	—	—
3AE	1.20	-6.44	0.90	3.50	3.50	—	—	—	—	—	—	—
3AH	1.20	7.80	0.90	3.10	3.10	—	—	13.33	—	—	—	—
3AX	12.82	0.00	0.00	—	—	—	32.59	—	—	—	—	—
3AL	10.20	0.00	0.00	8.95	14.23	—	—	—	—	—	—	—
3AM	13.80	0.00	0.00	7.35	15.83	—	—	—	—	—	—	—
3AN	11.97	-5.91	2.83	1.81	1.81	31.87	129.08	329.72	876.69	-15.70	11.17	-2.89
3BZ	6.75	0.00	0.90	15.21	8.18	8.18	231.89	94.06	—	54.36	—	—



~~SECRET/SPECIAL HANDLING~~

~~SECRET/SPECIAL HANDLING~~

Table 7.4-8 — Member coordinates and direction cosines

BY: D. DUQUETTE		TITLE: SCANNING		PAGE:									
DEPT:		DATE: 6/8		PROJECT: 9400									
Joint No	Initial	Initial Coordinates			Final Coordinates			U Direction Cosine			V Direction Cosine		
		X <sub>i</sub>	Y <sub>i</sub>	Z <sub>i</sub>	X <sub>f</sub>	Y <sub>f</sub>	Z <sub>f</sub>	u <sub>x</sub>	u <sub>y</sub>	u <sub>z</sub>	v <sub>x</sub>	v <sub>y</sub>	v <sub>z</sub>
1	JAB	0.21	-6.55	0.73	0.21	0.00	0.73	0	1.0	0			
2	JAC	0.21	6.55	0.73	0.21	0.00	0.73	0	-1.0	0			
3	JAD	1.20	0.00	0.90	1.20	-2.75	0.90	0	-1.0	0	1.6706	0	0.98595
4	JAE	1.20	0.00	0.90	1.20	2.25	0.90	0	1.0	0	1.6706	0	0.98595
5	JAF	0.204	-2.75	1.072	3.32	-2.75	3.00	0.8595	0	1.6706	0	1.0	0
6	JAG	0.204	2.25	1.206	3.32	2.25	2.50	0.8595	0	1.6706	0	1.0	0
7	JAH	1.20	-2.75	0.90	1.20	-6.55	0.90	0	-1.0	0	1.6706	0	0.98595
8	JAI	1.20	2.25	0.90	1.20	6.55	0.90	0	1.0	0	1.6706	0	0.98595
9	JAJ	1.20	-6.55	0.90	1.20	-6.44	0.90	0	1.0	0	0	0	1.0
10	JAK	1.20	6.55	0.90	1.20	7.80	0.90	0	1.0	0	0	0	1.0
11	JAL	6.75	-6.44	0.90	1.20	-6.44	0.90	-1.0	0	0	0	0	1.0
12	JAM	6.75	6.44	0.90	1.20	6.44	0.90	-1.0	0	0	0	0	1.0
13	JAN	6.75	-2.86	0.90	6.75	-6.44	0.90	0	-1.0	0	0	0	1.0
14	JAO	6.75	5.00	0.90	6.75	6.44	0.90	0	1.0	0	0	0	1.0
15	JAP	7.80	-2.86	0.90	7.80	-2.86	4.06	0	0	1.0	1.0	0	0
16	JAQ	7.80	6.44	0.90	10.11	6.44	0.90	1.0	0	0	0	0	1.0

MEMBER COORDINATES AND DIRECTION COSINES

~~SECRET/SPECIAL HANDLING~~

~~SECRET/SPECIAL HANDLING~~

Table 7.4-9 — Member coordinates and direction cosines

MEMBER COORDINATES AND DIRECTION COSINES		INITIAL COORDINATES			FINAL COORDINATES			U <sub>i</sub> DIRECTION COSINES								
MEMBER NO.	MEMBER	X <sub>i</sub>	Y <sub>i</sub>	Z <sub>i</sub>	X <sub>f</sub>	Y <sub>f</sub>	Z <sub>f</sub>	U <sub>11</sub>	U <sub>12</sub>	U <sub>13</sub>	U <sub>21</sub>	U <sub>22</sub>	U <sub>23</sub>	U <sub>31</sub>	U <sub>32</sub>	U <sub>33</sub>
17	SBE SBI	6.75	0.0	0.90	6.75	-2.86	0.90	0	-1.0	0	0	0	0	0	0	0
18	SBE SBI	6.75	0.0	0.90	6.75	5.00	0.90	0	1.0	0	0	0	0	0	0	0
19	SBL SBE	9.45	0.0	0.0	6.75	0.0	0.90	-1.0	0	0	0	0	0	0	0	0
20	SAL SBL	12.82	0.0	0.0	9.45	0.0	0.0	-1.0	0	0	0	0	0	0	0	0
21	SAL SBL	12.82	0.0	0.0	14.45	0.0	0.0	1.0	0	0	0	0	0	0	0	0
22	SAL SBL	14.45	0.0	0.0	13.80	0.0	0.0	-1.0	0	0	0	0	0	0	0	0
23	SBL SAL	9.45	0.0	0.0	10.20	0.0	0.0	1.0	0	0	0	0	0	0	0	0
24	SAL SAL	10.20	0.0	0.0	10.20	-5.91	2.83	0	0	0	0	0	0	0	0	0
25	SAL SAL	13.80	0.0	0.0	13.80	-5.91	2.83	0	0	0	0	0	0	0	0	0
26	SAL SBR	11.97	-5.91	2.83	9.72	-4.17	7.21	-43211	33323	83500	-14105	89281	42777	0	0	0
27	SAL SBR	11.97	-5.91	2.83	9.72	-8.23	-1.27	-43211	44429	78479	-14105	89281	42777	0	0	0
28	SAL SBT	11.97	-5.91	2.83	16.18	-5.37	2.57	99000	12722	66976	-14105	89281	42777	0	0	0

E 103 B 66 ENGINEERING ANALYSIS SHEET

h4

~~SECRET/SPECIAL HANDLING~~

~~SECRET/SPECIAL HANDLING~~

Since it was then necessary to reduce this matrix to a thirty-nine element square array, a matrix partitioning routine was utilized. The structural equation

$$\{F\} = (K)\{x\} \quad (1)$$

was partitioned in the form

$$\begin{matrix} F_1 & A & B & x_1 \\ F_2 & = & B^T & C & x_2 \end{matrix} \quad (2)$$

such that the forces ( $F_1$ ) were the forces at the dynamic degrees of freedom assigned to the structure and the forces ( $F_2$ ) were zero. The two resulting simultaneous equations were then solved for ( $F_1$ ),

$$\{F_1\} = [A - BC^{-1} B^T] \{x_1\} \quad (3)$$

which was in the form of  $\{F\} = [K]\{x\}$ . Therefore the reduced stiffness matrix was obtained as

$$[K'] = [A - BC^{-1} B^T] \quad (4)$$

and had an order of 39.

The model was given the capability to be used in an evaluation of the effects of bearing preload on gain by including eight additional degrees of freedom at the bearing locations. This was done by adding springs in parallel with the "base valued" existing bearing springs with care being exercised to maintain joint equilibrium. The values of these springs may be adjusted to reflect a particular set of preload conditions and the stiffness matrix modified accordingly.

The model has the capability to be forced at the pitch torquer, the roll torquer, or both simultaneously. Torques are applied to both the rotor and the stator, thus incorporating the effects of the reactive forces and its ensuing contribution to the structural transfer function. Because the system is being excited by a torque and not by a known rotor displacement, the procedure to match results to Fig. 7.1-3 involves the additional mathematical step of rationing the component response to the rotor response. This fact precludes the use of the digital plotting routines.

Figs. 7.4-21, 7.4-22, and 7.4-23 are plots of preliminary analysis on the model. The first two are responses for excitation at the pitch torque, while the third is for excitation at the roll torquer.

#### Effects of Ground Springs

It became obvious from earlier results obtained during random and shock loads work that the ground springs were extremely important to the low frequency modes of the structure. For this reason, it was decided to add the ground spring system, complete with cross coupling terms.

Limitations of the computer program precluded the simple insertion of an  $18 \times 18$  stiffness to account for the stiffness at the three pedestal feet; so an equifilent  $6 \times 6$  matrix was developed.

This was accomplished by extracting an  $18 \times 18$  flexibility matrix from the influence coefficients supplied by the customer, transforming this data to a common point (producing

~~SECRET~~/SPECIAL HANDLING

a  $6 \times 6$  matrix for that point). This matrix was transferred from the vehicle coordinate system and then inverted to obtain a stiffness matrix. The end result was a  $6 \times 6$  matrix in the scanner coordinate system that completely described and ground springs and that could be attached directly to an existing point JAN on the model.

In order to establish the validity of these derived stiffnesses, a separate analysis of the scanner treated as a resiliently supported rigid body was performed. This analysis involved the six degrees of freedom of that mass. The derived stiffness matrix was used as the [k] matrix and the [m] matrix was calculated for the point of attachment. The six frequencies and associated mode shapes were determined and were compared to derived data from the loads model. Good frequency agreement was obtained when the effects of the mass and inertia differences was accounted for. The normalized mode shapes were in excellent concord with their loads counterparts shown in Fig. 7.3-3. The rigid bodied frequencies and associated mode of response are:

1st frequency	12.8 hz	rotation about z, small motion in y
2nd frequency	15.1 hz	rotation about x, motion in z
3rd frequency	69.3 hz	motion in y
4th frequency	105.89 hz	rotation about y
5th frequency	538.2 hz	motion in z and y

These springs were then added to Model VI and the frequency spectrum was swept with inputs at both the pitch and roll torques. This preliminary run indicated an excited frequency of approximately 65 cps. This occurred as a rotation in about the z axis at the mirror. It is believed that this is primarily response of the third rigid body mode. At this time, data is not sufficient to quantitatively assess this response in terms of transmissibility nor was the computer run sufficiently detailed to indicate the level of response, if any, of the just two rigid body modes. Another note of interest was that the first resonance of the scanner hard mounted (recall 165 hz) had been decreased to approximately 90 hz. Results of further work will be presented at the formal PDR.

Future Work

A general precis of essential future dynamic analysis will be given with no attempt at flow order or schedule. The analysis listed above has been, in the main, performed on the unbalanced roll design. The loads portion reflects an earlier design while the transmissibility studies treat the most up to date unbalanced design with minor modifications. While it is generally felt that the balanced design will balance with more desirable dynamic features, the full impact to the design ventered by a shift to form unbalanced to balanced can only be appreciated and understood by a complete analysis of the balanced design. This analysis includes:

1. A loads study
  - Launch lock requirements
2. Structural dynamics study
  - a. Effects of having preload due to isothermal change
  - b. Effects of bearing preload due to temperature gradients
  - c. Mass and stiffness effects for various pointing angles
  - d. Sensitivity of response to structural damping.

~~SECRET~~/SPECIAL HANDLING

~~SECRET/SPECIAL HANDLING~~

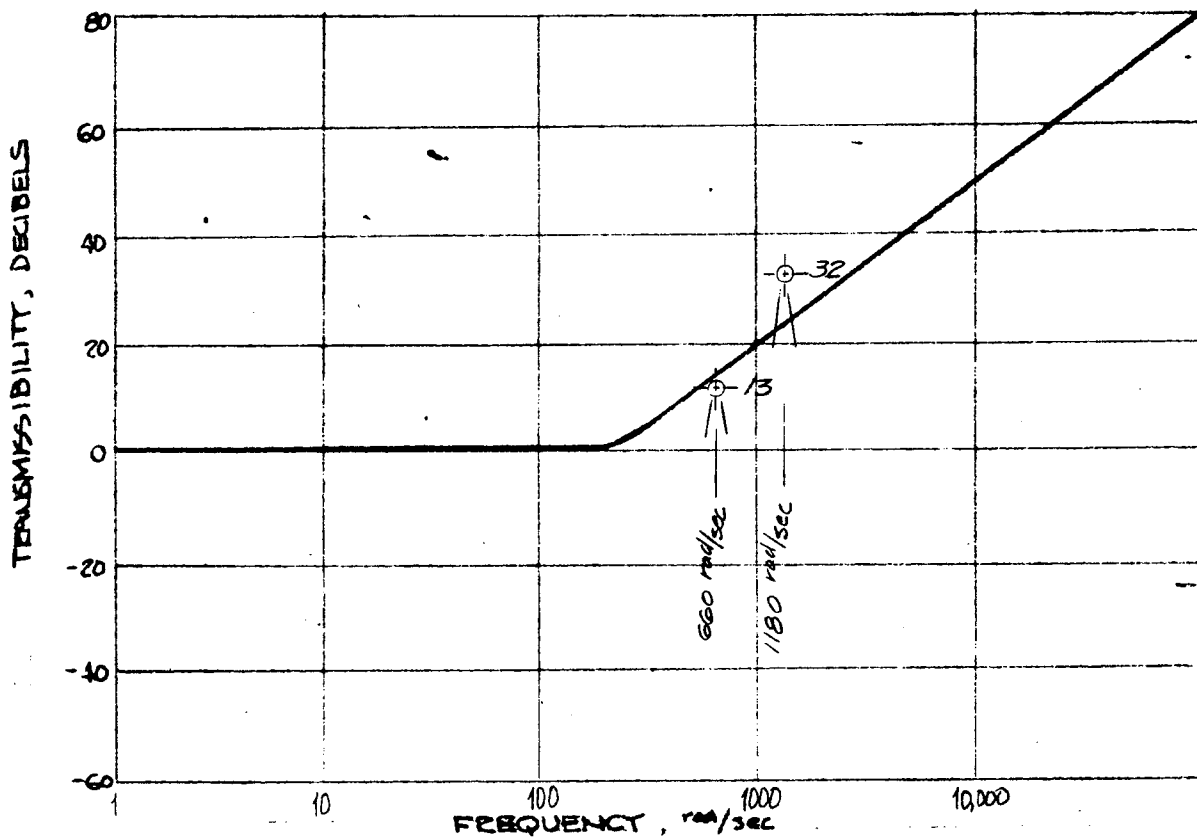


Fig. 7.4-21 — Transmissibility plot of pitch gyro mount for pitch torquer input on Model VI

~~SECRET/SPECIAL HANDLING~~

~~SECRET/SPECIAL HANDLING~~

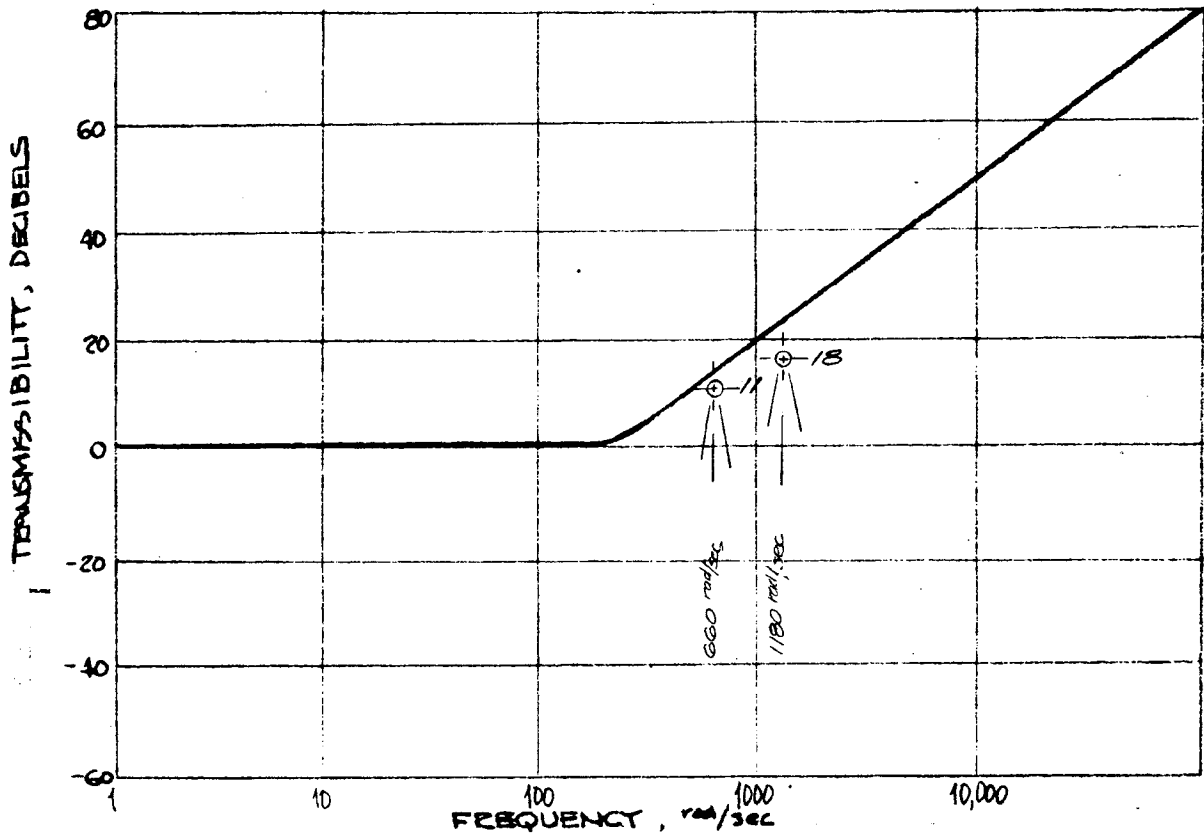


Fig. 7.4-22 — Transmissibility plot of mirror about pitch axis for pitch torquer input on Model VI

~~SECRET/SPECIAL HANDLING~~

~~SECRET/SPECIAL HANDLING~~

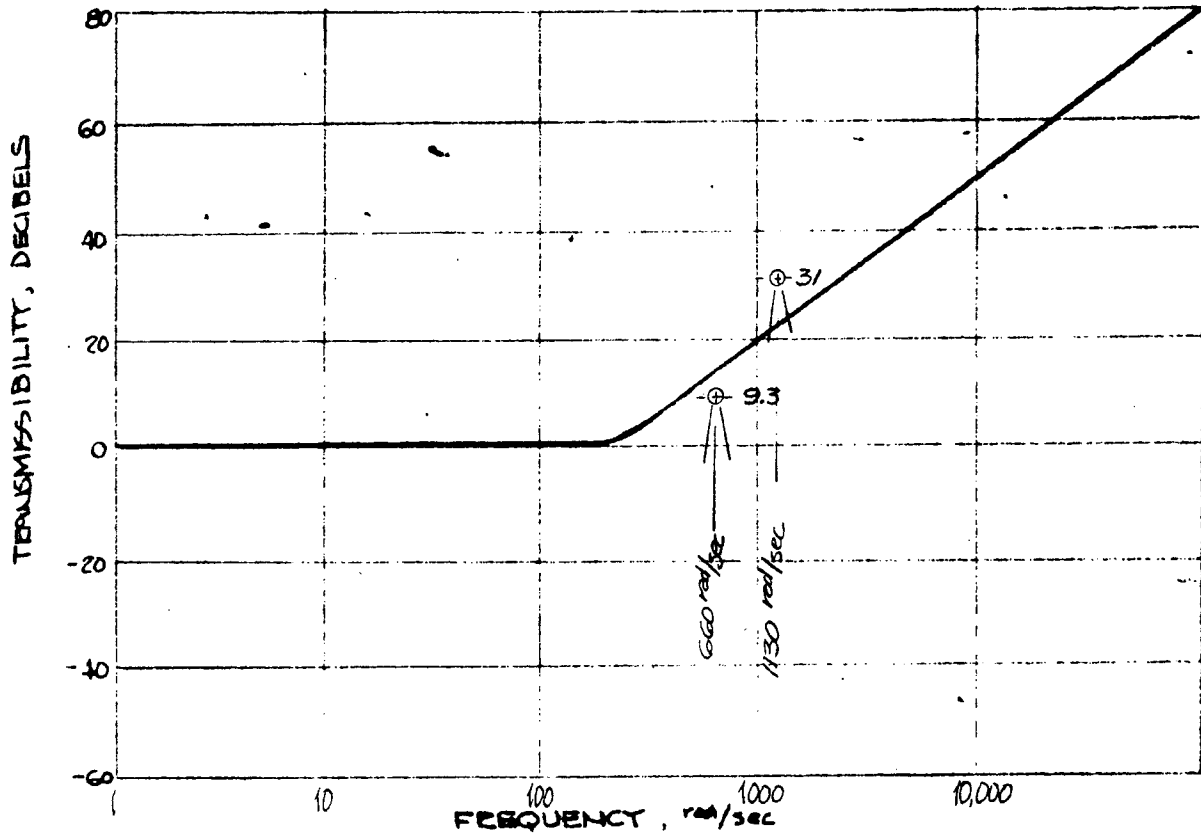


Fig. 7.4-23 — Transmissibility plot of roll gyro mount for roll torquer input on Model VI

~~SECRET/SPECIAL HANDLING~~

~~SECRET~~/SPECIAL HANDLING

## 8. THERMAL CONSIDERATIONS

### 8.1 THERMAL DESIGN CRITERIA

The successful design of a thermal control system depends upon its ability to maintain certain critical components within prescribed temperature limits. These limitations are determined by the various performance criteria, environmental effects, and by design considerations. These limitations are essentially thermal, optical, and mechanical in nature.

#### 8.1.1 Thermal Limitations

Customer-furnished gyros and gyro amplifiers are furnished for and mounted to the roll and pitch axes. In order to prevent excessive power drain or overheating, the roll and pitch axes must be maintained between 0 and 100 °F.

#### 8.1.2 Optical Effects

Since we are dealing with a diffraction limited system, the total wave front deformation of the light bundle leaving the eye piece must be within  $\lambda/4$  wave. This in turn means that the deflection of the scan mirror must be limited to considerably less than this, and accordingly the scan mirror design becomes quite critical.

There are two major causes of mirror thermal deflections. These are due to changes in temperature level, and to axial gradients within the mirror itself.

#### Temperature Level Changes

When an unrestrained flat mirror is subjected to a uniform temperature change, there is no change in its surface contour. However, when this mirror is potted into a bezel, a uniform temperature change causes a mechanical interaction between the bezel, mirror, and potting compound. This is due to their gross differences in modulus and expansion coefficients.

This effect has been eliminated in the design of the bezel which is covered in Section 4.5. The design range used is 0 to 100 °F which is the design range for the gyros and gyro amplifiers.

#### Gradient Effects

When an unrestrained flat mirror is subjected to an axial gradient it deforms into a shallow sphere. This introduces astigmatism into the system which causes a loss of resolution. The nominal bending permitted is 0.020 wave.

Since the potting compound offers very little resistance to such bending the only way it can be reduced is by either selecting a mirror with a low expansion coefficient or by limiting the absorbed heat flux on the mirror. Since the latter solution involves substantial configuration

~~SECRET~~/SPECIAL HANDLING

~~SECRET~~/SPECIAL HANDLING

changes it was not implemented. Bending caused by axial gradient is limited by the choice of mirror material. Cer-Vit was chosen, which has an expansion coefficient of  $0.083 \times 10^{-6} \text{ } ^\circ\text{F}$ .

The details of this analysis indicating the effects of the heat flux upon the mirror is shown in Section 8.4.1. Total surface deflections are discussed in Section 4.5.D.3.

### 8.1.3 Mechanical Limitations

In addition to the above mentioned optical effects, the thermal environment can cause changes in scanner dimensions, which in turn would affect the bearing loads and, hence the PSD. This class of problems is summarized below.

#### Bearing Gradients

Analysis indicate that bearing gradients do not constitute a major problem. Temperature differences of  $10^\circ\text{F}$  between the inner and outer race are not considered serious.

#### Scanner Level Changes

Changes in the scanner temperature level will result in a change of load on the bearings. This is mitigated somewhat by the fact that the scanner and the bearings have very nearly the same expansion coefficients. A maximum level change of  $70^\circ\text{F}$  can be tolerated before an increase in PSD becomes serious.

#### Structural Temperature Differences

Structural temperature differences could cause changes in the bearing PSD. For instance, if the yoke is at a temperature significantly different than the bezel, the pitch axis bearings preload will be changed. Also, temperature differences between the roll shaft and roll housing will cause changes in the roll axis preload. This effect is reduced by designing flexures fitting at the end of the roll and pitch axes to take up these loads. Presently they are being designed to accommodate temperature differences of  $20^\circ\text{F}$ .

~~SECRET~~/SPECIAL HANDLING

~~SECRET/SPECIAL HANDLING~~

## 8.2 DESIGN CONCEPT

There are essentially two methods whereby the temperature of a satellite can be controlled. A description of each and their advantages and disadvantages is presented below.

### 8.2.1 Active

This method uses thermostatically controlled heaters to maintain temperature. This could be handled by either bonding heaters to the inside of the shroud or directly to the scanner. The exterior of the shroud would be painted with a mosaic having a low  $\alpha/\epsilon$  ratio. This would ensure a heat sink for the heaters. Insulating blankets are fastened between the heaters and the heat sink to minimize power consumption.

The advantage of such a system is that it provides close control over the temperature level as well as gradients. Temperature control of less than  $1^\circ\text{F}$  is possible. In addition to close control of the temperature level, it is not sensitive to degradation of the paint mosaic. Its major disadvantages are an increase in weight due to the blankets, thermostats, and batteries. Furthermore, this type of system could not control the temperature of the scanner during actual use without a prohibitive expenditure of power.

### 8.2.2 Passive

This method controls the temperature by judicious trade-off of a variety of physical parameters. The exterior of the shroud is painted with a mosaic having a solar absorbtivity and infrared emmissivity that provides a particular average temperature range. The scanner would then be thermally linked to the shroud.

The advantage of such a system is that it is lighter than an active system. It can be used to maintain gradients below specified values.

Its disadvantages are that it cannot provide close control over temperature level ( $\pm 400^\circ\text{F}$  is typical), it is subject to degradation in space, and its design is generally more difficult than an active system.

Also, as in the active system, it provides no control during the active portion of the mission.

### 8.2.3 Description of Control System

Since there is no requirement for precise control of the temperature level, a passive system was selected. The major factors in design of this control system are described below.

#### 8.2.3.1 Environment

The environment to which the scanner is subjected includes:

- Solar
- Albedo
- Earthshine
- Radiator heating
- Space
- Plume heating
- Molecular heating

~~SECRET/SPECIAL HANDLING~~

~~SECRET~~/SPECIAL HANDLING

All the above affect the scanner to some degree. Control is achieved by isolating the scanner from those environmental loads which subject it to the greatest variations in temperature, and linking it to those which undergo the smallest variation.

8.2.3.2 Shroud

The most important component in the control system is the shroud. The shroud, shown schematically in Fig. 8.2-1 is insulated on all surfaces, except that surface parallel to the earth. This is done to insulate the scanner from those sources having the greatest energy variation and linking it to the earth which undergoes the smallest variation.

Paint Mosaic

The shroud exterior is painted with a mosaic which will yield acceptably low temperature. The three materials selected are as follows:

White Thermatrol Paint	(Dow Corning 92-007)
Black Kemacryl Paint	(Sherwin Williams M49BC12)
Pressure Sensitive Aluminum Tape	(Mystik 7402)

All of the above have been successfully used on other space programs.

Those surfaces subjected to plume heating will be painted all white. The other insulated surface will be painted with Thermatrol and striped with the aluminum tape. The lower surface, which is the control surface, will be painted all white. However, it may also be striped with black paint if subsequent analysis indicates it is so necessary.

Insulating Blanket

The interior of the shroud, except for the control surface, will be insulated with a multilayer insulation blanket. Present plans call for 30 layers of aluminized Kapton, each separated by a layer of Tissuglass. The blanket will be sewn together with nylon thread and fastened to the shroud by Velcro fasteners.

The radiator will also contain a blanket which thermally isolates the scanner from it. This blanket is the responsibility of either the vehicle contractor or the AO contractor.

All internal surfaces of the shroud and blanket will be painted black.

~~SECRET~~/SPECIAL HANDLING

~~SECRET~~/SPECIAL HANDLING

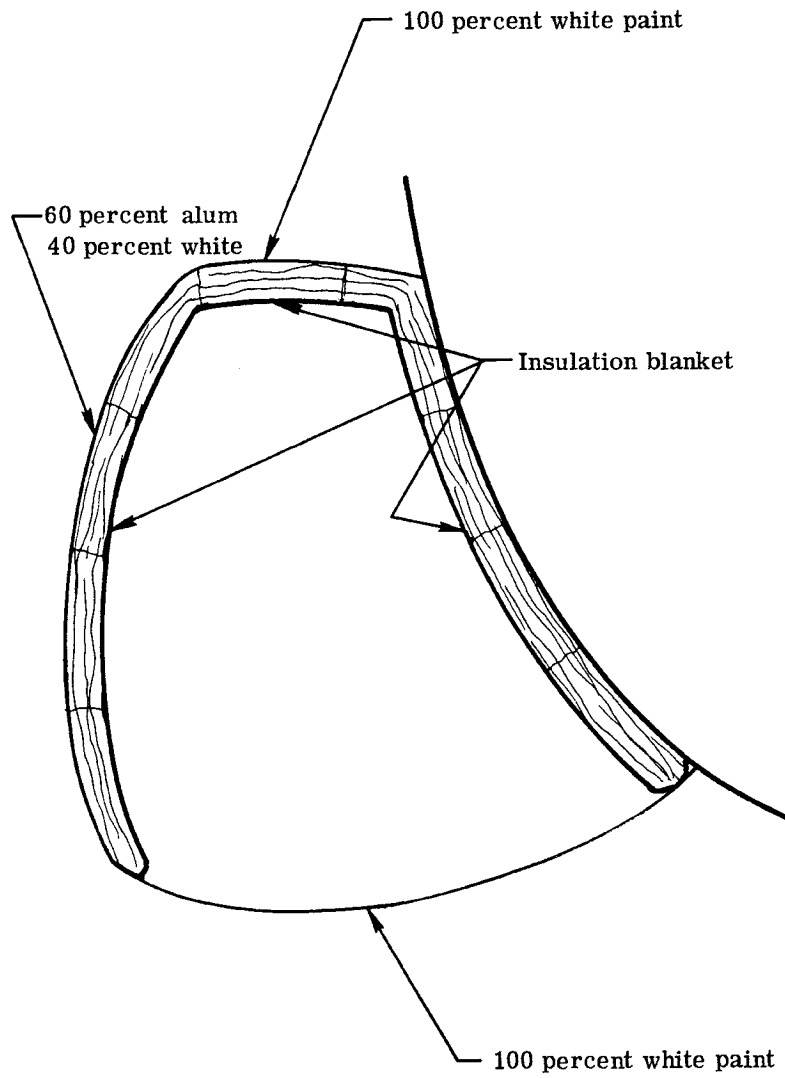


Fig. 8.2-1 — Shroud schematic

~~SECRET~~/SPECIAL HANDLING  
8.2-3

~~SECRET~~/SPECIAL HANDLING

8.3 ANALYSIS

For an object to be in thermal equilibrium, the heat stored in the object must equal the net heat transferred in to and out of the object. The following equation describes this equilibrium condition:

$$Q_{\text{stored}} = Q_{\text{radiation}} + Q_{\text{conduction}} + Q_{\text{convection}} \\ + Q_{\text{external flux}} + Q_{\text{internal power}}$$

where,

$Q_{\text{stored}}$	= the amount of heat stored in the object
$Q_{\text{radiation}}$	= the net heat transferred by radiation between the object and all other objects within its field of view
$Q_{\text{conduction}}$	= the net heat transferred by conduction between the object and all other objects to which it is mechanically connected
$Q_{\text{convection}}$	= the net heat transferred by convection between the object and other objects by the surrounding gases
$Q_{\text{internal power}}$	= the heat generated within the object due to Joule heating
$Q_{\text{external flux}}$	= the net heating from the surrounding environment. For spacecraft, the heat sources are generally solar, albedo, earthshine fluxes and, for near-earth orbits, molecular heating.

8.3.1 Method of Solution

The exact solution to the above thermal energy equation involves the solution of nonlinear, integral differential equations for which a closed form solution is virtually impossible. By replacing the real continuous system with a series of discrete isothermal elements, considerable mathematical simplification results. The coupling of these elements follows from the basic heat transfer/electrical analogy. This analogy can be shown for the simple case of heat flow through a thermal resistance, being analogous to the flow of direct current through an electrical resistance.

$$q = \frac{\Delta T}{R} \qquad i = \frac{\Delta E}{R_c} \qquad (8.3-1)$$

Some current theory can be applied to general heat transfer problems. One of these concepts, the idea of nodes, is well suited for thermal problems. By letting a thermal mass, which is nearly isothermal, be considered a node, and by assuming discontinuous temperature variation from node to node, the general heat balance equation can be rewritten for a node, as follows:

$$(mC_p)_i \frac{dT_i}{d\theta} = \sum \sigma A_i \tau (T_j^4 - T_i^4) + \sum \frac{T_j - T_i}{R_{ij}} + A_i q_{Ei} + Q(\theta) \qquad (8.3-2)$$

~~SECRET/SPECIAL HANDLING~~

This mathematical representation of the Equation 8.3-1 is the nodal heat balance encompassing the various modes of heat transfer and energy storage previously described. It is obvious that the temperature of each node is dependent upon the temperature of the other nodes in the system; thus, a temperature history for a particular node can be obtained only from the solution of n simultaneous equations. The solution, though long and complex, is readily applicable to computer solution by finite difference methods. Thus, the constituents of the equation can be input to the computer, and the final solution yields temperature histories for all the nodes of the thermal model.

8.3.2 Mathematical Model

To obtain accurate answers from solution of the above set of equations, care must be taken to ensure that the assumption of isothermality of the individual nodes is not violated.

8.3.2.1 Heat Stored

The heat stored term of equation is:

$$(mC_p) \frac{dT}{dt} \quad (8.3-3)$$

Thetum  $(mC_p)$  represents the thermal capacity of the node, and is determined by summing the products of mass and specific heat over all the various components constituting the node.

8.3.2.2 Radiation Conductances

The radiation conductance between nodal pairs in Equation 8.3-3 is a function of the surface radiation properties (emissivity and absorptivity), surface area of the nodes, and the geometric form factors between them. From the assumption of diffuse radiation (equal distribution of radiant flux density to all directions in space) and Lambert's cosine law, the basic equation for the geometric view factor can be determined as

$$F_{ij} + \frac{1}{A_i} \int_{A_i} \int_{A_j} \frac{\cos \phi_i \cos \phi_j dA_i dA_j}{\pi r_{ij}^2} \quad (8.3-4)$$

The integration of Equation 8.3-4 is difficult, except for very simple configurations. For certain specific geometries, integrated values for  $F_{ij}$  are available in the literature; computer codes which are available are used for more complex configurations.

From the area of each node, its emissivity, and the geometric view factors between various nodes, the reflecting view factor (or script F,  $\tau_{ij}$ ) can be determined. This reflecting view factor takes into account the multiple reflections of radiant energy which can take place within the system. For example, if only one source and one sink are present in an enclosure, it can be shown that

$$\tau_{ij} = \frac{1}{\frac{1}{F_{ij}} + \left(\frac{1}{\epsilon_i} - 1\right) + \frac{A_i}{A_j} \left(\frac{1}{\epsilon_j} - 1\right)} \quad (8.3-5)$$

Analytical determination of  $\tau_{ij}$  is extremely difficult for most configurations, and it is usually obtained from available computer code solutions.

~~SECRET/SPECIAL HANDLING~~

In most heat transfer systems, radiating surfaces are assumed to be completely diffuse. This assumption while good for black surfaces, may introduce significant error in analysis of highly specular surfaces. Since systems have components with highly specular surfaces, specularity must be considered if a high degree of accuracy is to be achieved in related thermal analyses. Computer codes have been used to handle such problems.

#### 8.3.2.3 Conduction Resistances

The conduction resistances,  $R_{ij}$ , are based on the electrical resistance analogy. The thermal conduction path between nodes can be characterized by a network of resistors such that each resistor represents a particular part of the overall resistance to thermal conduction. The solution of the electrical network provides the total resistance or conductance.

The electrical analogy allows the evaluation of the structural thermal resistance from point  $i$  to point  $j$  using the following basic equation:

$$R_{ij} = \frac{\Delta X_i}{k_i A_i} + R_{c_{ij}} + \frac{\Delta X_j}{k_j A_j}$$

where  $R_{ij}$  = Total resistance between  $i$  and  $j$   
 $k$  = Conduction Length  
 $A$  = Cross-sectional area  
 $R_c$  = Contact resistance (where applicable)

The most difficult component to evaluate in the determination of the individual resistances is the resistance between physically adjacent parts of the system. Mechanical attachment produces a "contact resistance" to conductive heat transfer. Determination of appropriate values of the contact resistance requires the appraisal of contact pressure, surface finish, and amount of contact area; from these quantities, the contact resistances can be estimated.

#### 8.3.3.4 Convection Resistances

The convection resistances,  $R_{ij}$ , are also based on the electrical analogy and are again characterized by a network of resistances. The convective resistance is

$$R_{ij} = \frac{1}{hA} \quad \begin{array}{l} A = \text{area} \\ h = \text{heat transfer coefficient} \end{array}$$

Although conduction is the primary mode of heat transfer in aircraft, there is no convection in space because of the lack of atmosphere. Only during the prelaunch or ground cooling phases is convection normally significant.

#### 8.3.3 Boundary Conditions

The boundary conditions of the spacecraft are used in conjunction with the thermal model composed of nodes and thermal resistances. These boundary conditions consist of the environmental heat fluxes plus the temperatures of the surrounding vehicle. The radiant heat fluxes incident on the surface of the optical system are divided into three classes: direct isolation, earshine, and albedo. Direct isolation is the radiant energy which comes directly from the sun and strikes the system. The second component of the incident heat flux, the earth shine is the energy radiated

~~SECRET/SPECIAL HANDLING~~

~~SECRET/SPECIAL HANDLING~~

from the earth by virtue of its having a finite temperature greater than zero. The third component of the heat flux striking the system is the albedo. This is the solar energy which is reflected by the earth.

8.3.3.1 Description of Nominal Conditions

The nominal conditions considered in this analysis are as follows:

Solar max = 440 Btu/hr-ft<sup>2</sup>  
Albedo max = 38%  
Earthshine max = 68 Btu/hr-ft<sup>2</sup>  
Duty Cycle = 10 minutes/orbit for 10 consecutive orbits

The orbital parameters are used for an 80 nautical mile perigee, 180 nautical mile apogee orbit. The flight path is assumed to be North-South orbit with perigee at 55° north latitude. The vehicle radiator temperature used is that corresponding to an 80/180 noon orbit, the pressure wall is assumed to be at 70 °F, and the molecular heating rates used are defined in EC-331B.

8.3.3.2 Off Design Consideration

The condition for the off design orbits are as follows for a cold and a hot orbit.

	<u>Hot</u>	<u>Cold</u>
Solar	460 Btu/hr-ft <sup>2</sup>	425 Btu/hr-ft <sup>2</sup>
Albedo	44%	32%
Earthshine	74.7 Btu/hr-ft <sup>2</sup>	61.3 Btu/hr-ft <sup>2</sup>
Pressure wall	80°F	60°F
Orbit	75/125	200 circular
Duty Cycle	12 min/orbit for 10 orbits	5 minutes/orbit for 10 orbits.

The other operational parameters are the same as in Para. 8.3.2.1.

~~SECRET/SPECIAL HANDLING~~

#### 8.4 RESULTS OF THERMAL ANALYSIS

A detailed thermal analysis of the scanner and bezel was completed using the nominal boundary conditions described in paragraph 8.3.3.1. The results are described below.

##### 8.4.1 Scanner Mirror

A thermal model of the configuration was constructed per Itek Drawing no. 906001. This is shown in Fig. 8.4-1. As shown, the bezel was represented by four nodes, and the scan mirror by two nodes. The RTV potting compound was represented by a single node. Local heat sources on the rear cover of the bezel are the gyro amplifier and the gyro. These were simulated by one and two nodes, respectively. Table 8.4-1 summarizes the thermal properties of the materials used.

To simplify calculations, the elliptical scan mirror was circularized by the following equation:

$$d^1 = \sqrt{D_{MAJ} \times D_{MIN}}$$

where  $D_{MAJ}$  = major diameter of mirror  
 $D_{MIN}$  = minor diameter of mirror

The equivalent circular diameter is 12.25 inches.

Radiation constants and conduction resistors were computed between all adjacent nodes. The bezel dishes were linked by both radiation and conduction.

Heat sources of 5.5 watts and 50 watts were applied to the gyro amplifier and gyro, respectively. To simulate warm-up of these, each was "turned on" 15 minutes prior to start of telescope operation. Upon attaining a temperature of 160°F, the gyro temperature remained constant. After the 15-minute warm-up, the shroud is opened and both the inner shroud and scanner interact radiatively with albedo, earthshine, and space. Following a 10-minute observation period, the power is turned off and the shroud is closed, remaining closed for the remaining 65 minutes of the orbit. This was repeated for 10 orbits. This was then followed by six inactive orbits. The history of the shroud is shown in Fig. 8.4-2.

##### 8.4.1.1 Models Studied

Two thermal models were analyzed in this study. The first had a high emissivity coating (0.9) on both the rear surface of the mirror and the opposite surface of the inner bezel dish. The second model had a low emissivity coating (0.1) on both these surfaces.

Selection of these coatings will permit a comparison between them of temperature and gradients. The data can then be used to evaluate both optical and structural performance of the mirror. It is thus reasonable to select the proper coating which will minimize optical and structural degradation induced by heat transfer to and within the mirror.

Both models were run while simulating a nominal mission day. This consists of ten 10-minute operational orbits followed by six inactive orbits.

##### 8.4.1.2 Temperature Histories

The resulting temperature histories for each case are shown in Figs. 8.4-3 and 8.4-4. Included in these figures are temperature data for nodes 1 and 7 on the bezel, and nodes 3 and 4 on the scan mirror. The temperatures of nodes 1 and 7 exhibit a "sawtooth" pattern, the period

~~SECRET/SPECIAL HANDLING~~

~~SECRET/SPECIAL HANDLING~~

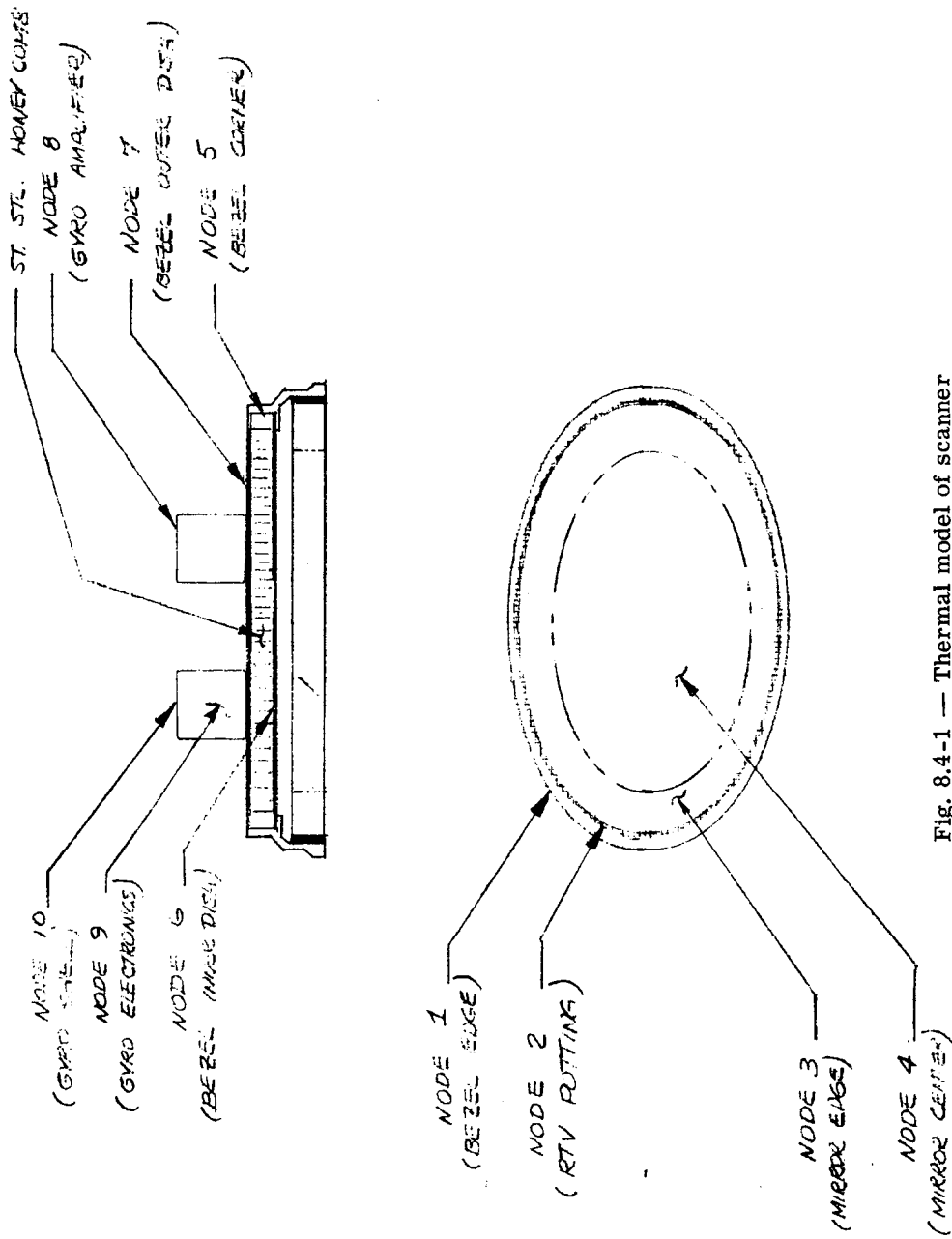


Fig. 8.4-1 — Thermal model of scanner

~~SECRET/SPECIAL HANDLING~~

~~SECRET~~/SPECIAL HANDLING

Table 8.4-1 Thermal Properties of Materials

<u>Material</u>	<u>(#/in<sup>3</sup>)</u>	<u>C<sub>p</sub>(BTU/#°F)</u>	<u>K(BTU/hi ft° F)</u>	<u>ε</u>
Beryllium	0.066	0.44	105	0.9*
S.S Honeycomb	0.0052	0.14	8	—
Cer-Vit	0.09	0.217	0.968	0.06*
RTV	0.049	0.36	0.18	0.9

\*Emissivity of 0.9 and 0.1 used in cases 1 and 2, respectfully

~~SECRET~~/SPECIAL HANDLING

~~SECRET/SPECIAL HANDLING~~

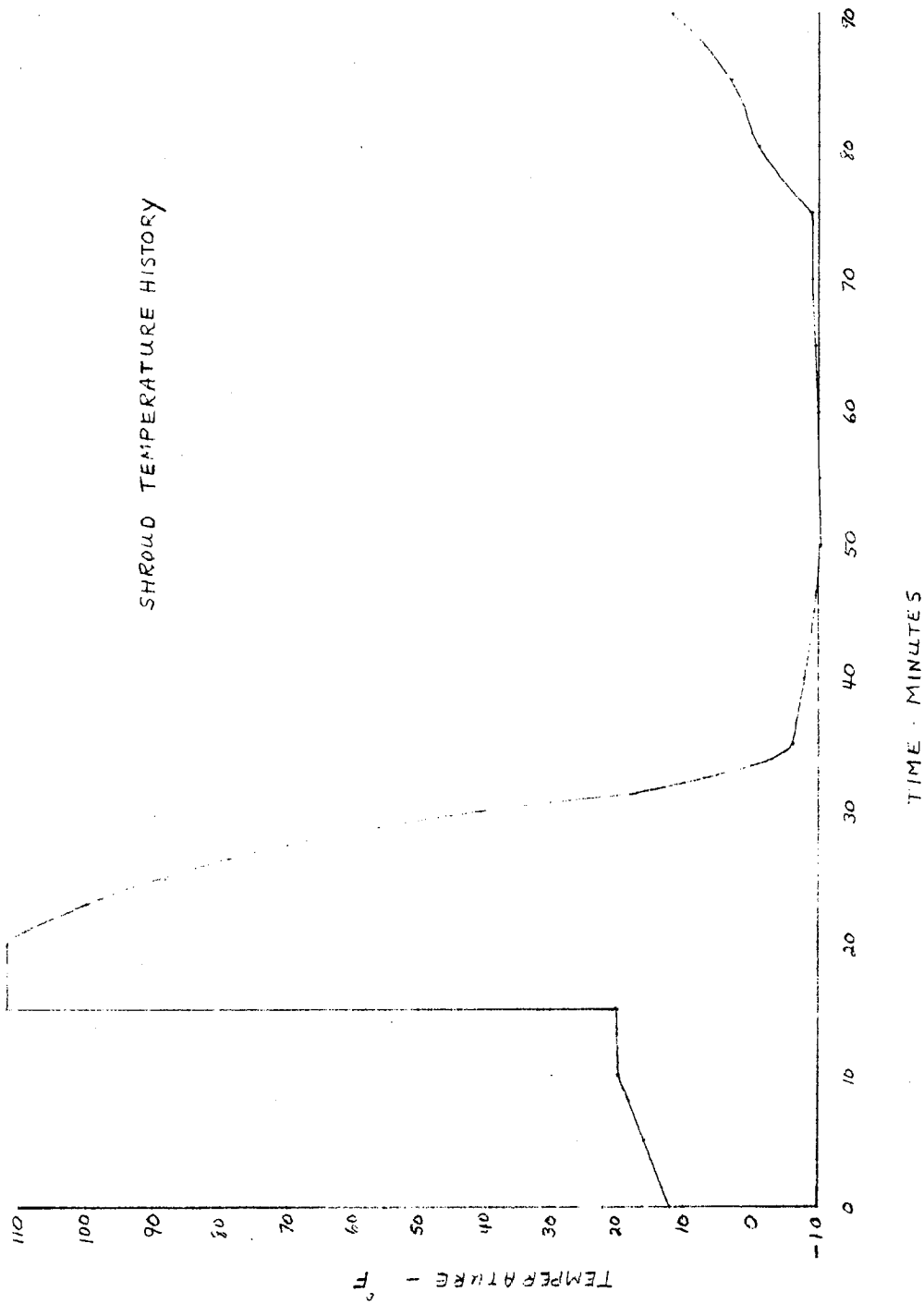


Fig. 8.4-2 — Shroud temperature history

~~SECRET/SPECIAL HANDLING~~  
8.4-4

~~SECRET/SPECIAL HANDLING~~

NEW SCAN/BEZEL CONFIGURATION

BEZEL TYPE: DOUBLE DISH  
ORBIT: 80/180 NOON  
OPERATION: 10 MIN/ORBIT  
MIRROR BACK: HIGH  $\epsilon$  (0.9)

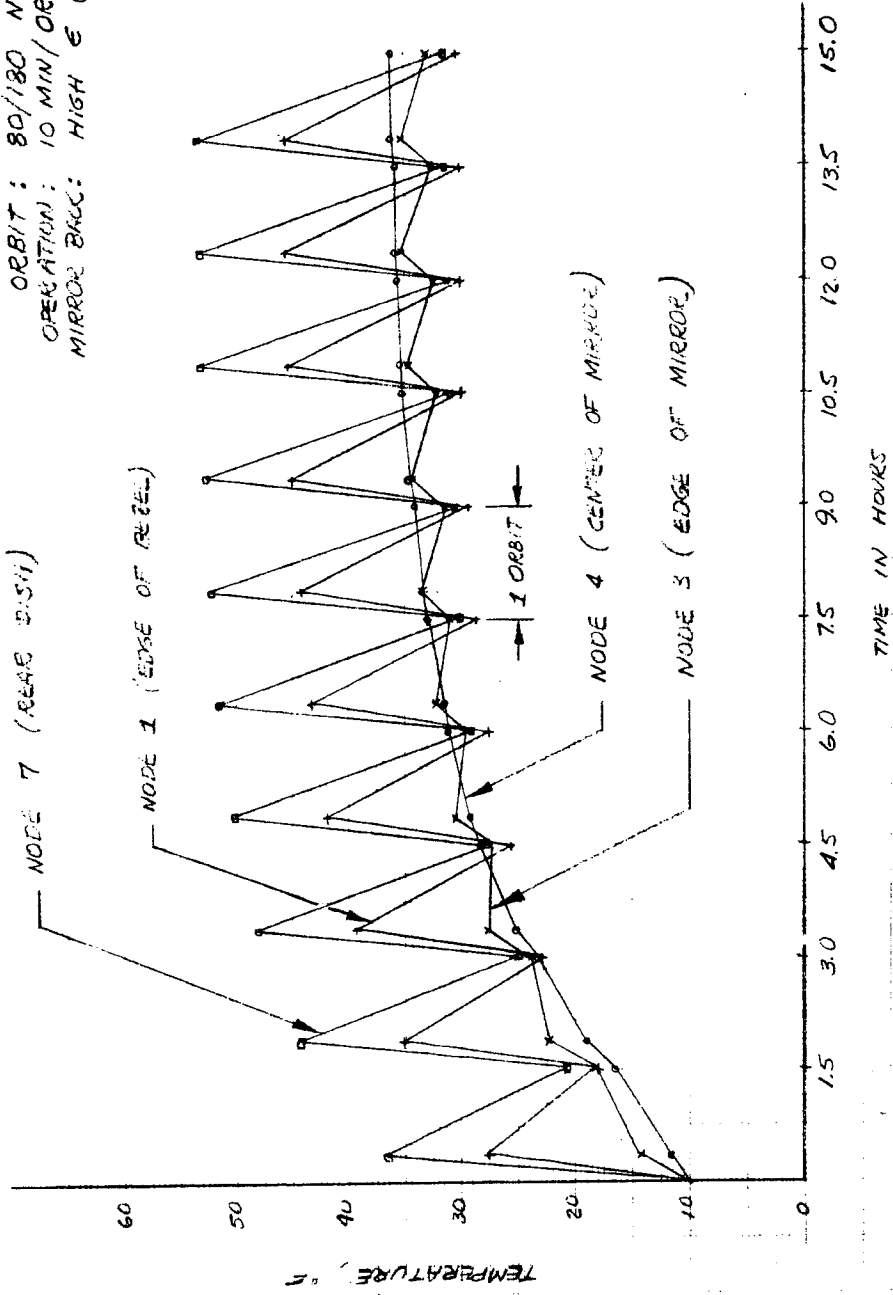


Fig. 8.4-3 — Temperature history for new scan/bezel configuration, high emissivity

~~SECRET/SPECIAL HANDLING~~  
8.4-5

~~SECRET/SPECIAL HANDLING~~

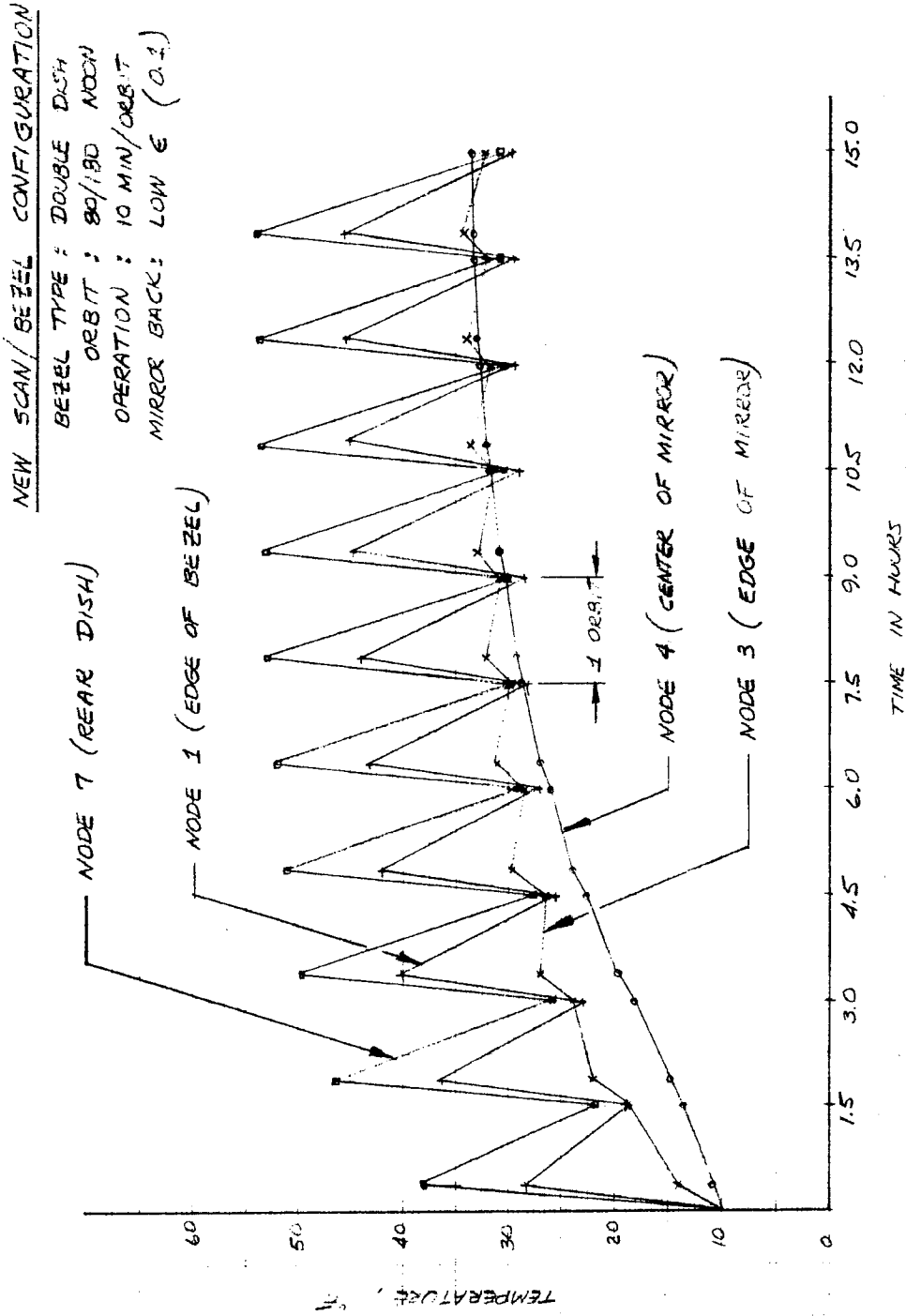


Fig. 8.4-4 — Temperature history for new scan/bezel configuration, low emissivity

~~SECRET/SPECIAL HANDLING~~

## ~~SECRET~~/SPECIAL HANDLING

period of each being 1.5 hours. These represent the temperatures attained by each during the course of each orbit. Upon the start of the gyro and gyro amplifier at the beginning of each orbit, these temperatures rise rapidly. They are further increased by albedo, earthshine, and shroud heating which occurs during the 10-minute observation period. The maximum temperatures during each orbit occur at the end of the observation period, at which time the shroud is closed and the bezel begins to cool rapidly. The temperature does not return to its initial value at the end of each orbit but does return at the end of a 24-hour day.

The "sawtooth" effect is less pronounced in node 3 of the mirror, and barely ascertainable in node 4. This is indicative of the high thermal mass of these nodes. Node 3 is thermally coupled to the edge of the mirror and the bezel through the potting, and undergoes greater variations.

The effect of varying the emissivity of the rear of the mirror and bezel dish is observed in Figs. 8.4-3 and 8.4-4. For the low emissivity coating ( $\epsilon = 0.1$ ), the radiation exchange between the bezel and mirror is reduced considerably. Conduction through the RTV potting then becomes the primary mode of heat transfer. Using the high emissivity coating ( $\epsilon = 0.9$ ) increases the radiant exchange between the mirror and the bezel, thus increasing the temperature of the mirror.

### 8.4.1.3 Optical Histories

The temperatures and heat rates from this analysis were incorporated as boundary conditions in evaluating optical performance of the mirror. In this analysis the mirror was represented as a 10.1-inch-diameter surface, corresponding to the diameter of the light bundle measured normal to the optical centerline at the scanner. From Fig. 8.4-1 it is seen that the mirror is not held on its edges, but is potted with RTV about its entire perimeter. Thus, as a first approximation, the mirror may be considered to behave as an unrestrained plate, and may be analyzed as such. A review of the heat rates in the mirror indicated that the axial heat flux dominates. Therefore, the heat rates on each face of the mirror were applied as boundary conditions to determine the axial temperature, gradients, and resulting edge sag of the mirror.

Figs. 8.4-5 and 8.4-6 are sag histories for each case studied, taken over a 5-orbit period. A positive sag indicates a concave mirror when viewed from its front surface; a negative sag indicating a convex mirror as seen from its front surface. These figures indicate the influence of the high and low emissivity coating on the rear surface of the mirror and inner bezel dish for the 5 minutes into the operation period when the positive flux from earthshine and albedo reduce the net heat load into the mirror, thereby reducing edge sag. Following operation, the thermal shroud closes, and the cold shroud and warm bezel interact with the mirror to cause a maximum heat load and maximum edge sag in the mirror. During the remainder of the orbit, the bezel and shroud cool to temperatures below that of the mirror, reducing both the net heat load and the sag on the mirror. An axial gradient of  $0.4^\circ\text{F}$  exists during maximum heating.

Fig. 8.4-6 reveals a significantly different edge sag history for the mirror. For this low emissivity (0.1) case, the bezel is warmer than the mirror. Due to the low emissivity, however, little radiation interchange occurs between these. The result is near total dependence of mirror sag upon the heat flux on its front surface. This is evidenced by the plot of edge sag versus time. Upon opening the shroud, the net positive heat flux induces an opposite sag, which reverses again following the observation period. A maximum axial gradient of  $0.26^\circ\text{F}$  occurs during the operation period.

From Figs. 8.4-5 and 8.4-6 it is seen that the maximum edge sag for the high and low emissivities were  $+0.02$  waves and  $-0.013$  waves, respectively. A review of detailed temperature

~~SECRET~~/SPECIAL HANDLING

~~SECRET/SPECIAL HANDLING~~

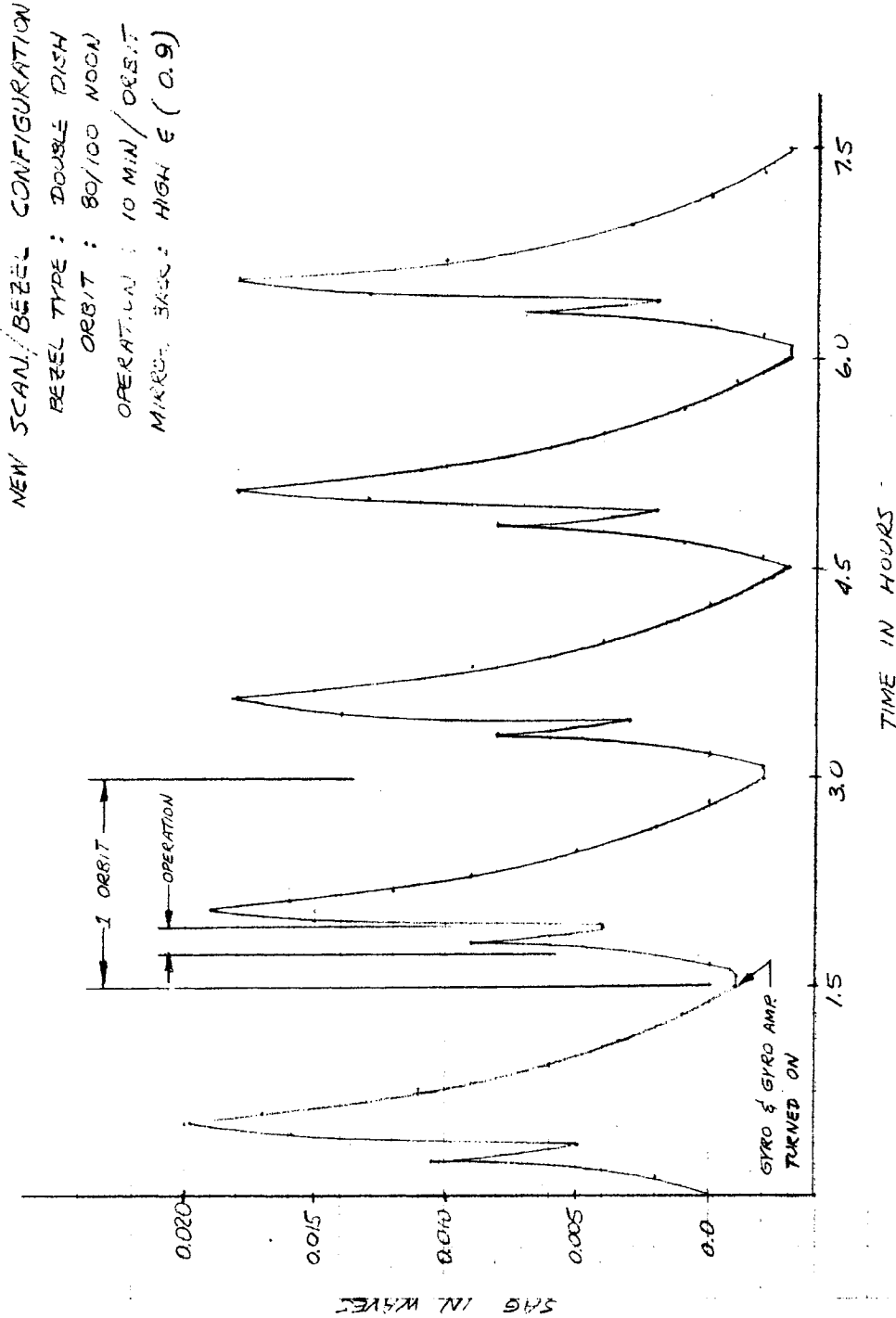


Fig. 8.4-5 — Sag history for new scan/bezel configuration, high emissivity

~~SECRET/SPECIAL HANDLING~~

~~SECRET/SPECIAL HANDLING~~

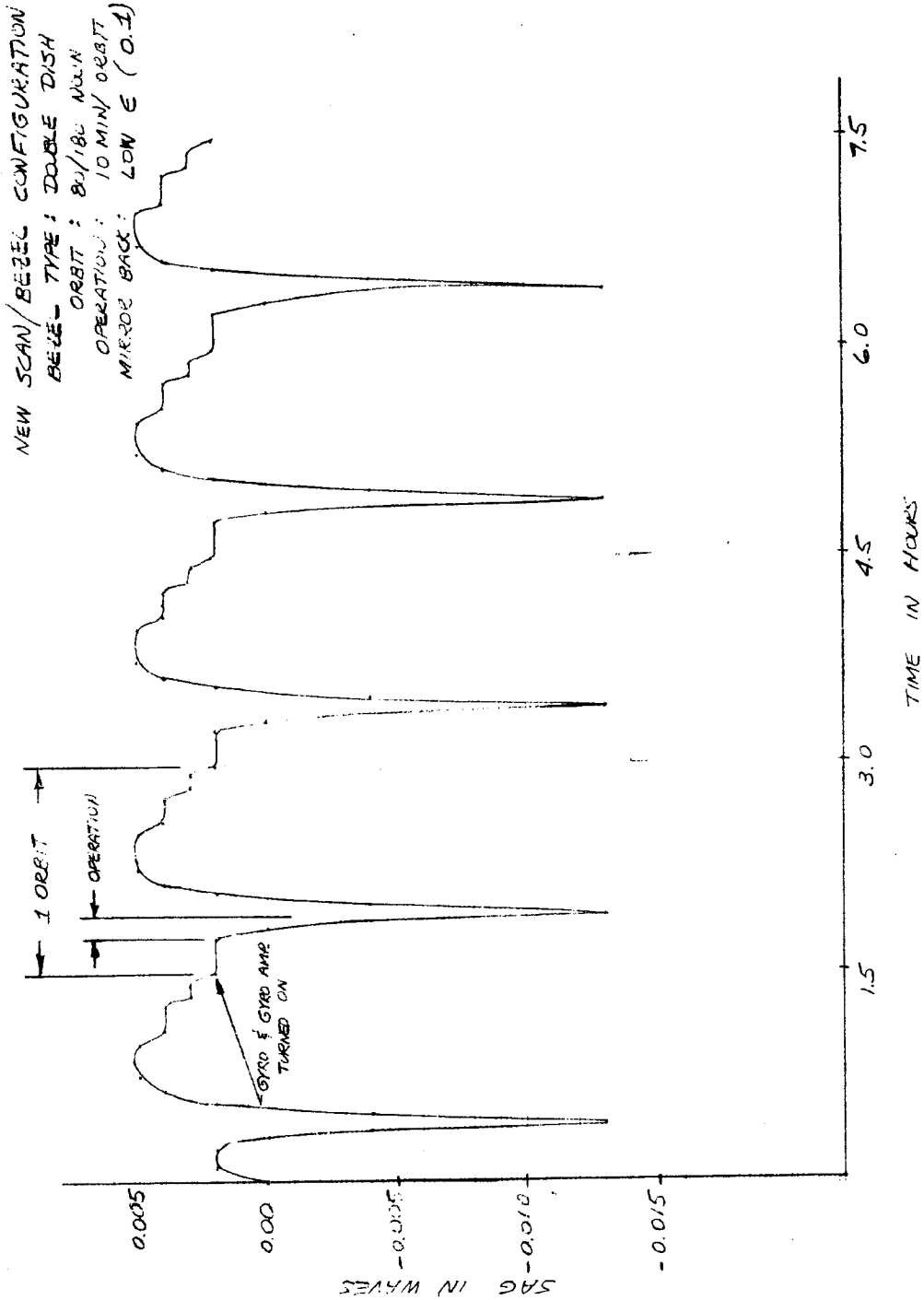


Fig. 8.4-6 — Sag history for new scan/bezel configuration, low emissivity

~~SECRET/SPECIAL HANDLING~~

## ~~SECRET~~/SPECIAL HANDLING

data for radial gradients between nodes 3 and 4 indicated a gradient of  $3.2^{\circ}\text{F}$  for the high emissivity case and  $4.1^{\circ}\text{F}$  for the low emissivity case. It is apparent that use of low emissivity coatings will reduce edge sag in the mirror, but will increase the radial by about  $1^{\circ}\text{F}$ . This data will be further analyzed to evaluate further optical and structural performance.

### 8.4.2 Scanner Assembly

#### 8.4.2.1 Description of Math Model

The scanner was broken down into 60 nodes, describing the scanner mirror and bezel, the pitch and roll gyros and amplifiers, the pitch and roll encoders, the pitch and roll motors, and the pedestal. Particular effort was made to determine the thermal gradients across the bearings located near the pitch and roll motors and encoders.

The boundary conditions applied to this model were the shroud temperatures calculated from previous preliminary system thermal analyses. The orbit simulated was an 80/180-nm noon orbit assuming the nominal geophysical constants.

Fig. 8.4-7 describes the general node layout for the scanner analysis. Nodes 1 through 11 describe the encoder with nodes 1 and 3 representing the inner and outer races of the pitch encoder bearings. Nodes 14 through 27 describe the roll encoder with nodes 14 and 56 representing the inner and outer races of the inboard bearings and node 16 and 56 describing the inner and outer races of the roll encoder bearings. Node 31 is the mirror; node 32 is the potting, and node 33 is the bezel, while node 34 is the pitch gyro amplifier and nodes 35 and 36 are the pitch gyro external and internal portions. The yoke is represented by nodes 37 through 43, as shown in Fig. 8.4-7. The roll gyro external and internal portions are represented by nodes 44 and 45, and node 46 represents the roll amplifier. Nodes 47 through 51 represent the pitch motor with nodes 51 and 48 representing the inner and outer races of the bearings. Nodes 52 and 53 represent the pedestal area and node 54 represents the pressure wall. Nodes 55 through 57 represent the roll motor with node 55 representing the joint case for the roll and encoder, and nodes 57 and 56 representing the inner and outer races of the outboard bearings.

During the active periods, the mirror and portions of the yoke and motor housings are exposed to albedo and earthshine fluxes as well as radiation to outer space. In addition, the gyros are thermostatically controlled so that they heat to 160 degrees internally during operation. These are activated 15 minutes prior to actual use.

#### 8.4.2.2 Temperature Histories

The results of the thermal analyses on the scanner plotted in the following figures. Fig. 8.4-8 is a plot of the average bezel and yoke temperatures for ten active orbits. The yoke experiences approximately 15-degree oscillations per orbit and the temperature builds up to a maximum of  $48^{\circ}\text{F}$  at the end of 10 active cycles. The bezel similarly experiences temperature oscillations and the temperature builds up to a maximum of  $43^{\circ}\text{F}$ . The temperatures of the bezel are somewhat lower than reported in Section 4.1.2 because of the difference in the math model. This does not affect, however, the findings of either section. Fig. 8.4-9 is a plot of the average yoke and bezel temperatures of the 10th active orbit only. As can be seen, the maximum average temperature difference between the bezel and the yoke is  $3.5^{\circ}\text{F}$  and occurs during the tenth cycle. Figs. 8.4-10 through 8.4-14 are the temperature histories of the pitch motor, pitch encoder, in-board bearings, roll encoder, and outboard bearings, respectively. Table 8.4-2 presents a summary of the maximum temperature differences experienced across each set of bearings. In all of the data, time

~~SECRET~~/SPECIAL HANDLING

zero is the beginning of gyro warm-up, time 15 minutes is the beginning of the observation and time 25 minutes is the end of the observation.

#### 8.4.3 Future Analysis

The shroud temperatures used in this analysis were determined from preliminary system analysis. Studies are now underway to calculate detailed shroud temperatures which will be more representative of the flight hardware. When the information is available, this analysis will be updated.

##### 8.4.3.1 Off Design Conditions

The current studies will also include the off design conditions in Section 8.3.2.2. The temperatures calculated from these studies will be used as boundary conditions for the scanner and the effects analyzed.

##### 8.4.3.2 Possible Tradeoffs

The results of off design updated temperature will be evaluated to determine the tradeoffs in optical, thermal, electrical and mechanical design so as to enhance the total system. Possible changes in the scanner and shroud thermal control coating and insulation will be analyzed at this time.

~~SECRET~~/SPECIAL HANDLING

~~SECRET/SPECIAL HANDLING~~

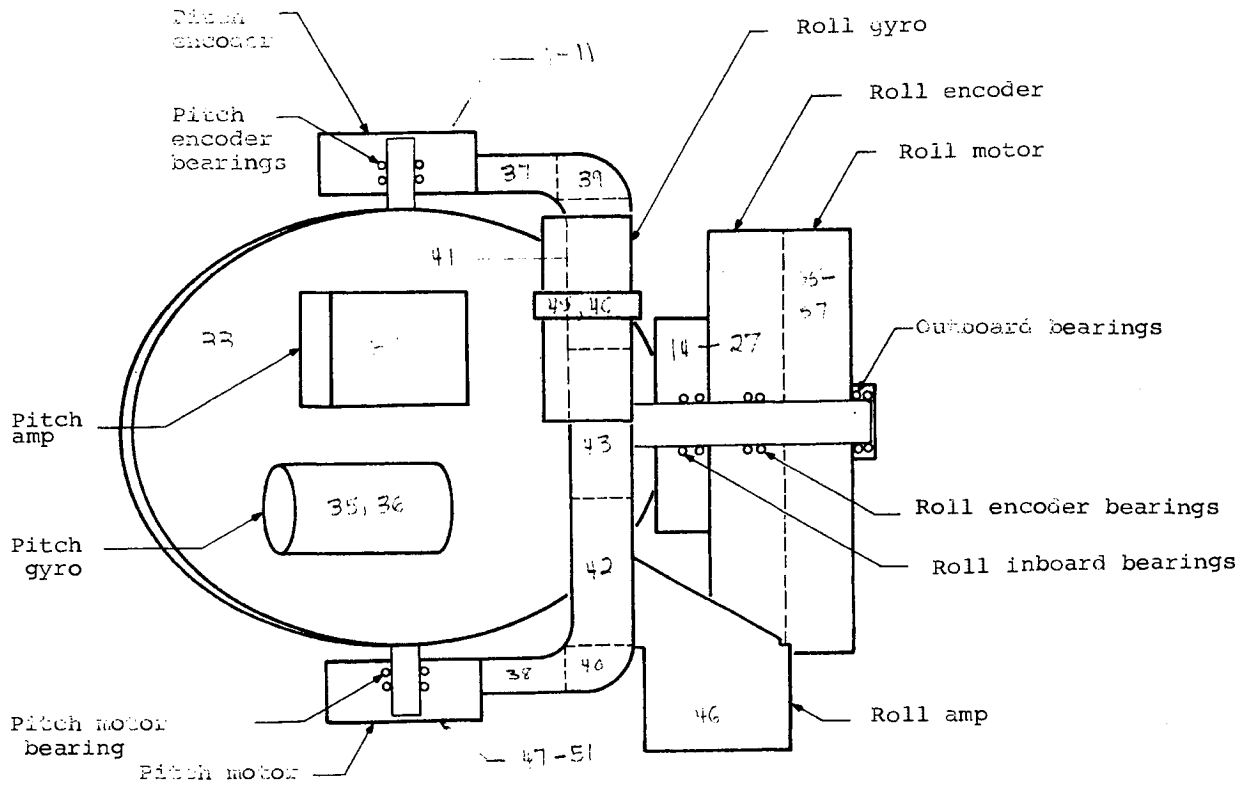


Fig. 8.4-7 — General node layout for scanner analysis

~~SECRET/SPECIAL HANDLING~~

~~SECRET/SPECIAL HANDLING~~

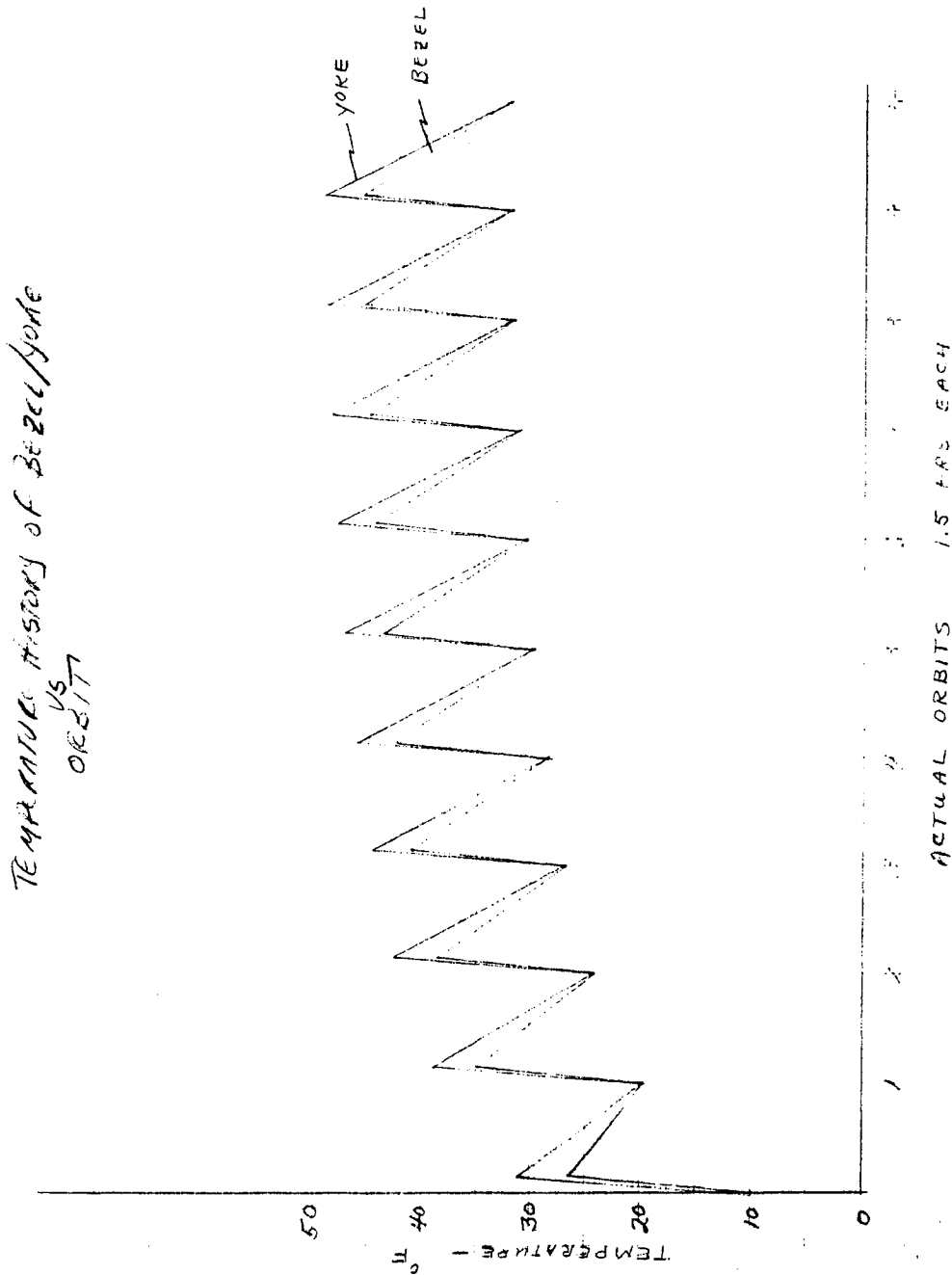


Fig. 8.4-8 — Temperature history of bezel/yoke for 10 active orbits

~~SECRET/SPECIAL HANDLING~~  
8.4-13

~~SECRET/SPECIAL HANDLING~~

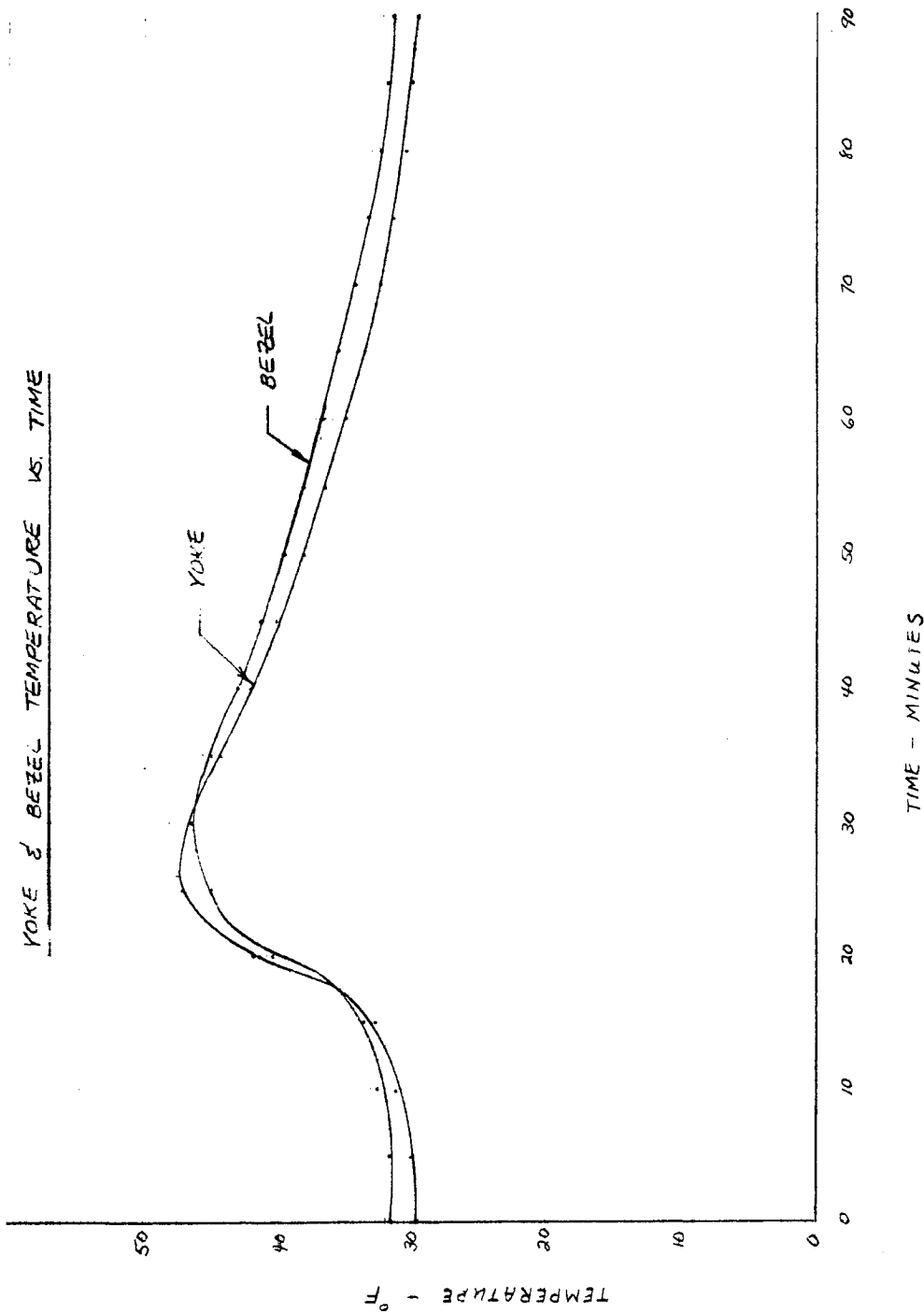
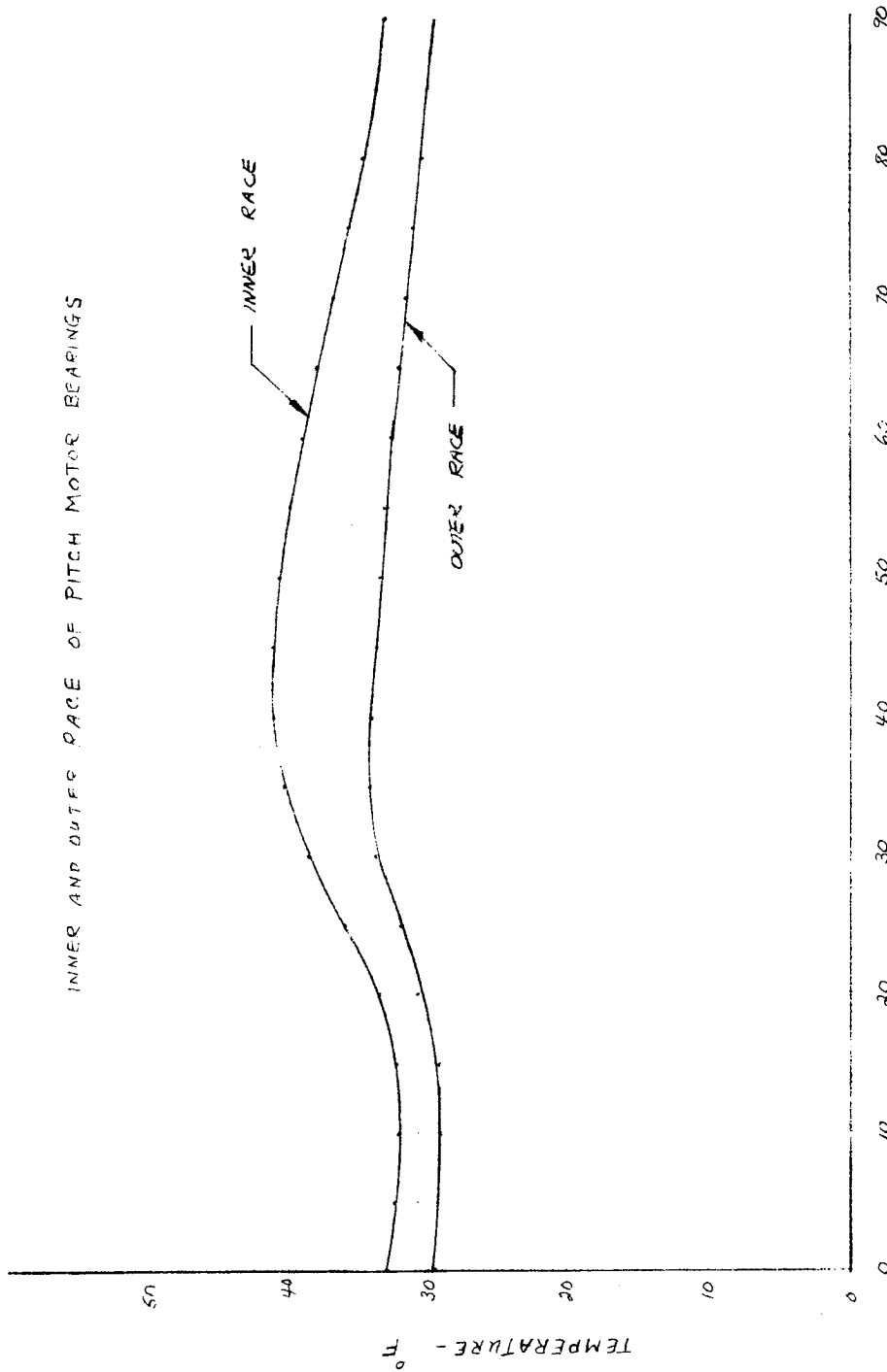


Fig. 8.4-9 — Average yoke and bezel temperatures for 10th orbit only

~~SECRET/SPECIAL HANDLING~~  
8.4-14

~~SECRET/SPECIAL HANDLING~~



TIME - MINUTES  
Fig. 8.4-10 — Pitch motor temperature histories

~~SECRET/SPECIAL HANDLING~~

~~SECRET/SPECIAL HANDLING~~

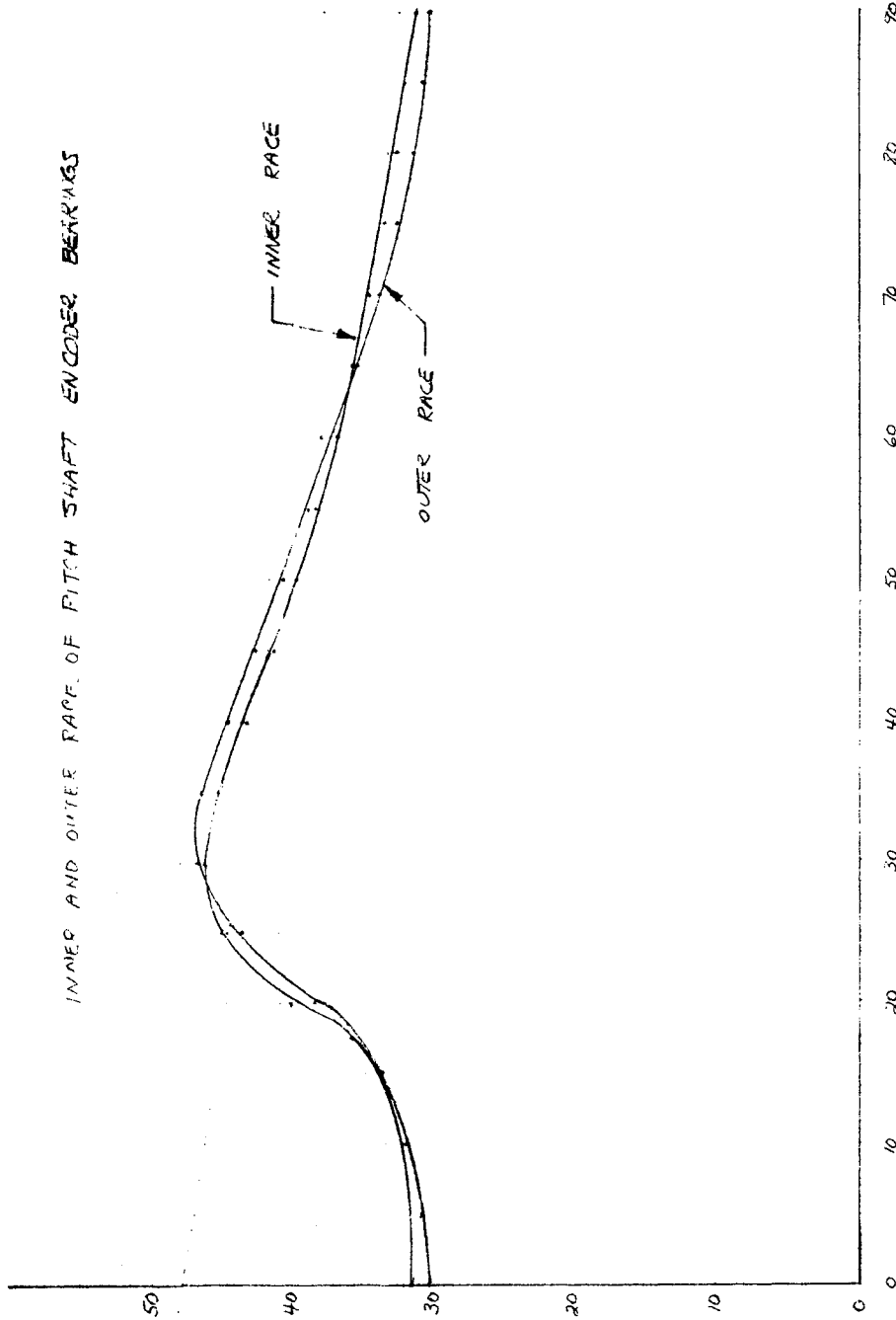


Fig. 8.4-11 — Pitch encoder temperature histories

~~SECRET/SPECIAL HANDLING~~

~~SECRET/SPECIAL HANDLING~~

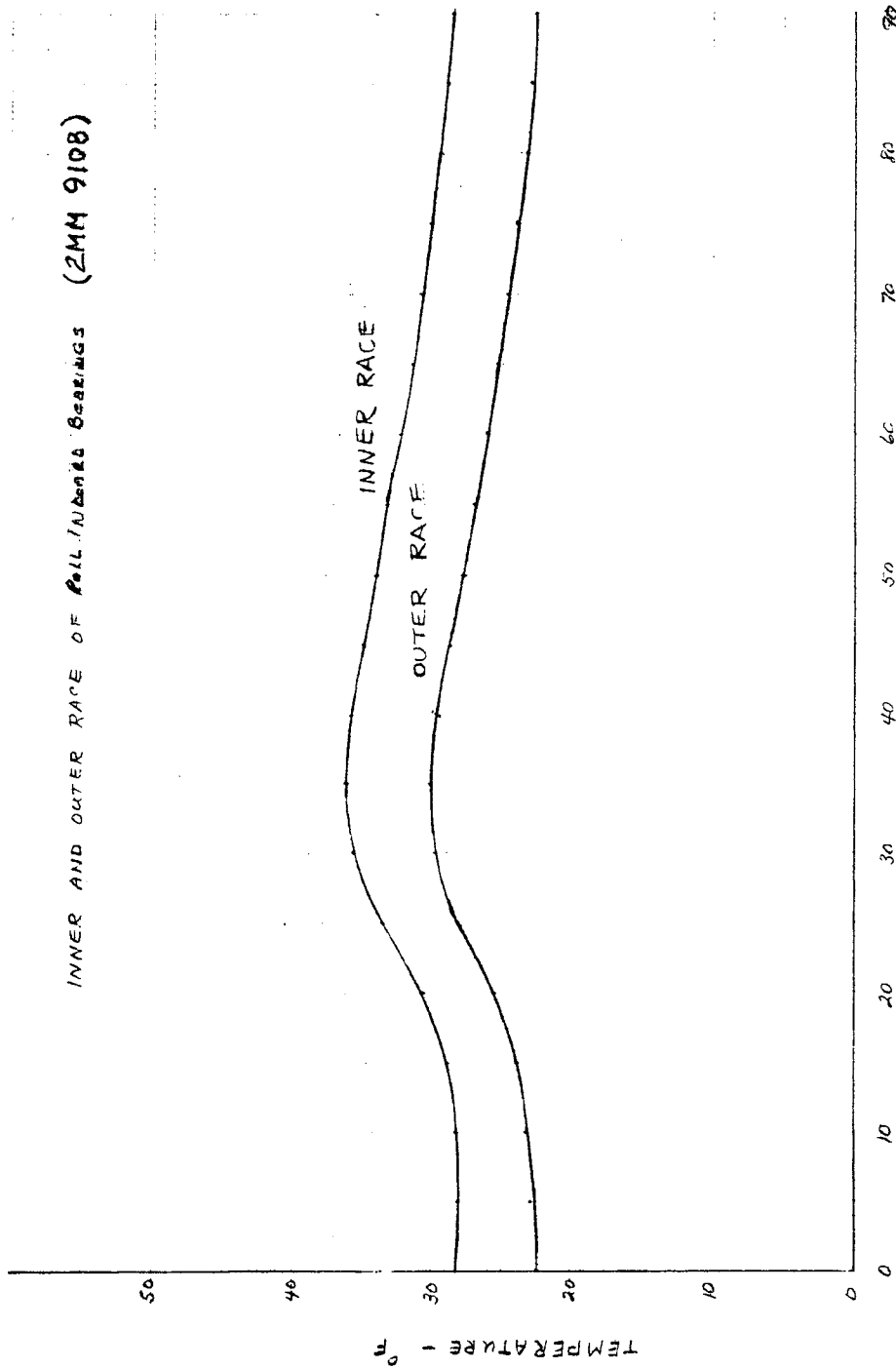


Fig. 8.4-12 -- Inboard bearings temperature histories

~~SECRET/SPECIAL HANDLING~~

~~SECRET/SPECIAL HANDLING~~

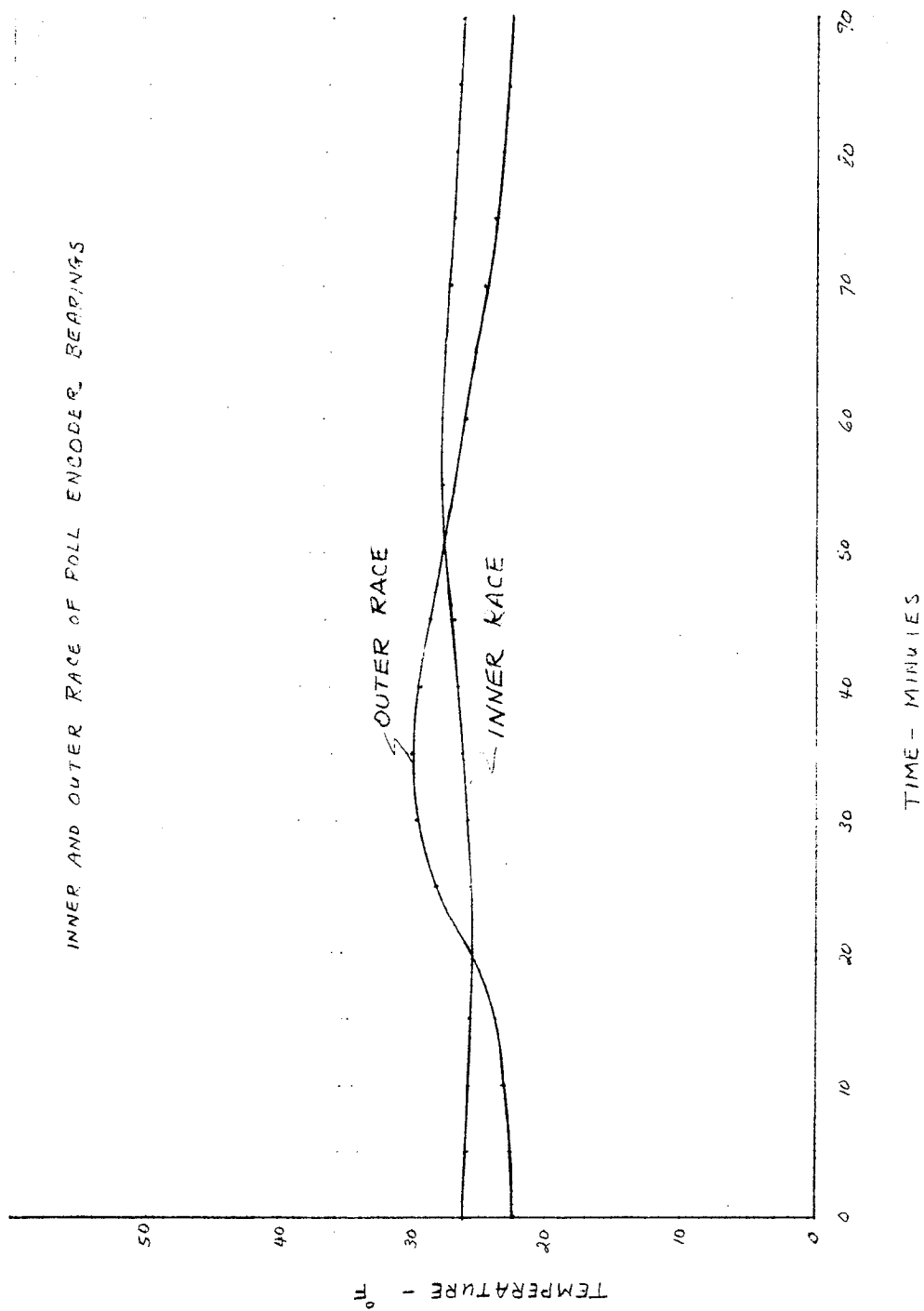


Fig. 8.4-13 — Roll encoder temperature histories

~~SECRET/SPECIAL HANDLING~~

~~SECRET/SPECIAL HANDLING~~

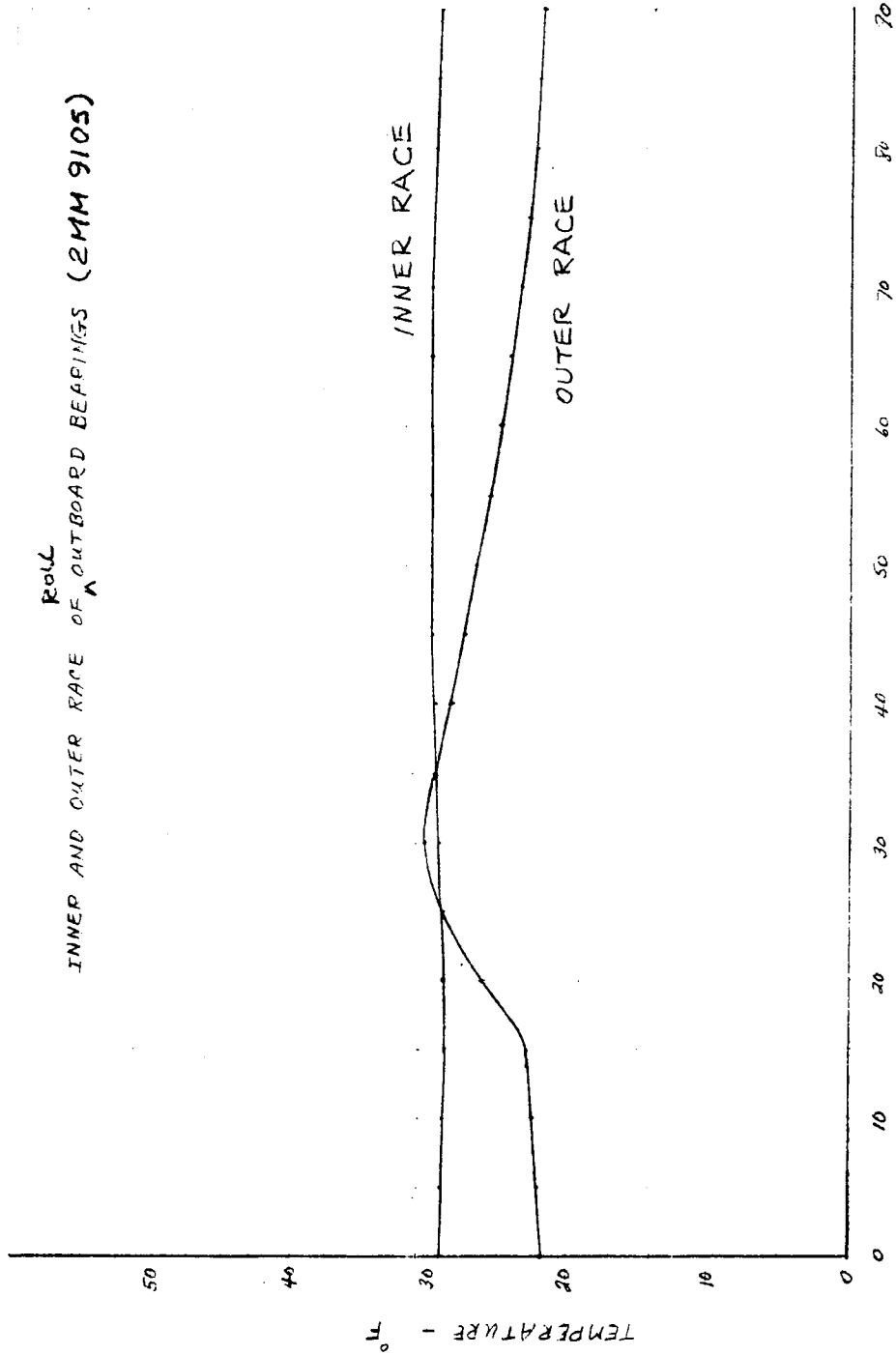


Fig. 8.4-14 — Outboard bearings temperature histories

~~SECRET/SPECIAL HANDLING~~  
8.4-19

~~SECRET~~/SPECIAL HANDLING

Table 8.4-2 — Maximum Thermal Bearing Gradients

Bearing Set	Gradient*
Pitch Motor	+ 7.3°F
Pitch Encoder	± 2 °F
Inboard	+ 6.3°F
Roll Encoder	± 3.8°F
Outboard	+ 7.4°F

\* + indicates inner race hotter

- indicates outer race hotter

## ~~SECRET/SPECIAL HANDLING~~

### 8.5 MIRROR/BEZEL

#### 8.5.1 TDT-1 Tests

The thermal/optical development test series includes a test just completed on the mirror double dish bezel design of October 1967, and a test scheduled in October 1968 for the latest scanner configuration. Both tests have the following objectives:

1. To determine the figure of the mirror under steady-state temperature conditions for the range of 70 to 150°F
2. To determine the response of the figure of the mirror to typical transient thermal conditions.

Also, the upcoming test will prove the mirror/bezel design under steady-state and transient thermal conditions. The test just completed will provide empirical data for verification of analytical methods, and familiarizes personnel with fabrication and testing of a low-expansion Cer-Vit mirror and bezel assembly. A complete report of this test will be published shortly. A brief description will be presented here.

The bezel configuration is shown in Fig. 8.5-1. It was instrumented with copper thermocouples and SR-4 strain gauges. Blanket heaters, 0.02-inch thick, were attached to simulate typical absorbed heating loads for the transient tests. Gyro and amplifier package heaters were also mounted on the rear of the bezel. Thermocouples were cemented to the rear surface of the mirror. The mirror bezel was mounted at one end of the vacuum chamber inside a thermally controlled shroud as shown in Fig. 8.5-2. A Fizeau interferometer was mounted outside the chamber and aligned with the mirror through an optical window in the chamber. The interferometer is a sensitive tool that measures surface figure by interference fringes and records them on film. The vacuum chamber was used to eliminate currents that degrade the performance of the interferometer. Also, the test setup was mounted on a seismic block to minimize vibration. A control panel was located to one side of the chamber. The test setup is shown in Fig. 8.5-3 and 8.5-4.

After a check-out of the test equipment, the steady-state test was performed. A number of interferometric, temperature, and strain gauge baseline readings were taken at ambient temperature and pressure. Then the chamber was pumped down and a vacuum of 1,000 microns or better was maintained throughout the test. Temperature levels of 90, 100, 130, and 150°F were provided by controlling the thermal shroud. Each level was maintained 18 hours. Data readings were taken every 1/2 hour, the first 9 hours, and every hour the second 9 hours.

The transient tests consisted of testing the mirror/bezel under four conditions, two duty cycles for two background temperatures. With vacuum conditions being maintained, the shroud was activated to a temperature level of 140°F and the mirror/bezel was allowed to soak at that temperature. After steady state had been reached, the gyro, amplifier, and bezel heaters were turned on to simulate typical absorbed heat loads. The heaters were turned off after 10 minutes and the assembly then soaked 80 minutes. That constituted one 90-minute transient cycle. This cycle was repeated 8 times and then the assembly was allowed to soak an additional 12 hours. A second power cycle was run at the 140°F background level. This cycle had power on 24 minutes and off 66 minutes. Both power cycles, the 10/80 and 24/66, were repeated for a background temperature of 50°F. These two power cycles represent nominal and maximum duty cycles to which the mirror/bezel are designed. The two temperature levels show the effect of background temperature.

The data is presently being assembled and evaluated for a final report. A more detailed discussion of the results and conclusions will be presented in the test report.

~~SECRET/SPECIAL HANDLING~~

~~SECRET~~/SPECIAL HANDLING

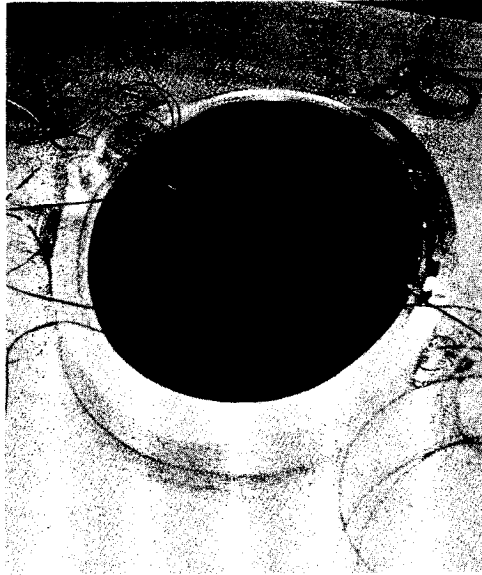


Fig. 8.5-1 — Back of aluminum bezel with cover off

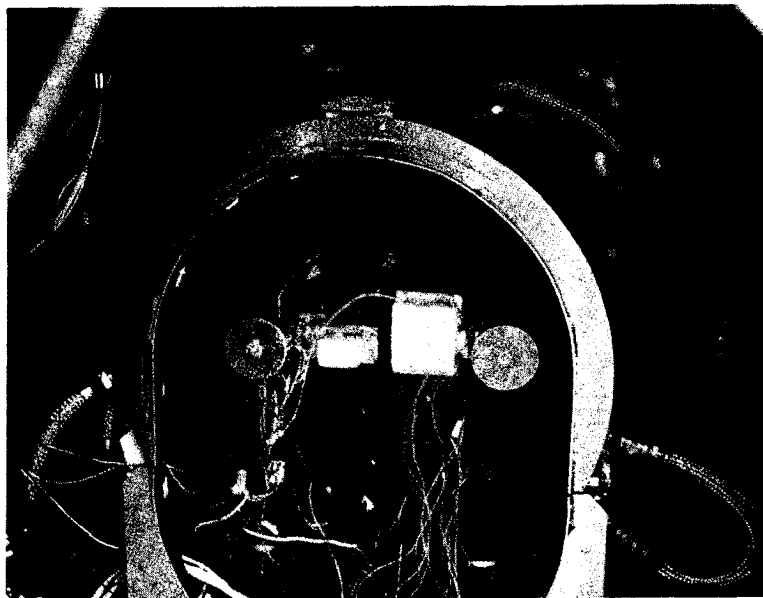


Fig. 8.5-2 — Mirror/bezel assembly mounted in thermal shroud in vacuum chamber

~~SECRET~~/SPECIAL HANDLING

~~SECRET~~/SPECIAL HANDLING

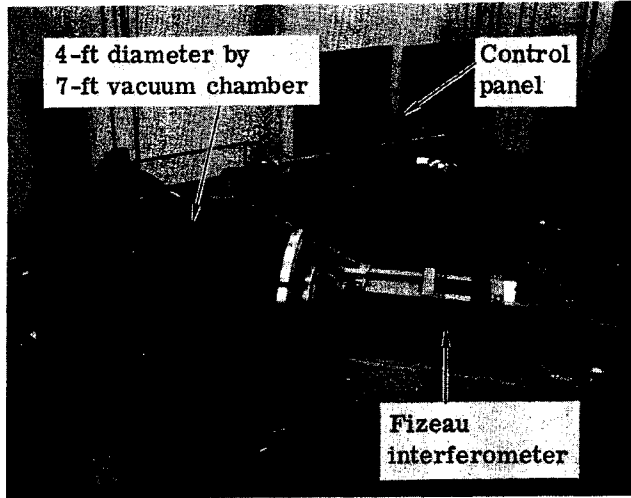


Fig. 8.5-3 — TDT-1 test setup



Fig. 8.5-4 — Control panel for TDT-1

~~SECRET~~/SPECIAL HANDLING

~~SECRET~~/SPECIAL HANDLING

## 9. SCANNER STRUCTURAL CONSIDERATIONS

### 9.1 GENERAL CONSIDERATIONS

The scanner structural design is based on the following three fundamental considerations:

1. The design must be strong enough to adequately resist the internal stresses caused by the random vibration and shock environment during launch and ascent
2. The design must be stiff enough to meet the transmissibility requirements during the operating condition
3. The design must be as light as possible without compromising its basic structural integrity.

During launch and ascent the scanner is subjected to a random vibration and shock environment. The dynamic analysis of the scanner in this environment yields the acceleration loadings on the various components. These acceleration loadings are converted to statically equivalent loads which are then applied to the various scanner components to determine their internal stress levels. For steady state considerations  $3\sigma$  values are used, while for fatigue considerations  $2\sigma$  values are used.

Once determined, the value of the internal stress level of a particular component is compared to the material allowable through the margin of safety expression, which defines the excess strength in the part. No component shall have a margin of safety of less than 0 when compared to the yield strength of the material while using a safety factor of 1, nor shall it have a margin of safety of less than 0 when compared to the ultimate strength of the material while using a safety factor of 1.4. For fatigue considerations, the material fatigue strength is treated as an ultimate strength and a safety factor of 1.4 is used.

In addition, since various elements of the scanner are extremely sensitive to small distortions, the permanent deformation of any component must be kept small enough to prevent impairment of bearing performance and optical performance. Since, as a rule, excessive permanent deformation is undesirable in most structures, it is common practice to adopt an arbitrary amount of tolerable distortion. Material test engineers have determined that in most structures 0.002 inch per inch of permanent set is reasonable. The stress corresponding to this distortion is defined as the yield strength of the material. In instrument applications such as this, however, it is appropriate to refer to a value known as the precision elastic limit. The precision elastic limit of a material is that stress which will produce 1 microinch per inch ( $1 \times 10^{-6}$ ) of permanent strain. The beryllium products selected for the design are HP-40 and XT-40 (roll shaft), or equivalents. The precision elastic limits of these two products are 8,000 psi and 12,000 to 15,000 psi, respectively. While no formal analysis has been performed as of this writing, preliminary indications are that the present design is satisfactory. A detailed analysis in this area will be performed to substantiate these preliminary findings.

The scanner transmissibility requirements are fully discussed in Section 7.

~~SECRET~~/SPECIAL HANDLING

~~SECRET/SPECIAL HANDLING~~

## 9.2 COMPONENT STRUCTURAL CONSIDERATIONS

### 9.2.1 Yoke

The yoke supports the scanner mirror and bezel and allows for pitching motions. At one end of the yoke, the bezel is attached through the torque housing while at the other end it is attached through the encoder housing. The encoder disc was originally mounted directly to the pitch shafting while its detector was mounted rigidly to the encoder housing. Analysis of the relative deflection between the disc and detector indicated that the clearance (0.0015 inch) between the two was inadequate to prevent contact under dynamic loading. This problem was solved by mounting the encoder disc on its own set of bearings, directly to the encoder housing. This results in both the disc and detector being mounted to the same piece of structure and thereby minimizes relative deflections.

The other side of the pitch shaft is connected to the torquer housing through a diaphragm which permits deflections in the plane of the yoke but resists loads perpendicular to the yoke. This feature is necessary to allow for thermal expansion of the mirror/bezel relative to the yoke. The maximum effective temperature difference between the two is approximately 20 °F. The diaphragm will allow the relative expansion of the two pieces to occur without exceeding the pitch axis bearing preload.

The basic structural section of the yoke, coupled with a specific material, is dictated by stiffness considerations in order to achieve the required frequency.

The original specifications called for locked rotor frequencies of 300 radians per second. This level was deemed adequate to minimize the structural response contributions to gyro output error. In order to obtain a fundamental level of 300 radians per second, each spring-mass system that comprises the parent structure must have a frequency higher than the fundamental one. This implied that the yoke-mirror system's frequency had to be greater than 300 radians per second. The precise amount greater depended on the rest of the system. In our case, the value required was 350 radians per second.

In the revised specification, EC331B, paragraph 3.1.1.1.8, the systems vibrational characteristics are defined in terms of a frequency response curve. This curve gives the same information as the more familiar structural transmissibility plots. The curve has a cutoff frequency of 300 radians per second. Weighing the role that the yoke plays in the overall response picture in a manner similar to that discussed above, the yoke-mirror system must have a frequency considerably greater than 300 radians per second. Although preliminary analysis indicated that the yoke should be approximately four times stiffer to meet the transmissibility requirements, more detailed analysis reveals it should be approximately eight times stiffer.

Materials considered for the yoke were primarily aluminum and beryllium. Under the original specifications, it appeared that the required structural-dynamic characteristics could be met with aluminum within a reasonable weight and space envelope. However, the increased stiffness required by the new specification would result in an aluminum yoke that is not only considerably heavier but prohibitively large in terms of the existing severe space restrictions. Due to these factors, the preliminary design configuration is a beryllium yoke, of two piece box construction. The cover is bonded to the channel section with Eccobond 45 (Emmerson & Cumming, Canton, Mass.) to form a closed box. Mechanical fasteners are also used as a backup in the event of bond failure.

The analytical work presented herein was done for the unbalanced scanner design and prior to the incorporation of the diaphragm on the torquer end of the pitch axis. In addition, the analysis

~~SECRET/SPECIAL HANDLING~~

~~SECRET/SPECIAL HANDLING~~

was performed using the preliminary dynamic loads. The geometrical changes incorporated in the planned design do not significantly effect stress levels. The diaphragm on the pitch axis has the effect of essentially causing in-plane yoke loading to be reacted by one arm rather than both arms. The preliminary dynamic analysis indicated in-plane yoke loading of 528 pounds which resulted in primary stress levels on the order of 5,000 pounds per inch<sup>2</sup>. The more recent dynamic loads analysis indicated a reduced in-plane loading of 383 pounds but since the load must now be resisted by one arm this results in primary stress levels on the order of 7,200 pounds per inch<sup>2</sup>.

This value is still within the PEL of the material used for yoke fabrication. Additional design changes to thicken cross sections will further reduce the primary stress levels.

### 9.2.2 Roll Shaft

The roll shaft must be stiff enough to meet the transmissibility requirements during the operating condition, strong enough to adequately resist the flexural stresses resulting from the bending moment produced by the scanner mirror and associated components during random vibration, and compact enough to meet the geometrical requirements imposed by the roll axis torquer and encoder. In addition, the design must incorporate a hole large enough to permit electrical cabling to run along its length without touching in order to minimize steady state torque and torque ripple values.

Materials considered for the shaft have been beryllium and stainless steel. The present design is beryllium with a weight of approximately 0.7 pounds. Stress levels are the governing criteria with a beryllium design, with the stiffness requirement being slightly exceeded. The steel design weighed approximately 2.1 pounds, with the stiffness requirement being the governing criteria and the stress requirement more than adequate. The beryllium design was selected due to its light weight.

In the original baseline design, the torque motor rotor was located near the aft bearings, in an area of low shaft flexural moment. The encoder for this design formed an integral part of the front plate. Recently, however, it was felt that placing the encoder in back of the roll axis torquer would provide for a better design interface and increase the accessibility of the encoder unit should servicing be necessary. This required a reduction in the forward diameter of the shaft from 1.375 inches to 1.28 inches to accommodate the torquer motor rotor.

Since the shaft is threaded in order to receive the retainers for the bearings, torquer and encoder, areas of high stress concentration are present. In order to predict these stress concentrations, the radius at the root of the threads must be controlled. Accordingly, the threads on the shaft will be manufactured in accordance with MIL-S-8879A, "General Specification for Screw Threads, Controlled Radius Root with Increased Minor Diameter." Treating the thread as a single notch, the worst anticipated theoretical stress concentration factor is approximately 4.85. While it is recognized that a series of closely spaced notches represents a smaller degree of stress concentration than a single notch, results of photoelastic tests by Hetenyi on the Whitworth thread shape indicate only a small reduction in the end threads.\* Hence, it is felt that treating the threads as a single notch is not unduly conservative. Since beryllium is a brittle material, full notch sensitivity has also been assumed, i.e., that the full theoretical value is realized. For these reasons then, although the maximum nominal stress in the shaft is approximately 15,000 psi, the maximum stress value that should be compared to the fatigue strength of the material is

---

\* Peterson, R. E., "Stress Concentration Design Factors."

~~SECRET/SPECIAL HANDLING~~

~~SECRET/SPECIAL HANDLING~~

approximately 67,000 psi. This value occurs in the threads just aft of the torque motor rotor and reflects a load reduction from 3r to 2r values, a safety factor of 1.4, and the thread stress concentration factor.

The particular grade of beryllium recommended for the fabrication of the roll shaft is XT-40, manufactured by the Beryllium Corporation, or extruded I-400, manufactured by the Brush Beryllium Company. This material is produced by the hot extrusion of a hot pressed beryllium block with a minimum beryllium oxide content of 4.25 percent. It offers an ultimate tensile strength of 90,000 psi and a yield strength of 52,000 psi. There is very little published data on the rotation beam fatigue characteristics of this material. One available piece of information regarding these characteristics is included in the Appendix 9A. The referenced curve indicates that the reversed bending endurance limit of the material is 56,000 psi, a reasonable value considered in the light of available axial fatigue data.

Using the margin of safety experience, a comparison of the endurance limit with the predicted fatigue stress of Section F-F in the shaft, yields a negative value of 16 percent (M.S. = 0.16). In other words, the load on the shaft at this location is 16 percent greater than its predicted load-carrying capacity.

The existing roll torque motor design was sized to provide the torque necessary to drive the unbalanced baseline configuration with a minimum amount of weight. The torque necessary to drive the balanced configuration is less. Preliminary calculations indicate that increasing the hole diameter in the torque motor rotor from its existing optimum value of 1.28 inches to 1.5 inches will result in a torque capability decrease of 10 percent. This reduction leaves a torque capability that is consistent with the balanced design requirements. The diameters of the shaft in the deficient area, can therefore be reared sufficiently to provide a positive margin of safety. The predicted increase is approximately 1/8 of an inch.

If the unbalanced design is used, the hole in the torque motor rotor cannot be increased, and the shaft diameter, in turn, cannot be increased. In this case, the alternatives are to change the shaft material to stainless steel with a consequent weight increase of approximately 1.4 pounds, or to move the torque motor aft on the shaft into a region of lower flexural moment.

The threads will be machined onto the shaft. Subsequent to the machining operation, the shaft will be heat treated at approximately 1,400 °F for 20 minutes to remove deformation twinning. It will then be chemically etched to remove 0.0015 inch of material to eliminate microscopic surface cracks. As a result of the chemical etching operation, the threads will be reduced to a class 2 fit.

### 9.2.3 Front Plate

The roll housing front plate is an integral part of the cylindrical portion of the roll housing and supports the forward end of the roll shaft through the forward roll axis bearings.

Originally, this component housed the detector and associated electronic equipment for the roll axis optical encoder. The encoder disc itself was mounted rigidly to the roll shaft. Analysis of this design showed that the relative deflection between the disc and detector under dynamic loading was sufficient to close the clearance gap (0.0015 inch) between the two components. This was caused by the flexibility of the roll shaft and bearings. The possibility of affixing a metal rim around the outside periphery of the disc was investigated as a solution. The purpose of the metal rim was to minimize any movement of the encoder disc by having it contact a stop and thus reacting load. The resulting stress in the disc was prohibitively large for glass and the scheme was abandoned. The problem was solved by mounting the disc on its own bearings directly to the

~~SECRET/SPECIAL HANDLING~~

~~SECRET~~/SPECIAL HANDLING

forward housing plate. The forward plate in this configuration was not only a primary load path, but an integral part of the roll encoder. The plate had to serve a dual function, i.e., provide adequate strength to resist the internal stresses incurred by the dynamic environment, and provide adequate rigidity to ensure that deflection of the plate was maintained small enough to provide positive clearance between the disc and detector. The analysis shown in Appendix 9A indicates that these requirements were met.

Recently, however, the encoder and roll axis torquer location were reversed to increase encoder accessibility. Moving the roll axis torque motor forward in this fashion provides the additional advantage of increasing the roll shaft stiffness between the torquer and yoke.

This configuration requires the forward plate to be stiff enough in relation to the aft plate to preclude excessive axial deflection in this latter element, to provide a rigidity compatible with the transmissibility requirements, and to limit permanent deformation to a level compatible with the bearing requirements. Although an analysis of this plate to determine its conformance to the above requirements has not yet been completed, the analysis of the previous front plate/encoder (Appendix 9A) indicates that they can be met with material thicknesses on the order of 0.25 inches.

#### 9.2.4 Aft Plate

The roll housing aft plate is mechanically attached to the cylindrical portion of the roll housing and supports the aft end of the roll shaft through the rear roll axis bearings.

Several requirements have resulted in the present design of this component. These requirements are as follows:

1. The plate must incorporate a diaphragm in order to provide sufficient flexibility in the out-of-plane direction to prohibit unloading of the preloaded bearing pair due to tolerance buildup between the mating parts and due to thermal gradients between the roll housing and the shaft. The maximum expected tolerance buildup is 0.002 inch while the maximum anticipated thermal gradient between the roll housing and the shaft is 20 °F which would result in an unrestrained axial shaft deflection of approximately 640 microinches
2. Sufficient strength must be provided in the in-plane direction to adequately resist the loads incurred by the dynamic environment. In addition, the flexure must be rigid enough to preclude buckling due to these same loads, and to supply an in-plane stiffness consistent with the transmissibility requirements
3. The component should be of minimum weight for consistency with its intended environment.

From buckling considerations and transmissibility consideration, it is desirable that the selected material have a large modulus of elasticity. However, for the out-of-plane flexibility requirement, it is desirable to have a material with low modulus. Beryllium has a high modulus and low density. Consequently, if the plate can be made thin enough to satisfy the out-of-plane flexibility requirements and still maintain the in-plane requirements, it would appear to be an attractive selection.

The present diaphragm thickness is 1/32 inch (0.03125) and the material is beryllium. Analysis (Appendix 9A) indicates that the in-plane and out-of-plane requirements are fulfilled and the weight is minimized.

~~SECRET~~/SPECIAL HANDLING

~~SECRET/SPECIAL HANDLING~~

Pedestal

The scanner pedestal supports the entire scanner assembly. It is mounted to the vehicle pressure wall through three standoffs which are provided by the vehicle contractor. The pedestal consists of three legs which attach to these standoffs and resist loads. Originally, a space truss was considered; however, due to the proximity of the scanner assembly to the vehicle, space limitation precluded this approach.

Initially, aluminum was selected for the pedestal material to provide the required strength and to keep stiffness low in order to minimize scanner shock loading. It has since been determined that the pedestal material should be beryllium in order to provide a stiffness consistent with the transmissibility requirements. The appropriate analyses are shown in Appendix 9A.

~~SECRET/SPECIAL HANDLING~~

~~SECRET/SPECIAL HANDLING~~

## 10. TEST PLAN

### 10.1 GENERAL DESCRIPTION

The first scanner which will undergo extensive functional and environmental tests is the nondeliverable engineering model. This scanner will be subjected to development testing to ascertain the functional characteristics of a total scanner assembly under varying test conditions. The test cycle will begin with a performance test covering areas of:

1. General operation
  - a. Power mode operation—open loop
  - b. Acceleration—velocity profiles
  - c. Signal outputs—encoder, gyro
  - d. Power measurements
2. Detailed operation
  - a. Scan field
  - b. Encoder position readout
  - c. Redundant drive mode
  - d. Scanner gimbal torques

These functional parameters will be measured and data will be recorded to form a pre-environmental baseline. This baseline will form a frame of reference against which all past environmental functional data will be evaluated.

~~SECRET/SPECIAL HANDLING~~

~~SECRET~~/SPECIAL HANDLING

## 10.2 TESTING

Thermal-vacuum testing of the scanner is planned during the development phase. This test will expose the scanner to an environment which closely simulates flight operation. Thermal profiles imposed will follow the predicted temperature levels and the scanner will undergo interferometric tests to determine mirror figure. Temperature histories will be determined by instrumenting the scanner with temperature sensors and recording their outputs. The data gathered during this test will constitute the first phase of the test on the scanner. A second phase of thermal-vacuum testing is planned under simulated flight conditions to verify the operational parameters of the scanner. The specimen will be subjected to the environment and electrically exercised using the SATS Test and Checkout Console. Data relating to operational criteria will be recorded, analyzed and compared to ambient baseline data.

~~SECRET~~/SPECIAL HANDLING

## ~~SECRET/SPECIAL HANDLING~~

### 10.3 DEVELOPMENT TESTS

#### 10.3.1 Resonance Search on Scanner Vibration Fixture

The scanner vibration fixture with the scanner, or dummy load, attached will be subjected to a sinusoidal sweep test on an electrodynamic shaker in three axes through the frequency range from 5 to 2,000 hz to identify the amplification and bandwidth of each fixture resonance greater than three. The fixture will be modified until the dynamic coupling between fixture and scanner is reduced to the specified levels. This test will be conducted on the Ling Model 249 vibration exciter in the Itek Environmental Laboratory.

#### 10.3.2 Sinusoidal Vibration—Low Level

After the vibration fixture has been checked out, the scanner will be subjected to a sinusoidal sweep in three axes to measure the following characteristics: (1) resonances, (2) Q-factors at resonance, and (c) mode shapes at resonance. The expected maximum input during the sinusoidal sweep will be 2.0 g (peak acceleration) except at low frequencies where the double amplitude will be limited to 0.1 inch. This test will be conducted on the Ling Model 249 vibration exciter in the Itek Environmental Laboratory.

#### 10.3.3 Random Vibration

The scanner will be subjected to a wide-band random vibration input similar to the qualification spectrum. The frequency limits will be 5 and 2,000 hz. The random vibration input will have a Gaussian distribution, but instantaneous acceleration peaks will be limited to three times the overall root mean square acceleration level. The applied vibration power spectral density will be equalized within a tolerance of  $\pm 3$  db between 10 and 2,000 hz. Test duration will be 5 minutes. The response of accelerometers mounted on the specimen will be recorded. This test will be conducted on the Ling Model 249 vibration exciter in the Itek Environmental Laboratory.

#### 10.3.4 Calibration Shock Test

This test is intended to identify the modifications to be made to the pyrotechnic shock test fixture for the scanner in order to obtain the specified shock response spectrum at the scanner/fixture mounting interface. It will involve the process of stiffening and or dampening the fixture to shape the correct input, as well as experimenting with the amount of explosives, location of charges, and method of mounting charges on the fixture. The technique of explosive firing will be developed. Shock response spectra of the input will be analyzed using the proposed MB Electronics N980 Shock Spectrum Analyzer.

#### 10.3.5 Pyrotechnic Shock

The scanner will be installed in a special shock fixture which will allow the simulation of a part of the vehicle structure. Explosive charges in metal pots on the fixture will be detonated to impart a shock to the scanner. At the mounting points of the test specimen accelerometers will be installed to monitor the acceleration-time history of the shock pulse. The electrical signal from the accelerometer will be recorded on the proposed magnetic tape recorder and subsequently analyzed using a Shock Spectrum Analyzer to ensure conformance with the specified response spectrum. The scanner will be subjected to shocks in each direction of the three mutually perpendicular axes. This test will be performed at a facility designated by the Customer or one built by Itek. The main emphasis during this phase will be the establishing of test techniques and explosive parameters.

~~SECRET/SPECIAL HANDLING~~

~~SECRET~~/SPECIAL HANDLING

10.3.6 Acoustic Test

It is planned to test all external pieces, i.e., the shroud, scanner, fixed fold mirror, and window at the same time as an assembly. The fixture will allow for the simulation of some vehicle structure. The fixture and specimens will be soft mounted in a reverberant chamber and subjected to a diffuse sound field with an overall sound pressure level of 159 db. This test will be done at Wyle Laboratories, Huntsville, Alabama.

NOTE

A request for an attenuated level is being processed because of the contractor's aerodynamic fairing.

~~SECRET~~/SPECIAL HANDLING

## ~~SECRET/SPECIAL HANDLING~~

### 10.4 SCANNER PERFORMANCE TEST PLAN

Test methods designed to ensure compliance with specifications have not yet been finalized. Work toward this end is progressing as part of the effort directed toward the SATS development. The following represents the current status of these plans.

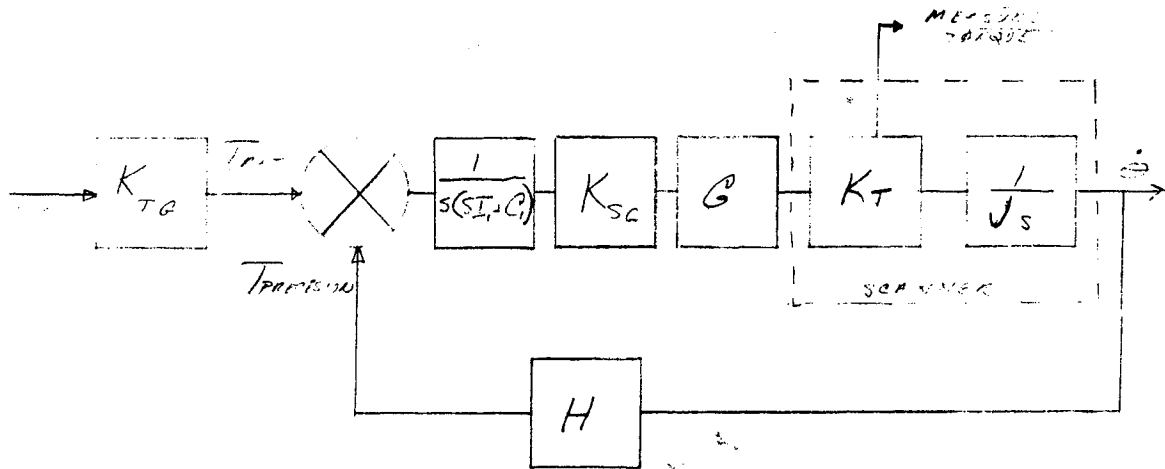
#### 10.4.1 Torque

It is proposed to measure torque values by operating the torque motors so that the gimbals are driven at typical rates, and measuring the motor current under these conditions. This method will require the predetermination of a torque versus motor current characteristic curve. Such a curve will be established in a test fixture prior to scanner assembly.

#### 10.4.2 PSD

Measurement of PSD requires that the scanner bearings be relieved of scanner load to avoid distortion of the noise data. It is proposed to accomplish this by supporting the scanner on its roll axis with a long wire to relieve the weight of the rotating mass. Measurement of current requirements of the motor would then be a reflection of instantaneous torque.

Both of the above test methods are, of course, closed loop procedures. It is intended to close the loop with the gyro. The following servo block diagram has been suggested to use the gyro for rate feedback.



where  $C_1$  = output axis damping coefficient  
 $I_1$  = gimbal polar moment of inertia  
 $K_{SG}$  = gimbal pickoff sensitivity  
 $K_{TG}$  = gyro torque sensitivity  
 $H$  = gyro wheel angular momentum

~~SECRET/SPECIAL HANDLING~~

~~SECRET/SPECIAL HANDLING~~

#### 10.4.3 Acceleration

The acceleration capability of the scanner will be tested by applying rate commands to the scanner and recording the gyro rate output. This signal will then be manually differentiated to obtain acceleration values.

#### 10.4.4 Encoder

It is proposed to test the encoders apart from the scanner for the purposes of measuring encoder accuracies since gimbal rate errors would contribute some factor to any error determined by measuring encoder output. For this reason, a precision air bearing rate table will be used to test encoders prior to scanner assembly. Once assembled to the scanner, the encoders will be checked precisely at the zero references position and at the extreme ends of gimbal travel.

#### 10.4.5 Transmissibility

It is proposed to measure system transmissibility by exciting the torquer motors and measuring gyro output using the system described in the above diagram in an open loop configuration.

~~SECRET/SPECIAL HANDLING~~

~~SECRET~~/SPECIAL HANDLING

## 11. RELIABILITY AND SAFETY ANALYSIS REPORT SUMMARY

Appendix 11A includes the detailed reliability analysis and safety report per MSMR-112. The design data upon which these analyses are based are preliminary and subject to change. Included are the parts, materials, processes used, and application data to the extent presently defined; figure of merit analysis; failure and hazard made analysis; life limited device evaluation; and a list of reference documents. The results of this analysis are summarized below.

### 11.1 PARTS USE AND APPLICATION DATA

The present design includes six nonstandard part types which will require contractor approval per MSMS-126. Preliminary nonstandard parts lists have been submitted which identify these items (reference 9400-68-576, 29 March 1968; 9400-68-605, 23 April 1968). Formal requests for approval will be made upon completion of the detailed part specification. The encoders, torquer, and bearings are the scanner critical components and require specification, review, and approval per EC 331B, paragraph 3.2.2.3 and AN-EC 331B-2. The specifications for components requiring special approval were submitted on 4 April 1968 (reference 9400-68-566). The most recent design data for the encoder (both pitch and roll) utilizes 4 device categories which are nonstandard and require contractor review and approval (Section 1 of Appendix 11A identifies these items). Historical use data is being obtained in order to prepare the formal request for approval on these items.

~~SECRET~~/SPECIAL HANDLING

~~SECRET/SPECIAL HANDLING~~

## 11.2 MATERIALS USE AND APPLICATIONS DATA

The inorganic materials in the present design are principally beryllium, glass, and stainless steel (see Section 2 of Appendix 11A). Surface treating of the beryllium with black anodizing and painting will be done for thermal control and to prevent stray light reflection and for protection against corrosion. The stainless steel maintaining hardware will be passivated (black where reflection may be a problem).

The organic (nonmetallic) materials are listed in Section 2 of Appendix 11A. A preliminary list was submitted in response to PDR Action Item no. 74 on 3 January 1968 (reference 9400-68-462). The following nonmetallic materials are presently being considered for use and do not appear on DR1111.

### NOTE

DR1111, materials approved for the Mission Module, was removed from the contract. Itek, therefore, has no list of approved materials for the external environment. DR1111 is presently being used as a guide on verbal direction from the contractor.

1. RTV-40 GE
2. Kernacryl Thermal Paint, Sherwin Williams
3. LCA-4 adhesive, Bacon, Indiana
4. Glyptal, GE
5. Teflon insulated wire
6. Silicone jacketed flat cable.

~~SECRET/SPECIAL HANDLING~~

~~SECRET~~/SPECIAL HANDLING

### 11.3 PROCESS USE AND APPLICATION DATA

Fifteen processes have been identified with the fabrication of the scanner. Of these processes, five are defined in Itek standard processes specifications which have been submitted to the contractor for approval. These process specifications did not contain outgassing criteria. The appropriate changes are being formulated for resubmission. The nonstandard processes required for the scanner will be submitted for approval upon completion of the specifications. Preliminary information is included in Section 3 of Appendix 11A.

~~SECRET~~/SPECIAL HANDLING

~~SECRET/SPECIAL HANDLING~~

#### 11.4 RELIABILITY FIGURE OF MERIT

The apportioned scanner reliability MTBF was established at 13,300 hours (see Section 4 of Appendix 11A). The baseline is based upon the initial RFMA and represents a series configuration. The following comparisons are also based on a series configuration:

1. Initial PDR MTBF is 13,300 hours
2. Internal Design Review, March 1968, MTBF is 15,600 hours
3. Current Scanner MTBF is 38,216 hours.

It can be seen that the predicted MTBF has more than doubled the last prediction. This reliability improvement can be related to the following:

1. Reduced complexity of the encoder from the previous estimate.
2. The number of gimbal bearings has been reduced. The number of bearings in the roll housing has been reduced to 12 from 20.
3. Elimination of a separate launch lock mechanism for pitch axis. One lock for both roll and pitch using redundant pyros is provided.
4. The K factors suggested for use by the contractor for "high reliability" parts improves the predicted MTBF.

~~SECRET/SPECIAL HANDLING~~

~~SECRET/SPECIAL HANDLING~~

### 11.5 FAILURE MODE AND EFFECTS ANALYSIS

The FMEAS (see Section 5 of Appendix 11A) must assume a solution to the present scanner design problems and successful demonstration under the simulated environmental conditions of the qualification test. Potential problems are ranked as critical, major, minor, and safe in accordance with the effect on A/O performance or safety and the likelihood of occurrence (reference RE101D). No critical problem areas were identified (i.e., disabling failure modes having a significant probability of occurrence during the mission). There were seven failure modes identified which could represent (major) problem areas. They are as follows:

1. Time variation in pointing alignment due to changes in pressure or breathing which would alter the vehicle shape, such as, to move the scanner relative to the vehicle axis.
2. Loss in resolution due to image jitter which could be caused by frictional changes in any of the contributors to PSD (e.g., bearings, cablings, lubricant, retaining hardware, etc.).
3. Encoder disc failure (emulsion or glass) would disable the affected A/O.
4. Failure of the stator permanent magnet within the torquer would disable the scanner.
5. If the scanner is not put into the stow position before the shroud is closed, damage to both areas may occur.
6. For an unbalanced design or release, premature firing of the launch lock EED's would allow free movement of the scanner when exposed to the dynamic environment. The possibility would exist of substantial damage to the shroud, scanner and/or vehicle pressure wall.
7. Unable to release launch lock due to jamming of the mechanism.

~~SECRET/SPECIAL HANDLING~~

~~SECRET~~/SPECIAL HANDLING

#### 11.6 HAZARD MODE AND EFFECTS

The following potential hazard modes have been identified:

1. Possible injury (eye) to test personnel of EED case ruptures during preflight checkout. Special safety procedures must be followed by all maintenance personnel when testing these devices.
2. Damage to pressure wall or window by the scanner (unbalanced) in the event of premature launch lock release.
3. The scanner structure will be beryllium. This metal produces toxic dust particles during machining operations. Although it is not expected that any machining, filing or drilling will be performed in the field, all personnel should be aware of the hazards of working this metal.

~~SECRET~~/SPECIAL HANDLING

~~SECRET~~/SPECIAL HANDLING

11.7 LIFE LIMITED DEVICES

This analysis did not reveal any life limited devices that would fall within the storage period of 5 years. Further investigation is required to provide backup analysis or data for the EED's, and lubricants.

~~SECRET~~/SPECIAL HANDLING

~~SECRET~~/SPECIAL HANDLING

11.8 REPORT EFFECTIVE DATE

The engineering data used for these analyses represent information available as of 25 June 1968. Listed in Section 8 of Appendix 11A are the drawings and specification applicable to this report.

~~SECRET~~/SPECIAL HANDLING

~~SECRET~~/SPECIAL HANDLING

## 12. QUALITY ASSURANCE

### INSPECTION

Several areas of the scanner assembly require special quality considerations. These have been identified as supplier selection and control, cleanliness and special processes.

Of the three bearing suppliers considered thus far, two have been surveyed (Split Ball Bearing and New Hampshire Ball Bearing) and third (Fafnir Bearing Co.) is anticipated in the near future. Results indicate both of the suppliers surveyed are acceptable.

Torque motors are brushless type and will be procured from Aeroflex Labs Inc., a sole source supplier. Although this manufacturer has been surveyed and accepted it is recognized that close controls will be required.

Because scanner locks are pyrotechnic devices they will require special considerations and a qualification program. Although no specification is available at this time one supplier (Atlas Chemical Co.) has been considered because of related experience in this type work.

The encoders are under subcontract to Wayne-George Division of Itek Corporation. A special QA and Reliability program is under way at that facility in order to meet our unique requirements.

All beryllium parts (trunnion, scan bezel, bezel cover, gimbal, yoke pedestal and main drive housing) will be procured from suppliers approved for use on this program.

Gyros, although customer furnished, will undergo electrical inspection. Because Itek does not have gyro testing capability, gyro testing is planned at an outside test lab.

The majority of the foregoing components will require source inspection by Itek personnel. In addition, test reports, analysis, X rays and certifications will be mandatory.

Two important inspection considerations during the fabrication cycle will be cleanliness and special processes. Cleanliness requirements will be imposed on those parts that cannot be subsequently cleaned at the next higher assembly. These same parts will be inspected and sealed in containers at the source. Subassembly will take place under class 100 clean conditions and precautions will be taken to ensure class 10,000 during testing.

The majority of inspection will be performed in-process, as against final. In this way critical alignments can be checked and recorded on-the-spot. The two special processes that have been identified at this time are bearing cleaning (relubrication) and mirror potting. Bearing cleaning procedure is still under investigation and mirror potting procedure rough draft is complete.

~~SECRET~~/SPECIAL HANDLING